Contact Metamorphic Processes in the Etive Aureole, Scotland

A Thesis Submitted to The University of Manchester for the Degree of Doctor of Philosophy in the Faculty of Science

1999

Mohssen Moazzen

Department of Earth Sciences
The University of Manchester

(DYFQA)

Table of Contents

Table of Contents	2
List of Figures	9
List of Tables	14
List of Plates	16
Abstract	18
Declaration	19
Acknowledgements	20
Dedication	21

Chapter 1 Introduction

1.1 Contact Metamorphism	22
1.2 Important problems in contact metamorphism that still need to be addressed	25
1.3 Specific objectives	27
1.4 Methodology	28
1.5 Structure of the thesis	28

Chapter 2 Geology of the Etive area in the Grampian Highlands of Scotland

2.1 Introduction	30
2.2 Geographical setting of the Etive area in the Grampian Highlands	32
2.3 Structural evolution of the Grampian Highlands	33
2.4 Stratigraphy of the Dalradian Supergroup in the Grampian Highlands and the Etive area	34
2.4.1 Lithostratigraphy of the Etive area	37
2.5 Structural Geology of the Dalradian Supergroup in the Grampian Highlands and the Etive area	40
2.6 Regional metamorphism of the Dalradian Supergroup	44

2.7 Age of regional metamorphism 47
2.8 Magmatic activities associated with Dalradian 49
2.8.1 Magmatic activities in the Etive area 51
2.9 Contact metamorphism of the Dalradian rocks by the 'Newer Granites' 55
2.9.1 Contact metamorphism in the Etive area 57

Chapter 3 Petrography and geochemistry of the Etive Igneous Complex

3.1 Introduction 58
3.2 Field relations 58
3.2.1 Internal contacts in the igneous rocks 59
3.2.2 Contacts with the country rocks 59
3.2.3 Dykes 62
3.3 Petrography of the main intrusive rocks 63
3.3.1 Cruachan intrusion 63
3.3.2 Meall Odhar intrusion 67
3.3.3 Quarry intrusion 67
3.4 Geochemistry 72
3.4.1 Major and trace elements variation 72
3.4.2 Rock classification 73
3.4.3 Magmatic characteristics 75
3.4.4 Minor and trace elements 77
3.4.5 Tectonomagmatic features 80
3.5 Mineral chemistry 82
3.5.1 Feldspar 82
3.5.2 Biotite 86
3.5.3 Amphiboles 88
3.5.4 Pyroxenes 92
3.5.5 Oxide minerals 94
3.6 Thermobarometry of igneous rocks 94
3.6.1 Barometry 95
3.6.2 Two-feldspar thermometry 97
3.6.3 Ternary feldspar thermometry 98
3.6.4 Opx-Bt thermometry 99

3.6.5 Hbl-Pl thermometry 100
3.6.6 Opx-Cpx thermometry 101

Chapter 4 Structural Geology of the Dalradian Supergroup in the Etive area

4.1 Introduction 103
4.2 Loch Creran sub-area 104
4.3 North Bonawe sub-area 109
4.4 South Bonawe sub-area 113
4.5 South Loch Awe sub-area 115
4.6 North Loch Awe sub-area 119
4.7 Summary 127

Chapter 5 Petrography of the metamorphic rocks

5.1 Introduction 130
5.2 Metamorphosed basic rocks 130
5.2.1 Regional metamorphic metabasites 131
5.2.2 Contact metamorphic metabasites 132
5.2.3 Retrogressive alteration of metabasic rocks 136
5.2.4 Distribution of the mineral zones and isograds in the metabasic rocks 136
5.3 Petrography of the non-graphitic pelites and semi-pelites 143
5.3.1 Regional metamorphic pelites and semi-pelites 143
5.3.2 Contact metamorphic pelites and semi-pelites 144
5.3.3 Retrogressive alteration of the pelitic rocks 159
5.3.4 Distribution of the mineral zones and isograds in the pelitic rocks 159
5.4 Petrography of the graphitic pelites and semi-pelites 162
5.4.1 Regional metamorphic graphitic rocks 162
5.4.2 Contact metamorphic graphitic rocks 163
5.4.3 Retrograde alteration of the graphitic rocks 170
5.4.4 Distribution of mineral zones and isograds in the graphitic rocks 172

5.5 Petrography of calc-silicates and marbles 173
5.5.1 Regional metamorphic calc-silicates and marbles 173
5.5.2 Contact metamorphic calc-silicates and marbles 173
5.6 Petrography of the meta-andesites 179

Chapter 6 Petrography of pelitic and semi-pelitic migmatites

6.1 Introduction 180
6.2 Field relation of Etive migmatites 181
6.2.1 Migmatites with small-scale leucosomes with pull-apart structures 181
6.2.2 Migmatites with small-scale cross-cutting leucosomes 182
6.2.3 Migmatites with medium-scale leucosomes 187
6.3 Mineralogical classification of migmatites 187
6.3.1 Qtz+Kfs±Ms leucosomes 187
6.3.2 Qtz+Kfs+Crd-bearing leucosomes 189
6.3.3 Garnet-bearing leucosomes 189
6.3.4 Orthopyroxene-bearing leucosomes 189
6.4 Chemical characteristics of leucosomes in migmatites 189
6.5 Evidence for partial melting 192
6.6 Discussion 195
6.6.1 Controls on leucosome shapes 195
6.7 Conclusions 197

Chapter 7 Mineral chemistry of the metamorphic rocks

7.1 Introduction 198
7.2 Mineral chemistry of metabasic rocks 198
7.2.1 Amphibole 199
7.2.2 Biotite 203
7.2.3 Plagioclase 204
7.2.4 Clinopyroxene 207
7.2.5 Orthpyroxene 207
7.2.6 Other minerals 208

7.3 Mineral chemistry of the pelitic and semi-pelitic rocks 211
7.3.1 Muscovite 211
7.3.2 Biotite 211
7.3.3 Cordierite 216
7.3.4 K-feldspar 220
7.3.5 Plagioclase 220
7.3.6 Spinel 220
7.3.7 Garnet 221
7.3.8 Orthopyroxene 223
7.3.9 Other minerals 224

Chapter 8 Metamorphic Reactions

8.1 Introduction 229
8.2 Metamorphism of basic rocks 230
8.2.1 Choice of compatibility diagrams 231
8.2.2 Regional metamorphic metabasites 231
8.2.3 Lower Hornblende Zone 232
8.2.4 Upper Hornblende Zone 233
8.2.5 Lower Clinopyroxene Zone 233
8.2.6 Upper Clinopyroxene Zone 238
8.2.7 Orthopyroxene Zone 238
8.3 Comparison with other aureoles involving basic rocks 238
8.4 Contact metamorphism of pelitic and semi-pelitic rocks 240
8.4.1 Choice of projections 240
8.4.2 Quartz-bearing pelites and semi-pelites 240
8.4.2.1 Regional metamorphic assemblages 240
8.4.2.2 Biotite and Cordierite Zones (Zone I) 241
8.4.2.3 Andalusite Zone (Zone II) 241
8.4.2.4 Andalusite-K-feldspar Zone (Zone III) 243
8.4.2.5 Partial melting within the Spinel Zone (Zone VI) 244
8.4.3 Quartz-absent pelites 244
8.4.3.1 Corundum Zone (Zone V) 245
8.4.3.2 Spinel Zone (Zone VI) 245
8.4.3.3 Sillimanite Zone (Zone VII) 246
8.4.4 Pressure estimation using a petrogenetic grid 248

8.5 Contact metamorphism of pelitic and semi-pelitic rocks in the W aureole 250
8.6 Constraints on fluid activity 252
8.7 Conclusions 252

Chapter 9 Geothermobarometry

9.1 Introduction 254
9.2 Thermodynamic basis for thermobarometry 254
9.3 Activity-mole fraction relations 256
9.4 Calculating activities of real phases 257
9.4.1 Cordierite and spinel activities 258
9.4.2 Pyroxene activities 258
9.4.3 Biotite activities 259
9.4.4 Feldspar activities 259
9.4.5 Garnet activities 260
9.5 Criteria for selecting rocks for P-T calculations 261
9.5.1 Rock equilibrium 261
9.5.2 Practical approach to collecting analyses for thermobarometry 262
9.6 THERMOCALC 263
9.7 Error estimation in thermobarometry 263
9.8 Geothermometry 264
9.8.1 Spinel-Cordierite thermometry 264
9.8.2 Garnet-Biotite thermometry 266
9.8.3 Garnet-Cordierite thermometry 269
9.8.4 Biotite-Orthopyroxene thermometry 270
9.8.5 Orthopyroxene-Clinopyroxene thermometry 271
9.8.6 Calcite-Dolomite thermometry 272
9.8.7 Amphibole-Plagioclase thermometry 274
9.9 Geobarometry 276
9.10 Constraints on a_{H2O} during contact metamorphism 277
9.10.1 Calculation of aH_2O from cordierite water contents 279
9.10.2 Calculation of a_{H2O} in high grade pelitic rocks using other dehydration equilibria 281
9.10.3 Calculation of a_{H2O} in high grade metabasites 283
9.11 Conclusions 285

Chapter 10 Discussion and Conclusions

10.1 Introduction 288
10.2 Conclusions and Discussion 288
10.2.1 Emplacement of the Quarry Diorite 288
10.2.2 Partial melting in the aureole 289
10.2.3 Implications for fluid behaviour 290
10.2.4 Problems of deducing reactions in inner-aureole rocks 292
10.2.5 Implications of geothermometric and geobarometric results 293
10.3 Scope for future work 293

Appendices

Appendix 1 XRF whole rock analysis 295
A1.1 Sample preparation 295
A1.2 Analysis and processing 295
A1.3 Limitation of the technique 295
A1.4 Quality assessment-comparison of internal standards 296
Appendix 2 Whole rock chemistry of igneous samples 297
Appendix 3 Electron Microprobe 302
A3.1 Sample preparation 302
A3.2 Machine Used 302
A3.3 Operation Condition 302
Appendix 4 Microprobe Results of Igneous Minerals 304
Appendix 5 Microprobe Results of Metamorphic Minerals 313
Appendix 6 F contents of biotites in pelites from WD microprobe analyses 353
Appendix 7 Ion Probe set-up 355
A7.1 Sample preparation 354
A7.2 Standards used 354
A7.3 Ion Probe setting-up 354
Appendix 8 Activity models for biotite, garnet and plagioclase 357

References 360

List of Figures

Figure 2.1 Distribution of Dalradian Supergroup and its subdivisions 31

Figure 2.2 Geographical setting of the studied area 33

Figure 2.3 Geological map of the Etive area 38

Figure 2.4 Structural map of the Etive area 42

Figure 2.5 Cross section across the Dalradian rocks in the Etive area 43

Figure 2.6 Metamorphic map of the Dalradian Supergroup 45

Figure 2.7 Distribution of the peak regional metamorphic pressures in Dalradian rocks 48

Figure 2.8 Location of the main granitoid intrusions in the SW Scotland 50

Figure 2.9 Geological map of the Etive igneous complex 53

Figure 2.10 Distribution of dykes in the Etive area 54

Figure 3.1 Sketch drawing of field relations amongst different igneous rocks 60

Figure 3.2 Equal area rose diagram for dyke trends in the Etive area 64

Figure 3.3 Locality of igneous rock samples in the study area 65

Figure 3.4 Variation diagram for the Etive igneous rocks 74

Figure 3.5 Classification of the Etive igneous rocks using Qtz-Kfs-Pl diagram 76

Figure 3.6 Classification of the Etive igneous rocks using $(K_2O+Na_2O)/SiO_2$ diagram 76

Figure 3.7 Classification of the Etive igneous rocks using An-Ab-Or diagram 78

Figure 3.8 Molar $Al_2O_3/(CaO+Na_2O+K_2O)$ diagram for Etive igneous rocks 78

Figure 3.9 Na_2O versus K_2O diagram for the Etive igneous rocks 79

Figure 3.10 K_2O versus SiO_2 diagram for the Etive igneous rocks 79

Figure 3.11 Comparison of the trace element distribution in the Etive igneous rocks 81

Figure 3.12 Comparison of the trace element distribution in the Etive igneous rocks 82

Figure 3.13 K/Rb diagram for the Etive igneous rocks 83

Figure 3.14 Nb/Y diagram for the Etive igneous rocks 83

Figure 3.15 Rb/(Nb+Y) diagram for the Etive igneous rocks 84

Figure 3.16 Y/SiO_2 diagram for the Etive igneous rocks 84
Figure 3.17 Rb/SiO_2 diagram for the Etive igneous rocks 85
Figure 3.18 Classification of igneous feldspars using An-Ab-Or diagram 87
Figure 3.19 Zoning profiles in igneous plagioclases 87
Figure 3.20 TiO_2-FeO-MgO triangular diagram for igneous biotites 89
Figure 3.21 Classification of the igneous biotites using SAF diagram 89
Figure 3.22 Classification of igneous amphiboles using (Na+K)/Si diagram 91
Figure 3.23 Ca+Na+K versus Si diagram for igneous amphiboles 92
Figure 3.24 Composition of igneous pyroxenes in Wo-En-Fs triangular diagram 93
Figure 3.25 Estimates of the crystallisation pressure of the Etive igneous Complex 96
Figure 3.26 Triangular Qtz-Ab-Or diagram for Etive igneous rocks 96
Figure 3.27 Two feldspar thermometry of the Etive igneous rocks 99
Figure 3.28 Two pyroxene thermometry of the Etive igneous rocks 101
Figure 4.1 Sketch map of the locality of the sub-areas in the Etive area 104
Figure 4.2 Symbols used in the structural maps 105
Figure 4.3 Structural map of the Loch Creran sub-area 106
Figure 4.4 Stereoplot for structural features in the Loch Creran sub-area 107
Figure 4.5 Structural map of the North Bonawe sub-area 110
Figure 4.6 Schematic block diagram for structures in the North Bonawe sub-area 109
Figure 4.7 Stereoplot for bedding and D_1 deformational phase in the North Bonawe sub-area 111
Figure 4.8 Stereoplot for D_2 and D_3 deformational phases in the North Bonawe sub-area 111
Figure 4.9 Structural map of the South Bonawe sub-area 114
Figure 4.10 Stereoplot for bedding, D1 and D2 deformational phases in the South Bonawe sub-area 115
Figure 4.11 Structural map of the South Loch Awe sub-area 118
Figure 4.12 Stereoplot for structural data from the South Loch Awe sub-area 117
Figure 4.13 Structural map of the western part of the North Loch Awe sub-area 120
Figure 4.14 Structural map of the eastern part of the North Loch Awe sub-area 121

Figure 4.15 Sketch block diagram of F_2 fold with "S" asymmetry 122
Figure 4.16 Sketch block diagram of F_2 fold with "Z" asymmetry 122
Figure 4.17 Sketch block diagram of structures in North Loch Awe sub-area 123
Figure 4.18 Stereoplot for bedding and D_1 phases in the North Loch Awe sub-area 124
Figure 4.19 Stereoplot for D_2 deformational phase in the North Loch Awe sub-area 125
Figure 4.20 Stereoplot for D_3 deformational phase in the North Loch Awe sub-are 125
Figure 4.21 Direction of the F_2 folds axial traces 127
Figure 4.22 Axial traces of the F_2 folds in the North Loch Awe sub-area 128
Figure 5.1 Distribution of sample localities, metamorphic zones and isograds in metabasites 139
Figure 5.2 Distribution of minerals in regional and contact metabasites in the Loch Awe area 140
Figure5.3 Distribution of sample localities, metamorphic zones and isograds in pelites and semi-pelites in the Loch Awe area 147
Figure 5.4 Distribution of sample localities in pelites and semi-pelites in the Bonawe area 167
Figure 5.5 Distribution of sample localities in pelites and semi-pelites in the Creran area 168
Figure 6.1 K_2O versus Na_2O diagram for leucosome 194
Figure 6.2 Distribution of trace elements in leucosome 194
Figure 7.1 Classification of metamorphic amphiboles 200
Figure 7.2 (Mg+Fe) versus Al^{iv} diagram for metamorphic amphiboles 201
Figure 7.3 Relationship between Ti content of amphiboles and distance from the igneous contact 202
Figure 7.4 $Mg/(Mg+Fe^{2+})$ content of amphiboles versus distance from the igneous contact 202
Figure 7.5 Al (total) in amphiboles versus distance from the igneous contact 203
Figure 7.6 Plot of Na concentration in amphiboles versus distance from the igneous contact 203
Figure 7.7 Classification of biotites in metabasites 205
Figure 7.8 Plot of Mg/(Mg+Fe) in metabasic biotites 205
Figure 7.9 Histogram of plagioclase composition in metabasites 206

Figure 7.10 Relationship between An mole% in plagioclase and distance from the igneous contact 207
Figure 7.11 Wo-En-Fs triangular diagram for pyroxenes in metabasites 209
Figure 7.12 classification of muscovites in the (semi)pelitic rocks 212
Figure 7.13 Classification of biotites in the (semi)pelitic rocks 214
Figure 7.14 Relationship between fluorine content in pelitic biotites and distance from the igneous contact 215
Figure 7.15 Relationship between Mg/(Mg+Fe) value for pelitic biotites with distance from the igneous contact 215
Figure 7.16 Histogram of Mg/(Mg+Fe) values for cordierite 216
Figure 7.17 Relationship between Mg/(Mg+Fe) value of cordierites and distance from the igneous contact 218
Figure 7.18 Relationship between H_2O (wt%) in cordierites and distance from the igneous Contact 220
Figure 7.19 Composition of K-feldspar plotted on An-Ab-Or diagram 222
Figure 7.20 Composition of spinels plotted on a Mg-Fe^{2+}-Mn diagram 225
Figure 7.21 Compositions of spinels plotted on a Cr-Al-Fe^{3+} diagram 225
Figure 7.22 Composition of regional and contact metamorphic garnets plotted on the (Ca+Mn)-Fe^{2+}-Mg diagram 226
Figure 7.23 Zoning profiles across the regional and contact metamorphic garnets 227
Figure 7.24 Composition of orthopyroxene from the psammitic rocks plotted on the Wo-En-Fs diagram 228
Figure 8.1 Mineral parageneses of metabasites plotted on NA-A-C-(FM) diagram 234
Figure 8.1 Continued 235
Figure 8.2 Projection of regional and low-grade contact metabasites on AFM diagram 236
Figure 8.3 Metabasite parageneses plotted on AC(FM) diagrams 237
Figure 8.4 AFM projections of Qtz-bearing metapelites 242
Figure 8.5 AFM projection of garnet-bearing metapelites 243
Figure 8.6 SFM projections of Qtz-absent metapelites 247
Figure 8.7 Petrogenetic grid showing the metamorphic reaction successions in pelitic rocks 251
Figure 9.1 Opx-Cpx thermometry of metabasites 273
Figure 9.2 Cal-Dol thermometry of regional metamorphic rock 275
Figure 9.3 Temperature -distance relation within the aureole 275

Figure 9.4 Barometry using amphibole composition in metabasites 276
Figure 9.5 Thermobarometry in pelitic rocks 278
Figure 9.6 Experimental data of Mirwald, *et al.,* 1979 for
cordierite dehydration 282
Figure 9.7 Water activity-distance relation within the aureole 282
Figure 9.8 Estimation of water activity in Sillimanite Zone pelitic sample 284

List of Tables

Table 2.1 Main subdivision of the Dalradian Supergroup 35

Table 2.2 Stratigraphic sequence in SW Scotland 39

Table 2.3 Major faults in the SW and Central Highlands 41

Table 2.4 History of igneous activities in the Etive area 44

Table 2.5 Pelitic isograd reactions in the Barrovian type mtamorphism 46

Table 3.1 Field information on dykes in the Etive area 63

Table 3.2 Representative mineral assemblages in the igneous rocks 68

Table 3.3 Representative analyses from igneous feldspars 73

Table 3.4 Representative analyses from igneous biotites 86

Table 3.5 Representative analyses from igneous amphiboles 88

Table 3.6 Representative analyses from igneous pyroxenes 90

Table 3.7 Representative analyses from igneous oxide minerals 93

Table 3.8 Results from Hbl-Pl thermometry of igneous rocks 94

Table 3.9 Results from Hbl-Pl thermometry 101

Table 5.1 Mineral assemblages in metabasites 137

Table 5.2 Summary of the mineral zones, assemblages and isograds in metabasites 143

Table 5.3 Mineral assemblages in non-graphitic pelites 145

Table 5.4 Mineral assemblages in graphitic pelites and semi-pelites 164

Table 5.5 Mineral assemblages in calc-silicates 175

Table 6.1 Chemical composition of leucosome 192

Table 7.1 Representative analyses of amphiboles in metabasites 199

Table 7.2 Representative analyses of biotites in metabasites 204

Table 7.3 Representative analyses of plagioclases in metabasites 206

Table 7.4 Representative analyses of clinopyroxenes in metabasites 208

Table 7.5 Representative analyses of orthopyroxenes in metabasites 209

Table 7.6 Representative analyses of chlorite, garnet calcite and epidote in metabasites 210

Table 7.7 Representative analyses of muscovite in pelites 212

Table 7.8 Representative analyses of biotites in pelites 213

Table 7.9 Representative analyses of cordierite in pelites 216

Table 7.10 H_2O content in cordierites 219

Table 7.11 Representative analyses of K-feldspar in pelites 221
Table 7.12 Representative analyses of plagioclase in pelites 223
Table 7.13 Representative analyses of spinel in pelites 224
Table 7.14 Representative analyses of garnet in pelites 226
Table 7.15 Representative analyses of orthopyroxene in psammites 228
Table 8.1 Summary of metamorphic reactions in pelites 249
Table 9.1 Results from the cordierite-spinel thermometry 266
Table 9.2 Results from the garnet-biotite thermometry 268
Table 9.3 Results from the garnet-cordierite thermometry 270
Table 9.4 Results from the orthopyroxene-biotite thermometry 271
Table 9.5 Results from the orthopyroxene-clinopyroxene thermometry 272
Table 9.6 Results from the amphibole-plagioclase thermometry 274
Table 9.7 a_{H2O} in pelitic rocks 280
Table 9.8 a_{H2O} in metabasites 283

List of Plates

Plate 3.1 Contact between igneous and country rocks 61

Plate 3.2 Andesitic xenolith in the granodiorite 61

Plate 3.3 Photomicrograph of hornblende granodiorite 69

Plate 3.4 Photomicrograph of hornblende monzodiorite 69

Plate 3.5 Photomicrograph of pyroxene diorite 70

Plate 3.6 Photomicrograph of Meall Odhar alkali-granite 70

Plate 3.7 Photomicrograph of two-pyroxene diorite 71

Plate 3.8 Photomicrograph of pyroxene diorite 71

Plate 4.1 Photomicrograph of crenulation cleavage in pelitic rocks 108

Plate 4.2 Photomicrograph of S_1 slaty cleavage and D_2 deformational phase 108

Plate 4.3 Photomicrograph of S_1 slaty cleavage and S_2 crenulation cleavage from the North Bonawe sub-area 112

Plate 4.4 Photomicrograph of S_2 crenulation cleavage in pelitic rocks of Ardrishaig Phyllite 112

Plate 4.5 F_1 and F_2 folds in calc-silicates of Ardrishaig Pyllite 116

Plate 4.6 Tight F_1 fold and F_2 fold in calc-silicate from the south Bonawe sub-area 116

Plate 4.7 F_2 fold with 'S' asymmetry in Ardrishaig Phyllite 126

Plate 4.8 S_1 slaty cleavage and S_2 crenulation cleavage in the pelitic rocks from the North Loch Awe sub-area. 126

Plate 5.1 Photomicrograph of regional metamorphic greenschist 141

Plate 5.2 Photomicrograph of high-grade contact metamorphic metabasite 141

Plate 5.3a Photomicrograph of Opx-Cpx-Hbl hornfels (PPL) 142

Plate 5.3b Photomicrograph of Opx-Cpx-Hbl hornfels (XPL) 142

Plate 5.4 Photomicrograph of And-Kfs-Crd-Ms-Bt hornfels 152

Plate 5.5 Photomicrograph of And-Kfs-Crd-Ms-Bt hornfels 152

Plate 5.6 Photomicrograph of Spl-And-Crd-Kfs hornfels 153

Plate 5.7 Photomicrograph of Spl-Crn-And-Crd-Kfs hornfels 153

Plate 5.8 Photomicrograph of Sill-Spl-Crn-Crd-Kfs hornfels (PPL) 154

Plate 5.9 Photomicrograph of Sill-Spl-Crn-Crd-Kfs hornfels (XPL) 154

Plate 5.10 Textural evidence for reaction And=Sill (PPL) 155

Plate 5.11 Textural evidence for reaction And=Sill (XPL) 155

Plate 5.12 Photomicrograph of Sil-And-Spl-Crd-Kfs-hornfels 156

Plate 5.13 Photomicrograph of contact-metamorphic and regional-metamorphic garnets 156
Plate 5.14 Photomicrograph of garnet-bearing leucosome (PPL) 157
Plate 5.15 Photomicrograph of garnet-bearing leucosome (XPL) 157
Plate 5.16 Photomicrograph of Opx-bearing leucosome (PPL) 158
Plate 5.17 Photomicrograph of Opx-bearing leucosome (XPL) 158
Plate 5.18 Photomicrograph of graphitic, semi-pelitc hornfels 171
Plate 5.19 Photomicrograph of Crn-bearing graphitic hornfels 171
Plate 5.20 Photomicrograph of scapolite-diopside hornfels 177
Plate 5.21 Photomicrograph of wollastonite-garnet-diopside-titanite hornfels 177
Plate 5.22 Photomicrograph of garnet-diopside-wollastonite hornfels (PPL) 178
Plate 5.23 Photomicrograph of garnet-diopside-wollastonite hornfels (XPL) 178
Plate 6.1 Migmatite with pull-apart structure 183
Plate 6.2 Hand specimen of migmatite with pull-apart structure 183
Plate 6.3 Migmatites with pull-apart and breccia structures 184
Plate 6.4 Sketch drawing of migmatites in Plate 6.3 183
Plate 6.5 Photomicrograph of leucosome and mesosome in migmatites (PPL) 185
Plate 6.6 Photomicrograph of leucosome and mesosome in migmatites (XPL) 185
Plate 6.7 Migmatites with cross-cutting leucosomes 186
Plate 6.8 Migmatites with cross-cutting and randomly oriented leucosomes 186
Plate 6.9 Photomicrograph of migmatites with cross-cutting leucosomes (PPL) 188
Plate 6.10 Photomicrograph of migmatites with cross-cutting leucosomes (XPL) 188
Plate 6.11 Migmatites with medium-scale leucosomes 190
Plate 6.12 Medium-scaled, sub-parallel leucosomes 190
Plate 6.13 Photomicrograph of medium-scaled leucosomes 191
Plate 6.14 Leucosomes in sample MM141 191
Plate 6.15 Photomicrograph of sample MM192D from a leucosome 192

Abstract

The intrusion of the Etive igneous complex, one of the Caledonian 'Newer Granites' into Dalradian metasedimentary and metabasic rocks of the S.W. Grampian Highlands during the Devonian caused contact metamorphism, producing a thermal aureole up to 2 km wide.

The highest temperature of the igneous rocks, during emplacement, was about 1000°C and the fluid content of the dioritic rocks was probably low.

At least three phases of ductile deformation occurred during regional metamorphism, prior to the contact metamorphism. The main deformational phase in the southern part of the aureole was the D_2 phase, represented by an intense S_2 crenulation cleavage.

Contact-metamorphic mineral assemblages are developed in basic, (semi)pelitic and calcareous rocks. In the southern segment of the aureole, adjacent to the Quarry Diorite, four metamorphic zones were distinguished in basic rocks; Hbl Zone, Hbl+Ep+Cpx Zone, Hbl+Cpx Zone and Hbl+Cpx+Opx Zone, and seven metamorphic zones were mapped in the (semi)pelitic rocks: Bt Zone, Crd Zone, And Zone, And+Kfs Zone, Crn Zone, Spl Zone and Sil Zone. Chemically suitable pelites and semi-pelites from the Upper Spl Zone and Sil Zone underwent partial melting. The contact-metamorphic zones are concentric and there is no structural control on the distribution of the zones, but original layering (bedding) and S_2 crenulation cleavage have influenced the distribution of the leucocratic veinlets in some migmatites.

The compositions of amphiboles and plagioclases in metabasites vary systematically with distance from the igneous contact (contact-metamorphic grade). The F content of biotite and H_2O content of cordierite also vary with distance from the igneous contact.

Metamorphic reactions are deduced for metabasites and pelites on the basis of mineral chemistry and phase relations in selected projections. When plotted on a petrogenetic grid, the sequence of reactions in pelites indicates a pressure of ca. 2 kbar for the contact metamorphism.

Application of thermometry to rocks with low-variance assemblages gives a temperature of ~550°C for the regional metamorphic rocks outside the aureole, ~650°C for And-Kfs Zone, ~700°C for Crn Zone, ~750°C for Spl Zone and ~800-850°C for Sil Zone. Barometry of pelitic assemblages yields a pressure of ca. 2 kbar for the contact-metamorphism. Water activity calculations suggest that contact-metamorphic reactions were water-saturated in the And Zone, And+Kfs Zone, Crn Zone and Lower Spl Zone and were water-undersaturated in the Upper Spl Zone and Sil Zone. Melting reactions were water-saturated at the onset of anatexis, but the subsequent melting reactions were water-undersaturated.

Declaration

No portion of the work referred to in the thesis has been submitted in support of an application for another degree or qualification at this or any other university or other institute of learning.

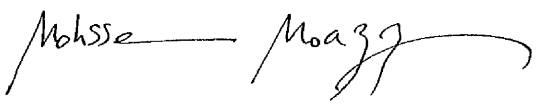

Mohssen Moazzen

Copyright and Intellectual Property Rights

The ownership of any intellectual property rights, which may be described in this thesis is vested in the University of Manchester, subject to any prior agreement to the contrary, and may not be made available for use by third parties without the written permission of the University, which will be prescribe the terms and conditions of any such agreement.

Further information on the conditions under which disclosures and exploitation may take place is available from the Head of Department of Earth Sciences.

Acknowledgements

Firstly I would like to express my deepest gratitude to Dr. Giles Droop. I am indebted to him for his extremely patient tutoring in thermodynamics, mineralogy and metamorphism. This thesis would not have been possible without Dr. Droop's help and support. I thank Prof. Henderson for his guidance and proof-reading of the thesis. Also I thank Dr. A. Pawley for her help and comments on the thesis. Many thanks go to Dr. K. Brodie for her advice and fruitful discussion and to Dr. J. Treagus for his support and comments on Chapters 2 and 4. He provided some of the samples from the Etive area. I am grateful to Prof. Ben Harte, Prof. Simon Harley and Dr. Richard Hinton from the University of Edinburgh for their help during my SIMS session in Edinburgh. Dr. Chinner from the University of Cambridge provided samples from the Harker collection. I thank Dr. Richard Pattrick, Dr. Rob Gowthrope and Dr. Dave Polya for their help and support during my studies in Manchester. Valuable support was also provided by Dave Plant, Steve Caldwell and Tim Hopkins with microprobe analysis. I am also grateful to Paul Lythgoe and Tim Jensen for helping me to analyse my rocks. I thank Richard Hartley from Drawing Office and Sue Maher for processing my photos. Harry Lock and Dave Wright provided the field work facilities. Many thanks to all staff in thin sectioning Lab. I would like to thank the many landowners in the Etive area, especially Scottish Power and Mr. Smith of the Castle Estate for giving me access to their lands, and the people of Argyll for their friendliness and for occasionally giving me lifts. Also I would like to thank the kind people of Taynuilt, especially Tom and Margaret McLellan for their hospitality during my stay there.

I would like to take this opportunity to thank the Iranian Ministry of Culture and Higher Education for a grant to support my Ph.D. studies.

Last but not least, I thank my wife for her support, my daughter who endured diminished parental attention from me during my studies, and my father and mother for their continued help and support.

This Thesis is Dedicated to The Great Nation of Iran and to my Family

1.1 Contact Metamorphism

Contact metamorphism is a type of metamorphism, which takes place in heated rocks in the vicinity of contacts with intrusive igneous rocks. The metamorphosed part of the country rocks is known as an 'aureole'. Many contact aureoles are hosted in unmetamorphosed rocks but some aureoles are developed in rocks of the greenschist and amphibolite facies of regional metamorphism.

The history of development of the knowledge of contact metamorphism can be divided into three main periods. The first period was an era of pioneering studies of contact metamorphism in late 1800s and early 1900s. The second period is from early 1900s to the mid-1960s, during which careful petrographic studies provided a framework for an increased appreciation of the importance of minerals, mineral assemblages and reactions. Third period was from the mid-1960s onwards when the use of electron microprobe in petrological studies developed.

The study of contact metamorphism dates from 1817, when MacCulloch described the hardened schists in the contact aureole of the Ballachulish igneous complex in Scotland. Rosenbusch (1877) studied the spotted slates known as the Steiger Schiefer around the Barr-Andlau granite. He described three zones, based on general descriptive characteristics: *knotentonschiefer*, or knotted clay slate, *knotenglimmerschiefer*, or knotted mica schist, and '*hornfels*'. Goldschmidt (1911) studied the contact metamorphism in the Oslo area of Norway. He described different classes of hornfelses, based on assemblages of relatively small number of minerals. Eskola (1914) described the mineral assemblages in contact aureole in the Orijärvi district of Finland and by comparing the parageneses in the Oslo and Orijärvi aureoles, introduced the concept of metamorphic facies (Eskola, 1915). Another outstanding, classic work on contact metamorphism is the Tilley's (1924) paper on the assemblages in the contact aureole of the Carn Chois diorite (Comrie aureole) in Scotland.

In the second period, studies of contact metamorphism focused on increasingly detailed petrography, combined with wet chemical analysis of whole rocks and selected minerals. Some of the classic studies of this period includes: Onawa aureole, Maine (Philbrick, 1936; Moore, 1960), Donegal aureole, Ireland (Pitcher *et al.*, summarised in Pitcher & Berger, 1972), Tono aureole, Japan (Seki, 1957), Kisokoma aureole, Japan (Oki, 1958), aureoles in the Santa Rosa range, Nevada (Compton, 1960) and Cupsuptic aureole, Maine (Hardwood, 1966).

Reverdatto (1970) provided a summary of work prior to the development of electron microprobe.

The development of electron microprobe analysis enhanced the development of the contact metamorphic investigations dramatically. Among many well documented modern studies of contact metamorphism of pelitic rocks, notable examples include: the Steinach aureole, Bavaria (Okrusch, 1969, 1971), the Ronda aureole, Spain (Loomis, 1972a,b), the Cashel aureole, Ireland (Treloar, 1981), the aureole of the Duluth complex, Minnesota (Labotka, *et al.,* 1981, 1984), the Kiglapait aureole, Labrador (Speer, 1982; Berg & Docka, 1983), the Strontian aureole, Scotland (Tyler & Ashworth, 1982; Ashworth and Tyler, 1983), the Newer Gabbro aureoles, Scotland (Droop and Charnley, 1985), the Laramie aureole, Wyoming (Grant and Frost, 1990), the Lexington aureole, Maine (Dickerson & Holdaway, 1989) and the Ballachulish aureole, Scotland (Pattison and Harte, 1985,1991; Pattison, 1987, 1991).

The notable modern studies of contact metamorphism of limestones and calcareous rocks include: the Adirondacks aureole, New York (Tracy *et al.,* 1978; Valley and Essene, 1980), the Alta aureole, Utah (Moore and Kerrick, 1976), the Adamello aureole, Italy (Bucher-Nurminen, 1982), the Ballachulish aureole, Scotland (Masch and Heuss-Aβbichler, 1991), the Boulder aureole, Montana (Rice, 1977b), the North Peak aureole, Utah (Labotka *et al.,* 1988) and the Beinn au Dubhaich aureole, Skye, Scotland (Hoersch, 1981; Holness, 1992).

Well studied aureoles in the basic rocks include: the Cuillin aureole, Skye (Ferry *et al.,* 1987), the Skaergaard aureole (Manning and Bird, 1991), the Karmutsen aureole, Vancouver Island (Kuniyoshi and Liou, 1976; Shive *et al.,* 1991) and the Laramie aureole, Wyoming (Grant and Frost, 1990; Russ-Nabelek, 1989).

Although contact and regional metamorphism have traditionally been separated according to scale and to the spatial relationship to intrusive heat source, this separation has long been questioned. Belts of regional metamorphism typically contain abundant intrusives (Kerrick, 1991) and it is still not completely clear if intrusives collectively increase the regional thermal gradient and thus are a primary cause of regional metamorphism. Some investigators have regarded low-pressure/high-temperature regional metamorphism as regional-scale contact metamorphism (e.g. Spear, 1993).

Contact metamorphism can affect any rock type. Pelitic rocks usually form a wide range of contact-metamorphic pelitic mineral isograds and mineral zones and contact-metamorphic pelitic mineral assemblages vary systematically with pressure and temperature (Pattison, 1991). For this reason, aureoles in pelitic rocks have been studied widely (see references above).

The contact metamorphism of calcareous rocks has been the subject of numerous studies (see above). Because the bulk composition of the typical calcareous rock protoliths tend to be closely restricted to the simple system, CaO, MgO, SiO_2, H_2O and CO_2, the complex solid solutions that produce high-variance assemblages are not a problem in the study of the contact metamorphism of calcareous rocks. The phase relations among the large number of mineral phases in the rather simple calcareous systems are relatively amenable to study by detailed petrogenetic grids in which the stability of mineral assemblages can be related to pressure, temperature and fluid composition.

The study of contact metamorphic metabasites is more problematic. The reactions that occur during the contact metamorphism of metabasites have not been well established because of the large number of major chemical components in typical basic rock compositions and because of the high variation brought about by the extensive solid solutions in the major participant minerals. Therefore many studies of contact metamorphism have only briefly reviewed the metamorphism of basic rocks.

Contact metamorphism occurs on a relatively short time-scale. It is not usually polymetamorphic, unless it overprints existing regional metamorphism. Contact metamorphism normally occurs at essentially constant pressure as its duration is usually too short to allow significant erosion to occur during heating. All these

characteristics make a contact metamorphic aureole an ideal natural laboratory for the study of metamorphic processes. Information gained from the study of aureoles can thus help Earth Scientist understand the thermal evolution of the crust.

1.2 Important problems in contact metamorphism that still need to be addressed

Despite a wealth of knowledge on contact metamorphism, especially on metamorphic reactions and P-T conditions of metamorphism of pelitic and calcareous rocks, several important problems still need to be addressed. Some of these problems are as follows.

- More studies need to be done to assess the role of magmatism in the thermal evolution of contact metamorphic aureoles. The related questions include: How, exactly, is magmatic heat transferred into the surrounding rocks. To what extent does magmatically-derived fluid interact with the wall rocks, how is it introduced, and in what direction(s) does it flow? What is the effect of several magmatic intrusions in an igneous complex on the country rocks, and can the addition of a second batch of magma initiate new pulses of contact metamorphism that is discernible in the rock record? Also, to what extent do magmatic processes taking place within thermal aureoles (in zones of anatexis) affect those that take place within the pluton that is supplying the heat? Do these magmas mix or exchange components in any way?
- More investigations are necessary to assess the kinetics of contact metamorphic reactions. The factors controlling the nucleation kinetics include: heating rate (Joesten, 1991), degree of reaction overstepping (Joesten, 1991; Kerrick *et al.,* 1991) and degree of correspondence between reactant and product mineral lattices (Worden *et al.,* 1992) but little is known about reaction mechanisms. Measurement of modal mineralogy would provide a necessary monitor of reaction progress during prograde metamorphism and might allow distinctions to be made between the progress of divariant and univariant reactions (e.g. Reinhardt and Rubenach, 1989).
- In the case of contact-metamorphosed basic rocks, there are few applicable mineral exchange geobarometers and geothermometers, and two-pyroxene thermometry is sufficiently precise only in iron-rich compositions.

- Further research is therefore required for the development of additional thermometers and barometers. As stated above, details of the phase reactions and reaction sequences in contact-metamorphosed basic rocks are poorly known.

Fluids play a significant role in contact metamorphism and thus deserve particular attention. The application of fluid-inclusion techniques to contact-metamorphic rocks could be helpful in constraining the evolution of fluid compositions, although traditional fluid-inclusion studies on contact metamorphism could be technically difficult due to the small size of the inclusions themselves (see Masch and Aβbichler, 1991). The main questions in rock-fluid interactions are, the extent of the presence of fluid and its infiltration capacity, the source of fluid (either from the crystallising pluton, or from dehydration and decarbonation of rocks within the aureole or from an external fluid source outside the aureole-pluton system), the composition of the fluid, the activity of fluid components in different parts of the aureole (outer aureole versus inner aureole, e.g. Moore and Kerrick, 1976; Bowman and Essene, 1982; Ferry, 1992), and the influence of fluids on contact metamorphic reactions and vice versa.

An attempt is made in this thesis to tackle some of the many inter-related questions concerning the behaviour of volatile components and fluids in thermal aureoles; specific questions to be addressed include:

(i) How variable are the activities of volatile components (especially H_2O and CO_2) within a thermal aureole, and how dependent is this pattern on bulk-rock composition?

(ii) Do all hornfelses crystallise in the presence of a fluid phase?

(iii) Within any one lithology, what is the relationship between the activities of volatile components and the identities of the devolatilisation and melting reactions? Are the reactions controlled by the volatiles (open-system behaviour) or are the volatile activities controlled by the reactions (closed-system behaviour)?

The thermal aureole of the Etive Complex, S.W. Scotland, is well suited for addressing these and related questions. It is one of the largest post-orogenic

Caledonian "Newer Granites" (Brown, 1991) of Siluro-Devonian age (Clayburn *et al.*, 1983), and is composed of a variety of igneous rocks including granite, granodiorite and diorite. Regionally metamorphosed sedimentary and basic country rocks of the Dalradian Supergroup underwent thermal metamorphism as a result of the intrusion, and a thermal aureole up to 2 km wide has developed. Contact metamorphism has affected a wide variety of Dalradian lithologies, including quartzites, psammites, graphitic pelites, non-graphitic pelites and semi-pelites, calc-silicates and metabasites. The greatest lithological variety occurs within the southern segment of the aureole, close to Loch Awe, where several units trend at high angle to the contact with the Quarry Diorite, the outermost ring-dyke of the Etive Complex. Anatectic migmatites have been formed in pelites and semi-pelites in this area, providing an opportunity to study the behaviour of volatiles in both melt-bearing and melt-free rocks. The aboundance of metabasites in the aureole also provides an opportunity to study phase relations and reactions in contact –metamorphosed basic rocks.

1.3 Specific objectives

The main objective of this thesis is a systematic study of the contact metamorphism of different lithologies within the Etive aureole. Despite the presence of a wide variety of country rock lithologies, the only published account of the contact metamorphism in the Etive area is the study by Droop and Treloar (1981) which was concerned entirely with thermobarometry. The large volume of igneous rocks, different intrusive pulses and the variety of lithologies in the aureole provide a suitable basis with which to study contact-metamorphic effects and processes within the aureole.

The main objectives of this study are:

- -Mapping and sampling the rocks within selected parts of the aureole and delineating the metamorphic zonal sequences in selected lithologies.
- -Characterising the igneous rocks to evaluate their thermal effects and fluid-bearing capacities.
- -Studying the structural geology of the aureole to find any possible structural controls on the distribution of mineral zones and isograds and microstructural controls on the development of hornfels and migmatite textures.

-Modelling the zonal sequences in terms of continuous and discontinuous metamorphic reactions.

-Estimating the peak metamorphic pressures and temperatures of contact metamorphism in different parts of the aureole, thereby assessing thermal and baric gradients within the aureole.

-Estimating the activities of fluid components (especially H_2O in selected lithologies.

-Assessing the role of any contact anatexis in the evolution of the aureole.

1.4 Methodology

Field work: Field work was carried out in four sessions which totalled about two months. About 300 localities were examined and more than 450 hand specimens were collected. All measurable structural features were recorded at each locality and all non-measurable features were described. Because of the varied nature of the lithologies (non-graphitic pelites and semi-pelites, graphitic pelites, quartzites, calc-silicate rocks and metabasites) outcropping in the southern segment of the aureole, the rocks there were mapped and sampled in more detail than in other parts of the aureole. The western segment of the aureole as mapped and sampled but no field work was carried out on the eastern and northern segments as the outcrop there is dominated by Grampian Group psammites and quartzites.

Laboratory work: Laboratory work involved optical microscopy of about 300 thin sections, XRF analyses of representative samples of igneous rocks, electron microprobe analyses of igneous and metamorphic minerals (by either energy-dispersive or wavelength-dispersive method), ion-probe analyses of water and CO_2 content in contact-metamorphic cordierites, mineral formula calculations and thermodynamic calculation of mineral equilibria.

1.5 Structure of the thesis

Chapter 2 is a brief literature review of the geology of the Grampian Highlands of Scotland with particular emphasis on the Dalradian Supergroup. This chapter provides a background for the study of the geology of the Etive area.

In Chapter 3, the petrography and geochemistry of the Etive igneous complex is described and discussed. The chapter begins with a brief description of the petrography of each intrusion in the complex; this is followed by a classification of

the rocks, and by studies of their geochemistry, mineral chemistry, and thermobarometry.

Chapter 4 documents the structural geology of the Dalradian Supergroup in the Etive area in terms of major and minor deformational phases and predominant structures in different parts of the aureole.

Chapter 5 presents the results of petrographic studies of the metamorphic rocks. The assemblage data are employed to construct maps of mineralogical isograds and metamorphic zones in different lithologies within selected parts of the aureole.

Chapter 6 deals with the partial melting of pelites and semi-pelites within the southern segment of the aureole and describes the field relations and textures of the partially melted rocks.

A study of the chemistry of the metamorphic minerals and their compositional variations within the aureole is presented in Chapter 7.

Building on these variations, Chapter 8 documents a study of the phase relations in pelites and metabasites in the southern segment of the Etive aureole, and of the metamorphic reactions responsible for the contact-metamorphic evolution of those lithologies.

In Chapter 9 independently calibrated thermometers and multi-equilibrium calculations are used to estimate peak contact-metamorphic temperatures and pressures in different parts of the aureole. Dehydration reactions and cordierite volatile contents are then used to place constraints on the activities of volatile species (particularly H_2O) in pelites and metabasites.

Chapter 10 provides a general discussion of the results on the contact metamorphism in the Etive aureole and its implication for the evolution of the Grampian Highlands of Scotland and discusses the findings in this research for the process of contact metamorphism in general. The chapter ends with suggestions for future studies.

Chapter 2

Geology of the Etive Area in the Grampian Highlands of Scotland

2.1 Introduction

The Etive igneous complex and its surrounding metasedimentary and metavolcanic rocks lie in the south west of Highlands. As a background for the geology of the Etive area, a summary of geology of Scotland, focusing on the Grampian Highlands is discussed briefly. The Grampian Highlands of Scotland is a portion of the Caledonides belt extending from the eastern coasts of North America to Scandinavia and Greenland (Lambert and McKerrow, 1976). Two major faults define the borders of the Grampian Highlands in Scotland. To the north, the Great Glen Fault, and to the south, the Highland Boundary Fault separate the Grampian Highlands from the other parts of Scotland. In most parts the Grampian Highlands is underlain by metasedimentary and metavolcanic rocks of the Dalradian Supergroup (Johnstone, 1975; Harrison and Pitcher, 1975; Johnson, 1983a). The rocks of this Supergroup crop out in a SW-NE trending belt from Islay in the Southwest Highlands to the Banffshire coast and the Shetlands Islands to the NE (Fig. 2.1). Dalradian Supergroup rocks underwent polyphase deformation and regional metamorphism from the Proterozoic to the Ordovician, during the Grampian Orogeny (Lambert and McKerrow, 1976; Johnson, 1991; Tanner and Leslie, 1994). Dewey (1969) and Lambert and McKerrow (1976) explained the Grampian Orogeny in a plate tectonics context. These authors considered it to be caused by the northward subduction of oceanic crust during the closure of the ancient Iapetus ocean (Lambert and McKerrow, 1976). Apparently this explanation is not consistent with geophysical evidence (Bamford *et al.*, 1976) which indicates a continental basement beneath the Dalradian rocks.

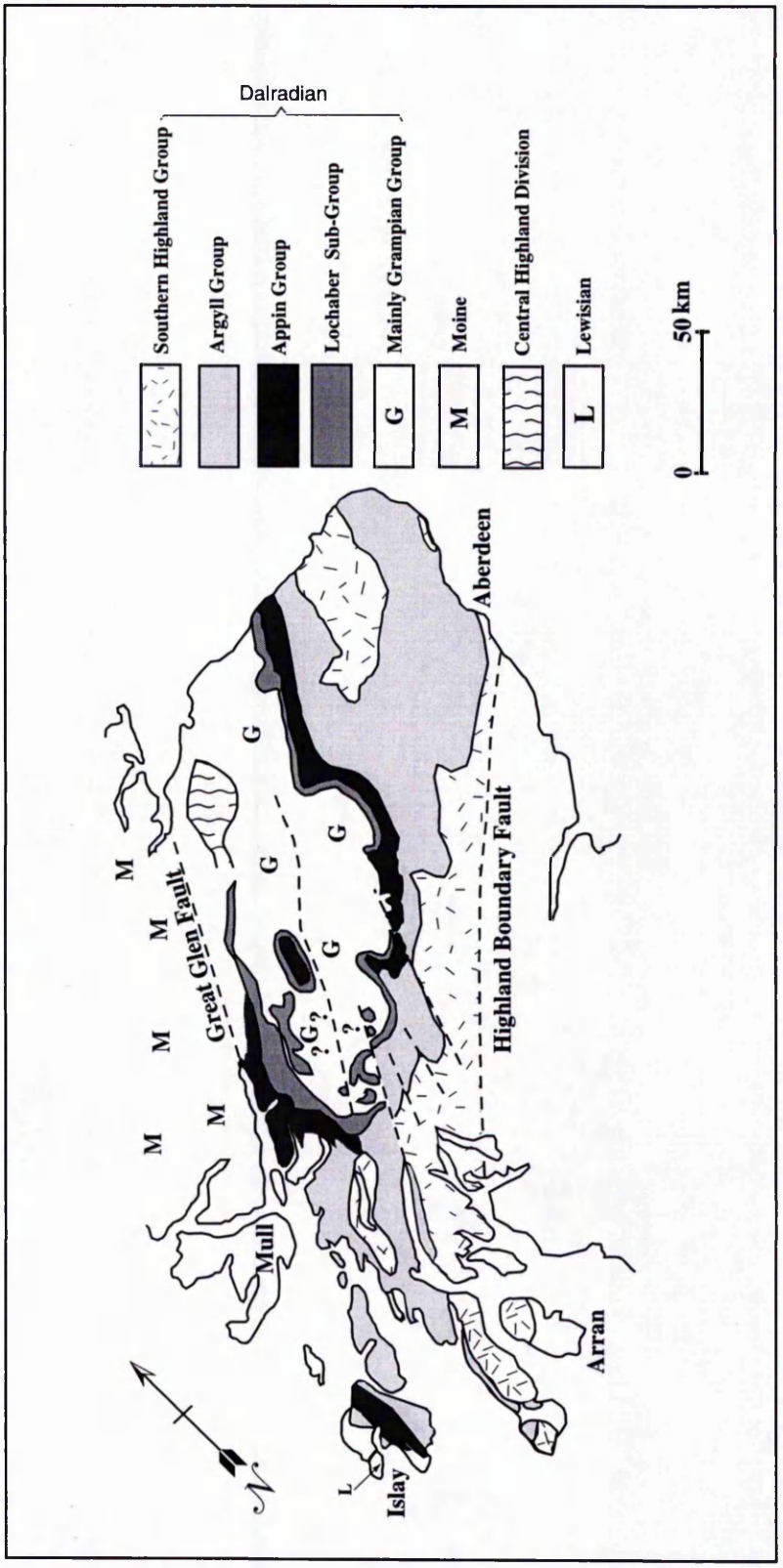

Fig.2.1. Distribution of Dalradian Supergroup and its subdivisions (after Harris and Pitcher, 1975).

Magmatic activities are spatially associated with the Grampian Orogeny. Deformed mafic and felsic igneous rocks called 'Older Gabbros' and 'Older Granites', respectively, (Watt, 1914; Read, 1919, 1923, 1961) intruded into the metasedimentary and metavolcanic rocks of the Grampian Highlands during or prior to the orogeny. Undeformed mafic and felsic rocks, called ' Newer Gabbros' and 'Newer Granites' (Read, 1919, 1923, 1961) intruded after deformation (see also Robertson, 1988). Contact metamorphism and partial melting of the Dalradian rocks around the 'Newer Gabbros and Granites' have been studied by many investigators (e.g. Tilley, 1924; Droop and Treloar, 1981; Tyler and Ashworth, 1982; Platten, 1982; Ashworth and Tyler, 1983, Platten, 1983; Droop and Charnley, 1985; Pattison and Harte, 1985; Pattison, 1987; Harte *et al.*, 1991).

2.2 Geographical setting of the Etive area in the Grampian Highlands

The Etive area is located in the south west of Scottish Highlands and within the Argyll and Bute districts of the Strathclyde region (Fig.2.2). The area is bounded by the Beinn Fhionnlaidh ridge to the north, by Loch Awe, Glen Shira and Glen Fyne to the south and southwest, by Glen Strae and Glen Orchy to the east and by Loch Creran and Loch Linnhe to the west. The main villages in this area are Dalmally, Taynuilt, Connel and Kilchrenan. Major lines of communication include A 85 (T) and the Oban to Glasgow rail link. Many other second class roads and forestry tracks facilitate access to the area.

There are two main types of topography. Firstly, there are the rough high dissected mountains mainly of granitic rocks such as Ben Cruachan (1101 m), Ben Starav (1078 m) and Stob Ghabhar (1101 m). Secondly, there is a more subdued topography which reflects the underlying geology of the Dalradian metamorphic succession, with long upstanding, rugged ridges largely consisting of quartzite, psammite and metabasite. Thermally affected rocks are more upstanding. The low smooth slopes and hollows are made of regionally metamorphosed metalimestone and metapelitic rocks.

Southwesterly flowing river valleys generally following the structural features of the Dalradian dominate the drainage pattern, a pattern emphasised by the Pleistocene glaciation. East of Ben Cruachan and Stob Ghabhar, the upland area drains towards

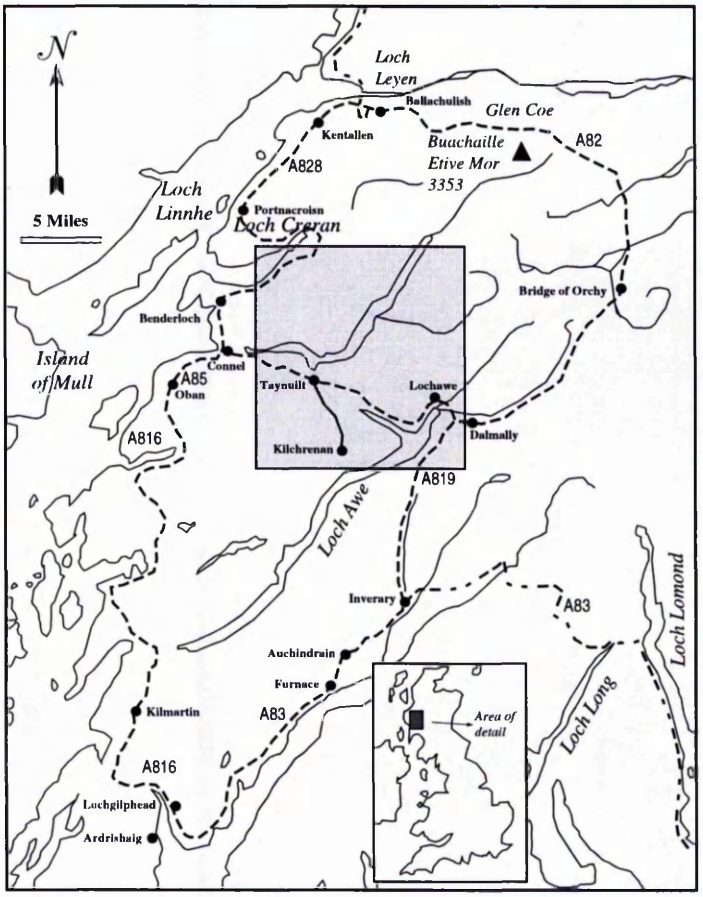

Fig.2.2 Geographical setting of the studied area in SW Scotland.

the rivers Strae and Orchy which discharge into Loch Awe, while to the west of Ben Cruachan, most of the granites drainage is to Loch Etive.

2.3 Structural Evolution of the Grampian Highlands

Geophysical studies indicate that the thickness of the crust in the Grampian Highlands is between 25-35 km, made of pre-Caledonian, Lewisian-type basement and 10-15 km thick overlying Dalradian Supergroup (Bamford *et al.*, 1977; Hall *et al.*, 1984; Hall, 1985; Westbrook and Borradaile, 1978; Hipkin and Hussain, 1983; Johnson, 1991). There are three models explaining the formation and evolution of the Dalradian depositional basin. Phillips *et al.* (1976) believed that the deposition of Dalradian metasediments was after the formation of the Iapetus Ocean. According to this model the Dalradian was deposited in a rifted basin, some distance away from the Iapetus Ocean to the south. Anderton (1980), based on sedimentary rocks and

volcanic rocks and the supposed northwards movement of the ice sheet (Spencer, 1971) which deposited the Port Askaig Tillite, concluded that the opening of Iapetus Ocean was after deposition of much of the Dalradian. The ice sheet must have grown and moved from continental crust to the south of the Dalradian (Anderton, 1980; see also Eylès and Eyles, 1983). In this model the Iapetus Ocean began to open during Southern Highland Group times, with extensive rifting causing rapid subsidence and volcanic activities in the Dalradian (Anderton, 1980). The third model is the pull-apart basin model of Graham (1986). In this model the entire Dalradian was deposited in the pull-apart basins, in a dextral transtensional region. Graham (1986) considered the Dalradian as a rifted margin with syn-depositional faults trending NE-SW. He recognised a number of important transverse NW-SE structures. The Cruachan lineament is suggested as being one of these NW-SE trending structures which controlled Dalradian sedimentation (Graham, 1986).

2.4 Stratigraphy of the Dalradian Supergroup in the Grampian Highlands And the Etive area

The first major attempt to work out the stratigraphic relations in the Dalradian Supergroup was the proposal of Ballapel and Iltay successions by Bailey (1922). Later Knill (1963) and Rast (1963) divided the Dalradian rocks into three divisions, upper, middle and lower parts. Rast and Litherland (1970) and Harris and Pitcher (1975) included the Appin Group (former Ballapel succession) and Grampian Group (former 'Central Highlands Granulites' or 'Younger Moines') as a part of the Dalradian Supergroup but Piasecki (1980) and Piasecki and van Breeman (1979a,b) showed that the basement of the Grampian Group is not certain and there is unconformity in some places. Anderton (1986) ruled out the inclusion of the Grampian Group in the Dalradian Supergroup but other authors (e.g. Johnson, 1991) have considered the Grampian Group as the fourth group of the Dalradian Supergroup by regarding the sedimentary transition between it and the Appin Group. The Dalradian Supergroup consists of four major groups. From the bottom to the top these are Grampian Group, Appin Group, Argyll Group and Southern Highlands Group (Table 2.1).

Table 2.1 Main subdivision of the Dalradian Supergroup (after Johnson, 1991).

Cambrian		Southern Highland Group (Upper Dalradian)	greywackes, shales and volcanics
		Argyll Group (Middle Dalradian)	well-sorted quartzite, pelites and limestones. Turbidite facies in places.
Vendian	?	Portaskaig Tillite	
		Appin Group (Lower Dalradian)	limestones, pelites, quartzites and laminated psammite-pelites.
Riphean	?	Grampian Group	psammite generally passes up without a break into Appin Group but is in tectonic contact in places.
		?????????	

Grampian Group: This group essentially consists of psammitic and semipelitic rocks which are regionally metamorphosed up to the amphibolite facies metamorphic grade. The nature of the contact between the Grampian Group and the underlying migmatitic rocks (Central Highlands Division) has been studied by Piasecki (1980), Piasecki and Temperley (1988), and Lindsey *et al.* (1989). They have considered different possibilities like basement and cover relation (Piasecki, 1980), unconformity (Piasecki and Temperley, 1988) and stratigraphical continuity locally. The contact between the Grampian Group and the overlying Appin Group is tectonic, graditional passage and unconformity in different localities (Winchester and Glover, 1988; Glover, 1993). The Grampian Group has been divided into subgroups in some localities (e.g. Schiehallion area, Thomas, 1980). Winchester and Glover (1988) have divided the whole Grampian Group into three, Ord Ban, Corrieyairack and Glen Spean subgroups based on the distinguishable lithofacies.

Appin Group: The Appin Group mainly consists of pelites, semipelites, quartzites, calc-silicate rocks and carbonates (Lambert *et al.*, 1981, 1982; Hickman and Wright, 1983; Rock *et al.*, 1986). There is a rapid alternation among these lithofacies (Wright, 1988). The Appin Group is divided into three subgroups. From the bottom to the top these are the Lochaber, Ballachulish and Blair Atholl subgroups. The Lochaber subgroup is divided into six units. Read (1923, 1936); Hinxman *et al.* (1923); Bailey (1934); Bailey and Maufe (1960); Peacock *et al.* (1968); Hickman (1975); Treagus and King (1978); Litherland (1980) and Anderton (1985, 1988) describe the lithology of these units. In the Lochaber-Appin area, the Ballachulish subgroup is divided into four formations, which are described by Bailey (1960);

Hickman (1975) and Litherland (1980). The Blair Atholl subgroup mainly consists of dark pelitic rocks and limestones. The thickness of the pelitic parts and the carbonate parts is different in different places. Based on the lithofacies changes some authors have divided this subgroup into formations locally (e.g. Appin area, Hickman, 1975; Firth of Lorn area, Rast and Litherland, 1970, Spencer, 1971; Glen Shee area, Upton, 1986).

Argyll Group: The Argyll Group has been divided into Islay, Easdale, Crinan and Tayvallich subgroups from the bottom to the top. The Islay Subgroup mainly consists of psammitic rocks with a base of Port Askaig Tillite (Spencer, 1971, 1981). In some localities there are dolomitic and quartzitic lithofacies in this subgroup which are named as different formations (e.g. Bonahaven Dolomite Formation in Port Askaig area, Klein, 1970, Spencer and Spencer, 1972, Fairchild, 1980, 1985; Islay Quartzite in the islands of Jura and Scarba, Anderton, 1976; Schiehallion Boulder Bed and Schiehallion Quartzite in the Schiehallion area, McCallien, 1927, Pantin, 1961, Harris, 1963; and Durn Hill Quartzite in the north of the River Isla area, Spencer and Pitcher, 1968).

The Easdale Subgroup consists of calcareous pelites and semipelites with local limestones. Like the preceding subgroups, this subgroup is divided into different formations locally. Some of these formations are the Jura Slate and Scarba conglomerate formation in the south-east Islay and south Jura areas (Anderton, 1979); Easdale Slate in the north of the Scarba area (Anderton, 1979); Degnish Limestone and Craignish Phyllite in the Shuna and Degnish Point areas (Knill, 1959; Roberts, 1966; Borradaile, 1973; Anderton, 1975); Shira Limestone and Slate in most parts of the south-west Highlands, Slema Slate, Slema Breccia, Culcharan Quartzite, Salachan Formation and Beinn Donn Quartzite Formation in the Benderloch area (Litherland, 1980); Ardrishaig Phyllite in the Loch Awe area (Roberts, 1966, Borradaile, 1973), Erins Quartzite, Stronachullin Phyllite, Stornoway Phyllite and Catherin's Graphitic Schist in the Knapdale area (Roberts, 1966) and Carn Mairg Quartzite and Ben Eagach Schist in a region from Tyndrum to the north of Loch Lyon.

The Crinan Subgroup, which crops out in the south-west Highlands, consists of Crinan Grits, which passes laterally into the Ben Lui Schist. Crinan Grits are made of psammitic rocks containing angular fragments of detrital feldspars, micas and

carbonates with interbedded black limestones and slates (Anderton, 1985). The Ben Lui Schist consists mainly of garnetiferous mica-schists, psammites and bands of limestones (Johnstone and Smith, 1965; Sturt, 1961). The distinguishable lithofacies of the Crinan Subgroup are named locally as formations, notably Craigievar Formation in the Tilly Fourie area (Read, 1955), Aberdeen Formation in the east and north of the Bennachie Granite (Munro, 1986), Ellon Formation in the Yathan valley (Read, 1952; Munro, 1986), Strichen Formation in the Ellon area (Kneller, 1988) and Cowhythe Psammite Formation in the region from Portsoy to the north-east of Huntly (Read, 1923).

The Tayvallich Subgroup mainly consists of the carbonate rocks of the Tayvallich Limestone and its equivalents, the Loch Tay Limestone and Deeside Limestone (Gower, 1973). The Tayvallich Volcanic Formation consists of limestones, clastic sediments and volcanic rocks. The volcanic rocks are mainly pillowed basic lavas and epiclastic volcanic rocks (Borradaile, 1973; Graham, 1976).

The Southern Highlands Group: This group contains the turbiditic rocks, typically metagreywackes, slates and phyllites. Metavolcanic 'green beds' make the basal part of the group (Harris *et al.,* 1978; Anderton, 1985). Several local successions have been established like Loch Avich Grit and Loch Avich Lavas in the core of the Loch Awe syncline (Borradaile, 1973); Glen Sluan Schist in the south-west of Loch Lomond (McCallien, 1929; Roberts, 1966); Ben Ledi Grit in the north-east of Loch Lomond (Mendum and Fettes, 1985) and Pitlochry Schist in the Killin area (Johnstone and Smith, 1965). Despite these local subdivisions, the whole Southern Highlands Group has been treated as a unique stratigraphical unit and its lithological variations is comparable with variations in each subgroups of the preceding groups of the Dalradian Supergroup.

2.4.1 Lithostratigraphy of the Etive area: The oldest rocks in the Etive area are metasediments of the Grampian Group (Fig. 2.3 and Table 2.2), which are known as the Eilde Flags, and comprise fine- to medium-grained micaceous psammite with intercalations of fine-grained quartzite (Thomas and Treagus, 1968).

The Appin Group consists of Lochaber Subgroup with the Glen Coe Quartzite at the bottom and the Leven schist at the top. The type section of the Appin Group on the north west side of the Etive area consists of fine-grained, locally pebbly, quartzites which pass laterally into a sequence of striped, graphitic pelite and semipelite. Rocks

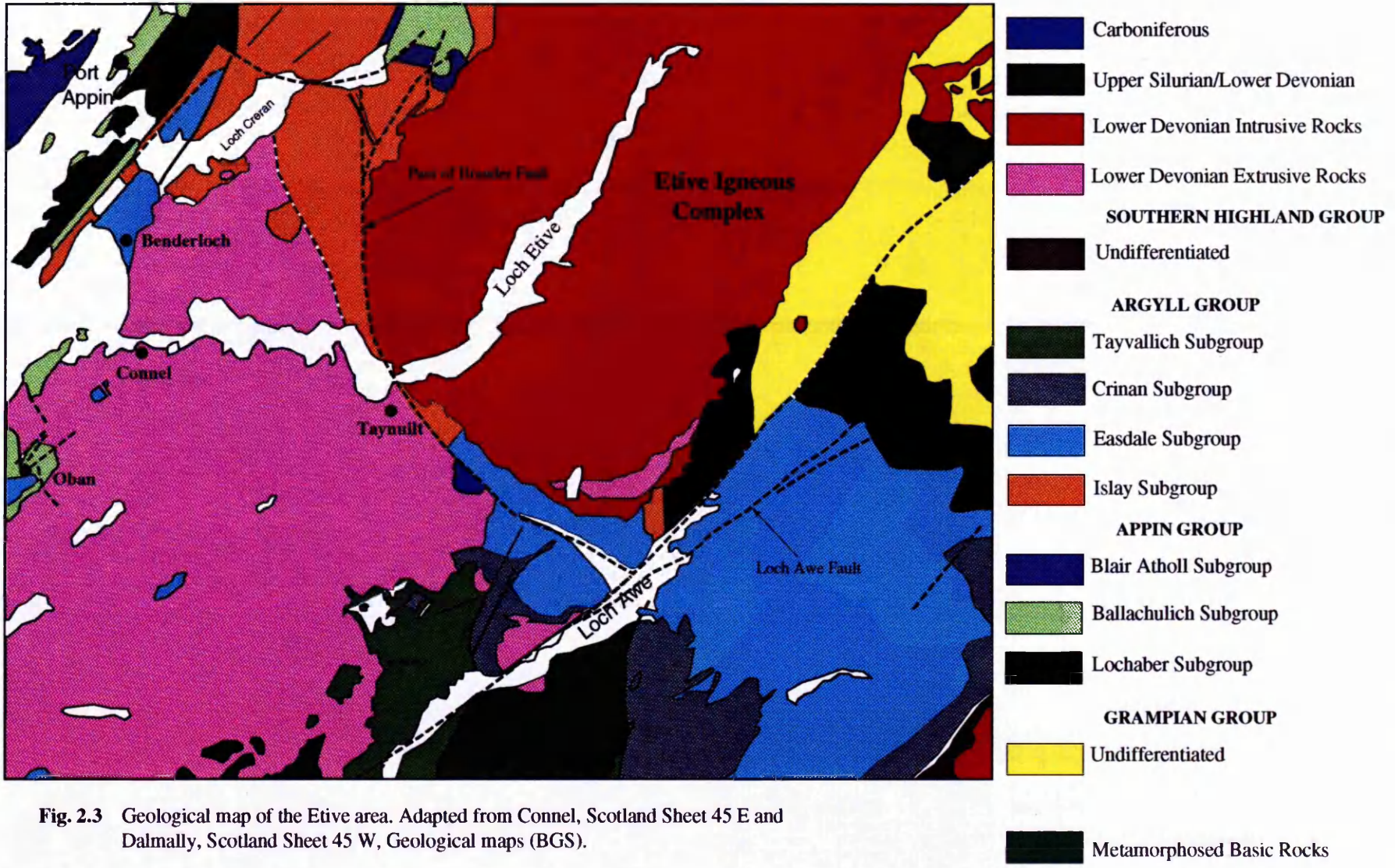

Fig. 2.3 Geological map of the Etive area. Adapted from Connel, Scotland Sheet 45 E and Dalmally, Scotland Sheet 45 W, Geological maps (BGS).

of the Easdale Subgroup represent the Argyll Group. The Islay Subgroup is exposed

Table 2.2 Stratigraphic sequence in Loch Awe, Dalmally and Loch Rannoch areas (after Johnson 1991).

Age	Group	Subgroup	Stratigraphic sequence
Lower Cambrian	Southern Highlands		Loch Avich Lavas<300m Loch Avich Grit<1100m Tayvallich Volcanics (590 Ma) 2000m Kilchrenan Conglomerate
	Argyll	Tayvallich Crinan Easdale	Tayvallich slate and limestone Crinan Grits 600-3000m Shira Limestone 5-300m Ardrishaig Phyllite>400m Degnish Limestone>20m Easdale Slate Pebbly Quartzite
Vendian	Appin	Blair Atholl Ballachulish Lochaber (transition)	 Leven Schist Glencoe Quartzite
Riphean	Grampian		Eilde Flags

near the village of Loch Awe and consists of a thin sequence of interbedded black slates and pebbly quartzite (Borradaile, 1973). The base of the Easdale Subgroup is marked by the Carn Mairg Quartzite, a medium-grained, flaggy quartzite with coarse pebbly bands (Roberts and Treagus, 1975). At the top of this quartzite, graphitic, pyrite-rich semipelitic rocks of the Ben Eagach Schist are deposited. The Ardrishaig Phyllite is a sequence of pelite, calcareous phyllite, thinly bedded sandy carbonates and fine-grained quartzite (Borradaile, 1973) which overlies the Ben Eagach Schsit. The Crinan Grits are the base of the Crinan Subgroup around Loch Awe, consisting of white quartzite. To the east of Loch Awe, the grits are impure quartzites with mica, feldspar and carbonates. The Tayvallich slates are laminated rocks with unsorted gritty zones. The Tayvallich Volcanic Formation is represented by meta-dolerite and meta-basalt sills within the Argyll Group. Some of these sills which are dated at 595 Ma by Halliday *et al.* (1989) are contemporaneous with the Tayvallich Volcanic Formation but the others are believed to be earlier, being emplaced from the Easdale Subgroup times (Anderton, 1985). The basal part of the Southern Highlands Group in the Etive area is made of Green Beds, a sequence of dark quartz-bearing

mica schist (Anderton, 1985). The highest formation of the Southern Highlands Group is the Beinn Bheula Schist, a sequence of deformed greywackes, schistose psammites and semipelites.

2.5 Structural Geology of the Dalradian Supergroup in the Grampian Highlands and the Etive area

The early structural studies of the Dalradian rocks are works by Clough (1897) in Cowal and Bailey (1910) in the Loch Leven area. These authors recognised the large-scale recumbent folds. Bailey (1922, 1934, and 1940) introduced two main structural units, the Iltay Nappe and the Ballapel Foundation separated by the Iltay Boundary slide. The recumbent folds of Bailey are early structures that have been refolded by later folds. The deformational episodes of the Dalradian rocks are labelled D_1, D_2, D_3,...etc in order of decreasing age. In the Central Highlands and the Schiehallion area the early recumbent folds are of D_1 and D_2 age while the latest deformational phases of open, upright folds are D_3 and D_4? (Roberts and Treagus, 1977, 1979; Thomas, 1979, 1980; Treagus, 1987), but in the Southern Highlands an even later? D_4 deformational phase has been recognised (Harris *et al.*, 1976; Bradbury *et al.*, 1979; Harte *et al.*, 1984; Mendum and Fettes, 1985). Bradbury (1985) categorised the deformational phases as 'Nappe Phases' and 'Late Nappe Phases' which now are considered as Early Grampian and Late Grampian deformations respectively.

The Early Grampian phases are responsible for the recumbent folds and associated faults (slides) and the Late Grampian Phases are responsible for the later small-scale folds.

Major Early Grampian (D_1 and D_2) structures are the Aberfoyle anticline or Tay Nappe, the Ben Lui Fold (Bailey, 1922, 1925; Read, 1955; Roberts and Treagus, 1977; Thomas, 1979, Bradbury, 1985), the Islay anticline in the Islay and Loch Leven area (Bailey, 1917, 1934; Roberts and Treagus, 1977), the Loch Awe syncline (Roberts and Treagus, 1977) and Ardrishaig anticline. In these structures, the D_1 structures are mainly the large-scale recumbent folds and the related slaty cleavages and the D_2 structures are linear structures like mullions, rods, mineral stretchings, small and large-scale tight folds and the related crenulation cleavage. The main Late Grampian (D_3 and D_4) structures are major folds with steep axial planes striking between NE-SW and E-W (Johnson, 1991). A good example for these structures is

the Ben Lawers syncline in Perthshire and the Ben Ledi antiform, which are responsible for refolding of the nose of the Tay Nappe. Also the common minor asymmetrical folds and small-scale open folds with NNE-SSW- trending axial planes are representative features of the Late Grampian deformational phases. It is believed that some lineaments controlling the basement and depositional regimes in the Dalradian basin have been active during the Late Grampian deformational phases. Examples are the Loch Lomond Lineament (Mendum and Fettes, 1985) and variably oriented shear zones of Ashcroft *et al.* (1984) in the NE.

Sub-parallel to Great Glen Fault and Highland Boundary Fault there are five major

Table 2.3 Characteristics of the major faults in the SW and central Highlands (adapted from Treagus, 1991). (sl=sinistral, de and dw = down to the east and west side dip-slip component respectively).

Fault	Displacement		Displacement Evidence
Ericht Fault	4km.sl	1.3km.dw	Disposition of the hinge of D_1 Kilmachrenan Syncline
Tyndrum Fault	4km.sl	2km.de	Position of the Garabal Hill complex related to the fault
Garabal Hill Fault	5km.sl	?	Garabal Hill granite is cut by this fault
Killin Fault	1.2km.sl	1.5km	Displacement in the D_3 Ben Lawers Syncline
Loch Tay Fault	6.5km.sl	few hundred meters	Glen Tilt igneous complex is cut by this fault

faults which have a significant effect on the lithostratigraphic boundaries of rock units in the Southwest and Central Highlands. Movement on these faults occurred late in the structural history (i.e. after all the major ductile deformation had ended), broadly at the same time as the intrusion of the late Caledonian Granites (Watson, 1984) (see section 2.8).

The main characteristics of the major faults in the SW and Central Highlands are summarised in Table 2.3.

In the Etive area, four deformational phases have been recognised by different investigators. The Early Grampian phases are D_1 and D_2 structures in the Loch Awe and Loch Creran areas. D_1 structures include the Barmaddy anticline (Borradaile, 1973); the Ardrishaig anticline (Bailey, 1938); the Toaig anticline; the Loch Dochard syncline (Bailey and McGregor, 1912); the Kilchrenan syncline; the Ballimeanoch

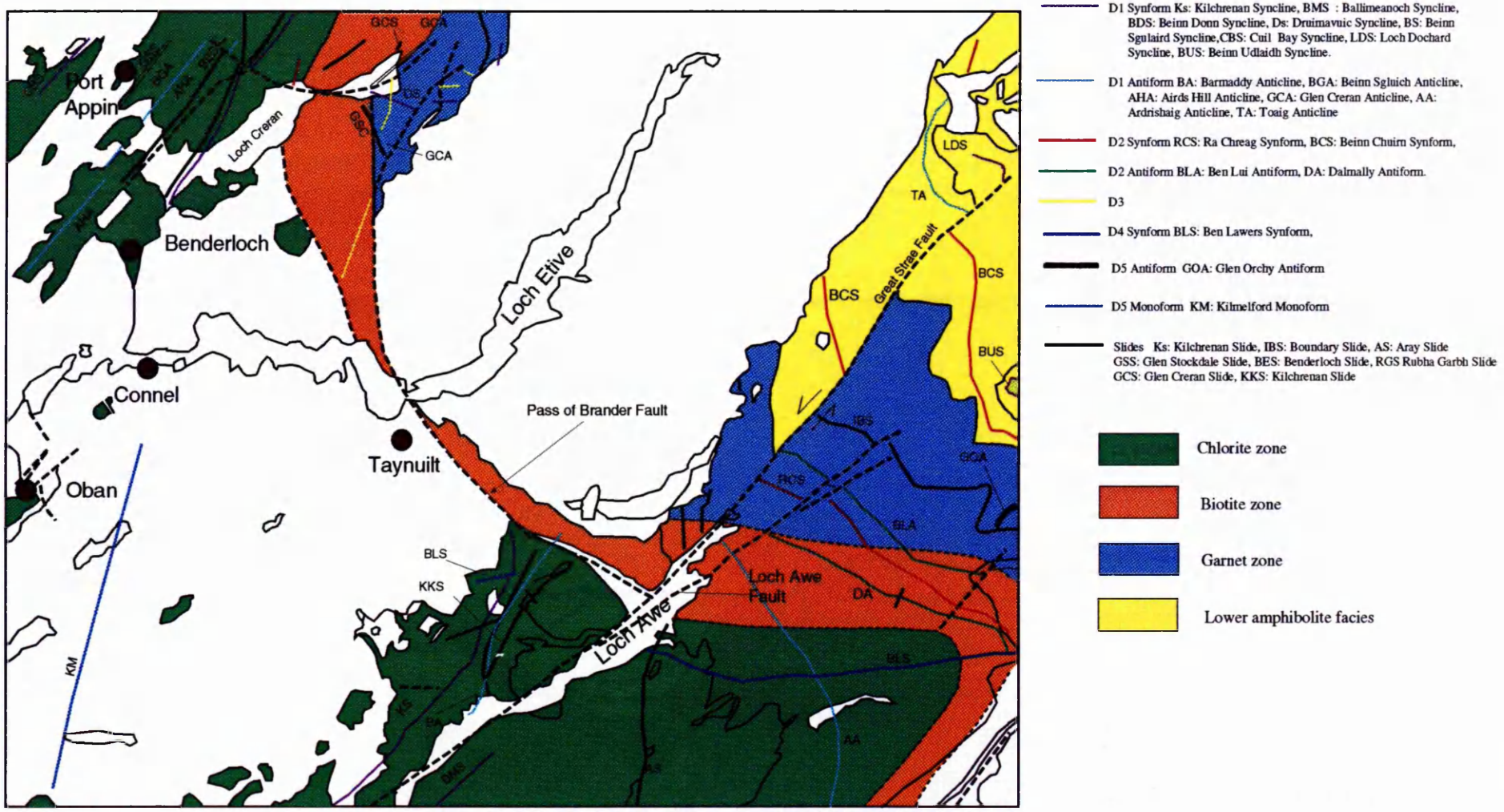

Fig. 2.4 Structural Geology and Metamorphic map of the Etive area. Adapted from Connel, Scotland Sheet 45 E and Dalmally, Scotland Sheet 45 W, Geological maps (BGS).

syncline and the Beinn Udlaidh anticline (Fig. 2.4). The Barmaddy anticline with the Ballimeanoch syncline forms the compound Loch Awe syncline (Fig. 2.4). The major D_2 structures are the Ben Lui antiform, Ra Chreag synform and Dalmally antiform. All of these folds are recumbent. Fig. 2.5 shows a cross section along the Ericht Fault in the Etive area, illustrating the main folds. The Late Grampian phases in the Etive area are poorly developed D_3 and D_4 structures in the Loch Awe area. The closely spaced crenulation cleavage axial planar to recumbent minor folds in the Pass of Brander area and weak westerly dipping S_3 crenulation cleavage in the north of Loch Avich area are the most important features (Borradaile, 1970). The D_3 folds are well developed in the Glen Creran and Alt Buidhe areas, where minor folds refold the earlier structures (Borradaile, 1973; Litherland, 1982). The D_4 deformational phase is represented by S_4 crenulation cleavage with NE- trends and SE- dips. This fabric is planar to both major and minor D_4 structures which have been correlated with the Ben Lawers synform (Borradaile, 1973).

Two main folds in the Etive area are the Ericht Fault and the Pass of Brander Fault. Ericht Fault has a 4 km sinistral horizontal movement component and 1.3 km down to the west side dip-slip component (Treagus, 1991, Table 2.3). The Pass of Brander Fault displaces the Lorne Lavas. These lavas are believed to overlie the Ericht Fault unconformably (e.g. southeast of Dalmally, Treagus, 1991). Therefore the Pass of Brander Fault post-dates the earlier movements on the Ericht Fault (Treagus, 1991). The Ericht Fault and the Pass of Brander Fault bound the Etive igneous complex and its aureole. The movement on the Pass of Brander Fault is more than 0.7 km (Treagus, 1991). The relation between igneous activities and faulting in the Etive area are given in Table 2.4.

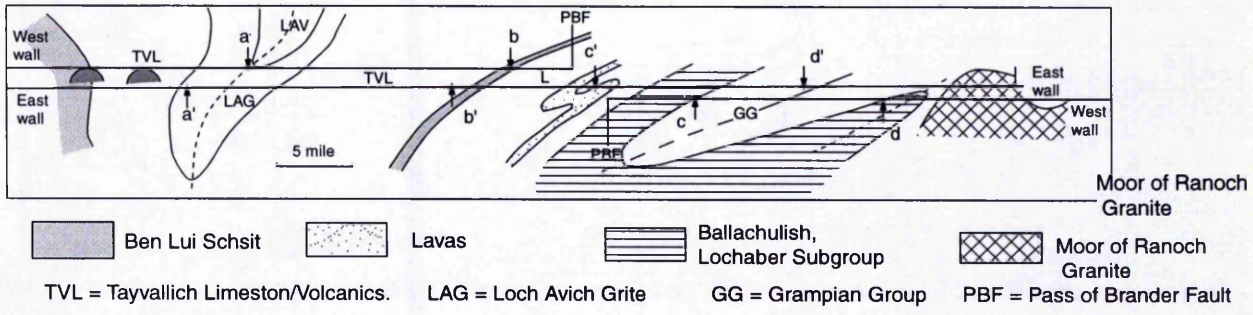

Fig. 2.5 Cross section across the Dalradian rocks, along Ericht Fault in the Etive area. After Treagus (1991)

Table 2.4 History of igneous activities and faulting in the Etive area (from Treagus, 1991)

Starav granite ring fractures, Pass of Brander initiation (down - throw to SW) and Ericht Fault reactivation locally (down throw to SE) (390±12 Ma, Clayburn *et al.*, 1983)
Porphyritic dykes (412±5 Ma, Thirwall, 1983)
Early intrusion of Etive igneous complex
Unconformable, Upper Silurian, Lorne Lavas (412±24 Ma)
Sinistral strike-slip
Intrusion of Moor of Rannoch "granite"
Dip-slip, down to NW movement
Folding of the Dalradian

2.6 Regional Metamorphism of the Dalradian Supergroup

The Scottish Dalradian is one of the best known metamorphic complexes in the world and its mapping dates back over 100 years (e.g. Barrow, 1893). Traditionally, metamorphic zones in the Dalradian are based on mineral assemblages in pelites and semi-pelites because such rocks are abundant in the Dalradian stratigraphy and show striking mineralogical changes with increasing grade. Barrow (1893), working in the east central Dalradian, mapped a series of metamorphic zones reflecting these changes, such that each successive zone (moving northwards from the Highland Boundary Fault) was characterised by a new 'index mineral'. These index minerals are in sequence: chlorite (lowest-grade), biotite, garnet, staurolite, kyanite and sillimanite (highest-grade). The upper part of the sillimanite zone is characterised by sillimanite+K-feldspar assemblages (e.g. Baker and Droop, 1983).

The concept of an 'isograd' as a line on the ground surface marking the first appearance of an index mineral (Tilley, 1925) coupled with the development of a rigorous phase diagram for pelitic mineral assemblages (the AFM projection: Thompson, 1957) prompted petrochemical studies on the metamorphic reactions responsible for the formation of Barrovian index minerals (e.g. Mather, 1970: biotite; Atherton, 1964: Garnet; Harte, 1975: staurolite; Chinner, 1965: kyanite; Chinner, 1965, 1966, Ashworth, 1975: sillimanite). These isograd reactions are summarised in Table 2.5.

The classic Barrovian type of regional metamorphism is one of three major types recognised in the Scottish Dalradian (Fig. 2.6) each reflecting different peak-

metamorphic P/T regimes, hence geothermal gradient. The Barrovian, or medium-P/T type, affects most of the central and SW Dalradian (Harte, 1975; Harte and Hudson, 1979; Atherton, 1977; Fettes, 1979). The NE Dalradian, on the other hand, records regional low-P/T ('Buchan type') metamorphism and is characterised by the zonal sequence biotite, cordierite, andalusite, staurolite, sillimanite, sillimanite+K-feldspar (e.g. Read, 1952; Hudson, 1980, 1985). Between the two, on the east coast at Stonehaven lies a small area of low-medium-P/T ('Stonehavian-type') metamorphism characterised by the existence of a distinct chloritoid zone (Chinner, 1967); here the zonal sequence is: chlorite, biotite, garnet, chloritoid,

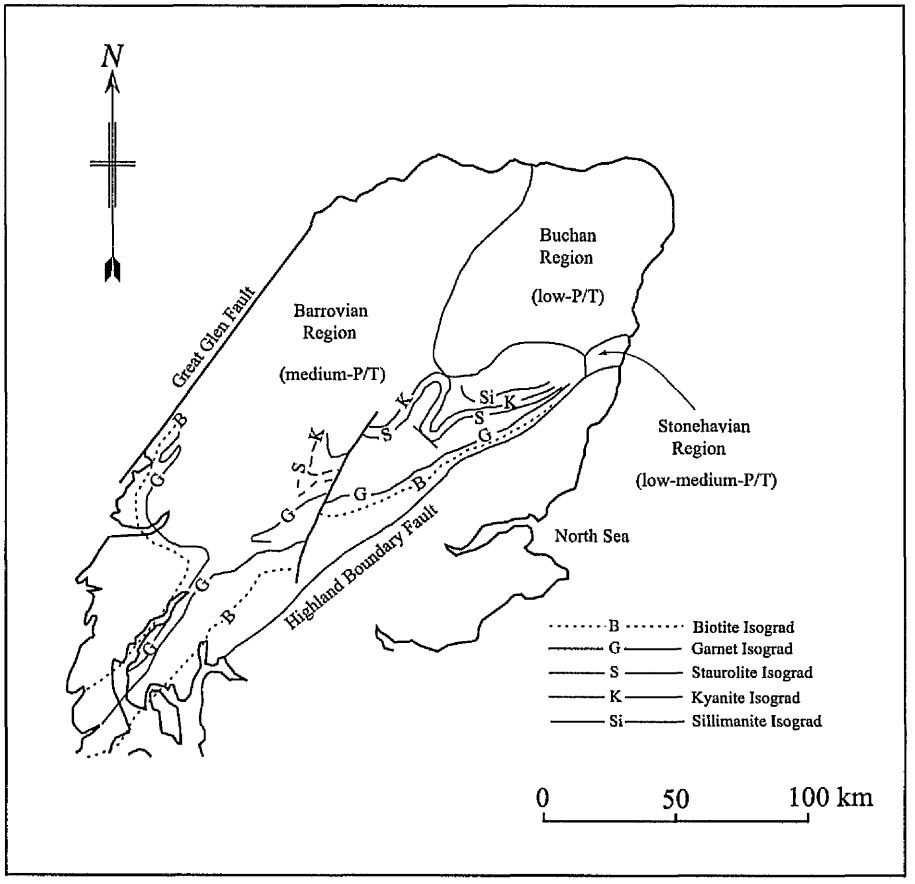

Fig.2.6 Metamorphic map and isograds of Barrovian zones for pelitic metamophic rocks of the Dalradian in the south-eastern Highlands (based on Fettes, 1979 and Chinner and Heseltine, 1979)

staurolite and sillimanite (Harte, 1975; Harte and Hudson, 1979; Droop and Harte, 1995).

Metabasites are common in the Dalradian. Those in the chlorite and biotite zones are greenschists and greenstones, while those in higher-grade zones are amphibolites, commonly garnet bearing. The garnet-in isograd in metabasites is very close to that in pelites (Fettes, 1979). Clinopyroxene-garnet amphibolites characterise the sillimanite + K-feldspar zone (Baker and Droop, 1983). Harte and Graham (1975) describe the mineralogy and reactions in chlorite- to garnet- zone metabasites from the SW Dalradian.

Many investigators have worked on the time relations between regional metamorphism and deformation of the Dalradian Supergroup (e.g. Rast, 1958; Sturt and Harris, 1961; Johnson, 1962, 1963; Harte and Johnson, 1969). They have employed porphyroblast-matrix relations and other microstructural criteria to work out when the metamorphic minerals crystallised relative to macrostructurally- defined phases of deformation. These studies show that the thermal peak of Dalradian metamorphism occurred between D_2 and D_3 deformational phases. Numerous studies have been made on the temperature (T) and pressure (P) conditions at the thermal

Table 2.5 Pelite isograd reactions in the Barrovian type metamorphism in the Scottish Dalradian (based on data from Chinner, 1960, 1965, 1966, 1967; Harte, 1975; Atherton, 1968).

Barrovian (western)			
Biotite in:		$Chl_f+Kfs=Bt+Chl_m(+Ms+Qtz+H_2O)$	C
Garnet in:		$Chl_f(+Ms+Qtz)=Grt+Bt+Chl_m(+H_2O)$	C
Staurolite in:		$Grt+Chl(+Ms)=St+Bt(+Qtz+H_2O)$	D
Kyanite in:	(i)	$St+Chl(+Ms+Qtz)=Ky+Bt(+H_2O)^*$	D
	(ii)	$St+Bt_m(+Qtz)=Ky+Bt_f(+H_2O)^*$	C
Staurolite out:		$St(+Ms+Qtz)=Grt+Ky+Bt(+H_2O)$	D
Barrovian (eastern)			
Biotite in:		$Chl_f+Kfs=Bt+Chl_m(+Ms+Qtz+H_2O)$	C
Garnet in:		$Chl_f(+Ms+Qtz)=Grt+Bt+Chl_m(+H_2O)$	C
Staurolite in:		$Grt+Chl(+Ms)=St+Bt(+Qtz+H_2O)$	D
Kyanite in:	(i)	$St+Chl(+Ms+Qtz)=Ky+Bt_f(+H_2O)^*$	D
	(ii)	$St+Bt_m(+Qtz)=Ky+Bt(+H_2O)^*$	D
Sillimanite in:		$Ky=Sil$	D
Staurolite out:		$St(+Ms+Qtz)=Grt+Sil+Bt(+H_2O)$	D
Sil+Kfs in:		$Ms+Qtz+H_2O=Sil+Melt$ (N.B. melt crystallises as Kfs+Pl+Qtz)	D

C: continuous reaction; D: discontinuous reaction. Phases in brackets are non-AFM phases. $Chl_fBt_fCrd_f$: relatively Fe-rich minerals; $Chl_mBt_mCrd_m$: relatively Mg-rich minerals. *depending on range of bulk-rock Fe/Mg ratios. Mineral abbreviations are from Kretz (1983).

peak of Dalradian regional metamorphism. Oxygen isotope thermometry (Kerrich *et al.*, 1977) yields T estimates of 300°C for the chlorite zone to 600°C for the kyanite zone. Thermobarometric studies based on equilibria among coexisting minerals have been carried out by Richardson and Powell (1976), Wells and Richardson (1979), Baltatzis (1979), Sivaprakash (1982), Baker and Droop (1983), Graham *et al.* (1983), Dempster (1983), Booth (1984), Baker (1985), Hudson (1985), McLellan (1985), Moles (1985), Watkins (1985), Dempster and Harte (1986), Beddoe Stephens (1990) and Bendall (1995). The results of these studies are summarised in Fig.2.7.

The distribution of the Barrovian regional metamorphic zones in the Etive area is shown in Fig.2.5. Although the pattern of metamorphic isograds reflects the major fold structures, there is an overall increase in grade toward the north and east from greenschist (chlorite and biotite zones) through epidote-amphibolite (garnet zone) into lower amphibolite facies. The pass of the Brander fault juxtaposes the original distribution of the chlorite and biotite zones and the Etive complex thermal aureole affects the position of regional garnet isograds.

2.7 Age of regional metamorphism

The earliest estimates of the latest age of sedimentation of the Dalradian Supergroup were based on palaeontological evidence and yield Lower Cambrian age using the trilobite *Pagetides* in the Leny limestone in the Southern Highland Group. (Pringle, 1940; Skevington, 1971). Later palaeontological evidence, particularly the acritarch assemblages reported by Downie *et al.* (1971) suggested that the Dalradian was younger. These assemblages possibly indicate an Arenig or Llanvirn age for upper part of Dalradian.

Using radiometric methods, metamorphic cooling ages for Dalradian have been well documented (e.g. Harte, 1988; Dempster, 1985; Dewey and Pankhurst, 1970; Harper, 1967; Brown *et al.*, 1965; Bendall, 1995). Most of the radiometric methods have involved either Rb/Sr or K/Ar dating of whole rock samples or specific minerals. Rb/Sr dating using muscovite, biotite, phlogopite, K-feldspar and albite gives a series of cooling (uplift) ages between 460-440 Ma (Powell and Phillips, 1985). The interpretation of whole rock ages is more complicated and gives various ages (Cliff, 1985). Ages obtained from specific minerals normally post-date the peak regional metamorphism.

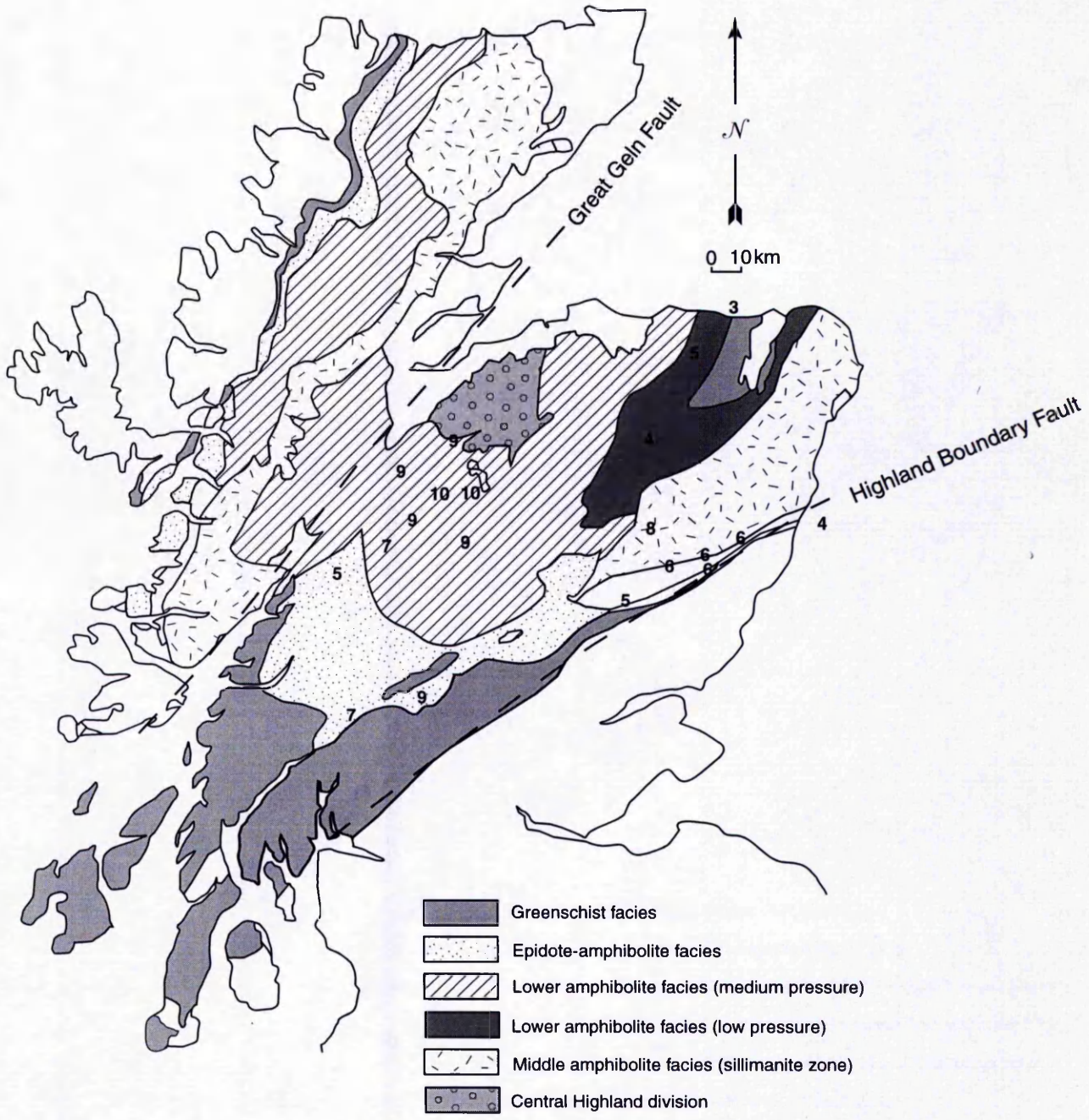

Fig. 2.7 Metamorphic zones and pressure distribution in Moine and Dalradian rocks. Figures are pressure in kbar. For source of data see text.

2.8 Magmatic activities associated with Dalradian

The igneous activities in the Scottish Caledonides are categorised into seven groups (Stephenson and Gould, 1995). This classification is based on the time relations of magmatism and is as below.

Pre-Tectonic Basic Magmatism: Pre-tectonic basic rocks or 'Older Basic Suites' are emplaced after the D_1 deformational phase and before the D_2 deformational phase. Some examples of these rocks are two-pyroxene-bearing gabbros underlying the boundary between the 'Central Highland Migmatitic Complex' and the Grampian Group (Highton, 1992); syn-depositional basic volcanic rocks like the Tayvallich volcanics (Graham, 1976; Leake, 1982) and metavolcanic material-bearing Farragon Beds (Graham and Bradbury, 1981;Goodman and Winchester, 1993). Halliday *et al.* (1989) dated the keratophyres (comagmatic with the Tayvallich volcanics) at 595±4 Ma and Graham (1976) and Graham and Bradbury (1981) studied the petrochemistry of the metamorphosed sills and lavas in the Argyll group.

Syntectonic Granitic Intrusions: The main syntectonic granites are the Ben Vuirich granite with a U/Pb zircon age of 590±2 Ma (Rogers *et al.*, 1989) (See also Tanner and Leslie, 1994); the Dunfallandy Hill granite (Bradbury *et al.,* 1976) which is pre- to early "D_3"in age and gneissose granites in the Milton of Clova area (Robertson, 1991; 1994). The Ben Vuirich and Dunfallandy Hill granites have high initial Sr isotope ratios and are S-type granites.

Syn- to Late- Tectonic Basic and Ultrabasic Intrusions: These intrusions were intruded during the D_3 (D_2 of most writers) deformational phase and shortly after the peak of the regional metamorphism. Small intrusions along the Portsoy-Duchroy Hill Lineament (Fettes *et al.*, 1986), Insch mass, Bogan Clogh mass (Busrewil *et al.*, 1973), Succoth-Brown Hill mass (Gunn *et al.,* 1990), the Huntly and Knock masses (Munro, 1970; 1984; Munro and Gallaghar, 1984), Portsoy mass (Munro, 1970; 1984; Munro and Gallaghar, 1984), Belhevie mass (Ashcroft and Boyd, 1976; Wadsworth, 1991) and Haddo House and Arnage masses (Gribble, 1967; 1968) are some examples of these intrusions. These rocks have yielded ages between 497 and 465 Ma (Brown *et al.*, 1965; Pankhurst, 1970).

Late-Tectonic Granitic Intrusions: These intrusions are divided into three suites by Stephenson and Gould (1995): north-eastern biotite-muscovite-granites which are S-type and are foliated and mostly are garnet-bearing, postdating the regional

metamorphism (Stephenson and Gould, 1995), north-western biotite-muscovite-granites which are S-type rocks and north-eastern diorites to granites which are I-type rocks. The U/Pb monazite age of some members of the first group is 470 to 475 Ma and Rb/Sr age is 435 to 470 Ma (Pankhurst, 1970; 1974; Pidgeon and Aftalion, 1978; Kneller and Aftalion, 1987). A 453±3 Ma Rb/Sr whole rock isochron age has been considered for the third group (Pankhurst, 1974).

Post-Tectonic Intrusions or 'Newer Granites': These intrusions make the main igneous activities in the Grampian Highlands. Read (1961) named them 'Newer Granites'. Plant (1986) divided these intrusions into three groups, based on petrographical characters. These groups are South Grampian Suite, Argyll Suite and Cairngorm Suite. The ages of emplacement of these intrusions are between 420 to 395 Ma (Brown *et al.*, 1965; Miller and Brown, 1965; Bell, 1968; Halliday *et al.*, 1979; Summerhayes, 1966; Pidgeon and Aftalion, 1978;

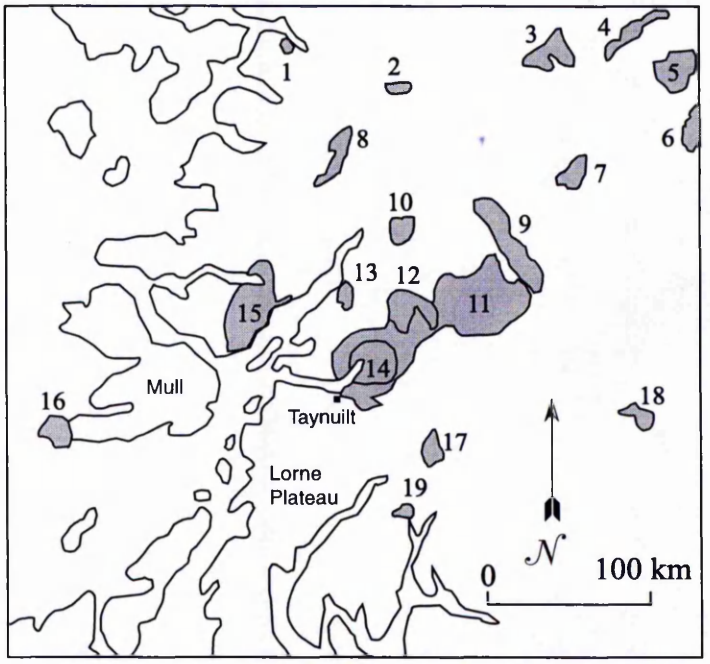

Fig.2.8 Location of the main granitoid intrusions in the SW Scotland (after Brown, 1991) 1.Ratagain, 2.Cluanie, 3. Foyers, 4. Glen Kyllachy, 5. Monadliath, 6. Cairngorm, 7. Strathspey, 8. Glen Dessary, 9. Strath Ossian, 10. Ben Nevis, 11. Rannoch Moor, 12. Glencoe, 13. Ballachulish, 14. Etive, 15.Strontian, 16. Ross of Mull, 17. Garabel Hill, 18.Comrie, 19.Arrochar.

Pankhurst, 1979; Clayburn, 1981; Haslam and Kimbell, 1981; Clayburn *et al.*, 1983; van Breemen and Piasecki, 1983; Harmon *et al.*, 1984; Turnell, 1985; Zaleski, 1983, 1985; Harrison and Hutchinson, 1987; Darbyshire and Beer, 1988; Rogers and Dunning, 1991). All of the intrusion have calc-alkaline and I-type isotopic and geochemical characters. Harmon and Halliday (1980) and Stevens and Halliday (1984) considered a mixed mantle-derived and lower crustal material source for these intrusions. The lithologies of intrusions are granite, diorite, tonalite, granodiorite and adamellite. The major 'Newer Granites' in the south west Highlands are Cluaire, Glen Dessary, Strontian, Ross of Mull, Ballachulish, Etive, Glencoe, Ben Nevis, Rannoch Moor and Strath Ossian (Fig. 2.8), all belonging to the Argyll suite.

Late- to- post-tectonic Minor Intrusions: Appinitic, lamprophyric, microdioritic and felsic plugs, sheets and dykes form these intrusions in the Grampian Highlands (Rock, 1991; Platten, 1991). Garabal Hill, Arrochar and Rubba Mor appinites have yielded U/Pb zircon and sphene ages of 422-429 Ma (Rogers and Dunning, 1991).

Volcanic Rocks of 'Lower Old Red Sandstone' Age: The Lower Old Red Sandstone Volcanics crop out in the Lorn Plateau and Glencoe and Ben Nevis area (Bailey, 1960; Kynaston and Hill, 1908). The lavas are potassic-calc-alkaline in type and are thought to be derived mainly from the mantle, with some crustal contamination (Groom and Hall, 1974; Thirlwall, 1981, 1982). A 400±5 Ma Rb/Sr isocron age was obtained by Clayburn *et al.* (1983) for these lavas.

2.8.1 Magmatic activities in the Etive area: The study of the geology of the Etive complex dates back over 180 years (MacCulloch, 1817). Kynaston and Hill (1908) and Bailey and Maufe (1916, 1960) studied the geology of the complex and the surrounding country rocks. Anderson (1937) divided the whole complex into three major petrographic facies namely 'Outer Cruachan Zone' composed of monzodiorite in the south and monzogranite in the north, 'Inner Starav Zone' made of monzogranite with a porphyritic margin and 'Meall Odhar Granite'which intruded the Cruachan facies. The complex is composed of five intrusive units ranging in lithology from diorite to granite (Frost and O'Nions, 1985; Batchelor, 1987) (Fig. 2.9). These are Quarry Intrusion, Cruachan Intrusion, Meall Odhar intrusion, Outer Starav Intrusion and Inner Starav Intrusion, from outer part (older) to the inner part

(younger) (Frost and O'Nions, 1985; Batchelor, 1987). There are abundant xenoliths of the Dalradian metasediments within the intrusion (Frost and O'Nions, 1985). Nockolds (1934) investigated the chemical and mineralogical affects of assimilation of the Dalradian xenoliths on the Quarry Intrusion. The Cruachan Intrusion is the main intrusion in the Etive complex and also is the most varied in lithology, which varies from granodiorite in the south, to a biotite granite in the north (Frost and O'Nions, 1985) and to monzodiorite in some parts (Batchelor, 1987). The Meall Odhar intrusion makes dyke-like bands composed mainly of perthitic orthclase and quartz-bearing pink leucogranite (Frost and O'Nions, 1985). Anderson (1973) has reported the existence of the andesitic xenoliths in the Meall Odhar Intrusion near the Beinn a'Bhridh screen. These xenoliths also have been observed by Frost and O'Nions (1985) at Bonawe Quarry. Batchelor (1987) identified two petrographic types of the Meall Odhar Intrusion: syenogranite and monzogranite. The Starav Intrusion represents the final phase of intrusion in the Etive complex. This intrusion has a porphyritic granite margin and a non-porphyritic pale granite core (Batchelor, 1987; Batchelor *et al.*, 1992). Batchelor *et al.* (1992) identified four phases of magmatic intrusion in the Starav Intrusion, based on studies of fluid inclusions in quartz. The first geochemical study of the Etive complex was carried out by Brown (1975). Groome and Hall (1971) in a study of the contemporaneous 'Old Red Sandstone Lorne Lavas' suite, concluded that the Etive magma chamber probably gave rise to the Lorne swarm of porphyritic dykes. Barritt (1983) attributed the high amounts of the heat-producing elements U and Th to the evolved nature of the Starav granitoids. Clayburn *et al.* (1983) using the isotopic evidence suggested an interaction between the juvenile melt from an enriched mantle source with lower crustal materials in the Etive magmatism, but Frost and O'Nions (1985) proposed an origin from recycled continental lithosphere for the Etive magmas generation. The third opinion is the incorporation of a mantle component into subducted sediments (Thirlwall, 1986). Clayburn et al. (1983) calculated a 401±6 Ma Rb/Sr whole rock age for the Etive complex, which is very close to the age of the Lorne Plateau basalts. This evidence with similar initial $^{87}Sr/^{86}Sr$ ratio suggests a possible co-magmatic source for the lavas and the 'Newer Granites'. Data from stream sediments showed Mo, Cu and Th anomalies around the Etive complex (Plant *et al.*, 1980).

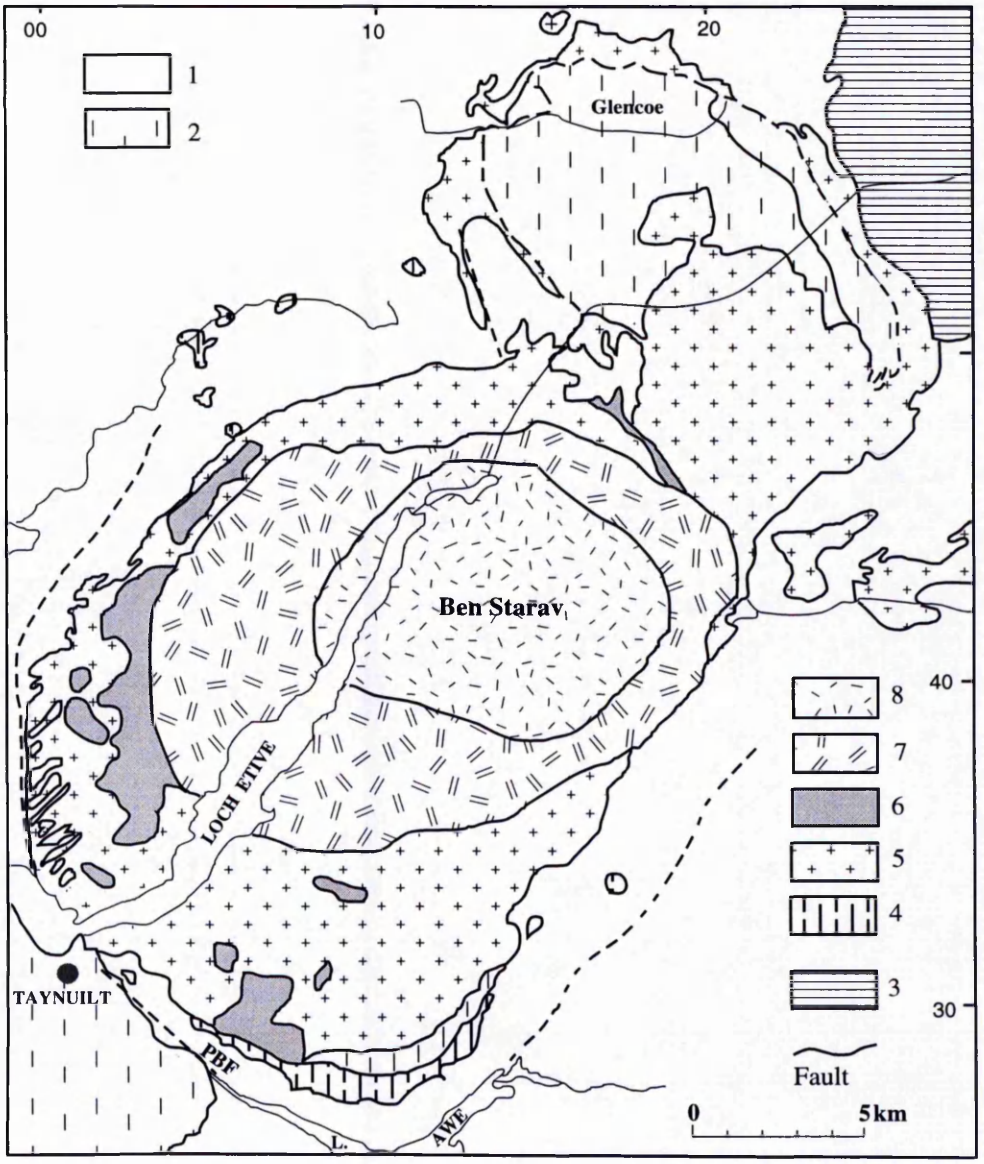

Fig. 2.9 The Etive Igneous Complex (partly after Anderson, 1973, adapted from Droop and Treloar, 1981). Lithologies: 1 Dalradian and Moine, 2 Lavas etc. of Lower Old Red Sandstone age, 3 Moor of Rannoch Granodiorite, 4 Quarry Diorite and Satellite Intrusion, 5 Cruachan Granodiorite, 6 Meall Odhar Granite, 7 Porphyritic Starav Adamellite, 8 Non-porphyritic Starav Adamellite. PBF= Pass of Brander Fault.

Three magmatic suites are spatially associated with the Etive granitoids. These are Glencoe Cauldron rocks, an elliptical outcrop of Lower Devonian age lavas to the Northwest of the Etive complex (Fig.2.9), composed of andesites with basalts and ignimbrites (Roberts, 1974b); Lorne Plateau lavas and late- Caledonian dykes. The early plutonic phases of the Etive complex are cut by a late-Caledonian swarm of mainly north-north-east-trending dykes comprising porphyrites, appinites, spessartites and olivine kersantites (Fig.2.10). Three suites may be distinguished: a) dykes that are truncated by the Cruachan phase; b) those that crosscut all the pre-Starav plutonic phases; c) rare microdiorites cutting the margin of the Starav Granite (Groome and Hall, 1974). The density of dykes decreases towards the Starav intrusion. The abundant porphyrite, felsite and lamprophyre sheets and dykes to the east of Glen Shira are related to the Garabal Hill-Glen Fyne plutonic complex (Groome and Hall, 1974). Post-Caledonian minor intrusions are represented by a

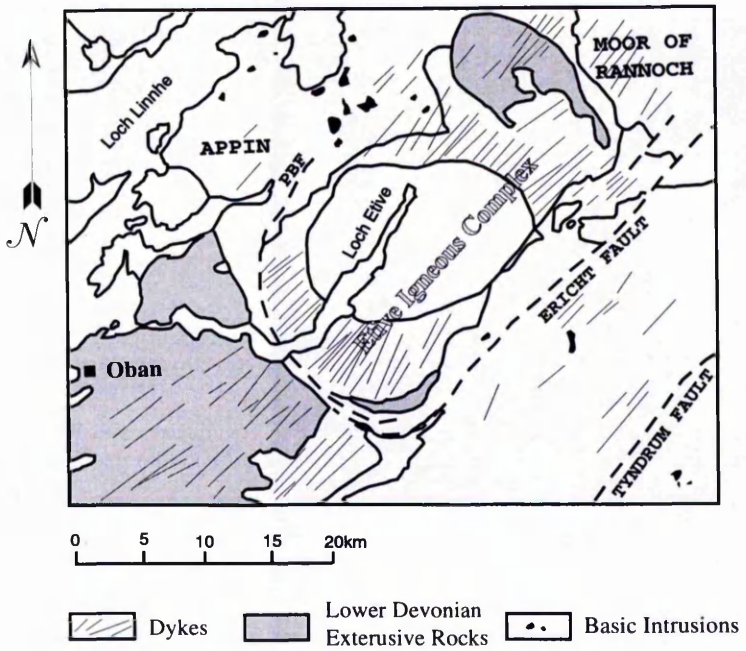

Fig 2.10 Distribution of dykes in the Etive area (adapted from Groome and Hall, 1974). The main trend of dykes is NE-SW.

suite of east to east-south-east trending Permo-Carboniferous quartz-diorite, camptonite and camptonitic dolerite dykes emplaced at c. 285±5 Ma (Groome and Hall, 1974).

2.9 Contact Metamorphism of the Dalradian Rocks by the 'Newer Granites'

The Newer Granites are intruded into the metasedimentary and meta-igneous rocks of the Grampian Group, Appin Group, Argyll Group, and Southern Highlands Group. In some cases, interesting assemblages of contact metamorphic minerals are developed in the aureoles of these granites. The aureoles around the Newer Granites, which have been studied in detail are the Comrie aureole, the Strontian aureole, the Foyers Complex aureole and the Ballachulish aureole.

Comrie aureole

One of the pioneering studies in the contact metamorphism of the Dalradian rocks by the 'Newer Granites' is the study of the Comrie aureole by Tilley (1924). The Comrie Granitic complex is intruded into the Dalradian rocks (Ben Ledi Grits and Aberfoyle slate-band, Tilley, 1924). Tilley (1924) defined three zones in the aureole, a) zone of spotted slates, b) zone of biotite development and c) zone of cordierite development. He divided the hornfelsic rocks into seven classes according to the different mineral assemblages, and derived some mineralogical reactions for the production of the metamorphic minerals.

Strontian Granodiorite aureole

The contact metamorphic aureole of the Strontian Complex is not obvious in the field. The most conspicuous change in the schists and gnisses, on approaching the igneous rocks, is an increase in deformational effects due to complex forceful emplacement (Munro, 1965). Probably the lack of a well developed hornfelsic aureole about the intrusion (Sabine, 1963) indicates emplacement while the country rocks were regionally hot (Watson, 1964). The aureole is strongly asymmetrical and the metamorphic zones are broader to the east of the intrusion. The asymmetry is attributed to a gradient in the background, regional temperature (Ashworth and Tyler, 1983).

The country rocks are meta-sediments of the Western Moinian, with a history of Precambrian as well as Caledonian regional metamorphism (Powell, 1974).

Despite poor field evidence for contact metamorphism, Ashworth and Chinner (1978) pointed out the formation of a new mineral assemblage near the contact. The occurrence of cordierite, and locally andalusite (Tyler and Ashworth, 1982), which

indicates lower pressure than in the slightly earlier regional climax (kyanite-sillimanite zonal sequences in the regionally metamorphosed rocks) is attributed to the thermal metamorphism (Tyler and Ashworth, 1982).

Ashworth and Tyler (1982) proposed a thermal model for the temperature distribution in the aureole and regionally metamorphosed rocks. According to this model, the peak temperature 2-km from the contact was below 645° C in the west and above 690° C in the east (Ashworth and Tyler, 1983).

Foyers Granite Complex aureole

The Foyers intrusion, east of Loch Ness in Central Highlands, is dated at 400 ± 10 Ma (Brown *et al.*, 1968) and is distinctly younger than the peak of the regional metamorphism. The intrusion consists of adamellite, granodiorite and tonalite and has intruded into the Grampian and Dalradian Supergroups.

The contact metamorphism around the Foyers Complex took place at a pressure of approximately 4kbar and low water activity (Tyler and Ashworth, 1982). This low a_{H2O} promoted the dehydration reaction that produces cordierite and K feldspar, which proceeded in the absence of melting at temperatures of approximately 650°C. Using the exchange equilibrium of Fe and Mg between garnet and biotite and between garnet and cordierite, Ashworth and Tyler (1983) calculated the maximum temperature of 650°C for the contact metamorphism.

Ballachulish aureole

The Ballachulish igneous complex is an "I-type" pluton (Harmon, 1983) which intruded into the Dalradian metasediments, mainly pelitic, semipelitic and calcareous rocks of the Appin group, the graphitic, sulphide-bearing Ballachulish slates and phyllite and quartzites of the Leven schist. The complex consists of a variety of igneous rocks including grey diorite, pink granite, two-pyroxene bearing monzodiorite and quartz diorite (Bailey and Maufe, 1960). The contact metamorphism of calc-silicates was studied by Heuss-Aßbichler and Masch (1991). Based on parageneses in these rocks he estimated a pressure of 2.8 ± 0.4 kb, with temperatures increasing from ~ 400°C before initial cordierite development in the pelites to ~750°C at the igneous contact. The contact metamorphism of pelitic rocks has been studied in detail by Pattison (1987) and Pattison and Harte (1985). The aureole contains an extremely well-defined sequence of prograde mineral-assemblage

zones in pelitic and semipelitic rocks (Pattison, 1987; Pattison and Harte, 1985). These zones are 'Marginal Zone' with Bt+Chl+Ms+Qz assemblage, 'Cordierite Zone' with Crd+Bt+Ms+Qz±Chl assemblage, 'Andalusite Zone' with Crd+And+Ms+Bt+Qz assemblage', Andalusite + Alkali feldspar Zone' with Crd+And+Kfs+Bt+Qz±Ms assemblage, 'Corundum Zone' with Crd+And+Bt±Crn+Kfs assemblage and 'Migmatite Zone' with Crd+And+Bt assemblage in the hornfelsic parts and Kfs+Qz in the melt parts (Pattison, 1987). The pressure obtained by Pattison (1991) is 2.8 to 3.2 kbars and the highest temperature is 750°C. Temperature of the country rocks before the intrusion is thought to be about 250°C (Pattison and Voll, 1991). Pattison (1985, 1991) described the contact metamorphic grade range from quartz-chlorite-biotite-cordierite-muscovite assemblages to high-grade muscovite-absent assemblages of biotite-cordierite-K feldspar with or without quartz and corundum. At the highest grade, partial melting of the country rocks occurred. The greatest extent of melting occurred in the Leven Schist in a 400 m wide zone of diatexites called the 'chaotic zone' (Pattison and Harte, 1985). The difference between the melting extent of the Leven Schist and Appin Quartzite is attributed to the lower amounts of magmatic fluids in equilibrium with Appin Quartzite (Pattison, 1985). Holness (personal communications) considered the role of the higher equilibrium quartz-fluid dihedral angle in the Appin Quartzite, which made it impermeable to aqueous fluids emanating from the crystallising pluton.

2.9.1 Contact metamorphism in the Etive area: The only work on the contact metamorphism of the country rocks around the Etive complex is the study by Droop and Treloar (1981). These authors have used calc-silicate and metapelitic assemblages for identification of the pressure in the southern section of the aureole. Calculated pressures lie within the range 1.0 to 2.0 kbars, corresponding to 3 to 6 km overburden during intrusion.

Chapter 3

Petrography and Geochemistry of the Etive Igneous Complex

3.1 Introduction

The main objective of this chapter is to provide a systematic petrographic and geochemical investigation of the different igneous rock types that comprise the main intrusive phases in the Etive complex. The eventual aim of studying the igneous rocks is to estimate the heat and fluid-bearing capacities of the rocks with a view to assessing their roles in the contact metamorphism of the surrounding metasediments.

This chapter is composed of seven parts. After the introduction, the field relations of igneous rocks are discussed in order to demonstrate the nature of the contacts and chronological order of emplacement. The next part deals with the detailed petrography of the rocks in each of the main intrusions. In the following parts, the geochemical and petrological aspects are considered. Mineral chemistry and petrogenetic aspects are then addressed. Eventually, some thermobarometric methods are applied to the igneous rocks of the Etive Complex to constrain conditions of crystallisation.

3.2 Field Relations

The igneous rocks of the Etive Complex are well exposed in several stream profiles in the southern and the northern sides of Loch Etive. Also the rocks outcrop in Bonawe Quarries and several other quarries to the south of Loch Etive and the north of the NE limb of Loch Awe along the Allt Mhoille stream. The rocks are well exposed around the Cruachan Reservoir, on the north of Loch Awe at the Monadh Driseig summit, and on the east of Loch Creran at the Meall Garbh and Glen Dubh summits.

3.2.1 Internal Contacts in the Igneous Rocks: Different phases of intrusions are present at Bonawe Quarries. At this locality the main rock body is the Cruachan intrusion which has different modal proportions of minerals in different parts. In some parts the rock is a granodiorite and in others it is mainly monzodiorite. At Bonawe Quarries the Cruachan intrusion is cut by microdioritic and microgranodioritic dykes. Apophyses of Meall Odhar pink leucocratic monzogranite (alkali-granite) are present in the Cruachan intrusion.

Figure 3.1a illustrates the relationships amongst the different rock types in the Cruachan intrusion in the eastern Bonawe Quarry (G.R.03183401). The Meall Odhar Granite is intruded into the Cruachan rocks, and both are cut by the later microdioritic dykes.

The contacts between adjacent intrusions are commonly sharp and distinctive (for example between Cruachan and Meall Odhar intrusions), but within a single intrusion gradational contacts are not uncommon. In the eastern Bonawe Quarry, a gradational change from granodiorite to monzodiorite (picked out by gradational increase in modal alkali feldspar) was observed at one locality (G.R. 03073402), proceeding upwards over a vertical distance of ca. 6 m, within the Cruachan intrusion. At the top of this 6 m unit, there is a sharp, sub-horizontal boundary between pinkish monzodiorite and overlying darker granodiorite. This feature is reminiscent of rhythmic layering. At this locality, also, there is a large (1×5m) flat-lying enclave of dark microdiorite, similar to the Quarry Diorite; this is interpreted as a large fragment of the Quarry Diorite broken off during emplacement of the Cruachan intrusion.

The intrusion of the later Meall Odhar leucogranite into the Cruachan intrusion rocks has caused fracturing and fragmentation of the rocks. Fig. 3.1b shows this effect in the eastern Bonawe Quarry.

In the Cruachan Reservoir area, near the dam (NN07822837), leucogranitic dykes and veins cut the rocks of the Quarry intrusion

3.2.2 Contacts with the Country Rocks: Contacts between igneous rocks and country meta-sedimentary or meta-igneous rocks are largely sharp and discordant. A metasomatic amphibole-rich layer generally accompanies contacts between granite or granodiorite and calc-silicate hornfels from mm scale to 2 cm thick. Plate 3.1 illustrates the contact between granodiorite from the Cruachan intrusion and calc-

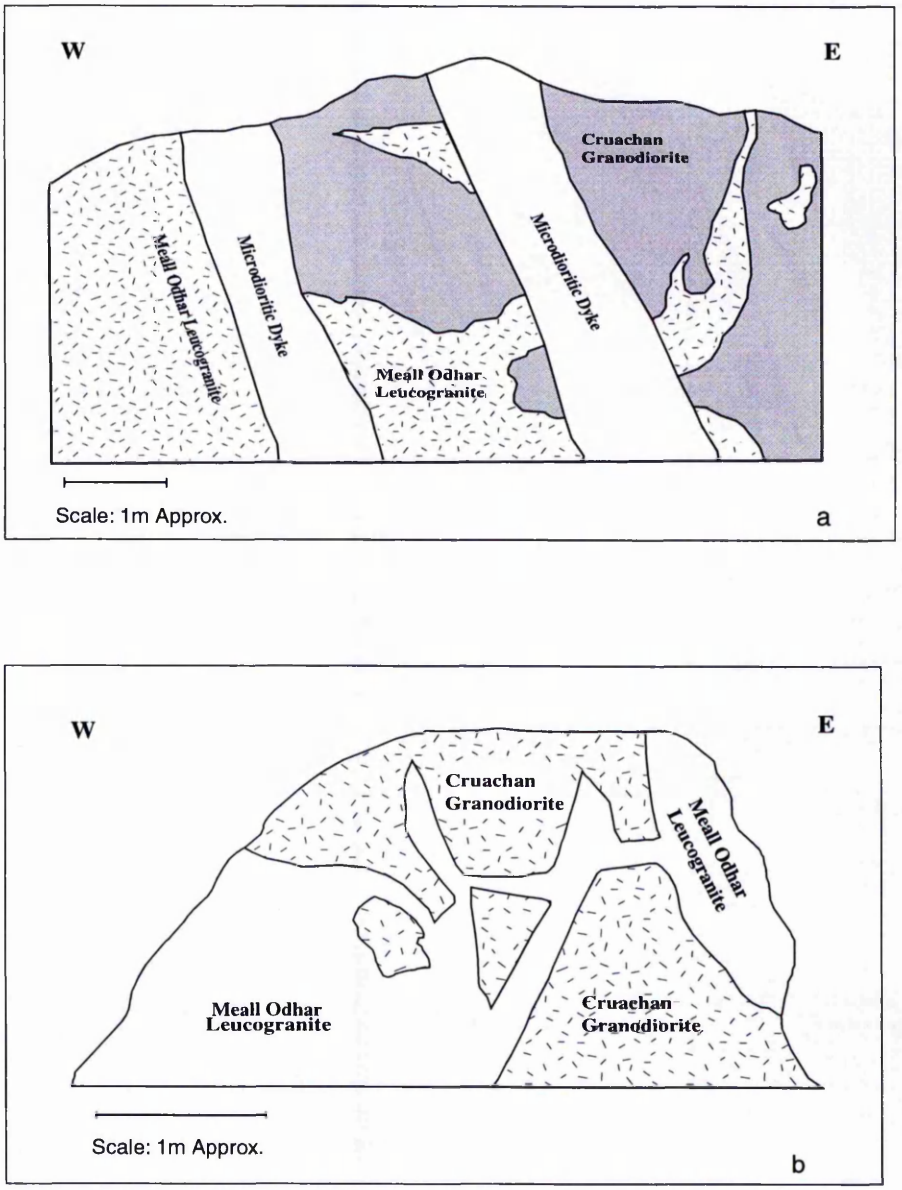

Fig. 3.1

a) Sketch drawing (section view) illustrating the different rock types in the Cruachan Intrusion rocks in the eastern Bonawe locality G. R. NN03183401.

b) Fragmentation of the Cruachan Intrusion rocks due to intrusion of the later Meall Odhar Granite. Section view, locality G.R. NN03183401.

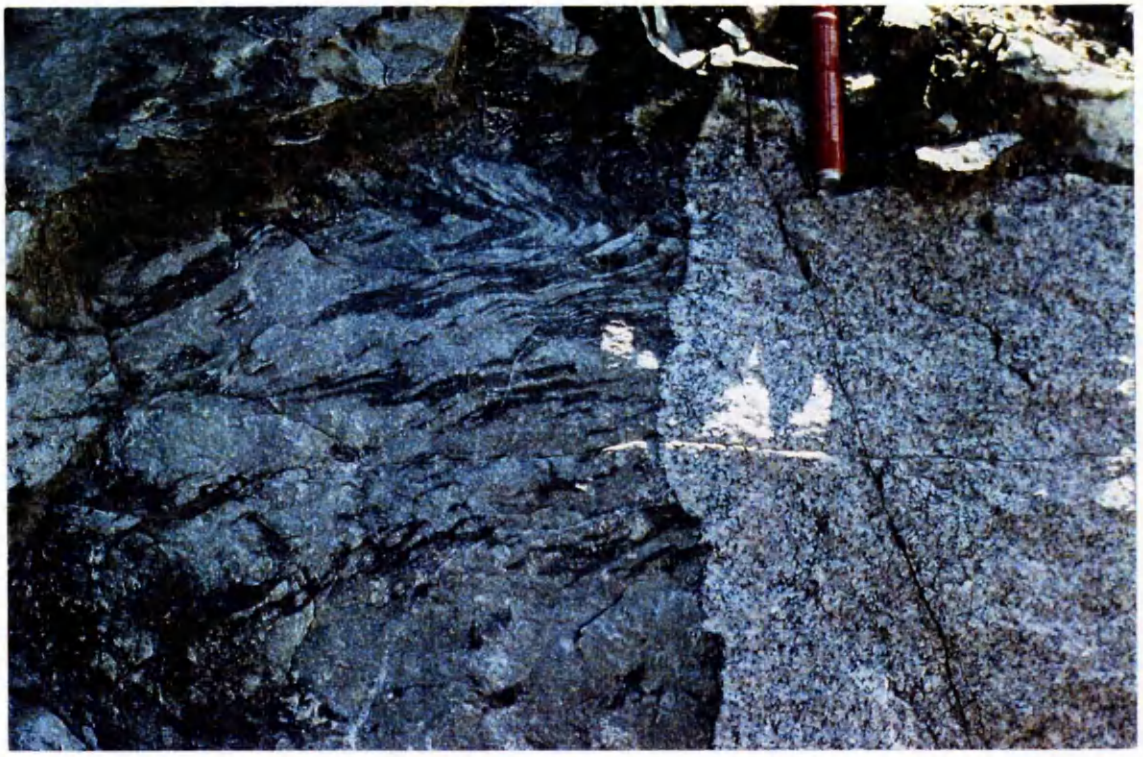

Plate 3.1 Contact between Cruachan Granodiorite and Calc-silicates from the Esdale sub-group at the locality G. R. NN020327, south of Loch Etive. The dark minerals at the contact are metasomatic amphiboles. Note the contact transects folds in the metasediments.

Plate 3.2 Andesitic xenolith in the granodiorite from the Cruachan intrusion at locality G.R. NN11592975, north Loch Awe area.

silicates from the Easdale subgroup at locality NN020327, which is a disused quarry on the south of Loch Etive. The amphibole-rich layer on the contact is visible in this plate. The contacts commonly truncate older (regional metamorphic) folds within the meta-sediments, but also locally follow the direction of lithological or structural anisotropy. On the outcrop scale contacts appear mainly steep. To the east of the complex, in the Loch Creran area, the Cruachan intrusion is in contact with the Creran Flags which mainly consist of quartzite, semipelite and psammites with minor carbonates and metabasites. Angular, commonly tabular xenoliths of metasediment are present in the Cruachan intrusion rocks near its contact on the east of Loch Creran (NN03244425).

In the area north of Loch Awe, the Quarry intrusion is in contact with the Leven Schists, Glencoe Quartzite, Islay Quartzite, Ben Eagach Schists and Ardrishaig Phyllites. In all cases the contact between the igneous rock and metasedimentary rock is more or less sharp and discordant.

In the old Quarry at the south side of Loch Etive (NN020327) and along the south shore of Loch Etive, large xenoliths and screens of calc-silicates and pelitic rocks of the Easdale Subgroup are present in the Cruachan intrusion. Also along the Blarcreen Burn stream, north of Loch Etive, xenoliths and screens of psammitic and semipelitic rocks of the Easdale subgroup are present in the Cruachan intrusion. The contact between the rocks of the Quarry intrusion and andesitic lavas around the Cruachan Reservoir at NN07832866 is sharp and the thermal effect of the diorite on the andesite is distinguishable by recrystallised hornblende and biotite. At NN11752965 on the stream bed, Quarry intrusion, andesitic rocks and Cruachan intrusion crop out and xenoliths of the andesitic rocks are present in the Quarry and Cruachan intrusions rocks. Recrystallised biotite reaches 1mm in size in some of these xenoliths. Plate 3.2 shows an andesitic xenolith in the granodiorite from the Cruachan intrusion at locality NN11592975, north of Loch Awe.

According to the field relations, the order of the emplacement of different intrusives from older to younger is: 1- Quarry Intrusion, 2- Cruachan Intrusion, 3- Meall Odhar Intrusion.

3.2.3 Dykes: As mentioned in section 2.8.1, a swarm of Late Caledonian dykes cuts the Etive Igneous Complex and its surrounding metasedimentary rocks. The main types of dykes in the studied area are dark, fine-grained microdioritic dykes and light

porphyritic dykes with plagioclase and biotite phenocrysts. The thickness of dykes varies from cm scale to 20 metres. The main trend of dykes is NNE-SSW (Fig. 2.10 Chapter 2).

Table-3.1- Field information on dykes in the Etive area. Readings are trends of dykes or dyke planes.

Locality	G.R.	Dyke Type	Direction (strike/dip)
Bonawe	NN0.377/3430	microdiorite	042/68S
Bonawe	NN0350/3419	microdiorite	120/08E
Bonawe	NN0082/3347	microdiorite	040
Inveresragan	NN0053/3366	porphyritic	047
Cruachan Reservoir	NN0824/2820	microdiorite	202/90
Cruachan Reservoir	NN0827/2822	porphyritic	185/80W
Cruachan Reservoir	NN0782/2837	microdioritic	063
Road to Reservoir	NN0830/2738	microdioritic	066/88N
Road to Reservoir	NN0830/2724	porphyritic	220/78SW
Road to Reservoir	NN0847/2693	porphyritic	027
Road to Reservoir	NN0908/2662	porphyritic	013/79E
Road to Reservoir	NN0991/2643	microdioritic	224/56NE
Road to Reservoir	NN1030/2639	porphyritic	170/78W
Road to Reservoir	NN1058/2640	lamprophyre	-

Table 3.1 includes some field information on dykes in the Etive area and Fig. 3.2 shows an equal-area rose diagram for these dykes. The pattern of dyke distribution indicates that a NNW-SSE-directed extensional regime was active in the SW Scottish crust during the Late Caledonian.

3.3 Petrography of the Main Intrusive Rocks

Several hand specimens and nineteen thin sections were examined from different intrusions in the Etive igneous complex. The main rock types in the southern part of the Etive Complex and locality of the studied samples are shown in Fig.3.3. Rock nomenclature is based on the modal classification of Streckeisen (1976). Texturally and mineralogicaly, all of the rocks are typical I-type granitoids without any mineralogical preferred orientation or deformation texture.

3.3.1 Cruachan Intrusion: The Cruachan intrusion is composed mainly of granodiorite and monzodiorite. The main varieties are hornblende granodiorite, hornblende monzodiorite and pyroxene-bearing diorite. One representative sample of each will be described.

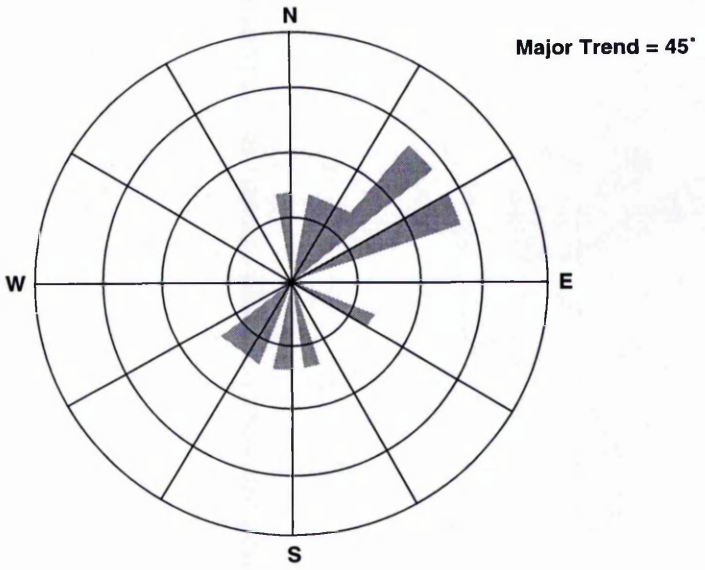

Fig. 3.2 Equal area rose diagram for dyke trends in the Etive area. The main trend of dykes is NE/SW (45°).

Hornblende Granodiorite (Sample MM3A, NN03503419): This is a medium grained rock. Amphibole and plagioclase are distinguishable in hand specimen. The length of hornblende reaches 3 mm and the length of plagioclase reaches 5 mm. In some parts of the rock, hornblende-rich areas are visible. Under the microscope (Plate 3.3), the rock consists of plagioclase, quartz, alkali-feldspar, amphibole, biotite and minor phases. Plagioclase is the dominant mineral. The length of the crystals is 0.5-3mm. Most of the crystals show very fine polysynthetic twinning. All of the plagioclases in the rock show optical zoning and are slightly altered to clay minerals. The extinction angle of plagioclases is 18-25", corresponding to andesine. Zoning is normal, i.e. from relatively Ca-rich cores to Na-rich rims (see section on mineral chemistry in this chapter). Quartz is not common and shows interstitial crystallisation and undulose extinction. Rare alkali feldspars (~4mm long) have poikilitic texture with inclusions of plagioclase, biotite, amphibole and opaque minerals. Amphiboles are green pleochroic hornblende. The amphibole crystals vary in size from 0.2 mm to 3mm. Some of the amphibole crystals have a biotite rim. There are also alternate layers of biotite and hornblende in some of the fibrous aggregates in the rock. The close textural relationship between biotite and amphibole in this sample indicates a possible alteration from amphibole to biotite. Greenish-brown to brown flakes of

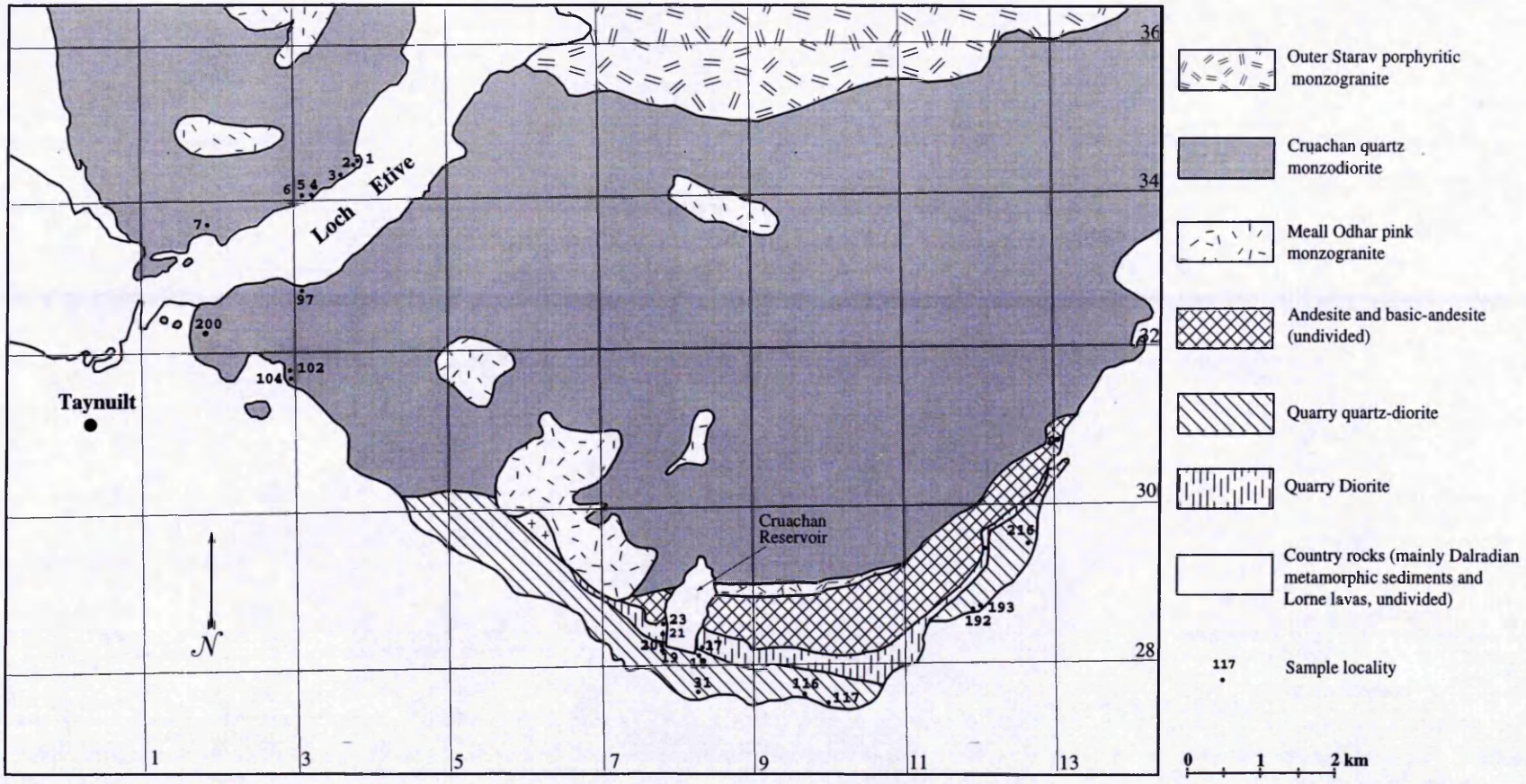

Fig. 3.3 Locality of igneous rock samples used in this study. The map also shows the distribution of the main intrusions in the southern part of the Etive Complex.

biotite in the rock have a strong pleochroism. A very fine-grained, high relief aggregate of minerals (possibly epidote) surrounds all of the biotite flakes (probably in amphibole to biotite alteration, Ca from amphibole, which cannot enter the biotite structure, accumulates in epidote around the biotite). Pleochroic haloes in the biotite are common. Minor phases are sphene with relatively large grains (1.5mm), opaque minerals (ilmenite and hematite), zircon and apatite.

Hornblende Monzodiorite (Sample MM5D, NN 03073402): This is a fine to medium grained rock with dark grey colour. Dark amphiboles and pale feldspars are visible. In the microscopic view (Plate 3.4), the rock consists of plagioclase, quartz, alkali-feldspar, amphibole, biotite and minor phases with a granular texture. The approximate mineral proportions are plagioclase ~45%, alkali-feldspar ~35%, quartz ~5%, amphibole ~5%, biotite ~5% and other minerals (mainly oxide minerals, sphene and epidote) ~5%.

Optically zoned plagioclases have fine polysynthetic twinning, are 0.2-2mm across, and are slightly altered to clay minerals. The extinction angle of plagioclases is 15-28", corresponding to andesine, and zoning is normal. Quartz is rare and shows undulose extinction. Large poikilitic crystals of both microperthitic and apparently non-perthitic microclines have inclusions of hornblende, biotite, plagioclase, oxide minerals, apatite and zircon. Amphiboles are green hornblendes with subhedral to anhedral shapes. Biotite appears as small, short flakes. Sphene, abundant apatite, zircon and secondary epidote are minor phases.

Pyroxene-bearing Diorite (Sample MM5E, NN 03073402): This rock is of medium grain-size with distinguishable amphiboles and plagioclases in hand specimen. In the microscopic view the rock has a granular texture. Twinned and zoned plagioclase, subhedral crystals of amphibole and fresh alkali feldspar are major minerals and quartz, biotite, oxide minerals, common zircon, apatite and rutile are minor phases. The approximate mineral proportions are plagioclase ~45%, quartz ~10%, alkali-feldspar ~20%, amphibole ~10%, biotite ~15% and other minerals ~5%. Some of the hornblende crystals contain tiny, irregular relicts of augite in their cores. Large perthites show poikilitic textures with inclusions of biotite, opaques, amphibole, plagioclase, apatite and zircon. Feldspars are slightly altered to sericite. Clinopyroxene becomes unstable and rimmed by amphibole as the hornblende and

K-feldspar amount increases. This is attributed to late-magmatic, pyroxene-consuming reaction of the type:

Cpx + Bi + 4 Qz = K-feldspar + Amphibole (Wones and Gilbert, 1982).

3.3.2 Meall Odhar Intrusion: This intrusion mainly consists of two petrographic types, the alkali-granite and the monzogranite.

Alkali-Granite (Sample MM 5G, NN 03073402): This rock is pink coloured, leucocratic, medium- to coarse-grained alkali-granite, with 3-5 mm long microclines. Under the microscope (Plate 3.6) the general texture of the rock is granular and myrmekitic texture is locally developed. Coarse perthitic alkali-feldspar is the predominant mineral, which is slightly altered to sericite and clay minerals. Quartz is the other major mineral, which fills the spaces between the blocky alkali-feldspar crystals. It shows undulose extinction. Plagioclase is rare. Chlorite (probably after primary biotite), rare oxide minerals, sphene and zircon are other minor phases. The approximate mineral proportions are alkali-feldspar ~65%, quartz ~25% and all other minerals ~10% .

Monzogranite (Sample MM3F.A, NN 03503419): This sample of Meall Odhar monzogranite with a granular texture consists of large, unaltered alkali-feldspars, less common plagioclase and quartz with minor amounts of biotite, zircon, apatite and opaque minerals. The approximate modal proportions of minerals are : alkali-feldspar ~55%, plagioclase ~20%, quartz~20 % and other minerals (mainly oxide minerals, rare biotite and rare secondary chlorite) ~5%.

3.3.3 Quarry Intrusion: This intrusion consists of two main petrographic types, two-pyroxene-bearing diorite and quartz monzodiorite.

Two-pyroxene-bearing diorite (Sample MM17, NN08192809): This rock is dark grey, fine- to medium-grained rock. The texture of the rock is granular and the major minerals are zoned and twinned plagioclases, abundant amphiboles, orthopyroxene, clinopyroxene, biotite, rare alkali feldspar and rare quartz (Plate 3.7). Most of the clinopyroxenes are rimmed by a hornblende envelope. The minor phases are ilmenite, apatite, zircon and secondary sericite. Clinopyroxenes are altered to amphibole and orthopyroxenes to biotite. These alterations are probably post-magmatic phenomena, which can be explained by the following probable sub-solidus hydration reactions:

$Opx + K\text{-feldspar} + H_2O = Bi + 3\ Qz$ (Wones and Eugster, 1965)

$Cpx + Bi + 4\ Qz = K\text{-feldspar} + Amph$ (Wones and Gilbert, 1982)

It seems that some of the biotites and amphiboles are not products of orthopyroxene and clinopyroxene alteration, according to the textural relations. They have probably crystallised directly from the silicate magma. The main low-temperature alteration products are actinolite after hornblende and clay minerals after plagioclase.

Quartz Monzodiorite (Sample Δ659, NN12082943): This rock is a medium- to coarse-grained rock with visible plagioclase, amphibole and alkali feldspar in hand specimen. Under the microscope (Plate 3.8) the main texture of the rock is granular and the main minerals are twinned and zoned plagioclases, perthitic alkali feldspar, hornblende, biotite and quartz. Minor phases are apatite, oxide minerals and zircon. Large plagioclases (up to 4mm) are slightly altered to clay minerals. Quartz is not common and shows interstitial crystallisation. Myrmekitic texture is developed in this rock.

Table 3.2 includes the mineralogical assemblages of the representative samples of Etive igneous rocks.

Table 3.2 Representative mineral assemblages in the igneous rocks of the Etive Complex. (X=Major Phase, O=Minor Phase, mineral abbreviations are after Kretz, 1983).

Sample No.	MM3A	MM5D	MM5E	MM5G	MM3f.a	MM17	D661
Rock Type	Hbl granodiorite	Hbl monzodiorite	px-monzodiorite	alkali granite	monzogranite	two pyroxene diorite	Qtz monzodiorite
Qtz	X	X	O	X	X	O	X
Pl	X	X	X	X	X	X	X
Kfs	X	X	X	X	X	O	X
Bt	X	X	O		O	X	X
Hbl	X	X	X			X	X
Opx						X	
Cpx			O			X	
Ap	O	O	O	O	O	O	O
Zirc	O	O	O	O	O	O	O
Ore	O	O	O	O	O	O	O
Tit	O	O	O	O		O	O
Ep		O			O		
Chl				A	A		

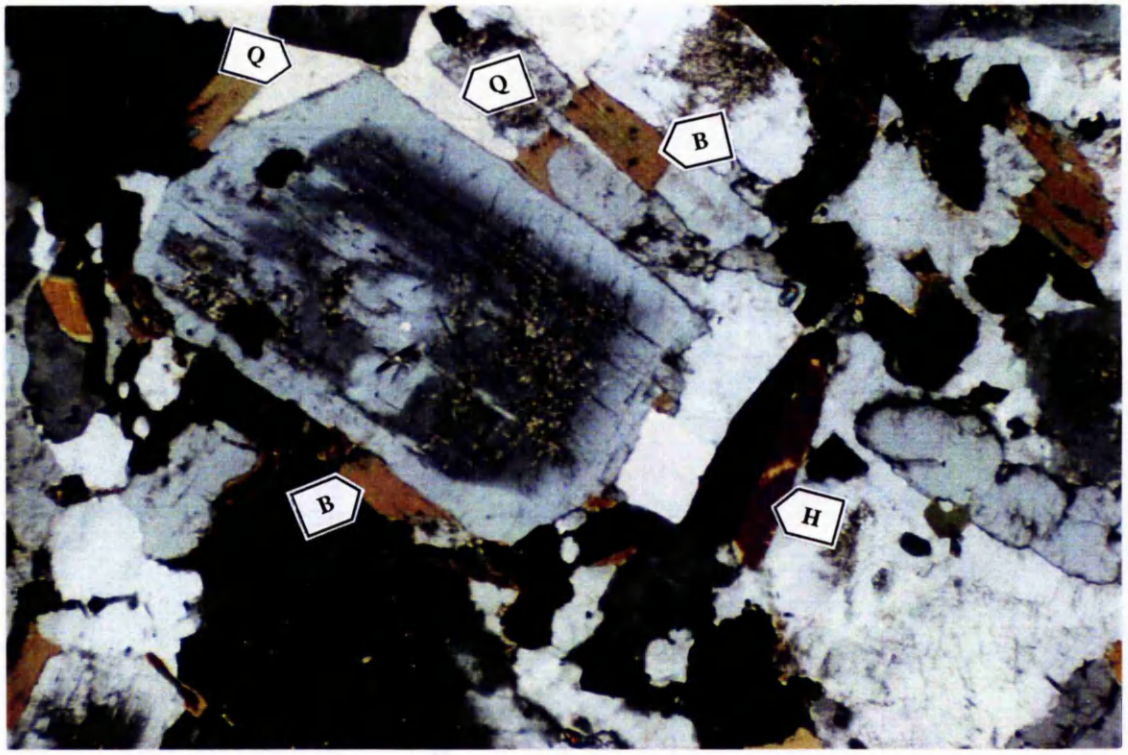

Plate 3.3 Hornblende Granodiorite sample MM3A (G.R. NN03503419) containing hornblende (H), quartz (Q), biotite (B) and large zoned plagioclase. XPL. Field of view 4.2 mm.

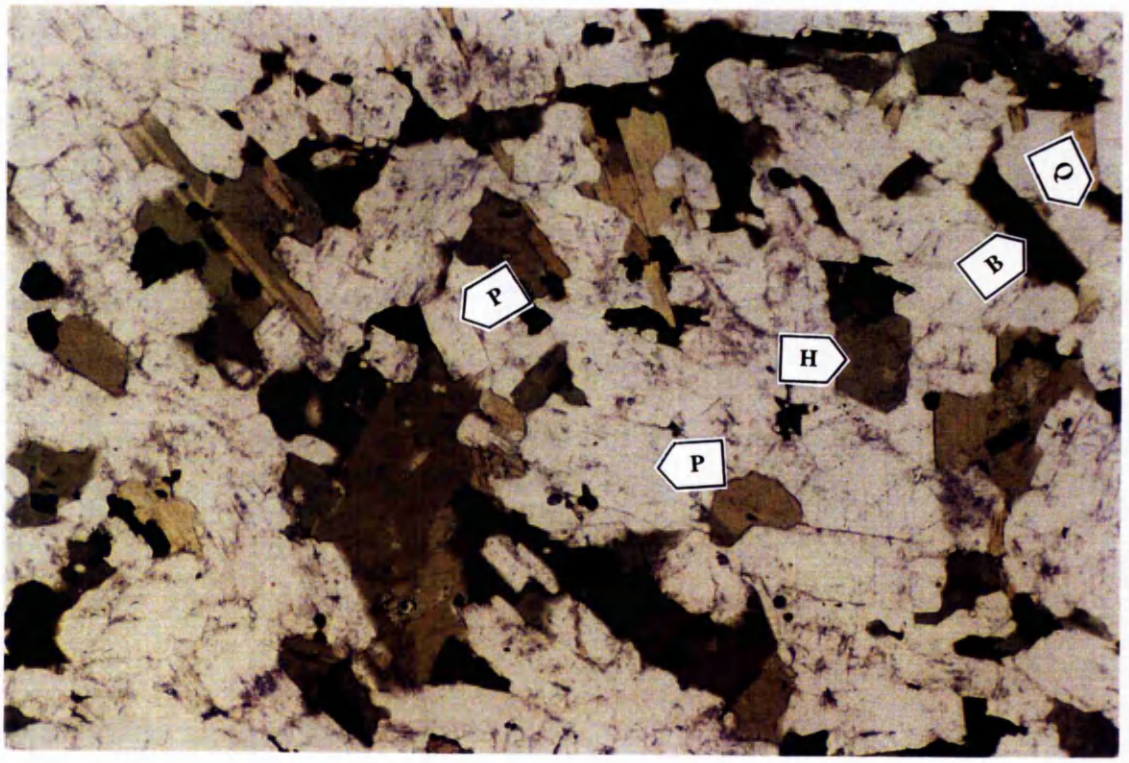

Plate 3.4 Hornblende Monzodiorite sample MM5D (G.R. NN03073402), containing hornblende (H), plagioclase (P), quartz (Q), biotite (B) and ore minerals (black). PPL. Field of view 4.2 mm.

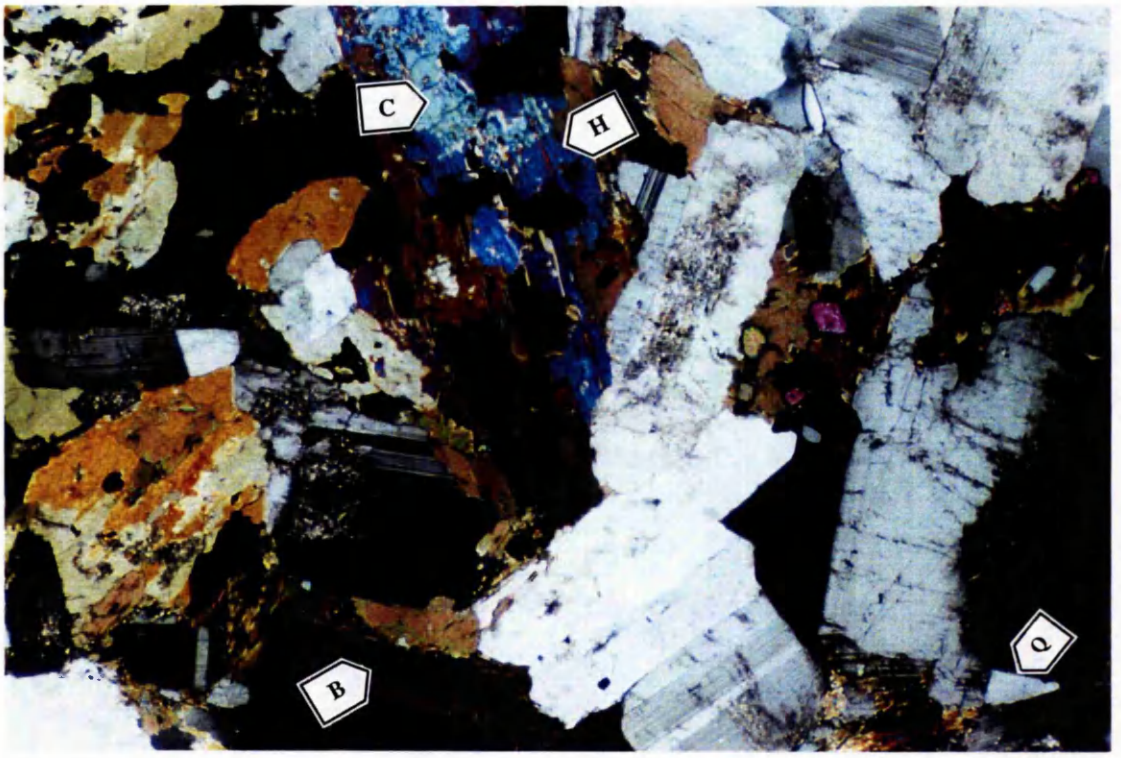

Plate 3.5 Pyroxene diorite sample MM5E (G.R. NN03073402), containing plagioclase with polysynthetic twining, biotite (B), hornblende (H) and quartz (Q) and zircon (high relief, euhedral diamond -shaped minerals). Clinopyroxene (C) is enclosed within the inner parts of hornblende. XPL. Field of view 4.2 mm.

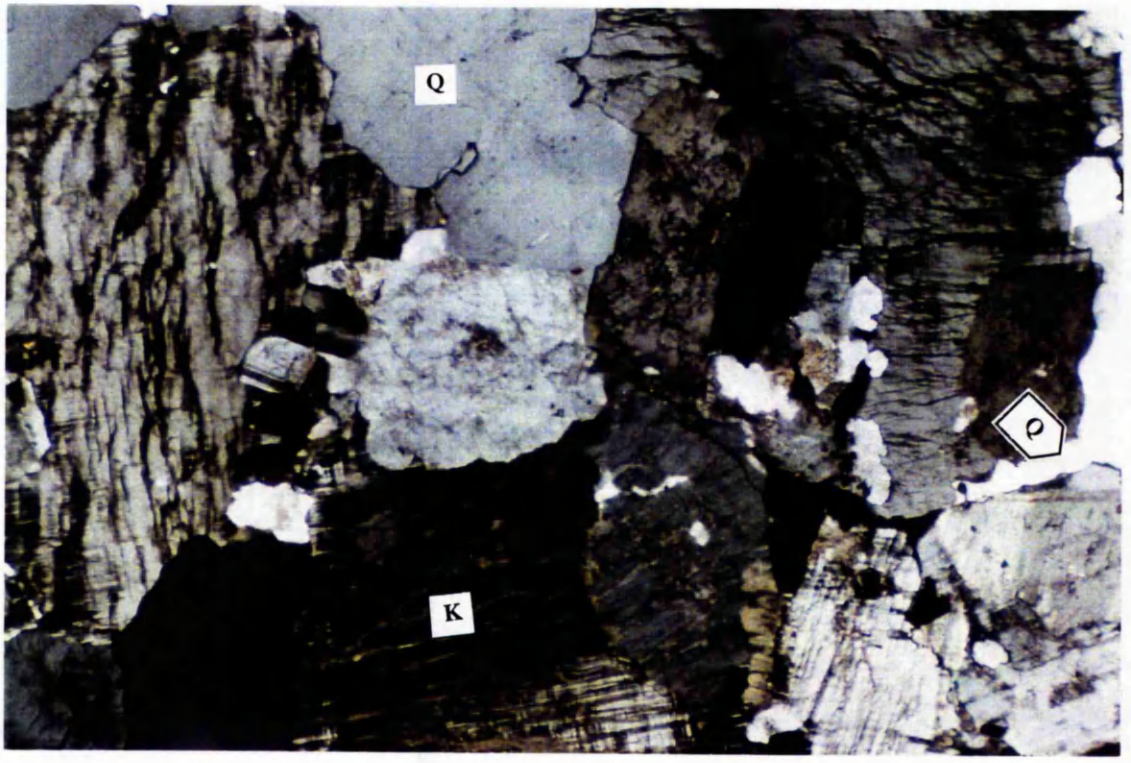

Plate 3.6 Meall Odhar alkali-granite sample MM5G (G.R. NN 03073402), containing quartz (Q) and K-feldspar (K). XPL. Field of view 4.2 mm.

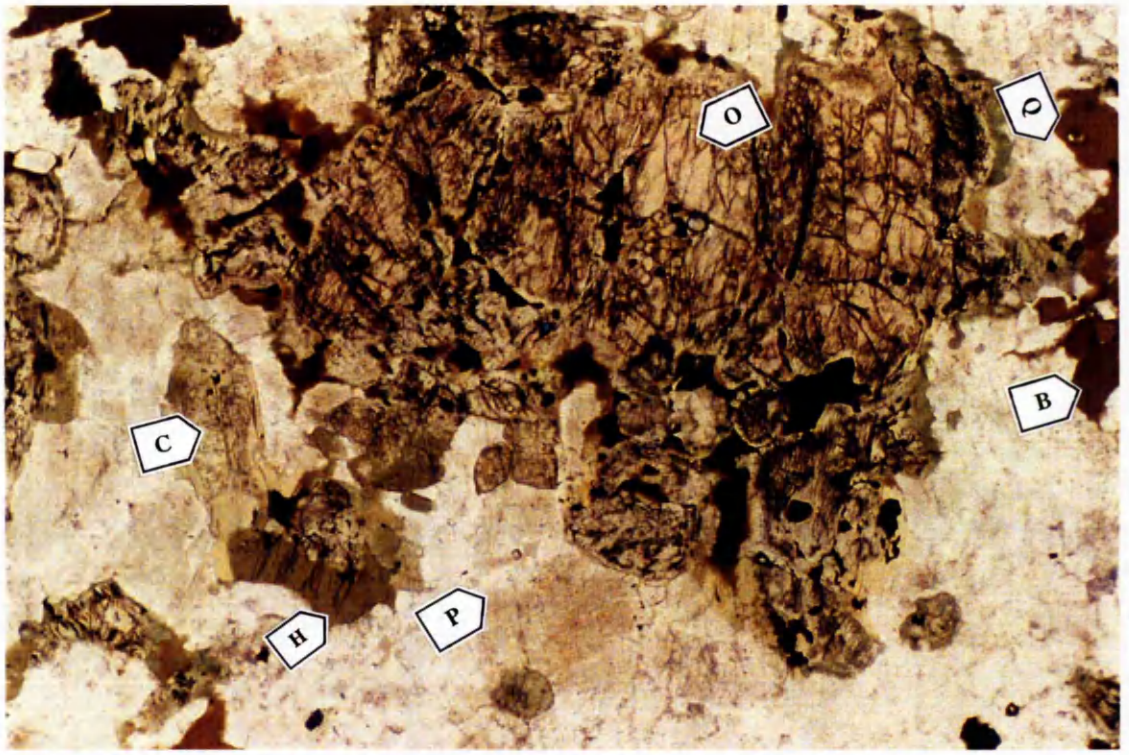

Plate 3.7 Two-pyroxene diorite sample MM17 (G.R. NN08192809), containing orthopyroxene (O), Clinopyroxene (C), quartz (Q), biotite (B), plagioclase (P), hornblende (H) and ore minerals (black). PPL. Field of view 1.6 mm.

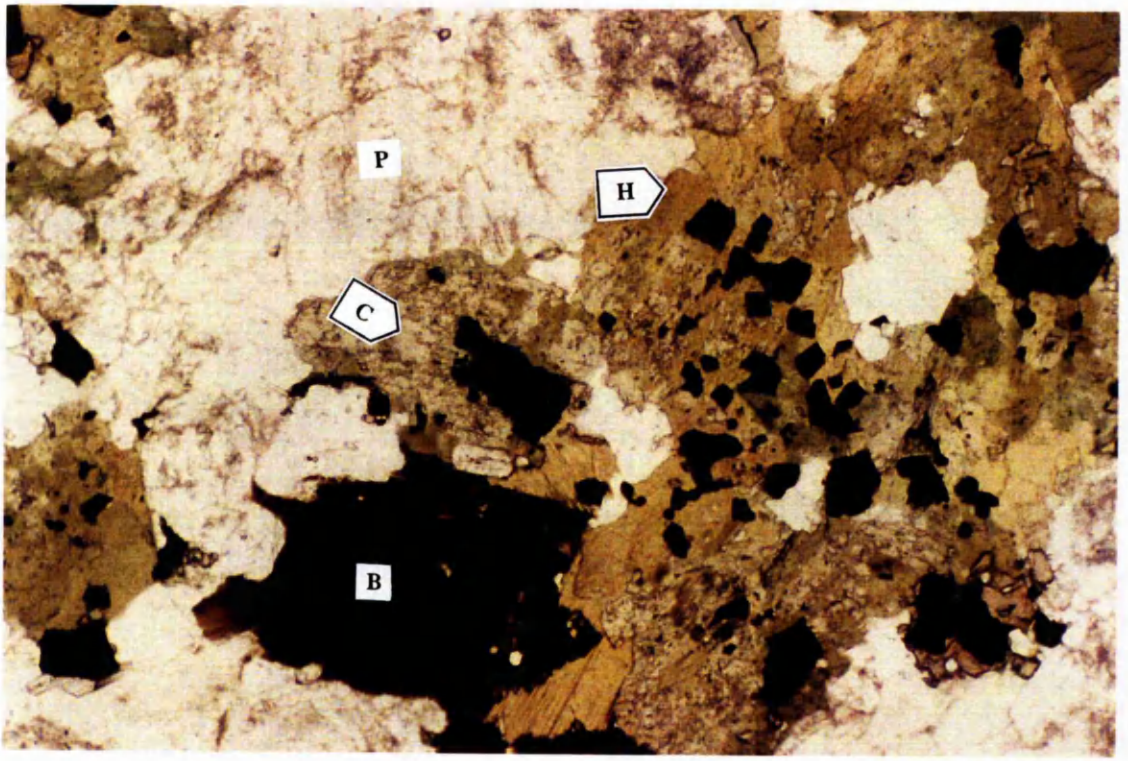

Plate 3.8 Pyroxene diorite, sample Δ659 (G.R. NN12082943), containing plagioclase (P), hornblende (H), clinopyroxene (C), biotite (B) and ore minerals (black). PPL. Field of view 4.2 mm.

3.4 Geochemistry

In order to undertake geochemical and petrogenetic studies of the Etive Igneous Complex, major and trace element data were obtained on 36 representative whole-rock samples. For apparatus, methods, procedures and standards see Appendix 1. CIPW norms were calculated using the computer program 'CIPW norm'. The amount of FeO was analysed in 8 representative samples of the different rocks by means of wet chemistry (determination of FeO wt% using ammonium metavanadate). The FeO/Fe_2O_3 ratio was calculated for each of the main rock types from the representative samples and the resulting ratio was used to calculate the FeO and Fe_2O_3 amounts in all of the respective analysed samples. Chemical compositions of the representative rocks are presented in Table 3.3; the chemical compositions of all of the analysed samples can be found in Appendix 2.

3.4.1 Major and trace element variation: For condensing and rationalising the data in Table 3.3 and Appendix 2, and for demonstrating the correlation between the main oxides and trace elements and SiO_2 proportion in the rocks, variation diagrams (after Harker, 1909) were constructed for Etive igneous rocks (Fig. 3.4).

In general, considering the TiO_2, P_2O_5, Fe_2O_3, K_2O, CaO, Sr, Rb and Ni versus SiO_2 variation diagrams in Fig.3.4, it can be seen that in all diagrams the variation of oxides or elements are close to linear trends but some show curvature and scattered behaviour. The relationship between weights percent Na_2O and amount of Zr and that of silica in the rocks are not clear, but K_2O and Rb increase as SiO_2 increases while TiO_2 decreases as the silica amount increases (Fig. 3.4). TiO_2 mainly accumulates in titano-magnetite and ilmenite (see section on mineral chemistry in this chapter). These minerals' concentration in the rocks decreases with increasing differentiation and silica enrichment. P_2O_5, FeO, MgO, CaO, Sr and Ni all show the same behaviour.

It is difficult to dismiss the possibility of contamination, assimilation or mixing phenomena using variation diagrams alone, but the normal and undistorted linear trends on the diagrams with the presence of normal zoning in most of the minerals, (mainly zoned plagioclases, see section on mineral chemistry in this chapter) indicate that fractional crystallisation was the most important process in the

Table.3. 3 Representative analyses of the igneous rocks from the Etive Complex. Samples MM17 and D659 are from Quarry Diorite, Samples MM3A, MM31D and MM5H are from Cruachan Intrusion and Sample MM5G is from Meall Odhar Granite.

Sample	MM17,	D659	MM3A	MM31D	MM5H	MM5G
			Major Oxides, wt%			
SiO2	61.90	59.95	57.14	55.31	63.35	76.58
Al2O3	16.25	18.28	18.15	17.07	17.90	12.68
Fe2O3	1.05	1.62	1.60	1.30	0.75	0.10
FeO	3.37	2.76	3.92	3.53	1.64	0.34
MgO	3.85	2.76	3.72	5.95	1.53	0.24
CaO	4.66	5.73	5.60	8.83	3.55	0.25
Na2O	4.54	4.67	4.55	3.59	4.93	3.59
K2O	2.79	2.81	2.65	2.03	3.60	5.33
TiO2	0.68	0.91	1.19	1.07	0.76	0.13
P2O5	0.30	0.42	0.54	0.56	0.25	BD
Total	99.39	99.91	99.06	99.24	98.26	99.24
			CIPW Norm			
Q	9.18	6.84	3.29	2.09	11.13	34.40
C	-	-	-	-	-	0.55
Or	16.49	16.61	15.66	12.00	21.28	31.50
Ab	38.42	39.52	38.50	30.38	41.72	30.38
An	15.72	20.62	21.28	24.47	16.08	1.24
Di	4.54	4.28	2.69	12.78	0.05	-
Hy	11.55	7.06	11.88	12.39	4.93	0.60
Hm	-	-	-	-	-	0.10
Mt	1.52	2.35	2.32	1.88	1.09	-
Ap	0.71	0.99	1.28	1.33	0.59	0.00
Ru	-	-	-	-	-	0.13
Il	1.29	1.73	2.26	2.03	1.44	-
Total	99.42	99.99	99.16	99.34	98.31	98.90
			Trace Elements, ppm			
Nb	15	13	16	10	8	BD
Zr	269	384	459	217	522	124
Y	39	39	31	27	31	33
Sr	1275	1614	1105	1401	1094	77
Rb	70	86	62	38	75	116
Zn	61	61	68	47	44	12
Cu	16	4	6	BD	BD	BD
Ni	12	11	BD	26	BD	BD
Cr	74	46	12	103	BD	BD
Ce	80	102	130	69	139	52
Nd	34	34	35	21	59	12
V	104	110	144	165	74	23
La	42	42	49	25	67	47
Ba	1363	1650	2003	1222	4005	159
Sc	12	14	17	18	5	6

evolution of the igneous rocks of the Etive Complex.

3.4.2 Rock Classification: The Etive igneous rocks are classified using chemical criteria. Because the normative mineralogies of the rocks are slightly different from

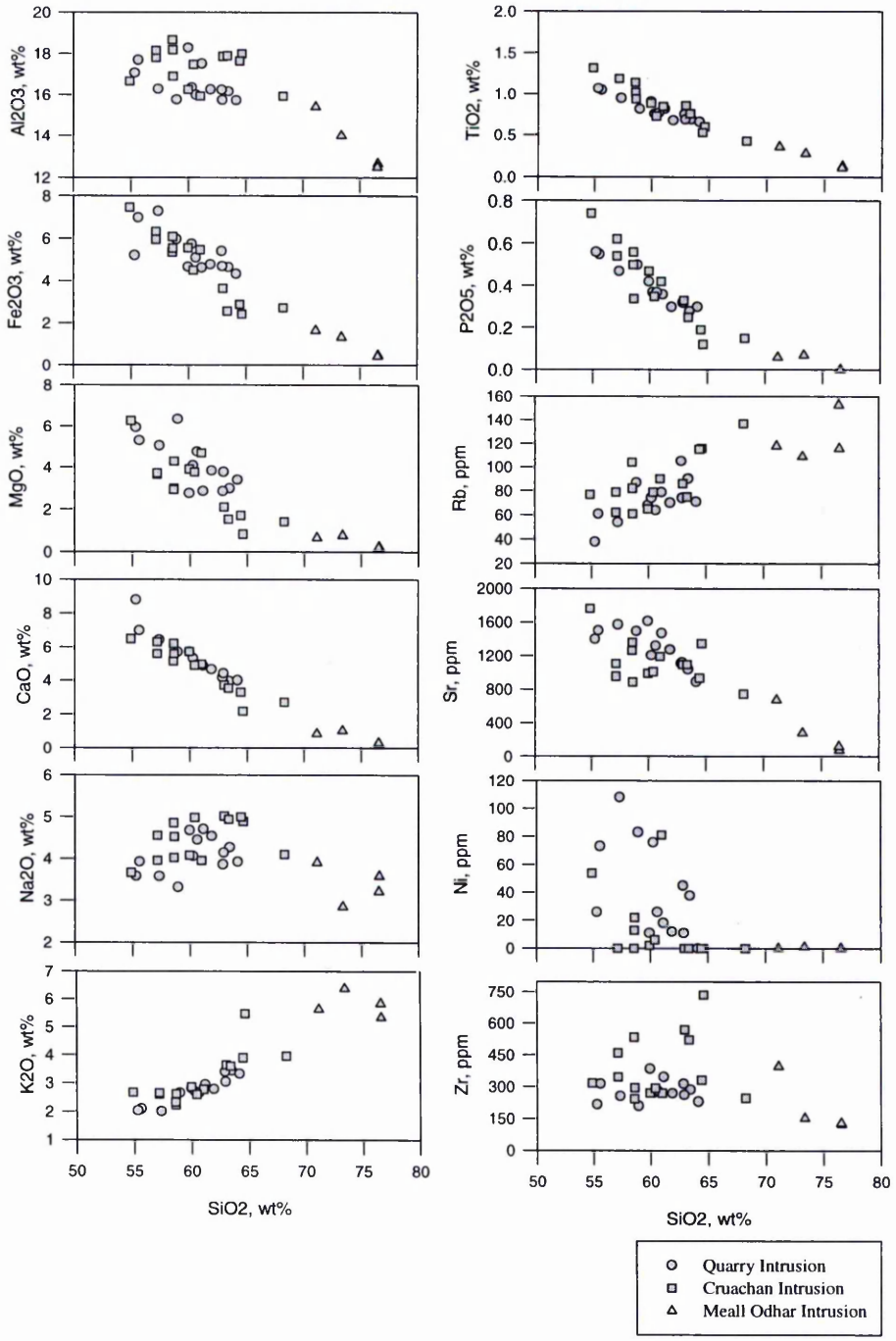

Fig. 3.4 Variation diagrams for the Etive igneous rocks. Fe, Ca and Ti oxides show linear trends. Trends of Mg, K, P and Sr oxides are close to linear.

the modal mineralogies, the nomenclatures of the rocks using different methods are different. In this study the Q-Kfs-Pl diagram of Streckeisen (1976) is used as the main criterion for rock classification (Fig. 3.5). In Figure 3.5, samples from the Quarry intrusion plot in the monzodiorite and quartz monzodiorite fields. Samples from the Cruachan intrusion mainly plot in the quartz monzodiorite field and all of the samples from the Meall Odhar intrusion plot in the granite field.

In the alkali versus SiO_2 diagram after La Maitre *et al.* (1989) (Fig. 3.6) all of the samples from the Quarry intrusion plot in the syeno-diorite field (corresponding to the monzodiorite field of the Streckeisen diagram in Fig. 3.5) and most of the samples from the Cruachan intrusion also plot in this field. All of the samples from the Meall Odhar intrusion plot in the alkali granite field. According to this diagram all of the rocks are alkaline (Fig.3.6). The normative An-Ab-Or triangular diagram (Barker, 1979; originally from O'Conner, 1965) is applicable to rocks with more than 10% normative quartz; it is based entirely upon the normative feldspar composition recast to 100% and represents a projection from quartz onto the feldspar face of the "granite" tetrahedron, Q-Ab-An-Or. This diagram was used for samples of Etive igneous rocks with more than 10% normative quartz (Fig.3.7). In this figure all of the samples from the Cruachan and Quarry intrusions plot in the granodiorite field and all of the samples from the Meall Odhar intrusion plot in the granite field.

3.4.3 Magmatic Characteristics: Based on the geochemistry of the major elements, granitoid magmas can be classified using three main criteria: alumina saturation, alkali ratio and K_2O:SiO_2 ratio.

Alumina saturation: This classification is based on the molar Al_2O_3 (A) against the molar amounts of $CaO+Na_2O+K_2O$ (CNK) (Shand, 1974). On this basis, four main types of granitoid magmas may be distinguished:

a) Haplogranitic magma which generates granites with only quartz plus feldspars. In this type of magma the molar ratio of the $Al_2O_3/(CaO+Na_2O+K_2O)$ is 1 (because in all varieties of feldspar, A/CNK=1). b) Peraluminous granitoid magmas with A/CNK >1. The existence of aluminous minerals such as aluminosilicates, cordierite, garnet and topaz are common mineralogical features for rocks from this type of magma. c) Metaluminous magmas with A/CNK <1. The most common minerals in the rocks of this type of magma are orthopyroxene, clinopyroxene, hornblende, biotite and magnetite. d) Peralkaline magmas with A < NK. In this type, the presence of sodic

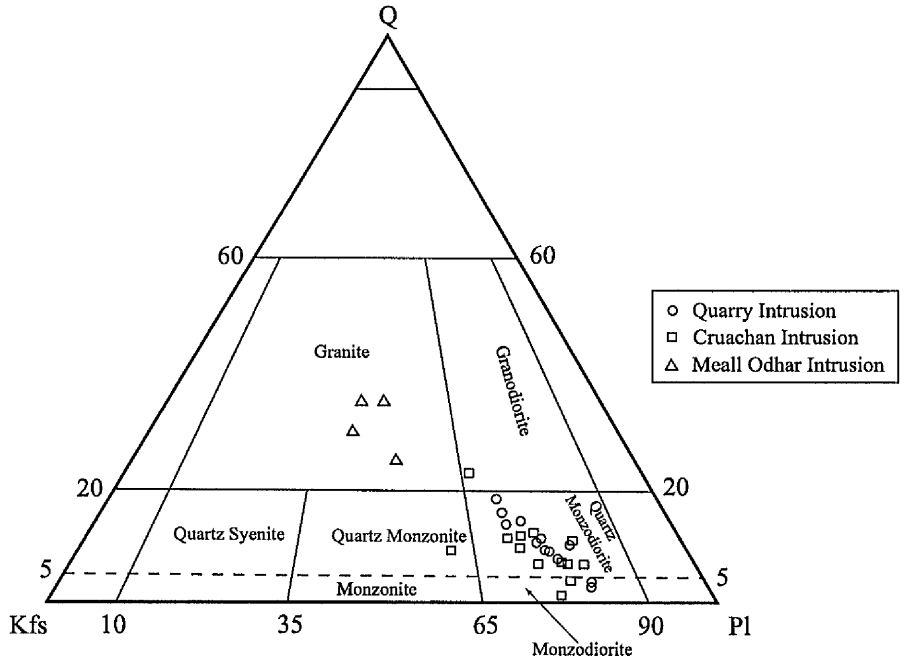

Fig. 3.5 Classification of the Etive igneous rocks using quartz-alkali feldspar-plagioclase diagram (after Streckeisen, 1976). Most of the samples from the Quarry and Cruachan Intrusions plot in the quartz-monzodiorite field and all of the samples from the Meall Odhar Intrusion plot in the granite field.

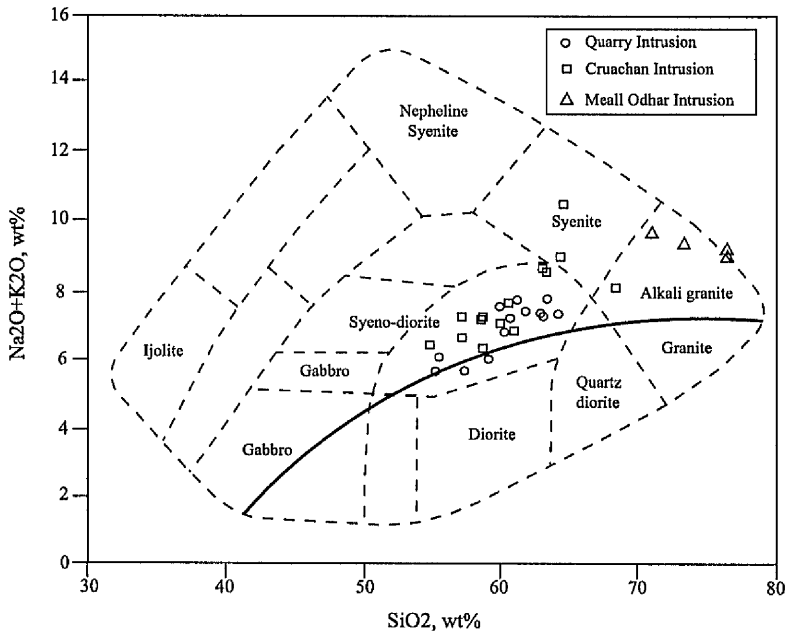

Fig. 3.6 Rock classification using the $(K_2O+Na_2O)/SiO_2$ diagram of Le Maitre, *et al.* (1989). The solid line separates the subalkaline rocks from alkaline rocks. Almost all of the Etive samples plot in the alkaline field.

ferromagnesian minerals, low modal biotite, and low amounts of CaO, Al_2O_3 are significant features.

Petrographical and geochemical studies of the Etive igneous rocks indicate that magmas were of a metaluminous nature. In the A/CNK versus SiO_2 diagram (Fig.3.8) most of the Etive samples plot in the metaluminous field. Two samples from the Cruachan intrusion are on the boundary and all of the samples from the Meall Odhar intrusion, having normative corundum, show a slightly peraluminous nature. In this diagram all of the samples plot in the I-type granitoid field. I-type granitoids have a magmatic source from mafic or intermediate igneous composition of ultimately upper mantle derivation, while S-type granitoids have a sedimentary or supracrustal source.

Alkali ratio: The K_2O versus Na_2O diagram is used for distinguishing I-type and S-type magmas. All of the Etive samples plot in the I-type field on this diagram (Fig.3.9).

K_2O versus SiO_2 diagram: This diagram also indicates the nature of the magmas. In this diagram almost all of the samples from the Etive Complex plot in the high-K calc-alkaline field (Fig. 3.10), indicating a probable nature between within-plate magmas and subduction related magmas.

3.4.4 Minor and trace elements: Minor and trace element concentrations in representative rocks from the Etive Complex are plotted on 'spider diagrams' (Figures. 3.11 and 3.12) allowing comparison of the abundance of trace elements in the main intrusions to those in the upper continental crust, lower continental crust, average continental crust and the primordial mantle. The first graph in figure 3.11 illustrates the 'spider diagram' for monzodiorite sample MM5D from the Cruachan intrusion (NN03073402). The trace element distribution in this rock generally shows the same pattern as the crust with slightly higher concentration of all of the elements except for a slight depletion in Nb. In the second graph, granodiorite sample MM3A (NN03503419) from the Cruachan intrusion shows the same pattern. The concentration of trace elements in this rock is higher than in average upper continental crust. The third graph in Fig. 3. 11 shows the relationships for diorite sample MM17 from the Quarry intrusion (NN08192809). It is apparent that the diorite is very close to the average crust in trace element composition. In comparison with the upper crust, the diorite variety of the Quarry intrusion is slightly

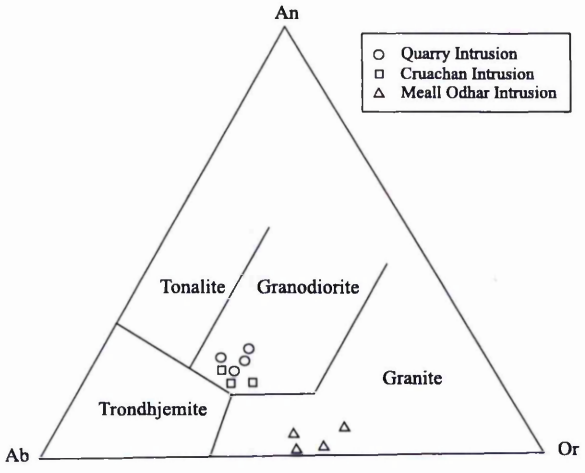

Fig. 3.7 Etive igneous rocks with more than 10% normative quartz in An-Ab-Or diagram (Barker, 1979). Samples plot in the granite and granodiorite fields.

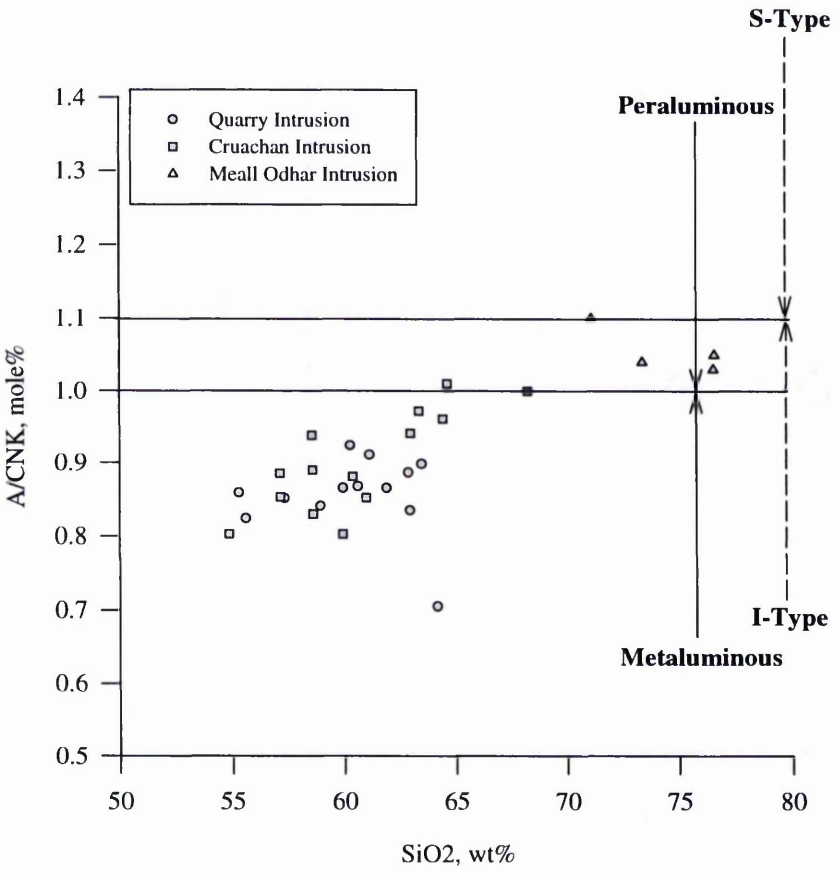

Fig. 3.8 Molar Al2O3/(CaO+Na2O+K2O) versus SiO2 showing metaluminuous and I-type characteristics of the Etive Complex. Peraluminuous and metaluminuous fields are after Shand, 1974 and I-type and S-type fields are after Chappel and White, 1974.

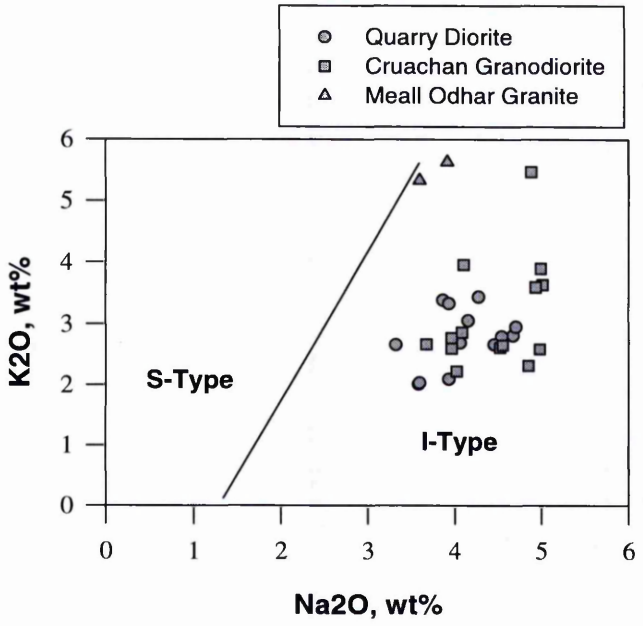

Fig. 3.9 N_2O versus K_2O diagram for Etive igneous rocks. All of the samples plot in the I-type field. Line dividing S-and I-type rocks based on the criteria of Chappell and White, 1974.

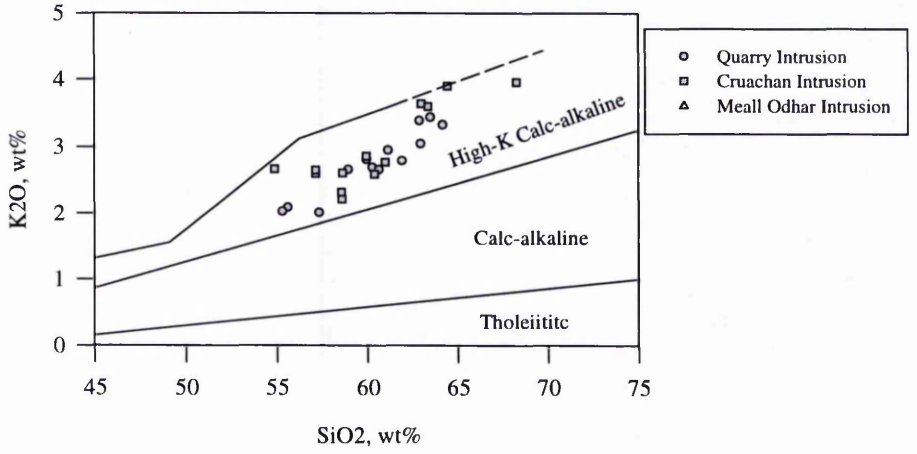

Fig. 3.10 All of the samples from the Etive Complex plot in the high-K calc-alkaline field of the K_2O/SiO_2 diagram. Field boundaries are from Ewart (1982).

depleted in Rb and Nb and in comparison with the lower crust it is slightly enriched in these elements. It is also enriched in Sr relative to all crust types shown. This enrichment in Sr possibly reflects the crystallisation of Sr-rich plagioclase during magmatic fractional crystallisation. Differences between the amounts of Rb and Nb in the Quarry diorite and lower crust can be attributed to the more mafic nature of the lower crust and the more felsic nature of the diorite.

The last graph in this figure illustrates the pattern of trace elements for Meall Odhar Granite sample MM5G (NN03073402); this is considerably different from the other patterns. Generally in the Meall Odhar Granite, La and Rb are enriched, while Sr, Ba, Sc and V are depleted. This pattern for Meall Odhar Granite reflects its high degree of differentiation. In the Meall Odhar Granite, the amount of Rb is as high as in the Upper Crust reflecting the incompatible behaviour of Rb during the main stage of magmatic fractional crystallisation. V, which mainly is a basaltophile element, is highly depleted in the Meall Odhar Granite.

In Fig. 3.12, spider patterns for the representative samples of the three outer intrusions of the Etive Complex are compared. The Meall Odhar Granite shows a different pattern due to its evolved nature. The spider diagrams for the Etive Igneous rocks show enrichment of trace elements in comparison with the average crust implying a partly continental origin for the magmas rather than a pure ultimate mantle source. This pattern corroborates Frost and O'Nions'(1985) model for the origin of Caledonian granite magmas by recycling of materials from the lower continental crust (Chapter 2, section 2.8.1).

Conventional wisdom suggests that high K/Rb ratios in the igneous rocks are typical of magmatic processes and that lower values can only be reached by fluid interaction (Clarke, 1992). The igneous rocks of the Etive Complex show relatively high K/Rb ratios (higher than 200) (Fig. 3.13), suggesting that magmatic processes were probably more important than hydrothermal processes in the Etive Complex.

3.4.5 Tectonomagmatic features: The idea of trying to relate the chemical features of magmas to different tectonic environments is attributed to Pearce and Cann (1971, 1973). These authors suggested that it is possible to use geochemistry to distinguish the basalts produced in different, known tectonic settings. Subsequently similar suggestions were made for granitoids. Plots of the Etive igneous rocks on the Nb/Y discriminant diagram (Pearce *et.al.* 1984) shows that the Etive complex has a

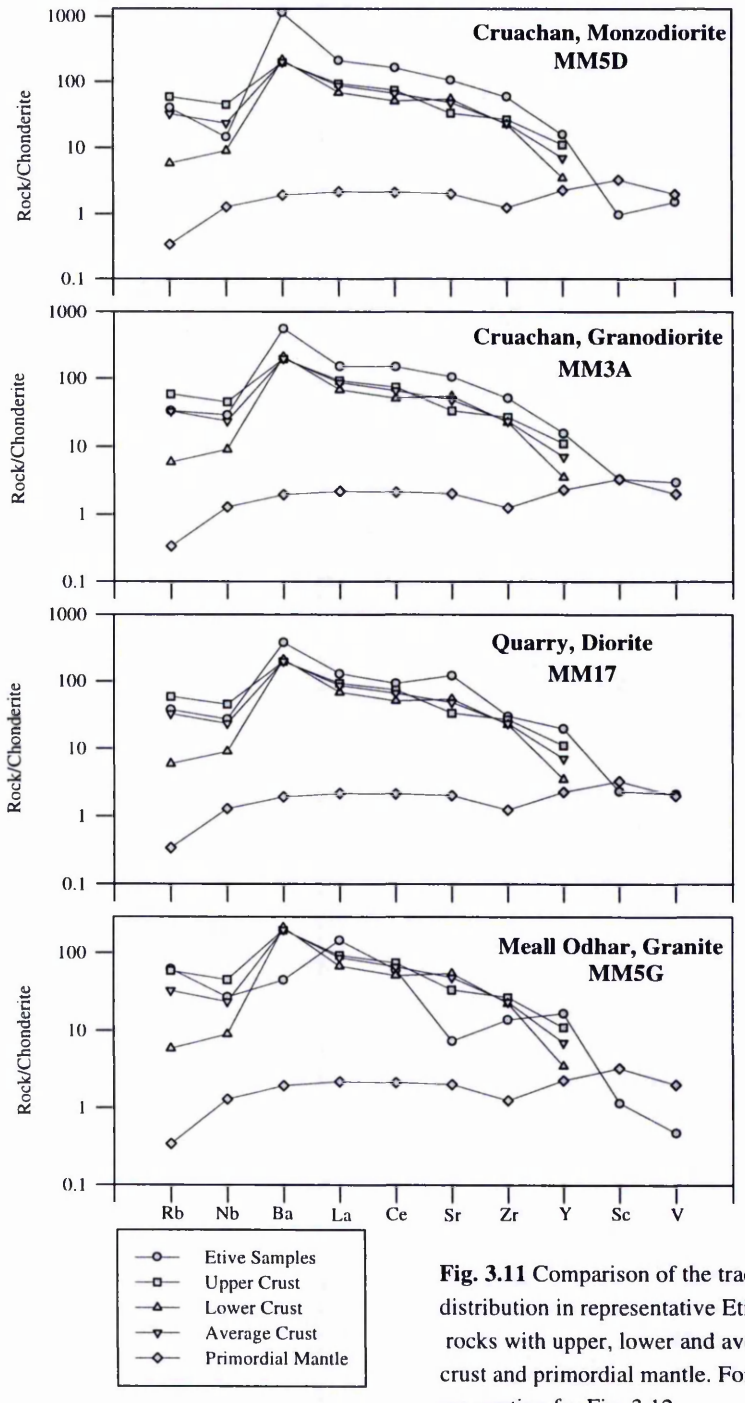

Fig. 3.11 Comparison of the trace element distribution in representative Etive igneous rocks with upper, lower and average continental crust and primordial mantle. For source of data see caption for Fig. 3.12.

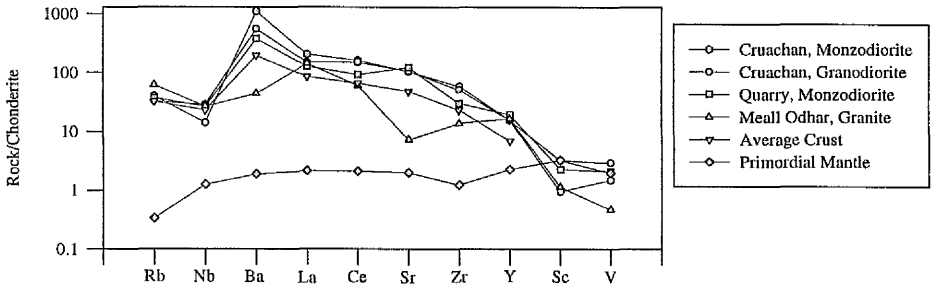

Fig. 3.12 Comparison of the trace element distributions in the different intrusions of the Etive Complex. The behavior of the Meall Odhar Granite is remarkably different from the other intrusions. Data for Chondrite from Wood *et al.*, 1979b, for upper crust from Taylor and McLennan, 1985, for lower crust and average of crust from Weaver and Tarney, 1984 and for primordial mantle from McDonough *et al.*, 1991.

transitional nature between within-plate granites and volcanic-arc and syn-collision granites (Fig. 3.14). The Rb/(Nb+Y) ratio appears to refute the syn-collision nature for Etive Complex and instead shows a within-plate or volcanic-arc nature (Fig. 3.15). In the Y/SiO_2 diagram the tectonic setting of the Etive complex is not clear (Fig. 3.16) but the Rb/SiO_2 diagram in Fig. 3.17 appears to confirm a within-plate tectonic setting for the Etive Complex.

3.5 Mineral Chemistry

Six fresh and optically well-defined representative samples from the igneous rocks were chosen for mineral chemistry studies. Minerals were analysed on polished, carbon coated slides using an energy dispersive (ED) microprobe. For sample preparation, machine set ups, analysing conditions and standards see Appendix 3. The results from mineral chemistry studies will be used for classification of major minerals, study of zoning in minerals and thermobarometry of the igneous rocks.

3.5.1 Feldspar: Feldspars from the igneous rocks of the Etive complex were analysed in six representative samples from the main intrusions. Three samples, MM5H, MM5K and MM5E were chosen from the Cruachan intrusion to represent

granodiorite, monzodiorite and pyroxene-bearing rocks respectively. Samples MM17

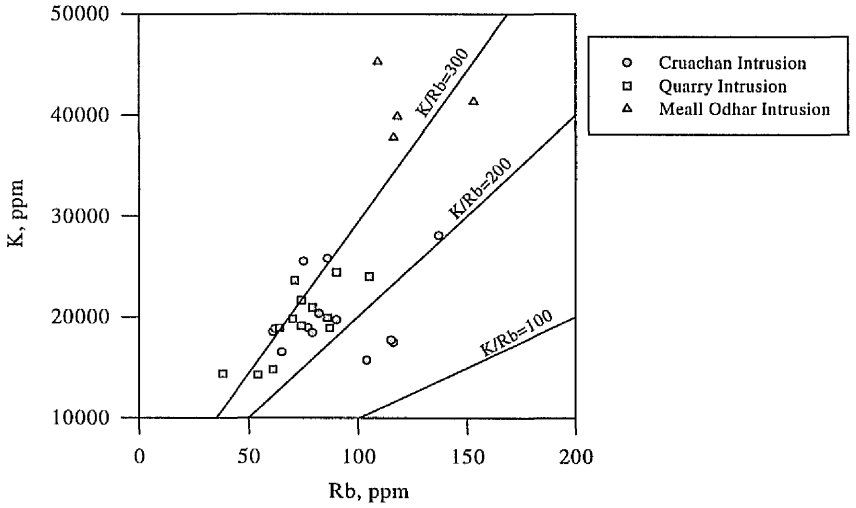

Fig. 3.13 K/Rb diagram (after Clarke, 1992) of the Etive samples. The Etive igneous rocks all have relatively high K/Rb ratios.

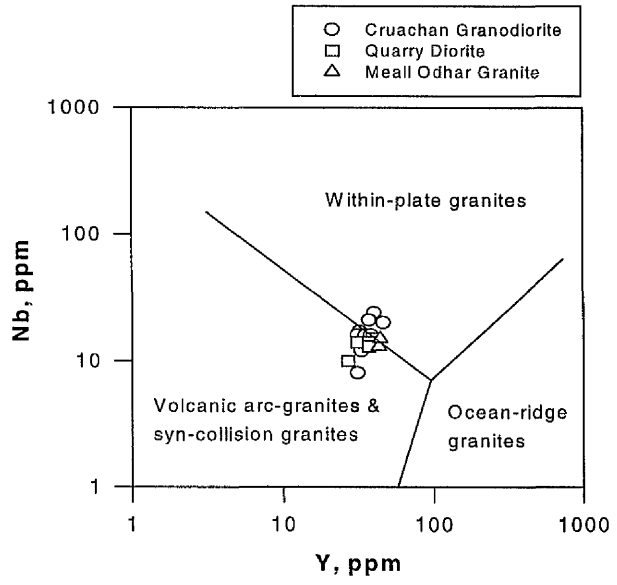

Fig. 3.14 Nb/Y diagram for tectonic setting of the granitoid rocks (after Pearce *et al.*, 1984) Etive Complex rocks plot on volcanic are granites + syn-collision granites and within-plate granites.

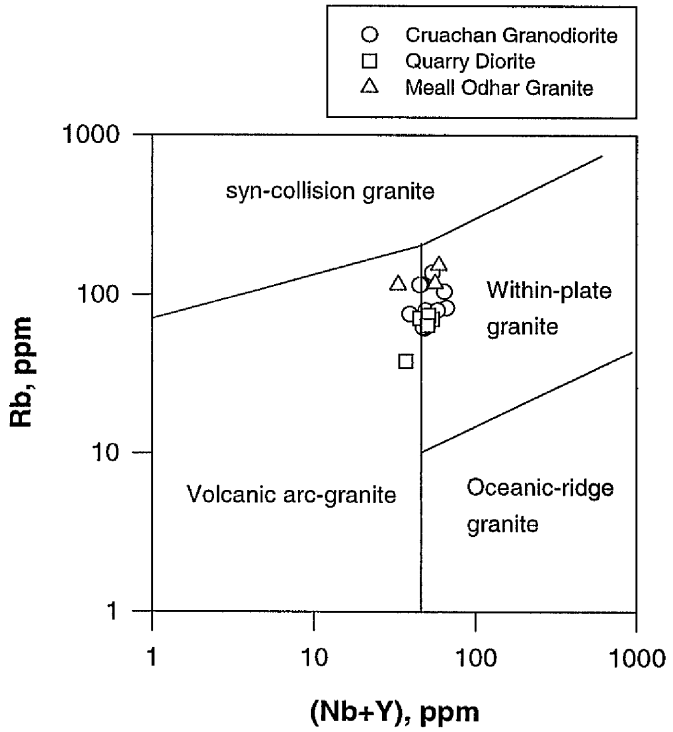

Fig. 3.15 Rb/(Nb+Y) diagram after Pearce *et al.*, 1984. Etive Complex rocks fit on the within-plate and volcanic are granites boundary.

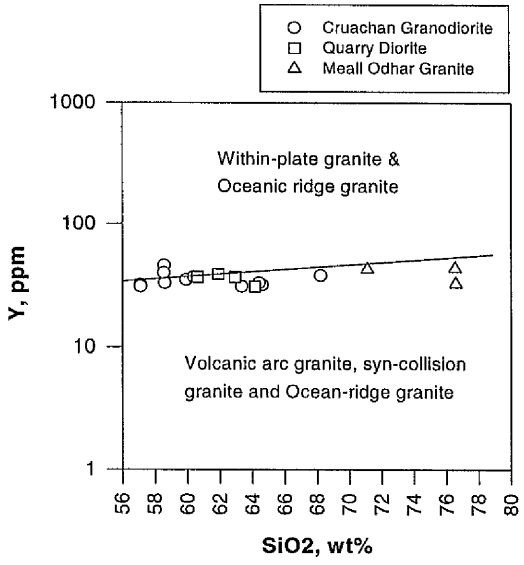

Fig. 3.16 Y/SiO2 diagram (after Pearce et al., 1984) for rocks of the Etive Complex. The tectonic environment of the Etive rocks is not clearly distinguishable.

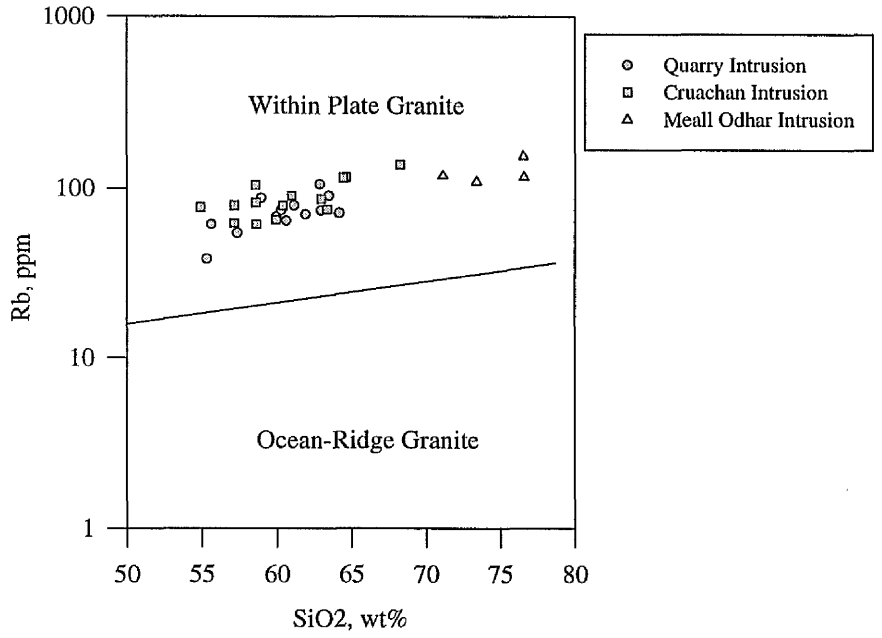

Fig. 3.17 Rb/SiO_2 diagram (after Pearce et al., 1984) showing that the Etive complex has within-plate affinities.

and Δ659 were chosen from the Quarry intrusion to represent two-pyroxene diorite and quartz diorite respectively, and sample MM5G, which is a leucogranite was chosen from the Meall Odhar intrusion. In all of these samples feldspar is clear and fresh with minimum alteration effects. In each sample 8-15 spots were analysed using ED microprobe. Where alkali feldspars are perthitic broad beam (~ 10 μm) analysis was performed to ensure the resultant analyses integrate the composition of the host and the lamellae. One optically defined crystal of plagioclase in each sample was examined for compositional zoning and construction of the zoning profile. Table 3.4 includes the representative analyses of feldspars in the Etive igneous rocks. The complete table of feldspar analyses is presented in Appendix 2. In Fig. 3.18 feldspars from the Etive igneous rocks are plotted on the An-Ab-Or triangular diagram. All samples plot within the proposed limit of feldspar solid solution (Parsons and Brown, 1983). According to this figure almost all of the plagioclases are poor in the Or end-member and all of the alkali feldspars are poor in the An end-member apart

Table 3.4 Representative analyses of feldspars in the igneous rocks from the Etive Complex.

Sample	MM17,Pl	MM17,Kfs	MM5E,Pl	MM5E,Kfs	MM5G,Pl	MM5G,Kfs
			Major Oxides, wt%			
SiO2	62.14	64.49	62.56	65.47	65.66	64.88
Al2O3	23.37	18.67	22.97	18.66	21.42	18.65
FeO*	0.41	0.00	0.39	0.10	0.27	0.17
MnO	0.00	0.00	0.00	0.00	0.00	0.05
MgO	0.02	0.13	0.00	0.11	0.01	0.05
CaO	5.09	0.21	4.55	0.09	2.42	0.35
TiO2	0.12	0.17	0.03	0.07	0.00	0.14
Na2O	8.64	1.17	8.87	1.11	10.16	1.40
K2O	0.26	14.68	0.24	15.18	0.20	14.44
Total	100.41	99.52	99.61	100.79	100.14	100.13
			Number of ions on the basis of 8 Oxygens			
Si	2.75	2.98	2.79	2.99	2.88	2.98
Al	1.24	1.02	1.21	1.00	1.11	1.01
Fe*	0.01	0.00	0.01	0.01	0.01	0.00
Mn	0.00	0.00	0.00	0.00	0.00	0.00
Mg	0.00	0.01	0.00	0.00	0.00	0.00
Ca	0.24	0.01	0.22	0.01	0.11	0.02
Ti	0.00	0.00	0.00	0.00	0.00	0.00
Na	0.74	0.10	0.77	0.09	0.87	0.13
K	0.01	0.86	0.01	0.89	0.01	0.85
Total	4.99	4.98	5.00	4.99	4.99	4.99

from some alkali feldspars from the Quarry intrusion and some outer parts of plagioclases from the Cruachan intrusion (granodiorite). X_{or}^{pl} (mole fraction of orthoclase in plagioclase) in the inner cores of plagioclases is from 0.004 to 0.015 and in the outer rim of the plagioclases is from 0.006 to 0.033. X_{an}^{kfs} is from 0.005 to 0.027. In other words nearly all of the feldspars are practically binary solid solutions rather than ternary. This aspect of the mineralogical composition of the Etive igneous feldspars is important from the feldspar thermometry point of view, which will be discussed later in this chapter. The microprobe work confirms the conclusions of the petrography, viz. that all of the plagioclase crystals in the Etive igneous rocks are zoned from An-rich cores to Ab-rich rims. Fig. 3.19 illustrates the zoning profile across plagioclases from different rocks. All analysed plagioclases show normal zoning.

3.5.2 Biotite: Biotites were analysed in samples from the Cruachan and Quarry intrusions. Table 3.5 includes representative analyses of biotites and Appendix 4 lists all analyses of igneous biotites from the Etive rocks.

The biotites are manganese-free and rarely contain chromium. The amount of titanium is about 0.48 atoms per formula unit on the basis of 22 oxygens (Figure

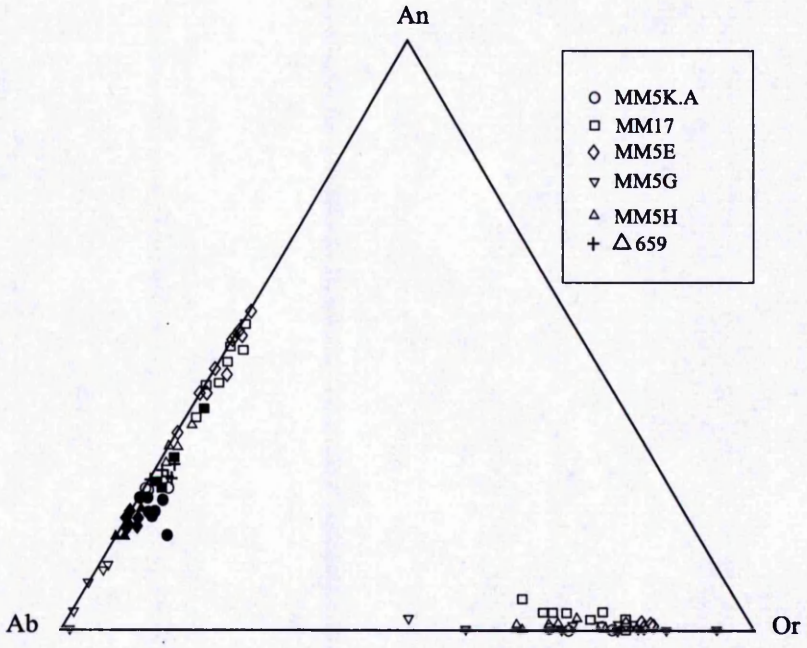

Fig. 3.18 Composition of the Etive igneous feldspars (mole%) in the An-Ab-Or diagram. The solid symbols indicate the outer rim of plagioclases and the open symbols (for plagioclases) indicate the inner core of the plagioclases.

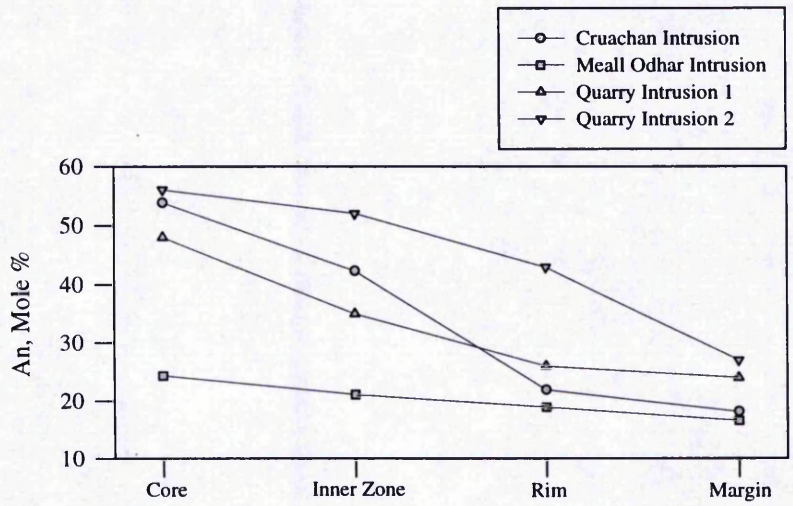

Fig. 3.19 Zoning in plagioclase crystals from different intrusions of the Etive Complex. All of the crystals show normal zoning (An-rich cores and Ab-rich rims).

3.20). The composition of biotites is plotted in the SAF diagram after Lambert (1959) in Fig. 3.21 the composition of biotites in this diagram lie close to the phlogopite-annite series. The fact that the biotites plot a small distance above the

Table 3.5 Representative analyses of biotites in the igneous rocks from the Etive Complex.

Sample	MM17	Δ659	MM5H	MM5K.B	MM5K.A	MM5E
			Major Oxides, wt%			
SiO2	37.45	36.84	37.31	37.31	37.52	36.59
Al2O3	13.00	13.41	13.67	13.42	13.45	13.08
FeO*	18.55	17.53	17.08	17.09	17.08	17.18
MnO	0.00	0.00	0.18	0.00	0.00	0.00
MgO	12.74	12.71	13.43	13.11	13.65	13.14
CaO	0.04	0.12	0.07	0.11	0.09	0.11
TiO2	3.72	4.49	4.28	4.47	4.41	4.61
Na2O	0.48	0.52	0.59	0.48	0.43	0.35
K2O	9.10	9.48	9.26	9.43	9.38	9.17
Cr2O3	0.00	0.09	0.00	0.02	0.03	0.00
Total	95.08	95.19	95.87	95.44	96.04	94.23
			Number of ions on the basis of 22 Oxygens			
Si	5.72	5.59	5.62	5.65	5.63	5.16
Al	2.34	2.40	2.43	2.40	2.38	2.36
Fe	2.37	2.22	2.15	2.16	2.14	2.20
Mn	0.00	0.00	0.02	0.00	0.00	0.00
Mg	2.90	2.88	3.01	2.96	3.05	3.00
Ca	0.00	0.02	0.01	0.02	0.01	0.02
Ti	0.43	0.51	0.48	0.51	0.49	0.53
Na	0.14	0.15	0.17	0.14	0.12	0.10
K	1.77	1.84	1.78	1.82	1.80	1.79
Cr	0.00	0.01	0.00	0.00	0.00	0.00
Total	15.67	15.62	15.67	15.66	15.62	15.16

phlogopite+annite-siderophyllite+eastonite line (on the muscovite side of the line) possibly suggests a small di-octahedral (muscovite+celadonite) component. No Fe^{3+} estimate has been made for the biotites; however Fe^{3+} cannot be responsible for the observed deviation from the ideal phlogopite+annite-siderophyllite+eastonite tie line, because considering some of the Fe as Fe^{3+} (which substitutes for Al^{3+}) would cause a shifting of analyses points to the left on the SAF diagram. Omission of Ti from the diagram could not be the reason either; the addition of the Ti^{4+} to Si^{4+}, for which it effectively substitutes via the coupled substitution $Si^{iv}+Al^{vi} \Leftrightarrow Al^{iv}+Ti^{vi}$, would cause the points to move further towards the S-apex away from the AF line in the diagram. In sample MM17 with the Opx-Bt assemblage, analyses of biotite were only carried out on biotites that were not in contact with orthopyroxenes (see thermobarometry section in this chapter).

3.5.3 Amphibole: Representative analyses of amphiboles from igneous rocks of the Etive complex are given in Table 3.6 and full analyses are provided in Appendix 4.

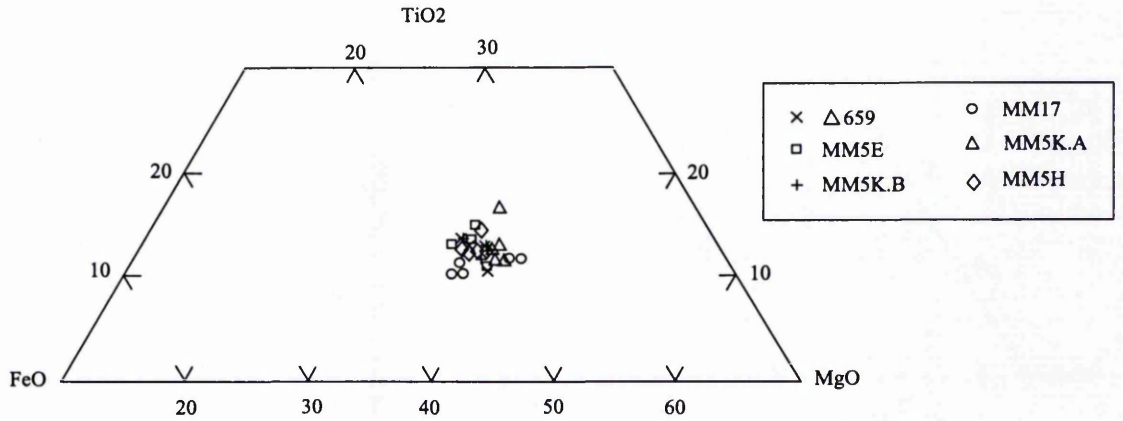

Fig. 3.20 TiO2-FeO-MgO triangular diagram for biotites from the Etive igneous rocks. All of the samples have about 4% TiO2 (~ 15% out of TiO2+FeO+MgO).

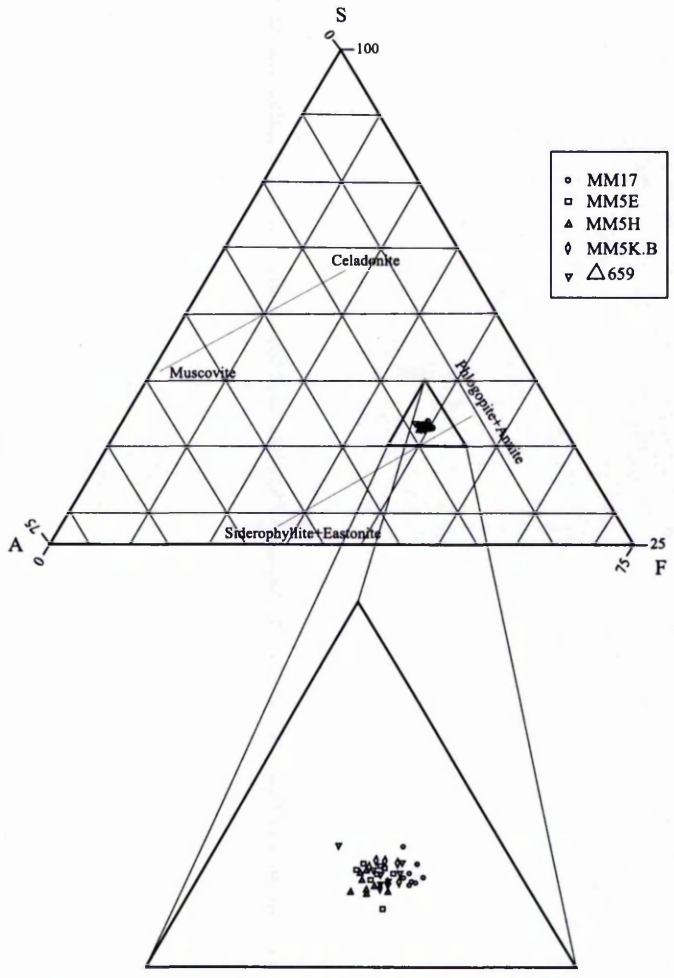

Fig. 3.21 Classification of the Etive igneous biotites in SAF diagram (after Lambert, 1959). S=(100×Si)/(Si+Al+Fe+Mn+Mg), A=(100×Al)/(Si+Al+Fe+Mn+Mg) and F=[100×(Fe+Mg+Mn)]/(Si+Al+Fe+Mn+Mg). The biotites plot close to the phlogopite-annite end of phlogopite+annite and siderophyllite+eastonite line towards the S apex indicating a small amount of dioctahedral component in the biotites.

Table 3.6 Representative analyses of amphibole in the igneous rocks of the Etive Complex.

Sample	MM17	Δ659	MM5E	MM5H	MM5K
			Major Oxides		
SiO2	49.94	48.29	49.82	50.18	49.97
TiO2	0.56	1.19	1.18	1.15	1.11
Al2O3	4.98	5.56	5.43	4.79	4.80
Cr2O3	0.02	0.06	0.04	0.12	0.01
Fe2O3	0.00	0.00	0.00	4.21	0.00
FeO	14.16	14.12	13.09	8.44	12.54
MnO	0.05	0.17	0.18	0.27	0.27
MgO	14.77	13.90	14.96	15.50	14.95
CaO	11.26	11.81	11.78	11.69	11.85
ZnO	0.00	0.07	0.00	0.00	0.00
Na2O	1.25	1.38	1.50	1.30	1.18
K2O	0.41	0.53	0.36	0.34	0.41
Total	97.40	97.17	98.34	98.00	97.09
			Number of ions on the basis of 23 Oxygen and 15 cations		
Si	7.33	7.15	7.24	7.22	7.34
Ti	0.06	0.13	0.13	0.12	0.12
Al	0.86	0.97	0.93	0.81	0.83
Cr	0.00	0.00	0.00	0.01	0.00
Fe^{3+}	0.00	0.00	0.00	0.46	0.00
Fe^{2+}	1.74	1.75	1.59	1.02	1.54
Mn	0.00	0.02	0.02	0.03	0.03
Mg	3.23	3.07	3.24	3.32	3.27
Ca	1.77	1.87	1.83	1.80	1.86
Zn	0.00	0.00	0.00	0.00	0.00
Na	0.37	0.40	0.42	0.36	0.34
K	0.08	0.10	0.07	0.06	0.08
Total	15.44	15.46	15.47	15.21	15.41

A few amphibole crystals in each rock were examined for any possible compositional zoning, but they appear to be homogeneous. All of the amphiboles have a Ca+Na content greater than 1.34, indicating that they are calcic amphiboles according to the classification of Leake (1978). For amphiboles, the Fe^{3+} and Fe^{2+} content were calculated (Droop, 1987). The amphibole analyses have oxide totals of between 96.62 and 99.07. No estimate of H_2O content has been made. Cation totals lie between 15.17 and 15.59 per formula unit per 23 oxygen. OH plus fluorine has been set at two. Fig. 3.22 illustrates the mineralogical composition of the Etive igneous amphiboles in the (Na+K) versus Si diagram (Leake, 1978). Most of the amphiboles plot in the hornblende field in this diagram. Some of the amphiboles from the Quarry intrusion (two-pyroxene diorite variety) plus a few samples from the

Cruachan intrusion plot in the edenite field. The vacancy on the A-site is between 0.30 and 0.62 atoms per formula unit for the Quarry intrusion and between

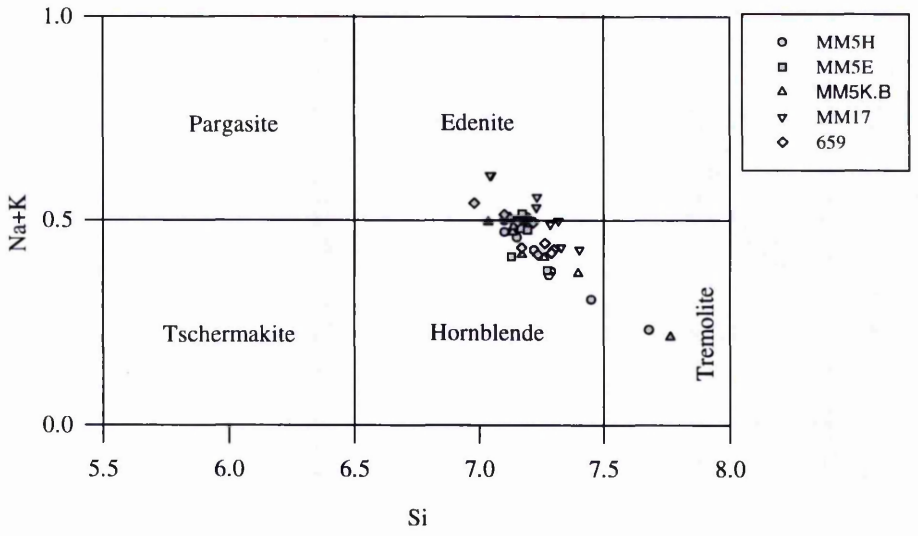

Fig. 3.22 Most of the amphiboles from the Etive igneous rocks plot in the hornblende field of the Leake (1978) diagram.

0.47 and 0.99 for the Cruachan intrusion; the potassium content varies from 0.08 to 0.16 atoms per formula unit for the Quarry intrusion and between zero and 0.09 atoms per formula unit for the Cruachan intrusion. The number of Mg atoms p.f.u. is between 2.62 and 3.53 for amphiboles from the Quarry intrusion and between 3.24 and 3.67 for the amphiboles from the Cruachan intrusion. This range shows that magnesium has a slight inverse proportion to iron (manganese is rarely detected). Calcium contents in amphiboles from the Quarry intrusion range from 0.76 to 0.89 atoms p.f.u. Aluminium accounts for 0.93 to 1.16 atoms per formula unit in the amphiboles from the Quarry intrusion, of which 0.19 to 0.27 is assigned to the T-site. The Fe^{3+} estimate yields no Fe^{3+} ions in the formula unit. Chromium is not common in these amphiboles; its concentration is up to 0.02 atoms p.f.u. Titanium is commonly present with a concentration up to 0.20 atoms p.f.u. Leake (1971) distinguished two main types of amphiboles, magmatic and post-magmatic, using the number of Ca+Na+K atoms versus the number of the Si atoms. By this criterion, all

of the analysed amphiboles from the Etive igneous rocks plot in the magmatic field (Fig. 3.23).

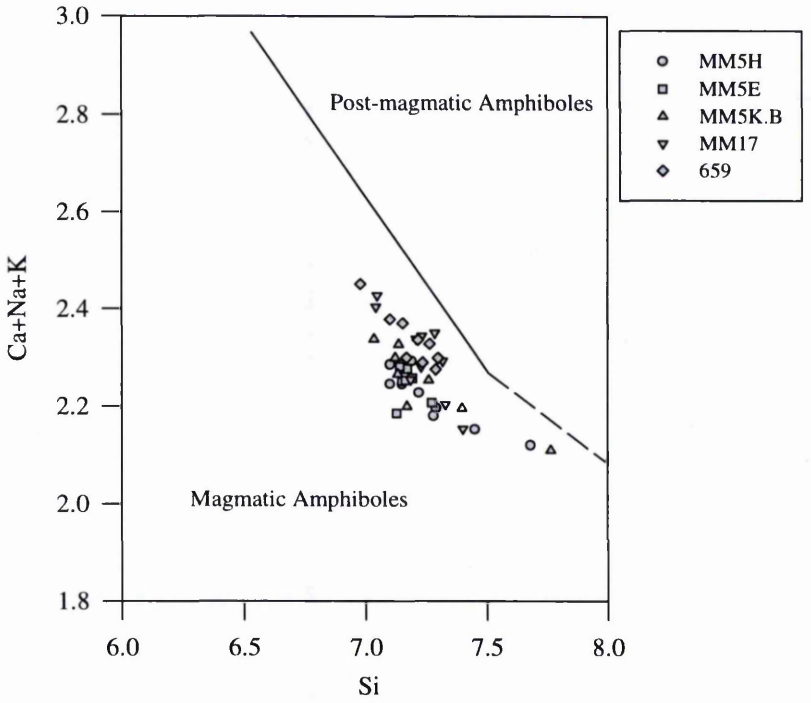

Fig. 3.23 Diagram of Ca+Na+K versus Si (after Leake, 1971) showing the compositional limit of magmatic and post-magmatic amphiboles in igneous rocks. All of the amphiboles from the Etive complex plot in the magmatic field.

3.5.4 Pyroxene: Pyroxenes were analysed in two samples from the Quarry intrusion representing two-pyroxene diorite and clinopyroxene-bearing monzodiorite. Pyroxenes appear to be homogeneous in these samples. Table 3.7 lists representative analyses of pyroxenes in these samples and Appendix 4 lists the full set of analyses. In clinopyroxenes, manganese and chromium are absent or occur in very low concentrations (less than 0.007 and 0.002 atoms p.f.u. respectively). Clinopyroxenes in the two-pyroxene-bearing diorite consist of ~41% wollastonite, ~45% enstatite and ~14% ferrosilite. Calcium varies from 0.79 to 0.82 atoms per formula unit occupying ~80 % of the M_2-site. In sample Δ659 wollastonite is ~56%, enstatite ~41% and ferrosilite ~13%. Fe^{3+} in clinopyroxenes is 0.06 to 0.09 and 0.02 to 0.09

Table 3.7 Representative microprobe analyses of pyroxenes in the Etive igneous rocks.

Sample	MM17, cpx	MM17, cpx	MM17, opx	Δ659, cpx	Δ659, cpx
			Major Oxides		
SiO2	52.86	52.77	52.97	53.75	53.98
TiO2	0.15	0.29	0.49	0.15	0.14
Al2O3	1.02	0.83	1.50	0.83	0.90
Cr2O3	0.29	0.07	0.04	0.30	0.04
Fe2O3	3.29	2.18	2.11	1.13	0.62
FeO	17.39	20.06	7.24	7.65	7.53
MnO	0.06	0.12	0.00	0.35	0.31
MgO	23.53	22.01	14.94	13.52	14.08
CaO	1.28	1.37	20.74	22.44	22.45
ZnO	0.00	0.12	0.00	0.13	0.00
Na2O	0.50	0.45	0.72	0.74	0.64
K2O	0.00	0.00	0.00	0.00	0.00
Total	100.37	100.27	100.75	100.72	100.69
		Number of ions on the basis of 6 Oxygen			
Si	1.94	1.96	1.95	1.99	1.99
Ti	0.01	0.01	0.01	0.00	0.01
Al	0.04	0.04	0.07	0.04	0.00
Cr	0.01	0.00	0.00	0.00	0.00
Fe^{3+}	0.09	0.06	0.06	0.03	0.02
Fe^{2+}	0.53	0.62	0.22	0.24	0.23
Mn	0.00	0.00	0.00	0.01	0.01
Mg	1.29	1.23	0.82	0.75	0.77
Ca	0.05	0.05	0.82	0.89	0.89
Zn	0.00	0.00	0.00	0.00	0.00
Na	0.04	0.03	0.05	0.05	0.05
K	0.00	0.00	0.00	0.00	0.00
Total	4.00	4.00	4.00	4.00	4.00

atoms p.f.u. in samples MM17 and Δ659 respectively. Orthopyroxenes from sample MM17 contain insignificant amount of Cr, Ti, Mn, and K. Na amounts are between 0.03 to 0.06 and Ca about 0.05 atoms p.f.u. The amount of Fe^{3+} is from 0.06 to 0.10 atoms p.f.u. Total Al in clinopyroxenes is from 0.06 to 0.08 and in orthopyroxenes is from 0.03 to 0.05 atoms p.f.u. Aluminium is mainly as Al^{iv}. In Fig. 3.24 end-member

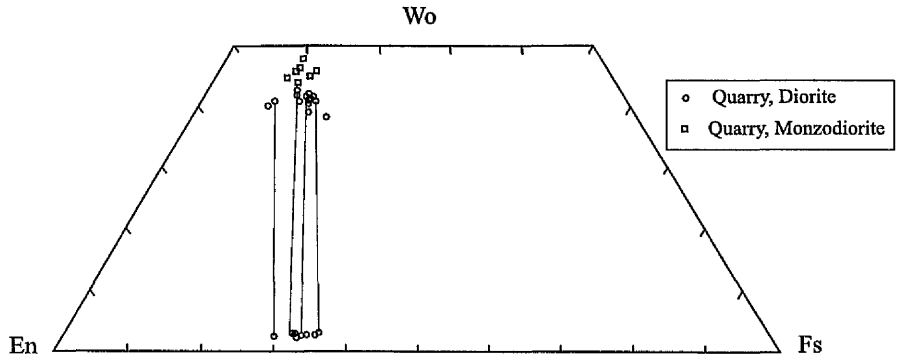

Fig. 3.24 Compositions of pyroxenes from Etive igneous rocks. Tie lines connect the crystals spatially close to each other.

Table 3.8 Representative microprobe analyses of Fe-Ti Oxide minerals in the Etive rocks.

Sample	MM5K.B	Δ659	MM5k.A	MM5E	MM17
SiO2	0.25	0.28	0.35	0.32	0.24
Al2O3	0.30	0.31	0.06	0.10	0.09
FeO*	90.10	90.44	39.15	49.96	48.45
MnO	0.00	0.00	8.95	2.37	1.05
MgO	0.04	0.09	0.04	0.11	0.14
CaO	0.04	0.10	0.02	0.03	0.08
TiO2	0.06	0.11	50.60	47.42	49.66
Cr2O3	0.40	0.15	0.10	0.03	0.07
Total	91.19	91.48	99.27	100.34	99.78
Si	0.02	0.02	0.02	0.01	0.01
Al	0.03	0.03	0.00	0.00	0.00
Fe*	5.91	5.98	1.62	2.17	2.07
Mn	0.00	0.00	0.39	0.10	0.04
Mg	0.01	0.01	0.00	0.00	0.01
Ca	0.01	0.01	0.00	0.00	0.00
Ti	0.01	0.00	1.94	1.85	1.91
Cr	0.01	0.01	0.00	0.00	0.00
Total	6.00	6.06	3.97	4.13	4.04

proportions of pyroxenes are illustrated in Wo-En-Fs triangular diagram. Clinopyroxenes are mainly augite in the two pyroxene bearing sample and in the clinopyroxene-bearing sample they are mainly salite according to the Poldervaart and Hess (1951) nomenclature.

3.5.5 Oxide Minerals: A few oxide minerals were analysed in each analysed sample. The main oxides are hematite (alteration product after original magnetite) and ilmenite. Table 3.8 includes the representative analyses of oxide minerals in the igneous rocks of the Etive Complex.

3.6 Thermobarometry

One of the main tasks of this chapter is to work out the temperature regime of the Etive igneous rocks to assess their role in the contact metamorphism of the surrounding metasediments. There are not many suitable assemblages in the Etive igneous rocks for thermobarometry. The methods applicable for barometry include the Al-in-amphibole barometry (Hammarstrom and Zen, 1986; Hollister *et al.*, 1987) and Na in the M_4 site versus Al^{iv} criteria (Brown, 1977). The most reliable results for pressure come from the metasediments in the Etive aureole (see chapter 9 on Thermobarometry). Droop and Treloar (1981) estimated a pressure of 1-2 kbars

using assemblages in metapelites and calcsilicates in the Etive thermal aureole, which will be considered a yardstick to evaluate the pressure estimations in the igneous rocks. For thermometry the main applicable methods are two- and ternary feldspar phase relations thermometry, orthopyroxene-clinopyroxene thermometry, orthopyroxene-biotite thermometry and amphibole-plagioclase thermometry. Each of these methods is employed and described in detail below.

3.6.1 Barometry: According to the calibration of Hammarstrom and Zen (1986), the amount of total Al in hornblende in calc-alkaline plutonic rocks can be used for estimating pressure. The relation between Al total (Al^T) in hornblende and pressure (in kbar) is expressed as $P=-3.92+5.03Al^T$ by these authors. Application of this equation to Etive igneous hornblendes indicates a pressure between 0.5 and 1 kbar for these rocks. The Al^T content of hornblende is suggested as an indicator of pressure to within ±3 kbar for crystallisation of plutonic rocks. From this barometer it can be deduced that the pressure of the Etive igneous complex was less than 4kbar at the crystallisation stage of hornblende. Application of an empirical correlation of Al total in hornblende with pressure (Hollister *et al.*, 1987) to the Etive igneous rocks gives pressures between 0.5 and 1 kbars. The error bars for this correlation, considered by Hollister *et al.* (1987) is ±1 kbars. Therefore the possible maximum pressure for hornblende crystallisation stage was 2 kbars.

If Brown's (1977) NaM_4 versus Al^{iv} diagram for metamorphic amphibole geobarometry is applicable to the products of igneous crystallisation, then the pressure of crystallisation of amphiboles in the Etive Complex is below 3 kbars (Fig. 3.25).

An-Ab-Or phase relations: Assuming a possible maximum pressure of 3 kbar, the CIPW-normative Ab-Or-Qz components of Etive igneous rocks are plotted in the residua system Ab-Or-Qz for P_{H2O} =3kbar after Tuttle and Bowen (1958) in Fig. 3.26. Samples from the Cruachan intrusion and Quarry intrusion plot away from the quartz-alkali feldspar boundary and ternary minima. All data plot in the low-T trough between binary (765° C at P_{H2O} =3kbar) and ternary minima. Samples follow a thermal trend from the binary minimum towards the ternary minimum, illustrating a possible differentiation trend produced by feldspar fractionation. Most of the samples from the Meall Odhar leucogranite (haplogranite) plot on, or close to the 3kbar cotectic line (heavy line on Fig. 3.26).

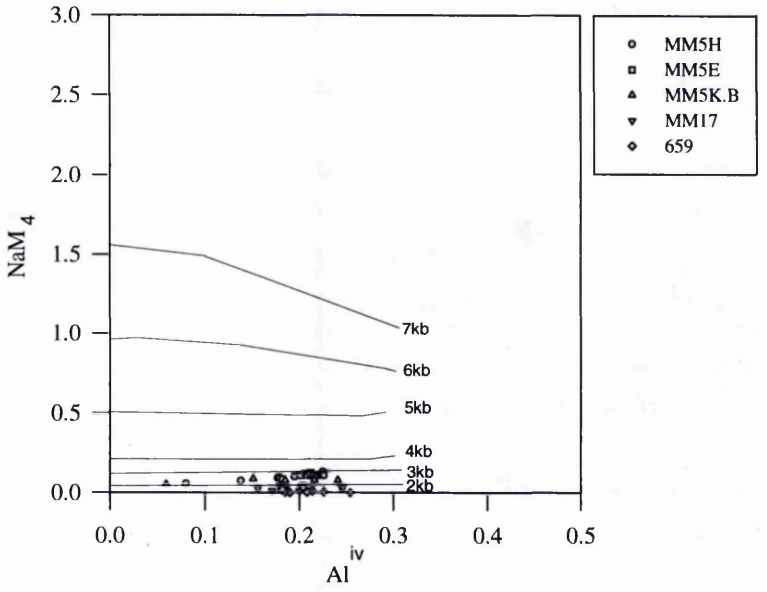

Fig. 3.25 Estimates of the crystallisation pressure of the Etive igneous amphiboles, based on the crossite (NaM4) content of amphiboles (after Brown, 1977). All of the amphiboles lie below the 3 kbar line.

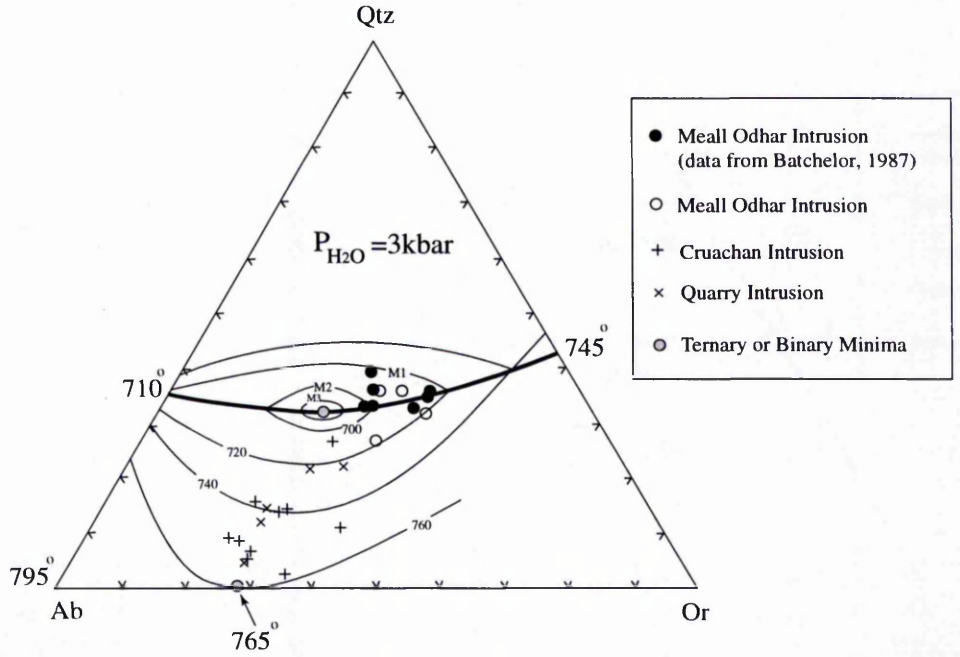

Fig. 3.26 Plotting the Etive igneous rocks on the Qtz-Ab-Or diagram. Samples from Cruachan and Quarry intrusions plot away from the quartz-feldspar field boundary and ternary minimum. Samples from the Meall Odhar Granite plot to the right side of the ternary minimum. All samples plot in a low-T trough between ternary and binary minima.

These samples are shifted towards Ab-depleted compositions. Therefore the water pressure in the crystallisation stage of leucogranite was lower than 3kbar (if 3kbar was the maximum pressure, the water pressure was lower than total pressure and leucogranitic magma was not water saturated). Lower water pressures (e.g. 1-2 kbar) will shift the cotectic/minimum intersections towards Ab-depleted compositions (M_1 and M_2 in Fig. 3.26) and to more quartz-rich compositions as well (Johannes, 1984; Weiss and Troll, 1991). The An content of the Meall Odhar haplogranite is insignificant and the displacement of rocks towards less Ab-rich compositions is not due to an An component in the liquid.

Although the barometers used are not precise, they are in reasonable agreement with 1-2 kbar pressure calculated by Droop and Treloar (1981). Therefore this range of pressure will used for temperature evaluation of the Etive igneous rocks.

3.6.2 Two-Feldspar Thermometry: The construction of the two-feldspar thermometer is based on the assumption that the compositions of the equilibrated coexisting feldspar pairs depend only on the pressure and temperature, for a given total feldspar composition. If equilibrium was attained only with respect to alkali exchange, the compositions also depend on Al-Si order in both frameworks (Brown and Parsons, 1981). Several empirical and semi-empirical two-feldspar thermometers have been proposed by different authors, based on the distribution of albite between coexisting plagioclase and alkali feldspar from natural assemblages (e.g. Ferry, 1978, Brown and Parsons, 1981; Haselton *et al.*, 1983). Most of the presently available two-feldspar thermometers fail to accommodate existing experimental data correctly (Brown and Parsons, 1981). Amongst the different two-feldspar thermometers, the graphical thermometer of Brown and Parsons (Brown and Parsons, 1981; Fig.2) and the thermometer of Haselton *el al.* (1983) which is based on calorimetric investigation of the excess entropy of mixing in albite-anorthite/sanidine solid solution, are probably more accurate (see Brown and Parsons, 1981). As mentioned in section 3.6 in this chapter, feldspars from the Etive igneous rocks can be considered as binary solid solutions. Therefore the application of two-feldspar thermometry seems to be reasonable for these rocks. For this purpose the means of the mole fractions of feldspar end-members in the plagioclases and alkali feldspars were calculated and the results were employed for thermometry. Because the plagioclases are zoned, the inner cores and the outer rims were treated separately. In

the equation of Haselton *et al.*(1983), which is presented below, temperature is in Kelvin and pressure is in bars:

$$T_K = \frac{(X_{or}^{kfs})^2(18810 + 17030\,X_{ab}^{kfs} + 0.364\,P) - (X_{an}^{pl})^2(28230 - 39520\,X_{an}^{pl})}{10.3(X_{or}^{kfs})^2 + 8.3143\,Ln\left\{\frac{(X_{ab}^{pl})^2(2 - X_{ab}^{pl})}{X_{ab}^{kfs}}\right\}}$$

Temperatures obtained from this thermometer are 670°C-780°C for the Cruachan intrusion, 411°C for the Meall Odhar intrusion and 473°C to 988°C for Quarry intrusion. In these data the first figure is the temperature obtained from the alkali feldspars and outer rims of plagioclases and the second figure is the temperature obtained from the alkali feldspars and inner cores of plagioclases. The outer rims of the plagioclases are more likely to be in equilibrium with the alkali feldspars. These temperatures probably correspond to sub-solidus re-equilibrium of the feldspars.

Brown and Parsons (1981) derived an improved graphical thermometer by making some modifications to Seck's (1971a & b) thermometer. X_{ab}^{pl} and X_{ab}^{kfs} in the Etive igneous feldspars are plotted in the graphical thermometer in figure 3.27. The cores of the plagioclases, which were probably not in equilibrium with alkali feldspars yield temperatures between 540°C to 800 °C for different samples, but the outer rims of the plagioclases which are believed to have been in equilibrium with alkali feldspars yield more clustered temperatures of about 400°C to 600°C for different samples from the Cruachan intrusion, about 470°C for the Meall Odhar intrusion and about 590°C for the Quarry intrusion. All of these temperatures are below the likely solidification temperature of a dioritic or granodioritic magma. Therefore all temperatures obtained reflect sub-solidus re-equilibrium of the feldspars.

3.6.3 Ternary Feldspar Thermometry: If the small amount of An in alkali feldspars and Or in plagioclases is taken into account, the Etive igneous feldspars may be treated as ternary solid solutions. In fact for feldspars in which ternary solid solution are substantial, feldspar thermometry is more problematic. However several ternary feldspar thermometers are provided by different authors (Seck, 1971; Elkins and Grove, 1990; Nekvasil and Burnham, 1985; Ghiorso, 1984; Furnham and Lindsley, 1988; Green and Usdánsky, 1986). Most of formulations of the feldspar

binaries, Ab-An and Ab-Or, and do not completely account for ternary composition. Ternary feldspar thermometry is based on the position of the isotherms on the

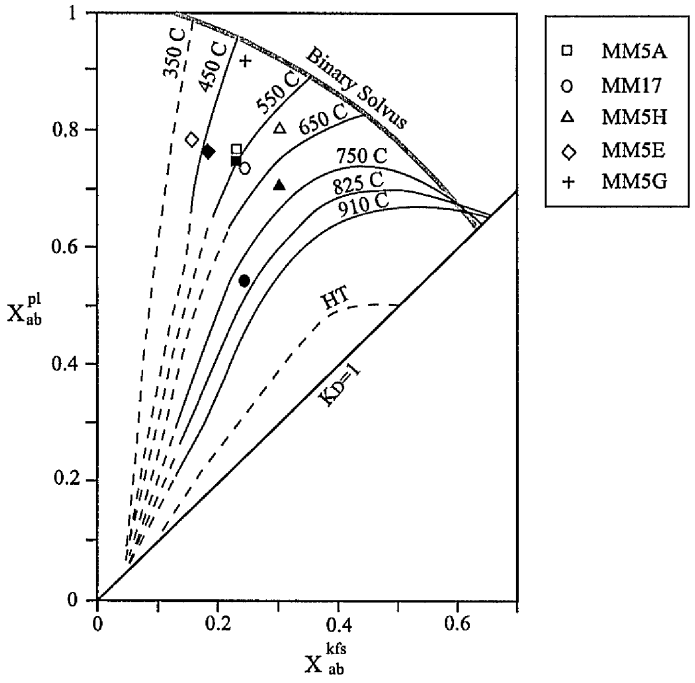

Fig. 3.27 Two feldspar thermometry of Etive igneous rocks using the graphical thermometer of Brown and Parsons (1981). Solid symbols indicate the cores of plagioclases and open symbols indicate the outer rims of plagioclases. The temperatures corresponding to the outer rims of plagioclases and alkali-feldspars are in the range 400-600°C.

An-Ab-Or ternary diagram as a function of water vapour pressure. Temperatures for the Etive igneous feldspars were calculated using six different models (by means of the SOLVCALC computer program, Wen and Nekvasil, 1994). The resultant temperatures in different samples are from 426°C to 757°C which are below the solidification temperature of the dioritic and granodioritic magmas, indicating the sub-solidus re-equilibrium of the feldspars.

3.6.4 Opx-Bt Thermometry: In sample MM17, which is a diorite from the Quarry intrusion, orthopyroxene and biotite are present. As mentioned in the petrography section in this chapter, two types of biotites are present in this sample, one spatially associated with orthopyroxene, which probably crystallised by sub-solidus hydration and the other, texturally remote from orthopyroxene grains, which probably precipitated directly from the magma. For Opx-Bt thermometry analyses of biotite were carried out entirely on the latter type. By employing the Opx-Bt thermometer of

Sengupta *et al.* (1990), a temperature of 710°C was obtained for the Quarry intrusion.

Hbl-Pl thermometry: This thermometer was calibrated by Blundy and Holland (1990) and Holland and Blundy (1994) and is constructed by using Al^{iv} content of amphibole coexisting with plagioclase in silica saturated rocks. The principle exchange vector in amphibole as a function of temperature is $(Na_{-1})^{A}(Al\text{-}_{1}Si)^{T1}$ and the appropriate reactions are:

Edenite + 4Quartz = Tremolite + Albite

Pargasite + 4Quartz = Hornblende + Albite

The equilibrium relation for these reactions used by Blundy and Holland (1990) for constructing the thermometer is:

$$T = \frac{0.677P - 48.98 + Y}{-0.0429 - 0.008314 \ln K}$$

and

$$K = \left(\frac{Si - 4}{8 - Si}\right) X_{Ab}^{Plg}$$

where Si is the number of atoms per formula unit in amphibole with P in kbar and T in K, the term Y represents plagioclase non-ideality, $RT\ln\gamma_{ab}$, from Darken's Quadratic Formalism (DQF) with Y = 0 for $X_{ab} > 0.5$ and $Y = -8.06+25.5(1-X_{ab})$ for $X_{ab} < 0.5$ (Blundy and Holland, 1990).

Plagioclases in the Cruachan Granodiorite are zoned crystals. The highest content of An in the core of the plagioclases is $X_{An} = 0.26$ and the lowest content is $X_{An} = 0.16$. Amphiboles are mainly homogeneous. For finding the overall atomic Si content in amphiboles, the mean of Si content in ten analysed amphiboles was calculated (n = 10, mean = 7.27, $\sigma = 0.17$).

Application of this thermometer gives the maximum temperature of 819°C at 2 kbars for Quarry Diorite (MM17) and 816°C for Cruachan Granodiorite (MM5E). Blundy and Holland (1990) have calculated the overall standard error of 38°C for the thermometer. The results from this thermometer are summarised in Table 3.9. The cores and rims of the plagioclases are treated separately.

3.6.6 Opx-Cpx Thermometry: Analyses from sample MM17 (diorite variety from the Quarry intrusion) are plotted on the graphical two-pyroxene thermometer of Lindsley (1983) (Fig. 3.28). For more details on the orthopyroxene-clinopyroxene

Table 3.9 Results from Hbl-Pl thermometry (Holland and Blundy, 1994). The upper and lower figures show the Edenite-Tschermakite and Edenite-Richterite equilibria respectively.

	2 kbars		4 kbars	
	Core	Rim	Core	Rim
MM5H	729	575	708	558
	731	684	734	686
MM5E	778	725	754	702
	814	712	816	713
MM17	801	755	776	730
	818	740	819	741
659	815	754	791	732
	789	702	792	705

thermometer calibration and method of thermometry see Chapter 9. The highest temperature from this diagram is 1000°C which is an acceptable temperature for the

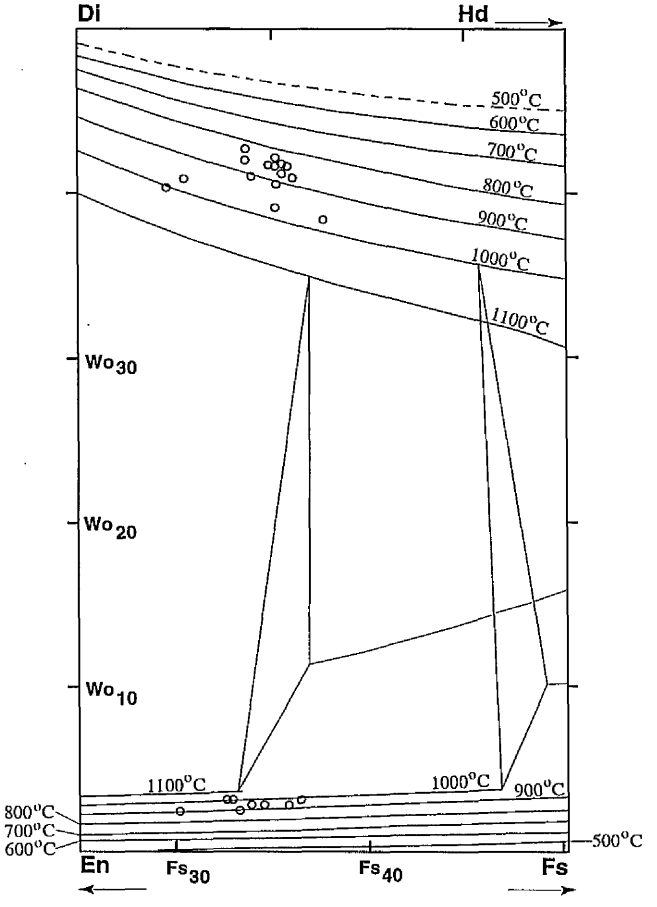

Fig. 3.28 Two pyroxene thermometry of the diorite from the Quarry Intrusion using the graphical thermometer of Lindsley (1983). The highest temperature of Opx and Cpx equilibrium is about 1000°C for a pressure of 3kbar. Lower temperatures are due to late stage re-equilibrium during cooling.

orthopyroxene and clinopyroxene crystallization stage. Other pyroxene pairs show an overall temperature of 900°C or lower, which are attributed to the later resetting of temperatures during cooling of the diorite. The two-pyroxene thermometer of Kretz (1981) gives a temperature of 832°C±60°C for the Quarry intrusion.

Chapter 4

Structural Geology of the Dalradian Supergroup in the Etive area

4.1 Introduction

In order to work out any possible influence of structures within the Etive aureole on distribution of contact metamorphic isograds and fluid flow paths, an outline of the structures in the Etive area is discussed in this chapter. This chapter is mainly based on structural information collected during field work. Data are provided on maps and on stereoplots in the text. The orientation of the planar surfaces in the field was recorded by means of a 3-figure strike and 2-figure dip direction (e.g. 123 / 37 SW). All linear structures were recorded as a plunge angle and plunge azimuth. (e.g. 40 / 225).

Deformational phases are described according to the method outlined by Spry (1969). A schistosity (S_n) is assumed to have developed synchronously with a phase of folding (F_n) and with a lineation (L_n). The first recognisable phase of deformation is defined as D_1 and subsequent phases are numbered accordingly. The description of folds follows the terminology of Fleuty (1964). Cleavages are classified according to the method of Powell (1979).

For structural (and lithological) mapping in the selected segments of the Etive aureole, 1: 10,000 scale maps enlargements of topographical 1: 25,000 scale maps were used.

The major structures in the Etive area are the Early Grampian structures (D_1 and D_2) such as the Aberfoyle anticline or Tay Nappe, the Ben Lui fold, the Loch Awe syncline and the Ardrishaig anticline and the Late Grampian structures (D_3 and D_4) such as the Ben Lawers syncline and the Ben Ledi antiform (see section 2.5 in chapter 2).

Regarding the different lithologies and geographical settings, the Etive area was divided into the following five sub-areas: (i) Loch Creran sub-area, (ii) North Bonawe sub-area, (iii) South Bonawe sub-area, (iv) South Loch Awe sub-area and (v) North Loch Awe sub-area (Fig.4.1). In each sub-area a typical locality, with the most comprehensive and clearest structural features is chosen as a key locality and described in more detail. The deformation history and geometry of each generation of structures is discussed for each area separately. At the end of the chapter, the overall structural characteristics of the Etive area are summarised. Fig. 4.2 shows the symbols used in all the structural maps in this chapter.

4.2 Loch Creran sub-area

The eastern side of Loch Creran consists of the Creran Flags, which are semi-pelitic rocks with interlayers of quartzite and metabasite. The bedding in the biotite-rich semipelite is well developed on a cm scale. 1mm to 1cm thick quartzite beds are present in the semipelites.

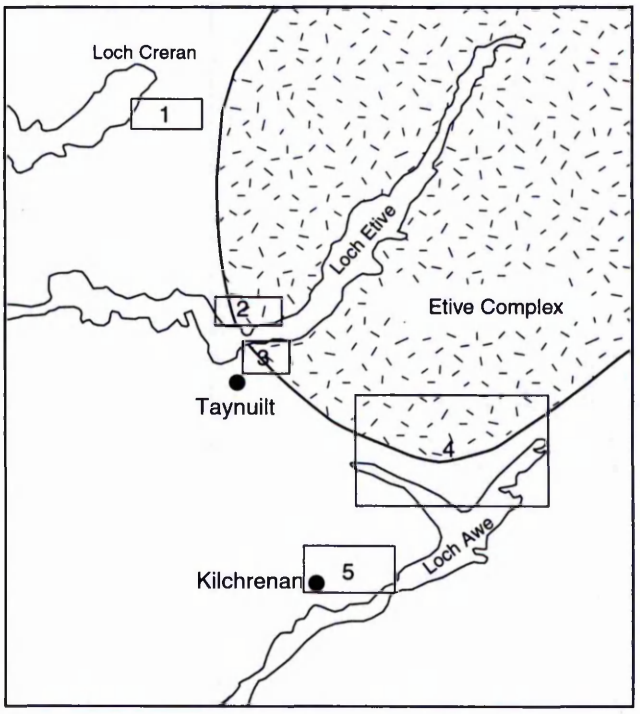

Fig. 4.1 Sketch map of the locality of the sub-areas in the Etive area. 1. Loch Creran sub-area, 2. North Bonawe sub-area, 3. South Bonawe sub-area, 4. North Loch Awe sub-area, 5. South Loch Awe sub-area.

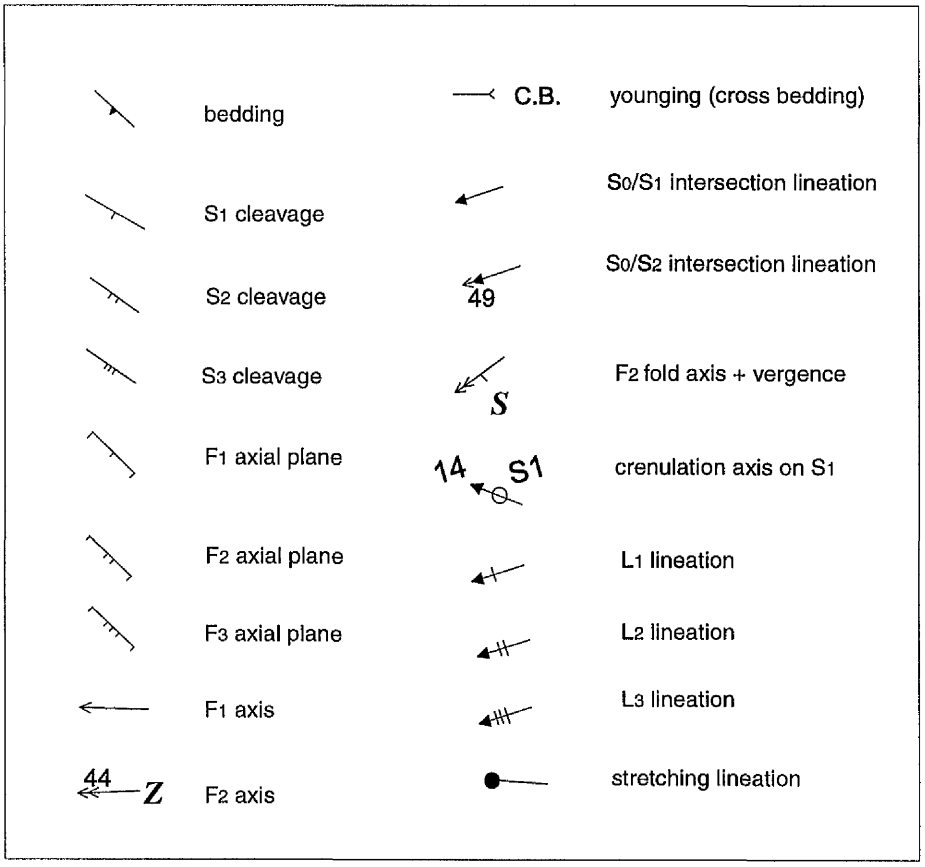

Fig. 4.2 Symbols used in the structural maps in this chapter.

In this sub-area the main structural feature is a fine, penetrative schistosity ("slaty cleavage"), which is a result of the parallelism of mica flakes in the semipelitic and psammitic rocks. The schistosity in the semipelite is strong. In the more pelitic rocks this schistosity is sub-parallel to the bedding or compositional layering, while in the more quartz-rich rocks the angle between the schistosity and bedding is higher. This schistosity is the earliest deformation feature in the Loch Creran sub-area (S_1) and is related to the D_1 deformation episode. The main linear structure in this sub-area is the bedding/S_1 schistosity (L_1) intersection lineation which is visible at the locality of NN00084483. Other major structural features of the D_1 phase were not found in this sub-area. Younger observed structural features in the Loch Creran sub-area include F_2 folds, which fold the S_1 schistosity. At NN01174467, the F_2 folds are open folds with wavelengths of 1 to 30 cm. A closely spaced crenulation cleavage (S_2) is developed axial planar to the folds. The axes plunge to the NW. Fig. 4.3 illustrates the structural map of the sub-area and Fig 4.4 shows the stereoplot for D_1

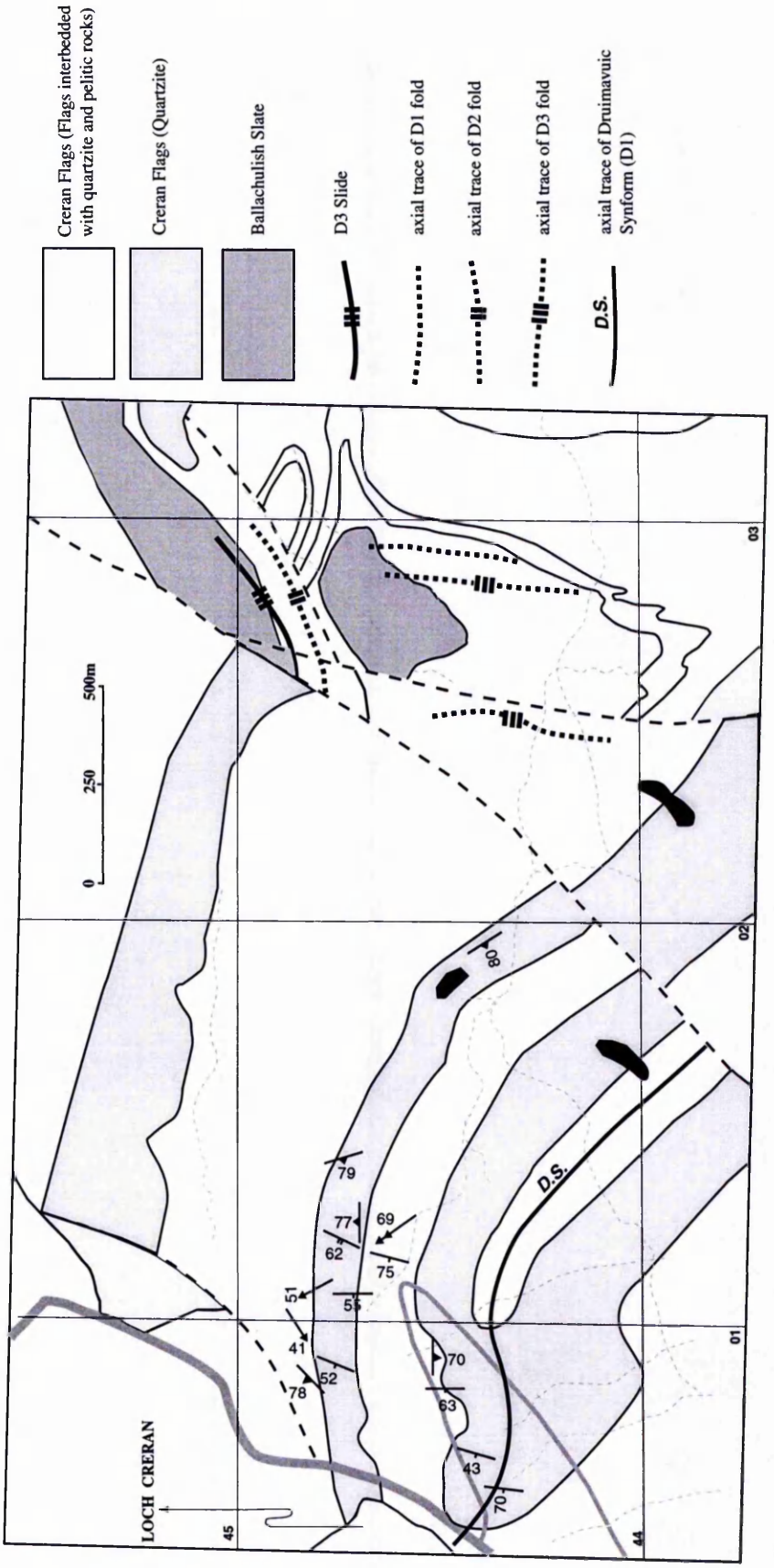

Fig. 4.3 Structural map of the Loch Creran sub-area. Boundaries and axial traces of D1, D2, D3 and D.S. are after Litherland (1982).

and D_2 structures which shows the bedding dips to the WSW and the S_1 cleavage dips to the WNW. According to the map in Figure 4.3, as Litherland (1982, Fig.1) has shown, the major deformational phase in this area is D_1 which is recognisable by means of S_1 schistosity. The minor structures are F_2 folds and S_2 crenulation cleavage, axial planar to the folds.

Plate 4.1 illustrates microstructures of pelitic rocks in the Loch Creran sub-area. The altered garnet is a syn-deformational phase, crystallising during the D_2 deformation phase. S_2 crenulation cleavage is well developed in this pelitic sample. Plate 4.2 shows S_1 and S_2 relations in pelitic rocks without garnet porphyroblasts. These samples are from the outer aureole without any significant thermal effects.

The Loch Creran sub-area is on the east side of the Glen Creran Slide and on the west limb of the D_1 Beinn Sgulaird recumbent syncline, which is a complementary fold to the Glen Creran Anticline (Litherland, 1982). These major structures control the D_1 deformation in this sub-area. Another major structure in the Loch Creran sub-area is the D_1 Druimaric Synform (Fig. 4.3).

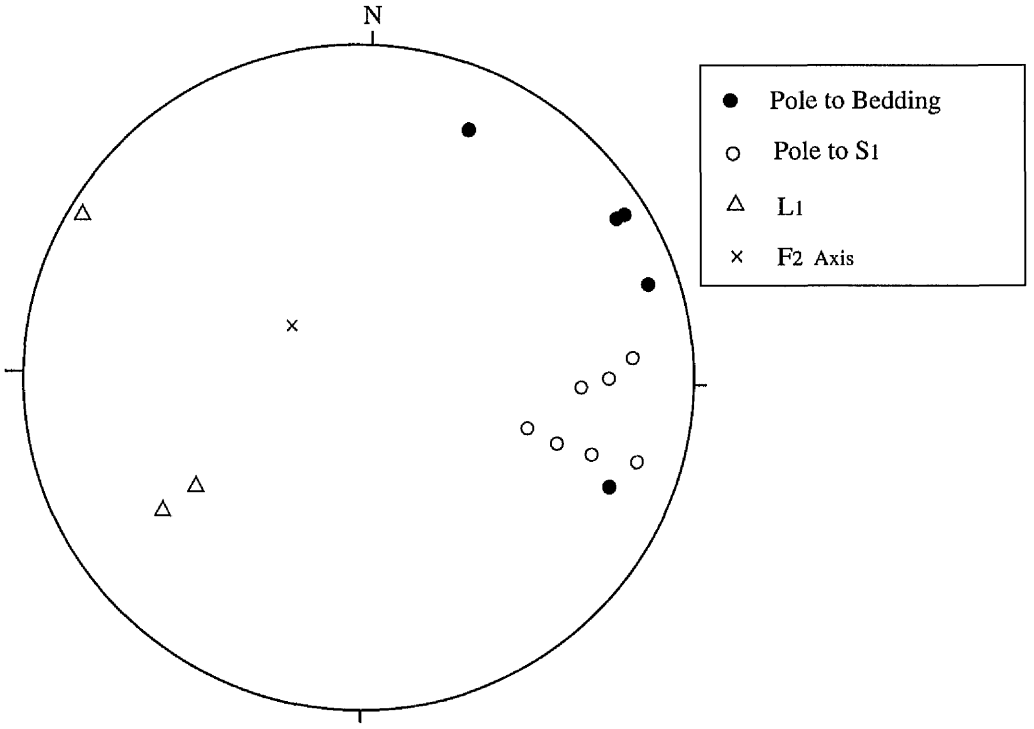

Fig. 4.4 Stereoplot for structural features in the Loch Creran sub-area. The bedding dip to the WSW and the S_1 cleavage dip to the WNW

Plate 4.1 S_2 crenulation cleavage in pelitic rocks from the Loch Creran sub-area. Altered garnet (Grt) is syn-deformational phase, crystallising during D_2 deformational phase. PPL. Field of view 5.5×3.5 mm.

Plate 4.2. S_1 slaty cleavage, which is folded by D2 deformational phase in the pelitic rocks of the Creran Flags in the Loch Creran sub-area. PPL. Field of view 5.5×3.5 mm.

4.3 North Bonawe sub-area

The main lithologies in the north Bonawe sub-area are Creran Flags and Culcharan Black Slates of the Easdale Subgroup. Figure 4.5 shows the structural map of the area. The dominant structure in the North Bonawe sub-area is the S_1 schistosity, which is affected by F_2 and S_2 structures and gently by S_3 and L_3 structures.

A typical locality in the Bonawe sub-area is at NN99583483. Figure 4.6 illustrates the relationship amongst the observed structural features at this type locality. Here the main lithology is black graphitic Easdale Slate. The D_1 deformation phase is represented by S_1 schistosity, which is sub-parallel to bedding. At NN00023425 tight to isoclinal microfolds lie in the S_1 schistosity which appears to be axial planar to the microfolds. Apparently these folds are F_1 folds. An L_1 stretching lineation is defined by elongation and preferred orientation of minerals especially sulphide minerals. D_2 deformation is represented by F_2 folds. These folds are steep-plunging open folds with a wavelength of 1-10 cm. The axial planar cleavage related to these folds (S_2) is almost at a right angle to the bedding and S_1 surfaces.

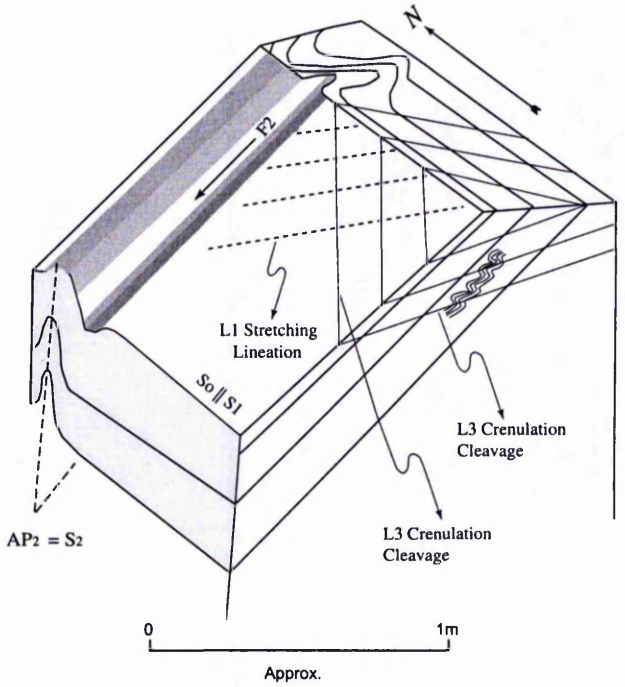

Fig. 4.6 Schematic representation of the relationships amongst the different deformational features at the locality NN99583483 in the North Bonawe sub-area. The major structures are D_2 folds.

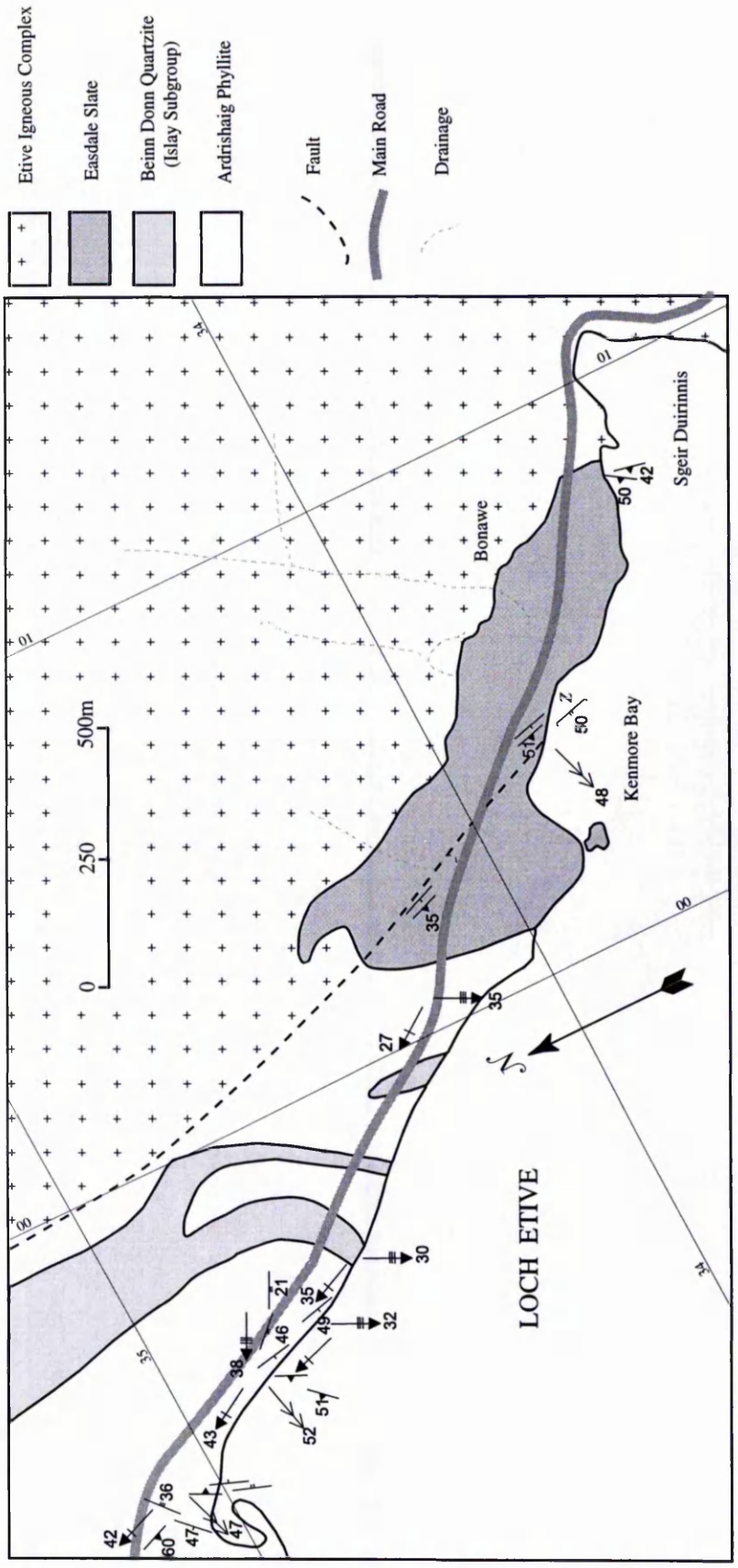

Fig. 4.5 Structural map of the North Bonawe sub-area. S1 schistosity is the dominant structure.

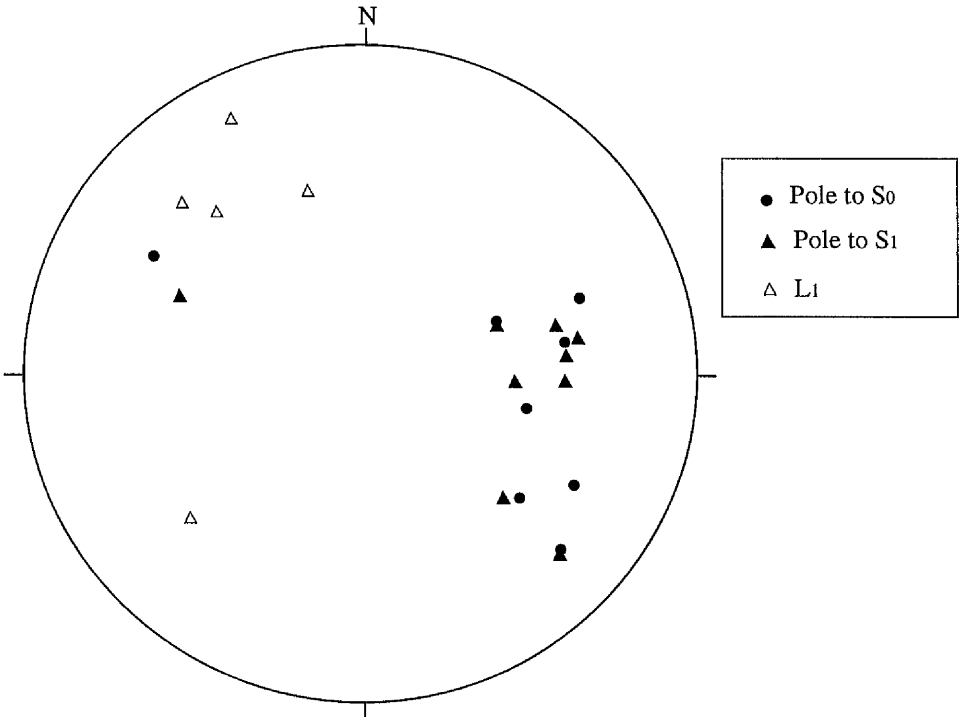

Fig. 4.7 Stereoplot for bedding (S0) and D1 deformation phase in the North Bonawe sub-area. The dip of S0 and S1 is mainly to the W and plunge of the L1 lineation is to the NW.

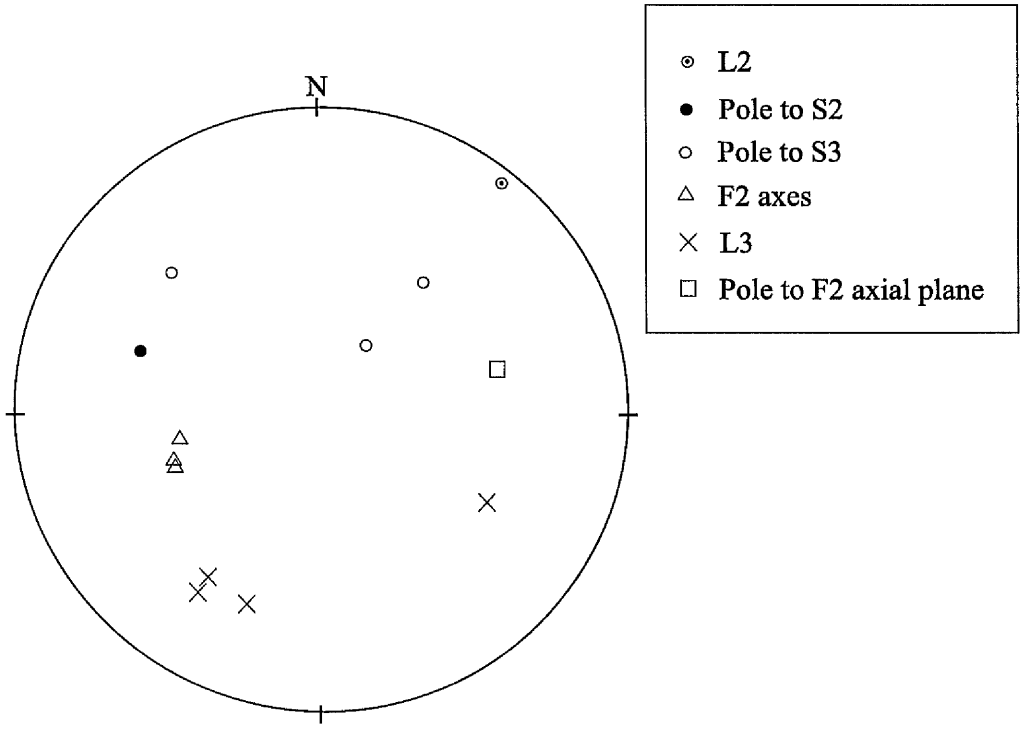

Fig. 4.8 Stereoplot for D2 and D3 deformation phases in the North Bonawe sub-area. The overall plunge of the F2 axes is SW and the main dip-direction of the S3 crenulation cleavage is S.

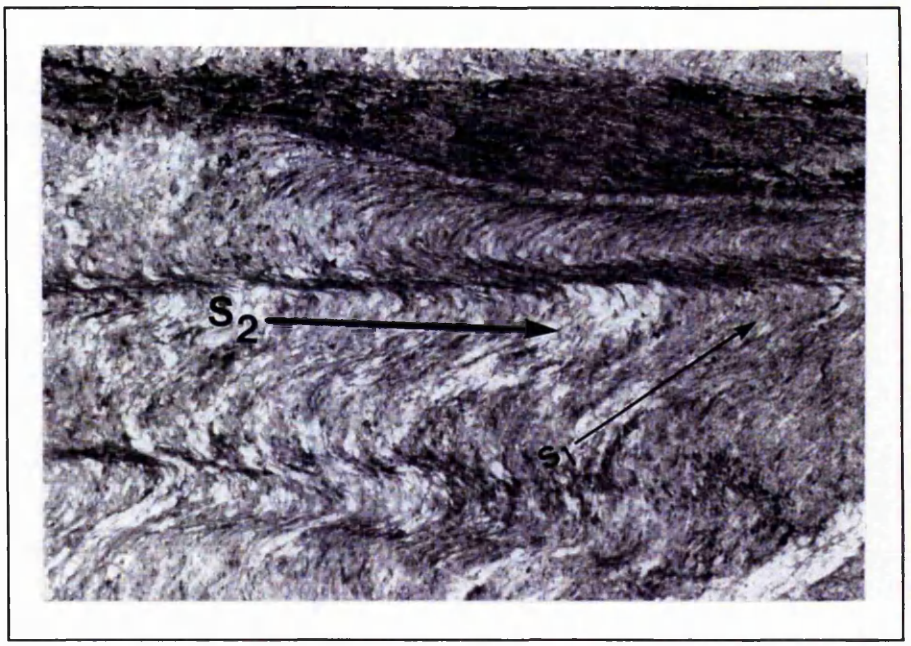

Plate 4.3 S1 slaty cleavage and S2 crenulation cleavage in the pelitic rocks from Ardrishaig Phyllite in the North Bonawe sub-area. PPL, field of view 5.5×3.5 mm.

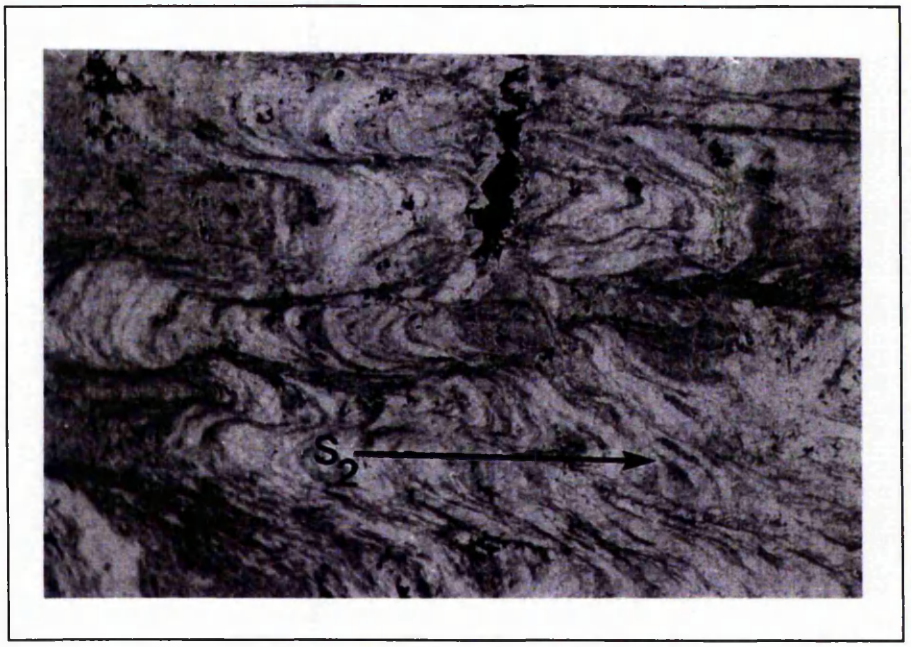

Plate 4.4 Well developed S2 crenualtion cleavage in the pelitic rocks of Ardrishaig Phyllite in the North Bonawe sub-area. PPL, field of view 5.5×3.5 mm.

D_3 deformation is recognisable by a gentle S_3 crenulation cleavage. L_3 lineation is a result of the intersection of S_3 crenulation cleavage and $S_0 \| S_1$ plane surfaces. In Fig. 4.7 the stereoplot for S_0 and D_1 deformational phase shows that the dip of these planar structures is mainly to the W and plunge of the L_1 lineation is to the SE. Fig. 4.8 is a stereoplot for D_2 and D_3 phases, which indicates SW-directed plunges for F_2 axes. This figure also shows a SW-directed overall plunge for the L_3 lineation and SE dip direction for the gentle S_3 crenulation cleavage. Plates 4.3 and 4.4 illustrate the S_1 and S_2 relations in samples from the North Bonawe sub-area. The lithology of these samples, which are from the outer aureole with minimum thermal effects, is Ardrishaig Phyllite.

4.4 South Bonawe sub-area

The main lithologies in the South Bonawe sub-area (the southern side of Loch Etive) are black slates of the Easdale Subgroup and the calcareous and semipelitic phyllites of the Ardrishaig Phyllite (Easdale Subgroup). At locality NN02573178 in the finely laminated biotite-rich pelites which are thermally metamorphosed, bedding (S_0) and early cleavage (S_1) are sub-parallel. The average strike and dip of the bedding and S_1 is approximately 152/33W. In the other localities along the Bonawe forestry track (eastern side of the River Awe), the strike and dip of the bedding and the earliest cleavage are more or less the same. The L_1 lineation is a stretching lineation. The D_2 deformation phase is represented by F_2 folds in the above-mentioned locality, which are 1-5 cm-scale tight to closed folds with Z asymmetry mainly plunging to the SW. The dominant structures in this sub-area are S_1 cleavage and F_2 folds. However at locality NN020327, which is a disused quarry near the Loch Etive shore, the strike and dip (Fig.4.10) of bedding and S_1 cleavage are not compatible with the overall strike and dip for these structures as measured in aureole rocks further SE. It can be deduced that the semipelitic and calcareous rocks in the quarry are large xenoliths in the Cruachan Granodiorite and not roof pendants.

The rocks at locality No. 206 (NN02573255) in Fig. 4.9 are large xenoliths with abnormal F_2 axis and axial plane directions. Fig. 4.10 illustrates the stereoplot for S_1 and S_0 plus F_2 axis structures in the South Bonawe sub-area. In this figure,

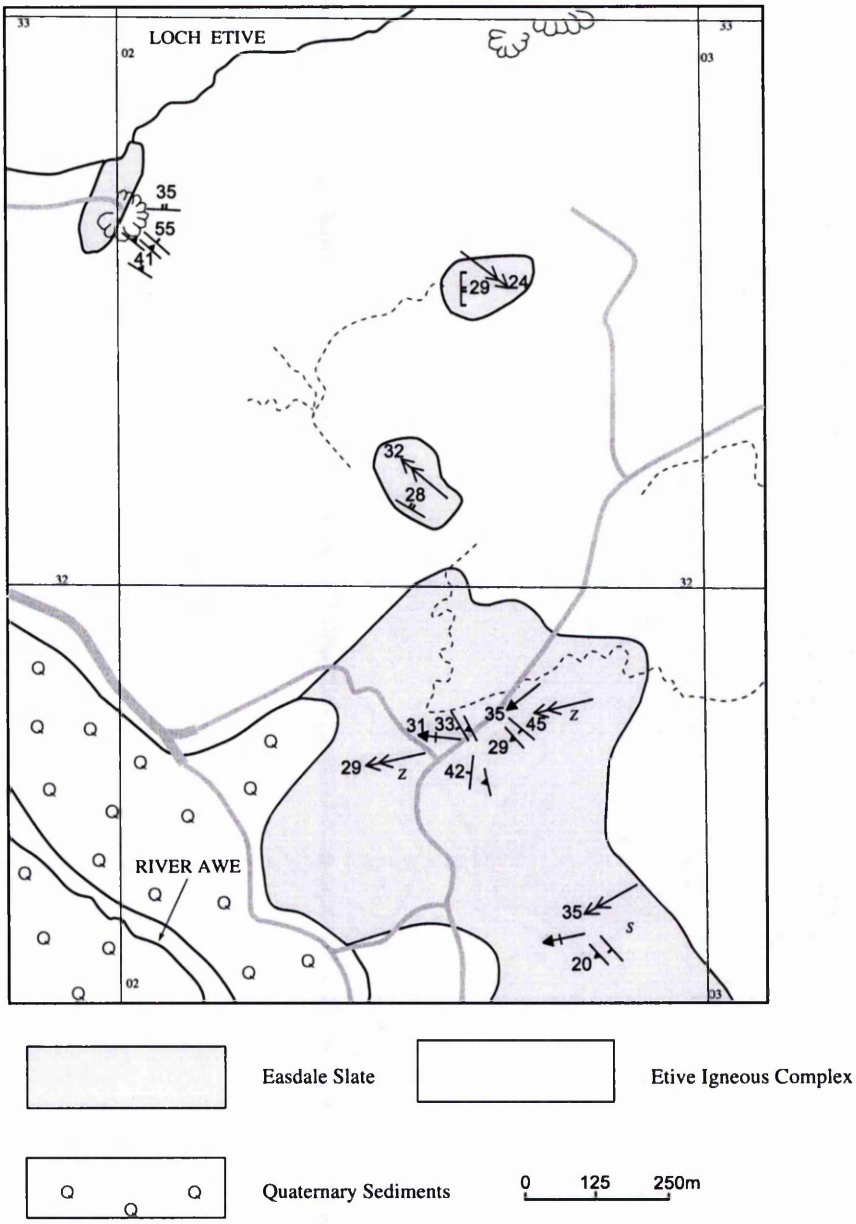

Fig. 4.9 Structural map of the South Bonawe sub-area. Large screens and xenoliths of the metasedimentary rocks have features with abnormal structural directions, which are not compatible with the overall trends of the structures.

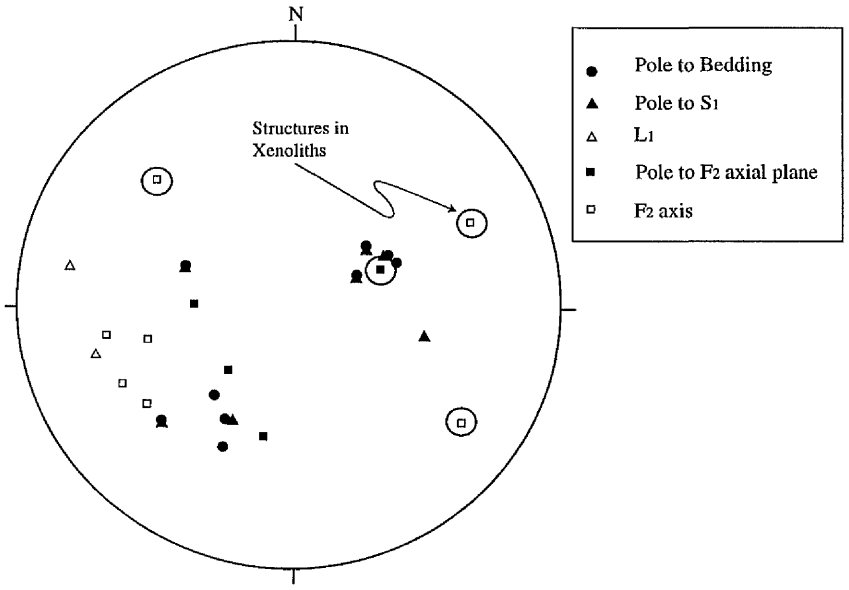

Fig. 4.10 Stereoplot for bedding, D_1 and D_2 deformational phases in the South Bonawe sub-area. South-west dipping S_0 and S_1 planes are *in-situ* structures and NE dipping S_0 and S_1 structures are attributed to the structures in the large xenoliths. The direction of the F_2 axes is SW.

south-west dipping S_0 and S_1 planes are *in-situ* structures while the NE dipping S_0 and S_1 structures are those in the large xenoliths. The overall orientation of the F_2 axes is SW. This sub-area and the north Bonawe sub-area lie on the west side of the Loch Awe Syncline. This syncline is an upright D_1 structure, which separates early folds with opposed facing directions (Roberts and Treagus, 1977). This major deformational phase is responsible for D_1 structures in both the North and South Bonawe sub-areas.

Plate 4.5 shows a mesoscopic relation between D_1 and D_2 deformation phases in calc-silicates of the Ardrishaig Phyllite in the South Bonawe sub-area. Plate 4.6 shows another example of D_1 and D_2 relation in calc-silicates. F_1 folds are refolded by later F_2 folds.

4.5 South Loch Awe sub-area

The main lithologies in the South Loch Awe sub-area (area close to the Kilchrenan village) are metamorphosed basic rocks (meta-dolerite and meta-gabbro), Ardrishaig phyllite (consisting of sandy limestone, quartzite and chloritic

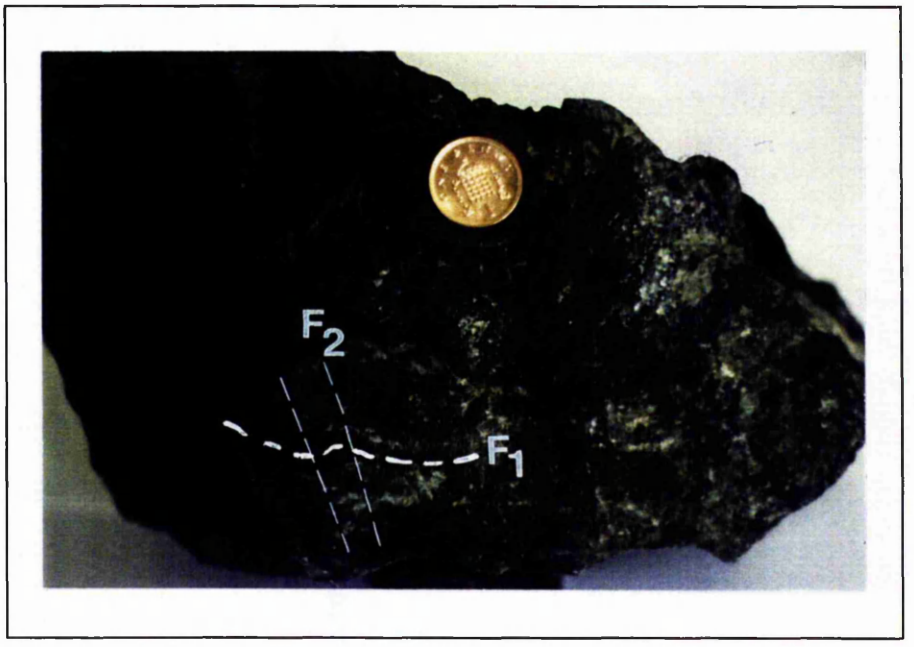

Plate 4.5 F1 fold in the calc-silicate rock of the Ardrishaig Phyllite from the South Bonawe sub-area, which is refolded by F2 fold. Locality NN020327.

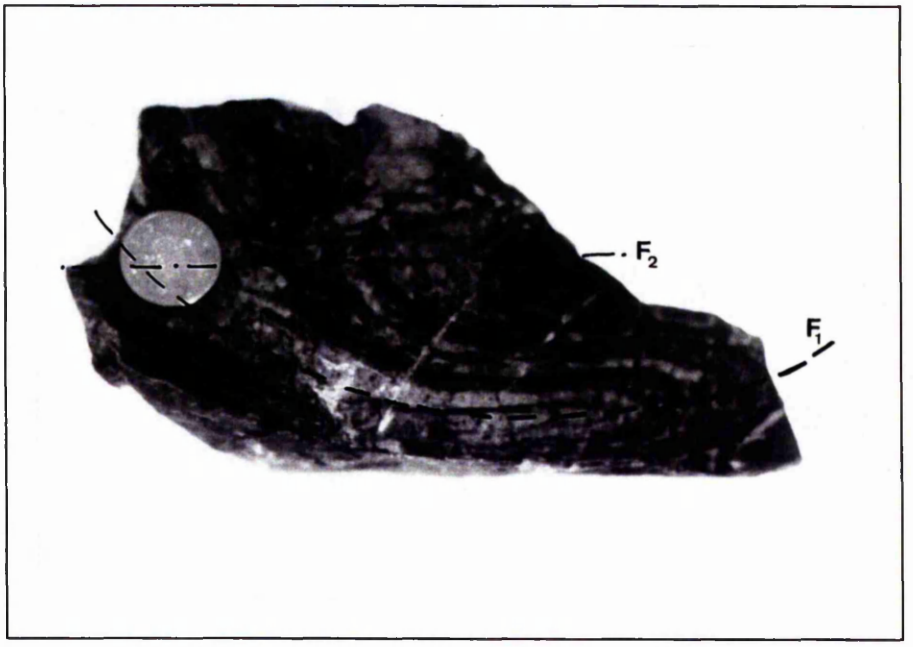

Plate 4.6 Tight F1 fold in the calc-silicate rock of Ardrishaig Phyllite, which is refolded by F2 fold. South Bonawe sub-area, locality NN020327.

slate) and limestones of Tayvallich subgroup. Fig. 4.11 is a structural map of this sub-area.

A typical locality in this sub-area is at NN07992561, which is a disused quarry. The main lithology in this locality is silvery grey to silvery brown Ardrishaig phyllite with about 2 cm thick interlayers of calc-silicates and quartzite. The rocks are well layered and strongly foliated. Within the phyllite the fine mm-scale bedding is sub-parallel to the dominant S_1 schistosity. The angle between bedding and S_1 schistosity is about 3-5° and bedding is steeper. D_1 deformation is represented by S_1 penetrative slaty cleavage and L_1 lineation, which is intersection of bedding and S_1 planes. The D_3 deformational phase is manifested as a fine L_3 crenulation lineation.

At locality NN05982266, in the Tayvallich limestone outcrop, the D_2 deformation appears as "Z"-shaped open to gentle asymmetrical folds on dm-m scales. The dominant schistosity in this sub-area is the S_1 schistosity and the dominant fold phase is F_2. In Fig. 4.12, the stereoplot for data from this sub-area indicates a west dipping direction for bedding and sub-parallel S_1 schistosity. The south Loch Awe sub-area lies on the east limb of the Loch Awe Syncline, the major D_1 structure in the area.

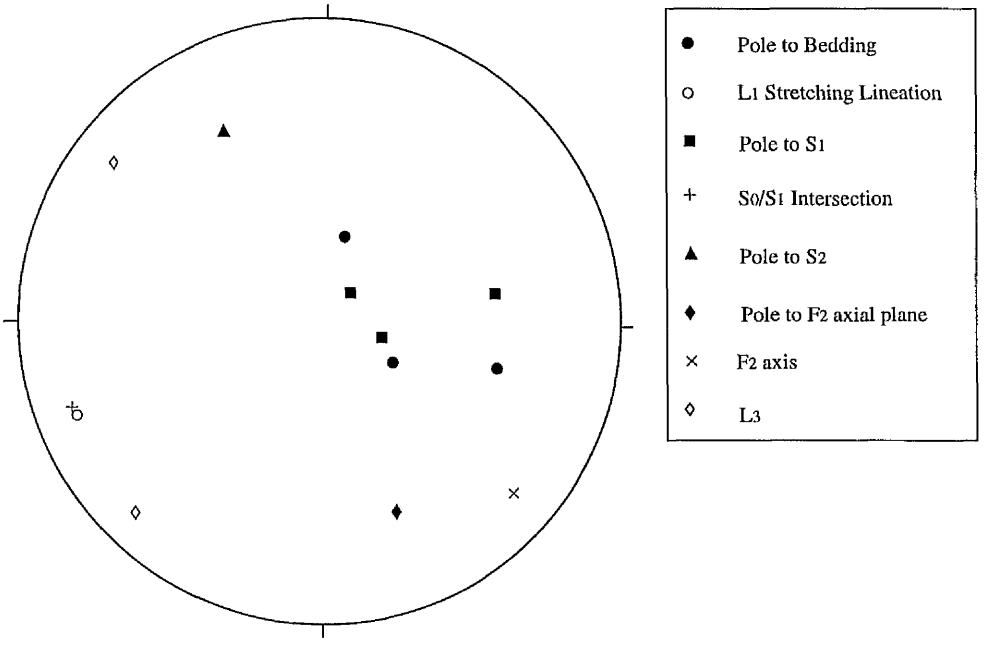

Fig. 4.12 Stereoplot for structural data from the South Loch Awe sub-area. The bedding dip is to the west, which is sub-parallel to the S1 slaty cleavage.

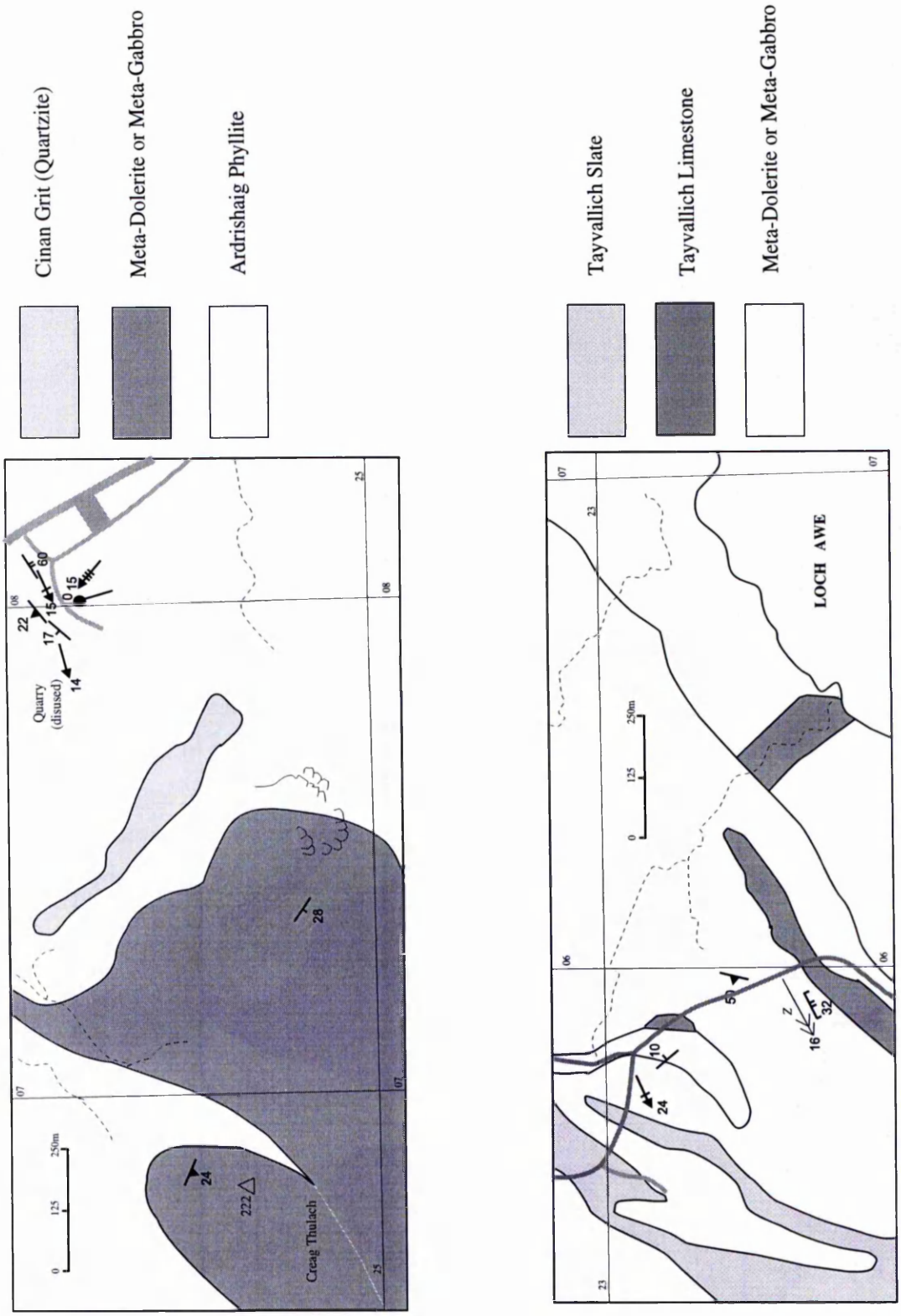

Fig. 4.11 Structural maps of the South Loch Awe sub-area.

4.6 North Loch Awe sub-area

The North Loch Awe sub-area has been studied in more detail than those discussed above. This sub-area extends from the western side of the Cruachan reservoir to the eastern side of Monadh Driseig. The structural data were collected in a series of N-S sections from the outer aureole toward the contact of igneous rocks. A set of data was also collected along the main road.

The North Loch Awe sub-area consists of a variety of meta-sedimentary rocks with meta-basic interlayers. The major lithologies are: Ardrishaig phyllite, graphitic and semipelitic schists of the Ben Eagach Schist with lenses of pebbly quartzite, Carn Mairg Quartzite, semipelitic flags of Islay Quartzite interbedded with black slates and quartzite, Leven Schists which are striped pelite with semipelite, thin quartzites, meta-basites and marble and eventually the Glencoe Quartzite which is a fine-grained, planar-bedded quartzite and is locally pebbly. The structural features are very well developed in some of these lithologies especially in the Ben Eagach graphitic schists.

The structure features of the North Loch Awe sub-area are also presented in the two separate maps (Figures 4.13 and 4.14). Bedding is well developed in calcareous rocks of the Ardrishaig phyllite as well as in the semipelitic rocks. The main trend of the bedding is NW-SE and dip direction is toward the SW-W. In the Ben Eagach schist, the bedding is on a fine scale and in the Carn Mairg Quartzite it is in mm-cm scale. In general in more pelitic rocks the dominant schistosity is sub-parallel to the bedding but in more psammitic rocks bedding is slightly steeper. At the localities NN12832943, NN12802929 and NN12732935 cross bedding is visible in the quartzite, which indicates younging to the west. D_1 deformation in this sub-area is represented by a penetrative slaty cleavage (S_1) which is slightly steeper than bedding at locality NN10792648. L_1 is represented as bedding and S_1 intersection (e.g. at locality NN10302639).

D_2 deformation is the most important phase in the North Loch Awe sub-area. Different features of this phase are recognisable. In the western part of the sub-area, (mainly in the Ardrishaig Phyllite) the S_2 crenulation cleavage (the dominant cleavage) is sub-parallel to the bedding and is well developed in semipelites, calcareous rocks and meta-basites. Other features of the D_2 deformation are F_2

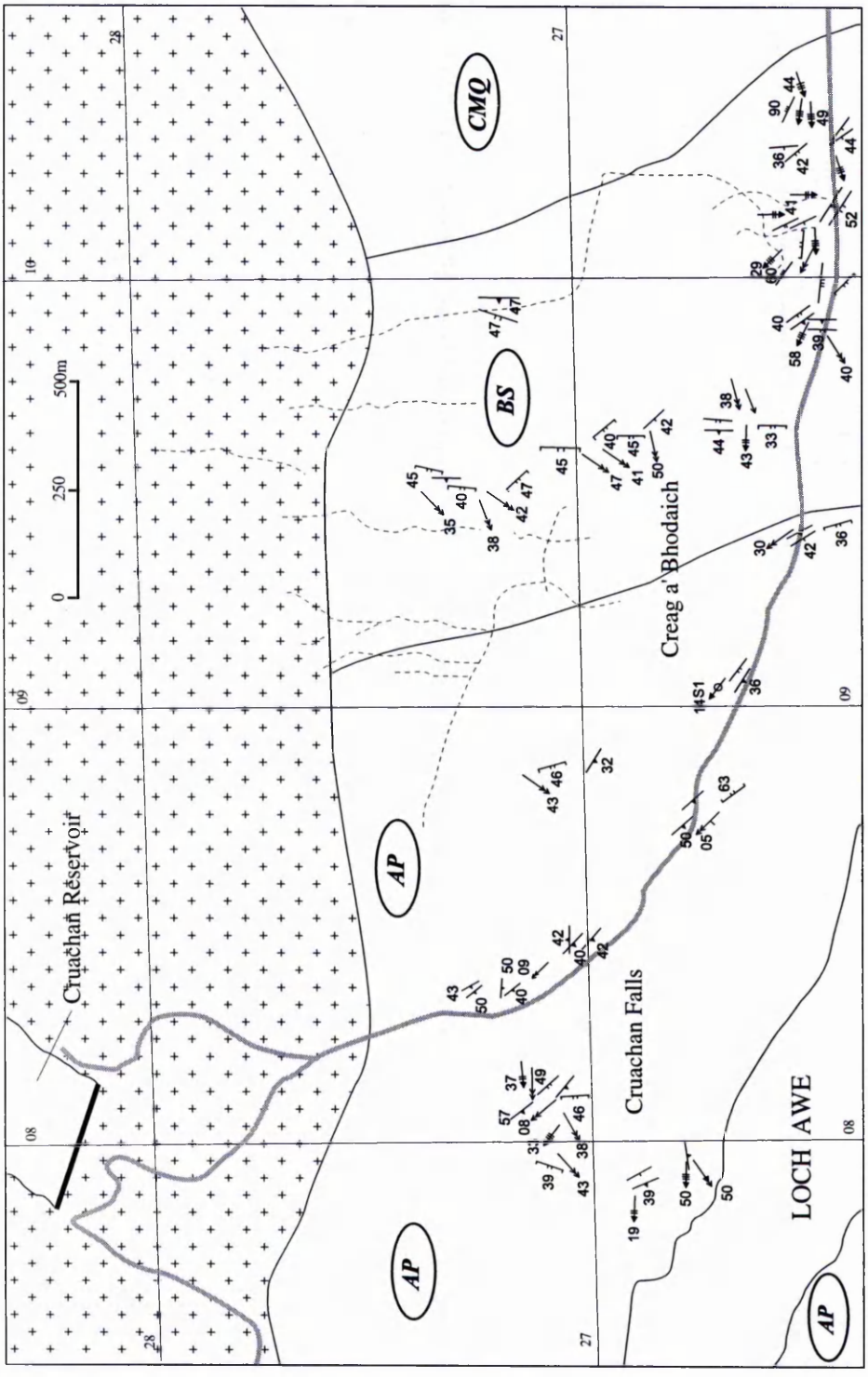

Fig. 4.13 Structural map of the western part of the North Loch Awe sub-area.

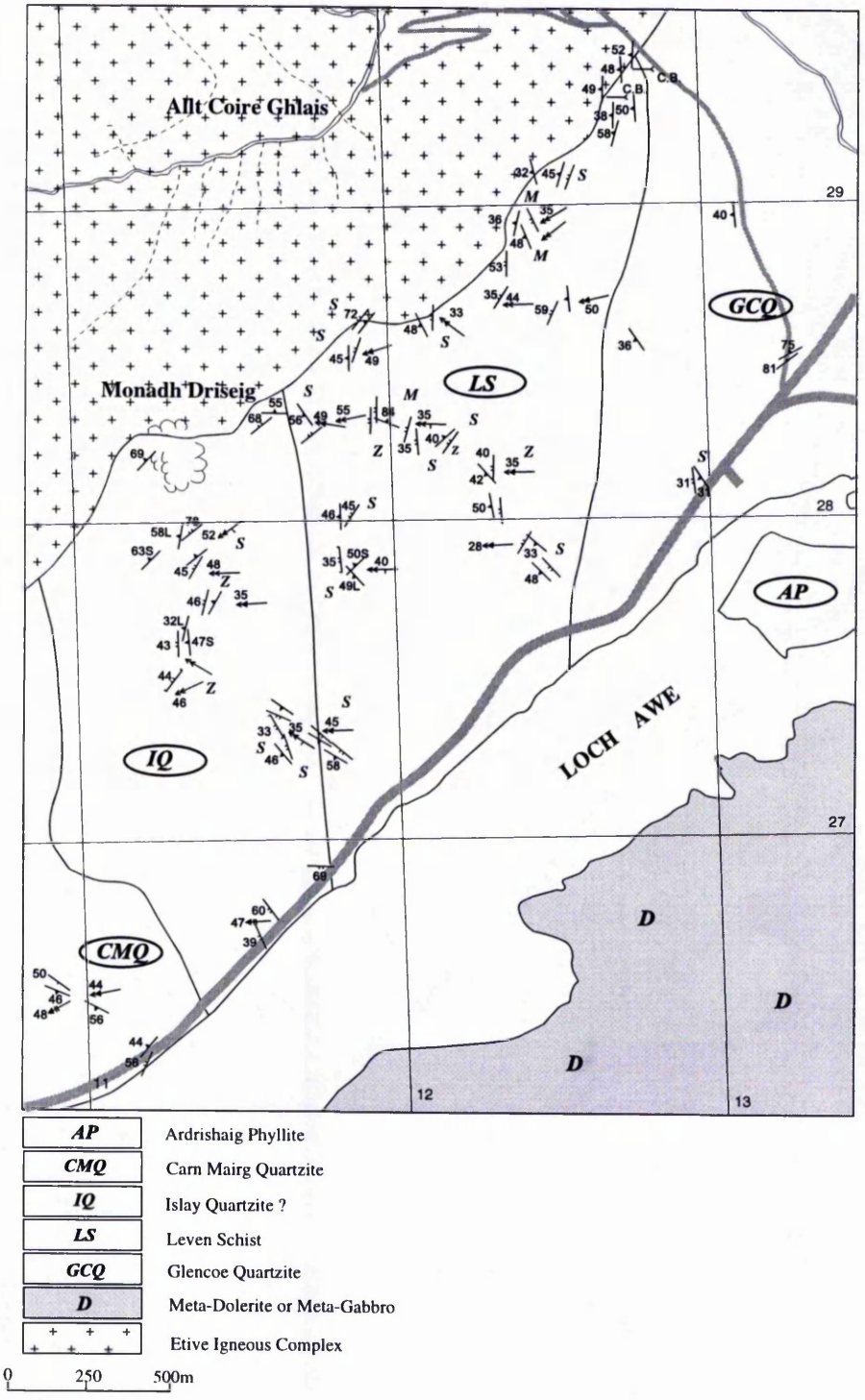

Fig. 4.14 Structural map of the eastern part of the North Loch Awe sub-area.

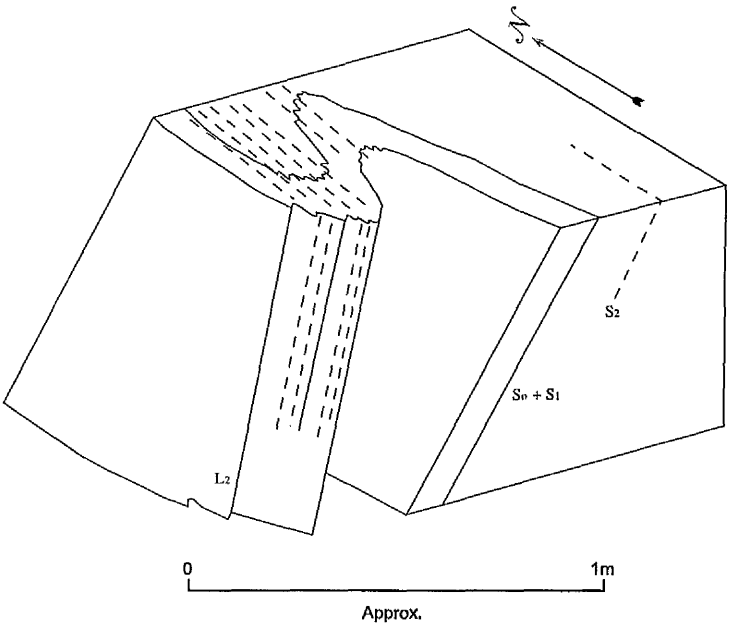

Fig. 4.15 A sketch block diagram of an open to closed F2 fold with 'S' asymmetry in the Leven Schist, North Loch Awe sub-area.

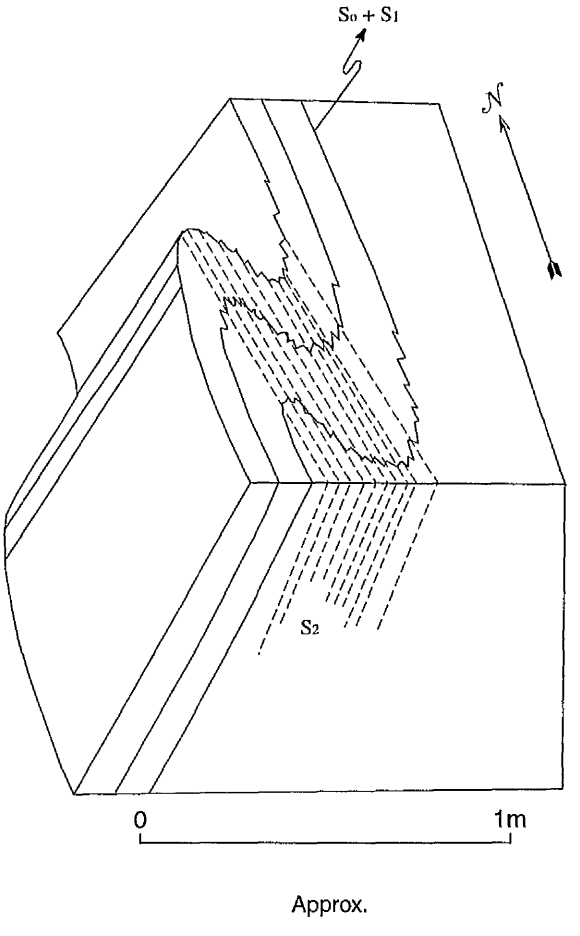

Fig. 4.16 A sketch block diagram of an open to closed F2 fold with 'Z' asymmetry in the Leven Schist, North Loch Awe sub-area.

folds. In the Ardrishiag Phyllite at locality NN08752677 the F_2 folds are 'S' shaped asymmetric folds with 10-30 cm wavelengths (Plate 4.7). In some localities the F_2 folds are chevrons with "Z" asymmetry. F_2 axes mainly plunge toward the SW. The L_2 lineation is a strong crenulation lineation (e.g. at NN09682660). Also the S_2/S_o intersection (L_2) is visible (e.g. at NN11442775). In the eastern part of the sub-area, in the Leven Schists, F_2 folds are well developed. These folds are open to closed folds with both 'Z' and 'S' asymmetry (Figures 4.15 and 4.16). In this part of the sub-area, L_2 lineation is represented by intersection of bedding and S_2 crenulation cleavage. At NN12582873 and NN12452795 this feature is easily definable.

The D_3 deformation is not very obvious. It can be seen only in a few localities (e.g. NN10172641, NN10302639 and NN10792648, Fig. 4.17). In these localities fine S_3 crenulation cleavage and measurable crenulation lineation are present.

In Fig. 4.18 a stereoplot for S_o, S_1 and L_1 structures are presented. The main direction of the bedding dip is SW, and the L_1 lineation plunges toward the SW. Fig. 4.19 is a stereoplot for D_2 deformation structures. The main direction of F_2 axes is SW, and the L_2 lineation plunges toward the SW.

Fig. 4.20 illustrates the stereoplot for D_3 deformation phase. The main direction of the L_3 lineation is W-SW.

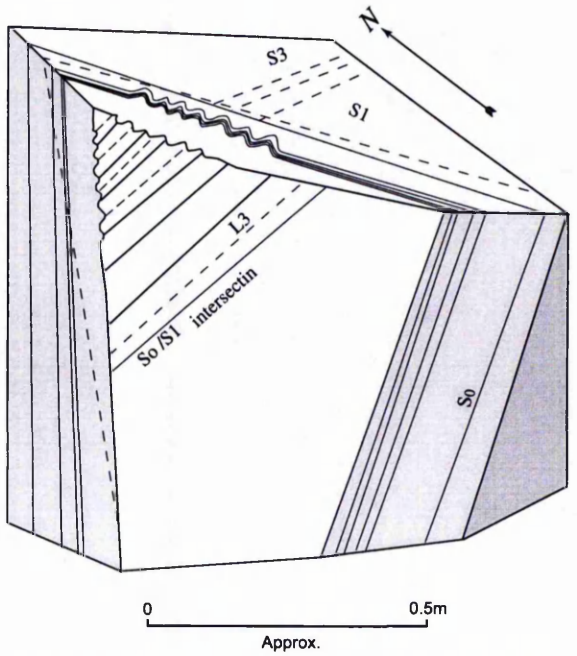

Fig. 4.17 A sketch block diagram of structural relationships at the locality NN10172641, North Loch Awe sub-area.

The major structures which control the structural features in this sub-area are Tay Nappe, Ardrishaig Anticline (D_1 structure) and Loch Awe Syncline (D_1 structure). The north Loch Awe sub-area lies on the eastern limb of the Loch Awe Syncline and the western side of the Ardrishaig Anticline or Tay Nappe, as suggested by S_o/S_1 at NN10792648. This anticline is a large recumbent fold with an axis which runs in a general NE-SW direction. The whole of the North Loch Awe sub-area lies on the lower limb of Tay Nappe in a stratigraphical sequence proved by sedimentary way-up inversion (see cross section in Fig. 2.5 in chapter 2).

The S_1 and S_2 relation in graphitic rocks of the Ben Eagach Schist is illustrated in Plate 4.8. S_2 crenulation cleavage is well developed in the Ben Eagach Schist.

The direction of the axial traces of F_2 folds were worked out using intersection of average of the slope of the erosion surface in the eastern side of the North Loch Awe sub-area with average of the S_2 cleavage planes and average of the F_2 axial planes (Fig. 4.21). The axial traces of F_2 folds are shown in the map of Fig 4.22. F_2 folds of the North Loch Awe sub-area are probably parasitic folds to the major D_2 Ben Lui fold. 'S' folds appear to dominate in this sub-area, suggesting that it is situated on the upper limb of the Ben Lui fold.

D_3 can be correlated with the Ben Lawers structure (see Shackleton, 1958).

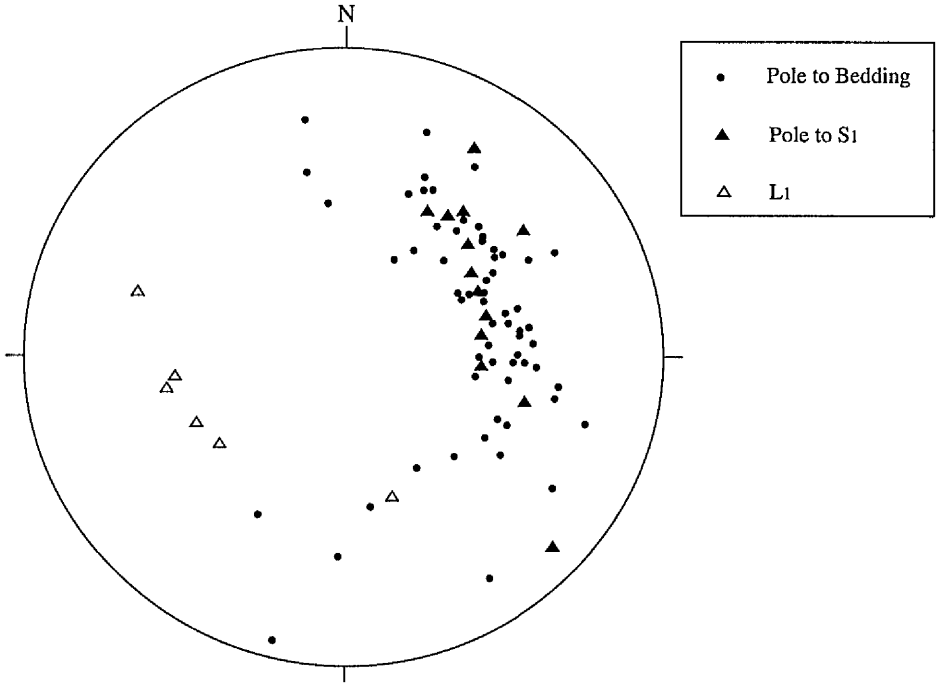

Fig. 4.18 Stereoplot for bedding and D1 deformational phase in the North Loch Awe sub-area. The main direction of the bedding dip is SW and L1 lineation plunges toward the SW. S1 is sub-parallel to S0.

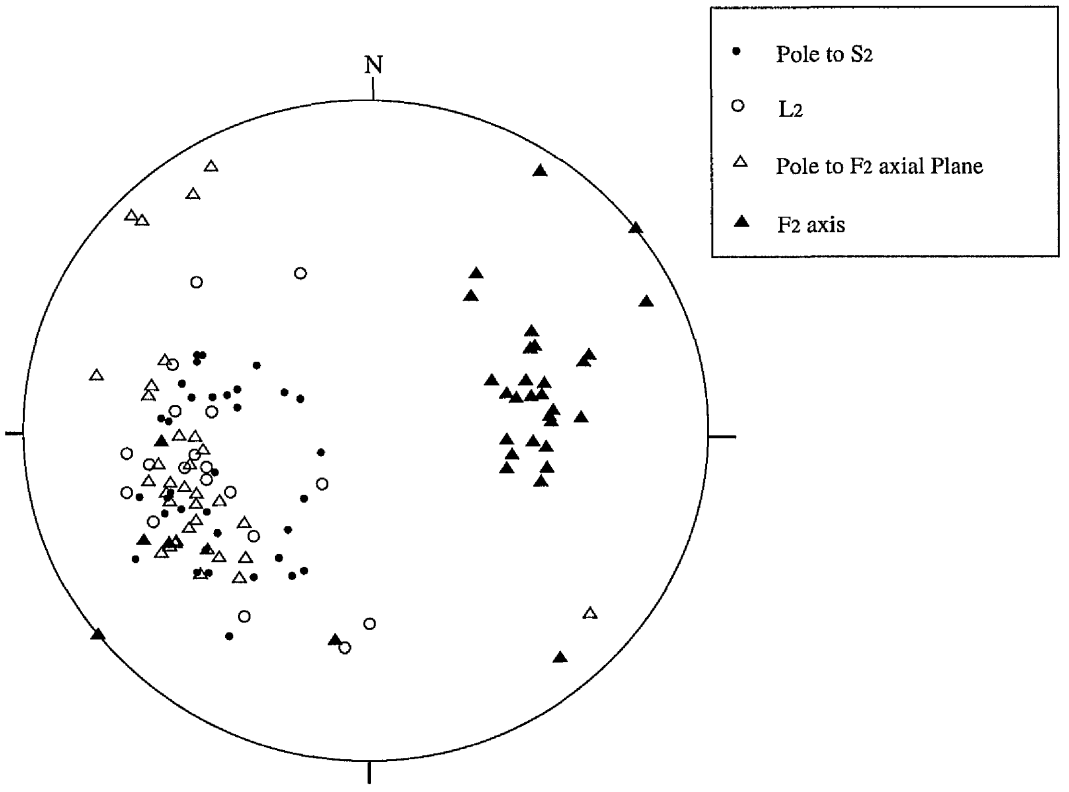

Fig. 4.19 Stereoplot for D2 deformational phase in the North Loch Awe sub-area. The main direction of F2 axes is to SW and the L2 lineation also plunges toward the SW.

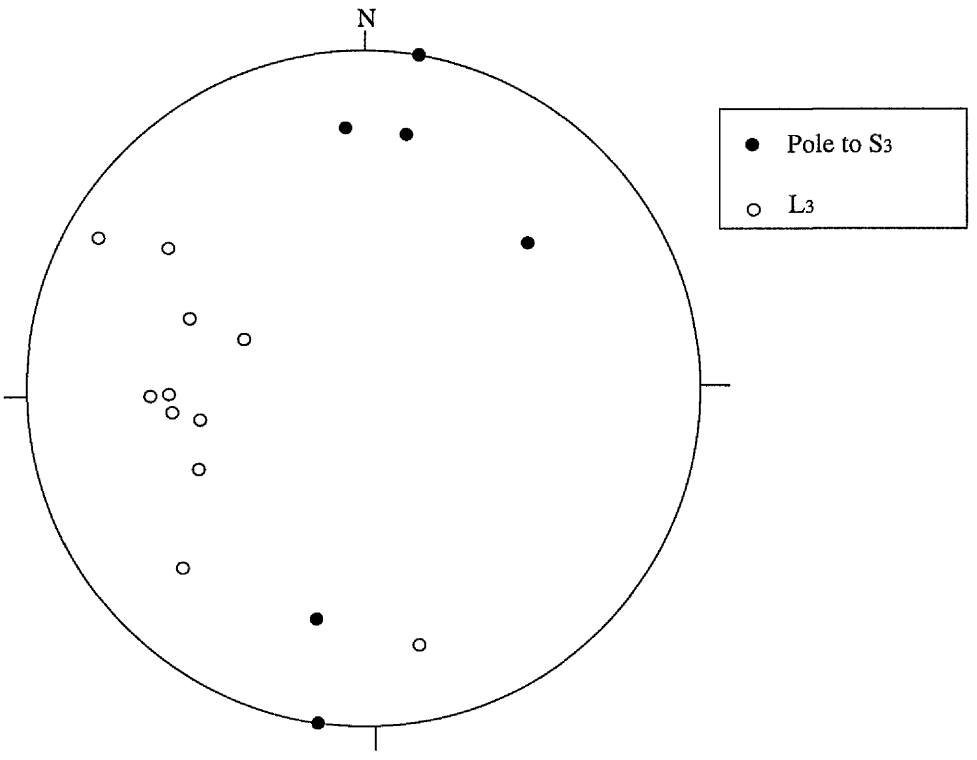

Fig. 4.20 Stereoplot for D3 deformational phase in the North Loch Awe sub-area. The main direction of the L3 lineation is E-W striking.

Plate 4.7 F2 fold with 'S' asymmetry in Ardrishaig Phyllite, North Loch Awe sub-area. Fold style is ptygmatic in places (locality NN08752677).

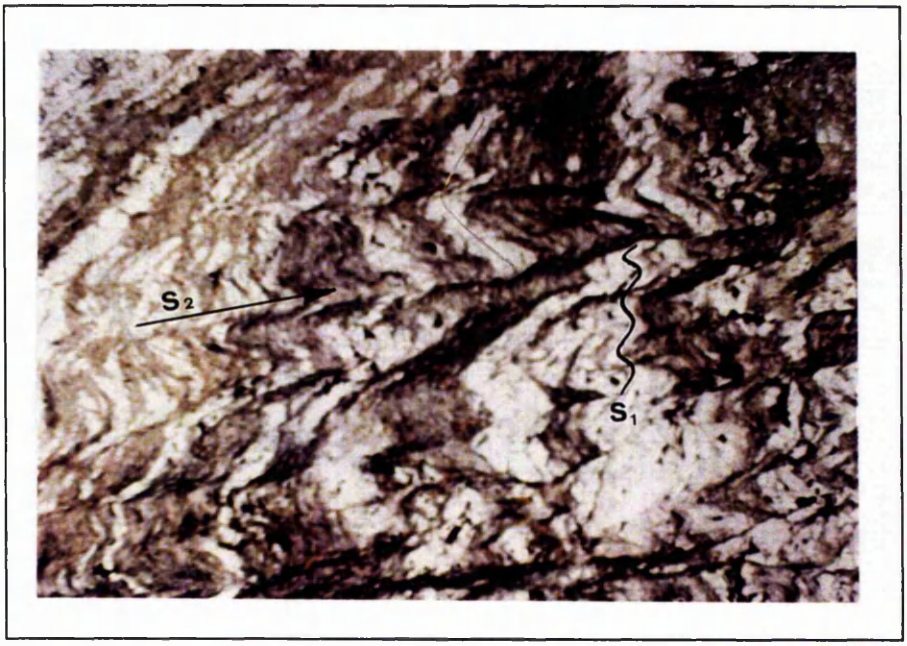

Plate 4.8 S1 slaty cleavage and S2 crenulation cleavage in the pelitic rocks of Ardrishaig phyllite, North Loch Awe sub-area. PPL, field of view 5.5×3.5 mm.

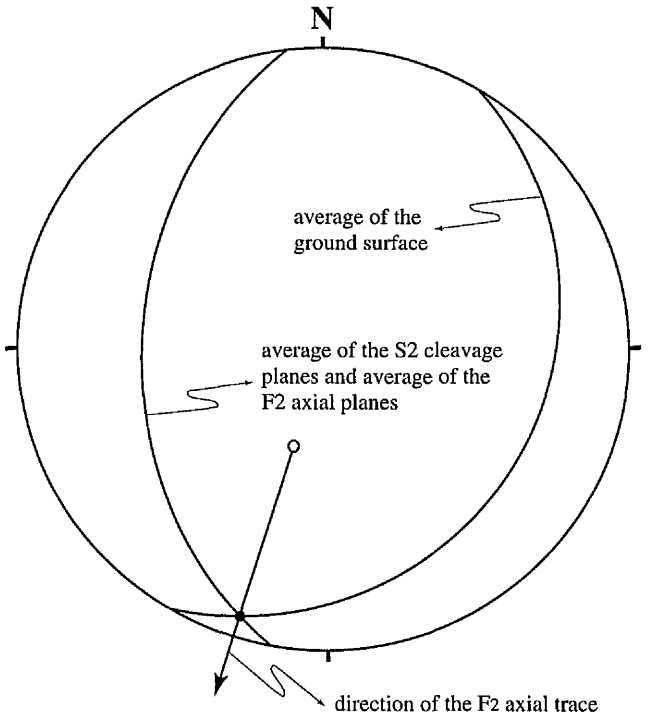

Fig. 4.21 Intersection of great circles representing the erosion surface on SE flank of Monadh Driseig (North Loch Awe sub-area) and average of S2 cleavage planes and F2 axial planes. The intersection indicates the direction of the F2 axial traces.

4.7 Summary

Three deformational phases were recognised in the Etive area as below:

-D_1 deformational phase which is represented by S_1 slaty cleavage and L_1 stretching lineation and S_0/S_1 intersection lineation.

-D_2 deformational phase which is represented by F_2 folds and S_2 crenulation cleavage mainly axial planar to the F_2 folds.

-D_3 deformational phase which is represented by a gentle S_3 Crenulation cleavage.

On the eastern side of the Etive area (Loch Creran sub-area) the S_1 schistosity of the D_1 deformational phase is the dominant structure. The overall strike direction of So and S1 in this sub-area is NW-SE (sub-parallel to the igneous contact) and the dip is to the SW.

In the Bonawe sub-area also the main structure is S_1 slaty cleavage with an overall NW-SE direction and SW dip.

In the Loch Awe sub-area S_o and S_1 also dip to the SW but the main structures are S_2 crenulation cleavage and F_2 folds of the D_2 deformational phase. The main strike

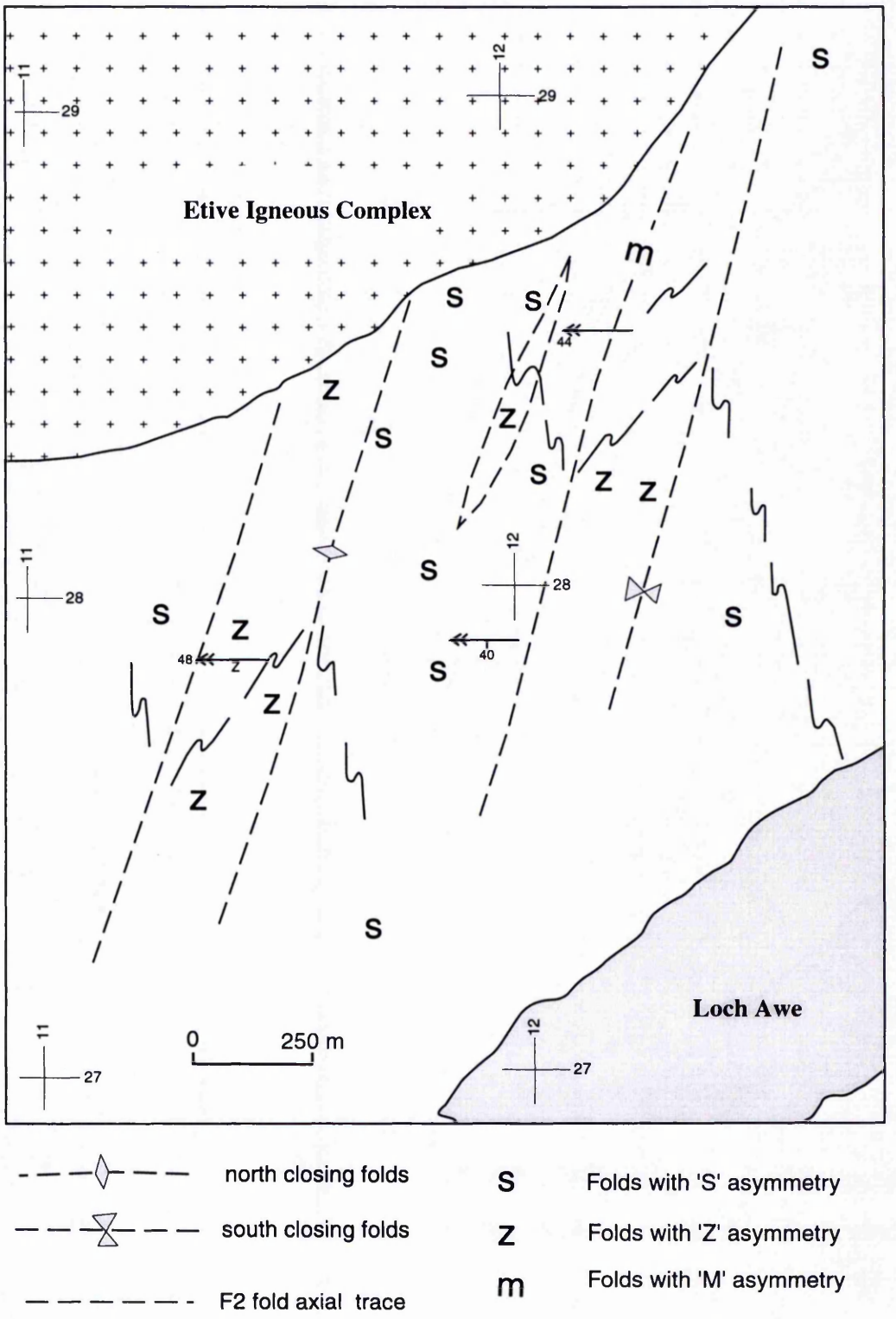

Fig. 4.22 Axial traces of the F2 folds in the North Loch Awe sub-area. Bedforms shown schematically.

direction of S_2 crenulation cleavage is NE-SW dipping to the NW and the main direction of F_2 axes is plunging to the SW.

5.1 Introduction

The main objective of this chapter is to provide a systematic petrographical investigation of different metamorphic rocks in the Etive aureole. The information from petrography will be used for: (i) choosing suitable mineral assemblages with low variance (i.e. a large number of mineral phases in equilibrium together) for mineral chemistry, phase relations and thermobarometric studies (ii) working out metamorphic zonal sequences in different Dalradian lithologies within the aureole and (iii) identifying possible contact metamorphic reactions. The main metamorphic rock types considered in this chapter are basic rocks, non-graphitic pelitic and semi-pelitic rocks, graphitic pelitic and semi-pelitic rocks, calc-silicates and marbles. 288 thin sections of metamorphic rocks were studied. 201 thin sections were made of samples collected during the field studies, 26 thin sections were donated by Dr. J. Treagus, 26 thin sections were donated by Dr. Droop and 35 thin sections (of samples collected and catalogued by Dr. Droop) were loaned from the Harker Collection, University of Cambridge.

Abbreviations for mineral names, used in this chapter are after Kretz (1983).
In this chapter the term 'Mineral assemblage' is used to describe the mineral association including peak metamorphic minerals, relict minerals and products of retrograde alteration whilst the term 'parageneses' is used to show the peak metamorphic minerals in equilibrium.

5.2 Metamorphosed Basic Rocks

Metamorphosed basic igneous rocks of the Dalradian Supergroup are mainly thin bands of pyroclastic or detrital volcanic materials in the Ardrishaig Phyllite in the Argyll Group of the south-west Highlands (Borradaile, 1973), the Tayvallich and

Loch Avich Volcanics which occur as frequently pillowed lavas and intercalated tuffs in the Southern Highlands Group (Harris and Pitcher, 1975), and contemporaneous and comagmatic suites of dolerite and gabbro sills which were intruded into the underlying sediments while the latter were still unconsolidated (Wilson and Leake, 1972; Borradaile, 1973; Graham, 1976; see section 2.8).

Pre-or early tectonic basic intrusions known as the Older Basic Intrusions are also well developed in the Argyll Group metasediments and the Loch Tay limestone. Numerous basic horizons are also found in the Ben Lui Schist. Isolated bodies of basic rocks are common in the south-eastern part of Loch Etive and south of Loch Awe.

The metabasic rocks in the Etive Aureole are intruded into the Glencoe Quartzite, Leven Schist, Islay Quartzite, and Ardrishaig Phyllite. They occur as sills and dykes. Nowhere in the aureole is there a continuous outcrop of metabasites from the outer aureole to the igneous contact. Therefore sample collection and field studies of the metabasic rocks have been done on separate bodies at different distances from the contact.

5.2.1 Regional metamorphic metabasites

The metamorphic rocks in the southern part of Loch Awe in the Kilchrenan area are greenschist-facies regional metamorphic rocks. Texturally two types of metabasites are recognisable: fine-grained, well-foliated and cleaved metabasites with a fine crenulation cleavage (possibly S_2), (e.g. location 92, NN05822300) and massive coarse-grained metabasites without obvious cleavage and with relict doleritic texture (e.g. NN04702297). Probably the fine-grained metabasites are after extrusive igneous rocks and the chilled margin of sills and dykes and coarse-grained rocks are after central part of doleritic sills and dykes and intrusives. The colours of the metabasic rocks are from dark green with visible amphiboles (actinolite), greenish-grey in fine-grained rock to light coloured metabasites with actinolite-rich and plagioclase-rich domains.

Three thin sections of the regionally metamorphosed basic rocks were examined and the following mineral assemblages were distinguished:

Act+Chl+Qtz+Pl+Ep+Cal±Bt [5.1]

Act+Chl+Qtz+Ep±Czo. [5.2]

Stilpnomelane was found in one sample of the regional metamorphic metabasites. It is brownish-green in this rock and has crystals of mm scale. Oxide minerals (hematite and ilmenite), zoisite, clinozoisite, apatite and sphene are minor phases in these rocks.

The main texture in the foliated rocks is the lepidoblastic texture due to the arrangement of chlorite flakes (Plate 5.1). Actinolite shows sub-hedral crystals mainly pseudomorphing igneous augite. Plagioclase also forms sub-hedral crystals. There are some patches of chlorite possibly after original olivine. In the massive rocks, relict doleritic texture is visible; actinolite is replacing igneous augite and ore minerals (ilmenite) have original doleritic texture with skeletal crystals.

Pleochroic actinolites with yellowish green to green colours are up to 1mm in length. Some of the crystals show simple twinning. Chlorite, which is a major phase in most of the rocks, has anomalous violet birefringence colour, which indicates its Fe-rich nature. Plagioclase which mainly is albite-rich (optical determination) is slightly altered to clay minerals and sericite. Biotite is present in tiny amounts with small flakes of greenish-brown colour. Muscovite flakes are up to 1.5 mm long with slightly green pleochroism probably owing to the Cr-bearing (fuchsite) composition. Epidote, calcite, apatite (occasionally as large idioblastic crystals), ilmenite and sphene are common minor phases.

5.2.2 Contact Metamorphic Metabasites

Forty-three thin sections of the thermally metamorphosed metabasites were studied and the following parageneses were distinguished :

Act+Chl+Bt+Ep+Qtz+Pl [5.3]

Act+Hbl+Chl+Cal+Pl+Ep+Qtz [5.4]

Hbl+Chl+Bt+Ep+Pl+Qtz±Ms [5.5]

Hbl+Pl+Cal+Qtz+Czo [5.6]

Hbl+Pl+Bt+Chl+Qtz [5.7]

Hbl+Bt+Cpx+Ep+Pl±Qtz±Czo	[5.8]
Hbl+Bt+Cpx+Pl+Qtz	[5.9]
Hbl+Cpx+Bt+Pl+Spl	[5.10]
Hbl+Cpx+Opx+Pl±Qtz	[5.11]
Hbl+Cpx+Opx+Bt+Pl±Qtz	[5.12]

Hematite, ilmenite, apatite and sphene are minor phases in most of the rocks. Retrograde chlorite, amphibole, calcite and epidote are present in some of the samples. Regional metamorphic garnet is present in three samples.

The metabasic rocks in the Etive Aureole can be divided into three categories according to their mineral assemblages: (a) assemblages with amphibole and without pyroxene (low-grade rocks); (b) assemblages with amphibole and clinopyroxene (medium-grade rocks) and (c) assemblages with amphibole and two pyroxenes (high-grade rocks).

a) Assemblages with amphibole and without pyroxene (low grade rocks):

The low-grade rocks generally have a lepidoblastic texture due to orientation of chlorite, hornblende and biotite. The first influence of thermal metamorphism observed as the igneous contact is approached is recrystallisation of biotite and actinolite. Hornblende is the first new contact-metamorphic mineral encountered. Crystallisation of hornblende has developed local microgranular textures in the low-grade rocks. In the samples with two amphiboles, actinolite and hornblende, actinolite is restricted to the inner core of hornblende-actinolite aggregates. Other minerals in these rocks are plagioclase, epidote, ilmenite and quartz.

Hornblende is the predominant mineral in the low-grade rocks. It has green to greenish-brown colour with subhedral crystals. Plagioclase is the other dominant mineral and has an albite-rich composition (~$An_{0\text{-}10}$, optical determination). Chlorite is stable in some of the samples but its birefringence colour is more greenish than the regional metamorphic chlorites probably due to a slightly higher Mg-rich composition. Biotite is well recrystallised and has strong pleochroism and dark brown colour (e.g. sample MM174, NN12542876). Epidote and/or clinozoisite, which are stable in the regional metamorphic metabasites, show an equilibrium texture with hornblende and biotite in some of the low-grade rocks. Quartz is present

in most of the samples but in some its existence is not easily proved by optical microscopy. Calcite, ilmenite, apatite, zircon and sericite are minor phases in the low-grade metabasites. The habits of the ore minerals are different from those in the regional metamorphic basic rocks. The doleritic texture of the oxide minerals has not survived contact metamorphism and skeletal oxides are changed to idioblastic crystals with granoblastic textures.

In some samples calcite crystals up to 1 mm occur. Apatite, which is a relict igneous mineral, occasionally shows large idioblastic crystals.

b) Assemblages with amphibole and clinopyroxene (medium-grade rocks):

Inherited lepidoblastic textures of regional origin are visible in some of the medium-grade rocks, but clinopyroxene, plagioclase and hornblende generally have granoblastic texture due to thermal metamorphism. Clinopyroxene occurs as fine-grained aggregates with a microgranular texture in the rocks far from the igneous contact, while it forms large crystals up to 1mm large with a granoblastic polygonal texture in the rocks closer to the contact. Hornblende is the dominant mineral in the rocks. It has granular texture and green to greenish-brown colour. Hornblende is elongated in the original actinolite layers in some of the samples. Plagioclase changes from albite to labradorite (optical determination) with decreasing distance from the igneous contact. Biotite is stable and is well recrystallised. Epidote is only stable in some of the medium-grade rocks and disappears as the igneous contact is approached. Chlorite is not stable in these rocks and the tiny amount of chlorite in some of the samples is a product of biotite alteration. Ti- bearing biotite is altered to chlorite and sphene. Calcite is present in some of the rocks but is not common. Opaque minerals (ilmenite), apatite, zircon and sphene are minor phases.

Despite the green colour of hornblende in most samples, hornblende crystals close to ilmenite commonly have a brown colour. Clinopyroxene near ilmenite also shows pleochroism. Apparently Ti diffusion from the oxide minerals has produced Ti-bearing hornblende and titano-diopsidic augite locally. Because Ti is not a very mobile element and also because of the relatively short duration of high-T condition in contact metamorphism, not all of the hornblende and clinopyroxene became saturated in Ti. The result is a spotted rock in which Ti diffusion profiles are present around ilmenites in the polycrystalline hornblende and clinopyroxene matrix.

c) Assemblages with amphibole and two pyroxenes (high-grade rocks):

Orthopyroxene appears in the high-grade rocks as medium to large (up to 3 mm) elongated and occasionally skeletal crystals. The overall texture of the rocks is granoblastic polygonal with well-crystallised grains of hornblende, plagioclase and pyroxene (Plates 5.2 and 5.3). Strongly pleochroic hornblende has greenish-brown to brown colour. Euhedral to subhedral crystals of plagioclase show polysynthetic twinning and some have optical zoning. Plagioclases in most samples are andesine to labradorite as determined by the Michel-Levy method but in sample MM141B the plagioclase is An-rich (~An_{90}). Biotite is present in some of the samples and shows strong pleochroism with a dark brown colour. Chlorite, epidote, clinozoisite and calcite are not present in the high-grade rocks. Sphene, ore minerals, apatite and zircon are minor phases.

The mineral changes during contact metamorphism can be summarised as below:

Actinolite: Actinolite is restricted to the regional metamorphic rocks and the low-grade contact-metamorphic rocks; in the latter it is restricted to the cores of hornblende-actinolite aggregates. At higher grades it breaks down to form hornblende.

Hornblende: Hornblende is the dominant mineral in most of the rocks. In the low-grade rocks it has green colour and with increasing grade (decreasing distance from the igneous contact) it becomes greenish brown to brown.

Biotite: Tiny flakes of green biotite are stable in the regional metamorphosed basites. It has recrystallised and has changed from green to brown in colour in the contact metamorphic condition. Biotite is not common in all of the samples but it is stable in the low-grade rocks and in the high-grade rocks adjacent to the contact.

Epidote and clinozoisite: Epidote or clinozoisite are stable in regional metamorphic metabasites and in the low grade contact metamorphic rocks. They disappear in the medium and high-grade rocks.

Plagioclase: Plagioclase is stable in the regional metamorphic rocks, low-grade contact metamorphic rocks and high-grade contact-metamorphic rocks. Apparently the mineralogical composition of plagioclase becomes An-rich by increasing the metamorphic grade.

Fig. 5.1 illustrates the mineral distribution in the regional and contact metamorphic basic rocks in the Etive aureole. Table 5.1 contains all full assemblages in the metabasic rocks in the Etive area.

5.2.3 Retrogressive alteration of metabasic rocks

Peak metamorphic mineral assemblages are altered (retrograded) to more hydrous and CO_2-bearing phases in some of the samples. The alteration is not wide-spread in the aureole and is restricted to some localities. For instance, some samples adjacent to the plutonic rocks are altered. Most of the studied samples from the metabasic rocks are very fresh without alteration. The main alteration products are chlorite after biotite, tremolite after pyroxene, epidote after clinopyroxene and hornblende and calcite after calcium-bearing phases. Tiny amounts of sericite in some samples is after biotite and feldspar. Prehnite in samples MM37C and MD3B is considered as an alteration product. Because of the limited extent of alteration within the aureole the amount of fluid was probably not appreciable in the early stages of cooling.

5.2.4 Distribution of the mineral zones and isograds in the metabasic rocks

According to the mineral assemblages presented in Table 5.1 and distribution of the assemblages in the Etive aureole (Fig. 5.2) four mineralogical zones are recognised in the metabasic rocks. These zones are discussed below.

Zone I (Regional metamorphic zone): This zone includes regional metabasites, which have experienced no contact metamorphic effect, and includes all assemblages with chlorite and actinolite. This zone can be divided into three sub-zones, including Act+Chl±Cal+Qtz and Act+Chl+Bt+Qtz assemblages and assemblages with hornblende and garnet. No systematic sample collection and zoneography was carried out in the regional metamorphic rocks. The first two assemblages were not seen in the southern segment of the Etive aureole (north of Loch Awe) and are studied in samples collected from greenschist-grade rocks. The presence of assemblages with garnet was deduced from the relict regional metamorphic assemblages in the aureole.

Zone II (Hornblende Zone): The first zone which appears in the southern segment of the Etive aureole is Zone II which includes assemblages containing contact

Table 5.1 Mineral assemblages in metabasites. X =major phase, O =minor phase, A =alteration product, R= altered mineral inferred from pseudomorph. Abbreviations after Kretz (1983).

Sample No.	G.R.	Act	Hbl	Chl	Bt	Pl	Qtz	Cpx	Opx	Cal	Ep	Czo	Ttn	Ore	Ms	Grt*	Prh	Ap	Zrc
MM88[R]	NN0686253			X	X	X	?			X	X		X	X				O	
MM94[R]	NN05502359	X		X		X	X			X	X		O	O				O	
MM98A[R]	NN02573187	X					X				O	O	O	O				O	
MD2A	NN11222725		X	O	X	X	X				O		O	O	O^A	X		O	O
MD3C	NN11072728		X	O^A		X	?			X		X		O					
MD3A	NN11072728	X		X	X	X	X				X		O	O				O	O
MM55	NN11742692		X	X	X	X	X			X	X			O		X			
MM57B	NN11402669		X	O	X	X	X							O				O	O
MM61F	NN10082593		X	X	X	X	?				X		O	O					O
MM127A	NN11652726		X		X	X	X						O	O	O^A				
MM174A	NN12542876		X	O	X	X				O	O			O					O
MM180A	NN13022814	O^A	X	O^A		X				X	X	X		O	O^A			O	
MD3B	NN11072728	O^A	X^R	O^A	X	X	X	X		O				O	O^A		X^A		
MD5B	NN11022756			X		X	X	X			X			O				O	O
MD11A	NN11912849		X			X		X		O			O	O					O
MM36G	NN08452702	O^A	X		X	X								O				O	O
MM37C	NN08472693		X	O^A		X		X		O	O		O	O	O^A		O^A	O	
MM49	NN07992703		X		X	X	X	X				O	O	O					O
MM50	NN08052709		X			X		X					O	O					
MM53A	NN07982679	O^A				X	X	X			O		O	O				O	O
MM127B	NN11652726	X^A		O^A	X		X	X			X			O		X			
MM138D	NN11252818	O^A	X	O^A	X	X	X	X					O	O	O^A			O	O
MM142	NN11502828	O^A	X	O^A	X	X	X	X		O	O			O				O	O
MM148A	NN11782812		X			X		X			O^A			O	O^A				
MM150	NN11852798		X			X	?	X		O	O			O	O^A				
MM187B	NN12052830		X	O^A		X		X			O^A			O					O
MM182C	NN12452795		X		X	X	?	X				X		O					O
MM188A	NN11992832	O^A	X	O^A	X	X		X		O	O^A		O	O					

* Regional metamorphic mineral.
R Regional metamorphic rock.

Sample No.	G.R.	Act	Hbl	Chl	Bt	Pl	Qtz	Cpx	Opx	Cal	Ep	Czo	Ttn	Ore	Ms	Grt*	Prh	Ap	Zrc
MM191	NN11912840		X	O^A	X	X		X					O	O					
MD8C	NN11092809		X			X	?	X	X		O^A		O	O				O	O
MD8D	NN11092809		X		X	X		X	X		O^A			O					O
MD11B	NN11912849		X		X	X	?	X	X		O^A			O					
MM113	NN09552734				X	X	X	X	X			O^A		O					
MM141B	NN11422828	O^A	X		X	X	X	X	X					O	O^A				O
MM162B	NN12722923		X	O^A	X	X	X	X	X					O	O^A				
MM164B	NN12572905		X		X	X	?	X	X					O					
MM165	NN12482896		X	O^A		X	X	X	X					O					O
MM166B	NN12482896		X		X	X	X	X	X					O					
MM167	NN12402890		X			X	X	X	X					O					
MM168A	NN12352880	O^A	X			X		X	X					O	O^A				
MM175	NN12582873		X	O^A		X	?	X	X			O^A		O					
MM192A	NN11902852		X		X	X		X	X^R					O					O
MM196A	NN12302877		X		X	X	X	X	X					O				O	O
MM196B	NN12302877		X		X	X	?	X	X					O					O
MM198B	NN12492911		X		X	X	?	X	X					O					O
MM223E	NN12622948		X		X	X	X	X	X					O					
MM227	NN 11972901		X		X	X	X	X	X					O					

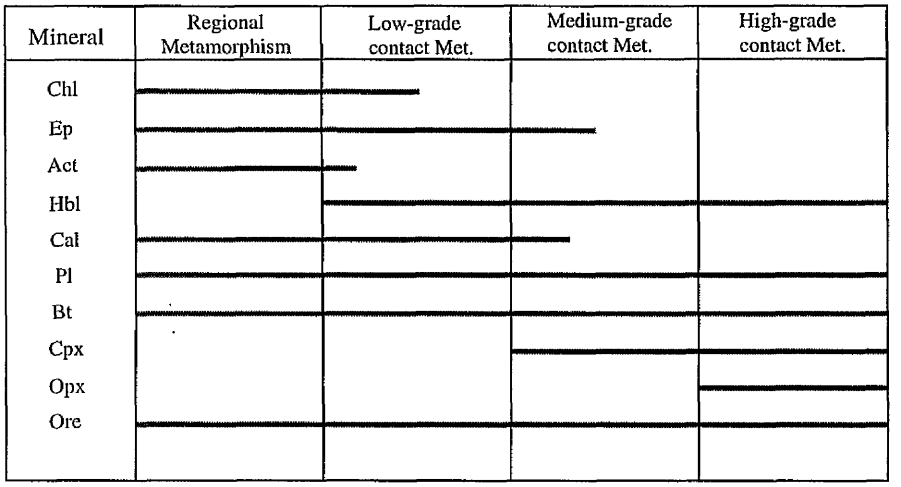

Fig. 5.1 Distribution of minerals in regional metamorphic and contact metamorphic metabasites according to their metamorphic grade.

metamorphic hornblende and biotite. Regional metamorphic actinolite, epidote and chlorite are stable in some samples from this zone. The width of this zone is about 300-350 m in the north Loch Awe area.

Zone III (Clinopyroxene Zone): This is the widest metabasite zone in the Etive aureole and includes assemblages containing clinopyroxene and hornblende with or without epidote. The width of this zone is about 650-800 m. This zone is divided into two sub-zones, based on the presence of epidote, which are sub-zone IIIA and sub-zone IIIB. Sub-zone IIIA contains all assemblages with Cpx+Hbl with epidote (and/or clinozoicite) and sub-zone IIIB represents the distribution of assemblages with Cpx+Hbl without epidote and clinozoisite. Stable epidote and clinozoisite are subhedral and are in mutual contact with other peak contact-metamorphic phases like Qtz, Hbl and Px , but epidotes produced by retrogression are fine-grained and are associated with other retrogressive products such as chlorite and sericite. Where epidote was found only in veins and not in the rock matrix, it was not considered as the peak contact-metamorphism phase.

Zone IV (Orthopyroxene Zone): This zone is the highest in metamorphic grade and includes all assemblages with Opx+Cpx+Hbl. The width of this zone is about 200m.

Fig. 5.2 illustrates the distribution of sample localities and mineral zones in the southern segment of the Etive aureole. Transition from Zone II to Zone III is marked by Cpx-in isograd, transition from Sub-zone IIIA to Sub-zone IIIB is marked by Ep-out isograd and transition from Zone III to Zone IV is marked by Opx-in isograd

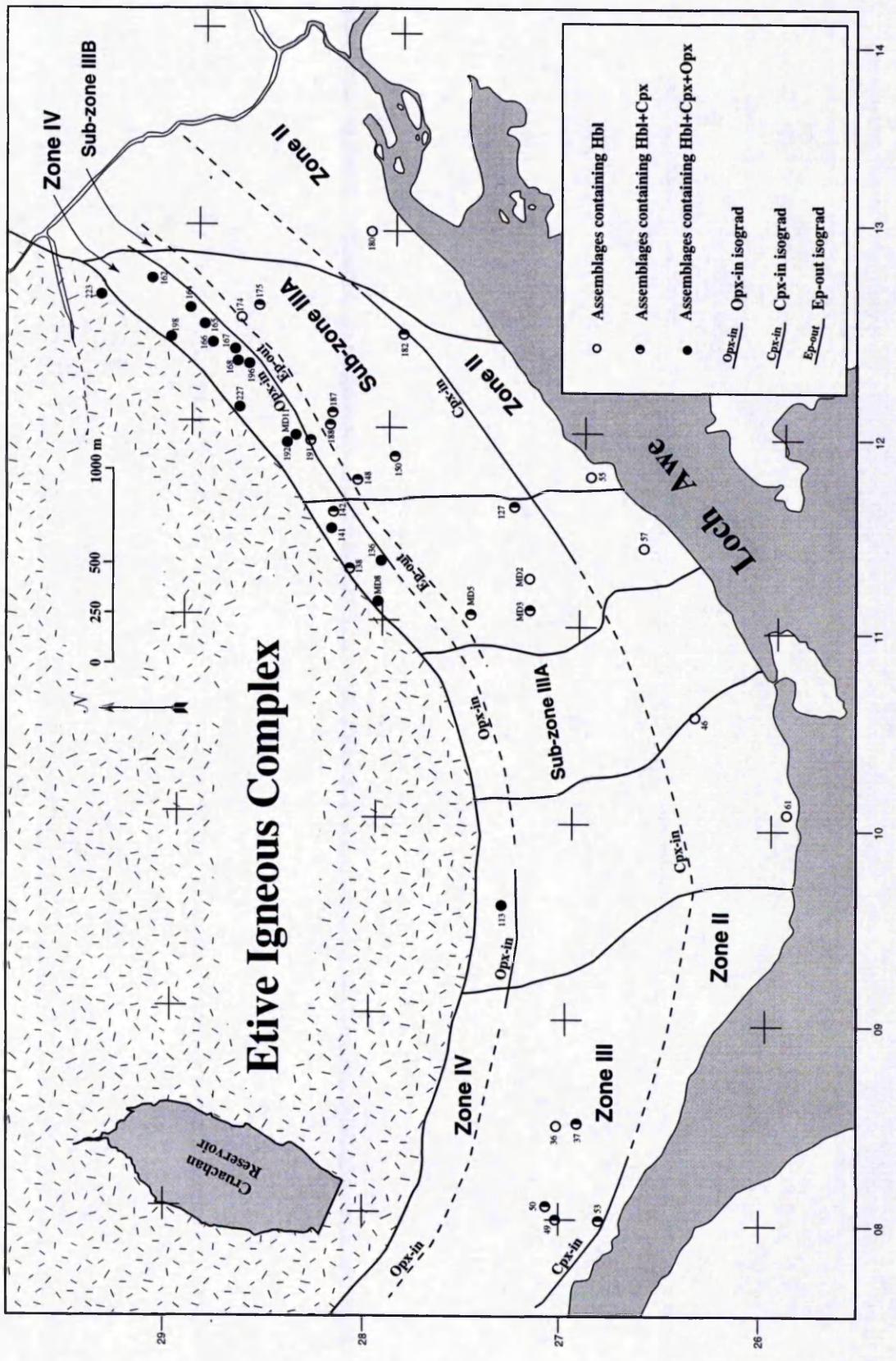

Fig. 5.2 Distribution of sample localities, metamorphic zones and isograds in metabasites in the North Loch Awe area.

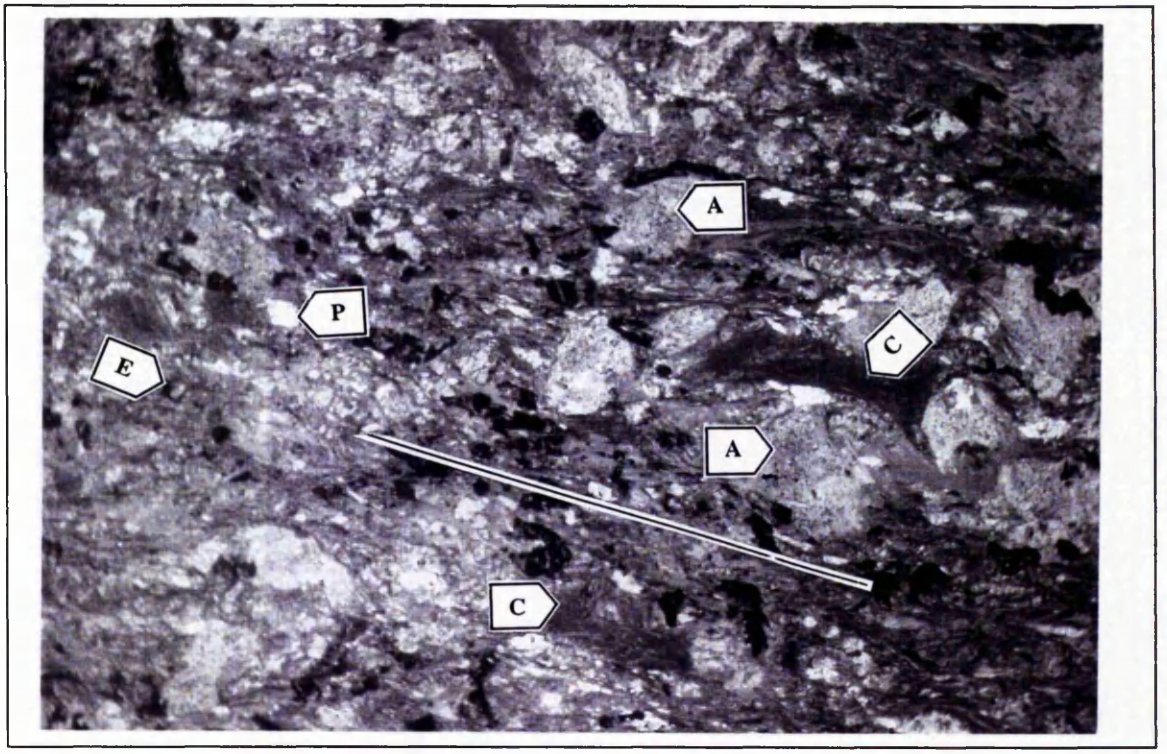

Plate 5.1 Regional metamorphic greenschist (MM94) containing actinolite (A), Chlorite (C), Plagioclase (P), epidote (E) and opaque minerals (black). Possible S_2 foliation is marked. PPL. Field of view 12×8 mm.

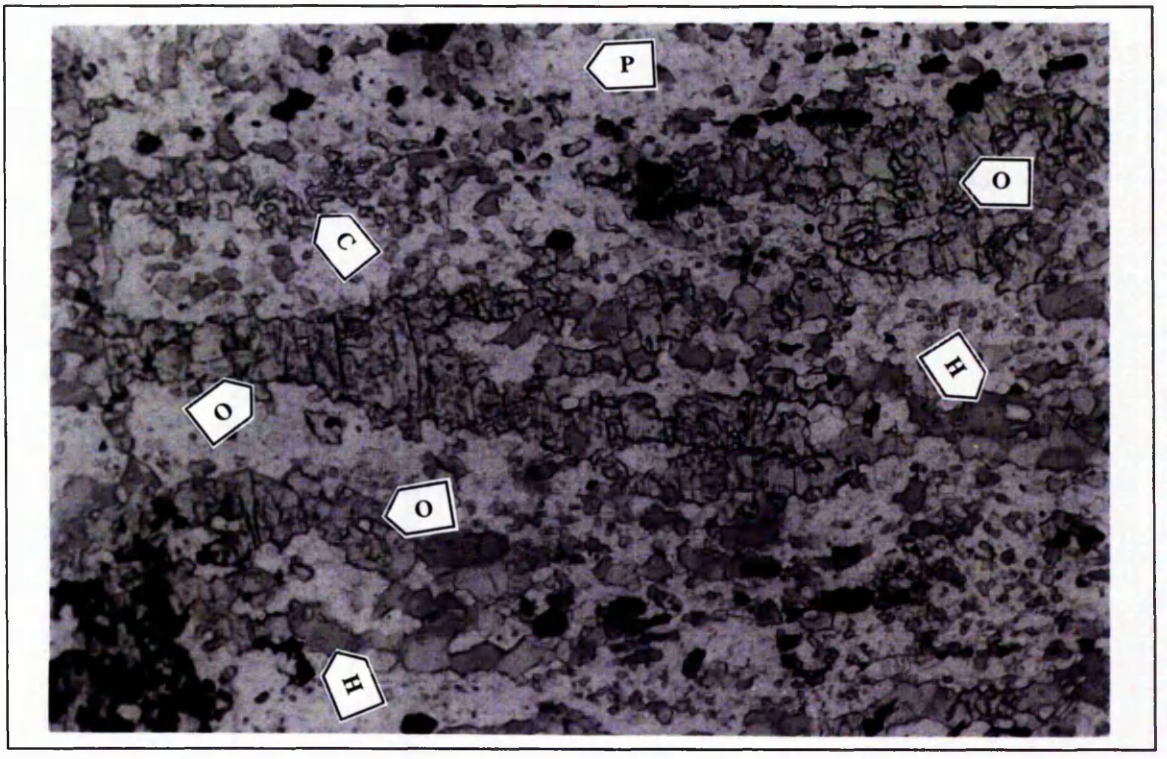

Plate 5.2 High grade contact-metamorphic metabasite (MM198B) containing orthopyroxene (O), clinopyroxene (C), hornblende (H), plagioclase (P) and opaque minerals (black). Granoblastic polygonal texture is well developed and all minerals show a high degree of textural equilibrium. PPL. Field of view 0.6×0.4 mm.

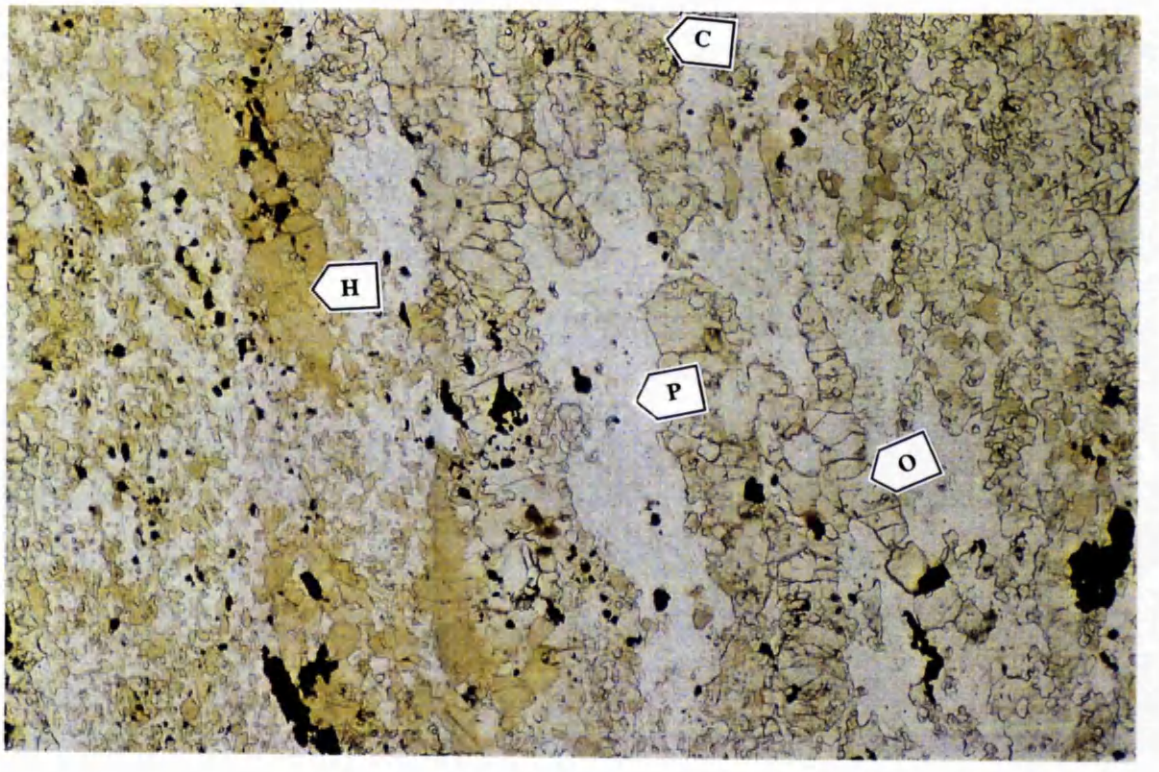

Plate 5.3a Mafic hornfels sample MM168A (G.R. NN12352880) containing orthopyroxene (O), clinopyroxene (C), hornblende (H), plagioclase (P) and ilmenite (black). PPL. Field of view 1.6mm.

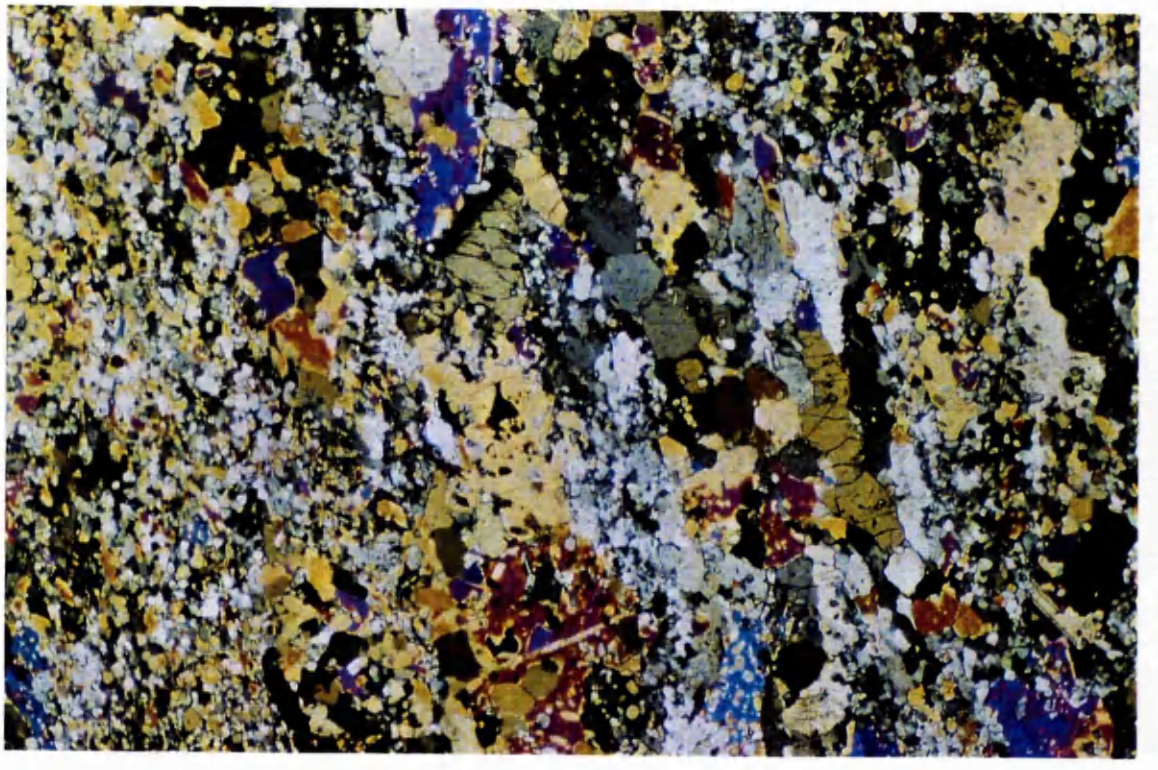

Plate 5.3b As above, in XPL, to show granoblastic polygonal texture.

Table 5.2 Summary of the mineral zones, diagnostic assemblages and isograds in the metabasic rocks

Zone	sub-zone	diagnostic assemblages	isograds
Zone I, Regional	Ia	Act+Chl±Cal+Qtz	
metamorphic	Ib	Act+Chl+Bt+Qtz	
metabasites	Ic	Hbl±Act+Grt±Bt+Qtz	
Zone II		Act+Hbl+Chl±Cal±Bt+Qtz+Ep±Czo	
Hornblende Zone		Hbl+Chl±Cal±Bt+Qtz+Ep±Czo	
Zone III	IIIa	Hbl+Cpx±Cal±Bt+Qtz+Ep (and/or Czo)	Cpx-in
Cpx-Zone	IIIb	Hbl+Cpx±Bt+Qtz	Ep-out
Zone IV Opx-Zone		Hbl+Cpx+Opx±Bt+Qtz	Opx-in

(Fig. 5.2). The Hbl-in isograd was not seen in the southern segment in the Etive aureole. Table 5.2 includes a summary of the mineral zones and isograds in the metabasic rocks. The possible metamorphic reactions responsible for formation of new contact metamorphic phases and mineral zones will be discussed in Chapter eight.

5.3 Petrography of the non-graphitic pelites and semi-pelites

The main pelitic rock body in the aureole is the Leven schist, which is exposed in the north Loch Awe area. This stratigraphic unit consists of striped pelites with semi-pelites, thin quartzite and thin marble bands. Other non-graphitic units are the Glencoe Quartzite which is a fine-grained quartzite, locally pebbly and psammitic, the Islay Quartzite which consists of semi-pelitic flags interbanded with slate and quartzite and the Carn Mairg Quartzite which is made of coarse pebbly quartzite, locally graded and psammitic. The unit named the Islay Quartzite crops out between the Leven Schist and Carn Mairg Quartzite and is not graphitic. The status of this quartzite is not very clear in the north Loch Awe area, but regarding stratigraphical relations, it is likely to be equivalent to the Islay Quartzite.

5.3.1 Regional metamorphic pelites and semi-pelites

Six thin sections from the regionally metamorphosed rocks of the Leven Schist, Islay Quartzite and Carn Mairg Quartzite were studied and the following parageneses were found:

Ms+Chl+Qtz+Bt+Pl+Grt [5.13]

Ms+Chl+Qtz+Bt+Pl [5.14]

Ms+Pl+Qtz [5.15]

Ms+Chl+Qtz+Bt+Cal [5.16]

The samples were collected from localities at Glen Orchy (close to the Bridge of Orchy), Glen Strea and along the Loch Awe shore, out of the thermal aureole. Fig. 5.3 shows the locality of samples in the north Loch Awe area. The regional metamorphic rocks are silvery, greenish grey garnet-mica schists and chlorite-muscovite schists, which are well foliated and schistose. Muscovite and chlorite flakes are visible on the foliation surface. Garnet (almost entirely altered to chlorite) is up to 3 mm in size. Under the microscope, the main texture of the rocks is lepidoblastic texture owing to orientation of the chlorite and muscovite flakes. Porphyroblastic texture is developed in the garnet-bearing rocks (garnet porphyroblasts). The garnets have S-shaped inclusion trails and are therefore syn-deformational. In some samples the main foliation (probably S_2) wraps the biotite and chlorite clots after garnet indicating pre- or syn-deformational crystallisation of original garnets. Apatite, titanite, oxide minerals (ilmenite), tourmaline and zircon are common minor phases in most of the studied samples. Table 5.3 includes the mineral assemblages in the studied non-graphitic rocks.

5.3.2 Contact metamorphic pelites and semi-pelites

Eighty seven thin sections from the pelitic and semi-pelitic rocks of the Leven schist, Glencoe Quartzite, Islay Quartzite and Carn Mairg Quartzite were studied. Samples were collected in several traverses from the outer aureole towards the contact of the igneous rocks. The following mineral parageneses were determined in the studied samples. All parageneses contain plagioclase and ilmenite except [5.25], which is without plagioclase.

Ms+Bt+Chl+Qtz [5.17]

Crd+Ms+Bt+Qtz [5.18]

Table 5.3 Mineral assemblages in non-graphitic pelites and semi-pelites. X=major phase, O=minor phase, A=alteration product. R= regional metamorphic mineral, C= contact metamorphic mineral.

Sample	G.R.	Chl	Bt	Ms	Qtz	Grt^{R}	Crd	And	Kfs	Sil	Crn	Spl	Grt^{C}	PL	Opx	Ilm	Zirc	Ap	Ttn	Tour	Ore
MM256B^{R}	NN18602747	X	X	X	X	X															O
MM255B^{R}	NN166273	X	X	X	X												O	O			O
MM255C^{R}	NN166273	X	X	X	X												O				O
MM43B	NN09912643	X	X	X	X																O
MM61E	NN10082593	X		X	X									X			O		O	O	O
MM61B	NN10082593	X		X	X												O				O
MM57A	NN11402669		X	X	X																O
MM56A	NN11562680	O^{A}	X	X	X									X			O	O			O
T802	NN111262			X	X																O
T801	NN104260	X	X	X	X									X			O		O		O
MM56B	NN11562680		X	X	X									X			O			O	O
MM288E	NN10832615	X	X	X	X																O
MM222	NN13372837	X	X	X	X	X	X							X			O	O		O	O
T950	NN117270	O^{A}	X	X	X		X														O
T952	NN123275		X	X	X		X							X				O	O		O
MM180B	NN13022814		X	X	X		X							X			O	O		O	O
MM153	NN12032771		X	O^{A}	X		X		X								O	O		O	O
MM182A	NN12452795	O^{A}	X	O^{A}	X		X		X								O	O		O	O
MM120	NN09982719		X	O^{A}	X		X		X								O	O			O
MD13	NN124281	O^{A}	X	O^{A}	X		X		X					X			O				O
MM125A	NN11772728		X	O^{A}	X		X	X	X					X							O
MM127D	NN11652726	O^{A}	X	O^{A}	X		X	X	X					X			O			O	O
MM126B	NN11742731	O^{A}	X	O^{A}	X		X	X													O
MM145B	NN11652831	O^{A}	X		X									X			O	O			O
MM154	NN12062760	O^{A}	X	O^{A}	X		X	X	X					X			O	O			O
MM144	NN11612834		X	O^{A}			X	X	X					X			O		O	O	O
MM155	NN12082746	O^{A}	X		X	X	X	X	X					X			O	O		O	O
MM181	NN12492787		X	O^{A}	X		X	X	X					X			O	O			O
MM186A	NN12092826		X	O^{A}			X	X	X								O				O
MD1	NN11392618		X	X	X		X	X	X								O	O		O	O
MD14	NN126279		X		X		X	X	X					X							O
MM121$_{a}$	NN09942710		X	O^{A}	X		X	X	X					X							
MM121$_{b}$	NN09942710		X	O^{A}			X	X	X		X			X			O	O			O
MM188C	NN11992832		X	O^{A}			X	X	X		X			X			O	O			O
MM188D	NN11992832		X	O^{A}			X	X	X		X			X			O			O	O
MM187A	NN12052830		X	O^{A}			X	X	X		X			X			O				O
MM185B	NN12202825		X	O^{A}			X	X	X		X			X			O				O
MM184B$_{a}$	NN12312818		X	O^{A}			X	X	X		X			X			O	O			O
MM184B$_{b}$	NN12312818		X	O^{A}	X		X	X	X					X			O	O			O
MM147	NN11772815		X	O^{A}			X	X	X		X			X			O		O		O
MM133$_{a}$	NN11442787		X				X	X	X					X							O
MM133$_{b}$	NN11442787		X		X		X	X	X			X		X							

Table 5.3 Continued.

Sample	G.R.	Chl	Bt	Ms	Qtz	Grt^{R}	Crd	And	Kfs	Sil	Crn	Spl	Grt^{C}	PL	Opx	Ilm	Zirc	Ap	Ttn	Tour	Ore
MM130B	NN11312749		X				X	X	X		X			X							O
MM129$_a$	NN11572755		X		X		X	X	X					X			O			O	O
MM129$_b$	NN11572755		X				X	X	X		X			X			O			O	O
MM128A$_b$	NN11642734	O^{A}	X	O^{A}	X		X	X	X												O
MD8B$_a$	NN112281		X				X	X	X		X						O		O		O
MD8B$_b$	NN112281		X		X		X	X	X					X			O		O		O
MM135A	NN11372795		X				X		X		X	X		X							
MM135B	NN11372795		X		X		X		X					X							O
MM134A	NN11392790		X		X	X	X		X				X	X				O			O
MM131B$_a$	NN11342763		X		X		X	X	X												O
MM131B$_b$	NN11342763		X				X	X	X		X	X									O
MM176	NN12642859		X		X		X	X	X			X		X			O	O			O
MM192B	NN11902852		X	O^{A}			X	X	X		X	X		X			O				O
MD5$_a$	NN110278	O^{A}	X	O^{A}			X	X	X		X	X		X							O
MD5$_b$	NN110278	O^{A}	X	O^{A}	X		X	X	X					X							O
MM151	NN11882786		X				X	X	X			X		X			O	O			O
MD12B$_a$	NN120284		X	O^{A}			X	X	X		X	X					O	O			O
MD12B$_b$	NN120284		X	O^{A}	X		X	X	X								O	O			O
MD7B$_a$	NN110279		X	O^{A}			X	X	X		X	X		X							O
MD7B$_b$	NN110279		X	O^{A}	X		X	X	X					X							O
MM146	NN11732834		X				X	X	X		X	X		X			O	O			O
MM171	NN12412878		X	O^{A}			X	X	X		X	X		X				O			O
MM174B	NN12542876		X				X	X	X			X		X			O	O			O
MM167C	NN12402890		X				X	X	X	X	X	X		X			O				O
MM169B	NN12322875		X				X	X	X	X		X		X			O				O
MM195C	NN12282874		X				X	X	X	X	X	X		X			O	O			O
MM166J	NN12482896		X				X		X			X		X			O				O
MM166F	NN12482896		X				X	X	X	X		X		X			O				O
MM166D	NN12482896		X				X	X	X	X	X	X		X			O	O			O
MM166C	NN12482896		X				X	X	X	X	X	X		X			O				O
MM166A	NN12482896		X				X		X				X	X			O				O
MM162A	NN12722923	O^{A}	X	O^{A}	X		X		X					X			O	O			O
MM162B	NN12722923		X				X	X	X	X		X		X			O				O
MM143	NN11572835		X				X	X	X	X	X	X		X			O	O			O
MM141A	NN11432828		X	O^{A}			X	X	X	X	X	X		X			O	O			O
MM197B	NN12412900		X				X	X	X	X	X	X		X			O				O
MM195A	NN12282874		X		X		X		X					X			O	O			O
MM197A	NN12412900		X	O^{A}			X	X	X	X	X	X		X			O	O			O
MM189A	NN11982835		X	O^{A}			X	X	X		X	X		X			O		O		O
MD9A^{Xn}	NN112283		X				X		X	X	X	X		X							O
MD9B^{Xn}	NN112283		X	O^{A}			X	X	X	X	X	X		X			O				O
MM193D	NN11932864						X		X	X	X	X		X					O		O
MM198C	NN12492911		X		X		X							X	X		O				O
MM138B	NN11252818		X		X		X							X	X		O				O

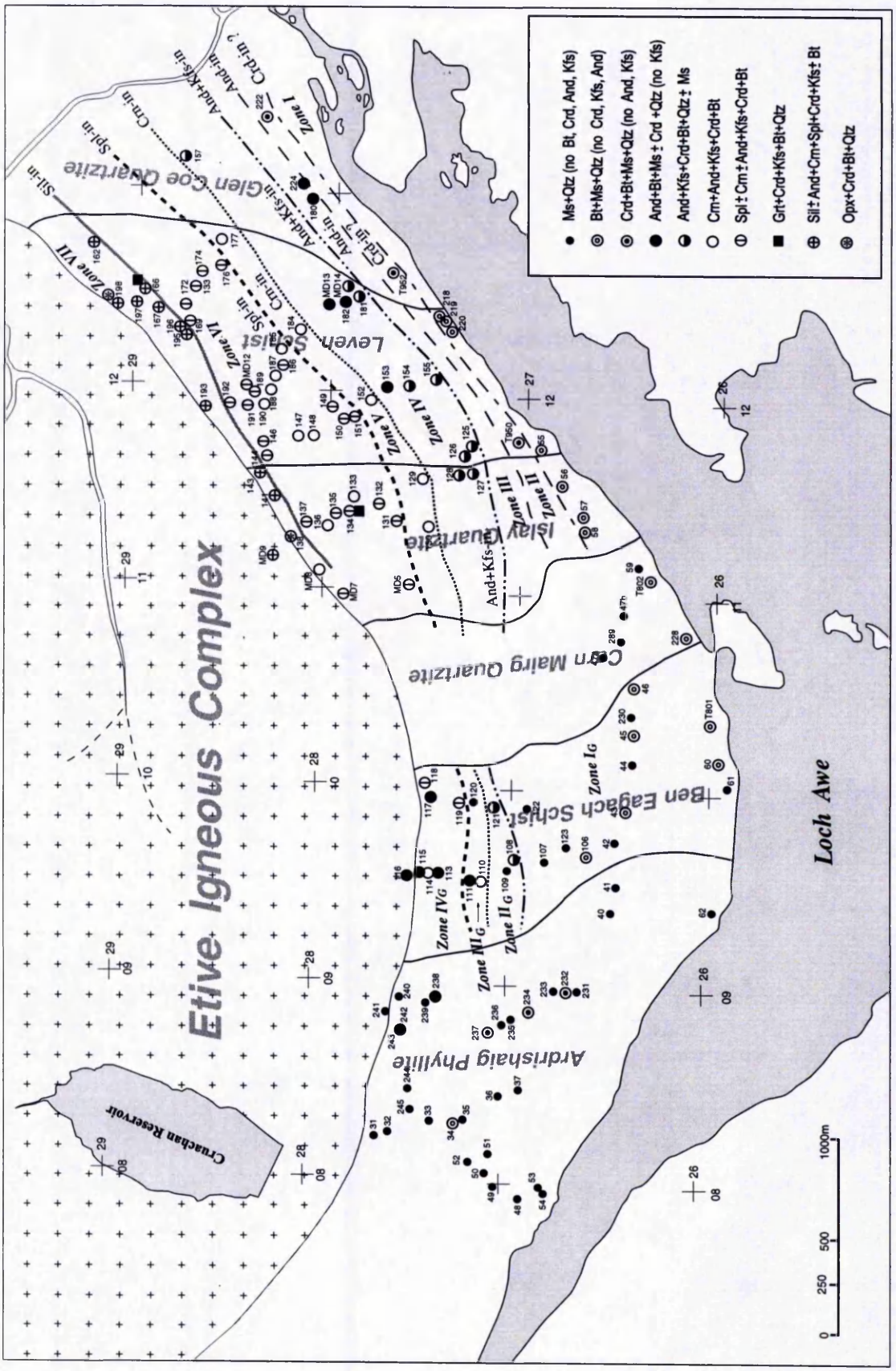

Fig. 5.3 Distribution of sample localities and mineralogical zones and isograds in the pelitic and semi-pelitic rocks in the North Loch Awe area. Lithologies from Scotland Sheet 45(E), Dalmally, BGS. All numbers representing samples have MM prefix in the map and in all figures and tables in the thesis unless otherwise is stated.

Crd+And+Bt+Qtz+Ms	[5.19]
Crd+Kfs+Bt+Qtz+Ms	[5.20]
Crd+And+Kfs+Bt+Qtz+Ms	[5.21]
Crd+And+Kfs+Bt+Qtz	[5.22]
Crd+Kfs+Bt+Qtz	[5.23]
Crd+And+Kfs+Bt	[5.24]
Crd+And+Bt+Qtz	[5.25]
Crd+And+Crn+Kfs+Bt	[5.26]
Crd+And+Crn+Spl+Kfs+Bt	[5.27]
Crd+Crn+Spl+Kfs+Bt	[5.28]
Crd+Spl+Kfs+Bt	[5.29]
Crd+And+Crn+Spl+Kfs	[5.30]
Crd+Sil+Crn+Spl+Kfs+Bt	[5.31]
Crd+And+Sil+Crn+Spl+Kfs+Bt	[5.32]
Crd+Sil+Crn+Spl+Kfs	[5.33]
Crd+Bt+Qtz+Kfs+Grt	[5.34]
Crd+Bt+Qtz+Opx	[5.35]

These parageneses can be divided into seven main groups: (1) parageneses without Crd, (2) parageneses with Crd±And±Kfs, (3) parageneses with corundum, (4) parageneses with spinel, (5) parageneses with sillimanite, (6) parageneses with contact metamorphic garnet and (7) parageneses with orthopyroxene. For full mineral assemblages in each sample see Table 5.3 and for distribution of the sample localities see Fig. 5.3.

(1) Parageneses without cordierite: The rocks of this category make the outermost part of the aureole. There are no obvious thermal effects on the rocks in field outcrops and hand specimens, except slight compaction of the rocks. The rocks are schistose and fissile with visible biotite and chlorite. Studied samples are from localities on the northern shore of the Loch Awe, localities adjacent to Loch Awe Hotel, and from road-side outcrops. Under the microscope, rocks have a lepidoblastic texture due to orientation of mica and chlorite flakes. The main mineral phases are Bt+Chl+Ms+Pl+Qtz. Apatite, zircon, oxide minerals (ilmenite) and

tourmaline are minor phases. There are two types of biotite in the rocks, one following the main foliation (probably S_2) which seems to be regional metamorphic biotite, the other overprinting the main foliation which is thought to be contact metamorphic in origin. If this deduction from the textural relations is correct, then the first effect of the contact metamorphism is recrystallisation of biotite in the aureole. Because contact metamorphic biotite is not easily distinguishable from regional biotite, biotite will not be considered as an index mineral for zoneography of the Etive aureole.

(2) Parageneses with cordierite, andalusite and alkali feldspar: In hand specimens the presence of cordierite is not obvious in the schistose rocks that crop out along the main road section in the north Loch Awe subarea. Under the microscope, cordierite is distinguishable, which is the first newly formed contact metamorphic mineral. It is altered to yellowish to orange-brown, fine-grained material (pinite) in sample T950 (GR NN123273). The main texture of the low grade cordierite-bearing rocks is lepidoblastic (arrangement of biotite and muscovite flakes, Plates 5.4 and 5.5), and the main assemblage is Crd+Bt+Ms+Qtz+Pl. Cordierite has crystallised both along the main foliation and locally in cordierite + biotite clots after regional garnet (or after chlorite which itself is after regional garnet) and clearly post-dates the S_2 crenulation cleavage. Chlorite becomes unstable as distance from the contact decreases. No Chl+Crd or Chl+And assemblages were found. The presence of cordierite is clear on the weathered surface of rocks in the higher grades (closer to the contact) where the mode and size of cordierites is appreciable. Altered cordierite makes small spherical or ellipsoidal holes on the weathered surface and has bluish colour on the fresh exposure of the rocks. Under the microscope, the amount of cordierite reaches up to ~40% (modal) of the rock. These rocks are well equilibrated texturally with granoblastic, polygonal textures with almost equal-sized biotites and subhedral to anhedral crystals of quartz. Cordierite forms relatively large poikiloblastic grains with inclusions of biotite, zircon and quartz. Pleochroic haloes are developed around zircon inclusions in the cordierite. The main assemblage of the rocks is Crd+Bt+Ms+Qtz+Pl. Apatite, zircon, ilmenite and tourmaline are common minor phases.

Cordierite coexists with alkali-feldspar in the higher-grade rocks. The main texture of these rocks is granoblastic, polygonal texture with subhedral crystals of alkali-feldspar. Andalusite-free rocks have the assemblage Crd+Bt+Qtz+Kfs+Pl±Ms. Andalusite-bearing hornfelses occur alongside these andalusite-free types in adjacent layers. Andalusite prisms stand out on the weathered surface of the andalusite-bearing rocks. It coexists with cordierite in lower-grade rocks and with alkali-feldspar at higher-grades. Andalusite-bearing rocks have a granoblastic texture with tabular, ragged and sometimes skeletal porphyroblasts of andalusite. The main assemblages are Crd+And+Bt±Qtz+Pl+Ms and Crd+And+Kfs+Bt±Qtz+Pl±Ms. According to Table 5.3, two types of assemblage may be distinguished in this category, quartz-bearing assemblages and quartz-absent assemblages. The latter is the result of quartz-consuming metamorphic reactions (see Chapter 8).

(3) Parageneses with corundum: As the grade of metamorphism increases (the distance from the contact decreases), corundum appears in the pelitic rocks of the inner aureole. Corundum-bearing rocks are well crystallised and the original schistosity is no longer present. The presence of corundum is not obvious in the field outcrops and in hand specimens. Under the microscope, corundum makes small round almost equigranular crystals, sometimes with ragged edges. Corundum is colourless in most of the samples, but in some samples it has a brownish-red colour, probably due to iron oxide in solid-solution. The main texture of the corundum-bearing rocks is granoblastic and the main assemblage is Crd+And+Crn+Kfs+Bt+Pl. Ilmenite, zircon, apatite and tourmaline are minor phases.

(4) Parageneses with spinel: Spinel forms dark-green crystals (hercynite) in the rocks. The main texture of the spinel-bearing rocks is granoblastic and the main mineral assemblage is Crd+Spl+Kfs+Bt+Pl±And±Crn. Plates 5.6 and 5.7 show two different parts of a spinel-bearing rock. Spinel is associated with Crd+And in Plate 5.6. Yellow pleochroic haloes are developed around zircon inclusions in cordierite. Spinels are dark-green to brownish-green in colour. In Plate 5.7, spinel is in association with And+Crd+Crn+Bt.

(5) Parageneses with sillimanite: Sillimanite occurs in the pelitic rocks very close to the contact (within 100 m) and in some xenoliths. Sillimanite forms elongated, prismatic crystals and fibrolitic sillimanite is absent. The main texture of the rocks is granoblastic and the characteristic mineral assemblages are Crd+Sil±And±Bt+Kfs±

Crn±Spl and Crd+Sil±And±Bt+Kfs±Qtz. Sillimanite is the only aluminosilicate in sample MM193D (G.R. NN11932864) within a few metres from the contact. There is no hydrous phase (i.e. biotite) in this sample. Plates 5.8 and 5.9 illustrate sillimanite needles in the pelitic rocks from the north Loch Awe area. Plate 5.12 illustrates the crystallisation of sillimanite on pre-existing andalusite, which is evidence for the prograde transformation of andalusite to sillimanite. Sillimanite is in equilibrium with Crd+Crn+Spl+Kfs in this sample. Sillimanite is retrogressed to andalusite in some samples. Non-equilibrium aggregates of And+Sil are seen in some samples, but sillimanite is completely retrogressed to andalusite in others. Plates 5.10 and 5.11 show aggregates of retrograde andalusite which are pseudomorphing original sillimanite prisms. This is one of two types of andalusite in this rock, the other having a tabular shape typical of prograde andalusite

(6) Parageneses with contact metamorphic garnet: Contact-metamorphic garnet (almandine-rich) has crystallised in a few pelitic rocks in the inner aureole. Contact-metamorphic garnet has formed close to the regional metamorphic garnet in sample MM134A (GR. NN11392790). In this unequilibrated rock, regional garnet is irregular in shape and is dusty in appearance (Plate 5.13). Contact-metamorphic garnet has a clear appearance and is idioblastic in shape. The assemblage is Grt+Bt+Qtz+Crd+Kfs+Pl with minor amounts of apatite and ilmenite. Contact-metamorphic garnet occurs in texturally equilibrated rocks at higher grades. Garnet is idioblastic in these rocks and is in equilibrium with Crd+Bt+Qtz+Pl+Kfs. Plates 5.14 and 5.15 show contact metamorphic garnets in sample MM166A from locality G.R. NN12482896.

(7) Parageneses with orthopyroxene: In the North Loch Awe area, orthopyroxene has only been found in two metasedimentary samples. These are semipelitic hornfelses (samples MM198C and MM138B) from ca. 10m from the diorite contact and contain the assemblage Opx+Crd+Bt+Pl+Qtz. The bulk of sample MM198C has a very fine-grained granoblastic texture, but the rock contains coarse irregular veins (leucosomes) of Opx+Crd+Pl+Bt+Qtz which are interpreted as the products of partial melting (see below and in Chapter 6).

(8) Other assemblages with melt: Many of the inner aureole rocks (within 300m from the contact, from Crn-bearing rocks upward toward the igneous contact) contain pale-coloured veins (leucosomes). These veins consist of quartz and alkali

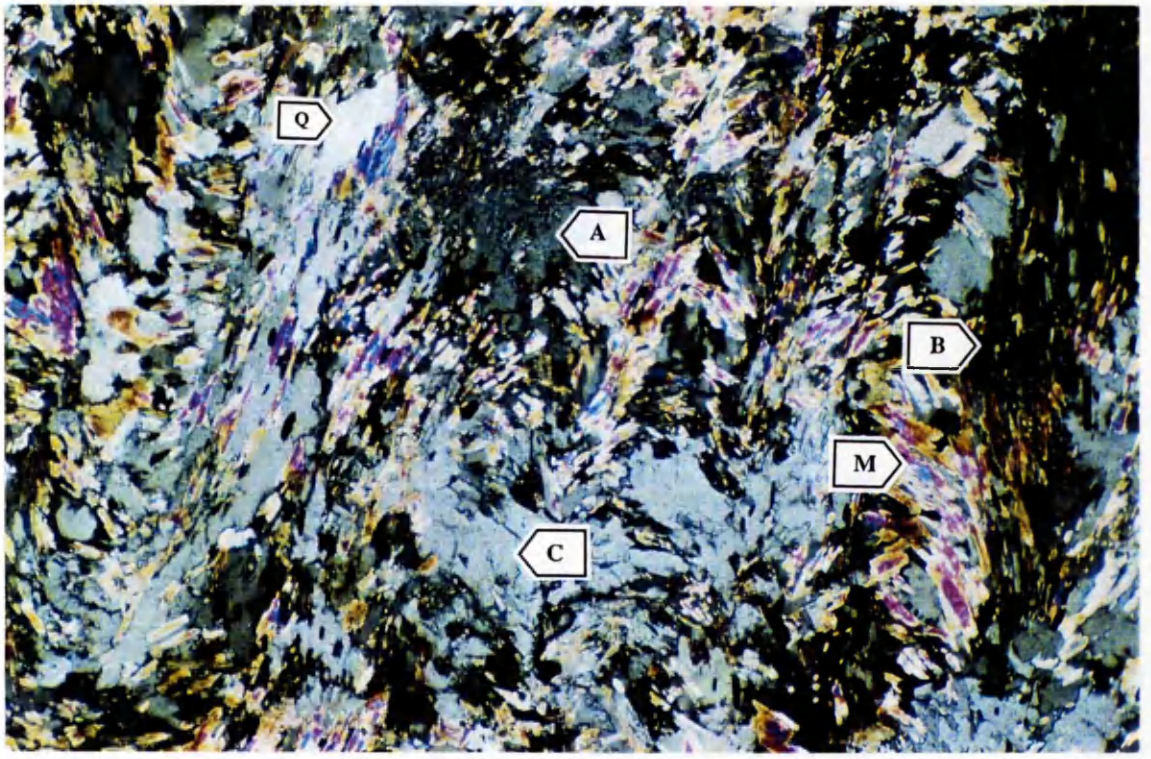

Plate 5.4 Sample MD1 (G.R. NN126525) containing muscovite (M) crystallised along the S_1 schistosity, andalusite (A), cordierite (C), biotite (B) and quartz (Q). XPL. Field of view 4.2mm.

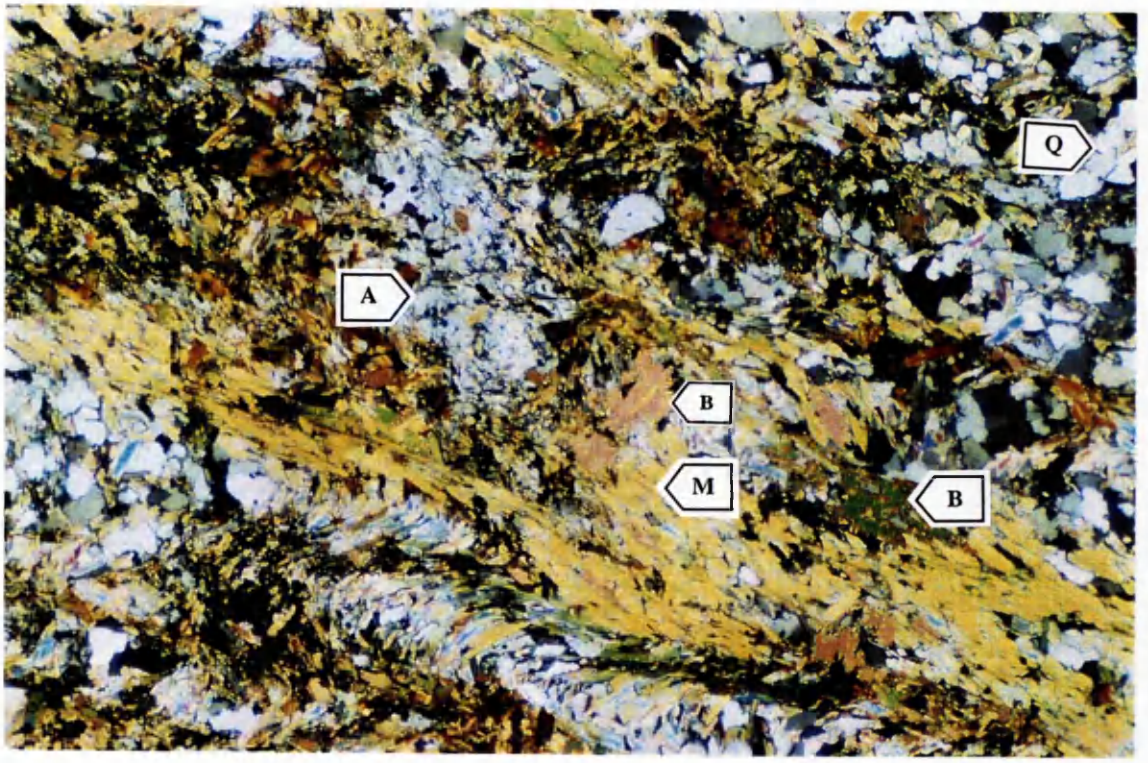

Plate 5.5 Other part of sample MD1. Muscovites (M) are aligned in the S_1 schistosity which has been crenulated to form the S_2 crenulation cleavage. Note large cross-cutting contact metamorphic biotites (B), andalusite (A) and granoblastic quartz (Q). XPL. Field of view 4.2mm.

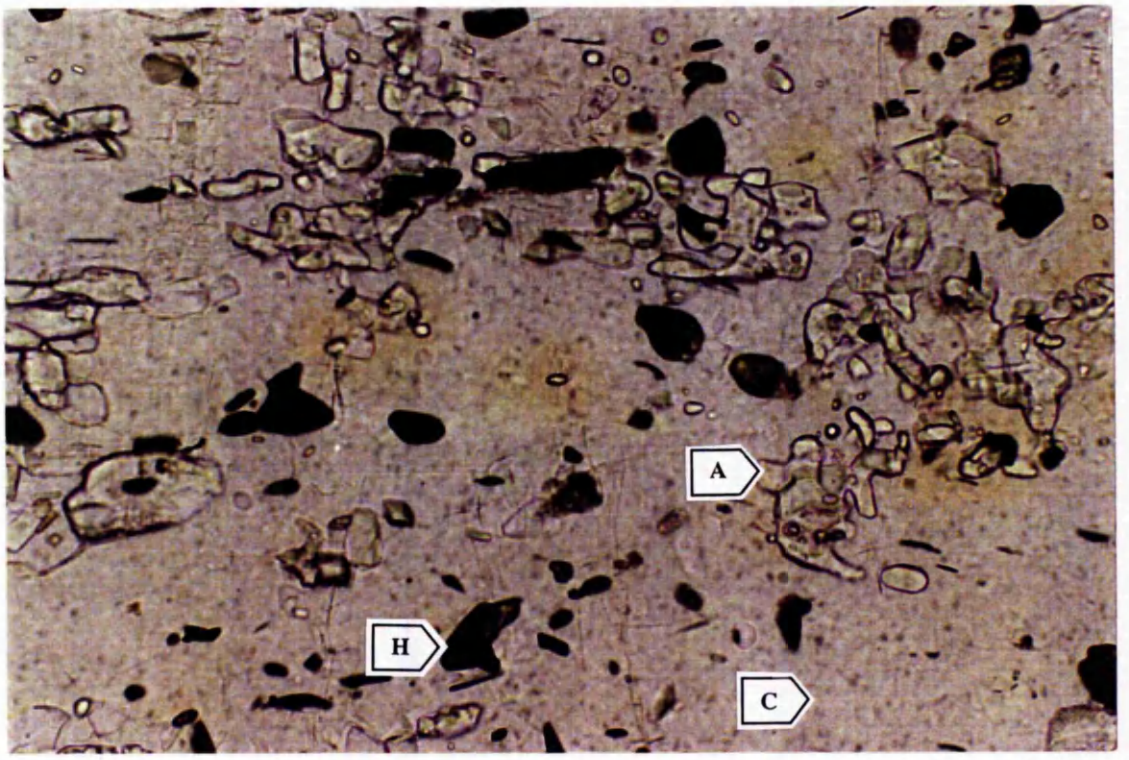

Plate 5.6 Pelitic hornfels sample MM166D (G.R. NN12482896) with coexisting hercynitic spinel (H), andalusite (A) and cordierite (C). Note pleochroic haloes around zircons in cordierite. PPL. Field of view 1.6mm.

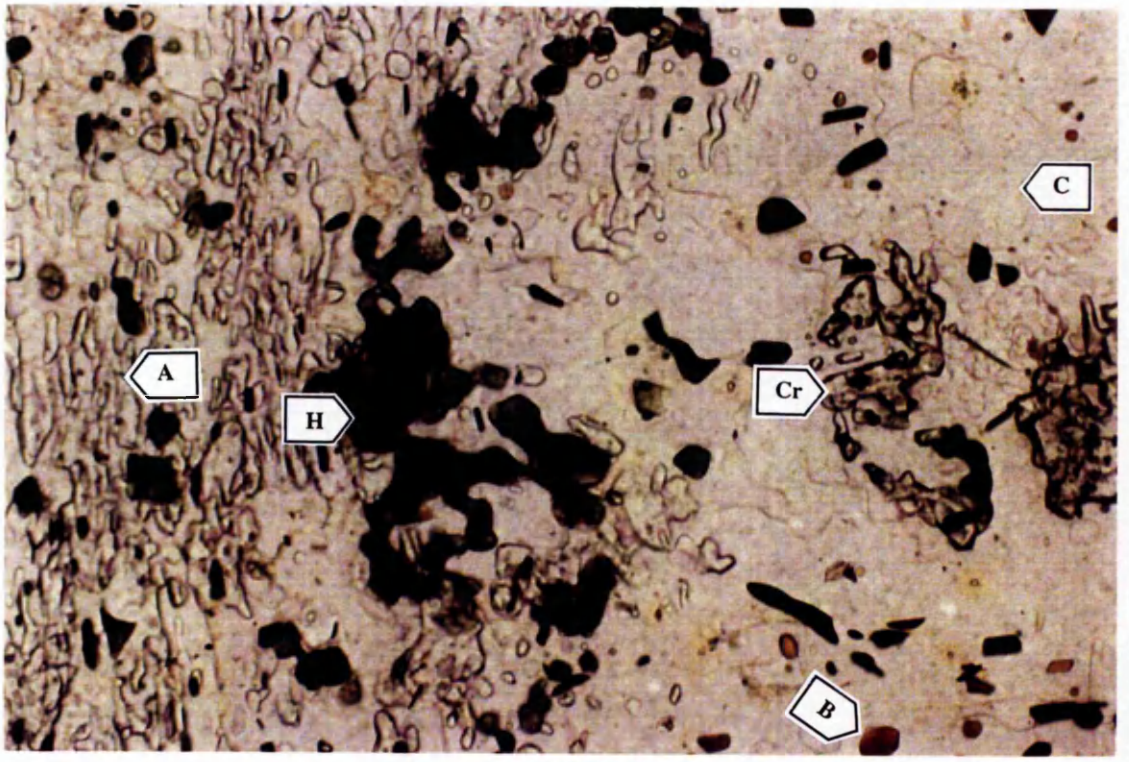

Plate 5.7 Coexisting corundum (Cr), cordierite (C), hercynitic spinel (H), andalusite (A) and biotite (B) in pelitic hornfels sample MM166D. PPL. Field of view 4.2 mm.

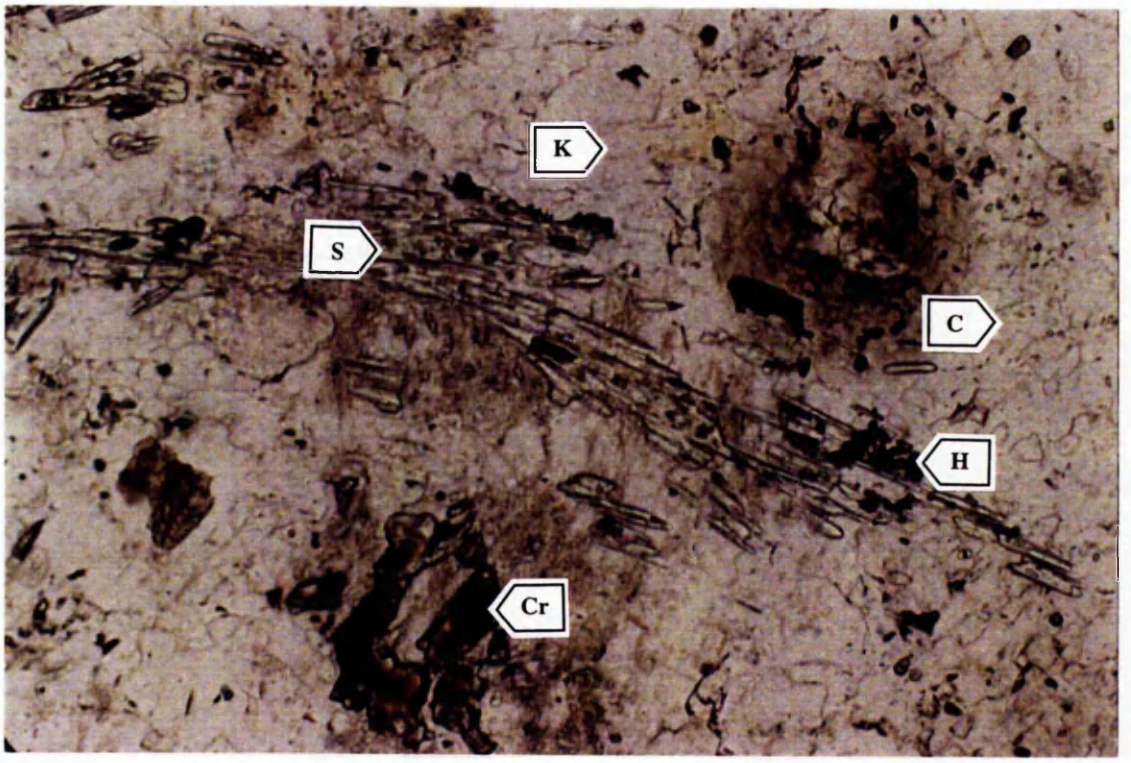

Plate 5.8 Pelitic hornfles sample MM193D (G.R. NN126531) showing coexisting sillimanite (S), corundum (Cr), spinel (H), cordierite (C) and K-feldspar (K). Acicular sillimanite is the only aluminosilicate in this rock. PPL. Field of view 4.2mm.

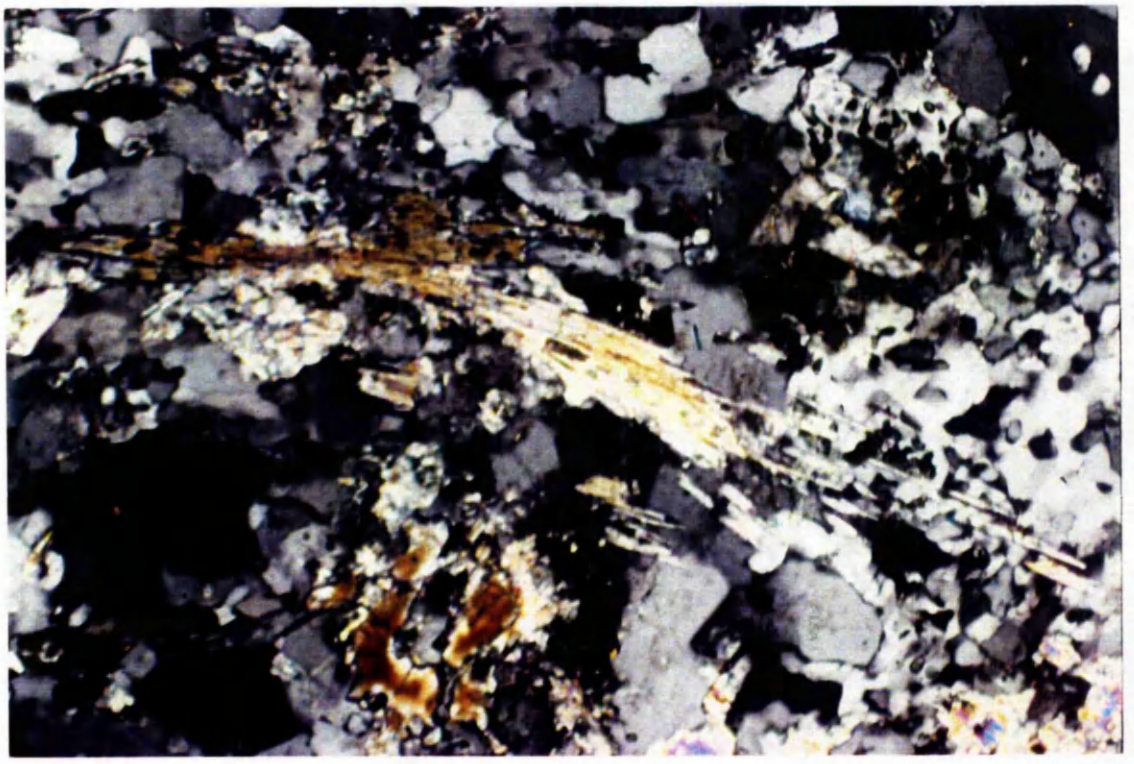

Plate 5.9 Sample MM193D, as above. XPL.

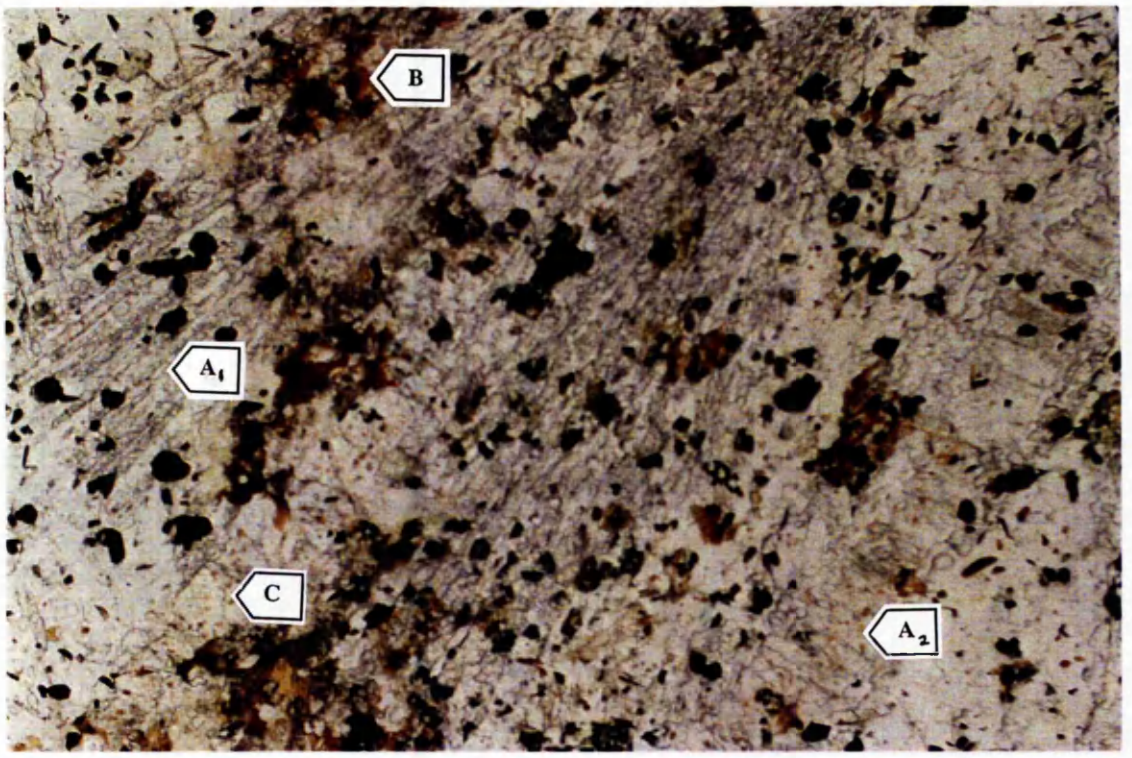

Plate 5.10 Pelitic hornfels sample MM195C (G.R. NN 12282874) showing large pseudomorph of andalusite (A_1) after sillimanite. This is textural evidence for the reaction Sil=And. Tabular andalusite (A_2) also occurs in the rock. PPL. Field of view 4.2mm.

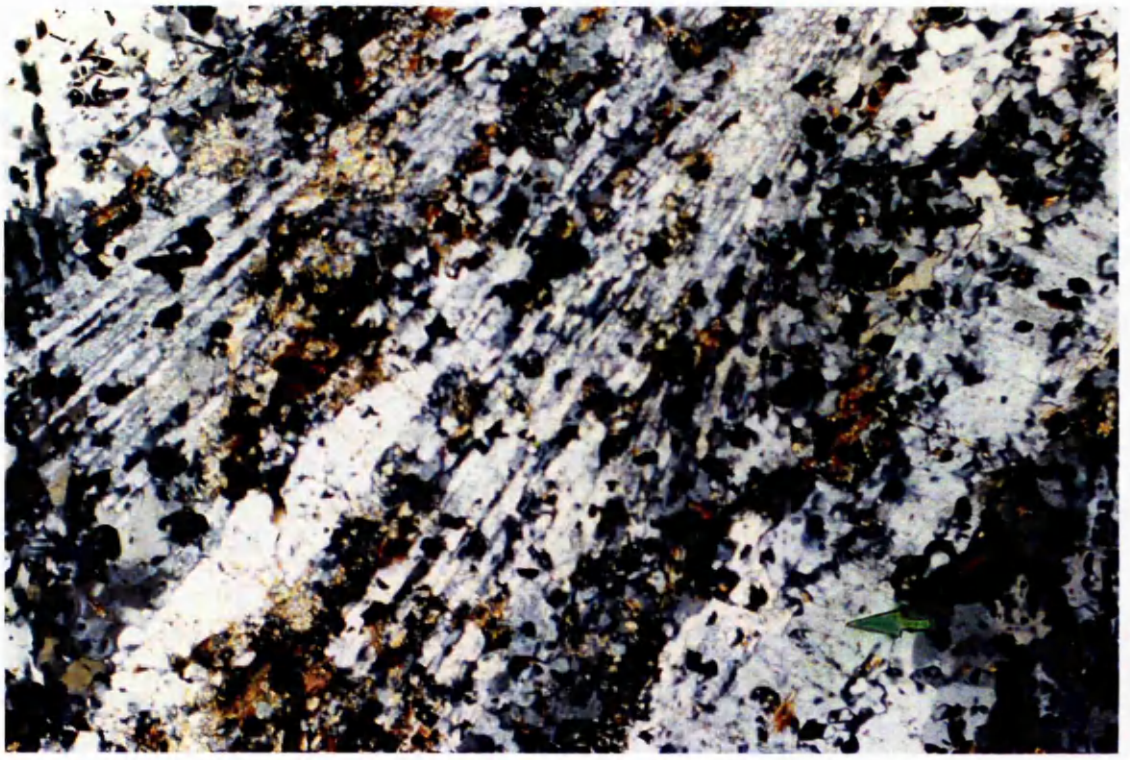

Plate 5.11 Pelitic sample MM193D, as above. Tabular andalusite is arrowed. XPL.

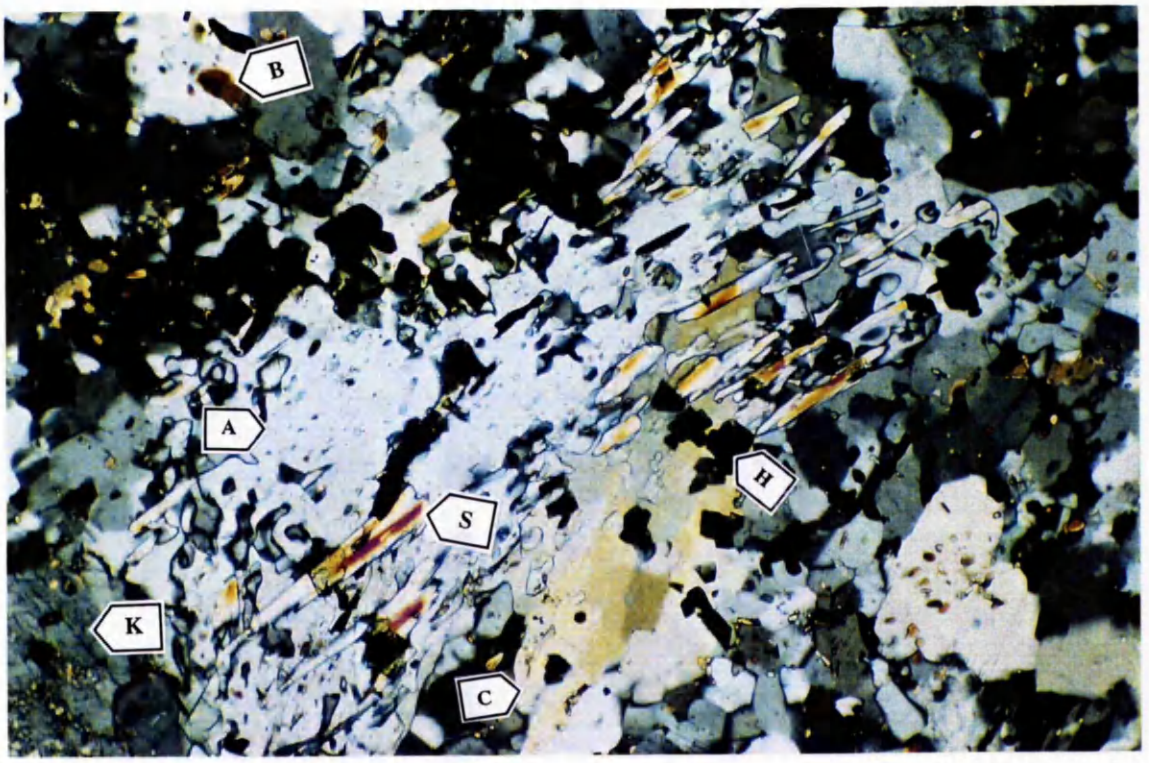

Plate 5.12 Pelitic hornfels sample MM167C (G.R. NN12402890) showing prisms of prograde sillimanite (S) overgrowing on andalusite porphyroblast (A). XPL. Field of view 1.6mm. Other minerals are K-feldspar (K), biotite (B), cordierite (C) and spinel (H).

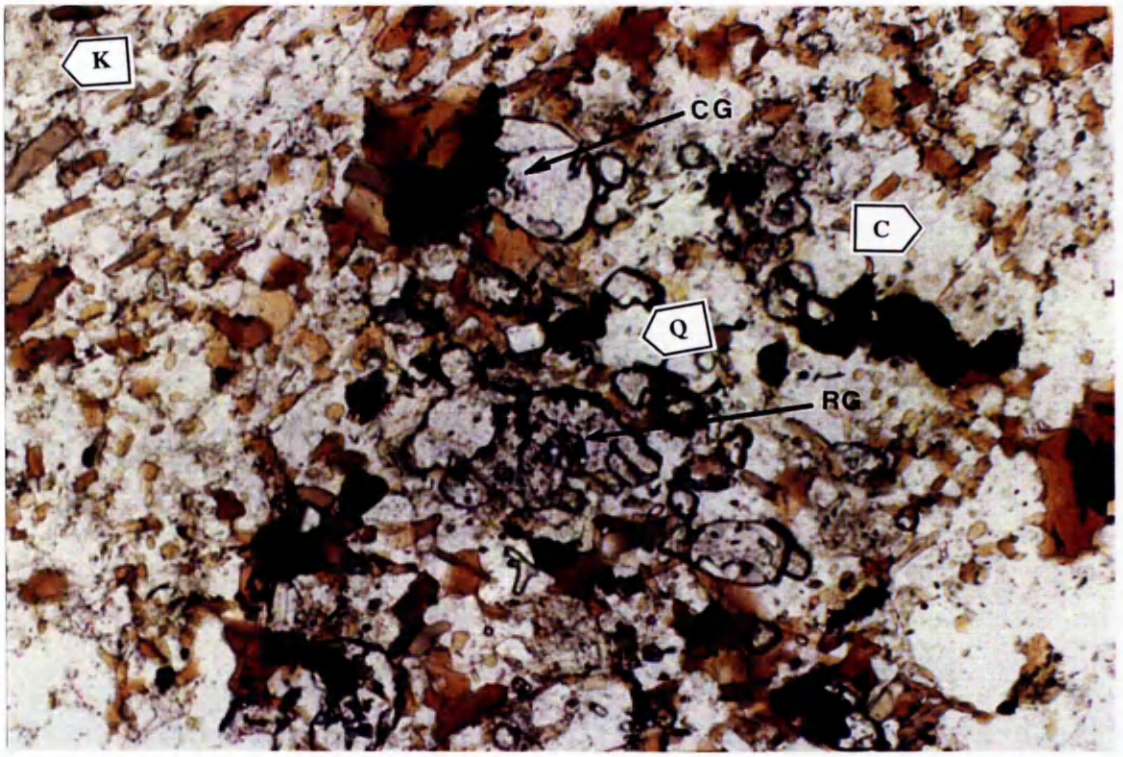

Plate 5.13 Pelitic sample MM134A (G.R. NN11392790) containing both contact metamorphic garnet (CG) and regional metamorphic garnet (RG). Other minerals shown include biotite (B), K-feldspar (K), cordierite (C), quartz (Q) and ilmenite (black). The regional metamorphic garnet has a dusty appearance and is irregular in shape but contact metamorphic garnet is clear and is sub-idioblastic in shape. PPL. Field of view 4.2mm.

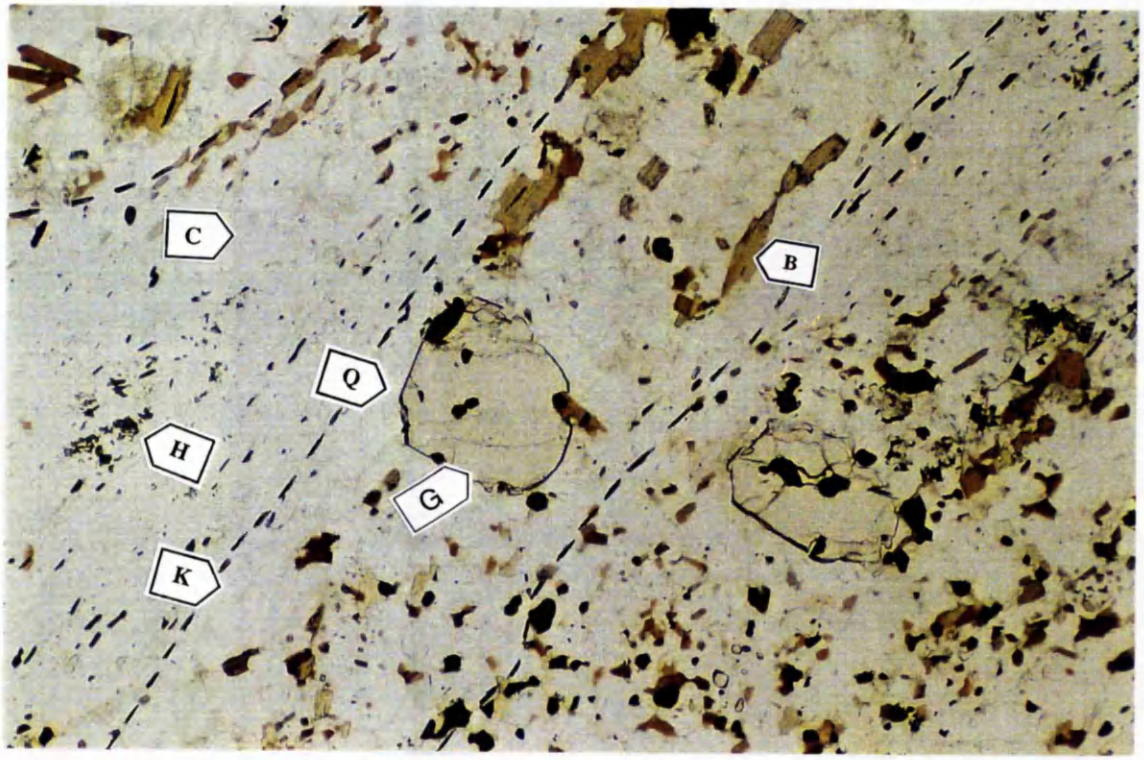

Plate 5.14 Pelitic hornfels sample MM165B (G.R. NN12482896), showing contact-metamorphic garnet (G) coexisting with biotite (B), cordierite (C), K-feldspar (K), quartz (Q) and ilmenite (black). Some cordierite grains contain clusters of tiny spinel granules (H) but the latter are nowhere in contact with other minerals. PPL. Field of view 4.2mm. For more description see caption for Plate 5.15.

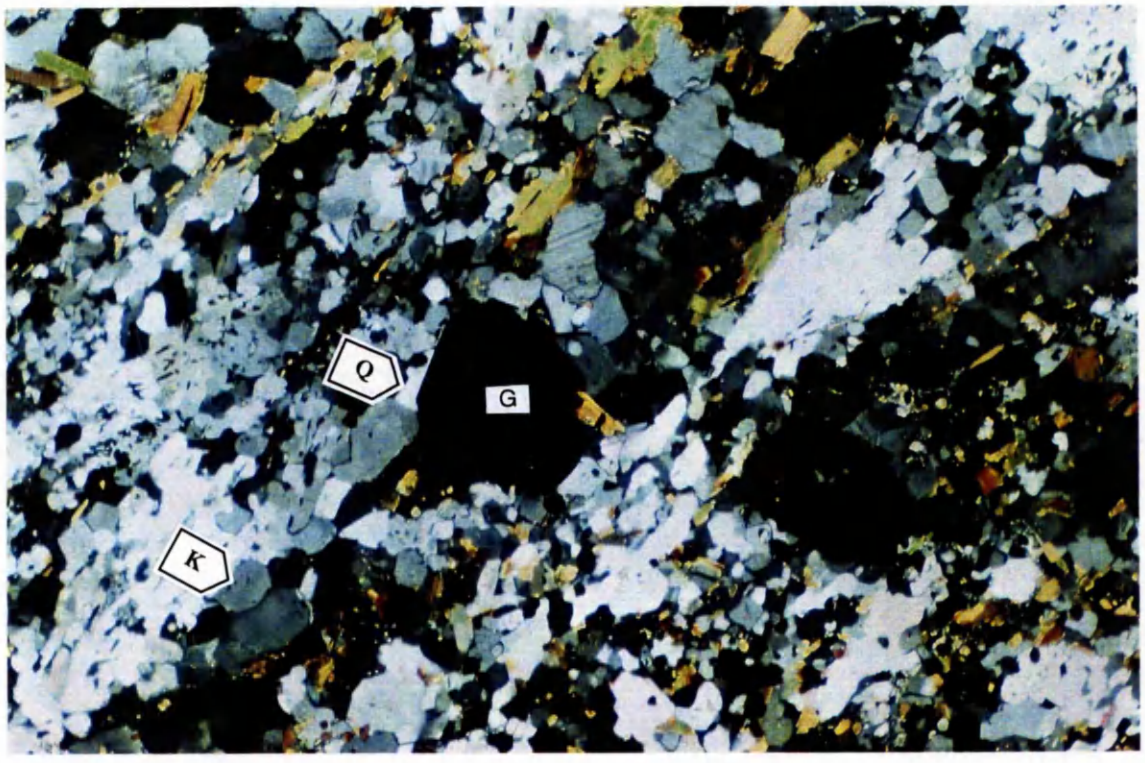

Plate 5.15 Pelitic hornfels sample MM165B, as above. The idioblastic garnet on the left-hand side of the photo is associated with a leucosome consisting of idioblastic K-feldspar (K) with interstitial quartz (Q) interpreted as crystallised melt. The probable boundary between melt and hornfels is marked by a dashed-line in Plate 5.14. XPL.

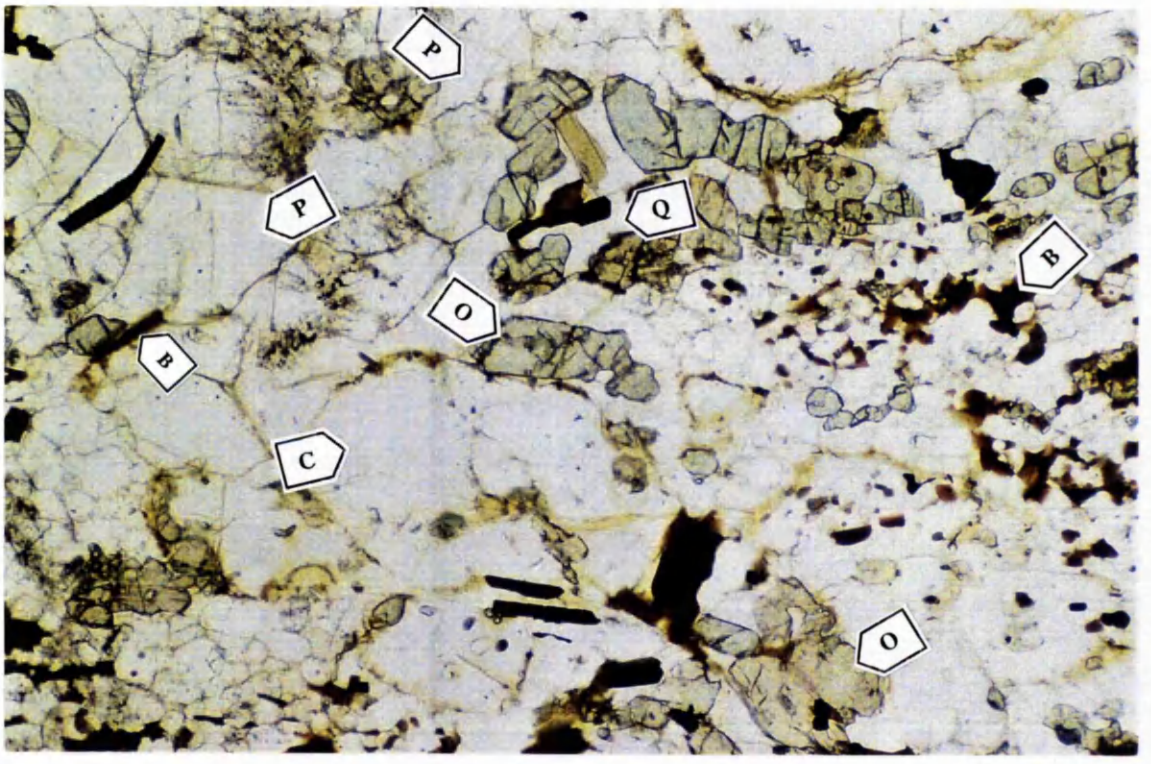

Plate 5.16 Semi-pelitic hornfels sample MM198C (G.R. NN12492911) showing medium-grained leucosome consisting of euhedral orthopyroxene (O), cordierite (C) and plagioclase (P) crystals with minor biotite (B) and interstitial quartz (Q). The mesosome (centre-right) is finer-grained, granoblastic, and lacks cordierite, PPL. Field of view 4.2mm.

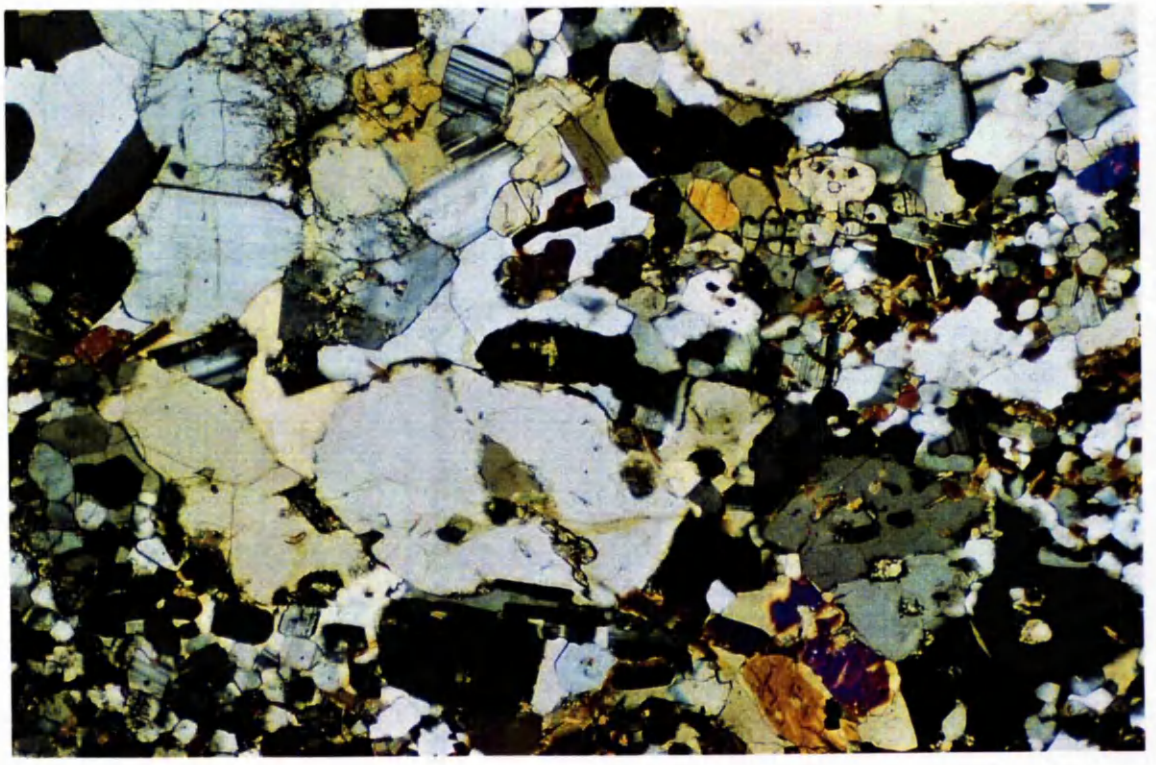

Plate 5.17 Semi-pelitic hornfels sample MM198C, as above. XPL.

feldspar ±cordierite±garnet with an igneous texture (i.e. blocky, euhedral alkali feldspars separated by cuspate interstitial patches of quartz). These veins are believed to be products of partial melting. The field relations and petrography of the partially melted rocks are discussed in more detail in Chapter 6.

5.3.3 Retrogressive alteration of the pelitic rocks:

Chlorite after biotite, muscovite after alkali feldspar, clay minerals after feldspar, and pinite after cordierite are the main alteration products in the pelitic and semi-pelitic rocks. Alteration (retrograde hydration) is not pervasive in the aureole and the inner aureole rocks are mainly fresh.

5.3.4 Distribution of the mineral zones and isograds in the pelitic rocks

Contact metamorphic non-graphitic rocks are divided into seven groups in section 5.3.2, according to their mineral assemblages. Considering the assemblages and also regarding the distribution of the samples in the north Loch Awe area (Fig. 5.3) the southern segment of the aureole is divided into seven mineralogical zones. These are the Biotite Zone (Zone I, including regional metamorphic rocks and contact metamorphic biotite-bearing rocks), the Cordierite Zone (Zone II), the Andalusite Zone (Zone III), the Andalusite+K-feldsar Zone (Zone IV), the Corundum Zone (Zone V), the Spinel Zone (Zone VI) and the Sillimanite Zone (Zone VII).

Zone I (regional metamorphic rocks and contact-metamorphic biotite-bearing rocks): This zone includes the regional metamorphic rocks with the parageneses:

Ms+Chl+Qtz+Bt+Grt,
Ms+Chl+Qtz+Bt
Ms+Pl+Qtz
Ms+Chl+Qtz+Bt+Cal

The boundary between regional-metamorphic rocks and contact-metamorphic rocks is not clear in the north Loch Awe area. The recrystallisation of biotite due to the contact metamorphism is not very clear in all samples and it is possible that the contact-metamorphic biotite isograd lies beneath Loch Awe, i.e. that all the

metamorphic rocks exposed on the North Loch Awe have undergone thermal metamorphism. The assemblage Bt+Chl+Ms+Qtz+Pl is the lowest contact-metamorphic assemblage with thermally recrystallised biotites.

N.B. Plagioclase and ilmenite are constituents of all mineral assemblages listed below, but have been omitted for brevity.

Zone II (Cordierite Zone): The appearance of cordierite is mappable in the north Loch Awe area. The presence of either fresh cordierite or pinite was used for locating the cordierite isograd. The characteristic paragenesis is:

Crd+Ms+Bt+Qtz.

Zone III (Andalusite Zone): Andalusite first appears after cordierite in the metamorphic grade sequence from the outer aureole towards the contact. Zone III includes assemblages with andalusite and cordierite or cordierite and alkali feldspar. The parageneses present are:

Crd+Kfs+Bt+Ms+Qtz
Crd+And+Bt+Qtz+Ms

Zone IV (Andalusite+Alkali Feldspar Zone): This zone is wider than the previous zones and includes assemblages with And+Kfs. The parageneses present are as follows:

Crd+Kfs+Bt+Qtz
Crd+And+Kfs+Bt+Qtz
Crd+Kfs+Bt+And+Ms+Qtz

Zone V (Corundum Zone): This zone is identified by the first appearance of corundum in the pelitic rocks. There are two types of pelite in this zone, quartz-bearing and quartz-deficient. The mineral parageneses present are:

Crd+And+Kfs+Bt+Crn

Crd+And+Kfs+Bt+Qtz.

Zone VI (Spinel Zone): This zone is the widest zone in the aureole (about 560m wide). The mineral parageneses present in this zone are:

Crd+And+Kfs+Bt+Qtz

Crd+And+Kfs+Bt+Spl

Crd+And+Bt+Kfs

Crd+And+Bt+Kfs+Crn

Crd+And+Kfs+Bt+Spl+Crn

Crd+Bt+Qtz

Crd+And+Kfs+Crn

Crd+Kfs+Bt+Spl

Crd+Kfs+Bt+Qtz

Crd+Kfs+Bt+Grt+Qtz

Crd+Kfs+Bt+Crn+Spl.

Zone VII (Sillimanite Zone): Upgrade of Zone VI sillimanite appears in the pelitic rocks. The parageneses present in this zone, in different bulk compositions, are as follows,

Crd+And+Bt+Crn+Spl+Kfs+Sil

Crd+Bt+Kfs+Qtz (semi-pelite)

Crd+And+Crn+Spl+Kfs

Crd+Bt+Kfs+Spl

Crd+Spl+Crn+Kfs+Sil

Crd+Sil+And+Bt+Kfs+Spl

Crd+Grt+Kfs+Bt+Qtz

Crd+And+Sil+Spl+Crn+Kfs

Crd+Sil+Bt+Spl+And+Kfs

Crd+Opx+Bt+Qtz

The first appearance of successive contact-metamorphic index minerals, peoceeding in an up-grade direction, was used to locate the mineral isograds in the north Loch Awe area. These isograds are Crd-in, And-in, And+Kfs-in, Crn-in, Spl-in and sillimanite-in (Fig. 5.3).

5.4 Petrography of the graphitic pelites and semi-pelites

The main graphitic units in the Etive area are Ben Eagach Schist and Ardrishaig Phyllite in the north Loch Awe area and black slates and associated psammites and quartzites of the Creran and Creagan Flags in the North Bonawe and Loch Creran areas. The psammites and quartzites are not graphite-rich in most of the studied samples, but because they are associated with graphitic pelites and semi-pelites will be considered as graphitic rocks in this chapter. The rock samples in the Bonawe area were collected along the Inversragan road section, in a traverse from the outer aureole to the contact of the igneous rocks and also from xenoliths in the igneous rocks exposed along the Blarcrean valley. The rocks are mainly Culcharan Black (graphitic) slates of the Easdale subgroup with calcareous interlayers. In the Loch Creran area, the samples were collected from the outer aureole towards the contact along the Glean Dubh and Druimavuic valleys. The locality of samples from the North Loch Awe, Bonawe and Loch Creran areas are shown in Figures 5.3, 5.4, and 5.5 respectively.

5.4.1 Regional metamorphic graphitic rocks:

Seven thin sections from the regional metamorphic graphitic rocks were studied and the following mineral parageneses were found:

Chl+Ms+Qtz	[5.36]
Chl+Ms+Qtz+Bt+Grt .	[5.37]

The samples were collected from the regional metamorphic rocks of the Ben Eagach Schist, Creagan Flags and Ardrishaig Phyllite, from localities close to Dalmally village, along the main road-side north of Barcaldine and along the main road-side

close to Awe village respectively. Table 5.4 includes mineral parageneses in the graphitic rocks.

The texture of all of these samples is lepidoblastic due to the arrangement of chlorite, muscovite and biotite. An S_2 crenulation cleavage is well-developed (e.g. sample MM 45B, Plate 5.18). Garnet porphyroblasts show syn-deformational textures and are partially altered to chlorite. Biotite is altered to chlorite in most of the samples. Some of the chlorite flakes, which are parallel to the main foliation, are believed to be prograde chlorite. Graphite is a major mineralogical component of the samples. Minor and accessory phases are ore minerals (mainly pyrite), zircon and titanite. There are carbonate minerals in some of the samples (e.g. sample MM256B, G.R. NN18602747, containing calcite and dolomite).

5.4.2 Contact metamorphic graphitic pelites and semi-pelites:

Sixty-eight thin sections from the thermally metamorphosed graphitic pelites and psammites were studied and the following mineral parageneses were determined:

Chl+Bt+Ms+Qtz	[5.38]
Bt+Ms+Qtz	[5.39]
Bt+Ms+Qtz+Crd	[5.40]
Bt+Ms+Qtz+Crd+And	[5.41]
Bt+Ms+Qtz+Crd+Kfs	[5.42]
Bt+Qtz+Crd+Kfs	[5.43]
Bt+Ms+Qtz+Crd+Kfs+And	[5.44]
Bt+Qtz+Crd+And+Kfs	[5.45]
Bt+Crd+Kfs+Crn	[5.46]
Bt+Crd+And+Kfs+Crn	[5.47]
Bt+Crd+Kfs+Crn+Spl	[5.48]
Bt+Qtz+Crd+Opx.	[5.49]

Graphite, pyrite, zircon, apatite, titanite and tourmaline are minor phases. The main parageneses at the lowest contact-metamorphic grade are Chl+Bt+Ms+Qtz and Bt+Ms+Qtz. No obvious thermal effect on these samples can be seen in hand

Table 5.4 Mineral assemblages of graphitic-pelites and semi-pelites. X=major phase, O=minor phase, A=alteration product, P=pseudomorph, E=Ex-mineral (altered to sericite). Rg=regional metamorphic rock, Xn=xenolith in igneous rocks.

Sample	G.R	Chl	Bt	Ms	Qtz	Grt^R	Crd	And	Kfs	Crn	Spl	Opx	Pl	Ilm	Zirc	Ap	Ttn	Tour	Ore	Ep	Cal
MM16Ca	NN00533366	O^A	X		X				X				X						O		
MM16B	NN00533366	O^A	X	X	X				X							O		O	O	O	
MM15B	NN00233409		X	X	X		X	X	X				O			O		O	O		
MM14B	NN00053422	O^A	X	X	X		X^P	X	?							O			O		
MM14A	NN00053422		X	X	X			X	X		O					O		O	O		
MM13	NN99703458		X	X	X			X	X				O			O			O		
MM12B	NN99603473	O^A	X	X	X		X^P	X										O	O		
MM11C	NN99583483		X	X	X			X					O		O			O	O		
MM11B	NN99583483	O^A		X	X													O	O		
MM10A	NN99433507		X	X	X			X											O	O	
MM9B	NN99403510		X	X	X		X						O					O	O		
MM84B	NN03904507			X	X	X									O	O	O	O	O		
MM69	NN00084483	X	X	X	X	X							X		O	O	O	O	O		
MM70	NN01084478		X	X	X	X	X						X		O	O	O	O	O		
MM71C	NN01174467		X	X	X								X		O	O	O	O	O		
MM71D	NN01174467		X	X	X	X	X						X		O				O		
MM72A	NN01424467		X	O^A	X	X	X						X		O			O	O		
MM75B	NN01964451		X	X	X		X	X					X		O		O		O		
MM82A	NN03164430		X	O^A	?	X^E	X	X	X				X			O			O		
MM83C	NN03244425		X	O^A			X^E	X	X	X			X		O				O		
MM43B	NN09912643	O	X	X	X								X						O		
MM45B	NN10302639	O	X	X	X													O	O		
MM34B	NN08302724	X^R	X	X^R	X								X			O			O		
MM36C	NN08452702	X	X	X												O			O		
MM39A	NN09082662		X	X^R	X								X						O		
MM60	NN10192596	O		X	X								X						O		
MM67	NN00704443		X	X	X								X		O		O	O	O		
MM74	NN01974451		X	X	X	X							O		O		O	O	O		
MM75A	NN01964451		X	X	X										O				O		
MM85A	NN07992561	X		X	X								X		O	O	O		O		
MM108A	NN09612692		X		X		X	X	X				O		O		O	O	O		

Sample	G.R	Chl	Bt	Ms	Qtz	Grt^{R}	Crd	And	Kfs	Crn	Spl	Opx	Pl	Ilm	Zirc	Ap	Ttn	Tour	Ore	Ep	Cal
MM110a	NN09532714		X				X	?	X	X									O		
MM110b	NN09532714		X		X		X	?	X	X									O		
MM111	NN09542720				X		X	X											O		
MM114a	NN09532740		X		X		X^{E}		?										O		
MM114b	NN09532740		X				X^{E}	X	?	X									O		
MM115	NN09552744		X	O^{A}	X		X		X				X		O		O		O		
MM124	NN09962711			X	X								O		O				O		
MM218^{Rg}	NN12412747	X		X	X										O				O		
MM256A^{Rg}	NN18602747	X		X	X										O		O		O		
MM256B^{Rg}	NN18602747	X	X	X	X	X									O	O		O	O		O+Dol
MM228G	NN10832615	X		X	X										O	O		O	O		O
MM228E	NN10832615	X	X	X	X								X		O			O	O		
MM228C	NN10832615	X		O^{A}	X	X	O												O		O
MM261	NN98054230	X		X	X								X		O						
MM232a	NN08982669	X	X	X	X								X		O			O	O		
MM234a	NN08892689		X	X	X								X		O			O	O		
MM236Aa	NN08892702		X	X	X								X		O			O	O		
MM237	NN08782709		X	X	X		?		X						O				O		
MM238A	NN08932737		X	O^{A}	X		X		X				X		O	O		O	O		
MM242	NN08772753		X		X		X		X				X			O			O		
MM243	NN08712752	O^{A}		O^{A}	X										O				O		
MM257A	NN96904305			X	X																
MM259^{Rg}	NN97724245	X		X	X										O				O		
MM260^{Rg}	NN97854236	X		X	X										O			O	O		
MM261^{Rg}	NN98054230	X		X	X								X		O				O		
MM262	NN99774255		X	X	X		?		X				X		O		O		O		
MM263	NN00244257		X	X^{A}	X		X						X					O	O		
MM265	NN00374257		X	X^{A}			X						X		O	O			O		
MM266	NN00324245		X		X										O	O			O		
MM267	NN00754207	O^{A}	X	X^{A}	X		X		X						O		O		O		
MM268	NN00874204		X	X			X		X				X		O		O		O		
MM269^{Xn}	NN01024205		X		X		X		X			X	X						O		
MM270	NN00674237	O^{A}		O^{A}	X		?		X				X		O		O		O		

Sample	G.R.	Chl	Bt	Ms	Qtz	Grt^{R}	Crd	And	Kfs	Sil	Crn	Spl	Opx	Pl	Ilm	Zirc	Ap	Ttn	Tour	Ore	Ep	
MM272	NN00593371		X	O^{A}	X		?		?					X						O		
MM273a	NN00643371		X	O^{A}	X		X		X							O				O		
MM275	NN00753380	O^{A}	X	O^{A}	X		X		X							O	O		O	O		
$MM280^{Xn}$	NN01063407	O^{A}	X	O^{A}	X		X		X				X							O		
MM281A	NN00943420			O^{A}			X		X		X	X				O			O	O		
MM289	NN01063302		X	O^{A}	X		?		X					X								
MM284	NN00783427		X	O^{A}	X		X		X					X		O		O		O		
MM283A	NN00833425		X	O^{A}	X													O		O		
MM282	NN00953427	O^{A}		O^{A}	X											O			O	O		

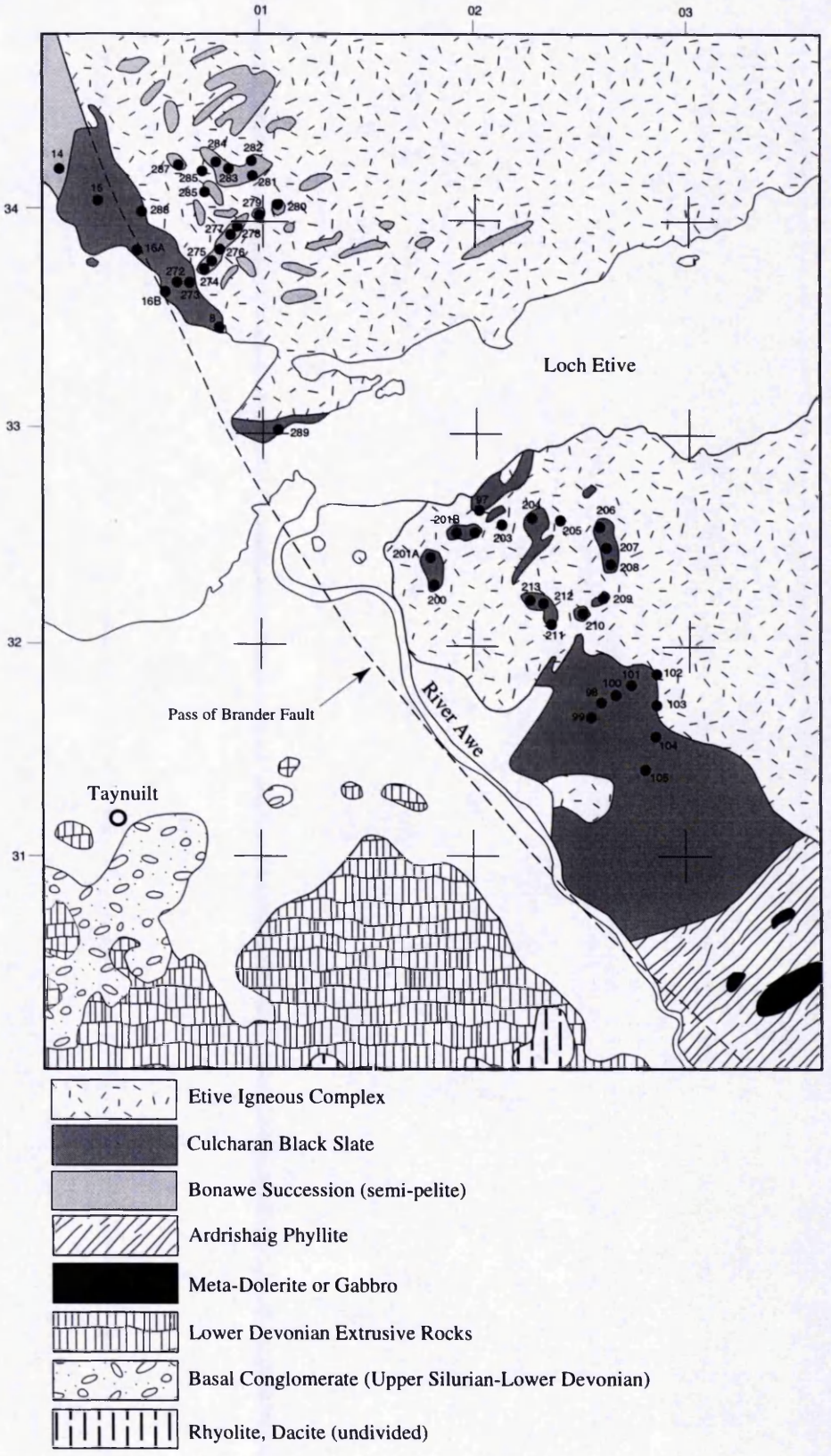

Fig. 5.4 Sample localities of graphitic pelites and semi-pelites and calc-silicates in the Bonawe area. Lithologies from Scotland Sheet 45(W), Connel, BGS.

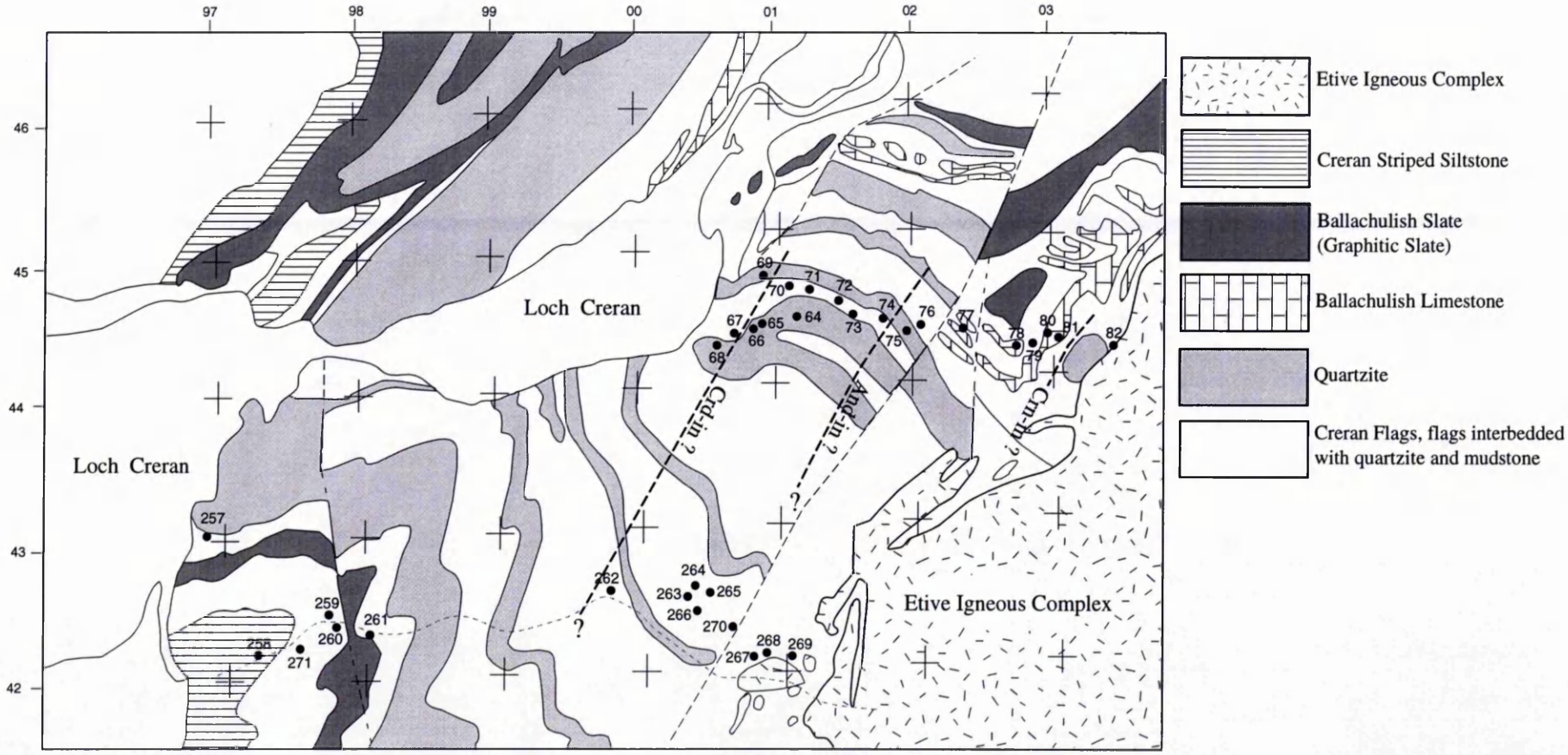

Fig.5.5 Distribution of sample localities of graphitic pelites and semi-pelites and calc-silicates in the Loch Creran area. Lithologies from Scotland Sheet 45(W), Connel, BGS.

specimens. The main texture of the rocks is lepidoblastic owing to the arrangement of chlorite, muscovite and biotite flakes. Under the microscope, biotite shows recrystallisation due to the thermal metamorphism. Some of the biotite flakes are not parallel to the main foliation and post-date the foliation. These biotites are believed to be contact metamorphic in origin. Chlorite is stable in low contact-metamorphic grades. Porphyroblasts of regional metamorphic garnet are present in some of the samples. Chlorite disappears as the grade of contact-metamorphism increases. Cordierite is the first newly formed contact-metamorphic mineral. The main texture of the low grade, cordierite-bearing rocks is lepidoblastic, with a schistosity defined by parallelism of muscovite and biotite flakes. Cordierite is altered to yellow isotropic material (pinite) in some of the samples. It has crystallised along the main foliation, replacing the pre-existing muscovite. No cordierite+chlorite association was found in the graphitic pelites and semi-pelites. Cordierite forms relatively large poikiloblastic crystals with inclusions of biotite, zircon and quartz in rocks closer to the igneous contact. The main mineral paragenesis of these rocks is Bt+Ms+Qtz+Crd ±Pl. Graphite, apatite, zircon, ilmenite and tourmaline are common minor phases. Andalusite has crystallised in peraluminous rocks. It forms chiastolite porphyroblasts in highly graphitic samples.

The S_2 crenulation cleavage is well preserved in these rocks and the arrangement of the muscovite and biotite flakes determine this crenulation (Plate 5.18). Porphyroblasts of chiastolite clearly post-date the S_2 cleavage. Andalusite is prismatic without chiastolitic texture in the slightly graphitic rocks, especially those closer to the igneous contact. The texture of these rocks is granoblastic with a vague original S_2 crenulation cleavage. Quartz and cordierite show equigranular polygonal textures. Microperthitic K-feldspar appears in higher-grade rocks. The main paragenesis of K-feldspar-bearing rocks are Bt+Qtz+Crd+Kfs and Bt+Qtz+Crd+And+Kfs. The K-feldspar-bearing rocks have a granoblastic polygonal texture and relict regional metamorphic textures such as foliation and crenulation cleavage are hardly distinguishable having been largely overprinted. Graphite, ilmenite, zircon, apatite, titanite and tourmaline are common minor phases in the rocks. Corundum forms small to medium-sized (up to ~0.3mm) crystals in the peraluminous pelitic rocks close to the contact (Plate 5.19). The paragenesis of the Crn-bearing rocks are Bt+Crd+Kfs+Crn and Bt+Crd+And+Kfs+Crn. These rocks

have a granoblastic polygonal texture and the original S_2 crenulation cleavage is not obvious. Spinel was found in a few samples of the graphitic pelites and semi-pelites. It forms dark-green (hercynite) crystals. The mineral paragenesis is Bt+Crd+Kfs+Crn+Spl. Orthopyroxene has crystallised in some semi-pelitic rocks and xenoliths in the north Bonawe area. It co-exists with Crd, Qtz and Bt, which together have a granoblastic texture. There are some veinlets in the high-grade rocks close to the contact and in xenoliths. These veinlets are made of Kfs+Qtz±Bt±Opx, and have igneous textures (i.e. idiomorphic K-feldspars with interestitial quartz) and are believed to be a product of contact anatexis of the graphitic (semi-)pelites. No sillimanite was found in the graphitic rocks. There are three possibilities accounting for this:

(i) Temperature was not high enough to produce sillimanite. The rocks in this part of the aureole are in contact with granite of the Cruachan intrusion not diorites.

(ii) Bulk composition of the inner aureole rocks was not suitable to produce sillimanite.

(iii) Pressure could have been different in eastern and western parts of the North Loch Awe area.

The first two possibilities are more likely to be reasons for the lack of sillimanite in the inner aureole rocks of the graphitic units. The distance between sillimanite-present localities and sillimanite-absent localities are not too much and difference in pressure is not likely to be the reason.

5.4.3 Retrogressive alteration of the graphitic pelites and semi-pelites:

Most of the graphitic pelites and semi-pelites are more altered than non-graphitic pelites and semi-pelites. The Kfs, Crd, Pl and Bt minerals are completely altered to sericite and pinite in some of the samples close to the contact. Alteration is widespread in the graphitic rocks and in some cases it is not possible to distinguish the peak contact metamorphic minerals.

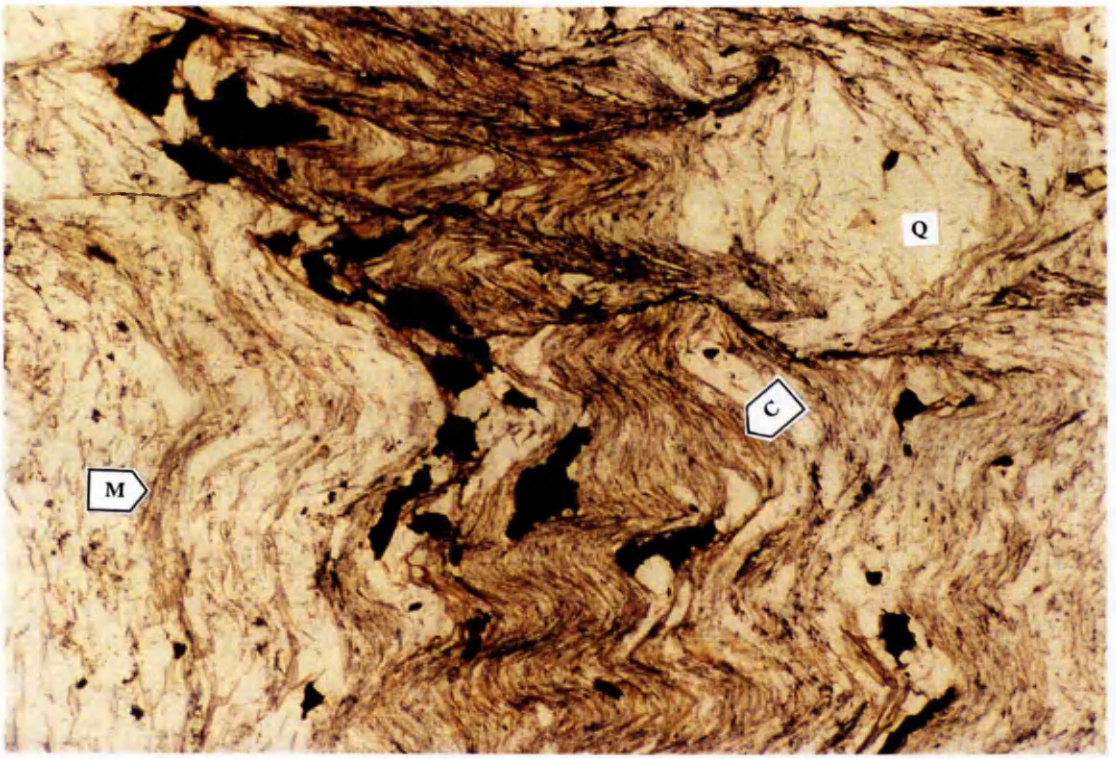

Plate 5.18 Graphitic, semi-pelitic hornfels sample MM45B (G.R. NN10302639) showing chlorite (C), muscovite (M), quartz (Q) and ilmenite (black). S_2 crenulation cleavage is well developed in the mica-rich graphitic part of the rock. PPL. Field of view 4.2mm.

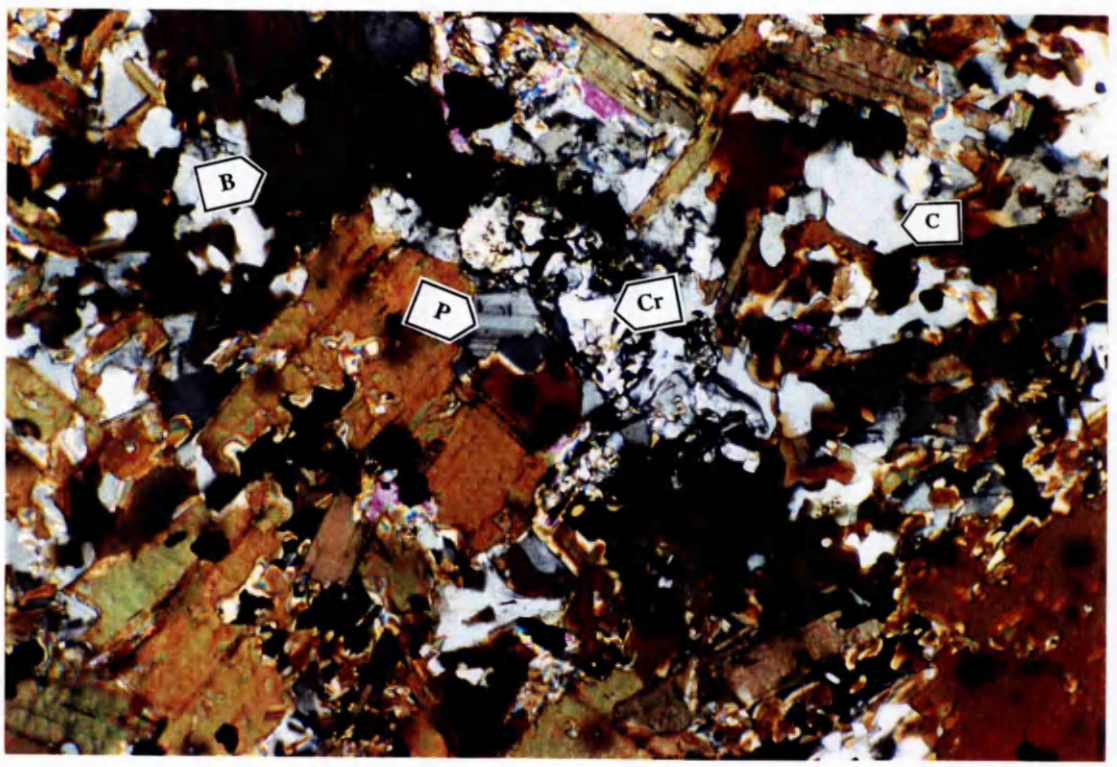

Plate 5.19 Graphite-rich pelitic hornfels sample MM83C (G.R. NN03244425) containing graphite, biotite (B), plagioclase (P), corundum (Cr), cordierite (C) and ilmenite (black). XPL. Field of view 1.6mm.

5.4.4 Distribution of mineral zones in the graphitic rocks:

It is possible to locate the mineralogical zones in the graphitic rocks in the Etive aureole according to Table 5.4 and sample locations in Fig. 5.3. Five mineralogical zones have been mapped in the graphitic rocks of the North Loch Awe area (Fig. 5.3):

Zone I_G (Cordierite zone): No fresh cordierite was found in the samples from the outer aureole rocks in the North Loch Awe area. Because the samples are altered, it is not clear whether there was no cordierite in these rocks prior to alteration or if all of the cordierite crystals are altered. Considering the width of this zone and the next zone, which is the And+Kfs zone, it is reasonable that the altered rocks of Zone I_G had cordierite once, which has since been altered. The existence of yellowish pinitic materials in some of the samples supports this assumption. Considering all these facts, Zone I_G is considered to be a cordierite zone.

Zone II_G (And+Kfs zone): The two characteristic parageneses in this zone are Bt+Ms+Qtz+Crd+Kfs+And and Bt+Qtz+Crd+And+Kfs. An andalusite zone (without Kfs) was not distinguished in the graphitic rocks of the North Loch Awe, probably because of the semi-pelitic and psammitic nature of the rocks, which do not allow andalusite crystallisation prior to muscovite + quartz breakdown.

Zone III_G (Crn zone): The parageneses in this zone are Bt+Crd+And+Kfs+Crn and Bt+Crd+Kfs+Crn.

Zone IV_G (Spl zone): The only paragenesis in this zone is Bt+Crd+Kfs+Crn+Spl.

Because of (i) the semi-pelitic nature of most of the rocks and lack of the index minerals in most of the studied samples, (ii) the widespread alteration in the graphitic rocks, and (iii) the small sampling density, the zoneography and location of mineral isograds for these rocks are not as precise as for non-graphitic rocks. The positions of isograds in the graphitic rocks of the North Loch Awe area though not precise, still permit comparison between isograds in the graphitic and non-graphitic rocks. This comparison shows that the And+Kfs-in isograd in the graphitic rocks is much closer to the contact than the And+Kfs-in isograd in the non-graphitic rocks. Also the Sil-in isograd is not developed in the graphitic rocks. These differences are attributed to higher temperature affecting the non-graphitic pelitic rocks (they are in contact with diorite) and lower temperature affecting the graphitic pelites (in contact with granodiorite).

Fig. 5.5 shows the sample location and distribution of the mineral zones and isograds in the graphitic rocks of the Loch Creran area. Three isograds are located in this area, which are the Crd-in, And-in and Crn-in isograds.

5.5- Petrography of calc-silicates and marbles

The main carbonate-bearing lithologies in the Etive area are Ardrishaig phyllite in the North Loch Awe and Bonawe areas and Creran Flags and Ballachulish Limestone in the Loch Creran area. The Ardrishaig Phyllite and Creran Flags are composed of interlayered (semi-)pelites and calc-silicates. {N.B. for samples in which calc-silicate rocks and (semi-)pelite are distinctly interlayered on a cm-scale (i.e. smaller than the size of a thin section), only the calc-silicate portion is described here}. In the mineral assemblage table (Table 5.5), the alphabetical suffixes to the sample numbers refer to different samples from one locality, when the letter is capital (e.g MM38A, MM38B, MM38C,...). The small letters (e.g. 273a and 273b) denote the different lithological portions in a single thin section.

5.5.1 Regional metamorphic calc-silicates and marbles:

Three thin sections from the regional metamorphic calc-silicates and marbles were examined and the following mineral assemblages were determined:

Cal+Dol+Qtz	[5.50]
Cal+Qtz+Pl+Kfs+Ms+Chl	[5.51]
Cal+Qtz+Pl+Ttn+Chl	[5.52]

These samples were collected from the localities near Dalmally village and localities near the Kilchrenan village in the south Loch Awe area. Oxide minerals and zircon are accessory phases in these samples. Calcite, dolomite and quartz appear as equigranular crystals. The size of calcite and dolomite reach up to 1 mm in sample MM265B and they are fine-grained in others. There is a dominant foliation in the rocks (F_2).

5.5.2 Contact metamorphic calc-silicates:

Forty thin sections of contact-metamorphic calc-silicates were studied using optical microscopy and the following mineral assemblages were found:

Qtz+Pl+Cpx+Wo±Ttn	[5.53]
Qtz+Cpx+Grt	[5.54]
Cpx+Grt+Wo	[5.55]
Qtz+Pl+Cpx+Grt+Wo±Ttn	[5.56]
Cpx+Grt	[5.57]
Pl+Cpx+Ttn	[5.58]
Qtz+Pl+Cpx+Grt+Ttn	[5.59]
Qtz+Pl+Cpx+Tr+Ttn	[5.60]
Cal+Pl+Cpx+Wo+Ttn	[5.61]
Cal+Cpx+Scp+Kfs	[5.62]
Cal+Cpx+Grt+Wo±Ttn	[5.63]
Cal+Cpx+Grt+Ep?	[5.64]
Cal+Qtz+Pl+Cpx+Grt+Ttn	[5.65]
Cal+Qtz+Pl+Cpx+Tr	[5.66]
Cal+Qtz+Cpx+Grt+Wo+Ep?	[5.67]
Cpx+Wo+Phl	[5.68]
Cal+Pl+Cpx+Grt+Wo	[5.69]
Cal+Pl+Cpx+Ttn+Ep	[5.70]
Cal+Pl+Cpx+Grt+Kfs+Ttn+Ep+Prh?	[5.71]
Cal+Tr+Ep+Ms	[5.72]
Cal+Dol+Tr	[5.73]
Cal+Qtz+Cpx+Wo+Scp	[5.74]
Cpx+Wo+Ttn	[5.75]
Cal+Qtz+Pl+Kfs+Ms	[5.76]
Cal+Qtz+Pl+Ttn	[5.77]
Cal+Cpx+Wo+Ttn+Zo	[5.78]
Cal+Qtz+Tr+Ep	[5.79]
Cal+Qtz+Tr+Ttn+Ep+Czo	[5.80]
Cal+Qtz+Pl+Cpx+Ttn+Ep	[5.81]

Table 5.5 Mineral assemblages in limestones and calc-silicates. X=major phase, O=minor phase, A=alteration product. R=regional metamorphic rock.

Sample	G.R.	Cal	Dol	Qtz	Pl	Cpx	Grt	Wo	Scp	Tr	Kfs	Phl	Ttn	Zo	Czo	Ep	Ilm	Prh	Ap	Ms	Chl	Ore	Zrn
Δ86	NN020327			X	X	X		X					X										
TA82	NN020327			X		X	X																
TA87	NN020327					X	X	X															
TA88	NN020327					X	X	X															
Δ96	NN020327			X	X	X	X	X			O		O										
Δ95	NN020327					X	X																
TT19	NN020327			X	X	X		X			O		O										
TT11	NN020327				X	X							X						O				
TA790	NN020327			X	X	X	X						O					O^A		O	O		
TT7	NN020327					X	X	X														O	
TT21	NN020327			X	O	X					O		O										
TT8	NN020327	X			X	X		X					X										
126514	NN020327			X	X	X	X	X			X		O					O^A					O
MM16C	NN00533366	X				X			X		O												
MM33B	NN08302738	X		X		X		X			O		O										
MM34G	NN08302724	X				X	X	X					O										O
MM36C	NN08452702	X				X	X			O^A						O							
MM38G	NN08752677	X		X	X	X	X						O										
MM39D	NN09082662	X		X	X	X				X													
MM39Ea	NN09082662	X		X		X	X	X								O						O	
MM39Eb	NN09082662					X		X				X	O							X			O
MM40B	NN09402648	X			X	X	X	X					O										
MM53A	NN07982679			X	X	X				X			O						O				O
MM63Cb	NN08712640	X			X	X							O			O							
MM63D	NN08712640	X			X	X	X				X		O			O		X	O			O	O
MM77A	NN02334435	X								X^A						O				X			O
MM78A	NN02454431	X	X							X						O						O	
MM81C	NN03024434	X		X		X		X	X														
MM81D	NN03024434	X				X	X	X															
MM82B	NN03164430					X		X					O										O
$MM85C^R$	NN07992561	X		X	O						O								O	X	X	O	O
$MM87^R$	NN06852538	X		O	X								O								X	O	O
MM162C	NN12722923	X				X		X					O	O									
MM232b	NN08982669	X		X						X						O					X	O	O
MM234b	NN08892689	X		X	?	?				X			O		O	O						O	
MM236A	NN08892689	X		X	X	X							X			O			O			O	O
MM237b	NN08782709			X		X				O^A						O							
MM238Bb	NN08932737	X		?	?	X	?		X				O			O							
MM243b	NN08712752	X		X		?				X													
MM244	NN08452749	X		X	?	X	X	?															
MM256b	NN18602747	X	X	X																		O	O
MM273b	NN00643371			X		X		X					X										
MM288	NN00413405	X		X		X		X	?														

Qtz+Cpx+Ep	[5.82]
Cal+Cpx+Scp+Ttn+Ep	[5.83]
Cal+Qtz+Tr	[5.84]
Qtz+Cpx+Wo+Ttn.	[5.85]

Zircon, oxide minerals and apatite are common accessory minerals in most of the samples. The full assemblages of the studied calc-silicates and marbles are summarised in Table 5.5. The first obvious influence of the thermal metamorphism on the calc-silicates is recrystallisation of calcite. In sample MM39D (G.R. NN09082662), calcite shows a granoblastic mosaic texture. Clinopyroxene appears as fine-grained (~0.2mm) to medium-grained (~0.5mm) crystals in higher grades. It is colourless to pale green and occasionally shows simple twining. In general, the Cpx-bearing calc-silicates are pale green, fine-grained, hard hornfelses with dark semi-pelitic interlayers. The main texture of these rocks is granoblastic. Scapolite is present in some samples (Table 5.5 and Plates 5.20). It forms tabular, colourless grains with low to moderate relief. Its cleavage is visible parallel to the length of the crystals. In some of the samples, it forms relatively large (up to 1.5 mm long) crystals with poikiloblastic texture with inclusions of calcite and diopside. The birefringence of scapolite is up to second order violet in sample MM16C (G.R. NN00533366), which probably reflects its Na-rich or marialite-rich composition. Grandite garnet has crystallised in rocks with suitable chemistry. It forms fine-grained (up to 0.2 mm) crystals. It has crystallised along some layers in some of the samples, which are inherited compositional layering from the original sedimentary rocks (Plates 5.21 and 5.22). Idioblastic grains of medium-sized (0.5 to 1mm) garnet are twinned and pleochroic in sample MM63D (G.R. NN08712640). Wollastonite appears as randomly oriented acicular and tabular crystals up to 2mm in length (Plates 5.28 and 5.29). Poikiloblastic wollastonite in an assemblage of Cal+Grt+Wo+Ttn contains inclusions of clinopyroxene and titanite in sample MM40B (G.R. NN09402698) (Plate 5.21). Plagioclase appears as small tabular crystals with polysynthetic twinning (e.g. sample 126514) and occasionally optical zoning. K-feldspar forms fine-grained crystals of microcline with tartan texture in K-feldspar-bearing calc-silicates. Biotite is present in some of the samples (e.g. sample MM16B, G.R. NN00533366) and forms

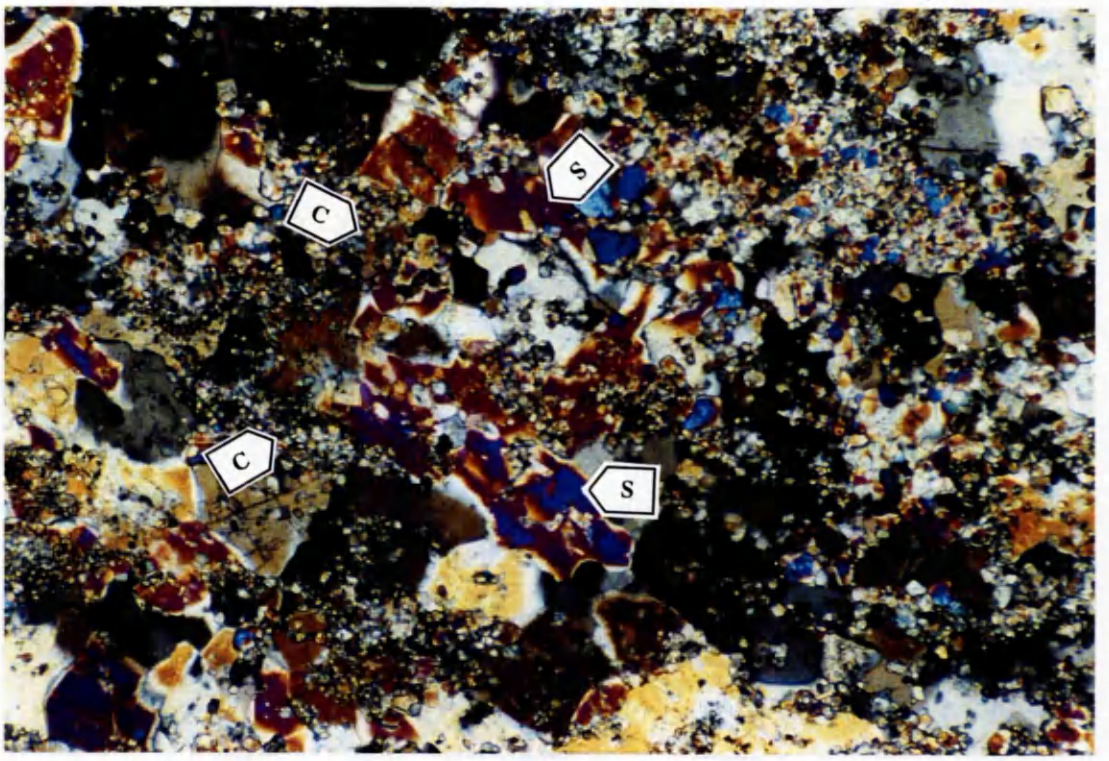

Plate 5.20 Calc-silicate hornfels sample MM16C (G.R. NN00533366) containing tabular scapolite (S) and fine- to medium-grained clinopyroxene. The rocks has a granoblastic texture. XPL. Field of view 1.6 mm.

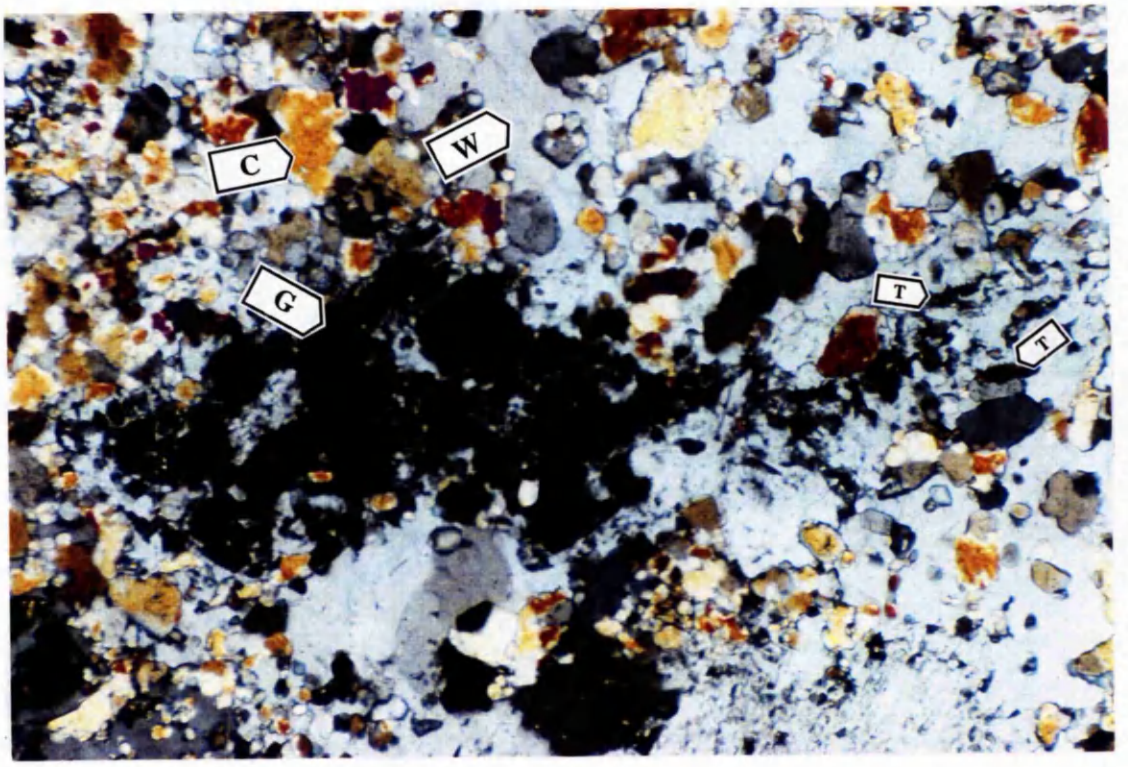

Plate 5.21 Calc-silicate hornfels sample MM40B (G.R. NN09402698), containing porphyroblastic wollastonite (W) with inclusions of clinopyroxene (C) and titanite (T). Isotropic mineral in the left-centre of the photo is garnet (G). XPL. Field of view 1.6 mm.

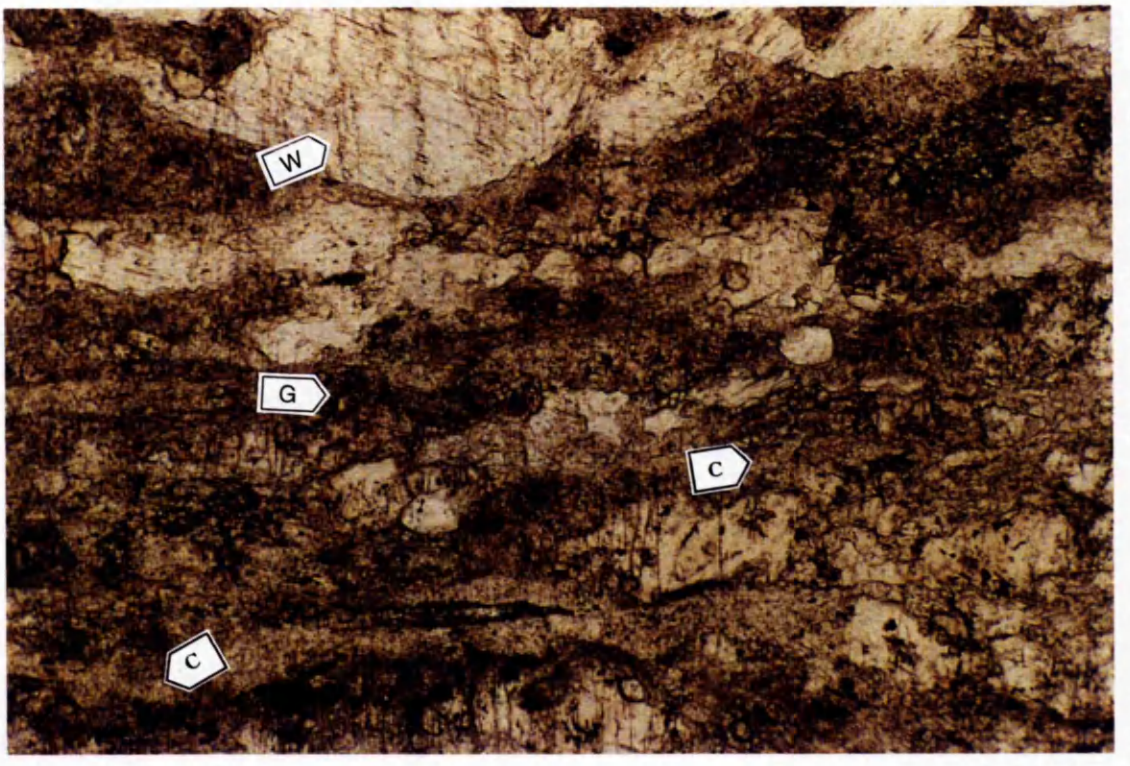

Plate 5.22 Calc-silicate hornfels sample MM34G (G.G. NN08302724), containing garnet (G), clinopyroxene (C) and wollastonite (W). Garnets are crystallised along the original layering (bedding) in the chemically suitable parts of the rocks. PPL. Field of view 1.6 mm.

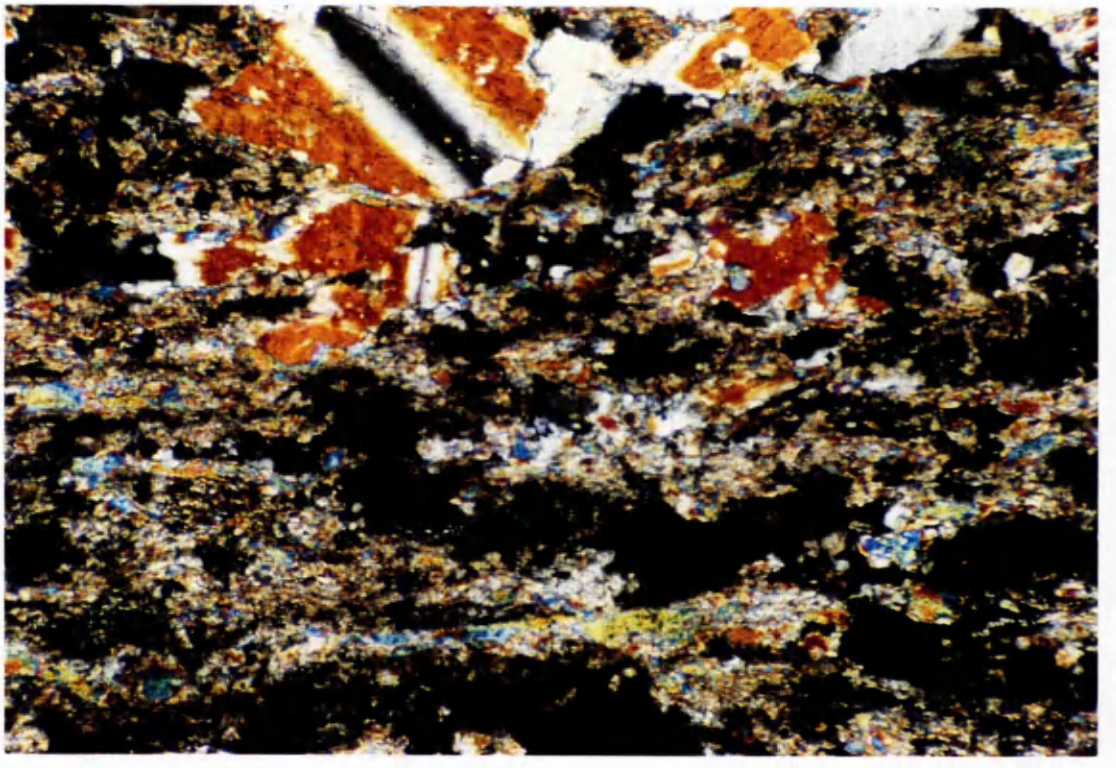

Plate 5.23 As above in XPL to show the twinning in wollastonite.

small flakes (~0.1 mm long). Titanite has wedge-shaped crystals and is relatively large (~0.5 mm) in some of the samples (e.g. TA86, G.R. NN126507). In sample MM77A (G.R. NN02334435), calcite is the dominant mineral and serpentine and tremolite are present. The serpentine occupies separate equidimensional domains, which reflects its probable retrogressive origin after olivine. Tremolite forms fine fibrous aggregates and is apparently a retrogressive product of clinopyroxene.

There is no clear pattern in the distribution of mineral assemblages in calc-silicates in relation to the distance from the igneous contact. Even samples relatively far from the contact (e.g. sample MM40B, G.R. NN 09402648), from localities corresponding to Cordierite Zone in the pelitic rocks contain wollastonite, diopside and garnet. I was not able to locate metamorphic zones and isograds in calc-silicates because of the relatively small number of samples and lack of clear pattern in distribution of assemblages in the studied calc-silicates.

5.6 Petrography of andesitic rocks

There is a screen of andesitic rocks in the north Loch Awe area in the plutonic rocks, which is in contact with Cruachan Granodiorite to the north and Quarry Diorite to the south. Four thin sections of andesitic rocks were studied. Samples were collected from the rocks close to the Cruachan Reservoir and outcrops along the Altt Mhoille stream. The mineral assemblage of these rocks is Qtz+Pl+Hbl with appreciable amounts of oxide minerals and accessory amounts of zircon and apatite. The rocks have a relict porphyritic texture with phenocrysts of hornblende and plagioclase. Plagioclase shows polysynthetic twinning and hornblende shows simple twinning. The former is altered to clay minerals and the latter is altered to biotite. The matrix of the andesitic rocks is recrystallised due to the contact-metamorphism and has a granoblastic texture. Probably the highly altered state of the rocks is because of the fluidal effects of the Cruachan Granodiorite.

Chapter 6
Petrography of pelitic and semi-pelitic migmatites

6.1 Introduction

Migmatites are mixed metamorphic and igneous rocks (Sederholm, 1967) containing light, leucosome and dark, mesosome components. Four possibilities for generation of leucosomes are proposed by investigators:

i) The leucosomes may have been derived from partial melting of the host rock (Holmquist, 1921; Mehnert, 1968; Wylie and Tuttle, 1961; von Platten, 1965; Johannes, 1983, 1988).

ii) The leucosomes may have formed by solid-state differentiation of mafic and felsic materials during metamorphism (White, 1966; Gresens, 1967; Fisher, 1973; Ashworth, 1985).

iii) Introduction of alkali elements during metasomatism can produce the leucosomes (Olsen, 1985).

iv) Leucosomes may have been produced by injection of granitic melt into metamorphic rocks (Sederholm, 1907, 1913, 1934; Buddington, 1948).

More than one factor may be active in the generation of migmatites and a combination of field and laboratory studies is required to interpret the processes involved, the scale of melting and any melt gain or loss during migmatisation.

Most of the studies of migmatites deal with migmatites in regional metamorphic terrains. Few cases of migmatisation of pelitic rocks within contact metamorphic aureoles have been studied. In the Grampian Highlands of Scotland, migmatised pelitic and semi-pelitic rocks around Caledonian granitoid intrusions have been studied by some authors (e.g. Platten, 1982, 1983; Pattison and Harte, 1988; Harte *et al.*, 1991) who concluded that partial melting is the dominant process by which they originated. In the Etive Aureole the pelitic and semi-pelitic rocks of the Leven schist have been migmatised adjacent to the igneous contact. In this chapter the field relations and petrography of the migmatites are described in an attempt to elucidate

their mode of origin. I shall demonstrate that, as in the case of the other studied Caledonian aureoles (e.g. Ballachulish), the Etive migmatites formed by partial melting.

In the South segment of the Etive aureole, migmatites occur within about 200m of the contact of the pluton in compositionally suitable rocks. The migmatites are best developed on the eastern side of the summit of Monadh Driseig. Some xenoliths within the Cruachan Intrusion in the North Bonawe area are also migmatised. The migmatites contain pale veinlet-shaped domains and dark domains. The pale veinlets are mainly composed of quartz and K-feldspar, and are believed to be produced from the crystallisation of a silicate melt (see below). The dark domains are hornfelses rich in restitic ferromagnesian minerals. In the text, the term "leucosome" is used for pale veinlets and the term "mesosome" is used for dark domains. The term "migmatite" is used for the rocks because they are a mixture of metamorphic rocks (hornfelses) and crystallised leucocratic veins fills. Migmatites in the Etive Aureole can be classified according to their mineralogy and field relations. It should be mentioned that the extent of migmatisation in the Etive Aureole (both in terms of leucosome proportion and exposed area of migmatites) is small in comparison with similar aureoles such as Ballachulish (Harte *et al.,* 1991). There are no diatexites comparable to the "Chaotic Zone" of Pattison and Harte (1988) in the area studied.

6.2 Field relations of Etive migmatites

The migmatites of the Etive aureole are classified according to their field relations and structures in the following section.

6.2.1 Migmatites with small-scale leucosomes with pull-apart structures: In this type of migmatite, leucosomes are associated with breccia-like ("agmatic") structures in the hornfelses. The leucosome occupies the spaces between pieces of hornfels, which gives a brickwork appearance to the migmatites. Plate 6.1 illustrates a photograph of this type of migmatite. Horizontal veinlets are almost perpendicular to the vertical ones but do not cut them. Particularly good exposures of this type of migmatite are found at locality NN12302850 eastern side of Monadh Driseig and west of Glen Strae. Plate 6.2 shows a polished slab of migmatite with pull-apart-structured leucosomes. In this sample the K-feldspar and quartz-rich veinlets are intruded into the spaces between the cordierite-rich hornfels mesosomes. This plate clearly shows the pull-apart effect on the hornfels mesosome. The leucosomes are

either at right angles to the S_2 crenulation cleavage or run along the cleavage. Plates 6.3 and 6.4 are other illustrations of these migmatites. Fragments of cordierite-rich hornfels mesosomes with breccia-like structures are shown in Plate 6.4. Mesosome fragments are 'floating' in leucosome. The brick-like mesosome fragments are elongated parallel to the original compositional layering (bedding) and separated by relatively thick (1-3mm) leucosome veinlets. A second set of much finer leucosomes has formed parallel to the former S2 crenulation cleavage. Under the microscope, the mesosome is made of cordierite-rich hornfels with andalusite and biotite. The leucosome is made of K-feldspar and quartz, the latter with an interstitial texture. Plates 6.5 and 6.6 illustrate the appearance of the migmatites with pull-apart structures under the microscope. It is clear that the leucosome part is virtually free of ferromagnesian minerals, but the mesosome contains biotite and cordierite (Plate 6.5). The interstitial texture of quartz is clear in Plate 6.6. K-feldspars are euhedral (especially where projecting into quartz) to subhedral. In Plate 6.5, K-feldspars in the leucosome part are cloudy.

Migmatites with pull-apart structures in the Etive Aureole are similar to migmatites with pull-apart and breccia-like structures from the Ballachulish Aureole described by Pattison and Harte (1988) and Harte *et al.* (1991).

6.2.2 Migmatites with small-scale cross cutting leucosomes: The leucosomes cross cut the original layering, S_2 crenulation cleavage and other leucosome veinlets in this type of migmatite. Plate 6.7 shows a photograph of this type of migmatite, in which two sets of leucosomes may be distinguished. One set of leucosomes runs approximately parallel to the length of the photograph (perpendicular to the S_2 crenulation cleavage which runs from the top to the bottom of the photograph), and a second set of cross-cutting leucosomes is at ca. 70° to the former set. In Plate 6.8, leucosomes are oriented randomly and cut each other and the S_2 crenulation cleavage. The thickness of leucosomes in this type of migmatite is a few mm and they can be traced for a few tens of centimetres. Under the microscope, the mesosome contains cordierite, biotite, andalusite, spinel and ore minerals and has a granoblastic/poikiloblastic texture typical of the inner-aureole hornfelses (see Chapter 5). The leucosome is made of quartz and K-feldspar. Plate 6.9 shows microscopic view of this type of migmatite. Cloudy K-feldspar is clearly visible in PPL view. Coarse-grained, igneous-textured leucosome is easily distinguishable from

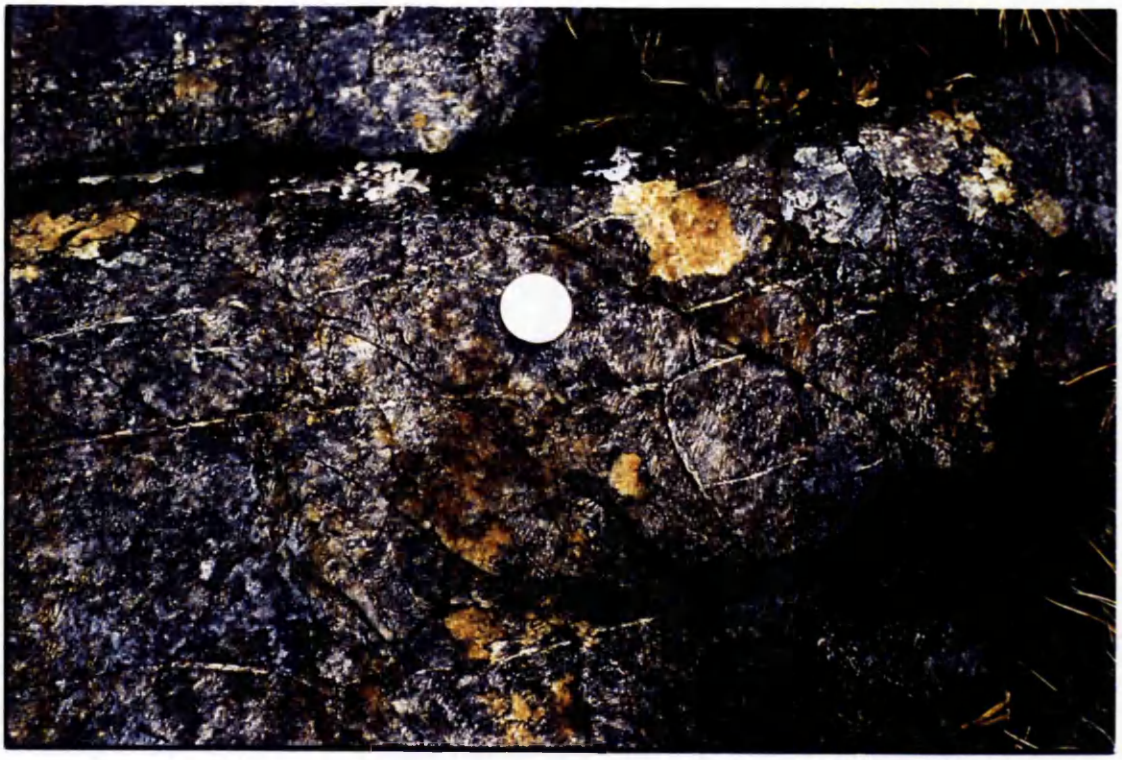

Plate 6.1 Migmatite with pull-apart structures from locality NN12302850. Thin veinlets (~10mm thick) of leucosome within a cordierite-rich hornfelsic matrix have brickwork appearance. Note also thin leucosomes parallel to the former S_2 crenulation cleavage oriented diagonally top right to bottom left of photo. Diameter of coin used for scale: 24 mm.

Plate 6.2 A cut and polished hand specimen of migmatite with pull-apart structure. One set of leucosomes are parallel to the former S_2 crenulation cleavage and the other set cut the crenulation. Dark spots on the rock surface shows cordierite-rich patches. The scale bar is 1 cm I ong.

Plate 6.3 Migmatites with pull-apart and breccia structures. Fragments of cordierite-rich hornfelsic mesosomes are surrounded by leucosomes. Diameter of coin used for scale: 24 mm.

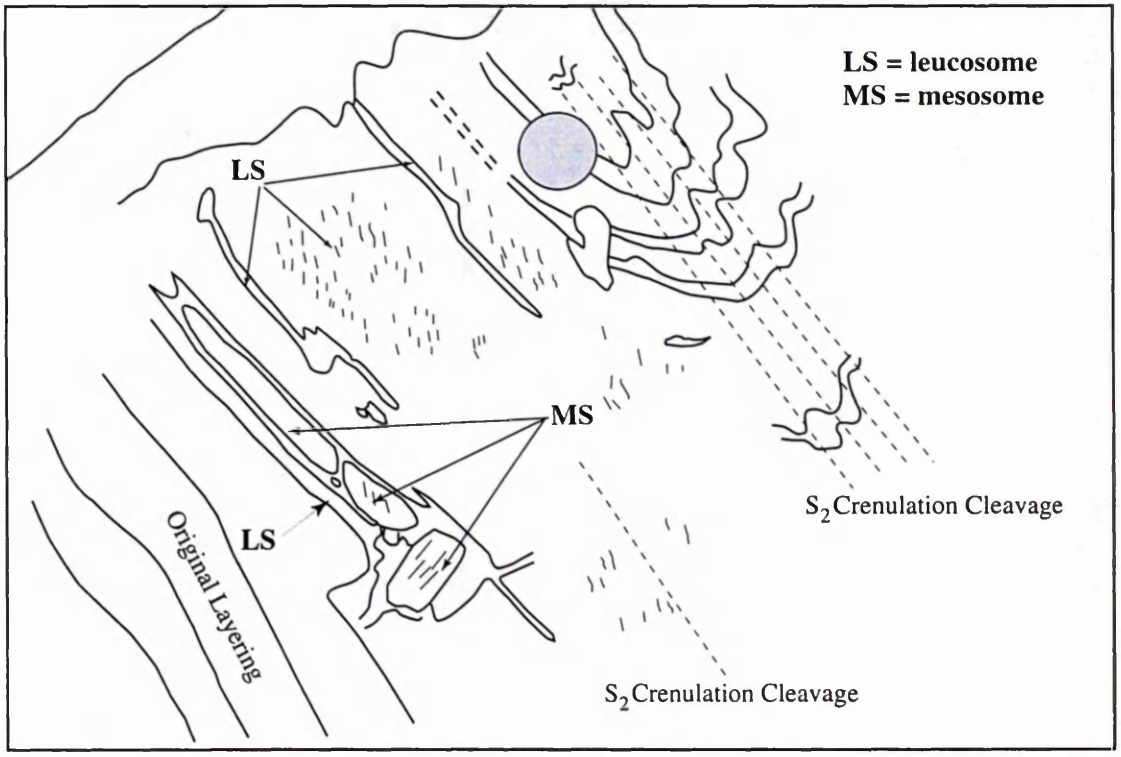

Plate 6.4 A sketch drawing of the above photograph to show the details of leucosome-mesosome relations. Note that the thicker leucosomes have formed parallel to the original compositional layering (bedding) while the thinner ones have formed parallel to the former S_2 crenulation cleavage.

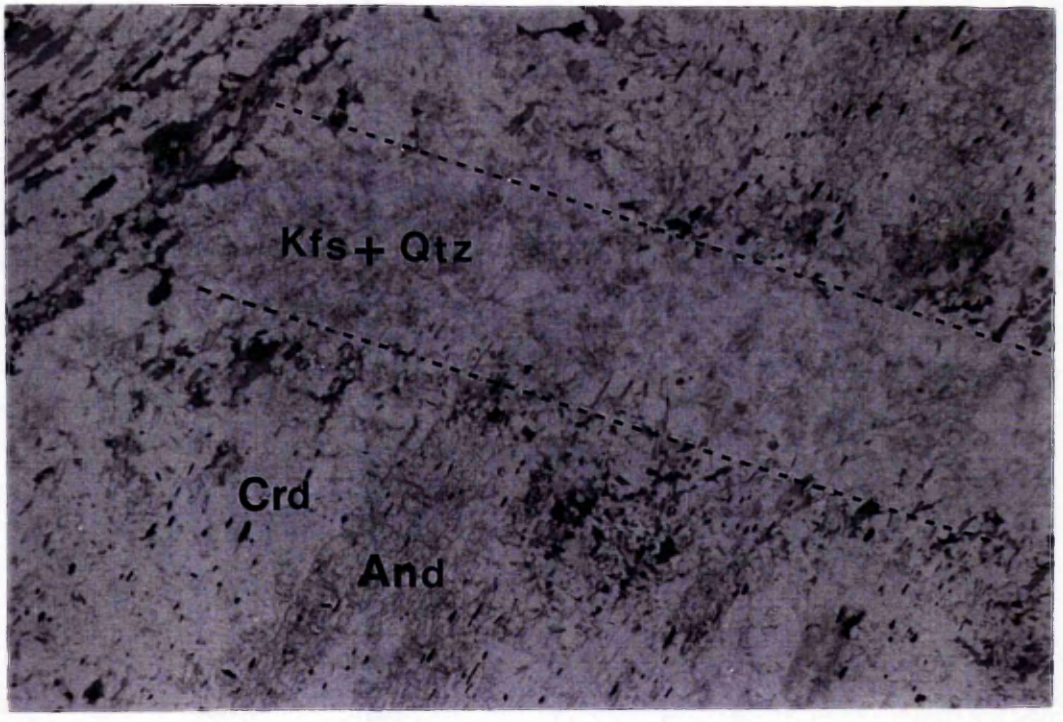

Plate 6.5 Leucosome and mesosome in sample MM186A, locality NN12092826. The leucosome is composed of quartz (Q) and K-feldspar (K) and the mesosome is composed of cordierite+andalusite+K-feldspar+quartz+biotite+ore minerals. K-feldspar in the leucosome has a cloudy appearance and quartz has an interstitial-xenomorphic texture. The boundary between the leucocratic and mesocratic parts is shown by a dashed-line. PPL, field of view is 4.2mm.

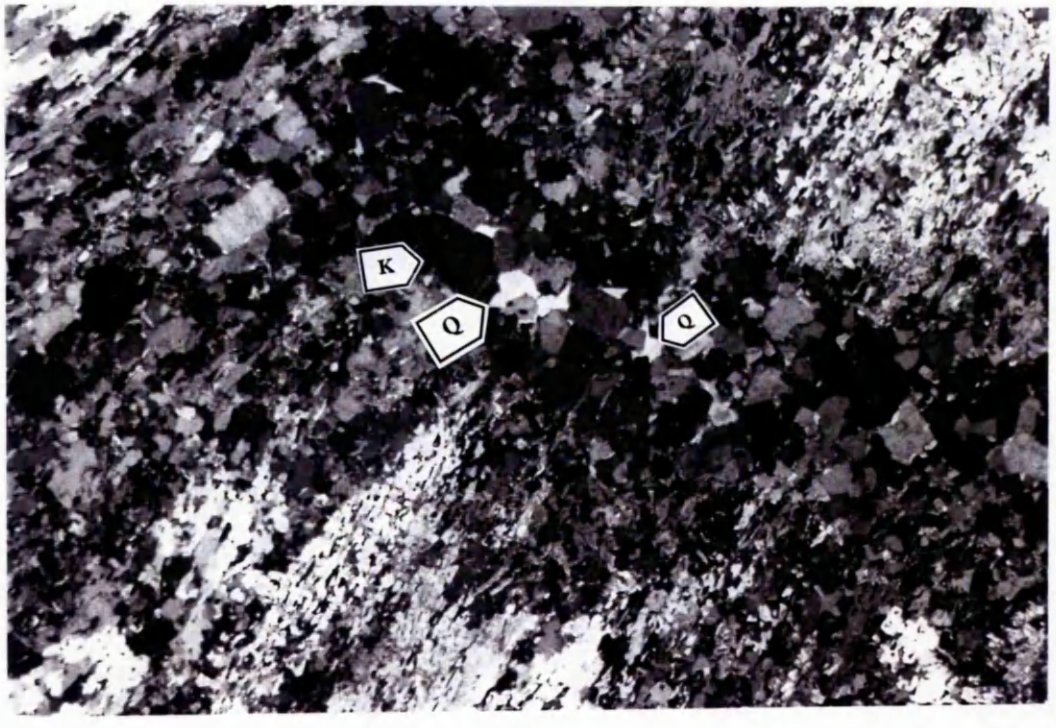

Plate 6.6 As above in XPL to show the interstitial xenomorphic texture of quartz and euhedral to subhedral texture of K-feldspar.

Plate 6.7 Migmatites with cross-cutting leucosomes. Leucosomes veinlets parallel to the length of the photograph (perpendicular to the S_2 crenulation cleavage) are cut diagonally by a second set of veinlets. Locality NN12302850. Diameter of coin used for scale is 24 mm.

Plate 6.8 Migmatites with cross-cutting leucosomes with randomly oriented veinlets. Locality NN12302850. Diameter of coin used for scale: 24 mm.

the fine to medium-grained mesosome hornfels in Plate 6.10. In the former, quartz shows very clear interstitial-xenomorphic texture, filling the cavities between K-feldspars. A film of quartz can be seen between K-feldspars, where K-feldspar is more abundant than quartz. The euhedral to subhedral habit of the K-feldspars is visible. Migmatites with small-scale cross-cutting leucosomes are present in the partial-melting zone, close to the former types of migmatites. Good exposures were found at locality NN12302850 in north Loch Awe area, in the Leven Schist.

Migmatites with medium-scale leucosomes: In this type of migmatites, leucosomes are about 15-40 mm thick and they can be traced for a few metres. Plate 6.11 illustrates the field appearance of this type of migmatite. Here, veins of leucosome are sub-parallel to one another and they cut both the folded compositional layering (bedding) and the S_2 crenulation cleavage perpendicularly. The S_2 crenulation cleavage is axial planar to the F_2 folds in Plate 6.11. Plate 6.12 shows sub-parallel leucosomes, which are cut by some thin diagonally oriented veins of leucosome. These diagonal veins are thicker in places and make a pool of melt locally around an island of hornfels. Two cases are marked in Plate 6.12. Under the microscope, the leucosomes have an igneous texture with interstitial-xenomorphic quartz and euhedral to subhedral cloudy K-feldspars (Plate 6.13). Some subhedral, relatively coarse biotite flakes are associated with quartz and K-feldspar. Small flakes of muscovite may also be found. In migmatites close to the igneous contact, the modal proportion of muscovite in the leucocratic part is higher. Plate 6.14 is a microphotograph of the leucosomes with interstitial-xenomorphic quartz and euhedral to subhedral cloudy K-feldspar plus fine- to medium-grained muscovite. The amount of biotite is lower than that of muscovite. Probably muscovites are retrograde alteration products after biotites. At locality NN11902852, the leucosomes are large enough to be sampled for chemical analysis. Plate 6.15 illustrates the microscopic appearance of leucosome sample MM192D. The rock consists of cloudy K-feldspar and interstitial quartz.

6.3 Mineralogical classification of migmatites

Four groups of migmatites can be distinguished in the Etive aureole, based on the mineralogy of the leucosomes. These groups are as follows.

6.3.1 Qtz+Kfs±Ms-bearing leucosomes: Euhedral to sub-hedral crystals of K-feldspar with perthitic texture are separated by cuspate interstitial patches of quartz in

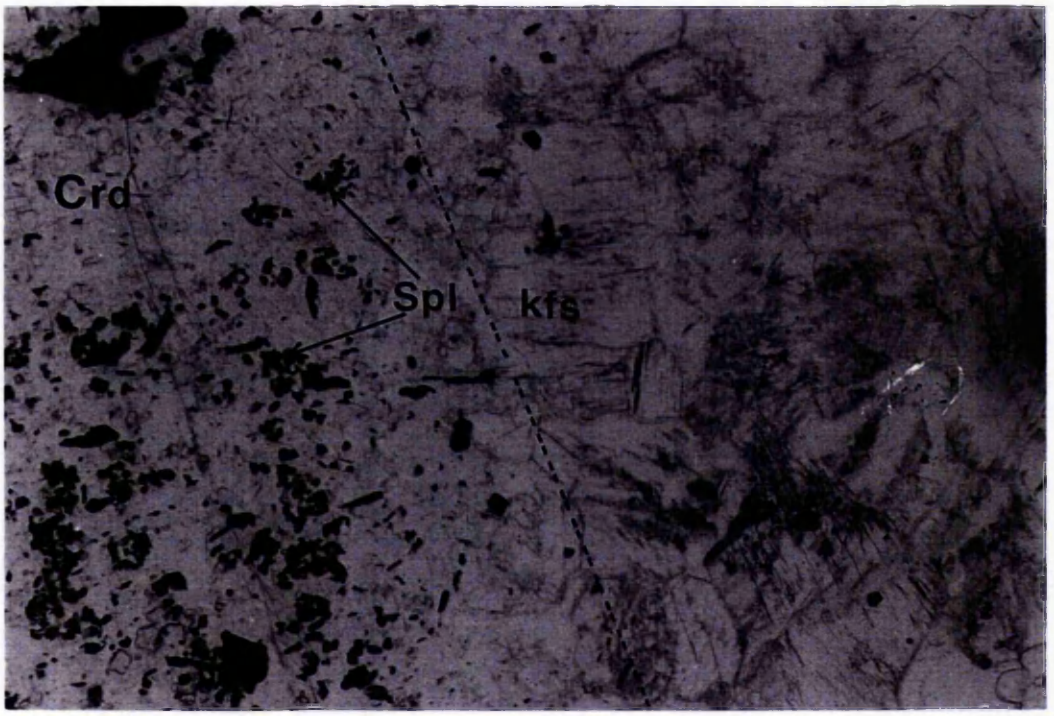

Plate 6.9 Microscopic view of migmatites with cross-cutting leucosomes in sample MM167C from locality NN 12402890. The leucocratic part is composed of interstitial-xenomorphic quartz and euhedral to subhedral cloudy K-feldspar. The mesocratic part is composed of cordierite (Crd), K-feldspar, Spinel (Spl), biotite and ore minerals ±andalusite. The boundary between leucosome and mesosome is marked by a dashed-line. PPL. The length of field of view is 1.6mm.

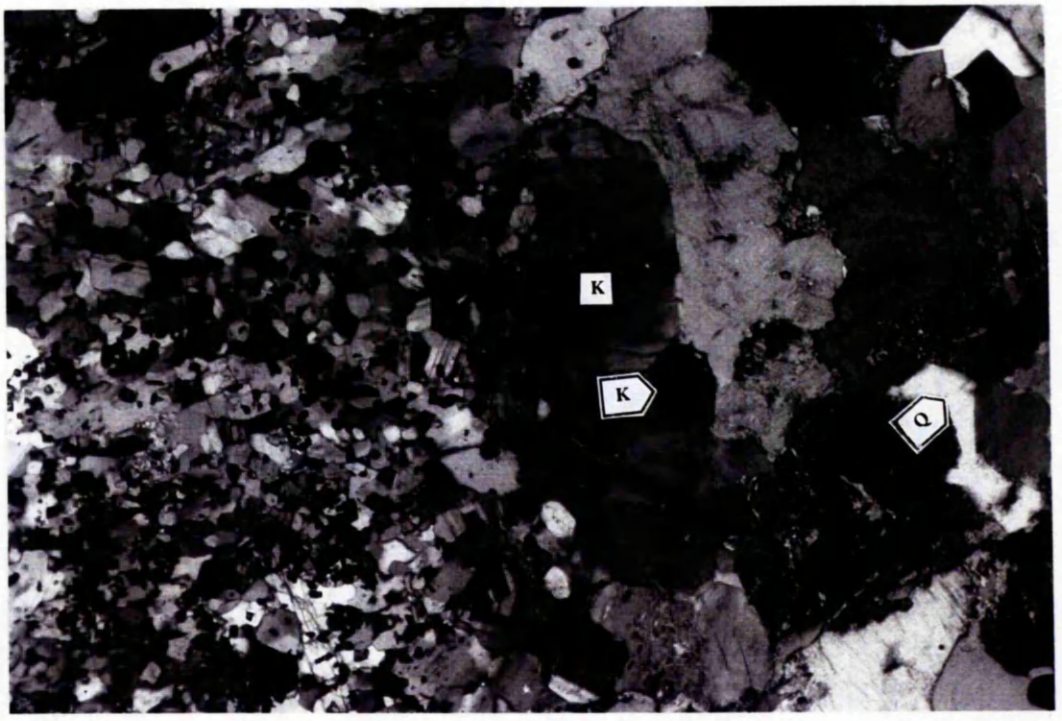

Plate 6.10 as above in XPL to show the interstitial-xenomorphic texture of quartz and euhedral to subhedral texture of K-feldspar.

this type of leucosome. Minor muscovite is present in some of the samples. Plates 6.13 and 6.14 show examples of this type of leucosome.

6.3.2 Qtz+Kfs+Crd-bearing leucosomes: Subhedral to euhedral cordierites are present in some leucosome veinlets. Cordierite is associated with interstitial quartz and perthitic K-feldspar. This assemblage can be found in sample MM166C from locality NN12482896.

6.3.3 Garnet-bearing leucosomes: Euhedral crystals of almandine-rich garnet (see Chapter 7) occurs in association with interstitial quartz and perthitic K-feldspars in some of the leucocratic parts of migmatites. Plates 5.14 and 5.15 (Chapter 5) show an example of garnet-bearing leucosomes.

6.3.4 Orthopyroxene-bearing leucosomes: Orthopyroxene, quartz and cordierite have crystallised in veinlets in some semi-pelitic and psammitic rocks. The hornfels mesosome composed of orthopyroxene, quartz, biotite, cordierite and ore minerals. Plates 5.16 and 5.17 (Chapter 5) show an example of an orthopyroxene-bearing migmatite. The composition of fine-grained orthopyroxenes in hornfels is different from the composition of coarse-grained orthopyroxene in the leucocratic part. Pyroxenes in leucosomes are more Fe-rich (see Fig. 7.24).

6.4 Chemical characteristics of leucosomes in migmatites

The sample MM192D was analysed by means of XRF for major and trace elements. The analysis is listed in Table 6.1. This sample is broadly granitic in terms of its major oxides but is different from the Etive igneous rocks in detail. Fig. 6.1 shows the Na_2O versus K_2O diagram for sample MM192D, which plots in the S-type field of the diagram where all samples from the Etive igneous rocks plot in the I-type field of this diagram (see Fig. 3.9). Fig. 6.2 shows the concentration of trace elements in sample MM192D, normalised for chondrite values. The Etive leucosomes are mineralogically similar to the I-type Meall Odhar Granite, which contains quartz and alkali-feldspar, but the trace element distribution patterns are different. The leucosomes are enriched in Ba (like samples from the Cruachan and Quarry intrusions) while the Meall Odhar Granite is depleted in Ba (Fig. 6.2). The other clear difference between the trace element concentrations in leucosomes and igneous rocks is the concentration of Zr. Zr is highly depleted in the leucosome in comparison with the igneous rocks. The concentration of Rb is higher in the leucosomes.

Plate 6.11 Migmatites with medium-scale leucosomes up to 40mm thick and a few metres long. Veinlets are parallel and cut S_2 crenulation cleavage, which is axial planar to the F_2 folds. Locality NN12302850.

Plate 6.12 Medium-scaled sub-parallel leucosomes which are cut by some thin diagonally running veinlets of leuocosome. Hornfels mesosome islands in a pool of leucosome are marked by arrows (see text for more explanation).

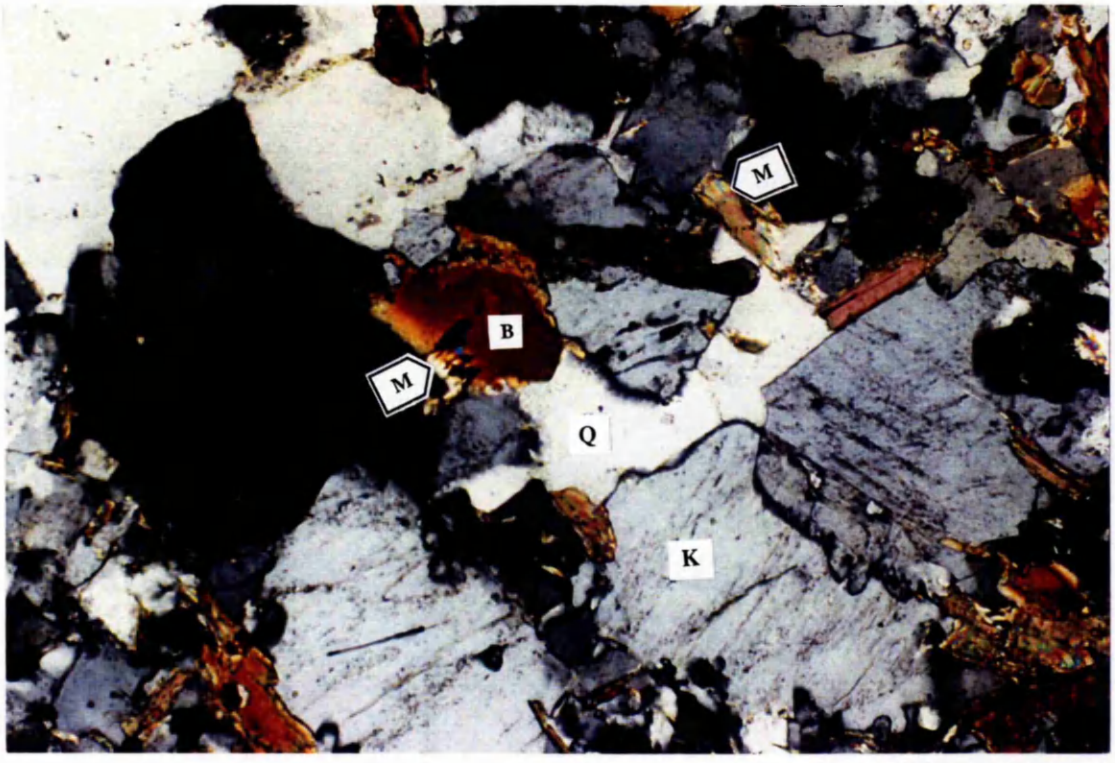

Plate 6.13 Microscopic view of a part of medium-scale leucosome consisting of interstitial-xenomorphic quartz (Q), sub-hedral K-feldspar (K) and biotite (B), Small flakes of muscovite (M) are probably retrograde alteration products after biotite. Sample MM147, Locality NN11772815. XPL. The length of field of view is 1.6mm.

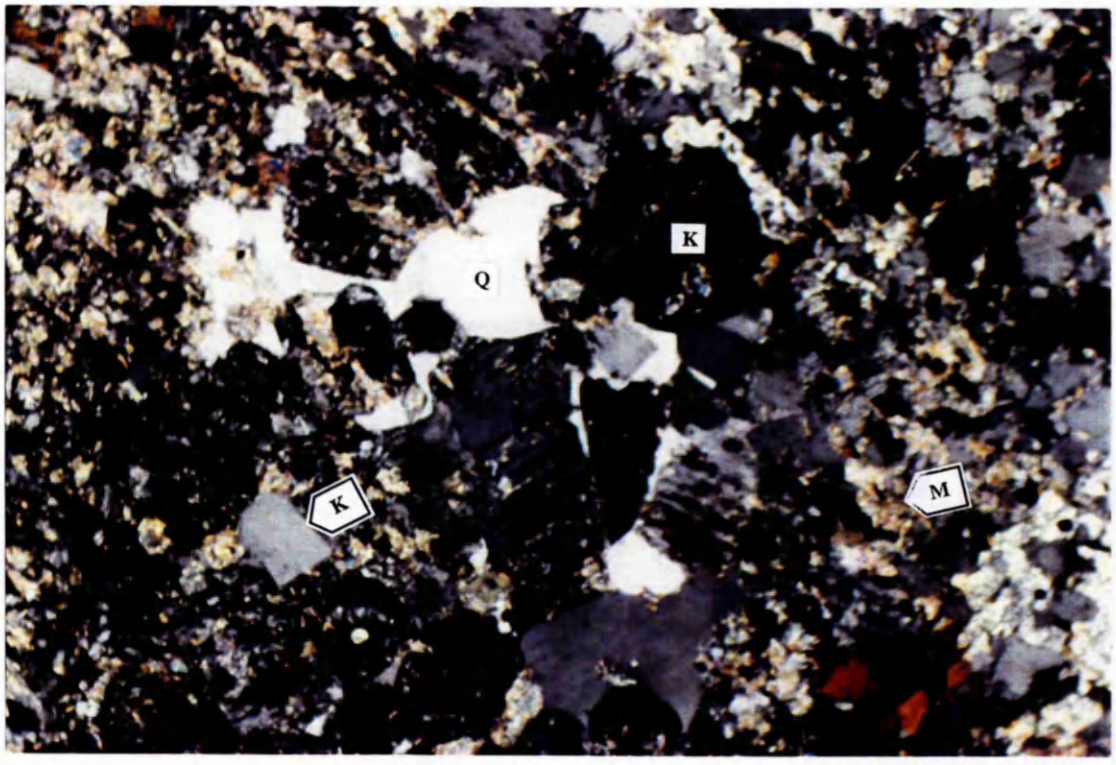

Plate 6.14 Leucosomes in sample MM141 from locality NN11432828, consisting of interstitial quartz (Q), euhedral to sub-hedral K-feldspar (K) and muscovite (M). Muscovite is probably after biotite. XPL,

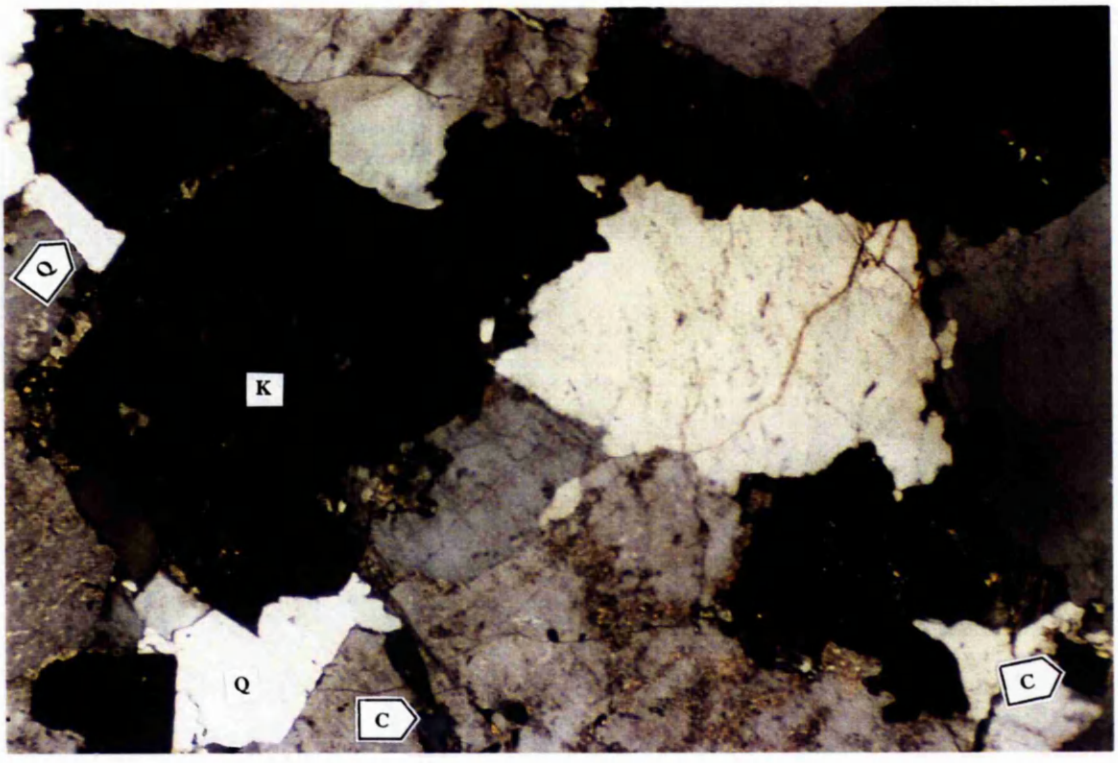

Plate 6.15 Sample MM192D from a leucosome in the migmatites with medium-scale leucosomes from locality NN11902852. The rock is composed of interstitial-xenomorphic quartz (Q), cloudy K-feldspar (K) and minor amounts of chlorite (C). The latter seems to be a retrogressive alteration product of biotite. XPL. The length of field of view is 4.2mm.

Table 6.1 Chemical composition and CIPW norm of leucosome sample MM192D. BD = below detection limit.

Major oxides	Value, wt %	CIPW norm	Value, %	Trace elements	Value, ppm
SiO2	72.78	Quartz	25.09	Nb	9
Al2O3	14.75	Corundum	1.18	Zr	54
FeO	0.31	Orthoclase	55.14	Y	50
MgO	0.37	Albite	15.57	Sr	197
CaO	0.65	Anorthite	1.23	Rb	227
Na2O	1.84	Hypersthene	1.36	Zn	10
K2O	9.33	Ilmenite	0.15	Cu	4
TiO2	0.08	Apatite	0.81	Ni	BD
MnO	BD	Total	100.53	Cr	4
P2O5	0.35			Ce	37
Total	100.46			Nd	16
				V	BD
				La	18
				Ba	814
				Sc	5

6.5 Evidence for partial melting

The following lines of evidence strongly suggest, when taken together, that the migmatites of the Etive Aureole were produced by partial melting of the local

metasedimentary country rocks, and that their leucosomes are essentially crystallisation products of anatectic melt.

(i) Leucosome morphology: many of the Etive leucosomes have vein-like morphologies and show intrusive, cross-cutting relationships with respect to primary compositional layering (bedding) in the metasediments. This indicates that they formed by the crystallisation of a discrete, mobile, low-viscosity phase that filled fractures in the rocks. This observation rules out formation of the Etive migmatites by solid-state differentiation. The mobile fracture-filling phase could have been either a hydrothermal fluid or, more likely (for reasons explained below), a silicate melt. The fact that the veins are generally thin and relatively short suggests that the fracture-filling phase was derived locally. None of the veins appear to be connected to large igneous bodies of the Etive intrusive suite, suggesting that the leucosomes are unlikely to have formed by injection of granitoid melt from the Etive intrusions.

(ii) Leucosome distribution: The fact that leucosomes are restricted to pelitic and semi-pelitic layers, and virtually absent from interlayered quartzites and metabasites strongly suggests a bulk-chemical control on their formation. Pelitic and semi-pelitic rocks are known to have lower minimum melting temperatures than mafic rocks. This suggests that the Etive migmatites could have been formed by anatexis. If so, the melts produced either crystallised very close to their sites of generation, or only migrated short distances (a few metres at most) before crystallising.

(iii) Textural contrast between leucosomes and mesosomes: The Etive leucosomes possess igneous textures, consistent with crystallisation from (or in the presence of) a melt, whereas the mesosomes have textures indicative of crystallisation in the solid state. The contrast is evident in both grain shape and grain size.

The leucosomes contain cloudy, euhedral to subhedral, blocky K-feldspars, occasionally rimmed by a fine albite layer, and interstitial-xenomorphic quartz. The grain-size of the leucosomes is generally larger, on average, than that of the mesosome. These features, plus the local granophyric intergrowth of quartz and feldspar, are commonly associated with granites and pegmatites (Mehnert, 1968). Pattison and Harte (1988) considered the cloudy appearance of K-feldspar as evidence for crystallisation from a melt. The interstitial-xenomorphic quartz grains

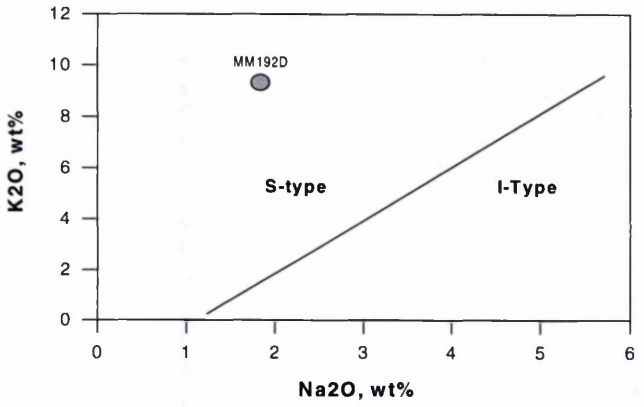

Fig. 6.1 K_2O versus Na_2O diagram for migmatite leucosome sample MM192D. The sample plots in the S-Type field. The line separating S-and I-Type rocks is based on the criteria of Chappell and White (1974).

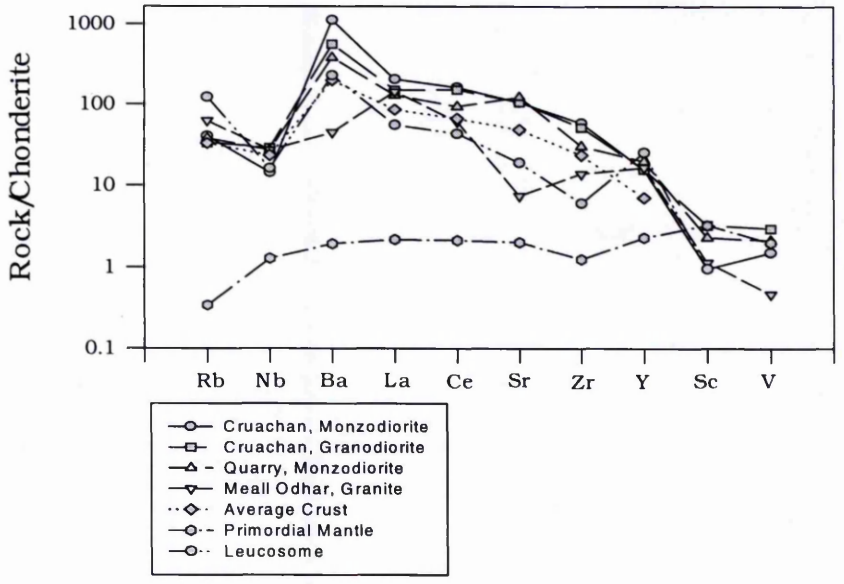

Fig. 6.2 Distribution of trace elements in leucosome sample MM192D in comparison with trace element distributions in Etive igneous samples and primordial mantle. The general trends of trace element distribution in the leucosome and Etive igneous rocks are similar but Zr is depleted in leucosomes.

are locally in optical continuity suggesting their crystallisation from the melt at a late stage (after crystallisation of much of the K-feldspar) so that they take the shape of the remaining pools of melt.

Where ferromagnesian minerals, such as garnet, cordierite or orthopyroxene occur in the Etive leucosomes, they are generally coarser, more euhedral, and contain fewer inclusions, than grains of the same minerals in the adjacent mesosomes. Such textural contrast has been noted in many migmatite occurrences (e.g. Waters and Whales, 1984; Powell and Downes, 1990) and have been ascribed to melt-fluxed growth of these minerals in leucosomes as the solid products of incongruent melting reactions.

(iv) Bulk chemical composition of leucosomes: The bulk chemistry of the analysed leucosome is essentially (leuco-)granitic, and thus more consistent with an origin by crystallisation from a melt than from a hydrothermal fluid.

Possible origins of leuco-granite melts in the Etive Aureole are (a) minor intrusions of the Meall Odhar granite suite, and (b) melts produced by anatexis. There is a wealth of experimental data showing that the initial melts produced by anatexis of pelitic rocks are granitic (e.g. Clemens and Wall, 1981; Clemens and Vielzeuf, 1987; Vielzeuf and Hollaway, 1988; Patino Douce and Johnston, 1991; Stevens *et al.*, 1997). The fact that the Etive leucosomes do not resemble the Meall Odhar suite either petrographically (they are a different colour and contain different mineral assemblges) or geochemically strongly suggests an anatectic origin, which is further supported by their S-type characteristics.

6.6 Discussion

6.6.1 Controls on leucosome shapes: If, as argued above, the Etive leucosomes originated by crystallisation of anatectic melt, it is appropriate to consider the factors that controlled their shapes.

The leucosomes in migmatites with pull-apart and breccia structures (e.g. Plates 6.3, 6.4) clearly reflect melt collection in structurally controlled sites. In many cases, the contacts between compositional bands (i.e. bedding planes) have acted as sinks for the collection of melt. On a smaller scale, melt has also gathered along former S_2 crenulation cleavage planes. These zones of coalescence could reflect either (a) the location of melting reactions in the rocks, or (b) zones of weakness in which dilation and hence melt accumulation, was possible, or (c) both. Bedding

planes commonly mark abrupt changes in bulk composition, reflected in changes in modal mineralogy, which are likely to be mirrored by changes in physical properties such as viscosity, thermal expansion etc. Because of this, bedding planes could easily be anomalously weak zones at high temperature, and hence possible sites of fractures, dilation and melt accumulation. The crenulation cleavage planes, on the other hand, are more pervasive and perhaps therefore less likely to have been anomalously weak zones. Immediately prior to partial melting, the original micaceous regional S_2 crenulation cleavage would have been annealed and, although still physically recognisable, would have consisted of a modal layering (e.g. quartz-rich vs. quartz-free, see Plates 6.3 and 6.4) but no preferred orientation of biotite. The main effect of this would probably have been the domainal distribution of the sub-assemblages required as reactants in melting reactions (e.g. cordierite/andalusite + biotite + K-feldspar + quartz + H_2O, see Chapter 8) Thus the former S_2 crenulation cleavage could well have controlled the actual locations at which melting reactions were initiated.

The vein-like leucosomes imply that the rocks have undergone brittle fracturing, and that the melts have been allowed to migrate (albeit only short distances) from their sites of generation. Though some fractures probably exploited bedding planes (see above), many clearly transect both bedding and S_2 (e.g. Plate 6.11), some in apparently random orientation (e.g. Plate 6.7, 6.8). Two possible origins can be considered for the fractures: (a) they were caused by stress set up by the intruding Quarry Diorite; (b) they were caused by stresses set up by the process of partial melting. The fact that the fractures only occur in migmatised rocks argues against the first explanation. In principle, partial melting has the potential to set up large stresses in the rocks on account of the volume change of the melting reaction. Fluid-present melting reactions, in which H_2O is a reactant, have negative ΔV and are thus unable to cause rock fracture by dilation. Fluid-absent reactions, on the other hand, have positive ΔV (Clemens and Droop, 1998). If the permeability of the rocks is low (as is probably the case in hornfelses) melt produced by such a reaction is likely to accumulate faster than it can percolate away, and the rock will dilate; stresses built up will eventually be over-pressured by melt and will fracture. This is analogous to "hydrofracturing" of rocks by over-pressuring by aqueous fluid (Nicolas and Jackson, 1982).

Conclusions

The principal conclusions of this chapter are as follows:

(i) Intrusion of the Quarry Diorite into rocks of the Leven Schist Formation resulted in the formation of anatectic migmatites within ca. 200m of the contact (i.e. within the Upper Spinel and Sillimanite Zones).

(ii) Partial melting was restricted to pelitic and semi-pelitic bulk compositions.

(iii) Partial melts were of S-type leuco-granitic composition.

(iv) The volume of anatectic melt generated was very small, and the melts crystallised close to the sites at which they were generated.

(v) In the Sillimanite Zone, euhedral garnet, cordierite and orthopyroxene crystallised locally in leucosomes as the solid products of incongruent partial melting reactions.

(vi) Partial melting was commonly accompanied by brittle fracturing of the rocks, possibly "hydrofracturing" caused by the volume increase involved in fluid-absent melting reactions.

(vii) The pre-existing structures in the metasediments, notably compositional layering (bedding) and annealed S_2 crenulation cleavage, locally exerted some influence on the way the melt bodies collected to form leucosomes, probably reflecting either zones of tensile weakness or sites of melt generation or both.

7.1 Introduction

The chemistry of the peak metamorphic minerals in the regionally and thermally metamorphosed rocks is studied in this chapter. The results from the mineral chemistry are important for classification of minerals, working out any possible changes in chemistry of the minerals due to contact metamorphic grade, and calculating the activities of the end-members which will be used for constructing phase diagrams and estimating pressure and temperature. The chemistry of minerals is studied in two main metamorphic rock types: (i) metabasic rocks and (ii) pelitic and semi-pelitic rocks. Samples were collected from regional metamorphic rocks outside the Etive aureole and also in traverses from the outer aureole toward the igneous contact in the selected segments of the aureole. More than ten analyses were carried out on each phase in each thin section. When zoning was found, zoning profiles were constructed where appropriate. The chemistry of different types of minerals will be treated one by one for each major metamorphic rock type. Some representative mineral analyses are provided in the text. For a full set of analyses see Appendix 5. Details of apparatus, set-up condition, procedures, standards and criteria for accepting or rejecting analyses, are presented in Appendix 3.

7.2 Mineral chemistry of metabasic rocks

Minerals in fourteen metabasites were analysed by energy dispersive spectrometry. Minerals analysed include amphibole, biotite, plagioclase, clinopyroxene, orthopyroxene, chlorite, epidote, regional metamorphic garnet and ore minerals, though not all occur together in a single sample. The mineral chemistry is considered in the context of the four main metamorphic zones mapped in the

Loch Awe area, namely Zone I (regionally metamorphosed metabasites), Zone II (metabasites with contact metamorphic hornblende), Zone III (metabasites with contact-metamorphic clinopyroxene, with or without epidote), and Zone IV (metabasites with orthopyroxene). For description of these zones see Chapter 5.

7.2.1. Amphibole: Table 7.1 lists representative analyses of amphiboles in the metabasites. Amphiboles appeared to be homogeneous in all analysed samples. Formulae have been calculated to 23 oxygens, and Fe^{3+} contents estimated on charge-balance criteria assuming ΣSiTiAlCrFeMnMgCa=15.00 per 23 oxygens (Droop, 1987). The amphibole analyses have oxide totals of between 96.13% and 98.52%; no estimation for H_2O has been made. Cation totals lie between 15.12 and 15.64. Fig. 7.1 shows the classification of metabasite amphiboles using the diagram of Leake (1978). All of the amphiboles from the regional metamorphic rocks plot in the tremolite field of this figure. One sample was analysed from Zone II. Amphiboles are

Table 7.1 Representative microprobe analyses of amphiboles in metabasic rocks.

Oxide,Wt%	MM166B	MM196A	MM141B	MM198B	MM165	MM148A
SiO2	53.80	50.83	51.47	45.36	48.27	41.67
TiO2	0.57	1.28	0.13	2.14	1.48	0.55
Al2O3	2.78	4.92	3.58	8.24	6.19	15.02
Cr2O3	0.29	0.28	0.18	0.00	0.11	0.00
Fe2O3	0.00	0.00	0.00	0.00	0.00	1.43
FeO	9.41	12.45	14.38	17.35	14.12	10.36
MnO	0.03	0.01	0.25	0.00	0.00	0.03
MgO	18.30	15.35	14.41	11.35	13.78	13.13
CaO	11.36	11.11	11.21	11.18	11.06	12.44
Na2O	0.64	1.00	0.50	1.43	1.24	3.02
K2O	0.15	0.23	0.05	0.73	0.46	0.23
Total	97.33	97.46	96.16	97.78	96.71	97.88
Atoms to 23 Oxygens, 15 cations						
Si	7.68	7.40	7.59	6.80	7.17	6.12
Ti	0.06	0.14	0.01	0.24	0.16	0.06
Al	0.47	0.84	0.62	1.46	1.08	2.59
Cr	0.03	0.03	0.02	0.00	0.01	0.00
Fe^{3+}	0.00	0.00	0.00	0.00	0.00	0.16
Fe^{2+}	1.12	1.52	1.78	2.18	1.76	1.27
Mn	0.00	0.00	0.03	0.00	0.00	0.00
Mg	3.89	3.33	3.17	2.54	3.05	2.86
Ca	1.74	1.73	1.77	1.79	1.76	1.95
Na	0.18	0.28	0.14	0.42	0.36	0.86
K	0.03	0.04	0.01	0.14	0.09	0.04
Total	15.20	15.31	15.14	15.57	15.39	15.91

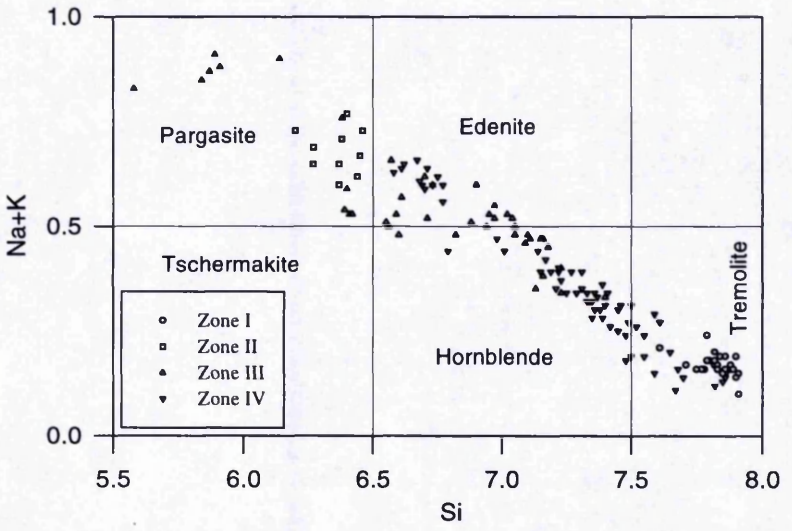

Fig. 7.1 Classification of amphiboles in metabasites using Leake's (1978) diagram. All amphiboles from contact metamorphic samples fall into the broad category of hornblende, although amphiboles from Zone II plot in the pargasite field, amphiboles from Zone III and IV plot in the hornblende, edenite and pargasite fields.

pargasite in this sample. Amphiboles from Zone III plot in the hornblende, edenite and pargasite fields and amphiboles from Zone IV plot mainly in the hornblende field. Some retrogressive amphiboles in samples from Zone IV plot in the tremolite field. The proportion of vacancies on the A-site in the amphiboles from Zones I, II, III and IV is between 0.83-0.93, 0.37-0.49, 0.01-0.66 and 0.41-0.90 respectively. The potassium content [atoms per formula unit (apfu) on the basis of 23 oxygens] varies from 0.00-0.01, 0.07-0.09, 0.04-0.13 and 0.02-0.18 in amphiboles from Zones I, II, III and IV respectively. The amount of Ti is between 0.00-0.01, 0.04-0.06, 0.03-0.18 and 0.10-0.27 (apfu) in amphiboles from Zones I, II, III and IV respectively. Cr ranges from 0.00 to 0.05 apfu. Fig. 7.2 illustrates the $Mg+Fe^{2+}$ versus Al^{iv} relation for amphiboles. A negative relation is apparent when amphiboles from all zones are included, reflecting Mg and Fe-tschermak substitution, i.e. $(Mg,Fe^{2+})^{vi}+Si^{iv} \Leftrightarrow Al^{vi}+Al^{iv}$. When the amphibole analyses from the different metamorphic zones are compared, it appears that chemical composition varies with contact metamorphic

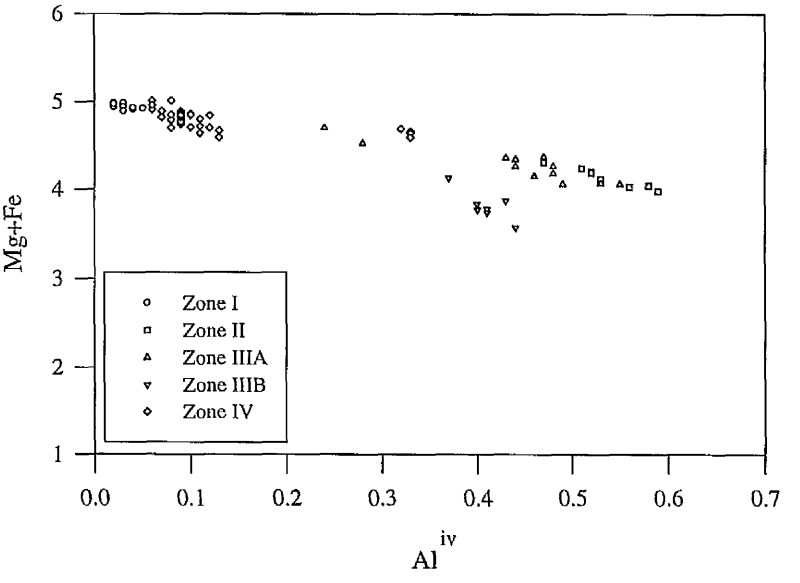

Fig. 7.2 (Mg+Fe) vs. Al^{iv} diagram for amphiboles in metabasites. In all samples, (Mg+Fe)/Al^{iv} shows a negative relationship, demonstrating tschermak substitution.

grade. To demonstrate these changes, a set of diagrams is constructed in which chemical variables are plotted as a function of distance from the igneous contact. Ti concentration is plotted against distance from the contact in Fig. 7.3. Samples in Zone I are from regional metamorphic metabasites which are far from the igneous contact. This figure shows that the Ti concentration in amphibole generally increases as distance decreases (i.e. as temperature increases). Variation of $Mg/(Mg+Fe^{2+})$ with distance from the contact is illustrated in Fig. 7.4. Amphiboles from the regional metamorphic rocks are actinolites with relatively high $Mg/(Mg+Fe^{2+})$ values. There is not a clear pattern in this figure. Probably bulk rock composition controls the $Mg/(Mg+Fe^{2+})$ ratio in amphiboles. A plot of Al concentration in amphiboles with distance from the contact is presented in Fig. 7.5. Apparently there is no obvious relationship between total Al and distance. The highest amount of Al is in amphiboles from Zone IIIB. The Al concentration of amphiboles from Zone IV is

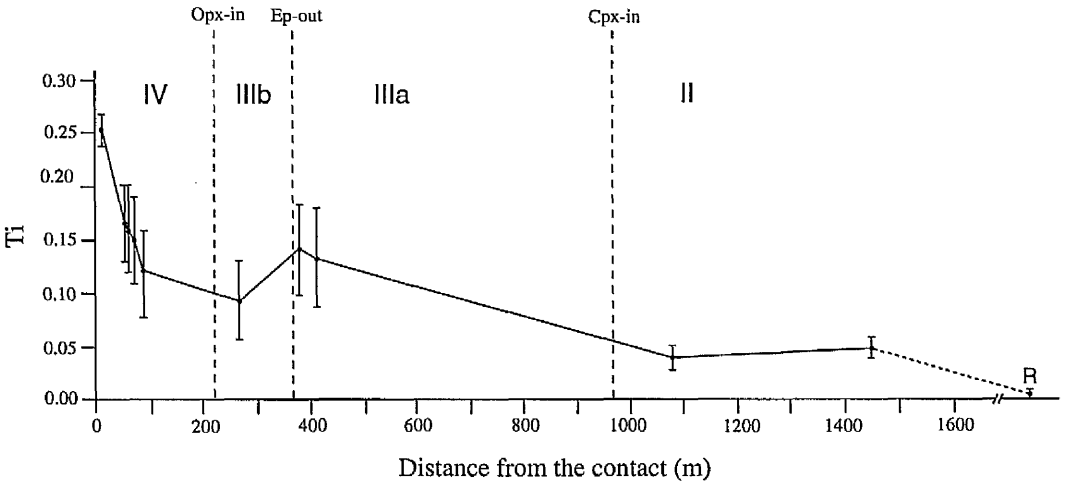

Fig. 7.3 Relationship between Ti concentration in amphiboles and distance from the igneous contact in the aureole in the N Loch Awe area. R: regional metabasite in the S Loch Awe area. Note that as the distance decreases, the amount of Ti in amphibole increases.

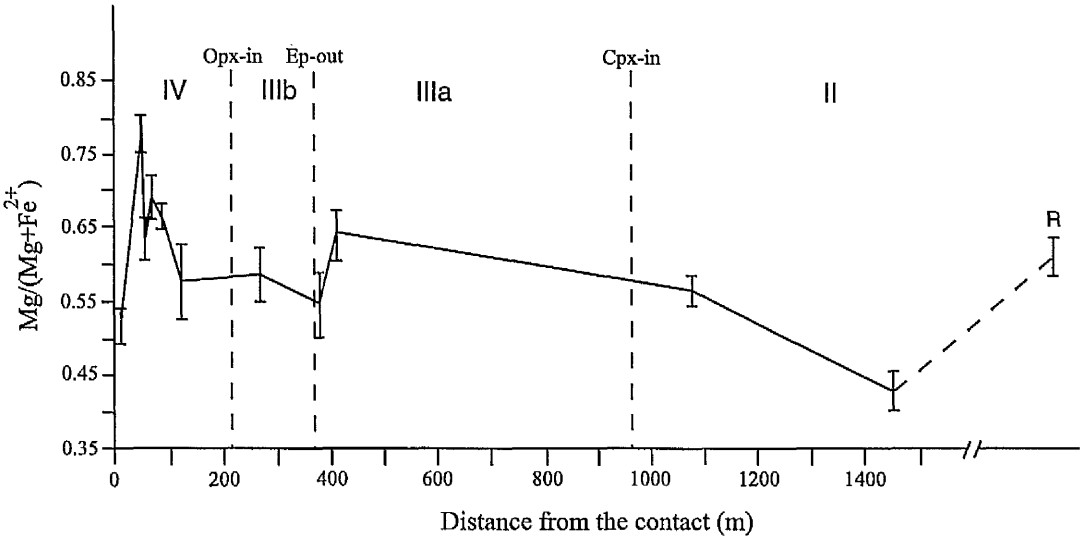

Fig. 7.4 Plot of $Mg/(Mg+Fe^{2+})$ in amphiboles versus distance from the igneous contact in the aureole in the N Loch Awe area. There is no clear relationship.

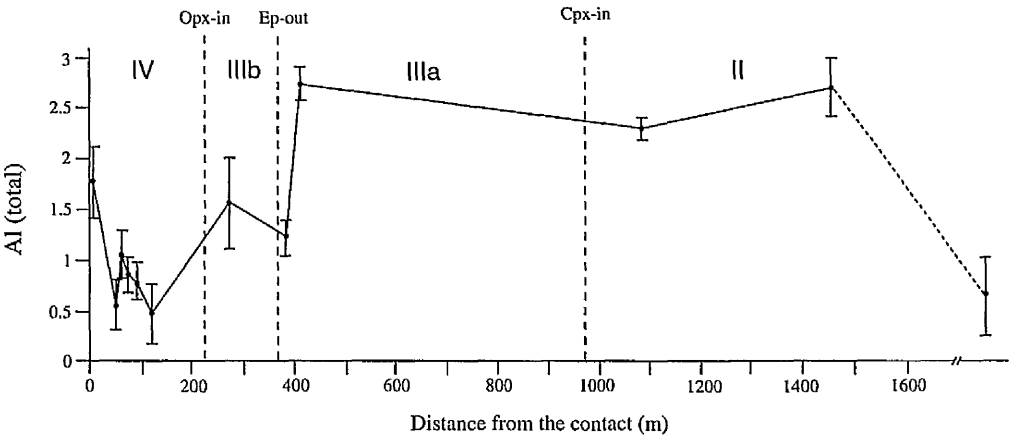

Fig. 7.5 Plot of total Al in amphiboles versus distance from the igneous contact in the N Loch Awe area. No clear relationship is apparent.

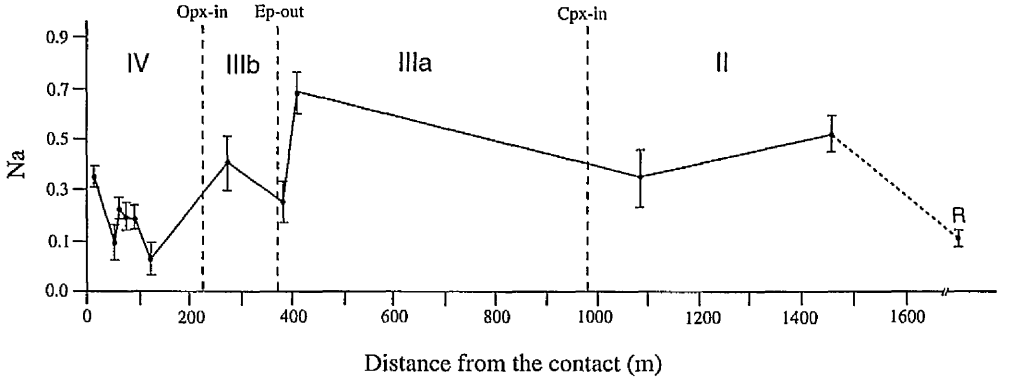

Fig. 7.6 Plot of Na concentration in amphiboles versus distance from the igneous contact in the North Loch Awe area. There is no clear relartionship but the pattern is very similar to that of Al(total) in Fig. 7.5.

low (between 0.47 and 1.62 apfu). There is no obvious relationship between Na content of amphibole and contact metamorphic grade (Fig. 7.6).

7.2.2. Biotite: Biotite is not present in all samples but it occurs in regional metamorphic metabasites and in pyroxene-hornfelses very close to the igneous contact. Table 7.2 lists representative analyses of biotite. Biotites are essentially homogeneous. Biotite formulae have been calculated to 22 oxygens, which gives cation totals of between 15.24 and 15.77.

Table 7.2 Representative microprobe analyses of biotite in metabasic rocks.

Oxide,Wt%	MM166B	MM196A	MM141B	MM198B	MM165
SiO2	37.84	38.00	36.79	35.82	36.09
TiO2	5.85	4.49	4.71	5.39	5.10
Al2O3	13.99	14.40	14.03	13.58	13.89
Cr2O3	0.33	0.33	0.39	0.06	0.23
FeO*	13.74	11.78	16.55	20.14	17.08
MnO	0.00	0.00	0.00	0.00	0.00
MgO	15.17	16.67	13.55	10.74	12.39
CaO	0.03	0.09	0.12	0.09	0.18
Na2O	0.50	0.54	0.51	0.36	0.36
K2O	8.97	8.85	8.51	9.15	8.96
Total	96.42	95.15	95.16	95.33	94.28
Atoms to 22 Oxygens					
Si	5.55	5.59	5.55	5.52	5.53
Ti	0.64	0.49	0.53	0.63	0.59
Al	2.42	2.49	2.49	2.47	2.51
Cr	0.04	0.04	0.04	0.00	0.02
Fe	1.68	1.45	2.09	2.60	2.19
Mn	0.00	0.00	0.00	0.00	0.00
Mg	3.32	3.66	3.04	2.47	2.83
Ca	0.00	0.02	0.01	0.02	0.03
Na	0.14	0.15	0.15	0.10	0.10
K	1.68	1.66	1.64	1.80	1.75
Total	15.47	15.55	15.54	15.61	15.55

* Fe total

The composition of biotites from metabasites are plotted on the diagram of Guidotti (1984) (Fig. 7.7). Biotites from all metamorphic zones plot close to the phlogopite-annite end-members. $Mg/(Mg+Fe^{2+})$ in biotites is plotted against distance from the contact in Fig. 7.8. Biotite was analysed in one sample from zone IV. No biotite was found in sectioned samples from sub-zone IIIA. Biotites in sectioned samples from the regional metamorphic rocks occur as tiny flakes inter-grown with chlorite (or altered to chlorite) and their analysis using EDS was not easy. According to the graph in Fig.7.7, there is not a clear relationship between $Mg/(Mg+Fe^{2+})$ values of metabasite biotites and distance from the contact.

7.2.3. Plagioclase: Table 7.3 lists representative analyses of plagioclase in metabasic rocks. In these rocks plagioclases do not exhibit optical zoning but polysynthetic twinning is common. In regional metamorphic rocks (Zone I) plagioclases are virtually albite with 0-10 mole per cent anorthite. Plagioclases from Zone II are also albite-rich with 5-10 mole per cent anorthite. The amount of anorthite in plagioclases

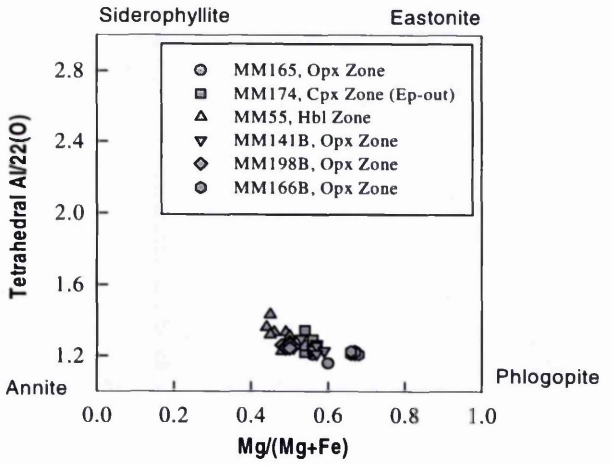

Fig. 7.7 Plot of biotites in the metabasites on diagram of Guidotti (1984). All biotites plot between phlogopite-annite ends. The amount of Mg/(Mg+Fe) is lower in biotites from the Hornblende Zone.

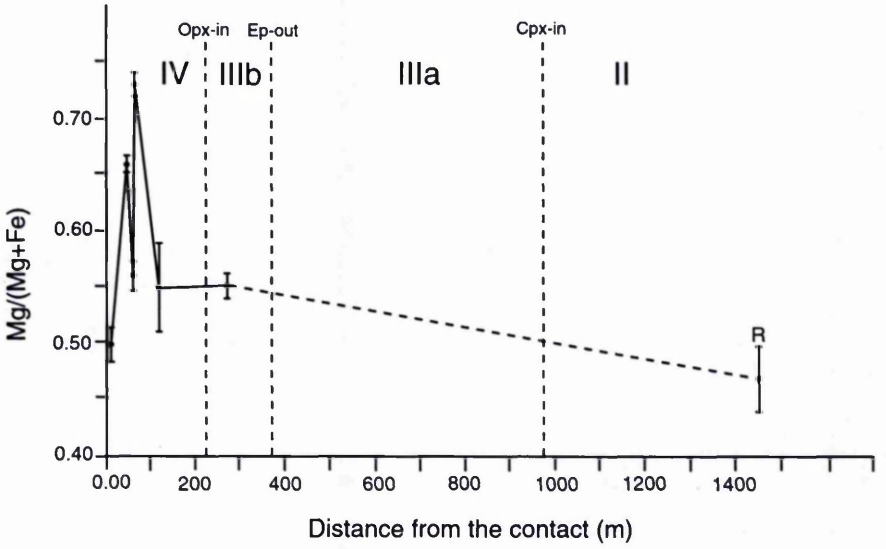

Fig. 7.8 Plot of Mg/(Mg+Fe) in metabasic biotites versus distance from the contact in the N Loch Awe area. There is no clear relationship.

from Zones IIIA is between 15-25 mole% corresponding to oligoclase. In Zone IIIB the An content reaches 45-55 (andesine to labradorite) and 60-85 (labradorite to bytownite) mole% in different samples from this zone. In samples from Zone IV the amount of anorthite is between 45-95 mole% which corresponds to the variation in An amount in different samples rather than zoning of plagioclases in a single sample.

Fig. 7.9 shows a histogram of frequency of An mole% in plagioclases from different metamorphic zones within the Etive aureole and regional metamorphic rocks. The variation of An mole% in plagioclases is clear from this figure. Fig. 7.10 shows the relationship between plagioclase composition and distance from the igneous contact.

Table 7.3 Representative microprobe analyses of plagioclase in metabasic rocks.

Oxide,Wt%	MM166B	MM196A	MM141B	MM198B
SiO2	55.93	51.06	45.45	55.38
TiO2	0.11	0.17	0.01	0.00
Al2O3	27.77	31.07	34.52	28.25
FeO*	0.17	0.37	0.17	0.21
MnO	0.00	0.00	0.00	0.06
MgO	0.09	0.08	0.23	0.04
CaO	9.83	14.01	18.24	10.57
Na2O	5.93	3.65	1.18	5.41
K2O	0.17	0.02	0.04	0.15
Cr2O3	0.03	0.03	0.04	0.04
Total	100.03	100.46	99.88	100.11
Atoms to 8 Oxygens				
Si	2.52	2.32	2.10	2.49
Ti	0.00	0.00	0.00	0.00
Al	1.47	1.66	1.88	1.50
Fe	0.01	0.01	0.01	0.01
Mn	0.00	0.00	0.00	0.00
Mg	0.01	0.00	0.02	0.00
Ca	0.47	0.68	0.90	0.51
Na	0.52	0.32	0.10	0.47
K	0.01	0.00	0.00	0.01
Cr	0.00	0.00	0.00	0.00
Total	5.01	4.99	5.01	4.99

The An content increases dramatically as distance from the contact decreases (i.e. as temperature increases). The sharp slope in the An mole%-distance curve can be

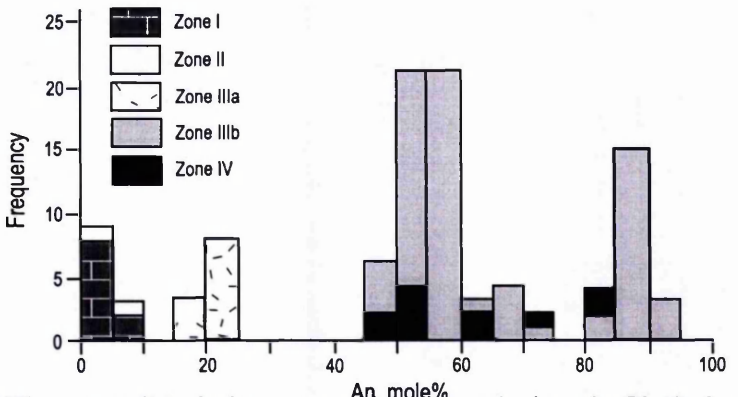

Fig. 7.9 Histogram of plagioclase compositions in metabasic rocks. Plagioclases in Zone I are albite-rich and plagioclases in the higher zones become An-rich.

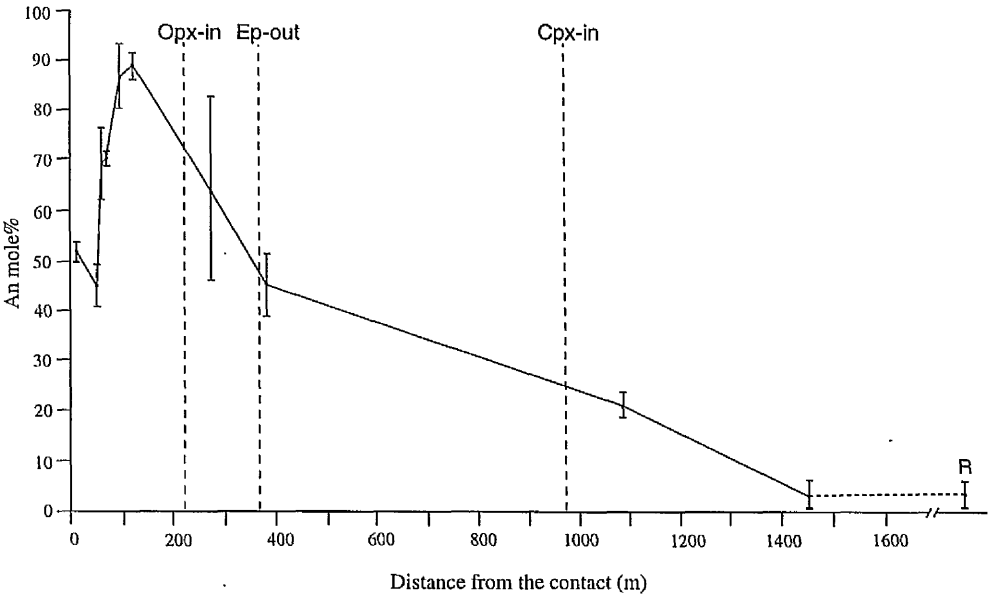

Fig. 7.10 Relationship between An mole% in plagioclase and distance from the contact in the N Loch Awe area. R: regional plagioclase in the S Loch Awe area. Plagioclase generally becomes more An-rich as distance from the contact decreases (metamorphic grade increases), but in very high grade rocks, plagioclase become more Ab-rich adjacent to the contact.

attributed to Ep-consuming reactions which produce An-rich plagioclases. There is a decrease in An content of plagioclases in samples close to the contact (less than 100 m). This is probably due to the effect of a hornblende-consuming reaction (see chapter 8).

7.2.4 Clinopyroxene: Table 7.4 lists representative analyses of clinopyroxene in metabasic rocks. Clinopyroxene formulae were calculated to 6 oxygens and cation totals assumed to be exactly 4.00 (Droop, 1987). All clinopyroxenes appear to be compositionally homogeneous. Manganese and chromium are absent or occur in very low concentrations (less than 0.007 and 0.004 apfu respectively). Calcium varies from 0.85 to 0.95 apfu. Octahedral aluminium accounts for 0.00 to 0.02 apfu on the M_1-site. Fe^{3+} concentration, which is estimated using charge-balance criteria (Droop, 1987), is between 0.01 and 0.07 and Ti amount varies from 0.00 to 0.01. Fig. 7.11 shows the composition of clinopyroxene (and coexisting orthopyroxene) from metabasic rocks (from Zones III and IV) on the wollastonite-enstatite-ferrosilite diagram. The amount of Wo is between 43% and 47%, the amount of En is between 37% and 45% and the amount of Fs is between 14% and 25%.

7.2.5 Orthopyroxene: Table 7.5 lists representative analyses of orthopyroxene in metabasic rocks. All crystals appeared to be homogeneous. Formulae have been

Table 7.4 Representative microprobe analyses of clinopyroxene in metabasic rocks.

Oxide,Wt%	MM166A	MM196A	MM141B	MM198B	MM165
SiO2	53.18	52.66	51.93	52.27	52.51
TiO2	0.18	0.33	0.22	0.05	0.11
Al2O3	0.94	0.89	0.56	0.84	0.70
Cr2O3	0.21	0.20	0.19	0.15	0.09
Fe2O3	1.53	0.99	1.17	1.40	2.46
FeO	7.53	9.64	12.59	11.31	8.74
MnO	0.07	0.10	0.32	0.00	0.12
MgO	14.97	13.94	11.89	12.41	12.98
CaO	21.12	20.90	20.83	20.96	21.87
Na2O	0.52	0.41	0.32	0.49	0.61
K2O	0.00	0.00	0.00	0.00	0.00
Total	100.26	100.06	100.02	99.88	100.19
Atoms to 6 Oxygens					
Si	1.97	1.97	1.97	1.98	1.97
Ti	0.00	0.01	0.00	0.00	0.00
Al	0.04	0.04	0.02	0.04	0.03
Cr	0.00	0.00	0.01	0.00	0.00
Fe^{3+}	0.04	0.03	0.04	0.04	0.07
Fe^{2+}	0.24	0.30	0.40	0.36	0.27
Mn	0.00	0.00	0.01	0.00	0.00
Mg	0.83	0.78	0.68	0.70	0.74
Ca	0.84	0.84	0.85	0.84	0.88
Na	0.04	0.03	0.02	0.04	0.04
K	0.00	0.00	0.00	0.00	0.00
Total	4.00	4.00	4.00	4.00	4.00

calculated to six oxygens and ferric iron content has been estimated on the basis of exactly 4.00 cations per formula unit. The amount of Cr, Ti, Mn and K is very small (less than 0.006) and the amount of Na is between 0.02 and 0.05 apfu. Ca varies between 0.03 and 0.05 apfu. Ferric iron calculations yield 0.02 to 0.07 Fe^{3+} apfu. The amount of Al is between 0.01 and 0.03 apfu. Fig. 7.11 presents the end-member proportions of orthopyroxenes which rages from 2% to 3% wollastonite, 51% to 69% enstatite and 28% to 47% ferrosilite.

7.2.6 Other minerals: Chlorite, epidote, carbonate minerals and regional metamorphic garnet were analysed in low-grade rocks and ore minerals were analysed in all analysed samples. Chlorite analyses were calculated to 28 oxygens (without considering H_2O, Cl and F) giving a total number of cations between 19.79

Table 7.5 Representative analyses of orthopyroxene in metabasic rocks.

Oxide,Wt%	MM166B	MM196A	MM141B	MM198B	MM165
SiO2	53.77	52.69	51.91	51.50	51.97
TiO2	0.22	0.19	0.16	0.07	0.16
Al2O3	0.36	0.29	0.25	0.44	0.43
Cr2O3	0.02	0.04	0.00	0.03	0.09
Fe2O3	1.50	1.09	0.83	2.00	2.22
FeO	20.56	24.75	26.94	27.37	25.90
MnO	0.00	0.03	0.43	0.23	0.25
MgO	22.70	20.04	18.23	17.23	17.84
CaO	0.79	0.83	1.13	1.01	1.12
Na2O	0.53	0.34	0.19	0.43	0.63
K2O	0.00	0.00	0.00	0.00	0.00
Total	100.45	100.29	100.07	100.33	100.60
Atoms to 6 Oxygens					
Si	1.98	1.98	1.98	1.98	1.98
Ti	0.00	0.00	0.00	0.00	0.00
Al	0.02	0.01	0.01	0.02	0.02
Cr	0.00	0.00	0.00	0.00	0.00
Fe^{3+}	0.04	0.03	0.02	0.06	0.06
Fe^{2+}	0.64	0.79	0.87	0.88	0.82
Mn	0.00	0.00	0.01	0.01	0.01
Mg	1.25	1.14	1.06	0.98	1.01
Ca	0.03	0.03	0.04	0.04	0.05
Na	0.04	0.02	0.01	0.03	0.05
K	0.00	0.00	0.00	0.00	0.00
Total	4.00	4.00	4.00	4.00	4.00

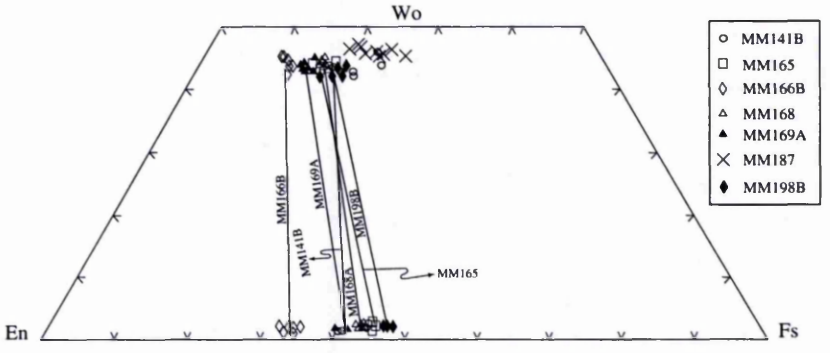

Fig. 7.11 Wo-En-Fs diagram showing the end-member proportions in orthopyroxenes and clinopyroxenes in metabasic rocks. Tie lines connect the average compositions of orthopyroxene and clinopyroxene in individual rock samples.

Table 7.6 Representative microprobe analyses of chlorite, garnet, calcite, epidote and ilmenite in metabasites.

Oxide wt%	MM94. Chlorite	MM55 Garnet	MM94. Calcite	MM94. Epidote	MM166B. Ilmenite
SiO_2	25.45	37.11	0.16	37.54	0.19
TiO_2	0.00	0.15	0.02	0.05	55.71
Al_2O_3	18.59	20.85	0.03	22.14	0.00
Cr_2O_3	0.09	0.07	0.00	0.21	0.22
FeO (Fe_2O_3 in Ep)	27.62	28.62	1.04	13.59	41.18
MnO	0.00	3.86	0.69	0.00	0.00
MgO	14.08	1.75	0.36	0.30	2.31
CaO	0.06	7.88	59.94	22.48	0.11
Na_2O	0.45	0.32	0.13	0.17	0.19
K_2O	0.07	0.00	0.00	0.00	0.04
Total	86.41	100.61	62.37	96.48	99.95
Number of oxygens	28	12	10	12.5	24
Si	5.54	2.97	1.68	3.12	0.04
Ti	0.00	0.00	0.00	0.00	8.22
Al	4.27	1.97	0.00	2.17	0.00
Cr	0.01	0.00	0.00	0.01	0.03
Fe	5.03	1.92	0.13	0.94	6.76
Mn	0.00	0.26	0.08	0.00	0.00
Mg	4.57	0.21	0.08	0.04	0.67
Ca	0.01	0.68	9.60	2.00	0.02
Na	0.19	0.05	0.03	0.03	0.07
K	0.02	0.00	0.00	0.00	0.01
Total	20.14	8.06	11.60	8.31	15.82

and 20.22 in regional metamorphic metabasites and 18.85 to 20.06 in low grade contact metamorphic rocks from Zone II. Amount of Fe is between 4.38 and 5.41 apfu. Epidote analyses were calculated to 13 oxygens (without considering H_2O, Cl and F) which gives a total number of cations between 8.60 and 8.65. The amount of Mg is between 0.01 and 0.09 apfu and amount of Fe is between 0.95 and 1.03 apfu. Amount of Ca is between 1.99 and 2.10 apfu. The carbonate minerals are calcite with about 0.04 apfu Mg (on the basis of 6 oxygens) and 0.60 apfu Fe. In one sample (MM55, GR, NN11742692) from Zone II, regional metamorphic garnet is present which shows that metabasic rocks from the Etive aureole area were metamorphosed regionally at least up to lower amphibolite grade. Garnet was analysed in this sample which is almandine-rich with low amounts of pyrope end-member and appreciable amounts of grossularite and spessartine end-members. This garnet is not zoned and its composition is ~ 3.86 wt% MnO, 1.75 wt% MgO, 7.88 wt% CaO and 28.62 wt% FeO. Cr is absent or occurs in very low amounts (less than 0.08 wt%).

Ore minerals were analysed in all samples. In all cases they are ilmenite with about 2 wt% MgO. Table 7.6 lists representative analyses of chlorite, epidote, garnet, calcite and ilmenite in the metabasic rocks.

7.3 Mineral chemistry of the pelitic and semi-pelitic rocks

Minerals in the optically defined sections from the pelitic and semi-pelitic rocks (mainly from the non-graphitic Leven Schist) were analysed. Analysed minerals include muscovite, biotite, cordierite, alkali feldspar, plagioclase, spinel, garnet, orthopyroxene and ore minerals, though not all occur together in a single sample. A few analyses were obtained from corundum, andalusite and sillimanite. The chemistry of the minerals is considered with reference to the seven main metamorphic zones: Biotite Zone (Zone I), Cordierite Zone (Zone II), Andalusite Zone (Zone III), Andalusite+K-feldspar Zone (Zone IV), Corundum Zone (Zone V), Spinel Zone (Zone VI) and Sillimanite Zone (Zone VII). For a full description of metamorphic zones see Chapter 5. The mineral chemistry of pelitic rocks will be discussed mineral by mineral.

7.3.1. Muscovite: Table 7.7 lists representative analyses of muscovite in the pelitic rocks. Muscovite formulae have been calculated on the basis of 22 oxygens assuming a total of four hydroxyl, fluorine and chlorine. The oxide totals are between 93.58 and 95.82 and the cation totals are between 13.94 and 14.08. The compositions of muscovites are plotted on an SAF diagram in Fig. 7.12. Muscovites from sample MM255D are regional metamorphic and muscovites in samples MM56A, MM56B and 181 are contact metamorphic. Muscovites in all samples plot close to the muscovite end-member of the muscovite-celadonite join. The celadonite (phengite) content of the regional muscovites are slightly higher. Mg ranges from 0.13 to 0.67 apfu. Chromium and manganese are 0.00 to 0.1 apfu. Titanium occurs in concentrations of 0.01 to 0.11 apfu and sodium and potassium vary from 0.08 to 0.28 and 1.63 to 1.83 respectively.

7.3.2. Biotite: Biotite is present in almost all studied samples (it is absent only in very high-grade sillimanite-bearing rocks). Some representative analyses of biotite are provided in Table 7.8. As with muscovite, biotite formulae have been calculated on the basis of 22 oxygens considering a total of four hydroxyl, fluorine and chlorine. The oxide totals of biotites are between 93.36 and 96.59. The majority of the

Table 7.7 Representative microprobe analyses of muscovite in pelitic rocks. Muscovites in samples MM255D and MD1A are regional metamorphic.

Sample	MM255D	MM56A	MM56B	MM181	MD1A*	MD1B*
SiO2	48.17	47.31	47.39	45.61	46.06	47.72
TiO2	0.65	0.74	0.83	0.97	0.53	0.38
Al2O3	30.18	30.06	31.82	33.17	36.58	34.03
Cr2O3	0.06	0.00	0.00	0.00	-	-
FeO	2.64	3.34	2.06	2.58	0.88	0.26
MnO	0.01	0.00	0.04	0.00	0.00	0.00
MgO	2.11	1.91	1.85	1.57	0.41	0.31
CaO	0.08	0.02	0.02	0.01	0.00	0.18
Na2O	0.58	0.47	0.34	0.47	0.08	0.33
K2O	10.00	10.34	10.64	10.46	10.08	0.35
Total	94.48	94.19	94.99	94.84	94.62	94.66
Number of atoms on the basis of 22 oxygens						
Si	6.50	6.45	6.36	6.15	6.12	6.35
Ti	0.06	0.08	0.08	0.10	0.05	0.04
Al	4.80	4.83	5.03	5.27	5.73	5.34
Cr	0.00	0.00	0.00	0.00	-	-
Fe	0.30	0.38	0.23	0.29	0.10	0.14
Mn	0.00	0.00	0.00	0.00	0.00	0.00
Mg	0.42	0.39	0.37	0.32	0.08	0.19
Ca	0.01	0.00	0.00	0.00	0.00	0.01
Na	0.15	0.12	0.09	0.12	0.02	0.08
K	1.72	1.80	1.82	1.80	1.71	1.68
Total	13.96	14.05	13.98	14.05	13.81	13.83

* From Droop and Treloar (1981)

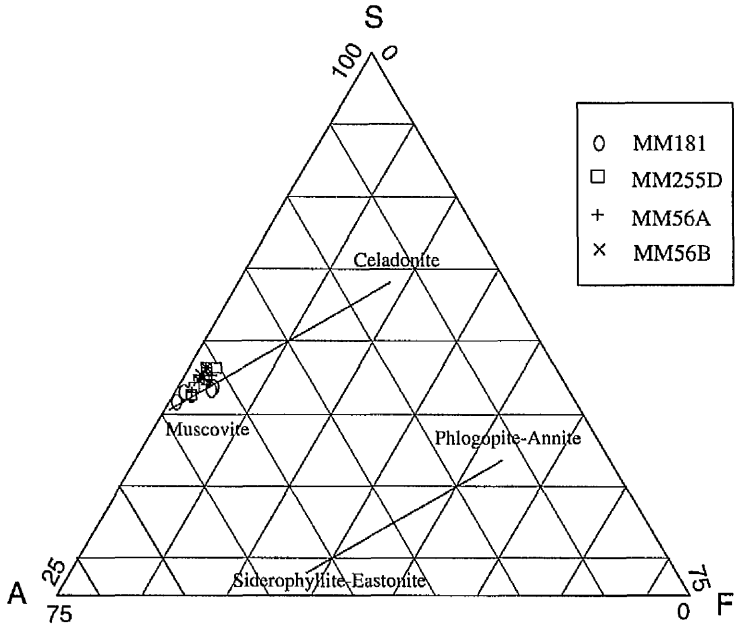

Fig.7.12 SAF diagram (after Lambert, 1959) for muscovites in the pelitic rocks. A=(100*Al)/(Si+Al+Fe+Mg+Mn), S=(100*Si)/(Si+Al+Fe+Mg+Mn), F={100*(Fe+Mg+Mn)}/(Si+Al+Fe+Mg+Mn). All of the samples plot close to the muscovite end of the muscovite-celadonite join. Muscovites in regional metamorphic rocks (sample MM255D) have a slightly higher celadonite (phengite) content.

Table 7.8 Representative microprobe analyses of biotite in pelitic rocks.

Samples	153	181	56A	151	197A	195C	189A	185B	225D
SiO2	34.49	34.80	35.91	35.11	35.48	33.64	34.84	33.96	33.25
TiO2	3.92	3.57	3.02	4.62	4.72	4.68	4.97	3.09	1.88
Al2O3	19.21	19.09	17.94	18.40	16.13	19.23	17.67	19.71	17.27
Cr2O3	0.07	0.04	0.06	0.17	0.12	0.39	0.00	0.06	0.00
FeO*	22.97	20.02	22.15	22.41	21.26	21.99	20.13	23.21	26.51
MnO	0.00	0.00	0.00	0.00	0.00	0.00	0.00	0.00	0.00
MgO	5.66	7.89	6.78	6.19	8.92	6.59	7.84	5.72	5.97
CaO	0.12	0.03	0.06	0.09	0.00	0.00	0.15	0.12	0.14
Na2O	0.52	0.50	0.39	0.44	0.41	0.24	0.49	0.49	0.48
K2O	9.38	9.45	9.28	9.39	9.32	9.22	8.99	9.10	7.83
Total	96.34	95.39	95.59	96.82	96.36	95.98	95.08	95.46	93.33
Atoms on the basis of 22 oxygens									
Si	5.30	5.32	5.52	5.35	5.41	5.17	5.35	5.27	5.38
Ti	0.45	0.41	0.34	0.53	0.54	0.54	0.57	0.36	0.23
Al	3.48	3.44	3.25	3.30	2.90	3.48	3.20	3.60	3.29
Cr	0.00	0.00	0.00	0.02	0.01	0.05	0.00	0.00	0.00
Fe	2.95	2.56	2.85	2.86	2.71	2.83	2.58	3.01	3.59
Mn	0.00	0.00	0.00	0.00	0.00	0.00	0.00	0.00	0.00
Mg	1.30	1.80	1.55	1.41	2.03	1.51	1.79	1.32	1.43
Ca	0.02	0.00	0.00	0.01	0.00	0.00	0.02	0.02	0.03
Na	0.15	0.15	0.12	0.13	0.12	0.07	0.15	0.15	0.15
K	1.84	1.84	1.82	1.85	1.81	1.81	1.76	1.80	1.62
Total	15.49	15.52	15.45	15.44	15.53	15.46	15.42	15.53	15.72

data lie around 95%. The cation totals are between 14.99 and 15.01, on the basis of 22 oxygens. Fig. 7.13 illustrates the composition of biotites on Guidotti's (1984) diagram. There is no important variation in composition of biotite in different mineralogical zones. Biotites in rocks from biotite, andalusite and corundum zones plot close to the annite corner in the diagram. Biotites are associated with orthopyroxene in sample MM198C from the sillimanite zone. Phlogopite contents of these biotites are higher.

For evaluation of F concentration in biotites, representative samples from different metamorphic zones were analysed using wavelength-dispersive microprobe (for details see Appendix 6). The amount of F is 0.10 to 0.15 apfu in biotites from the biotite zone, 0.15 to 0.26 apfu in biotites from the andalusite zone, 0.21 to 0.29 in biotites from the corundum zone, 0.10 to 0.24 in biotites from the spinel zone and 0.31 to 0.55 in biotites from the sillimanite zone. In one sample (sample MM 166A) biotites were separated mechanically and were analysed by wet chemistry. The amount of Fe_2O_3 in these biotites is 0.58 wt%.

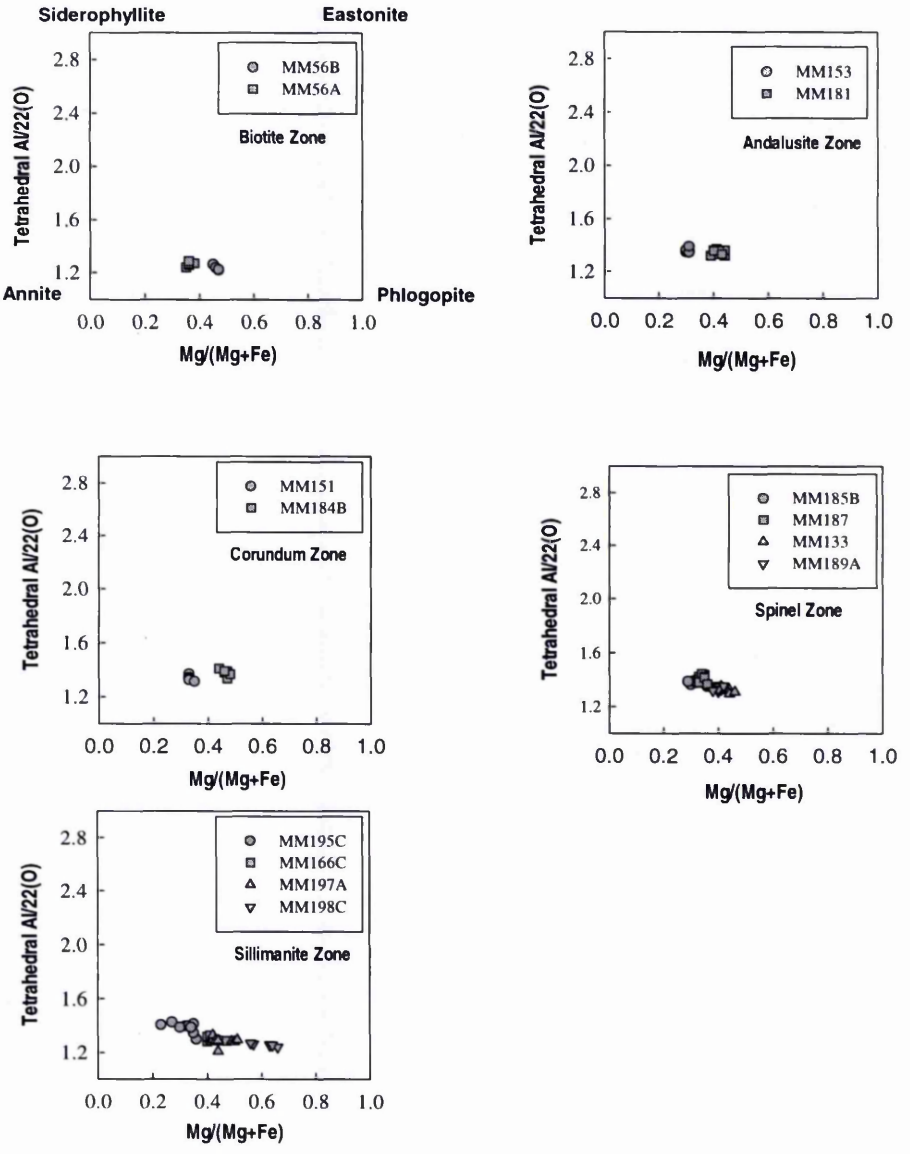

Fig. 7.13 Plot of contact metamorphic biotites in diagram of Guidotti (1984). All biotites plot between phlogopite and annite ends, closer to the annite end. There is no important difference in composition of biotites from different zones. Biotites in sample MM198C, associated with orthopyroxene, have the highest phlogopite content.

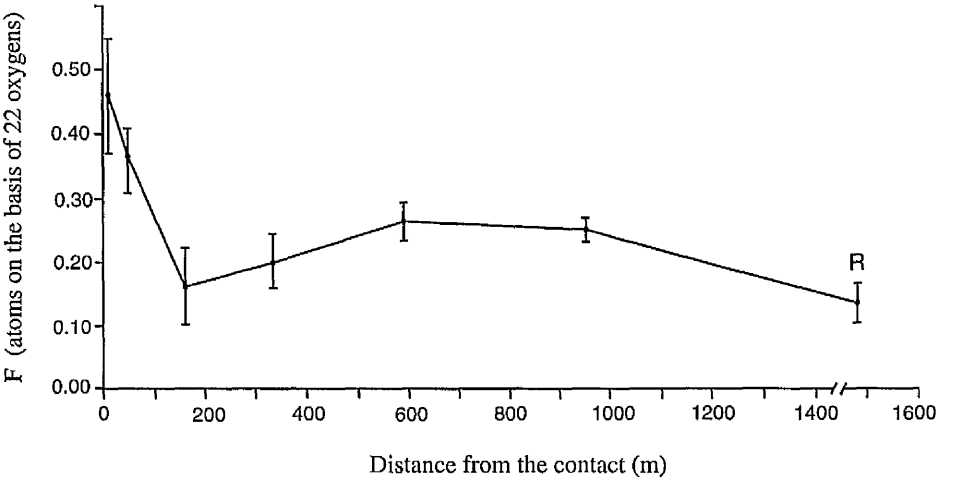

Fig. 7.14 Relationship between fluorine content in biotite and distance from the igneous contact in the N Loch Awe area. Close to the contact, the F content increases as distance from the contact decreases.

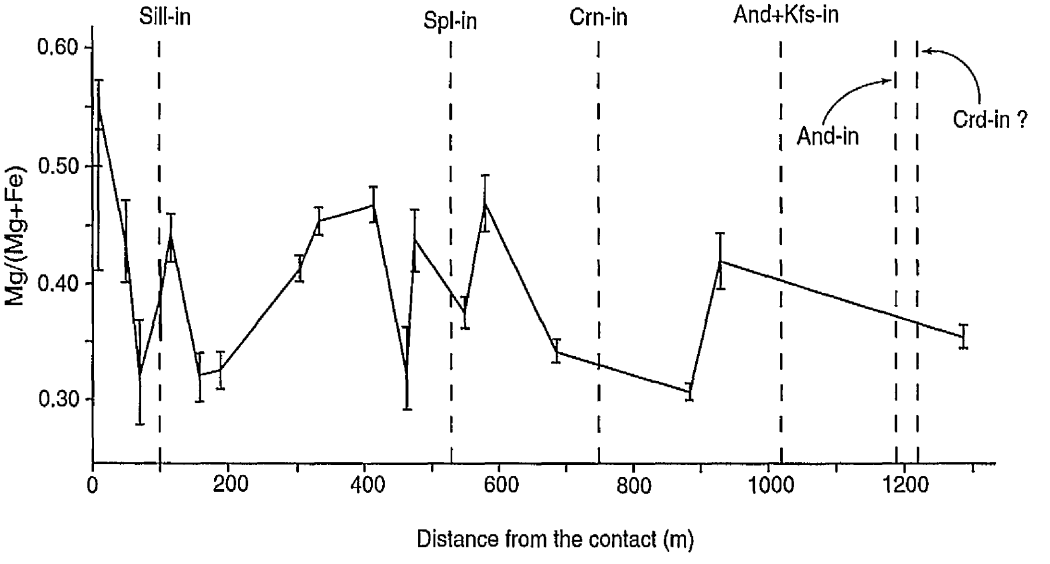

Fig. 7.15 Relationship between Mg/(Mg+Fe) value of biotite and distance from the contact. There is no clear pattern.

Fig.7.14 shows the relation between fluorine content and distance from the igneous contact. The F content of biotite increases as the distance from the contact decreases. Fig. 7.15 shows the distance-composition relationship for Mg/(Mg+Fe) in biotites. According to this figure, there is no relationship between Mg/(Mg+Fe) and distance from the contact. Even two different samples from the same locality (same distance from the contact) have different Mg/(Mg+Fe) values. The Mg/(Mg+Fe) value of biotites is probably controlled by whole rock chemistry.

7.3.3 Cordierite: Table 7.9 includes representative analyses of cordierite. Cordierites appeared to be homogeneous in all analysed samples.

Table 7.9 Representative microprobe analyses of cordierite in pelitic rocks.

Sample	MM198C	MM166A	MM166D	MM171	MM187	MD1*	MD9*
SiO2	48.93	47.99	47.67	47.42	47.27	48.43	48.16
TiO2	0.00	0.14	0.09	0.04	0.04	0.00	0.00
Al2O3	32.57	32.58	32.67	32.37	32.34	33.16	32.93
Cr2O3	0.08	0.03	0.03	0.00	0.00	-	-
FeO	9.15	11.77	11.66	11.64	12.10	9.99	12.18
MnO	0.24	0.17	0.17	0.23	0.17	0.17	0.14
MgO	8.22	6.57	6.51	6.49	6.37	7.00	5.96
CaO	0.02	0.05	0.06	0.00	0.03	0.02	0.00
Na2O	0.21	0.25	0.31	0.51	0.49	0.00	0.00
K2O	0.04	0.03	0.00	0.02	0.00	0.07	0.00
Total	99.46	99.58	99.17	98.72	98.81	98.84	99.37
Number of atoms on the basis of 18 oxygens							
Si	5.01	4.97	4.95	4.95	4.95	5.00	4.99
Ti	0.00	0.01	0.00	0.00	0.00	0.00	0.00
Al	3.93	3.97	4.00	3.99	3.99	4.03	4.02
Cr	0.00	0.00	0.00	0.00	0.00	-	-
Fe	0.78	1.02	1.01	1.06	1.06	0.86	1.06
Mn	0.02	0.01	0.01	0.01	0.01	0.02	0.01
Mg	1.25	1.01	1.00	0.99	0.99	1.08	0.92
Ca	0.00	0.00	0.00	0.00	0.00	0.00	0.00
Na	0.04	0.05	0.06	0.10	0.10	0.00	0.00
K	0.00	0.00	0.00	0.00	0.00	0.01	0.00
Total	11.03	11.04	11.03	11.10	11.10	11.00	11.00

* From Droop and Treloar (1981)

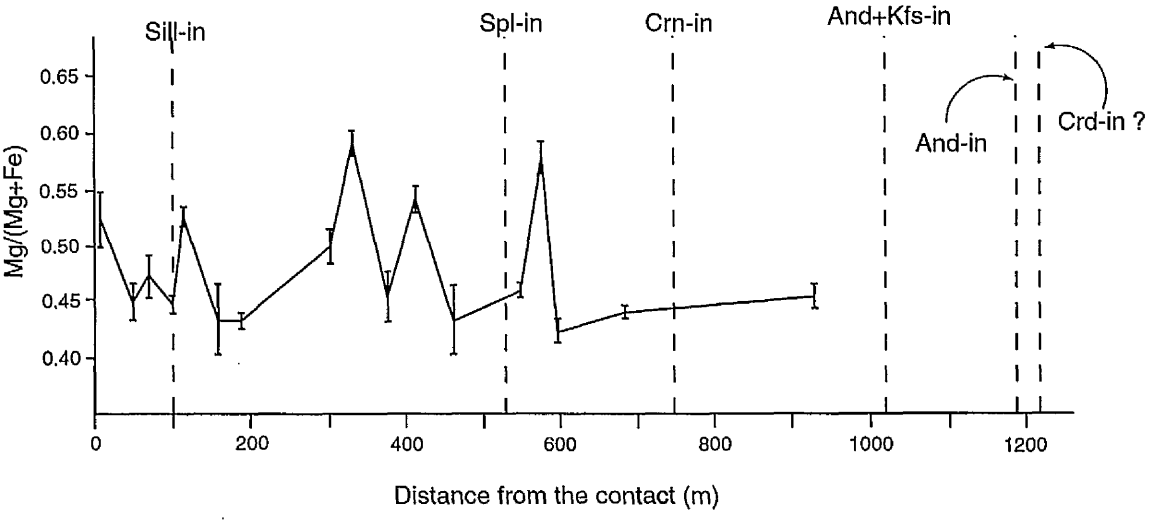

Fig. 7.16 Relationship between Mg/(Mg+Fe) value of cordierite and distance from the igneous contact in the North Loch Awe area. No obvious relationship is apparent.

Cordierite formulae have been calculated on the basis of 18 oxygens. The oxide totals of cordierite are between 97.03 and 100.46 and the cation totals are between 11.00 and 11.11. Fig. 7.16 illustrates the relationship between Mg/(Mg+Fe) values and distance from the contact. Apparently there is no relationship between these two factors and probably the whole rock chemistry of cordierite-bearing rocks define the Mg and Fe contents but the pattern seen in Fig. 7.16 is similar to the Mg/(Mg+Fe)-distance relationship for biotite in Fig. 7.15, suggesting a positive correlation between the Mg/(Mg+Fe) values of biotite and cordierite. The Mg/(Mg+Fe) values of cordierite from different metamorphic zones are illustrated in the histograms of Fig. 7.17. Cordierites from the corundum zone have the highest Mg/(Mg+Fe) values and cordierites from andalusite and andalusite+K-feldspar zones have the lowest.

Seven rocks with fresh cordierite were chosen for estimation of the H_2O and CO_2 content of cordierite from the different contact metamorphic zones. Secondary ion mass spectrometry (SIMS) was employed for H_2O and CO_2 analyses in cordierite. For details of machine settings, conditions and standards, see Appendix 7. Table 7.10 lists the water contents of cordierites from the pelitic hornfelses and Fig. 7.18 illustrates the relationship between H_2O content and distance from the contact. The tight clustering of cordierite water content in each sample suggests that retrogressive diffusion and leakage or influx of water through cordierite grains has been minimal, and thus the results for water contents reflect amount of water at the thermal peak of contact metamorphism. Fig. 7.18 shows that the H_2O content of cordierite remains essentially constant from the andalusite zone to the upper spinel zone but that it is significantly lower in the sillimanite zone. A possible reason for this pattern is discussed in Chapters eight and nine. The amount of water in cordierites of sample MD9, which is a xenolith in the Quarry Diorite, is as high as those in cordierites from the spinel and andalusite zones. Probably cordierite in xenoliths scavenges any water released by the crystallising magma during cooling. CO_2 is absent or is very low (less than 0.07 wt%) in cordierites from all the analysed samples except the xenolith sample, MD9, which has up to 0.398 wt% CO_2. This high CO_2 content can be attributed to the CO_2 content of the magmatic fluids in equilibrium with xenolith cordierites.

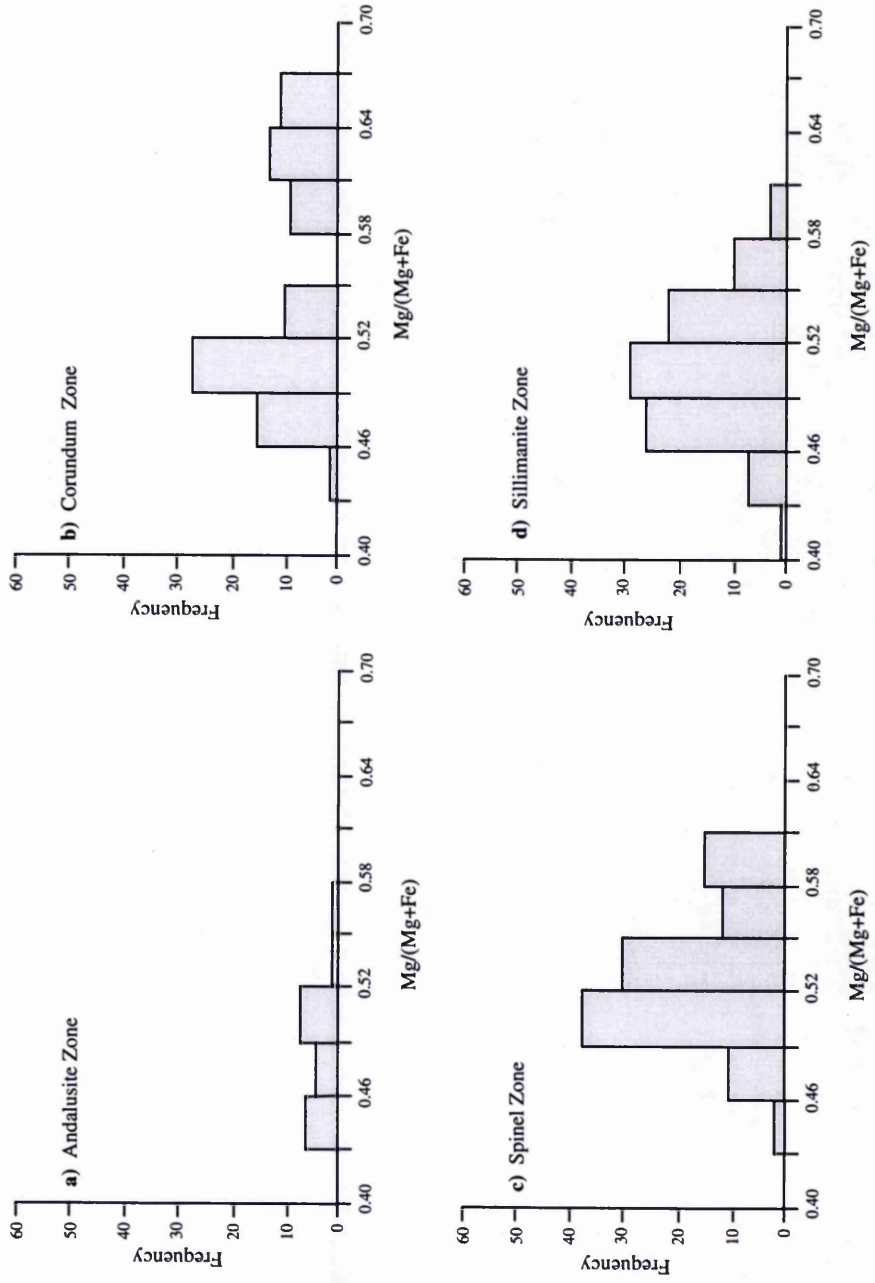

Fig. 6.16 Histogram of Mg/(Mg+Fe) value of cordierite in different contact metamorphic zones. Cordierites from the Corundum zone have the highest Mg/(Mg+Fe) values.

Table 7.10 $^{1}H/^{28}Si$ and $^{1}H/^{30}Si$ ratio (from SIMS) and water content of cordierites. X denotes the mean of the water content in each sample and SD denotes the standard deviation of the water content in each sample.

Sample	$^{1}H/^{28}Si$	wt% H_2O	
MM166D	0.1206	0.947	n=6
	0.1145	0.898	$\overline{X}$ = 0.896
	0.1109	0.869	SD= 0.058
	0.1113	0.872	
	0.1031	0.806	
	0.1255	0.986	
MM166A	0.1205	0.946	n=4
	0.1041	0.814	$\overline{X}$ = 0.883
	0.1097	0.859	SD= 0.050
	0.1165	0.913	
MM198C	0.1214	0.953	n=13
	0.1091	0.854	$\overline{X}$ = 0.944
	0.1343	1.057	SD= 0.058
	0.1145	0.898	
	0.1236	0.971	
	0.1170	0.918	
	0.1086	0.850	
	0.1230	0.966	
	0.1164	0.913	
	0.1187	0.932	
	0.1226	0.963	
	0.1223	0.961	
	0.1313	1.033	
MM187	0.1892	1.500	n=8
	0.1740	1.377	$\overline{X}$ =1.443
	0.1950	1.546	SD=0.078
	0.1684	1.332	
	0.1758	1.392	
	0.1738	1.376	
	0.1864	1.477	
	0.1947	1.544	
MM171	0.1677	1.326	n=11
	0.1703	1.347	$\overline{X}$ =1.516
	0.1963	1.557	SD=0.151
	0.2083	1.654	
	0.2054	1.630	
	0.2126	1.688	
	0.2241	1.781	
	0.1839	1.457	
	0.1744	1.380	
	0.1698	1.343	
	0.1907	1.512	
MD9	0.1630	1.289	n=5
	0.1878	1.488	$\overline{X}$ =1.613
	0.1938	1.537	SD=0.236
	0.2250	1.788	
	0.2464	1.961	
	$^{1}H/^{30}Si$	wt% H_2O	
MD1	0.5659	1.355	n=4
	0.5295	1.264	$\overline{X}$ =1.263
	0.5540	1.325	SD=0.095
	0.4672	1.108	

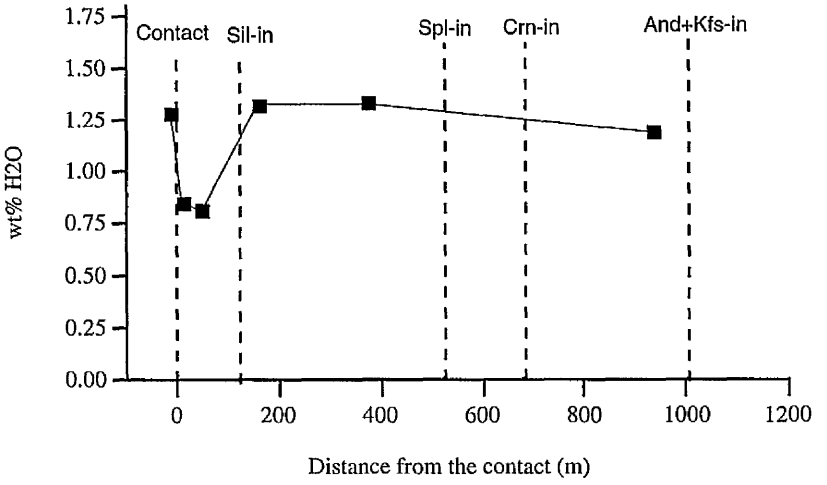

Fig. 7.18 Relationship between H_2O (wt%) in cordierite and distance from the igneous contact in the North Loch Awe area. The H_2O content remains approximately constant throughout the andalusite and spinel zones but is significantly lower in the sillimanite zone. The cordierite of the xenolith sample has a relatively high H_2O content.

7.3.4. K-feldspar: Representative analyses of K-feldspars are provided in Table 7.11. K-feldspar formulae are calculated on the basis of 8 oxygens. The oxide totals are between 99.16 and 101.31. Most of the data lie close to 100%. The cation totals are between 4.99 and 5.01. As the K-feldspars show perthitic texture, broad beams (~10 μm) were used to integrate the host and lamellae and so obtain the composition of the homogeneous K-feldspar prior to exsolution. The compositions of K-feldspars are plotted on the An-Ab-Or triangular diagram in Fig. 7.19. The proportion of orthoclase varies between 75 and 92 mole percent and the anorthite content is between 0 and 1 mole percent. K-feldspars from different metamorphic zones are treated separately in Fig. 7.19, but there is no trend in the data and K-feldspars from all zones appear to have same range of composition.

7.3.5. Plagioclase: Table 7.12 lists representative analyses of plagioclases in the pelitic rocks from the Etive aureole. Plagioclases exhibit optical zoning in some samples but it is not common. Study of zoned plagioclases by microprobe shows normal zoning (i.e. Ca-rich cores and Na-rich rims). The An content is between 1 and 54 mole percent.

7.3.6. Spinel: Table 7.13 shows representative analyses of spinel in the pelitic rocks. Formulae were calculated on the basis of four oxygens and the amount of Fe^{3+} was calculated using charge-balance criteria assuming a fixed cation total of 3.00. Oxide

totals are between 100 and 102. The analysed spinels contain no manganese and silicon, titanium and calcium are absent or in very low concentration (up to 0.01 apfu). The main divalent cations are Fe^{2+} and Mg. The amount of Fe^{2+} is between 0.67 to 0.84 apfu and the amount of Mg is between 0.10 and 0.15 apfu (Fig. 7.20).

Table 7.11 Representative microprobe analyses of K-feldspar in pelitic rocks.

Sample	MM155	MM181	MM171	MM149	MM134A	MM131B	MM195C	MM187	MM166C
SiO2	65.42	64.66	63.51	65.63	65.15	64.30	64.89	64.68	64.96
TiO2	0.09	0.19	0.28	0.24	0.18	0.29	0.25	0.39	0.16
Al2O3	18.53	18.45	19.54	18.65	18.68	19.23	19.41	19.45	18.79
Cr2O3	0.01	0.09	0.02	0.05	0.00	0.02	0.00	0.02	0.05
MnO	0.04	0.00	0.00	0.00	0.00	0.00	0.00	0.03	0.00
MgO	0.08	0.00	0.06	0.02	0.12	0.08	0.20	0.18	0.06
CaO	0.06	0.00	0.85	0.11	0.12	0.14	0.09	0.17	0.12
Na2O	0.82	1.09	1.45	2.03	1.84	1.79	1.68	2.17	2.27
K2O	15.75	15.05	13.65	13.77	13.84	14.10	14.47	13.57	13.36
FeO	0.15	0.15	0.13	0.00	0.05	0.25	0.24	0.03	0.00
Total	100.95	99.68	99.49	100.50	99.98	100.20	101.23	100.69	99.77
Number of atoms on the basis of 8 oxygens									
Si	2.99	2.99	2.93	2.99	2.99	2.95	2.95	2.95	2.98
Ti	0.00	0.00	0.01	0.01	0.00	0.01	0.01	0.01	0.00
Al	1.00	1.00	1.06	1.00	1.01	1.04	1.04	1.05	1.02
Cr	0.00	0.00	0.00	0.00	0.00	0.00	0.00	0.00	0.00
Mn	0.00	0.00	0.00	0.00	0.01	0.00	0.00	0.00	0.00
Mg	0.00	0.00	0.00	0.00	0.01	0.00	0.01	0.01	0.00
Ca	0.00	0.00	0.04	0.01	0.00	0.01	0.00	0.00	0.01
Na	0.07	0.10	0.14	0.18	0.16	0.16	0.15	0.19	0.20
K	0.92	0.89	0.80	0.80	0.81	0.83	0.84	0.79	0.78
Fe	0.00	0.00	0.00	0.00	0.00	0.01	0.01	0.00	0.00
Total	4.98	4.99	4.98	4.99	4.99	5.01	5.01	5.00	4.99

The Zn content of spinels is between 0.00 and 0.05 apfu. The trivalent cations, chromium, aluminium and Fe^{3+} are dominated by aluminium, which accounts for over 1.81 to 1.92 apfu. The amount of Fe^{3+} is between 0.07 and 0.21 apfu and chromium is absent or is up to 0.01 apfu (Fig. 7.21). In conclusion the spinels are dominated by the hercynite end member with up to 15% of Mg-spinel end member component. The amount of Zn-end member is low (up to 0.05 apfu Zn) and the amount of chromite component is insignificant.

7.3.7. Garnet: Garnet is present in regional metamorphic pelites and in a few samples from the contact metamorphic pelites. Table 7.14 contains representative analyses of garnet in the pelitic rocks. Garnet formulae were calculated on the basis of twelve oxygens and Fe^{3+} contents were estimated by fixing the number of cations at 8.00. The oxide totals are between 100.09 and 101.98. The number of silicons is between 2.93 and 2.98 apfu and the number of aluminiums is between 1.95 and 1.98

apfu, in both cases close to the ideal numbers of three and two respectively, giving good stoichiometry. Fig. 7.22 shows the composition of garnets on a (Ca+Mn)-(Fe^{2+})-(Mg) triangular diagram. Garnets from sample MM255D, which is a regional metamorphic pelite, are almandine-rich with 2.18 to 2.37 apfu Fe, 0.10 to 0.25

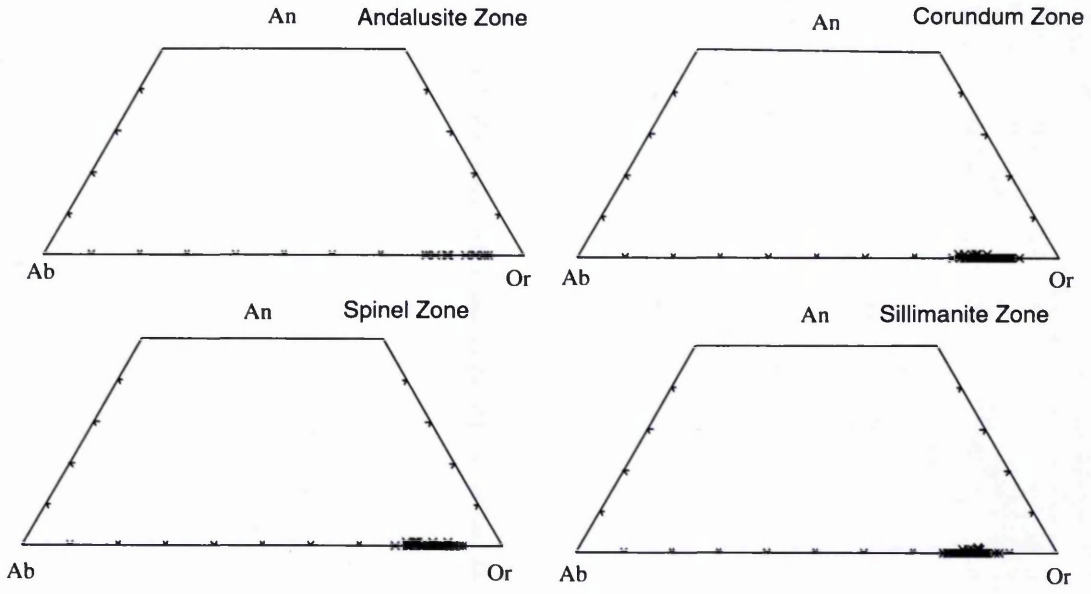

Fig. 7.19 Compositions of K-feldspars ploted on the An-Ab-Or triangular diagram (mole%) from different contact metamorphic zones. K-feldspar in all zones show the same range of composition.

apfu Mg, 0.46 to 0.70 apfu Ca. The amount of Mn is low between 0.00 and 0.01 apfu. Cr is absent or very low in amount (less than 0.007 apfu). In sample MM134A which is within the thermal aureole (Spl-Zone), two types of garnet are present (Chapter 5), one regional and the other contact metamorphic. The regional metamorphic garnet has a higher amount of Ca+Mn (Fig.7.22) and also is zoned (Fig. 7.23). Sample MM166A is a high-grade contact metamorphic pelite with unequivocal contact metamorphic garnet with well-developed textural equilibrium (Chapter 5). The garnets in this sample are almandine-rich with 2.36 to 2.41 apfu Fe, 0.42 to 0.46 apfu Mg and 0.07 to 0.08 apfu Ca. The amount of Ti is between 0.00 and 0.01 apfu and the Fe^{3+} content is between 0.09 and 0.16 apfu. The amount of Mn is between 0.12 and 0.17 apfu. Fig. 7.23 shows the zoning profiles across three garnet crystals in samples MM134A and MM166A. Fig. 7.23 a shows a traverse across the regional metamorphic garnet. The zonation is obvious and rims are Mn-rich, Ca,Mg-poor and cores are relatively Mn-

Table 7.12 Representative analyses of plagioclase in pelitic rocks.

Sample	MM138B	MM146	MM143	MM185B	MM193D	MM197A
SiO2	58.86	59.00	60.15	60.19	59.52	59.36
TiO2	0.03	0.00	0.06	0.00	0.00	0.06
Al2O3	25.72	25.61	25.56	25.38	25.03	26.24
Cr2O3	0.00	0.03	0.04	0.10	0.00	0.00
MnO	0.00	0.00	0.00	0.00	0.00	0.00
MgO	0.00	0.00	0.00	0.00	0.00	0.02
CaO	7.15	7.17	6.90	6.61	6.47	7.39
Na2O	7.12	7.22	7.70	7.74	7.78	7.12
K2O	0.23	0.19	0.14	0.09	0.05	0.18
FeO	0.12	0.11	0.15	0.24	0.17	0.13
Total	99.23	99.33	100.70	100.35	99.02	100.50
Number of atoms on the basis of 8 oxygens						
Si	2.63	2.65	2.66	2.68	2.68	2.64
Ti	0.00	0.00	0.00	0.00	0.00	0.00
Al	1.36	1.36	1.33	1.33	1.33	1.37
Cr	0.00	0.00	0.00	0.00	0.00	0.00
Mn	0.00	0.00	0.00	0.00	0.00	0.00
Mg	0.00	0.00	0.00	0.00	0.00	0.00
Ca	0.38	0.34	0.33	0.31	0.31	0.35
Na	0.62	0.63	0.66	0.67	0.68	0.61
K	0.01	0.01	0.01	0.00	0.00	0.01
Fe	0.00	0.00	0.00	0.01	0.00	0.01
Total	5.00	4.99	4.99	5.00	5.00	4.99

poor, Ca, Mg-rich. Figures 7.23b and 6.23c exhibit the zoning profiles in contact metamorphic garnets. There is no zonation in these garnets and all cation profiles appear as straight lines.

7.3.8 Orthopyroxene: Orthopyroxene occurs in some high grade psammitic and semi-pelitic rocks. It is associated with leucosomes (anatectic melt veins, Chapter 6) in some of samples. Table 7.15 includes representative analyses of orthopyroxenes. The formulae have been calculated on the basis of six oxygens and ferric iron contents have been estimated on the basis of 4.00 cations pfu.

Orthopyroxenes appeared to be homogeneous in the studied samples. The oxide totals are between 99.20 and 101.43. Orthopyroxenes contain insignificant amounts of, or an absence of, Cr, Ti, Mn, Na and K and small amounts of Ca (0.01 to 0.03 apfu). Ferric iron calculations yield 0.03 to 0.12 apfu Fe^{3+}. The end-member proportions of orthopyroxenes are presented in Fig. 7.25. The Wo content is between 0.013 to 0.019 mole. There are two types of orthopyroxene in sample MM198C. One

is fine-grained associated with fine-grained biotite and ilmenite and the other is coarse-grained, associated with coarse-grained cordierite (Chapter 5). According to

Table 7.13 Representative analyses of spinel in pelitic rocks.

Sample	MM197A	MM186	MM166C	MM146	MM171
SiO_2	0.08	0.05	0.07	0.08	0.02
TiO_2	0.17	0.19	0.03	0.12	0.00
Al_2O_3	54.33	56.25	56.77	57.74	57.37
Cr_2O_3	0.87	0.25	0.02	0.06	0.26
Fe_2O_3	5.27	3.07	3.97	3.21	2.81
FeO	36.03	34.68	36.94	36.17	36.94
MnO	0.00	0.00	0.00	0.00	0.26
MgO	2.78	2.81	2.42	2.99	2.61
CaO	0.00	0.00	0.07	0.07	0.00
ZnO	0.48	2.16	0.77	0.98	0.00
K_2O	0.04	0.00	0.00	0.03	0.00
Total	100.05	99.46	101.06	101.45	100.27
Number of atoms on the basis of 4 oxygens					
Si	0.00	0.00	0.00	0.00	0.00
Ti	0.00	0.00	0.00	0.00	0.00
Al	1.85	1.92	1.91	1.92	1.93
Cr	0.02	0.00	0.00	0.00	0.00
Fe^{3+}	0.11	0.07	0.08	0.07	0.06
Fe^{2+}	0.87	0.84	0.88	0.85	0.88
Mn	0.00	0.00	0.00	0.00	0.00
Mg	0.12	0.12	0.10	0.13	0.11
Ca	0.00	0.00	0.00	0.00	0.00
Zn	0.01	0.05	0.02	0.02	0.00
K	0.00	0.00	0.00	0.00	0.00
Total	3.00	3.00	3.00	3.00	3.00

Fig. 7.24 the coarse-grained orthopyroxene is more ferrosilite-rich than the fine-grained orthopyroxene in the same rock, suggesting that the two types have different origins.

7.3.9 Other minerals: Oxide minerals were analysed in all analysed samples. They are ilmenite in all of the studied samples. Analyses of corundum show up to 0.74% FeO (Fe total as FeO) which probably substitutes Al as Fe^{3+}. Andalusite and sillimanite are virtually pure Al_2SiO_5.

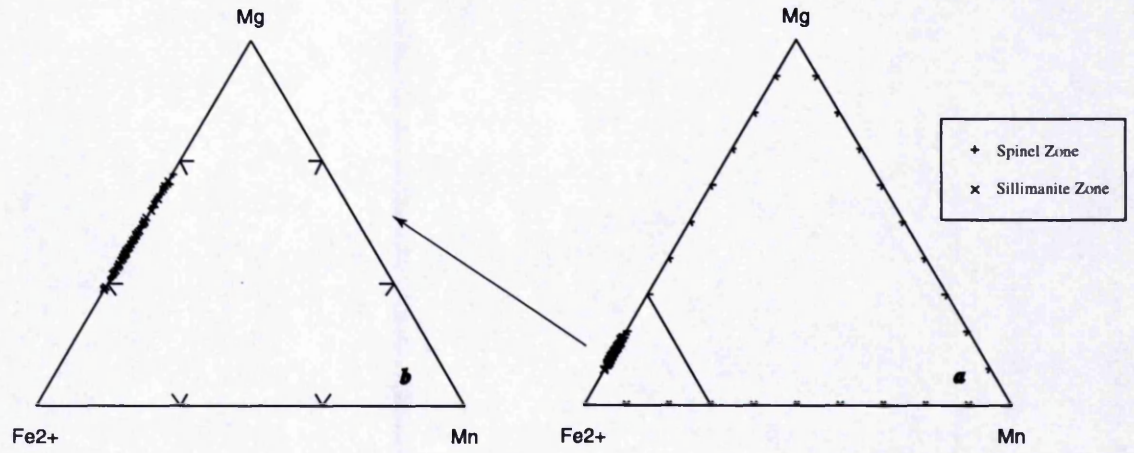

Fig. 7.20 Composition of spinels from the spinel and sillimanite zones. Spinels are mainly hercynite with a small amount of Mg-spinel component but no galaxite (Mn-Al spinel)

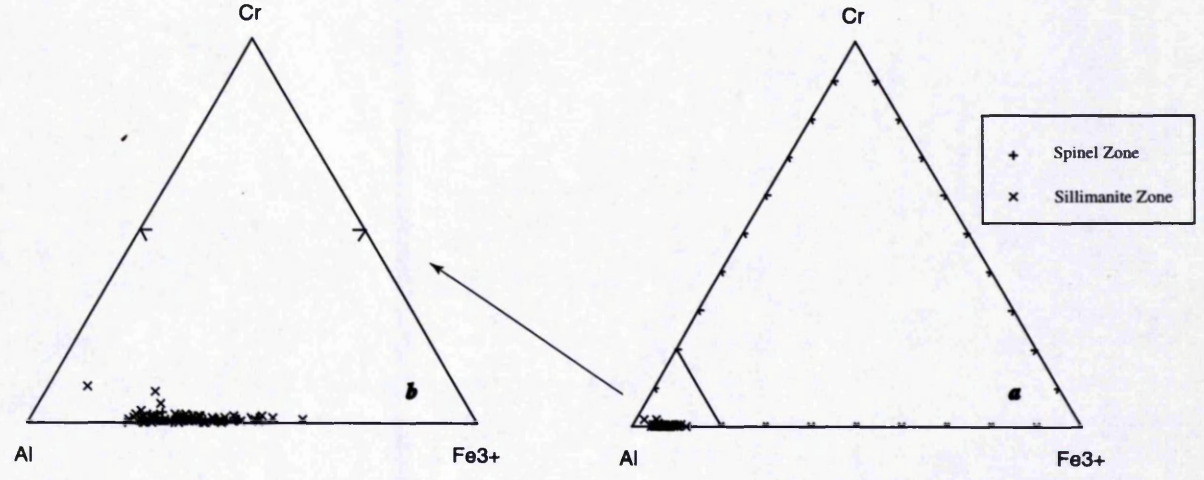

Fig. 7.21 Compositions of spinels plotted on a Cr-Al-Fe^{3+} diagram. The amounts of chromite and magnetite components are very low.

Table 7.14 Microprobe analyses of garnet in pelitic rocks. Garnets in samples MM255D and MM134A# are regional metamorphic minerals.

Sample	MM166A*	MM134A*	MM134A#	MM255D#
SiO2	37.03	37.56	37.72	37.18
TiO2	0.00	0.00	0.00	0.05
Al2O3	21.10	21.20	21.35	20.97
Cr2O3	0.09	0.11	0.09	0.04
Fe2O3	2.56	2.18	2.04	-
FeO	33.11	27.09	26.06	33.77
MnO	2.06	7.95	7.60	0.00
MgO	3.83	4.04	3.70	2.01
CaO	0.87	1.09	2.63	6.31
Na2O	0.24	0.24	0.27	0.29
K2O	0.00	0.02	0.00	0.00
Total	100.88	101.48	101.46	100.62
Atoms on the basis of 12 oxygens				
Si	2.95	2.96	2.97	2.98
Ti	0.00	0.00	0.00	0.00
Al	1.98	1.97	1.98	1.98
Cr	0.01	0.01	0.01	0.00
Fe3+	0.15	0.13	0.12	-
Fe2+	2.20	1.79	1.71	2.27
Mn	0.14	0.53	0.51	0.00
Mg	0.45	0.47	0.43	0.24
Ca	0.07	0.09	0.22	0.54
Na	0.04	0.04	0.04	0.04
K	0.00	0.00	0.00	0.00
Total	7.99	7.99	7.99	8.05

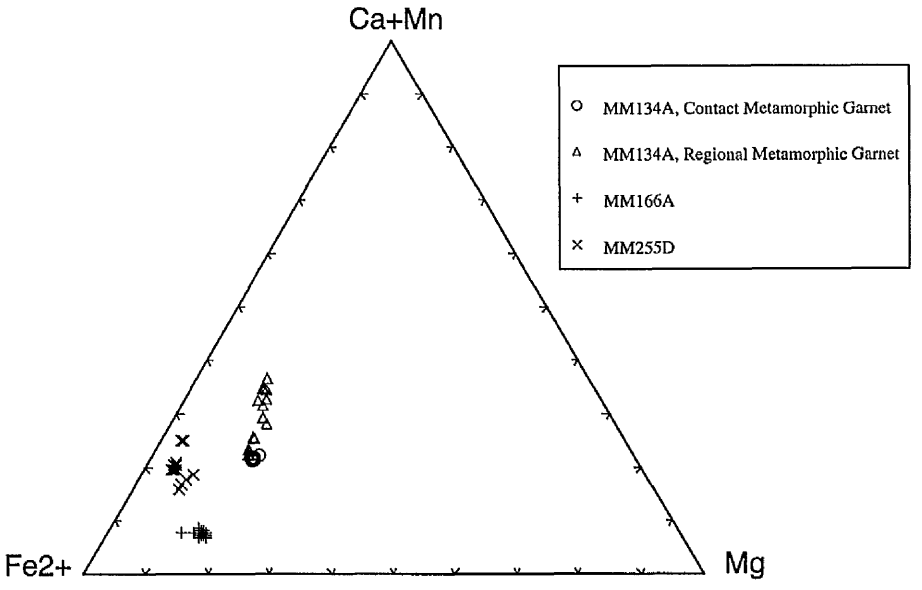

Fig. 7.22 Compositions of contact metamorphic and regional metamorphic garnets plotted on the (Ca+Mn)-Fe^{2+}-Mg diagram. Contact metamorphic garnets from the sample MM166A are almandine-rich. The amounts of spessartite and grossularite end-members are higher in the regional metamorphic garnets.

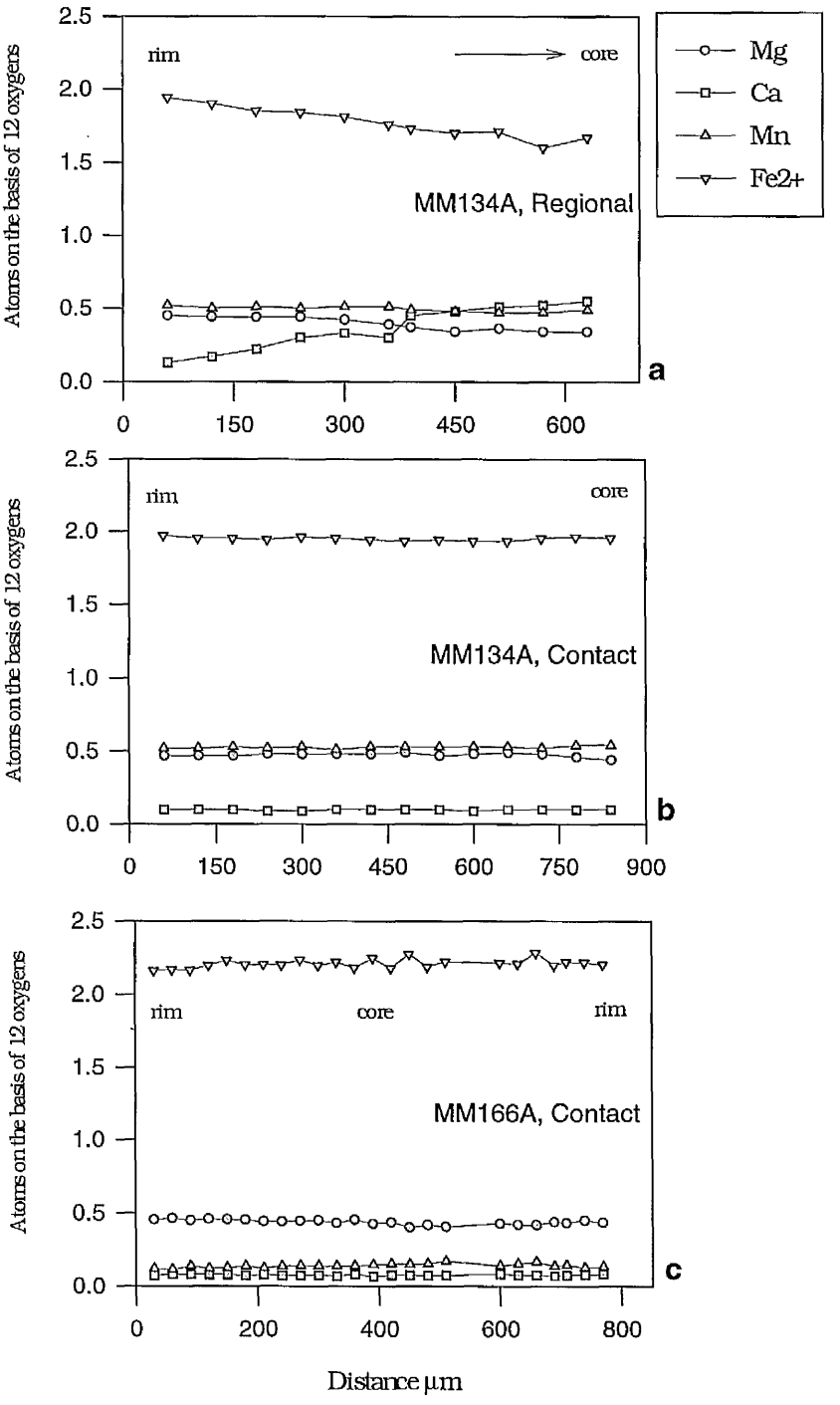

Fig. 7.23 Zoning profiles across contact metamorphic and regional metamorphic garnets. Regional metamorphic garnets (samples MM134Aa) are zoned with Ca-poor and Mg and Fe^{2+} -rich rims. Contact metamorphic garnets are homogeneous in composition.

Table 7.15 Representative analyses of orthopyroxene in psammitic rocks.

Sample	MM198C.f*	MM198C.c*	MM8B	MM138B
SiO2	51.50	49.42	53.46	52.33
TiO2	0.14	0.16	0.25	0.15
Al2O3	1.33	2.06	0.72	0.62
Cr2O3	0.00	0.00	0.10	0.00
Fe2O3	3.38	1.98	1.42	1.01
FeO	21.23	31.28	22.57	26.35
MnO	0.23	0.26	0.08	0.97
MgO	20.29	14.28	21.53	18.18
CaO	0.68	0.18	0.88	0.80
Na2O	0.64	0.42	0.43	0.42
K2O	0.03	0.02	0.00	0.00
Total	99.45	100.06	101.44	100.83
Number of atoms on the basis of 6 oxygens				
Si	1.94	1.94	1.97	1.98
Ti	0.00	0.00	0.01	0.00
Al	0.06	0.10	0.03	0.03
Cr	0.00	0.00	0.00	0.00
Fe3+	0.10	0.06	0.04	0.03
Fe2+	0.67	1.02	0.70	0.84
Mn	0.01	0.01	0.00	0.03
Mg	1.14	0.83	1.18	1.03
Ca	0.03	0.01	0.04	0.03
Na	0.05	0.03	0.03	0.03
K	0.00	0.00	0.00	0.00
Total	4.00	4.00	4.00	4.00

* f = fine-grained opx, c = coarse-grained opx.

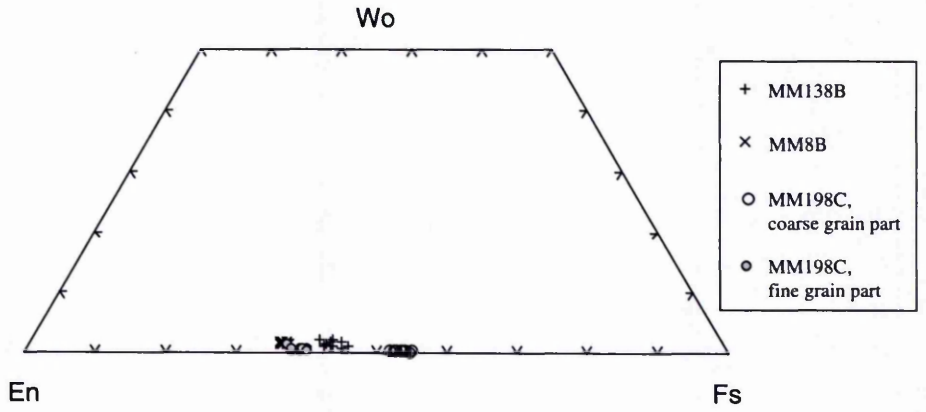

Fig. 7.24 Compositions of orthopyroxenes from psammitic rocks plotted on the Wo-En-Fs diagram. Coarse grained orthopyroxenes in sample MM198C are more Fe-rich than other analysed orthopyroxenes.

Chapter 8

Metamorphic Reactions

8.1 Introduction

The main objective of this chapter is to deduce the sequence of metamorphic reactions in different lithologies in different parts of the aureole. The original intention was to compare reaction sequences in all the P-T sensitive lithologies within the aureole (pelites and semi-pelites, metabasites and calcareous rocks). Because of the psammitic and quartzitic nature of rocks in the northern and eastern segments of the aureole, studies were restricted to the southern and western segments where P-T sensitive lithologies dominate. The most detailed information is available from the southern segment where thick metasedimentary units with intercalated metabasites trend at high angle to the igneous contact (Plate 3.1). An attempt will also be made to extract reaction sequences from the west segment of the aureole. Because of time limitations, calcareous rocks were omitted from this study.

The main reason for deducing metamorphic reactions sequences is to explain mineralogical changes due to temperature, pressure and compositional variables. The sequence of metamorphic reactions will be used to establish a facies series for the southern part of the aureole and to find out whether or not this facies series is isobaric (as expected). In principle one could compare different facies series in different parts of the aureole to find out if there is any pressure gradient within the aureole caused by later tilting of the igneous complex.

The facies series developed in a metamorphic terrain reflects the 'P-T array', the array of peak-metamorphic P-T points recorded by rocks collected from different localities on the erosion surface (England and Richardson, 1977). (This is also termed the "metamorphic field gradient" by various authors, e.g. Spear, 1993.) In normal contact metamorphism, heating is not accompanied by pressure changes. Thus, contact-metamorphic P-T paths taken by individual rocks are likely to be

assemblages is likely to be identical to the time sequence of reactions and assemblages in individual high-grade rocks, provided that heating was slow enough to allow equilibrium to be maintained in the process.

To be able to study all the above mentioned aspects, the following methods are employed:

-Looking at the sequence of mineral assemblages, paying attention to 'outgoing' phases and appearance of 'new' phases and assemblages at isograds.

-Analysis of phase relations by means of projections to determine compatibility relations and possible reactions. Discontinuous reactions appear as changes in tie-line topology (e.g. cross tie-line relations) and continuous reactions appear as changes in the positions of three-phase triangles with changing grade.

This chapter discusses the evidence for metamorphic reactions in two different lithologies in the Etive aureole (semi)pelites and metabasites. The chapter starts with metamorphism of basic igneous rocks, which had already been metamorphosed up to greenschist facies prior to contact metamorphism. The later part is concerned with metamorphism of (semi)pelites. A petrogenetic grid is used to place broad temperature and pressure limits on the crystallisation of pelitic rocks. More precise estimates for pressure and temperature are made in Chapter 9.

8.2 Metamorphism of basic rocks

The sequence of petrographical (Chapter 5) and chemical changes of minerals (Chapter 7) in the metabasic rocks are:

- Regional metabasites are composed mainly of Act+Chl+Ab+Ep(Czo)± Cal+Qtz±Stilp+Ttn.
- Hbl, Cpx and Opx appear in sequence as the grade of contact metamorphism increases and are used as index minerals to define the Hbl, Cpx and Opx Zones.
- Chl disappears in the upper Hbl Zone as thermal grade increases.
- Ep disappears within the Cpx Zone as thermal metamorphic grade increases.
- Pl becomes more Ca-rich as the distance from the contact decreases and ultimately at high grade (rocks adjacent to the contact) it becomes Na-rich again.
- Hbl becomes more Al-rich and Na-rich from the Opx-in isograd towards the contact but these changes are not very clear.
- Hbl becomes more Ti-rich as the contact metamorphic grade increases.

8.2.1 Choice of compatibility diagrams: Minerals in metabasites can be represented by components in the system FeO, MgO, CaO, Na_2O, Al_2O_3, SiO_2, K_2O, Fe_2O_3, TiO_2, H_2O and CO_2. Metabasic rocks display considerable chemical variability in this system. If a component resides in only one phase, the Phase Rule dictates that it is possible to ignore that component and the phase from consideration without altering the phase relations of the remaining phases. Almost all studied metabasites contain quartz, so projection from SiO_2 is possible. It is also reasonable to assume that fluids in low- and medium-grade metabasites (even calcite-bearing ones) were essentially H_2O and that the amount of CO_2 in the fluid, though finite, was very small (Graham *et al.*, 1983). Calcite is present in the regional metamorphic metabasites and low-grade contact metamorphic rocks, so one can assume that virtually all CO_2 is in calcite. Thus, CO_2 and calcite may both be ignored. TiO_2 is in either sphene or ilmenite. K_2O is in either stilpnomelane or biotite. Fe_2O_3 may be present in epidote and is assumed to substitute for Al_2O_3. Considering all these facts and assumptions, TiO_2, CO_2, K_2O, Fe_2O_3 can be ignored for projection and SiO_2 and H_2O can be considered as excess components. Therefore one ends up with the five components, CFMNA. Fe/Mg partitioning between amphibole and chlorite, amphibole and orthopyroxene and orthopyroxene and clinopyroxene is very small. Therefore, to a first approximation, Fe and Mg can be combined as one component. CAN(FM) tetrahedral diagrams (after Ernst, 1976) were constructed in this way and were used to project (from quartz and H_2O) the phases in metabasic rocks from different grades (Fig. 8.1). These diagrams permit investigation of metabasic rocks in the full NC(FM)ASH system. The problem with tetrahedral diagrams is that it is not possible to plot the three-dimensional position of points unambiguously on a piece of paper. Because of this problem, triangular diagrams are required to project the absolute position of each point. Different triangular projections are used for different grades because it is not possible to find the same common ('excess') phases throughout the whole section of metabasites in the aureole.

The AFM projection from quartz, albite, epidote and H_2O (Harte and Graham, 1975) is used for low-grade albite- and epidote-bearing rocks. The AC(FM) projection from plagioclase (actual compositions), quartz and H_2O (Spear, 1993) is used for the rocks.

8.2.2 Regional metamorphic metabasites: Mineral phases in regional metamorphic sample MM94 are plotted on the NA-A-C-(FM) diagram in Fig. 8.1.a. The mineral

paragenesis is actinolite, albite, chlorite, epidote and quartz. The chemical compositions of coexisting minerals in this rock are plotted on the AFM projection in Fig. 8.2.a and on the A-C-FM projection in Fig. 8.3.a.

8.2.3 Lower Hornblende Zone: The first influence of contact metamorphism on the regional metamorphic metabasites is the appearance of contact-metamorphic hornblende. Two processes were probably involved, recrystallisation of already existing hornblende and generation of new hornblende by reaction [8.1]. Some of the metabasic samples from the outer aureole in the Loch Awe area have relicts of regional metamorphic garnet. This implies that metabasites had already been metamorphosed up to the garnet-amphibolite facies prior to contact metamorphism. Therefore regional-metamorphic hornblende may have been present in the outer aureole in the Loch Awe area. Nevertheless, it is clear from the thin sections that decussate contact metamorphic hornblende is formed within the aureole in the Hornblende Zone.

Mineral phases in low-grade contact metamorphic metabasite from the lower Hornblende Zone (sample MM55) are plotted on the A-C-NA-FM projection in Fig. 8.1.b. The composition of minerals are plotted on the AFM projection in Fig. 8.2.b. The main result from the two projections in Fig. 8.2.a and 8.2.b is that actinolite in regional metamorphic rocks is more Mg-rich and Al-poor than hornblende in contact metamorphic rocks. Chlorite in regional rocks shows a variation in Al-content but contact metamorphic chlorite shows only a slight Mg-Fe variation.

Comparison of Figures 8.1.a, 8.3.a with Figures 8.1.b and 8.3.b shows that hornblende appears as the rocks become involved in contact metamorphism. The most likely reaction for hornblende generation from a greenschist precursor is:

$$Act+Ep+Chl+Qtz = Hbl + H_2O \qquad [8.1]$$

This reaction is an Fe/Mg continuous reaction. The large distance between regional metabasite samples and contact metabasite samples plus lack of systematic sampling from regional rocks towards the contact metamorphic rocks (because of natural restrictions i.e. Loch Awe) do not permit me to establish whether there is a continuous transition from actinolite to hornblende or a jump from actinolite to hornblende because of the Act-Hbl miscibility gap (Klein, 1969; Allen and Goldie, 1978; Grapes and Graham, 1978).

The transition from actinolite to hornblende in the Loch Awe area is considered as Hbl-in isograd (inferred but not seen).

8.2.4 Upper Hornblende Zone: Plagioclase is virtually pure albite in regional metamorphic rocks and low-grade contact metamorphic rocks. It becomes more Ca-rich as contact metamorphic grade increases. Fig 8.1.c shows schematic phase relations in sample MM180 from the Upper Hornblende Zone. The reaction:

$$Ep+Chl+Ab = Hbl+Pl\ (\pm Qtz+H_2O) \qquad [8.2]$$

which is an Fe/Mg- and Ca/Na-continuous reaction, is responsible for the formation of Ca-bearing plagioclase solid-solution (Fig. 8.1.c).

There is no clear relationship between the Al and Na contents of amphibole and contact metamorphic grade in Fig. 7.5, but an overall increase in Al content from the regional metamorphic amphiboles to the Hornblende Zone amphiboles is apparent. Also an overall increase in Al content of amphiboles from the Opx-in isograd towards the igneous contact is apparent. Considering a probable increase in the Al and Na content of amphiboles with contact metamorphic grade (Fig. 8.1d). the likely reaction for this compositional change is:

$$Hbl+Ep+Chl+Pl = \text{more Na,Al-rich Hbl}\ (\pm Qtz+H_2O) \qquad [8.3]$$

Reaction [8.3] is both Na/Ca- and Fe/Mg-continuous. Reactions [8.2] and [8.3] are both expressions of the single multi-variant reaction that controls the migration of the Hbl-Chl-Ep-Pl four-phase volume with increasing grade:

$$Hbl+Ep+Chl+Pl = \text{more Na,Al-rich Hbl+more Ca-rich Pl}\ (\pm Qtz+H_2O). \qquad [8.4]$$

This reaction is probably also responsible for the disappearance of Chl in the upper Hornblende Zone. The fan of Hbl-Pl-Ep tie-planes on the C-rich side of the four-phase volume in Fig. 8.1c has finite thickness. Therefore chlorite disappears as the Hbl-Ep-Pl plane bounding the four-phase volume rises up through the bulk composition, yielding the assemblage Hbl+Ep+Pl+Qtz.

8.2.5 Lower Clinopyroxene Zone: Further migration of the Hbl-Ep-Pl planes to more A-rich compositions causes Cpx to appear. The following reactions show these changes:

$$Hbl+Ep+Pl = \text{more Na,Al-rich Hbl+Cpx}\ (\pm Qtz+H_2O) \qquad [8.5]$$

$$Hbl+Ep+Pl = \text{more Ca-rich Pl+Cpx}\ (\pm Qtz+H_2O) \qquad [8.6]$$

These reactions are Fe/Mg- and Na/Ca-continuous respectively. They are both expressions of the single multi-variant reaction that controls the migration of the Hbl-Cpx-Ep-Pl four-phase volume with increasing grade:

$$Hbl+Ep+Pl = \text{more Na,Al-rich Hbl+more Ca-rich Pl+Cpx}\ (\pm Qtz+H_2O). \qquad [8.7]$$

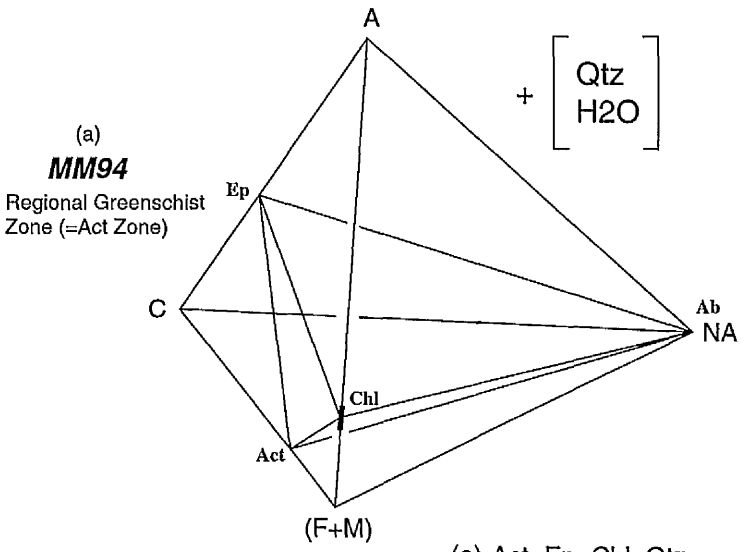

(a) Act+Ep+Chl+Qtz ⟶ Hbl+H2O
(Fe,Mg continuous)

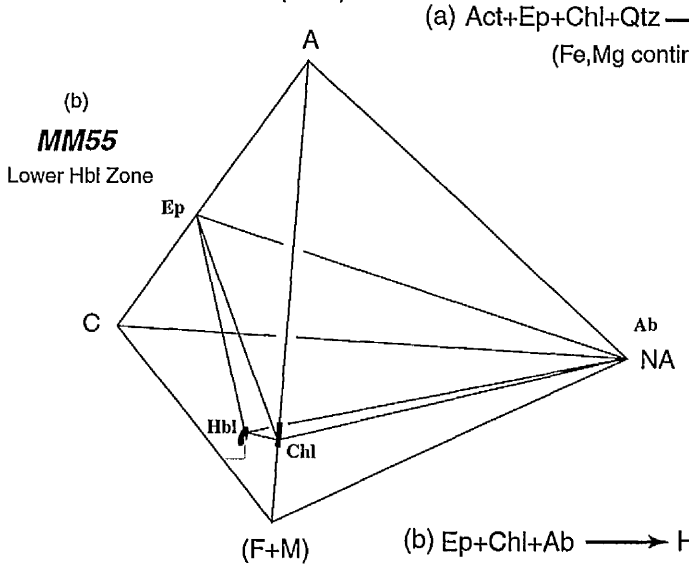

(b) Ep+Chl+Ab ⟶ Hbl+Pl(±Qtz+H2O)
(Fe,Mg and CaAl,NaSi continuous)

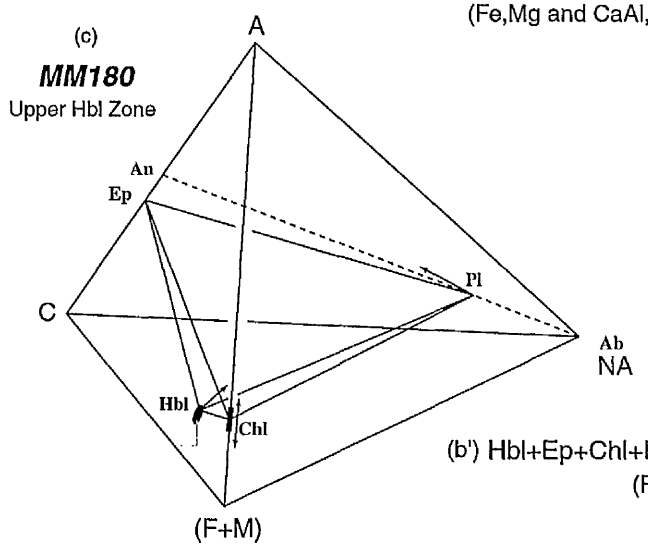

(b') Hbl+Ep+Chl+Pl ⟶ more Na,Al-rich Hbl(±Qtz+H2O)
(Fe,Mg and Na,Ca continuous)

8.1 Mineral parageneses of metabasites plotted on NA-A-C-(FM) tetrahedra (Ernst, 1976), and deduced metamorphic reactions.

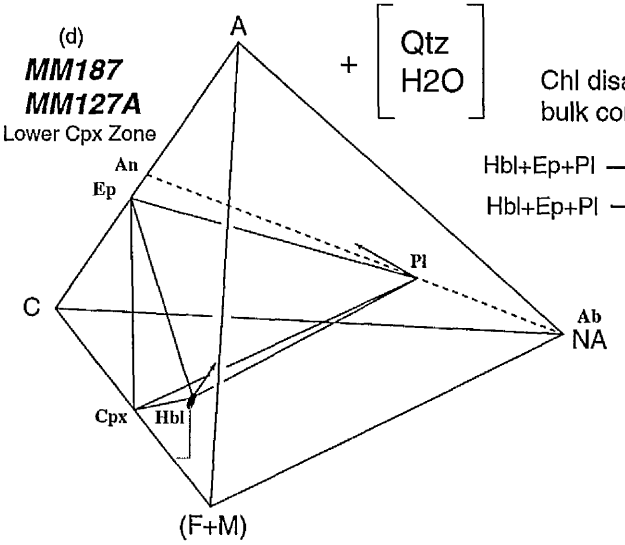

Chl disappears as the Hbl-Ep-Plss plane rises up through bulk composition and Cpx appears instead.

Hbl+Ep+Pl ⟶ more Na,Al-rich Hbl+Cpx(+H2O±Qtz)

Hbl+Ep+Pl ⟶ more Ca,Al-rich Pl+Cpx(+H2O±Qtz)

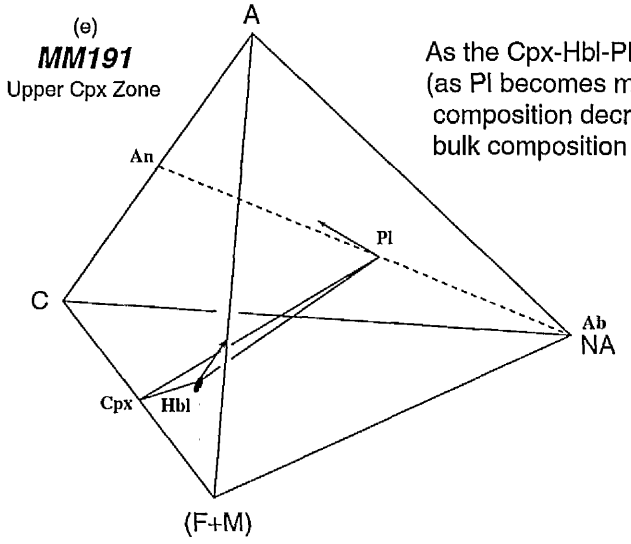

As the Cpx-Hbl-Pl plane moves towards more Ca,Al-rich compositions (as Pl becomes more calcic), the proportion of Ep in given bulk composition decreases. Eventually the Cpx-Hbl-Pl plane crosses the bulk composition and Ep disappears (effectively Ep⟶ An).

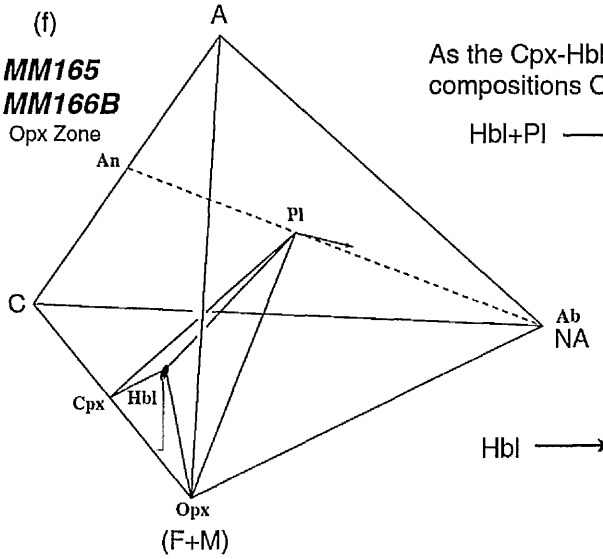

As the Cpx-Hbl-Pl plane continue to move to more Ca, Al-rich compositions Opx appears.

Hbl+Pl ⟶ Cpx+Opx+ more Ca-rich Pl(±Qtz+H_2O)

Hbl ⟶ Pl+more Na-poor, Al-rich Hbl+Cpx+Opx (±Qtz+H_2O)

Fig. 8.1 Continued.

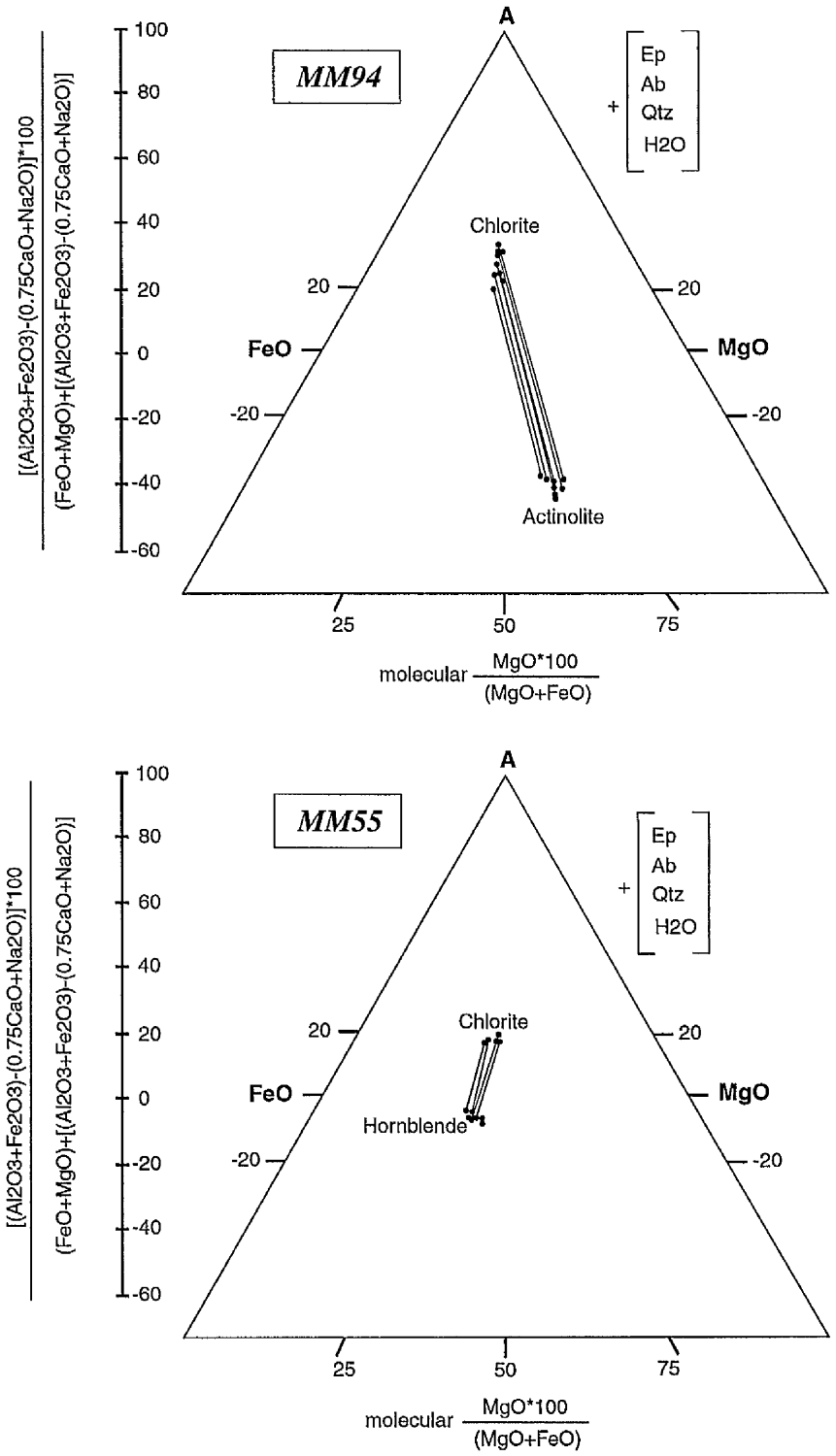

Fig. 8.2 Projection of regional metamorphic metabasite (MM94) and low-grade contact metamorphic metabasite (MM55) on the AFM diagram of Graham and Harte (1975). There is no significant change in chlorite composition but amphibole becomes more Al and Fe-rich as contact metamorphism occurs.

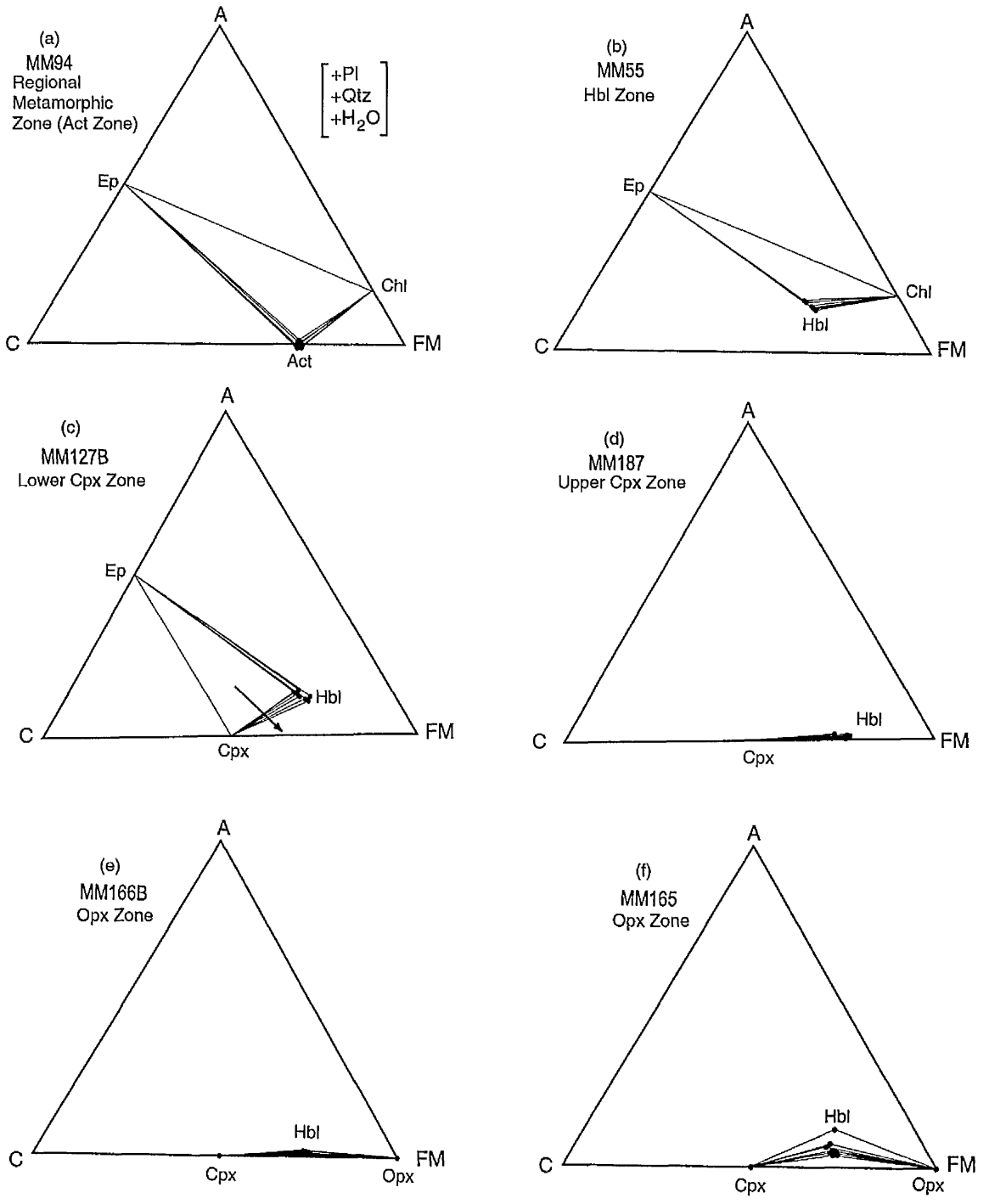

Fig. 8.3 Metabasite parageneses plotted on AC(FM) projection from plagioclase, quartz and H_2O. See text for explanation.

8.2.6 Upper Clinopyroxene Zone: The transition to the Upper Cpx Zone is marked by the loss of epidote from the assemblage. As the Cpx-Hbl-Pl plane in Fig. 8.1.d moves towards more Ca,Al-rich compositions (as Pl becomes more calcic), the proportion of epidote in any given bulk composition decreases. Eventually the Cpx-Hbl-Pl plane crosses the bulk composition and epidote disappears (Fig. 8.1e). Figures 8.3d and 8.3e illustrate the transition from the Lower Cpx-Zone (with Ep) to the Upper Cpx-Zone (Ep-free). The Ep-out isograd indicates this transition.

8.2.7 Orthopyroxene Zone: The next phase to appear with increasing grade is Opx. As the Cpx-Hbl-Pl plane continues to move towards the CA(FM) face of the tetrahedron (Fig. 8.1.f), orthopyroxene is produced by the continuous reaction (also see Figures 8.3e and 8.3f):

$$\text{Hbl+Pl} = \text{Cpx+Opx+more Ca-rich Pl } (\pm\text{Qtz+H}_2\text{O}) \qquad [8.8]$$

Within the Opx Zone plagioclase starts to become more Na-rich with increasing grade, while Hbl starts to become Na-poor but continues to become more Al-rich. The latter trend can be explained by the reaction:

$$\text{Hbl} = \text{Pl +more Na-poor, Al-rich Hbl+Cpx+Opx } (\pm\text{Qtz+H}_2\text{O}) \quad [8.9]$$

However, the reason for the reversal of the compositional trend of plagioclase is unclear. The Na enrichment of plagioclase is presumably derived from hornblende, which is becoming Na-poor, but if the projection conditions are fulfilled, the migration of the plagioclase corner of the Opx-Cpx-Hbl-Pl four-phase volume to more Na-rich compositions implies a reversal of reaction [8.8] (since no new phase has appeared). This would be nonsensical, as it would imply a reversal of thermal gradient within the inner aureole. One possible explanation for this trend is that the projection conditions are no longer fulfilled. There is some evidence (see Chapter 9) that hydrous fluid is absent from metabasites of the Opx Zone, invalidating the projection.

8.3 Comparison with other aureoles involving basic rocks

Because of the problems in studying contact metamorphic basic rocks (see Chapter 1), very few studies have described the mineralogical changes and metamorphic reactions that accompany prograde contact metamorphism of basic rocks. Most of these studies deal with aureoles developed around basic or ultrabasic intrusives, in basalts or low-grade regional metamorphic volcanites. A well-studied

example is the contact metamorphic basalts within the aureole around the Cuillin Complex in Skye, Scotland (Almond, 1964; Ferry, *et al.*, 1987).

The contact metamorphic zones within the thermally metamorphosed Karmutsen volcanics of Vancouver Island comprise a Zeolite Zone, Prehnite-pumpellyite Zone, Amphibole Zone, Clinopyroxene Zone and Orthopyroxene Zone, from the outer aureole towards the contact of the gabbroic pluton (Kunyioshi and Liou, 1976; Cho and Liou, 1987).

The intrusion of the Laramie Anorthosite Complex into amphibolites (Hbl+Pl±Qtz) has developed a contact aureole at Morton Pass, USA (Grant and Frost, 1990). Russ-Nabelek (1989) studied the reactions in the contact aureole. Breakdown of hornblende produced clinopyroxene and, as the contact metamorphic grade increases, orthopyroxene appears in the rocks. Olivine is found at the highest grade at temperatures in excess of 900°C (Russ-Nabelek, 1989). Russ-Nabelek (1989) found that the hornblende becomes richer in Al and Ti and poorer in Si as the contact metamorphic grade increases.

Of the three aureoles mentioned above, Morton Pass is most similar to Etive because it has formed at higher pressure (3kbar, Grant and Frost, 1990) than the other two aureoles. The sequence of the reactions in the Etive and Morton Pass aureoles are similar [Hbl→Cpx→Opx→(Olv)]. The only difference is the lack of olivine in the Etive aureole. This could be because of the lower inner aureole temperature in the Etive aureole (where intrusion is a diorite) compared to Morton Pass (where the intrusion is gabbroic). Alternatively, the lack of olivine may be a function of bulk composition; many of the Etive two-pyroxene hornfelses are quartz-bearing, suggesting that they may have tholeiitic chemistry. The chemical changes of hornblende in the Etive aureole is not very clear except for Ti, which shows a clear increase as the contact metamorphic grade increases as at Morton Pass.

According to the experimental studies of Spear (1981), hornblende breaks down to augite as the temperature increases and hypersthene and olivine are products of hornblende breakdown at higher temperatures. Spear (1981) also found that the amphibole composition changes during the breakdown reactions, becoming Al, Na, K and Ti-rich and Si-poor as the temperature increases. The breakdown of hornblende in the Etive aureole and generation of Cpx and Opx are consistent with

the experimental results of Spear (1981). The increase in Ti-content of amphiboles in the Etive aureole is also consistent with Spear's observation.

The deduced reactions for metabasic rocks in the Etive aureole are consistent with observed mineral assemblages and isograds and variations in the chemical compositions of plagioclase and, to some extent hornblende with contact metamorphic grade.

8.4 Contact metamorphism of pelitic and semi-pelitic rocks in the S aureole

The mineral assemblages in the pelitic and semi-pelitic rocks are discussed in Chapter 5. The distribution of mineral assemblages, metamorphic zones and isograds is illustrated in Fig. 5.3.

The phase relations and metamorphic reactions in the (semi)pelitic rocks are addressed in this section.

8.4.1 Choice of projections: Two sets of triangular diagrams are used, one for quartz-bearing rocks and one for quartz-absent rocks. The phase relations in the quartz-present rocks are studied on AFM diagrams projected from muscovite, quartz and water or K-feldspar, quartz and water (Fig. 8.5, Thompson, 1957). The phase relations in the quartz-absent rocks are studied using SFM diagrams (Pattison, 1991) projected from corundum, K-feldspar and water or from corundum, K-feldspar and melt. Phases projected on SFM diagrams from melt probably plot in almost the same places as those projected from water because minimum melts produced by pelitic anatexis can be considered as essentially chemically equivalent to Kfs+Qtz+H_2O (e.g. Grant, 1985; Stevens *et al.*, 1997). All projected assemblages contain plagioclase and ilmenite.

8.4.2 Quartz-bearing pelites and semi-pelites

8.4.2.1 Regional metamorphic assemblages: Regional metamorphic pelites contain assemblages Ms+Bt+Chl+Qtz+Pl and Ms+Qtz+Bt+Grt+Pl+Chl. Comparison of these mineral assemblages shows that they are related by the operation of the garnet-producing reaction :

$$Ms+Chl+Qtz = Grt+Bt+H_2O. \qquad [8.10]$$

This Fe,Mg-continuous reaction is known to be responsible for the appearance of garnet at the Grampian garnet isograd and for the Mg-enriched trend of coexisting garnet, chlorite and biotite within the garnet zone (Atherton, 1964).

8.4.2.2 Biotite and Cordierite Zones (Zone I): The first effect of the contact metamorphism on regionally metamorphosed rocks is the generation of new biotite (see section 5.3.2). which occurs partly by recrystallisation of regional biotite and partly by muscovite-consuming, cordierite-producing reactions (see below).

Cordierite is the first newly formed contact metamorphic mineral to appear (section 5.3.2) The main low-grade, cordierite-bearing assemblage is Crd+Ms+Bt+Qtz. This assemblage is plotted on an AFM diagram in Fig. 8.4.a. Biotites are plotted using microprobe analyses but cordierite is plotted schematically because all cordierites in the low-grade rocks are pinitized. Comparison of this assemblage with the regional metamorphic pelites and low-grade contact metamorphic pelites implies the operation of the following model divariant KFMASH reaction

$$Ms+Chl+Qtz = Crd+Bt+H_2O. \qquad [8.11]$$

Cordierite replaces regional metamorphic garnet and chlorite, the latter itself forming retrogressive pre-contact metamorphic pseudomorphs after regional metamorphic garnet in few samples. Replacement of regional garnet by cordierite suggests the following model KFMASH reaction:

$$Grt+Ms+Qtz+H_2O = Crd+Bt. \qquad [8.12]$$

This reaction, which is likely to be a disequilibrium reaction (since it probably occurred far outside the stability field of garnet) is a prograde fluid-consuming reaction (hydration reaction). The release of water from prograde dehydration reactions such as reactions [8.10] and [8.11] may have provided the water required for reaction [8.12].

8.4.2.3 Andalusite Zone (Zone II): Upgrade of the Cordierite Zone (Zone I), andalusite first apppears in pelitic rocks in the Andalusite Zone (Zone II). K-feldspar also appears in this zone, but not in andalusite-bearing rocks. The assemblages present in this zone are Crd+Kfs+Bt+Ms+Qtz and Crd+And+Bt+Qtz+Ms. The appearance of the assemblage Crd+Kfs suggests the progress of the divariant KFMASH reaction:

$$Ms+Bt+Qtz = Crd+Kfs+H_2O. \qquad [8.13]$$

The appearance of the assemblage And+Bt+Qtz upgrade of zones I and II (assemblage Ms+Crd+Bt+Qtz, Fig. 8.4.b) suggests the progress of the model divariant KFMASH reaction:

$$Ms+Crd = And+Bt+Qtz+H_2O. \qquad [8.14]$$

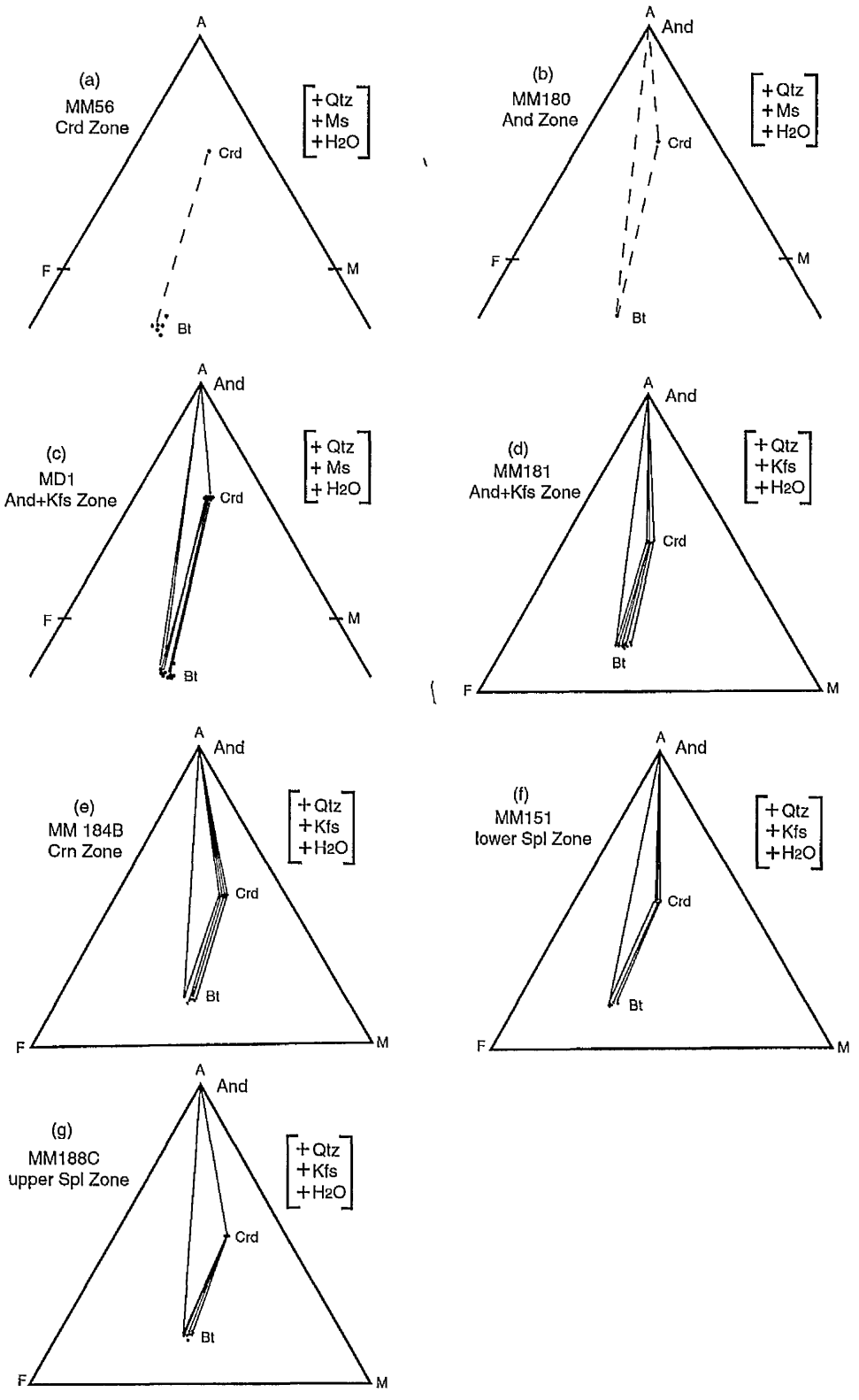

Fig. 8.4 Quartz-bearing pelitic parageneses plotted on AFM projection from quartz, muscovite or K-feldspar and H_2O. See text for explanation.

Evidence for this continuous reaction is provided by the slight movement of the And-Crd-Bt triangle to more Mg-rich compositions with increasing grade (Fig. 8.4a, b, and c).

8.4.2.4 Andalusite-K-feldspar Zone (Zone III): In the And + Kfs Zone the characteristic mineral assemblage in the less aluminous lithologies is Crd+Kfs+Bt+Qtz while those of aluminous pelites are Crd+And+Kfs+Bt+Qtz (Fig. 8.4d) and Crd+Kfs+Bt+And+Ms+Qtz (Fig. 8.4c). The major reaction for generation of And+Kfs-bearing assemblages is the univariant, discontinuous reaction

$$Ms+Qtz = And+Kfs+H_2O. \qquad [8.15]$$

In quartz-rich pelites and semi-pelites, muscovite is exhausted before quartz as the reaction [8.15] progresses. In quartz-poor pelites, quartz will be exhausted before muscovite, resulting in the production of quartz-absent assemblages (these are discussed separately in section 8.4.3 below). Only one sample containing the full univariant assemblage, Ms+Qtz+Bt+Crd+Kfs+And is found (Sample MD1).

The assemblage And+Crd+Bt+Kfs+Qtz persists until the middle Spinel Zone. In principle it should be possible to deduce the continuous reaction that must occur among these phases from the migration direction of the And+Crd+Bt triangle progressing from Fig. 8.4c to 8.4f. Migration towards more Fe-rich compositions would imply that reaction

$$And+Bt+Qtz = Crd+Kfs+H_2O \qquad [8.16]$$

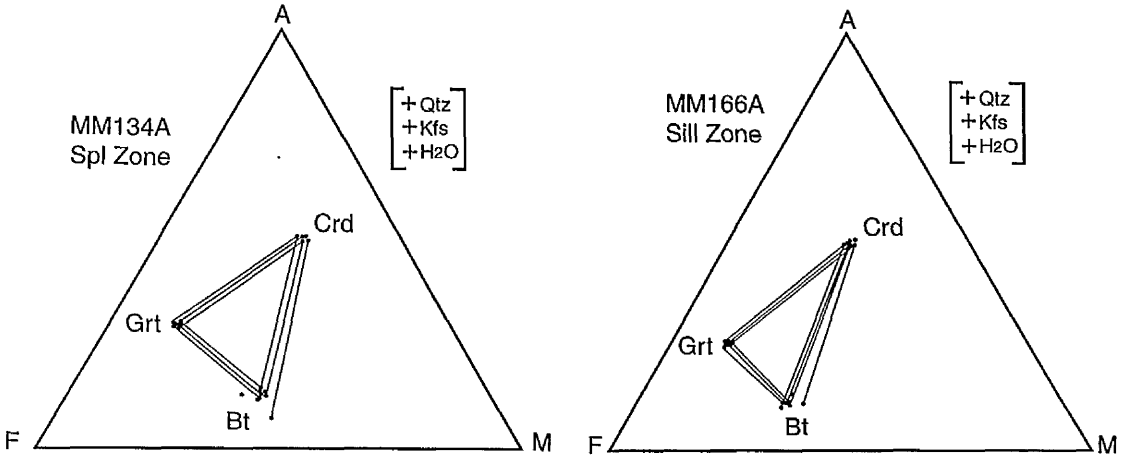

Fig. 8.5 Garnet-bearing metapelites plotted on AFM diagram, projected from quartz, K-feldspar and H_2O. See text for explanation.

while migration towards more Mg-rich compositions would imply the reverse. Unfortunately no clear trend is apparent in Fig. 8.4. However, in view of the fact that equilibrium curves for this reaction has a positive dP/dT slope with Crd+Kfs+H2O on the high-T side (Droop and Treloar, 1981; Holdaway and Lee, 1977), the forward version of reaction [8.16] (as written) is probably correct.

8.4.2.5 Partial melting within the spinel Zone (Zone VI): Quartzo-feldspathic leucosomes, interpreted to be a crystallised melt phase, first appear in the upper Spinel Zone (see Chapter 6). Considering the mineral assemblages below the onset of the partial melting (mainly Bt+Crd±And+Ksp+Qtz), the first melting reaction was probably the discontinuous water-saturated, congruent reaction:

$$Bt+Crd\pm And+Kfs+Qtz+H_2O = melt. \qquad [8.17]$$

(see Chapter 9 for the water activity variations within the aureole). The assemblage Bt+Crd±And+Kfs+Qtz persists beyond the first appearance of leucosomes ('melt-in' isograd) suggesting that none of the solid phases were used up by reaction [8.17]. The limiting phase is thus likely to have been aqueous fluid, a small amount of which would have been present in the (small) porosity. If reaction [8.17] consumed all available water, subsequent melting reactions must have been water-undersaturated.

Contact metamorphic garnet is associated with melt veins in rare quartz-bearing samples from the upper Spinel Zone and Sillimanite Zone (Chapter 5). These rocks lack Al-silicate. Instead of the Bt+And assemblage, these rocks contain Grt+Crd. Comparing the AFM projections (Fig 8.5 versus Fig. 8.4f) a crossed tie-line arrangement is apparent, indicating that a discontinuous reaction of the form Bt+And = Grt+Crd±other phases must have been responsible for the generation of garnet and disappearance of And in quartz-bearing rocks. As melt was clearly present, this reaction is likely to have been:

$$Bt+And+Qtz = Grt+Crd+Kfs+melt. \qquad [8.18]$$

According to Fig. 8.5 there is a movement of the Grt+Crd+Bt triangle to more Fe-rich compositions with increasing grade, suggesting the continuous reaction

$$Grt(\pm Kfs) = Crd+Bt(\pm Qtz\pm melt). \qquad [8.19]$$

8.4.3 Quartz-absent pelites

Many of the metamorphic reactions deduced for quartz-bearing pelites and semi-pelites consume quartz (e.g. [8.15] and [8.16]). This is because the phases K-feldspar and cordierite, which generally appear on the high-T sides of the reactions,

are themselves very Si-rich. Because of the operation of these reactions, quartz may be exhausted in pelitic rocks and quartz-absent assemblages may be developed as a result. The characteristic assemblages of the Corundum and Spinel zones have been generated in this way.

8.4.3.1 Corundum Zone (Zone V): The characteristic assemblage present in the quartz-absent pelitic rocks of the Corundum Zone is Crd+And+Kfs+Bt+Crn (Fig. 8. 6a). Prograde muscovite is absent in corundum-bearing assemblages but is likely to have been present in some rocks immediately prior to the formation of corundum. Although no rocks with the assemblage And+Crd+Bt+Ms+Kfs were actually found, the existence of such rocks is likely. In rocks with originally a small amount of modal quartz, muscovite would have been in excess in reaction [8.15], and all the quartz would have been used up. Thus muscovite would have been stable in the And+Kfs zone, but only in quartz-absent rocks. In such rocks, corundum can form by the univariant terminal muscovite-breakdown reaction:

$$Ms = Crn+Kfs+H_2O. \qquad [8.20]$$

As no other new minerals appear with corundum, this reaction is deduced to be responsible for the corundum isograd in the aureole.

Within the Corundum Zone, the most abundant quartz-absent assemblage is Crd+And+Kfs+Bt+Crn, which plots as an And-Crd-Bt triangle on the SFM projection from Crn, Kfs and H_2O (Fig. 8.6). A possible corundum-forming reaction involving these minerals is the KFMASH divariant reaction:

$$Bt+And = Crn+Crd+Kfs+H_2O. \qquad [8.21]$$

The textural association of Crn+Crd+Kfs in some of the samples suggests the progress of this reaction. However according to Figures 8.6.b to 8.6.d, the And-Crd-Bt triangle appears to slide slightly towards more Mg-rich compositions which would suggests the reverse of reaction [8.21]; this would be unlikely as it would imply prograde hydration. The reason for this anomaly is not known.

8.4.3.2 Spinel Zone (Zone VI): The Corundum Zone assemblage Crd+And+Bt+Crn+Kfs persists into the Spinel Zone. The new quartz-absent assemblages that characterise this zone are Crd+And+Spl+Bt+Crn+Kfs and Crd+And+Spl+Bt+Kfs. (see section 5.3.4). Although quartz occurs in the same thin sections as spinel in some Etive rocks, these two minerals have not been observed in contact, and the mineral assemblages of the spinel-bearing and quartz-bearing domains (layers) have been treated separately.

The development of Spl suggests the KFMASH univariant reaction:

$$Bt+And = Spl+Crn+Crd+Kfs+H_2O \qquad [8.22]$$

which is confirmed by the crossing of And+Bt and Spl+Crd tie lines in Figures 8.6.e to 8.6k.

If the compositions conform closely to the KFMASH system, the operation of this discontinuous reaction would be expected to result in the consumption of either And or Bt in the lower Spinel Zone. In fact, Al-silicate and biotite coexist in almost all quartz-absent pelites, and biotite only finally disappears in the uppermost Sillimanite Zone (Fig. 8.6.l). The persistence of the full reaction assemblage through the spinel and sillimanite zones (Figures 8.6e-k) indicates that something (presumably one or more non-KFMASH components) is causing reaction 8.22 to become continuous. Biotites from the inner Etive aureole contain relatively high Ti content, suggesting that Ti may be the additional component. There is petrological and experimental evidence (e. g. Stevens *et al.*, 1997) for the stability influence of Ti in biotite. Other possible components include F in biotite which is higher in the inner aureole rocks (Fig.7.14). There are several possible KFMASH continuous spinel-producing reactions amongst the minerals And, Bt, Crd, Spl, Crn and Kfs, including

$$Crn+Crd = Spl+And \qquad [8.23]$$

and

$$Bt+Crn\pm Crd = Spl+Kfs+H_2O. \qquad [8.24]$$

7.4.3.3 Sillimanite Zone (Zone VII): Within the Sillimanite Zone, sillimanite occurs as elongated, prismatic crystals and fibrolitic sillimanite is absent (section 5.3.2). The sillimanite-producing analogue of reaction [8.15]

$$Ms+Qtz = Sill+Kfs+H_2O \qquad [8.25]$$

cannot be considered as a potential sillimanite-forming reaction in the Etive aureole because all muscovite had already been consumed in other reactions well down-grade of the sillimanite-in isograd. Therefore the most likely reaction for sillimanite generation is the univariant reaction:

$$And = Sill. \qquad [8.26]$$

Textural evidence for reaction [8.26] exists in the form of prisms of prograde sillimanite overgrowing andalusite porphyroblasts (e.g. Plate. 5.12). Most sillimanite-bearing samples contain both polymorphs. Only one sample (MM193D) contains sillimanite as the only Al_2SiO_5 polymorph. Even at the highest grades, most of the Al_2SiO_5 is andalusite. This is probably due to the sluggish kinetics of the

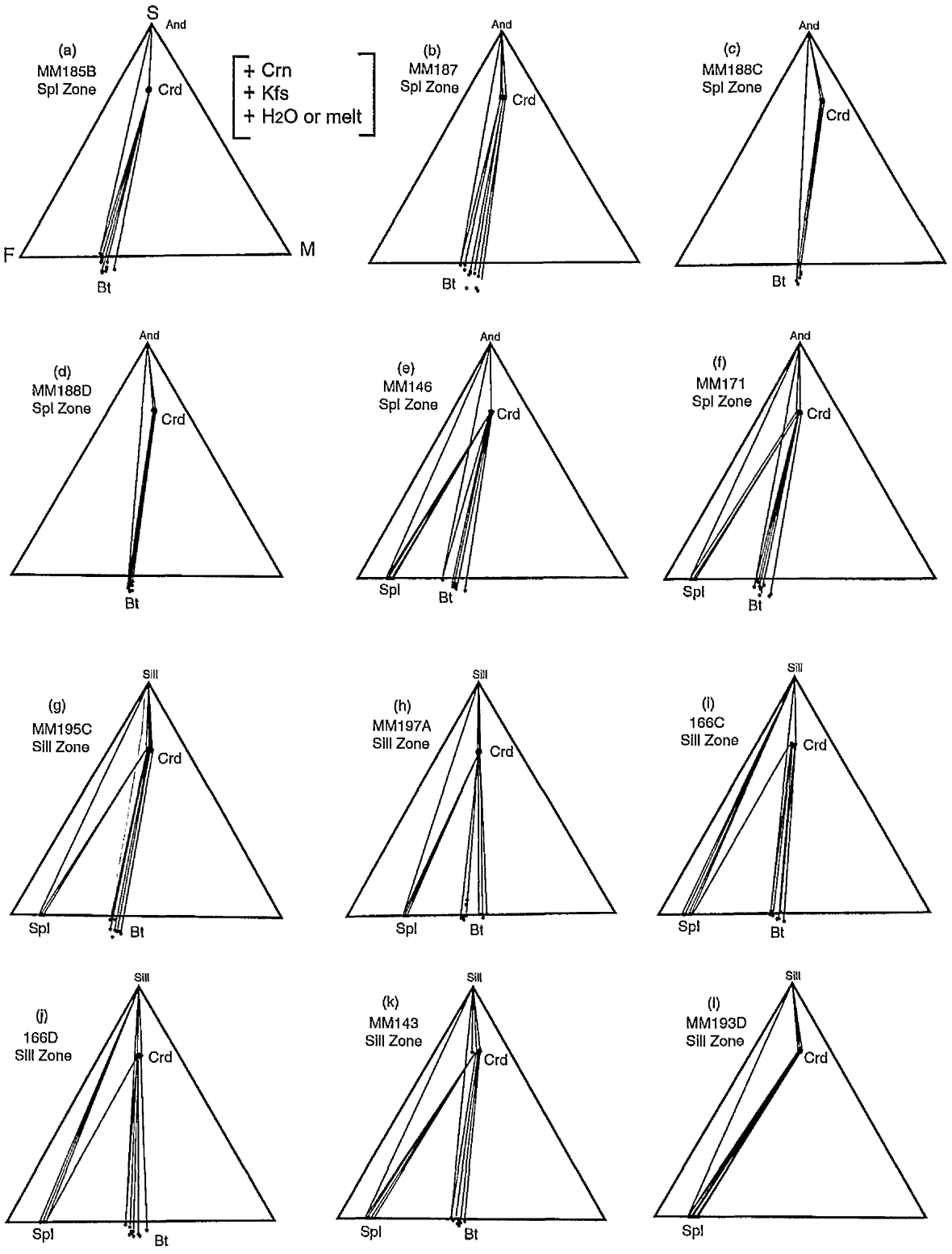

Fig. 8.6 Quartz-absent metapelitic parageneses plotted on SFM projection from corundum, K-feldspar and H_2O or melt. See text for explanation.

andalusite-sillimanite polymorphic reaction (Kerrick, 1990). In one sample (MM195C) acicular pseudomorphs of andalusite after sillimanite were found, which indicates the retrograde reaction :

Sill = And. [8.27]

The first appearance of sillimanite is due to reaction [8.27] and the coexistence of andalusite and sillimanite at higher grades is because of metastable persistence of andalusite within the sillimanite P-T stability field.

As mentioned above, there is no fibrolitic sillimanite in the studied samples. Vernon (1979) has argued that fluid presence is necessary for the production of fibrolite. The absence of fibrolite in the Etive Sillimanite Zone may be due to the absence of a discrete aqueous fluid during Sillimanite-Zone contact metamorphism. Since the main melting reaction deduced for quartz-bearing rocks in the upper Spinel Zone (reaction 8.18) is fluid-absent, it is likely that fluid-absent conditions also prevailed in the adjacent quartz-absent rocks. (Evidence for reduced H_2O activity in quartz-bearing and quartz-absent pelites is presented in Chapter 9).

The presence of quartzo-feldspathic leucosomes within otherwise quartz-absent Sillimanite Zone pelites suggest that a fluid-absent melting reaction such as

Sill+Bt = Spl±Crd+Crn±Kfs+melt [8.28]

has occurred. The localised occurrence of euhedral Crd grains within leucosomes at this grade is consistent with an incongruent melting reaction of this type.

Biotite is absent in the highest-grade pelitic rock in the Etive aureole (Fig. 8.6 l).

The Fe/Mg migration trend of pelitic mineral tie-triangles are not very clear for the quartz-absent rocks (Fig. 8.6). For high-grade rocks, this can be attributed to the water under-saturated state above the upper Spinel Zone. This would mean that the projection conditions are violated as a water-saturated condition is assumed for all rocks in the construction of the SFM diagrams.

The sequences of metamorphic reactions in quartz-bearing and quartz-absent assemblages are summarised in Table 8.1.

8.4.4 Pressure estimation using a petrogenetic grid

The petrogenetic grid of Pattison and Harte (1985, Fig. 8.7) was used to estimate the pressure of metamorphism in the Etive aureole. The observed sequence

Table 8.1 Summary of the metamorphic reactions in the quartz-bearing and quartz-absent rocks. Reactions in bold, assemblages in normal type. C denotes the continuous reactions and D denotes discontinuous reaction in the KFMASH system. Melting reactions in silica-poor pelites are uncertain. High-grade spinel-and biotite-bearing assemblages are not strictly within the KFMASH system owing to appreciable contents of Zn in spinel and Ti and F in biotite.

Silica-rich rocks (Quartz-bearing rocks at all grades)

Mineral Zone	Reactions and assemblages	
Cordierite Zone	Crd+Bt+Ms+Qtz	
	Crd+Ms = And+Bt+Qtz+H_2O	**C**
Andalusite Zone	Crd+And+Bt+Ms+Qtz	
	Ms+Qtz = And+Kfs+H_2O	**D**
Andalusite+K-feldspar Zone, Corundum Zone and Spinel Zone	Crd+And+Bt+Kfs+Qtz	
	Bt+And+Qtz = Crd+Kfs+H_2O	**C**
	Bt+And+Kfs±Crd+Qtz+H_2O = melt	**D**
	Bt+And+Qtz = Grt+Crd+Kfs+melt	**D**
	Grt+Crd+Bt+Kfs+Qtz+melt	
	[And = Sill] not seen	**D**
Sillimanite Zone	Grt+Crd+Bt+Kfs+Qtz+melt	

Silica-poor rocks (Quartz-absent rocks at high grade)

Mineral Zone	Reactions and assemblages	
Andalusite Zone	And+Crd+Bt+Ms+Qtz	
	Ms+Qtz = Kfs+And+H_2O	**D**
Andalusite+K-feldspar Zone	And+Crd+Bt+Ms+Kfs Not seen	
	Ms = Kfs+Crn+H_2O	**D**
Corundum Zone	And+Crd+Bt+Crn+Kfs	
	Bt+And = Crn+Crd+Kfs+H_2O	**C**
	And+Bt = Spl+Crd+Kfs+Crn+H_2O	**D**
Spinel Zone	And+Crd+Bt+Spl+Crn+Kfs	
	? Bt+And = Spl±Crd+Crn+Kfs+melt	**D**
	Crd+And+Spl+Crn+Bt+Kfs+melt	
	And = Sill	**D**
Sillimanite Zone	Sill+Kfs+Crd±Spl±Crn±Bt+melt	

of metamorphic reactions in the pelitic rocks can be reconciled with an isobaric sequence of reactions on the petrogenetic grid. The position of the reaction curves for the aluminosilicate polymorphs were calculated using THERMOCALC. Corundum first appears in the stability field of andalusite according to the mineralogical zonation in the Etive aureole. This means that the pressure of the metamorphism is lower than 2.5kbar, which is the intersection of Ms=Crn+Kfs+H_2O and And+Sill reactions curves and is marked with letter A on the grid. Also melt first appears in the andalusite stability field, indicating that the pressure of contact metamorphism is lower than 2.3kbar, which is the intersection of the Ab+Kfs+Qtz+H_2O = melt and And+Sill reaction curves and is marked with letter B on the grid. The most probable pressure for Etive aureole is about 2kbar, indicated with an arrow on the grid.

8.5 Contact metamorphism of pelitic and semipelitic rocks in the W aureole

All the information about metamorphic reactions discussed above comes from the southern segment of the aureole from the North Loch Awe area. The distribution of the metamorphic zones in the semi-pelitic and pelitic rocks from the Loch Creran area in the western segment of the aureole is shown in Fig. 5.5 and mineral assemblages are studied in section 5.4.2.

Most of the aureole is composed of psammitic rocks of the Creran Flags in the Loch Creran area. Therefore the density of the pelitic samples is low in this segment. Because of this problem, the exact location of isograds is not certain but the sequence of the mineral assemblages from the outer aureole towards the igneous contact is the same as in the southern segment in the Loch Awe area. The sequence of mineral assemblages are as follows:

Bt+Ms+Qtz

Bt+Ms+Qtz+Crd

Bt+Ms+Qtz+Crd+And and Bt+Ms+Qtz+Crd+Kfs

Bt+Crd+And+Kfs+Qtz

Bt+Crd+And+Kfs+Crn.

The only difference between the Loch Creran area and the Loch Awe area in terms of mineral assemblages is that the assemblages with spinel and sillimanite are absent in the Loch Creran area. This implies that the highest contact metamorphic temperature

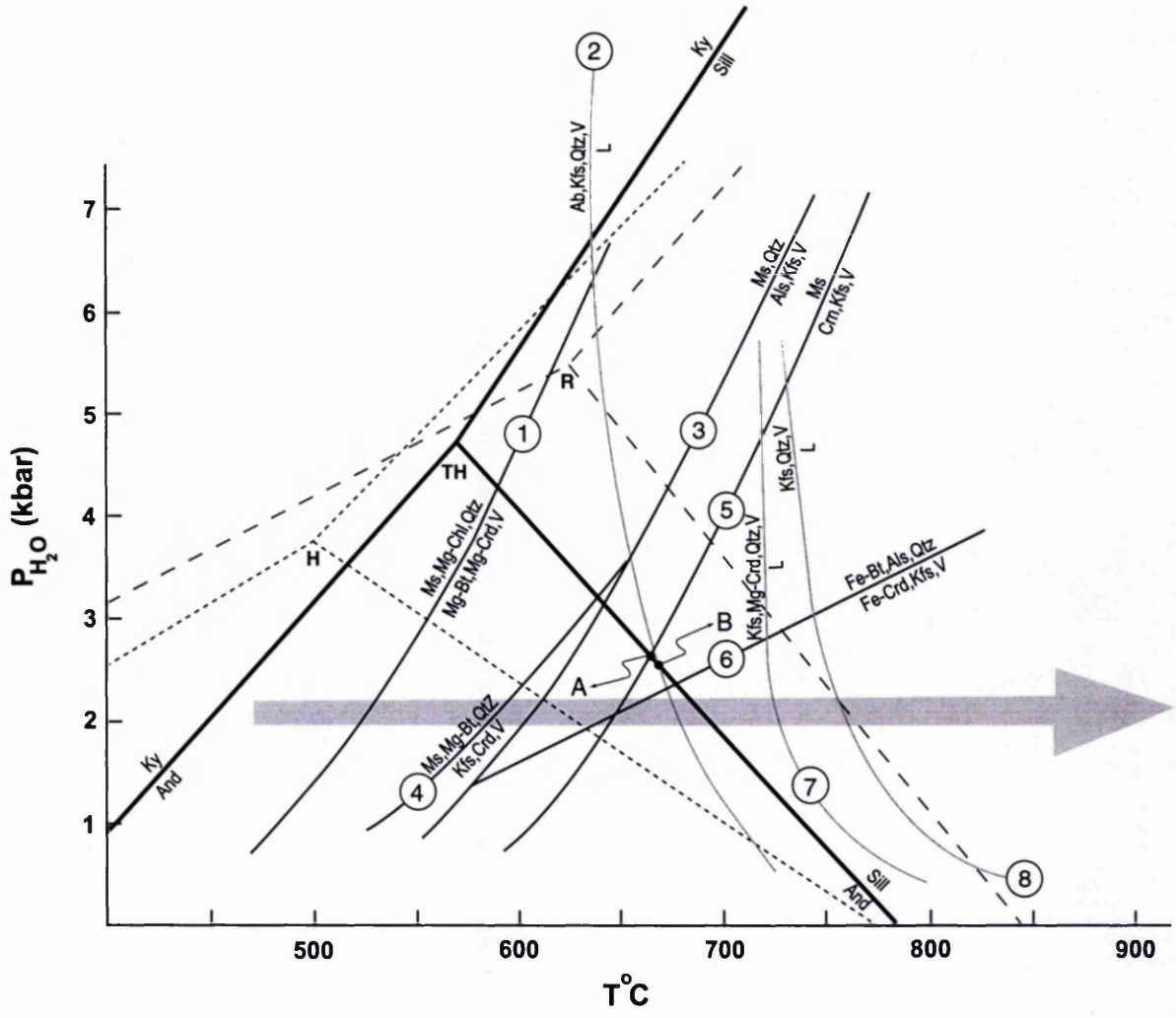

Fig. 8.7 Petrogenetic grid for low-pressure metapelites (after Pattison and Harte, 1985). Pressure of metamorphism in the Etive aureole is lower than the pressure of points A and B (see text). The large arrow shows the succession of metamorphic reactions in the Etive aureole, which corresponds to a pressure of about 2 kbar. H: Holdaway (1971); R: Richardson *et al.*, (1969); TH: THERMOCALC (version 4.2); (1): Seifert (1970); (2): Tuttle and Bowen (1958); (3): Chatterjee and Johannes (1974); (4): Seifert (1976); (5): Chatterjee and Johannes (1974); (6): Holdaway and Lee (1977); (7): Seifert (1976); (8): Shaw (1963).

at the Loch Creran area was lower than those of the Loch Awe area. Comparison of the igneous rocks in contact with the country rocks in these two areas (diorite in the Loch Awe area and granite in the Loch Creran area) shows that the assumption of the different temperatures seems to be valid.

The sequence of the mineral assemblages in the Loch Creran area implies the operation of reactions [8.13], [8.14], [8.15], [8.16], [8.20] and [8.21] from the outer

aureole towards the igneous contact. The similarity between the metamorphic reactions in the southern and western segments of the aureole shows that the metamorphism of the pelitic rocks follow the same isobaric facies series and the same P-T array in these two areas. As mentioned above, sillimanite is absent in the western segment of the aureole and corundum appears in the stability field of andalusite. This means that the pressure of metamorphism in the Loch Creran area was lower than the pressure for point A in Fig. 8.7 (lower than 2.5kbars). The similarity between the pressures of contact metamorphism in the southern and western segments shows that there was probably no significant tilting of the complex after its intrusion.

8.6 Constraints on fluid activity

Pelitic rocks in the Loch Awe area are graphite- and carbonate-free-rocks. Considering this mineralogical observation, water was probably the only significant component in the fluid during contact metamorphism. Most of the low- to medium-grade metamorphic reactions in the Loch Awe area release water (all reactions from [8.10] to [8.16] except [8.12]). Because of the dehydration nature of these reactions, the presence of aqueous fluid in the low- to medium-grade rocks during contact metamorphism, is very likely. The first melting reaction (e.g. [8.17]) was probably congruent and water-saturated and would thus have consumed water. The amount of free aqueous fluid contained within the hornfelses is likely to have been small because of their very low porosities, so that fluid would have been quickly used up. By using all of the aqueous fluid to form melt, the subsequent melting reactions (e.g. [8.18] and [8.19]) were probably water-undersaturated. Evidence from the water content of cordierite and calculations of the water activity in different metamorphic zones in Chapter 9 confirm these deductions.

8.7 Conclusions

As we saw in the metamorphic reactions of the pelitic rocks in this chapter, information from changing assemblages (i.e. discontinuous, cross tie-line relationships in the AFM and SFM projections) has been more useful than the continuous tie-line-sliding or three-phase-triangle-migration relationships for constraining metamorphic reactions in this study. Two reasons for this can be considered. First, there may be some extra component in the AFM (or SFM) phases

like Ti and F in biotite (see Fig. 7.14) which causes sliding of tie lines not to be systematic with increasing grade. Second, the projection requirements may not have been fulfilled in some of the projections. If the high-grade rocks were water-undersaturated the projection from H_2O is likely to give erroneous results.

Contact metamorphism of pelitic rocks is widely studied mainly because the mineral assemblages in these rocks vary systematically with pressure and temperature. Phase equlibria and thermobarometry of contact metapelites along with a brief description of well-studied pelitic aureoles are well summarised by Pattison and Tracy (1991). Using different facies series types, they have classified contact metamorphic pelites according to their pressure. They have considered four facies series and several sub-facies. The sequence of mineral assemblages in the Etive aureole corresponds to the 1b facies series of Pattison and Tracy (1991). The mineral assemblages in this facies series from the outer aureole towards the igneous contact are: Crd+Chl+(Ms,Bt,Qtz)→Crd+(Ms,Bt,Qtz)→Crd+(Kfs,Bt,Qtz)→Crd+And(Sill) +(Kfs,Bt,Qtz) and Crd±Grt+(Kfs,Bt,Qtz)→Opx±Grt±Crd+(Kfs,Bt,Qtz) (Pattison and Tracy, 1991).

Other well-studied examples of aureoles with this facies series are Ballachulish, Scotland (Pattison, 1989, Pattison and Harte, 1988), Lochnagar, Scotland (Chinner, 1962; Ashworth and Chinner, 1978), Lilesville, N. Carolina, U.S.A. (Evans and Speer, 1984), Liberty Hill, S. Carolina U.S.A. (Speer, 1981), Laramie, Wyoming, U.S.A. (Grant and Frost, 1990) and Hidaka, Japan (Shiba, 1988).

Ballachulish (about 8 km to the north of Etive) was intruded at a similar P (3 kbar; Pattison and Harte, 1985) as Etive. This implies that both Etive and Ballachulish were emplaced at a similar crustal levels. Considering this fact, the thickness of overburden over much of SW Dalradian at about 400 Ma was possibly uniform. Further constraints on thickness of overburden are provided in the next chapter.

9.1 Introduction

The main objectives of this chapter are to determine the peak-metamorphic P-T conditions of the contact-metamorphism and the surrounding regional metamorphism and to calculate the water activity during the contact-metamorphism. The results from barometry will be used to find out the depth at which the Etive complex was intruded into the Caledonian crust (at *ca.* 400Ma). The results from thermometry will be used to work out the peak contact-metamorphic temperature and to find out if this temperature is high enough for partial melting of the pelitic and semi-pelitic rocks (fluid-present or fluid-absent).

Independently calibrated geothermometers and THERMOCALC were employed for geothermobarometry.

9.2 Thermodynamic Basis for Thermobarometry

The thermodynamic basis for thermobarometry is well established (e.g. Wood and Fraser, 1977; Fraser, 1977; Essene, 1989). In a low-variance equilibrium assemblage containing several coexisting solid-solution minerals it is commonly possible to identify one or more reactions among the end-members present. If one such reaction is:

$$\underset{\text{phase p}}{aA} + \underset{\text{phase q}}{bB} = \underset{\text{phase r}}{cC} + \underset{\text{phase s}}{dD} \qquad [9.1]$$

where a, b, c, and d are the molecular coefficients of each end-member component A, B, C, and D, the equilibrium constant, K is defined as:

$$K = \left[\frac{(a_C^r)^c.(a_D^s)^d}{(a_A^p)^a.(a_B^q)^b}\right] \qquad [9.2]$$

where a_i^j is the activity (or effective thermodynamic concentration) of component i in phase j. For any given reaction, K is a function of pressure and temperature only. Therefore in principle it is possible to calculate an isopleth (a line on a P-T diagram corresponding to a particular value of K) for an equilibrium assemblage. If the necessary thermodynamic data are available for all the end-members of a given reaction, the P-T diagram may therefore be contoured with a set of isopleths. K can be calculated using the activities of end-members in the equilibrium assemblage and end-member activities can be estimated using the chemical analyses of coexisting minerals. Once K is found the P-T conditions of equilibrium are constrained to lie somewhere on the isopleth. Intersection of this isopleth with the isopleth of a second equilibrium in the same assemblage (same locality and same P-T) provides a fix for P and T of equilibrium. The error on such a P-T fix depends on (i) the errors on the intersecting isopleths (see section 9.7) and (ii) the "angle" at which the isopleths intersect. The error on the P-T fix will be small if the isopleths both have small errors and intersect at a large "angle".

The relation between K and $\Delta G^0_{(r)_{P,T}}$ which is the free energy change of the reaction at pressure and temperature of interest is:

$$\Delta G^0_{(r)_{P,T}} = -RT\ln K \qquad [9.3]$$

In this equation R is the gas constant and T is temperature in Kelvin.

At one bar pressure and the temperature of interest, the following equation may be used for calculating ΔG^0 :

$$\Delta G^0_{(r)_{1,T}} = \Delta H^0_{(r)_{1,298}} + \int_{298}^{T} \Delta C_p dT - T(\Delta S^0_{(r)_{1,298}} + \int_{298}^{T} \frac{\Delta C_P}{T} dT) \qquad [9.4]$$

where $\Delta H^0_{(r)_{1,298}}$, $\Delta S^0_{(r)1,298}$ and ΔC_p are the standard state enthalpy change, entropy change and heat capacity change of the reaction, respectively.

For an individual end-member, heat capacity can be expressed in polynomial form:

$$C_p = a + bT + cT^{-2} + dT^{-0.5} + eT^2 \qquad [9.5]$$

In this equation *a, b, c, d,* and *e* are coefficients that depend on the end-member in question.

Extrapolating $\Delta^0_{(r)1,T}$ from 1 bar to the pressure of interest yields:

$$\Delta G^0_{(r)\,P,T} = \Delta G^0_{(r)\,1,T} + (P-1)[\Delta V_s + \Delta(\alpha V)(T-298) - \Delta(\beta V)\frac{P}{2}] + n_i RT \ln f_i \qquad [9.6]$$

where ΔVs is the volume change for solid phases, f_i is the fugacity of any gas species present in the reaction, n_i is the molecular coefficient of the gas, α is the coefficient of isobaric volume expansion and β is the coefficient of isothermal volume compressibility. Combining equations 9.3 and 9.6 gives the equation:

$$0 = \Delta G^0_{(r)\,1,T}(P-1)(\Delta V_s + \Delta\alpha V)(T-298) - \Delta(\beta V)\frac{P}{2}) + n_i RTLnf_i + RT \ln K \qquad [9.7]$$

where $\Delta G^0_{(r)\,1,T}$ is given by equation 9.4. Provided that $\Delta H^0_{(r)\,1,298}$, $S^0_{1,298}$, $V^0_{1,298}$, α, β, *a, b, c, d* and *e* quantities are known for all end-member components in a reaction, and f_i is known as a function of pressure and temperature for the gas phases, then in principal equation 9.7 can be solved for temperature at any given value of pressure and vice versa.

9.3 Activity-mole fraction relations

At elevated P-T conditions the concentration of any end-member component A is not simply the chemical concentration but is the thermodynamic concentration or effective concentration which can be higher or lower than the chemical concentration. The effective concentration or *activity* of a component a_A, is defined in terms of the changes in the chemical potential of the component, μ_A at given P and T,

$$\mu_A = \mu^0_A + RT \ln a_A$$

where μ°_A is the chemical potential of pure A at the P and T of interest. Thus a_A adopts a maximum value of unity when A is pure; for a solid solution of A and other components, $0 < a_A < 1$. Suppose the end-member component A in equation [9.1] has the formula $Q_n[\ldots Si_jO_g]$ (where Q is an element that resides in each of n equivalent sites of type j per formula unit, and Si_jO_g signifies part of the formula in which no substitution occurs) and forms a solid solution mineral of formula $(Q,Z)_n\,[\ldots Si_jO_g]$. The activity of A is related to the mole fraction of Q atoms in the j site (X^j_Q). The following equation may be used for calculation of activity of component A:

$$a_A = (X_Q^j)^n \qquad [9.8]$$

This equation shows the simplest way of calculating the activities of end-members and assumes simple ionic mixing in site j, i.e., all available elements that can occupy the site (Q and Z in the present case) enter the mixing site j with equal ease. In other word this equation works when complete cation disorder or ideal mixing is the case. In real rock systems ideal mixing is rare because the elements occupying the same site generally have significantly different ionic radii and electronic configurations. Thermodynamically speaking, because H_{mix} (enthalpy of mixing) is never exactly equal to zero, natural rock systems with solid solution phases deviate from ideality. An activity coefficient (γ) is used to express the tendency of atom association ($\gamma<1$) or atom avoidance ($\gamma>1$) in non-ideal solid solutions. Regarding this tendency, the equation for activity on a given site is as follows:

$$a_A = (X_Q^j . \gamma_Q^j)^n \qquad [9.9]$$

where γ is the activity coefficient, and defines the probability of atomic association or avoidance. For a binary system in which A and B atoms are mixing on a site, γ_A is given by equation :

$$RT\ln\gamma_A = (1-X_A)^2 W_G \qquad [9.10]$$

where W_G is the "Margules interaction parameter" which represents the interaction energy of two types of ions on a crystallographic site. W_G defines the difference in the strength of an A-B bond in the solid solution compared to the average strength of A-A and B-B bonds. The above equation is applicable to symmetrical or regular solution mixing, which occurs when the strength of the A-B bond when X_A is close to zero is equal to the A-B bond strength when X_B is close to zero. When A-B bond strength is not constant with different X_A and X_B values, an asymmetrical mixing model with at least two interaction parameters is required. W is independent of composition but may vary with temperature and pressure.

9.4 Calculating activities for real phases

For pure phases used in thermobarometry (e.g. sillimanite, andalusite and quartz) which show essentially no mixing, activity is unity. Ideal mixing models are applied for biotite, muscovite, amphiboles, spinel and cordierite. A variety of solution models have been proposed for other phases of interest especially garnet and

feldspar. In this section some of the more popular models for each phase are considered. The activity expressions used in this study are located in Appendix 8.

9.4.1 Cordierite and Spinel Activities: Regarding the general formula for cordierite $(Fe,Mg)_2[Al_4Si_5O_{18}].nH_2O$, cation mixing is assumed to occur only between Fe^{2+} and Mg on a single octahedral site M. No Fe^{3+} is assigned for cordierite. The large channel site H (1 per formula unit) may accommodate molecular H_2O, CO_2 or may be vacant (Smith and Schreyer, 1962). For cordierites in which the H site occupancy has not been determined (and must therefore be calculated at each P and T at given a_{H2O} and a_{CO2}), the end-member activities are calculated as follows:

$$a^{Crd}_{Fe-Crd} = (X^{Crd}_{Fe^{2+}})^2 \qquad [9.11]$$

$$a^{Crd}_{Mg-Crd} = (X^{Crd}_{Mg})^2 \qquad [9.12]$$

Cordierite water content was determined in seven pelitic samples using the SIMS method (Chapter 7). There is no detectable CO_2 in cordierites in samples from the aureole. For these cordierites, the activities of anhydrous Mg-cordierite and Fe-cordierite were calculated using the following formulae:

$$a^{Crd}_{\substack{Mg-Crd \\ (anhydrous)}} = (X^{M}_{Mg})^2.(X^{H}_{o})^1 \qquad [9.13]$$

$$a^{Crd}_{\substack{Fe-Crd \\ (anhydrous)}} = (X^{M}_{Fe})^2.(X^{H}_{o})^1 \qquad [9.14]$$

where "*o*" denotes channel-site vacancy.

For spinel the Fe^{3+} component is calculated based on charge balance calculations. There appears to be no Fe^{3+} in the analysed spinels (Chapter 7) therefore the activities for end-members are calculated as follows:

$$a^{Spl}_{Spl} = (X^{Spl}_{Mg}) \qquad [9.15]$$

$$a^{Spl}_{herc} = (X^{Spl}_{Fe^{2+}}) \qquad [9.16]$$

9.4.2 Pyroxene activities: Ideal ionic mixing is assumed for pyroxenes in this study. Mixing occurs on three sites of pyroxene crystals, two octahedral sites, M1 and M2 and one T tetrahedral site. For Tschermak substitution a coupled substitution of

$Al^{M1}Al^{T}$ for $Mg^{M1}Si^{T}$ (Mg-Tsch) or $Al^{M1}Al^{T}$ for $Ca^{M1}Si^{T}$ (Ca-Tsch) occurs. This substitution shows that mixing on the M1 and T sites is not independent. Therefore by mixing on the M2 and M1 sites no extra entropy is introduced by Al-Si mixing on the T sites. For this reason no T-site terms appear in the *a*-X equations. Ca, Na and Mn are assumed to only occur in M2 site and Ti, Al^{vi} and Fe^{3+} in M1 site. Mixing between Fe^{2+} and Mg is assumed to occur equally on both sites (e.g. Perkins *et al.* 1985). The ideal, two-site model of Wood and Banno (1973) is used for calculating the activities.

The activities of three end-members, enstatite, ferrosilite and Mg-Tschermak component are:

$$a_{en}^{opx} = X_{Mg}^{M1}.X_{Mg}^{M2} \qquad [9.17]$$

$$a_{fs}^{opx} = X_{Fe^{2+}}^{M1}.X_{Fe^{2+}}^{M2} \qquad [9.18]$$

$$a_{Mg-tsch}^{opx} = X_{Al}^{M1}.X_{Al}^{M2} \quad . \qquad [9.19]$$

9.4.3 Biotite activities: Several models have been proposed to account for ideal mixing in biotites e.g. Indares and Martignole (1985), Holland and Powell (1990), Hoisch (1991) and Patiño Douce *et al.* (1993) but the data on the mixing characteristics of biotite is limited. In this study the models of Patiño Douce *et al.* (1993) which are based on experimental work from a natural metapelitic rock are used. These models take into account partial decoupling of Al^{vi} and Al^{iv} and excess octahedral mixing properties. Octahedral Ti and Al are attributed to the M2 sites, whilst the Fe/Mg ratios are assumed to be equal on both M1 and M2 sites. The ideal activity models are:

$$a_{phlogopite}^{Bt} = \frac{256}{27}(X_{Mg}^{M2})^2.(X_{Mg}^{M1}).(X_{Al}^{T}).(X_{Si}^{T})^3.(X_{K}^{A}).(X_{OH}^{H})^2 \qquad [9.20]$$

$$a_{eastonite}^{Bt} = 64(X_{Mg}^{M2}).(X_{Mg}^{M1}).(X_{Al}^{M1}).(X_{Al}^{T})^2.(X_{Si}^{T})^2.(X_{K}^{A}).(X_{OH}^{H})^2 \qquad [9.21]$$

Activities for annite and siderophyllite can be calculated by substituting Fe for Mg in these two models.

9.4.4 Feldspar activities: Feldspars display coupled substitution with Ca, Na and K substituting on an A site and Al with Si on a T site. Because there is only limited solid solution between Na and K (Deer *et al.*, 1992), mixing in feldspars is non-ideal.

Newton *et al.* (1980), using experimental data (Orville, 1972; Newton *et al.*, 1980) and statistical models (Kerrick and Darken, 1975) constructed an activity model for anorthite and albite. This model ignores the effect of small amount of potassium in plagioclase and Al-Si ordering on mixing. More recent models (Ghiorso, 1984; Green and Usdansky, 1986; Fuhrman and Lindsley, 1988) have taken account of the equilibrium between the albite, anorthite and orthoclase components in feldspars. Elkins and Grove (1990) using the experimental data from natural feldspars and thermodynamic formulations of Ghiorso (1984) and Fuhrman and Lindsley (1988) constrained the interaction parameters of the three feldspar components. In this study the model of Elkins and Grove (1990) is used. This model and that of Fuhrman and Lindsley (1988) yield similar results for a_{an}^{pl} and compare well with the calculated pressures and temperatures of the aluminosilicate stability field (Applegate and Hodges, 1994). The interaction parameters from the Elkins and Grove (1990) model are:

$W_{NaK} = 18810$ J/mol $W_{KCa} = 40317$ J/mol

$W_{KNa} = 27320$ J/mol $W_{CaK} = 38947$ J/mol

$W_{NaCa} = 7925$ J/mol $W_{NaKCa} = 125452$ J/mol

$W_{CaNa} = 0$ J/mol.

The equation used to calculate anorthite activities in this study is presented in Appendix 8.

9.4.5 Garnet activities: Non-ideal mixing among Fe, Mg, Ca and Mn in garnet is well established. This non-ideality is due to the differences in ionic radii of Ca^{2+}, Mg^{2+}, Fe^{2+} and Mn^{2+} and hence to the difference in strength of the Ca-Mg-Fe-Mn bonds in garnet. Several regular solution models have been developed for garnets mainly for Ca, Mg, Fe components. These models neglect the effect of Mn in garnet (e.g. Haselton and Newton, 1980). Quaternary mixing models for garnet have been proposed by Hodges and Spear (1982), Ganguly and Saxena (1984) and Berman (1990). The Berman model which is developed by mathematical programming of reversed phase-equilibria and the internally consistent standard state thermodynamic dataset of Berman (1988) is used in this study. Berman's model produces more consistently reasonable results than the models of Hodges and Spear (1982) and Ganguly and Saxena (1984) when compared to the aluminosilicate stability field

(Applegate and Hodges, 1994). The interaction parameters used in the Berman model have been derived for the quaternary system by examining mixing in binary systems. They are:

$W^{Grt}_{Ca-Ca-Mg} = 21560$ J/mol $\quad W^{Grt}_{Mg-Fe-Fe} = 3720$ J/mol

$W^{Grt}_{Ca-Mg-Mg} = 69200$ J/mol $\quad W^{Grt}_{Ca-Mg-Fe} = 58825$ J/mol

$W^{Grt}_{Ca-Ca-Fe} = 20320$ J/mol $\quad W^{Grt}_{Ca-Mg-Mn} = 45424$ J/mol

$W^{Grt}_{Ca-Fe-Fe} = 2620$ J/mol $\quad W^{Grt}_{Ca-Fe-Mn} = 11470$ J/mol

$W^{Grt}_{Mg-Mg-Fe} = 230$ J/mol $\quad W^{Grt}_{Mg-Fe-Mn} = 1975$ J/mol.

Garnet activity equations are as follows:

$$a^{Grt}_{gr} = (X^{VIII}_{Ca} \cdot \gamma^{VIII}_{Ca})^3 . (X^{VI}_{Al})^2$$

$$a^{Grt}_{py} = (X^{VIII}_{Mg} \cdot \gamma^{VIII}_{Mg})^3 . (X^{VI}_{Al})^2$$

$$a^{Grt}_{alm} = (X^{VIII}_{Fe} \cdot \gamma^{VIII}_{Fe})^3 . (X^{VI}_{Al})^2$$

The equations for calculating the activity coefficients (γ) are presented in Appendix 8.

9.5 Criteria for selecting rocks for P-T calculations

The most important considerations for the selection of a rock for P-T calculation purposes are (i) that the rock possesses enough minerals to enable one to write one or more balanced reactions among end-member components for which thermodynamic data are available, and (ii) the phases of interest were all in chemical equilibrium.

9.5.1 Rock Equilibrium: When a rock is subjected to a given pressure and temperature, chemical reactions and diffusion start among the phases in the rock until the mineral assemblage of the rock reaches its lowest free energy. After completion of reaction, if P-T conditions remain stable no chemical reaction or diffusion can take place between, or within the phases. In this state the rock is at chemical equilibrium. This state can sometimes be preserved in assemblages formed as a result of metamorphism. Although this does not necessarily represent peak metamorphic conditions, it is a record of the conditions when the chemical system closed. Continuous reaction equilibria are likely to close at different temperatures, so

some sub-systems within a rock may equilibrate at different P-T-time from others (e.g. Fraser and Lawless, 1978; Ellis and Green, 1985; Avchenko, 1986; Spear and Florence, 1992). In principle it is possible to test if chemical equilibrium has been achieved among phases or not. The criteria for equilibrium are:

(a) The variance (or number of degree of freedom), as given by the Gibbs' Phase Rule, must be greater than or equal to zero.

(b) All phases must be chemically homogeneous, i.e. without zoning.

(c) All phases should exist in mutual contact.

In practice (a) and (b) can be checked by microprobe analyses and (c) can be checked by microscope. Textural equilibrium in rock is commonly taken as an indication of a close approach to chemical equilibrium. Criteria for textural equilibrium are (Carswell, 1990):

(a) The interfacial angle between phases in contact for a given P-T and the mean radius of curvature along a grain boundary are constant.

(b) There are no reactions between phases e.g. symplectites, reaction rims etc.

(c) There is no strain stored within the grains, i.e., no undulose extinction, dislocations, etc.

These textural criteria are considered as much as possible for selecting the Etive metamorphic rocks.

9.5.2 Practical approach to collecting analyses for thermobarometry: Mineral analyses of all assemblages used for thermobarometry have been collected using ED microprobe (the approach is described in Appendix 3) and meet the stoichiometric acceptance conditions for each mineral (Appendix 3). To ensure the analyses are representative of the peak-recorded metamorphic condition, the analysis points have been selected using the following criteria:

(a) The chemical analyses are in a small area where all the phases of interest (including unanalysed phases such as andalusite) coexist in textural equilibrium.

(b) Analyses of phases involved in the same reactions where possible were not in contact to avoid resetting during cooling (this criterion especially was used for biotite analyses used in garnet-biotite and Opx-biotite thermometers as biotite easily re-equilibrates during cooling).

(c) The areas of analysis of individual grains display homogeneity.

9.6 THERMOCALC

There are few computer packages for calculating pressure and temperature in metamorphic rocks. The two main available packages are "GEOCALC" developed by Berman and Brown (1988) and Berman (1988), and "THERMOCALC" developed by Holland and Powell (1985), Powell and Holland (1988), Holland and Powell (1990) and Holland and Powell (1998). These two programs work on similar principles and produce comparable results (Holland and Powell, 1990). These programs use internally consistent thermodynamic datasets for calculation of pressure and temperature. The main differences between the two relate to the methods by which the datasets were derived. Berman and Brown (1988) used a linear programming method to optimise their data, while Holland and Powell (1985) used a least-squares method. The 1990 version of THERMOCALC (Holland and Powell, 1990) has a larger data base providing data for 123 end-members whereas the 1988 version of GEOCALC (Berman, 1988) provides thermodynamic data for 70 end-members. Version 2.4 of THERMOCALC (1995 update) was used in this study.

For creating the program, Holland and Powell (1985) took the best published values for the following molar thermodynamic variables: entropy, volume, compressibility, expansivity and heat capacity coefficients. Existing fugacity data for H_2O and CO_2 were fitted to complete polynomial equations. Standard state enthalpies of formation from the elements for all the end-members were optimised simultaneously using a least-squares approach. The data in this program are fully self-consistent, i.e. they have been optimised *simultaneously* with respect to a large dataset of experimental reversals on various equilibria, rather than *sequentially* (e.g. dataset of Helgeson *et al.,* 1978). THERMOCALC works by selecting a pressure value, and then varying values of temperature until the right hand side of equation 9.7 equals zero.

9.7 Error estimation in thermobarometry

There is no possible method for measurement of pressure and temperature in metamorphic rocks directly, therefore the calculation of many of the errors involved in thermobarometry is problematic. The errors are either random or systematic. The errors arise from both mineral analyses and thermodynamic data. The errors in the collection of the chemical analyses from which end-member activities and

equilibrium constants are calculated are random errors. These errors are from the electron microprobe measurements (machine errors) and from within-sample chemical variation, which can result from mineral zoning or alteration. Random errors can lead to large uncertainties in pressure and/or temperature estimation. This error is more likely to happen in measurement of end-members with low mole fractions. The random error from chemical variation can be reduced by analysing the cores of minerals and avoiding altered and retrograded phases and increasing the number of analyses statistically.

The systematic errors come from errors in data used in the dataset and calibrated thermobarometers. These errors are constant in the application of each individual activity model, or calibrated geothermometer or geobarometer. Only continuing experimental work on mineral end-members and correction of thermodynamic variables for them can reduce these errors.

The program THERMOCALC generates realistic errors for pressure and temperature estimates. The program allows the propagation of errors from uncertainties on the enthalpies of end-members together with errors from activity composition data through thermobarometric calculations, to give overall errors on pressure and temperature quoted as 1σ. The user can input errors generated from chemical variations in the form of standard deviation of mean calculated activities.

9.8 Geothermometry

Calibrated geothermometers are applied for pelitic, metabasic and calc-silicate rocks of the Etive area (some thermometers are applied to igneous rocks as well, Chapter 3). The cordierite-spinel, garnet-biotite, garnet-cordierite, and orthopyroxene-biotite thermometers are applied to the pelitic rocks, orthopyroxene-biotite, and orthopyroxene-clinopyroxene thermometers are applied for metabasic rocks and calcite-dolomite thermometer is applied to calc-silicate rocks and marbles. The results of these thermometers are described below for regional and contact metamorphic rocks.

9.8.1 Spinel-cordierite thermometry: The partitioning of Fe^{2+} and Mg between coexisting spinel and cordierite is temperature-dependent and relatively insensitive to pressure (Vielzeuf, 1983; Nichols *et al.*, 1992). The exchange reaction between spinel and cordierite is written as :

$$2MgAl_2O_4 + Fe_2[Al_4Si_5O_{18}] = 2FeAl_2O_4 + Mg_2[Al_4Si_5O_{18}] \quad [9.22]$$

spinel cordierite spinel cordierite

The distribution coefficient for this reaction is $K_D=(Mg/Fe)^{crd}/(Mg/Fe)^{spl}$. There are two calibrations for this reaction, Vielzeuf (1983) and Nichols *et al.* (1992). Vielzeuf (1983) used the natural assemblage of spinel+quartz+sillimanite+garnet from xenoliths in basaltic rocks for his calibration which is :

$$T^oK=-1.763/LnK_D+0.378. \quad [9.23]$$

Nichols *et al.* (1992) used synthetic and natural minerals for their calibration, which is:

$$T=\frac{29774+170P-2(RTLn\gamma_{herc}-RTLn\gamma_{spl})}{3.13+RLn\frac{(X_{herc}^{spl})^2.a_{Mg-crd}^{crd}}{(X_{spl}^{spl})^2.a_{Fe-crd}^{crd}}} \quad [9.24]$$

where T is in K, P in kbar. $RTLn\gamma_{herc}$ and $RTLn\gamma_{spl}$ can be calculated from appropriate equations given by Nichols *et al.* (1992, equation 18). The Vielzeuf (1983), Nichols *et al.* (1992) calibrations and THERMOCALC were used for spinel-cordierite thermometry of contact metamorphic pelitic rocks of the Etive aureole. In each sample with coexisting spinel and cordierite, ten or more analyses were taken from each of cordierite and spinel. The end-member activities were calculated assuming ideal mixing for these phases. The results of this thermometer are provided in Table 9.1. According to this table, the results from the Vielzeuf (1983) thermometer are higher than the results from the Nichols *et al.* (1992) calibration and the results from THERMOCALC are higher than the results from Nichols *et al.* (1992). Vielzeuf's calibration does not consider the small volume changes of reaction then there is no P-dependent term in the equation. Also this calibration is entirely based on natural minerals. The calibration of Nichols *et al.* (1992) takes the pressure effect on Fe-Mg distribution between spinel and cordierite into account. Also this calibration takes into account the Margules interaction parameters for Mg-Fe-Zn in spinel. Regarding these features, the Nichols *et al.* (1992) calibration is preferred for temperature estimation for coexisting Spl-Crd-bearing pelitic rocks. From the analysed samples for Crd-Spl thermometry, samples MM146, MM133B,

Table 9.1 Results from spinel-cordierite thermometry.

Sample	G.R.	NEA2	NEA3	Vielzeuf	THERM2	THERM3
MM146	NN11732834	674±50	679±50	880±50	709±290	722±290
MM133B	NN11442787	678	683	903	761±305	774±305
MM169B	NN12322875	645	650	829	653±263	665±263
MM197A	NN12412900	660	664	859	647±256	659±256
MM197B	NN12412900	606	610	766	514±193	524±193
MM166C	NN12482896	682	686	888	-	-
MM189A	NN11982835	727	732	986	779±322	792±322
MM195C	NN12282874	619	623	788	628±246	639±246
MM166D	NN12482896	704	709	933	838±359	851±359
MM171	NN12412878	598	602	747	540±212	550±212
MM193D	NN11932864	552	556	690	574±214	585±214

All temperatures are in °C. NEA2 and NEA3 = Nichols et al. (1992). Calibration at 2 and 3 kbars respectively. THERM2 and THERM3 = results from THERMOCALC at 2 and 3 kbars respectively. The first three samples are from the Spinel Zone and rest of the samples are from the Sillimanite Zone (see Fig. 5.3).

MM189A and MM171 are from the spinel zone and the rest of the samples are from the sillimanite zone (Table 9.1). Temperatures from Nichols *et al.* (1992) thermometry at 2 kbars pressure are 598-727°C for the spinel zone and 606-704 °C for the sillimanite zone. The results from THERMOCALC at 2 kbars pressure are 540-779 °C for the spinel zone and 514-838°C for the sillimanite zone. Sample MM193D is very close to the igneous contact and aluminosilicate in this sample is sillimanite only. Temperatures for this sample are 552 and 574°C at 2 kbars pressure from the Nichols *et al.* (1992) calibration and THERMOCALC respectively. These temperatures are the lowest in Table 9.1, which can be attributed to the retrograde re-setting of spinel-cordierite couple due to fluidal effects of the adjacent pluton. In comparison with temperatures obtained from metabasites using Opx-Cpx thermometry (see section 9.8.5), all temperatures from Crd-Spl thermometry in the inner aureole rocks are low, which is probably due to later re-setting of this couple. This implies that the Spl-Crd couple re-sets more easily than Opx-Cpx couple.

9.8.2 Garnet-biotite thermometry: Fe and Mg partitioning between coexisting garnet and biotite is strongly temperature dependent, and relatively independent of pressure. The exchange reaction between garnet and biotite can be written as:

$$\underset{\text{garnet}}{Fe_3Al_2Si_3O_{12}} + \underset{\text{biotite}}{KMg_3AlSi_3O_{10}(OH)_2} = \underset{\text{garnet}}{Mg_3Al_2Si_3O_{12}} + \underset{\text{biotite}}{KFe_3AlSi_3O_{10}(OH)_2} \quad [9.25]$$

The distribution coefficient for this reaction is written as: $K_D=(Mg/Fe)^{Grt}/(Mg/Fe)^{Bt}$. The calibrations for this reaction are more numerous than calibrations for any other thermometer. The earliest empirical calibrations are Frost (1962), Saxena (1969), Thompson (1976), Goldman and Albee (1977) and Holdaway and Lee (1977). The calibrations of Thompson (1976) and Holdaway and Lee (1977) which are based on temperature estimates from natural assemblages, are widely used by different authors. The first calibration based on experimental work was proposed by Ferry and Spear (1978). This calibration does not consider minor elements in garnet and biotite. When applied to garnets and biotites with considerable amounts of minor elements (Ca and Mn in garnet and Ti in biotite) there is a significant departure from the relationships of the calibration (Indares and Martignole, 1985). The effect of Ca and Mn in garnet and Ti in biotite has been studied by Indares and Martignole (1985), Hodges and Spear (1982), Pigage and Greenwood (1982), Ganguly and Saxena (1984) and Bhattacharya *et al.* (1992). Most of these studies rely on the experimental data of Ferry and Spear (1978). The Ti content in biotite from upper amphibolite and granulite facies rocks causes higher temperature estimations using calibrations of Thompson (1976), Goldman and Albee (1977) and Ferry and Spear (1978). Apart from the effect of minor elements in garnet and biotite, there is an additional problem in garnet-biotite thermometry in high grade rocks, which is re-equilibrium of Fe and Mg after peak metamorphic conditions, leading to under-estimate in temperatures. This re-equilibration has a much greater effect on biotite crystals than garnet crystals because the open crystal structure of biotite is more suitable for re-equilibrium than the close-packed structure of garnet (e.g. Loomis, 1975; Tracy *et al.*, 1976). By analysing biotite crystals far from garnets and by using samples with modally abundant biotite relative to garnet, this problem can be limited.

In each sample of the Etive aureole and regionally metamorphosed rocks, ten or more analyses were taken from garnet cores and biotites. Biotite inclusions in garnet and biotites in contact or close to garnets (less than 500 μm) were avoided. Eight different calibrations plus THERMOCALC were used for garnet-biotite thermometry. The results are given in Table 9.2.

This table shows that the temperature estimates from THERMOCALC, Ferry and Spear (1978), Pigage and Greenwood (1982) and Hodges and Spear (1982) are higher than other estimates and temperatures from the calibration of Indares and

Martignole (1985) are systematically lower than the results from the other calibrations. There is a divergence in the temperatures from Grt-Bt thermometry in Table 9.2. Temperatures are high from calibrations, which do not take into account the effect of minor components. Indares and Martignole (1985) showed that these high temperature

Table 9.2 Results from the Grt-Bt thermometer. Uncertainties for all thermometers is ±50.

Calibration	T	H&L	F&S	P&G	P&L	H&S	I&M	BEA	THERM
MM166A	Sill Zone								
1kbar	773	743	853	908	763	853	617	695(HW) 664(GS)	992
2kbars	782	747	858	913	756	859	622	696(HW) 666(GS)	1002
3kbars	791	752	863	918	748	864	628	697(HW) 668(GS)	1012
MM134A	Spl Zone								
1kbar	760	732	834	990	755	835	606	675(HW) 624(GS)	531
2kbars	769	737	839	995	748	840	611	676(HW) 626(GS)	536
3kbars	778	741	844	1000	740	845	616	677(HW) 628(GS)	542
MM255D	Regional metamorphic rock								
5kbar	550	540	521	636	559	536	423	-	-
6kbar	557	543	524	640	553	539	427	-	-
7kbar	564	547	528	643	547	543	430	-	-

T=Thompson (1976), H&L= Holdaway and Lee (1977), F&S= Ferry and Spear (1978), P&G= Pigage and Greenwood (1982), P&L= Perchuk and Lavrent'eva (1983) , H&S= Hodge and Spear (1982), I&M= Indares and Martignole (1985), BEA= Bhattacharya *et al.*(1992), THERM= THERMOCALC 4.2.
HW= mixing parameters for pyrope-almandine asymmetric solution after Hackler and Wood (1984).
GS= mixing parameters for pyrope-almandine asymmetric solution after Ganguly and Saxena (1984).

estimates were an artefact of the high Ti content in biotite from the high-grade rocks. This is best highlighted by the estimates given by THERMOCALC, which gives temperature in excess of 950 (up to 1012°C at 3 kbars), which are well in excess of the maximum temperature at which even Ti-saturated biotite can remain stable and therefore cannot represent the true temperature at which the biotite crystallised. Temperatures given by the calibration of Indares and Martignole (1985) are systematically lower than those given by all other calibrations. The lower temperatures are due to the introduction of interaction parameters for Ti and Al^{vi} in biotite and Mn and Ca in garnet, into the original calibration of Ferry and Spear (1978). These temperatures are lower than temperatures from Crd-Spl thermometer for the inner aureole rocks, suggesting that calibration of Indares and Martignole

(1985) possibly over-corrects the effect of the minor components. The calibrations of Bhattacharya *et al.* (1992), which include improved garnet Ca-Mn mixing data, give temperatures intermediate to those of Indares and Martignole (1985) and Ferry and Spear (1978). The temperatures given by the Bhattacharya *et al.* (1992) calibration, which uses the mixing parameters for pyrope-almandine asymmetric regular solution after Hackler and Wood (1984) are in good agreement with temperatures given by Crd-Spl thermometer for the inner aureole rocks. Therefore the calibration of the Bhattacharya *et al.* (1992) are taken to best estimate the temperatures of Grt-Bt-bearing pelites. The temperature given by this calibration for sample MM166A from the sillimanite zone is 696°C at 2 kbars and 676°C at 2 kbars for sample MM134A from the spinel zone. The temperature for sample MM255D from the regional metamorphic pelites is between 521°C to 559°C at 5 kbar pressure using calibrations of T, H&L, F&S, P&L, H&S (Table 9.2, see table for abbreviation).

9.8.3 Garnet-cordierite thermometry: The Fe-Mg exchange reaction between cordierite and garnet is:

$$2FeAl_2Si_3O_{12} + 3Mg_2Al_4Si_5O_{18} = 2Mg_3Al_2Si_3O_{12} + 3Fe_2Al_4Si_5O_8 \qquad [9.26]$$

garnet cordierite garnet cordierite

Thompson (1976) and Holdaway & Lee's (1977) calibrations for this reaction are based on empirical methods and natural samples. In these calibrations, ideal mixing for both garnet and cordierite are assumed. The calibration model of Bhattacharya *et al.* (1988) incorporates non-ideal mixing models for both garnet and cordierite, derived from the garnet mixing data of Ganguly and Saxena (1984) and data from natural coexisting cordierites. The calibration of Nichols *et al.* (1992) assumes ideal mixing for cordierite and non-ideal mixing for garnet. This calibration is based on combination of data for garnet and cordierite from earlier garnet-cordierite data and data from experiments in the spinel-cordierite-garnet-sillimanite assemblage. Two contact metamorphic samples from the Etive aureole contain coexisting garnet and cordierite. Sample MM166A is from the sillimanite zone and sample MM134A is from the spinel zone. In these samples more than ten analyses were taken from core of garnet (garnets are unzoned, Chapter 5) and clean unaltered cordierites far from

garnet crystals. For the calibration of Nichols *et al.* (1992), activities were calculated from the garnet data using the models of Berman (1990). The results of temperature estimation from this thermometer using calibrations of Thompson (1976), Holdaway and Lee (1977), Bhattacharya *et al.* (1988), Nichols *et al.* (1992) and THERMOCALC are given in Table 9.3.

Table 9.3 Results from the Grt-Crd thermometer.

Calibration	T	HL	BEA	NEA	THERM
MM166A	Sill Zone				
2kbars	808±75	766±75	747±65	777±50	965±221
3kbars	820±75	771±75	753±65	783±50	978±221
MM134A	Spl Zone				
2kbars	799±75	759±75	816±65	757±50	926±202
3kbars	805±75	764±75	821±65	762±50	939±202

T= Thompson (1976), HL= Holdaway and Lee (1977), BEA= Bhattacharya et al. (1988), NEA= Nichols et al. (1992), THERM= THERMOCALC 4.2.

The temperatures given by THERMOCALC are consistently higher than those given by all other garnet-cordierite calibrations. For the purpose of comparison of temperatures in various rocks and different thermometers, the calibration of Nichols *et al.* (1992) is used as it was formulated using updated experimental data and non-ideality in garnet is taken into account.

9.8.4 Biotite-orthopyroxene thermometry: The Fe-Mg exchange reaction between orthopyroxene and biotite can be written as:

$$3Fe_2Si_2O_6 + 2KMg_3AlSi_3O_{10}(OH)_2 = 3Mg_2Si_2O_6 + 2KFe_3AlSi_3O_{10}(OH)_2 \quad [9.27]$$

Opx biotite Opx biotite

This reaction has been calibrated by Sengupta *et al.* (1990). This thermometer was applied to coexisting biotite and orthopyroxene in two thermally metamorphosed metasedimentary rocks (compositionally equivalent to greywacke) and five metabasic rocks. Results are summarised in Table 9.4.

There is a large divergence in the temperatures given by Bt-Opx thermometry for all of the inner aureole rocks. The fine-grained part of sample MM198C has the highest

temperature among the meta-sedimentary rocks and the coarse-grained part has the lowest temperature. It is believed that the coarse-grained part is a product of partial melting of the coarse-grained part (see chapter 6). Possibly biotite and orthopyroxene are not in equilibrium in the fine-grained part. Temperatures for sample MM8B are low indicating a possible disequilibrium (re-setting) in this rock.

The highest temperature from the metabasites is 944°C in sample MM198B at 2 kbars, which is close to the temperature obtained from the Opx-Cpx thermometer (see next section).

Table 9.4 Results from Opx-Bt thermometry. Uncertainty is ±50°C.

Sample	*MM198C(f)*	*MM198(c)*	*MM8B*	MM196A	MM166B	MM165	MM198B	MM141B
1kb	867	367	587	575	882	857	938	912
2kb	873	371	592	579	887	862	944	917
3kb	881	375	597	584	892	867	949	922

Samples in italic font are meta-sedimentary rocks and sample in roman font are metabasites.
Temperatures are in °C. All meta-sedimentary rocks are from Sill Zone and all Metabasites are from Opx Zone.

9.8.5 Orthopyroxene-clinopyroxene thermometry: The amount of Ca in coexisting orthopyroxene and clinopyroxene is a function of temperature. The Ca content of clinopyroxene (augite) decreases with increasing temperature, while Ca in orthopyroxene (or pigeonite) increases (Lindsley, 1983). Opx-Cpx thermometry projects the compositions of coexisting pyroxenes to the Di-En (Fe-free) join and employs either a phase diagram or solution model for that join to yield temperatures. The earliest attempts to use this approach are Davis and Boyd (1966), Boyd (1969) and Boyd (1973). Following Boyd, almost all Opx-Cpx thermometers have neglected the effect of pressure. Later calibrations of this thermometers were made by Wood and Banno (1973) and Wells (1977), based on ideal mixing in clinopyroxene. Because of ideal mixing assumption for Cpx and large reaction enthalpy for Oen=Cen reaction, these calibrations are seriously in error (Holland *et al*, 1979; Lindsley et al., 1981; Davidson *et al.*, 1982). Saxena and Nehru (1975) proposed that both the clinopyroxene and orthopyroxene series must be treated as non-ideal solutions. Other Opx-Cpx thermometers that involve projection onto the Di-En join are Saxena (1976), Mercier (1976), Kretz (1982) and Lindsley (1983). The thermometer of Ishii (1975) is based on the natural occurrence of pyroxene in erupted

lavas and the Ross and Heubner (1975) graphical thermometer is based on unreversed experimental data at high temperatures. In this study thermometers of Kretz (1982) and Lindsley (1983) are applied to the two-pyroxene-bearing metabasic rocks of the Etive aureole. Kretz (1982) derived the following equation for temperature-dependence of the Mg-Fe distribution coefficient using a calibration of natural data and experimental data:

$$T = 1130/(\ln K_D - 0.505) \qquad [9.28]$$

where T is temperature in K and $K_D = [X^{opx}/(1-X^{opx})]/[X^{cpx}(1-X^{cpx})]$. The results from this thermometer are given in Table 9.5.

Table 9.5 Results from the orthopyroxene-clinopyroxene thermometer. All samples are from the Opx Zone.

Sample	MM196A	MM166B	MM165	MM141B	MM198B
Temperature	731±60°C	708±60°C	710±60°C	1197±60°C	760±60°C

The composition of pyroxenes from metabasic rocks of the Etive aureole are projected in the quadrilateral diagram of Lindsley (1983) (Fig.9.1). Corrections for non-quadrilateral components in the pyroxenes (Ac, Jd, FeCaTs, CrCaTs, AlCaTs in clinopyroxene and $NaR^{3+}Si_2O_6$, $NaTiAlSiO_6$, $R^{2+}TiAl_2O_6$ and $R^{2+}R^{3+}AlSiO_6$ in orthopyroxene) were carried out according to the procedure explained by Lindsley (1983), using the computer program QUILF (Anderson *et al.*, 1993). Lindsley and Anderson (1983) estimated a 30°C uncertainty in the placement of the isotherms in the quadrilateral diagram (Fig. 9.1). They have considered 20 to 30°C additional uncertainty due to errors from non-quadrilateral components. Therefore the thermometer probably is accurate to ± 50°C (Lindsley, 1983).

9.8.6 Calcite-dolomite Thermometry: The binary system calcite-dolomite contains a solvus, which closes up-temperature. This solvus can be used as a thermometer and can be applied to any rock containing coexisting calcite and dolomite (Bickle and Powell, 1977; Anovitz and Essene, 1987). The calcite limb of the asymmetrical solvus is shallower (i.e. with lower dT/dX) than the dolomite limb, and in practice only the solubility of Mg in calcite is of use. Addition of Fe to the system changes the width of the solvus. Bickle and Powell (1977) calibrated the solubility of Mg in calcite as a function of both temperature and Fe content. Advantages of using this particular calibration include: (i) the effect of

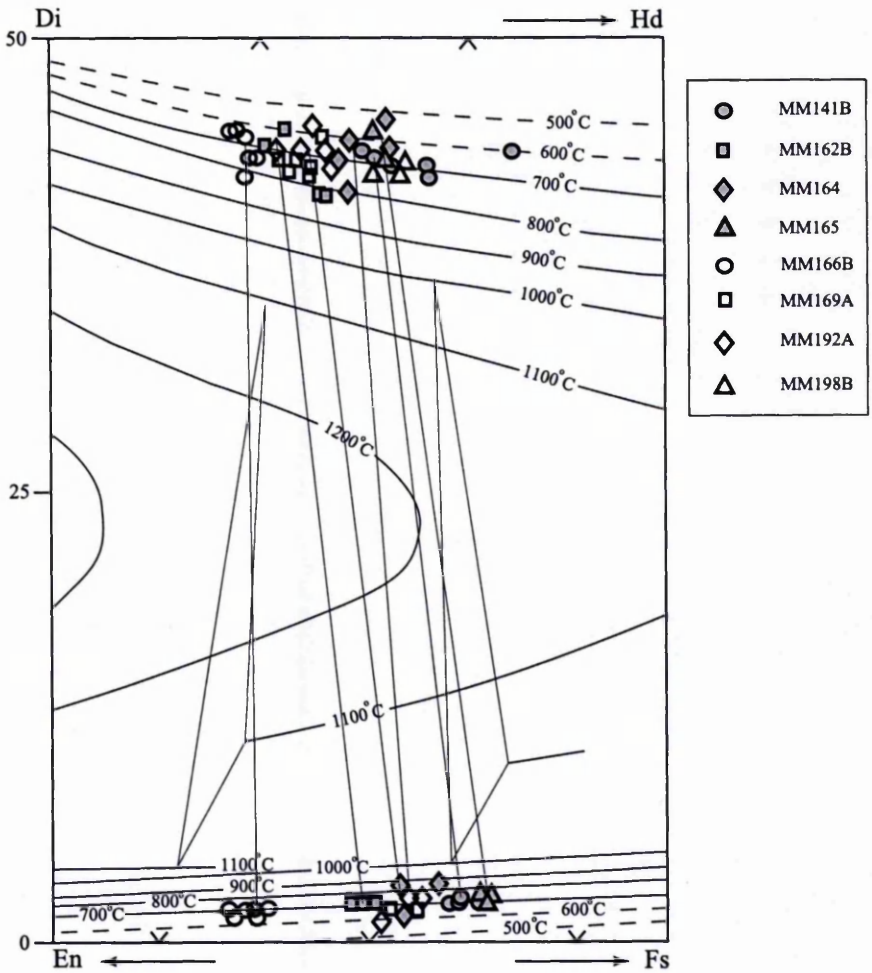

Fig. 9.1 Two-pyroxene thermometry (Lindsley, 1983) of metabasites. The highest temperature is about 820°C for a pressure of 3kbar. Tie lines connect the average composition of pyroxenes in each sample.

addition of iron on the calcite/dolomite solvus is taken into account; (ii) its diagrammatic form makes it easy to use, and provides a useful means of showing the variation in amount of Mg for different calcite analyses, due to different amounts of retrograde exolution of dolomite and/or recrystallisation.

Anovitz and Essene (1987) produced a calcite-dolomite thermometer of the form:

$$T = A(X_{Cal}^{MgCO3}) + \frac{B}{(X_{Cal}^{MgCO3})^2 + C(X_{Cal}^{MgCO3})^2 + D(X_{Cal}^{MgCO3})^2} \qquad [9.29]$$

where: A=-2360.0, B=-0.01345.0, C=2620.0, D=2608.0, E=334.0 and T in °K.

Equation [9.29] is applicable to iron-poor carbonates. Equation 31 of Anovitz and Essene (1987), was developed for ferroan calcite. This thermometer has the form :

$$T^{FeMg} = T^{Mg} + a(X_{Cal}^{FeCO3}) + b(X_{Cal}^{FeCO3})^2 + c(X_{Cal}^{FeCO3} / X_{Cal}^{MgCO3}) + d(X_{Cal}^{FeCO3} \times X_{Cal}^{MgCO3}) + e(X_{Cal}^{FeCO3} / X_{Cal}^{MgCO3})^2 + f(X_{Cal}^{FeCO3} \times X_{Cal}^{MgCO3})^2 \quad [9.30]$$

where: T^{Mg} = T from equation [9.29] above, a=1718.0, b=-10610.0, c=22.49, d=-26260.0, e=1.333, f=0.32837*10^7 and T in °K. The position of calcite-dolomite solvus is reasonably well known (±10°C) between 500 and 800°C. Outside of this range the error brackets widen and potential errors are rapidly increased (Anovitz and Essene, 1987).

The calcite-dolomite thermometer was used to estimate the temperature in the carbonate portion of sample MM256B from Tyndrum, which is a regional metamorphic rock (Fig. 9.2). The pelitic portion of this rock shows the upper greenschist (garnet zone) metamorphic grade. The mean of 34 analyses of calcite, co-existing with dolomite, gives the temperature of 474°C. The highest content of $MgCO_3$ in calcite (X_{MgCO3} = 0.0379) gives the temperature 523°C. The calculated temperature is 517°C when the $FeCO_3$ in calcite (X_{FeCO3}=0.0377) is taken into account.

9.8.7 Amphibole-plagioclase thermometry: The edenite-tremolite equilibrium in the form of the amphibole-plagioclase thermometer of Holland and Blundy (1994) was applied for nine metabasites. For detail on thermometer see section 3.6.5. The results are summarised in Table 9.6.

Table 9.6 Thermometry results from Amphibole-Plagioclase thermometer of Holland and Blundy (1994). Uncertainty is about 40°C. All samples are from the Opx Zone except sample MM127A which is from the Cpx+Ep Zone.

Sample	166B	198B	141B	165a	165b	127A	168A	162B	196A
T°C at 2.5kbar	658	858	777	742	778	591	731	828	780

The results from this thermometer are plotted against the distance from the igneous contact in Fig. 9.3. Temperature from sample MM166B is lower than other

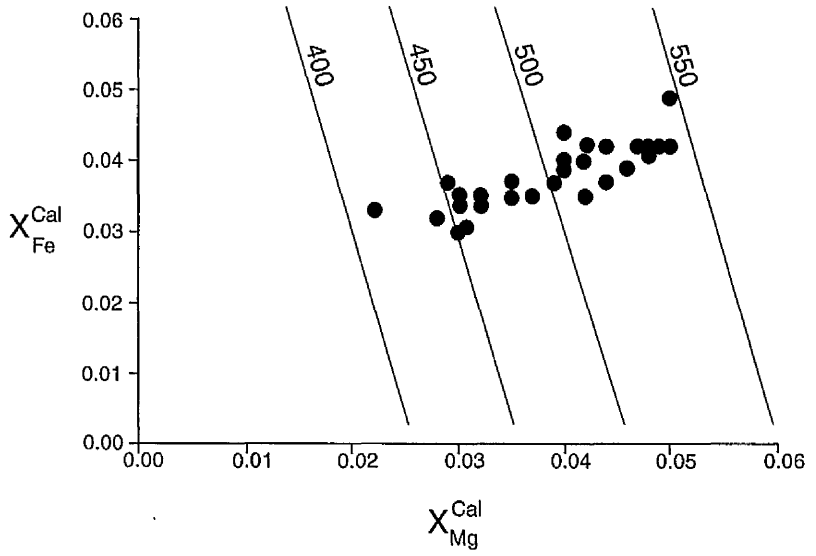

Fig. 9.2 Composition of calcite coexisting with dolomite in carbonate part of regional metamorphic sample MM256B from Tyndrum. Temperature contours (in T°C) are from Powell *et al.* (1984).

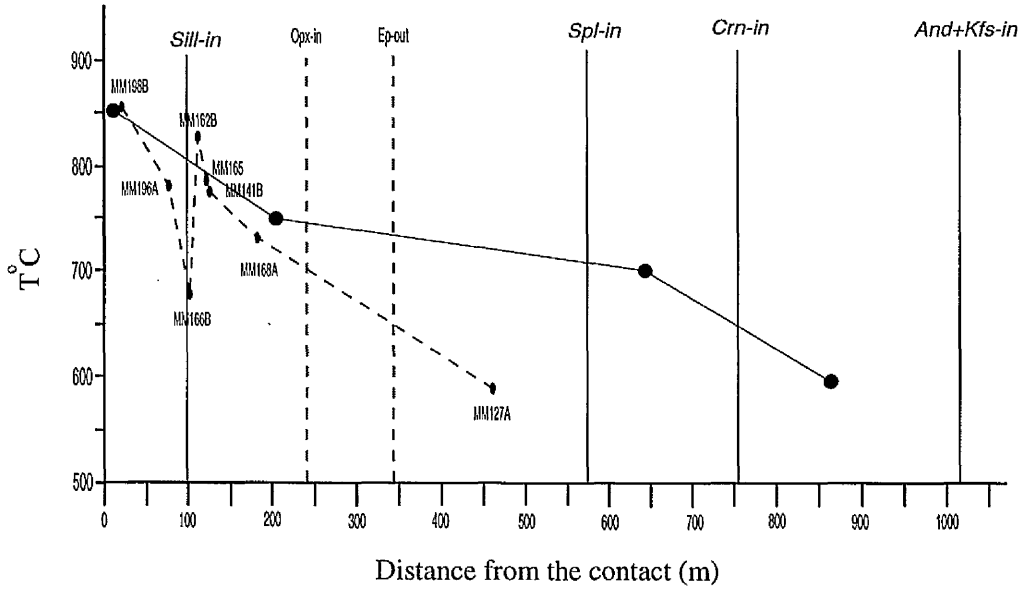

Fig. 9.3 Temperature-distance plot for metabasites (using Hbl-Pl thermometer, dashed line) and pelites (solid line, see Fig. 9.5).

temperature estimates from the inner aureole rocks, which could be because of the re-setting of amphibole-plagioclase pair during cooling or retrograde alteration.

9.9 Geobarometry

There is no suitable assemblage in the Etive aureole rocks to which one can apply independently calibrated geobarometers (e.g. the GASP barometer, Ghent, 1976). The only independently calibrated barometer is NaM_4 versus Al^{iv} barometer of Brown (1977). Using this barometer for metabasites gives a pressure less than 3kbar (Fig. 9.4).

In metapelitic rocks, pressure was estimated by the means of THERMOCALC in three low-variance rocks. Samples MM166D, MM171 and MD1 are from sillimanite-zone, spinel-zone and andalusite+K-feldspar-zone respectively. The water contents of cordierites in these samples were analysed using the SIMS method

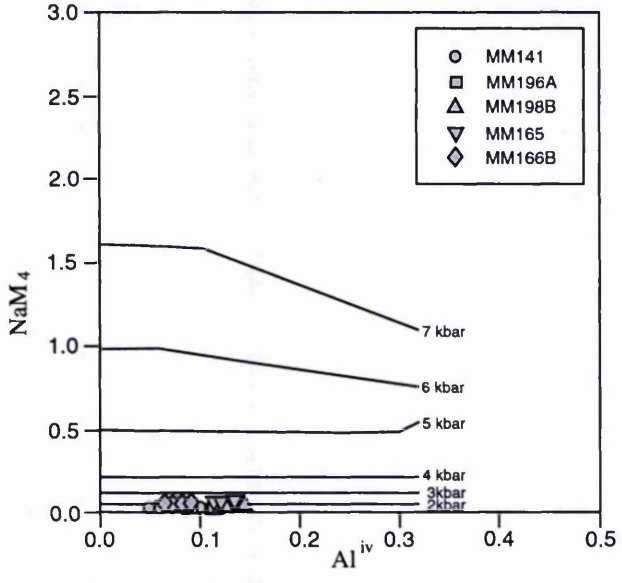

Fig. 9.4 Estimation of pressure of metamorphism of basic rocks using NaM_4 content of amphibole (after Brown, 1977). All of the amphiboles lie below the 3 kbar line.

(Chapter 7). Since the pressure estimation using dehydration reactions is dependent on the water activity and because the water activity in the aureole has not yet been established, fluid-absent reactions involving cordierite were therefore used for pressure estimation. Activity of anhydrous cordierite was calculated using equations 9.13 and 9.14 and the resultant activities were used to construct the THERMOCALC input data files.

The equilibrium curve for reaction

$$\text{Fe-Crd+5Crn} = \text{5Sill+2Herc} \qquad [9.31]$$

intersects the Sill=And equilibrium curve at 2.2 kbar in sample MM166D from the Sill-zone (Fig. 9.5). Strictly speaking, the And=Sill equilibrium provides a pressure minimum for this sample, since the reaction has clearly been overstepped. However, in view of the fact that the sample still contains much unreacted andalusite and was collected from very close to the Sill-isograd, andalusite and sillimanite may be assumed to coexist in this rock, and the And=Sill equilibrium may (within error) be used to define a P-T fix. Independent P-T fixes provided by the intersection of isopleths for reaction 9.31 with those of the cordierite-spinel and two-pyroxene thermometers all fall between 2 and 3 kbars (Fig. 9.5).

In Fig. 9.5 the equilibrium curves for reactions

$$\text{5And+2Herc} = \text{Fe-Crd+5Crn} \qquad [9.32]$$

$$\text{3And+2Phl+6Herc} = \text{Crd+7Crn+2Ann} \qquad [9.33]$$

intersect the And+Sill curve at 2.6 and 2.2 kbar respectively providing pressure maximum for sillimanite-free sample MM171 from the spinel-zone.

Intersections of equilibrium curves for reactions:

$$\text{Phl+2Ms+5Qz} = \text{3Cel+2And} \qquad [9.34]$$

$$\text{2Ms+3Crd} = \text{2Phl+8And+7Qz} \qquad [9.35]$$

$$\text{8Ms+5Crd} = \text{Phl+7Cel+18And} \qquad [9.36]$$

in Fig. 9.5 indicate a pressure of about 2.2 kbar for sample MD1 from the And+Kfs-zone. The intersection yields a temperature of about 570°C for the And+Kfs-zone. Although the uncertainties are relatively large, the pressure estimates from the different zones are in good agreement.

9.10 Constraints on a_{H2O} During Contact Metamorphism

The presence or absence of fluids, especially water, during peak metamorphic conditions is one of the most debated questions in metamorphic petrology. Assessing the role of water is very important for explaining some aspects of contact

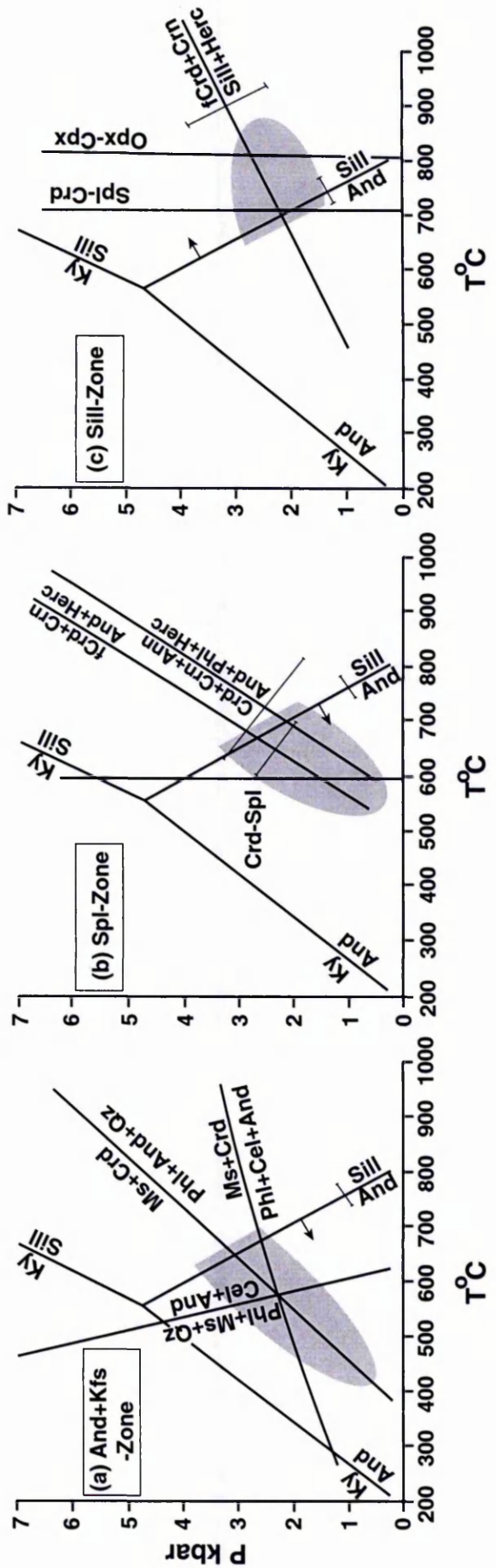

Fig. 9.5 Pressure and temperature estimation for And+Kfs Zone, Spl Zone and Sill Zone, using fluid-conservative reactions. Equilibrium curves for reactions in each rock intersect at about 2kbar pressure.

metamorphism and partial melting in the Etive aureole. Three different methods are used to estimate the water activity and its variation in different zones within the aureole. These are (i) the direct implications of the water content of cordierite, (ii) calculation of a_{H2O} using dehydration equilibria in high grade pelitic hornfelses, and (iii) calculation of a_{H2O} using the dehydration equilibrium

$$2Tr = 3En+4Di+2\beta Qz+2H_2O \qquad [9.37]$$

in the high grade metabasites.

9.10.1 Calculation of aH_2O from cordierite water contents: Water contents of cordierite were analysed in seven pelitic/semi-pelitic samples, one from the And+Kfs-zone, two from the Spl-zone, three from the Sill-zone and one xenolith sample (Chapter 7). Cordierite is known as a good sensor of H_2O activity in metamorphism and anatexis (Newton & Wood, 1979; Kurepin, 1985; Vry *et al.*, 1990; Harley, 1994). Mirwald & Schreyer (1977), Mirwald *et al.* (1979) and Kurepin (1981, quoted in Kurepin, 1985), have calibrated the solubility of H_2O in pure Mg-cordierite under H_2O-saturated conditions. Boberski and Schreyer (1990) showed experimentally that the solubility of H_2O in cordierite is largely independent of its Mg/Fe ratio. The volatile content of cordierite is less than its saturation value at the same P and T. Carrington & Harley (1996) have confirmed this by measuring the H_2O content of cordierite that had equilibrated with a series of granitic melts with different H_2O content at 900°C and 5 kbar. The dehydration reaction of Mg-cordierite can be written as:

$$\underset{\text{Mg-Cordierite}}{Mg_2Al_4Si_5O_{18}.H_2O} \rightarrow \underset{\text{Mg-Cordierite}}{Mg_2Al_4Si_5O_{18}} + \underset{\text{fluid}}{H_2O} \qquad [9.38]$$

(Helgeson *et al.*, 1978; Newton & Wood, 1979; Kurepin, 1985; Carey, 1995). Assuming $\Delta C_{p(r)} = 0$ for the above reaction we have:

$$0 = \Delta H^0_{(r)} - T\Delta S^0_{(r)} + P\Delta V_s + RTLnf_{H2O} + RTLnK \qquad [9.39]$$

where

Table 9.7 a_{H2O} in pelitic/semi-pelitic rocks of the Etive aureole, calculated using water content of cordierite.

Sample	Mean n	aH_2O
MM166D Sill Zone T=800°C	$\overline{X}$ =0.315 SD=0.020	$\overline{X}$ =0.456 SD=0.040
MM166A Sill Zone T=800°C	$\overline{X}$ =0.310 SD=0.018	$\overline{X}$ =0.435 SD=0.039
MM198C Sill Zone T=800°C	$\overline{X}$ =0.328 SD=0.020	$\overline{X}$ =0.468 SD=0.050
MM187 Spl Zone T=700°C	$\overline{X}$ =0.508 SD=0.027	$\overline{X}$ =0.833 SD=0.091
MM171 Spl Zone T=700°C	$\overline{X}$ =0.535 SD=0.053	$\overline{X}$ =0.916 SD=0.180
MD9 Xenolith T=850 °C	$\overline{X}$ =0.521 SD=0.057	$\overline{X}$ =1.120 SD=0.198
MD1 And Zone T=600°C	$\overline{X}$ =0.440 SD=0.033	$\overline{X}$ =0.568 SD=0.073

$$K = \frac{(X_{Mg})^2(1-n)a_{H2O}}{(X_{Mg})^2.n} = \frac{(1-n)a_{H2O}}{n} \qquad [9.40]$$

or:

$$a_{H2O} = \frac{n}{f(1-n)} \exp[\frac{\Delta S}{R} - \frac{\Delta H}{RT}] \qquad [9.41]$$

where n is the water content of cordierite, ΔS is the entropy change of reaction, ΔH is the enthalpy change of reaction, R is the gas constant and T is temperature in °K.
f is known as a function of P and T (Burnham *et al.*, 1969; Powell and Holland, 1988) and ΔS and ΔH can be extracted from the water-saturated data of Mirwald *et al.* (1979) or Kurepin (1985). The water-saturated data of Mirwald *et al.* (1979) which are presented in Fig. 9.6 are almost linear at low pressures, especially at pressures near 2 kbar (the pressure of interest as estimated above for the Etive aureole, Fig.9.5). Using the data of Mirwald *et al.* (1979) the following thermodynamic data for cordierite dehydration were calculated at 2 kbar: ΔS=87.825 JK^{-1} and ΔH=27550 J.

Using these data and the water contents of cordierite obtained from the SIMS (listed in table 7.10), a_{H2O} was calculated for each sample (Table 9.7).

Variation of a_{H2O} in cordierites from the Etive aureole is illustrated versus the distance from the igneous contact in Fig. 9.7. As this figure shows there is an abrupt decrease in a_{H2O}. a_{H2O} in the inner aureole rocks is low (between 0.418 and 0.454). The possible reasons for this are discussed below.

9.10.2 Calculation of a_{H2O} in high grade pelitic rocks using other dehydration equilibria

Geothermometry and geobarometry methods applied for the pelitic rocks from the inner aureole (Sill-zone) give a pressure of about 2 kbar and a temperature about 800 °C. Using obtained pressure and temperature, the activity of water in one contact-metamorphic garnet-bearing pelite (sample MM166A) was calculated by means of THERMOCALC. Equilibrium curves for reactions:

$$Phl+3East+12Qz = 4Kfs+3Py+4H_2O \qquad [9.42]$$

$$Ann+East+Qz = Phl+Kfs+Alm+H_2O \qquad [9.43]$$

were calculated at various water activities. The results are illustrated in Fig. 9.8 Considering a temperature of 800°C for sample MM166A (lower Sill-zone), a_{H2O} is lower than 0.5 (Fig. 9.8a, using reaction 9.42) and higher than 0.7 (Fig. 9.8b, using reaction 9.43). This result is compatible with direct water analyses of cordierite.

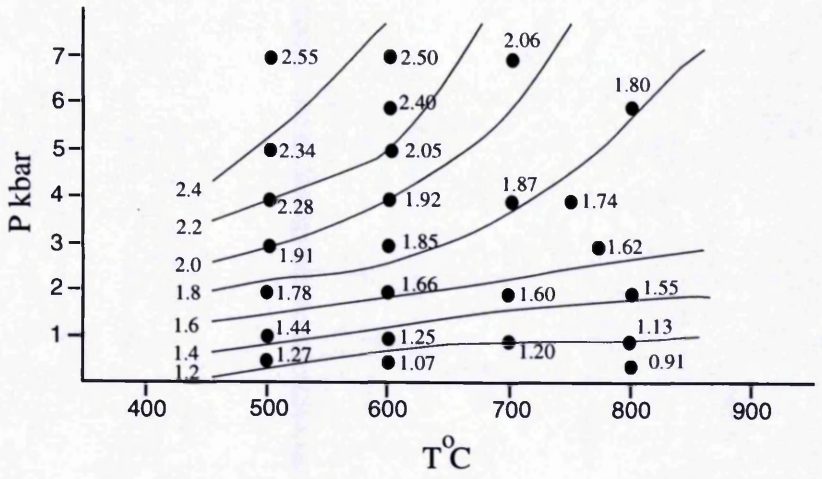

Fig. 9.6 The water-saturated data for cordierite (Mirwald *et al.*, 1979). The data are almost linear at low pressures.

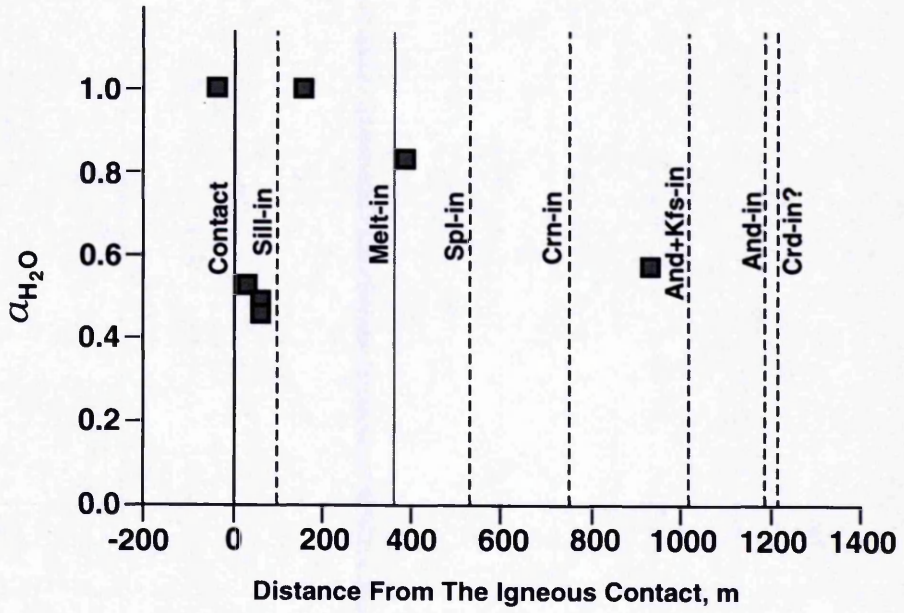

Fig. 9.7 Water activity in metapelites plotted against the distance from the igneous contact. There is an abrupt decrease in water activity in Sillimanite Zone.

9.10.3 Calculation of a_{H2O} in high grade metabasites: The dehydration reaction 9.37 can be used to determine the activity of water in the peak contact metamorphism of metabasites from the Opx-Cpx-zone. Thermodynamic data for tremolite are provided by Jenkins *et al.* (1991) and thermodynamic data for all other phases can be found in Holland & Powell (1990). The equilibrium constant (K) for the above reaction was calculated in eight metabasite samples and f_{H2O} were calculated using appropriate equations provided in Jenkins *et al.* (1991). Using the relation $RTLna_{H2O} = RTLn(\frac{f_{H2O}}{f^0_{H2O}})$ (Wood and Fraser, 1977), and polynomial equation (Powell and Holland, 1985), the water activities in the analysed samples were calculated. The results are presented in Table 9.8.

Table 9.8 Calcualted a_{H2O} in metabasites using tremolite dehydration reaction. All samples are from Opx Zone.

Sample	MM198B	MM196A	MM165	MM166B	MM141B	MM192A	MM164	MM162
f_{H2O}, kbar	0.00303	0.13648	0.06127	0.06157	0.27625	0.01233	0.05354	0.01149
a_{H2O}	0.00300	0.13553	0.06084	0.06114	0.27430	0.01224	0.05316	0.01141

Data in Table 9.8 show that f_{H2O} in metabasites is very variable and very low. The highest f_{H2O} is 0.28 kbar, which is about 1/8 total pressure (2 kbar). Probably the higher amounts in the above table are due to later retrograde hydration. If this assumption is true then the lowest amount in Table 9.7 is likely to be more representative of a_{H2O} in peak contact metamorphism of basic rocks. It means that the water activity during contact metamorphism of metabasites was extremely low in the inner aureole.

9.11. Discussion and Conclusions

The temperature of peak regional metamorphism obtained from Cal-Dol thermometry is about 550°C corresponding to greenschist to lower amphibolite facies of regional metamorphism. This estimate is made from a sample from Tyndrum about 8 km to east of the Etive aureole. Bendall (1995) has estimated a maximum temperature of 612°C (Grt-Hbl cation exchange thermometer) for metabasites from Tyndrum. He also has obtained a temperature of 577°C for a pelitic sample (THERMOCALC) for this area. The Cal-Dol temperature estimated here is consistent with Bendall's (1995) T estimates.

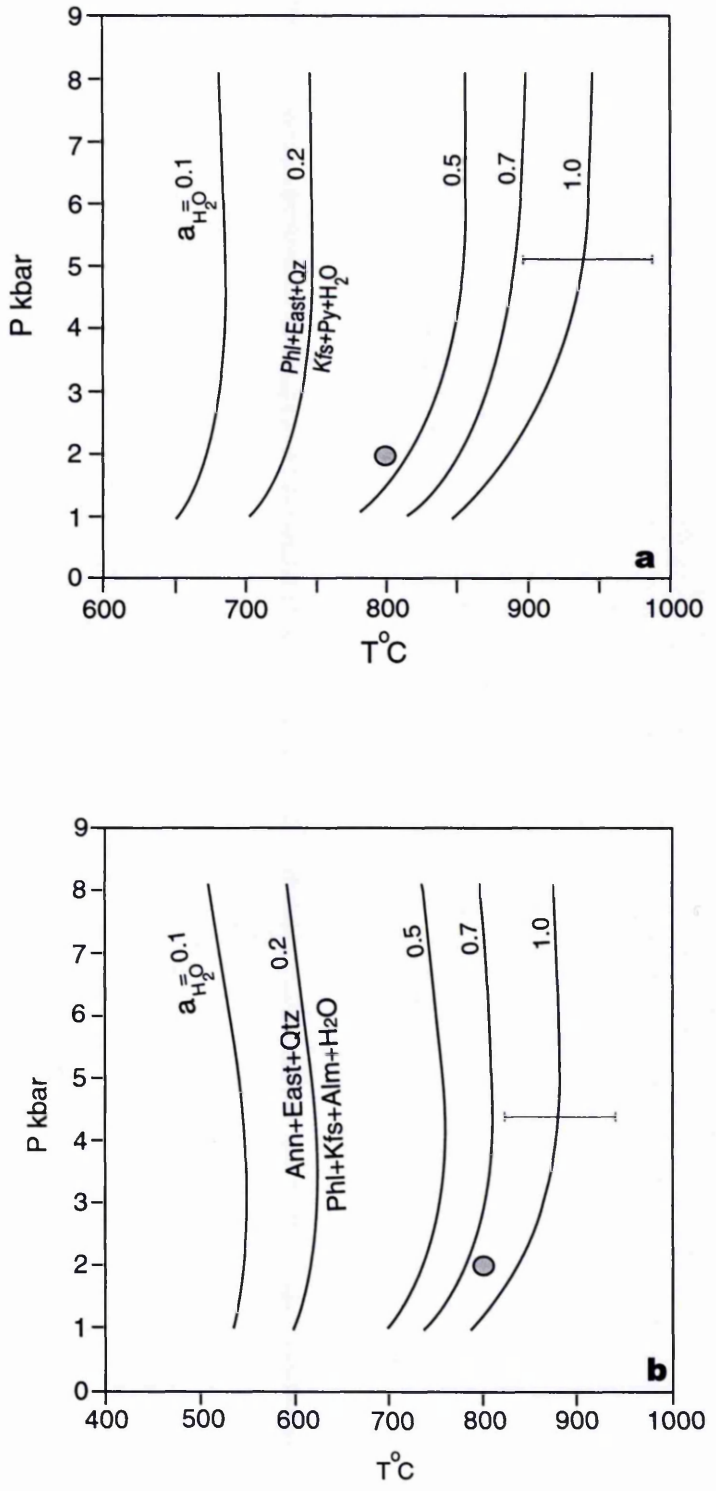

Fig. 9.8 Estimation of water activity in Sillimanite Zone garnet-bearing sample MM166A. Activity of water is slightly lower than 0.5 from Fig. 9.8a and slightly higher than 0.7 from Fig. 9.8b. Both Fig.'s show water undersaturated condition for the rock.

The maximum pressure for regional metamorphism in the Tyndrum area is about 7 kbar (Bendall, 1955). The garnet-grade, Barrovian type, regional metamorphic zone (see Fig. 2.6) covers the Etive aureole. P-T estimates for regional metamorphic rocks, outside the Etive aureole (this study and Bendall, 1995) are consistent with garnet-grade regional metamorphic zone (Fettes, 1979; Chinner, 1966).

There was probably no major tilting of the Etive igneous complex during emplacement, but because of lack of P estimates from the northern and eastern parts of the aureole and because of uncertainties in P estimates from the western part, it is not possible to rule out the possibility of tilting completely.

The pressure estimated for contact metamorphism in the southern part of the aureole (~ 2kbars) is in very good agreement with pressure estimated by Droop and Treloar (1981).

The contact metamorphic pressure (~ 2kbar) is much lower than the regional metamorphic peak pressure. 2 kbar pressure for contact metamorphism is equivalent to 6 km depth of burial, with a possible error of ± 1.5 kbar (± 4 km) (Fig. 9.5).

The Spl-Crd thermometry shows rather similar results for Spl Zone and Sill Zone rocks. The results from the Bt-Grt thermometry are very divergent. Probably the most reliable thermometers are Opx-Cpx (Lindsley, 1983), Grt-Crd (Nichols *et al.*, 1992) and Opx-Bt (Sengupta *et al.*, 1990) thermometers.

The highest temperature at the contact of the igneous rocks (Quarry Diorite) is ~ 850°C. Temperature estimated for different contact metamorphic zones are as follows: And+Kfs Zone, ~ 600°C; Crn Zone, ~ 700°C; Sp Zone ~750°C and Sill Zone ~800-850°C (Fig. 9.5). Considering a width of about 2 km for the aureole, the thermal gradient is very steep, about 125°C/km.

The tight within-sample clustering of cordierite H_2O contents (Table 7.10) suggests that retrogressive diffusive leakage or influx of H_2O through cordierite grains has been minimal, and thus that the measured H_2O contents reflect aH_2O at the thermal peak of contact metamorphism. Compared to regional metamorphic rocks, hornfelses in a contact aureole are likely to cool rapidly, which would tend to suppress retrogressive H_2O diffusion through cordierite.

With respect to calculated values of peak-metamorphic aH_2O (Table 9.7 and Fig. 9.7), the analysed hornfels samples fall into three groups:-

(i) Samples yielding high values of aH_2O (>0.8):- The two Zone VI and the xenolith fall within this group. The implication of the high aH_2O is that these samples crystallised in the presence of an aqueous fluid.

(ii) Samples yielding low values of aH_2O (0.4-0.5):- The three Zone VII samples fall in this group. In the absence of detectable CO_2 in their cordierites, aCO_2 in these samples must have been negligible, implying that they crystallised either under fluid-absent peak-metamorphic conditions or in the presence of an aqueous fluid containing a large proportion of either diluent species such as NaCl, CH_4, N_2 and HF. The former explanation is preferred here. Typical X_F of biotites in Zone VII pelites are ca. 0.18-0.25, (see Fig. 7.14), implying negligible HF contents in any fluid present (Askyuk and Zhukovskaya, 1994). Although it is theoretically possible for a metamorphic fluid to consist mainly of H_2O and CH_4, such a fluid would only be stable at very low fO_2, particularly in the absence of graphite (Lamb and Valley, 1985). No graphite has been detected in hornfelses of the Leven Schist formation (see Chapter 5). Without such a source of carbon, Zone VII hornfelses, which presumably evolved during heating through an aqueous-fluid-present stage analogous to peak conditions in Zone VI, would have no internal means of generation substantial quantities of CH_4 as they approached temperatures corresponding to the sillimanite isograd. Similarly, as the rocks' internal capacity for introducing NaCl and/or N_2 into a fluid was also minimal, there is no reason why the concentration of these componenets should have been so much higher in a fluid in Zone VII than elsewhere in the aureole.

Introduction of a NaCl-rich fluid from the adjacent Quarry Diorite seems unlikely in view of the high aH_2O recorded by the xenolith sample MD9A.

(iii) Samples yielding intermediate values of aH_2O:- The single Zone VI sample yields an aH_2O value of ca. 0.57, which is difficult to interpret in terms of fluid presence or absence.

Within the inner aureole, there is a dramatic decrease in aH_2O (proceeding up-grade) which correlates approximately with the sillimanite isograd (Fig. 9.7). and is up-grade of the melt-in isograd in quartz-bearing pelites. Up to the sillimanite isograd the rocks appear to have been fluid-bearing at the peak of contact metamorphism, while beyond it they were fluid-absent.

The sequence of reactions deduced in Chapter 8, for pelites involve the progression from dehydration reactions through fluid-present melting reactions to fluid-absent melting reactions. The consumption of H_2O by fluid-present melting reactions in upper Zone VI provides a mechanism for reducing aH_2O and initiating fluid-absent conditions close to the sillimanite isograd. The Zone VII samples lie entirely within the part of the section where fluid-absent melting reactions are thought to have dominated, and their low calculated aH_2O values support this conclusion. Further evidence for fluid-absent melting in Zone VII is the fact that most of the migmatites are breccia-like, suggesting that partial melting was accompanied by rock fracture. Fluid-present melting reactions, which generally have negative dP/dT slopes at low pressure and hence negative ΔV, are unable to cause fracture. Fluid-absent reactions, on the other hand, have positive dP/dT and ΔV (e.g. Clemens and Droop, 1998) and can result in rock dilation and fracture if melt is produced faster than it can percolate away by distributed grain-boundary flow.

Sample MM171, from the high-grade part of Zone VI, lies within the part of the aureole where at least quartz-bearing rocks have begun to melt. This sample is not itself quartz-bearing (Chapter 5), so it is not certain whether this rock had actually begun to melt (see Chapter 8). Thus, the high aH_2O calculated for this sample could reflect either dehydration or melting under fluid-present conditions. Further work on the H_2O content of cordierite in quartz-bearing Zone VI rocks is needed before fluid-present melting can be demonstrated unequivocally.

The presence of K-feldspar-rich leucosomes in the xenolith sample (MD9A) indicates that it, too, underwent melting, presumably at temperatures even higher than much of Zone VII, yet it seems to have experienced fluid-present conditions. As it cooled and crystallised, the Quarry Diorite would have expelled H_2O as a free fluid phase, which would have had access to the xenolith within it. Importantly, wall-rock hornfelses as close as 15m from the diorite contact do not seem to have been influenced by magmatically-derived fluid at the peak of contact metamorphism.

The low aH_2O calculated in the inner aureole metabasites are in agreement with the low aH_2O in the inner aureole pelites.

Chapter 10
Conclusions and Discussion

10.1 Introduction

The main aim of the present research has been a systematic study of contact metamorphism of different lithologies within the Etive aureole to elucidate the distribution of the metamorphic zones and isograds and to indicate the factors that control the metamorphic reactions.

The major achievements are summarised in this chapter and the results are discussed. The chapter ends with a section on scope for future work.

10.2 Conclusions and Discussion

10.2.1 Emplacement of the Quarry Diorite: Thermometry of the igneous rocks shows a maximum temperature of ~1000°C for Quarry Diorite (Opx-Cpx thermometer). According to the mineralogy of the Quarry Diorite, Opx and Cpx crystallised at an early stage of the magmatic crystallisation. Therefore the 1000°C temperature obtained from the equilibrium between these two minerals probably represents a temperature close to that at which the dioritic magma was initially intruded. The Quarry Diorite is the outermost ring intrusion in the southern part of the Complex, and is in direct contact with the Dalradian rocks. This intrusion was thus the major heat source for contact metamorphism in the southern part of the aureole.

Temperatures obtained for the igneous rocks from feldspar thermometry and Pl-Hbl thermometry are low, indicating late-magmatic re-setting of the thermometers. Probably any other contact metamorphic effects on the country rocks, because of the intrusion of the Cruachan Granodiorite (which has intruded after the Quarry Diorite) was not important in comparison with heat from Quarry Diorite in

the southern part of the aureole. The main source of the heat in other parts of the aureole was the Cruachan Granodiorite.

The high Rb/K ratio for the igneous rocks indicates the dominance of the magmatic activities during crystallisation rather than hydrothermal activities (Clark, 1992) and a possible low-fluid content for the rocks. A part of the magmatic fluid was consumed during the late-magmatic alteration of previous crystallised anhydrous minerals such as pyroxene and plagioclase to form hydrous minerals such as amphibole, biotite and sericite.

The contact between the igneous rocks and the country rocks is very steep. This fact should be considered in any attempt to model the thermal regime of the pluton and its aureole, based on the intrusion geometry. The large xenoliths and screens of country rocks within the complex may have contaminated the magmas to some extent.

The pattern and orientation of all mesoscopic structures within the aureole are similar to those outside the aureole. There is no evidence at all that the intruding pluton has cause any of the ductile deformation structures within the aureole i.e. there is no evidence for 'forceful' intrusion. The contact of igneous and country rocks is sharply discordant and truncates all structures in the wall rocks and the latter appear to have behaved in a purely brittle manner during interactions with magma.

The existence of numerous country-rocks xenoliths within the intrusive rocks, of concentric ring-dikes of different igneous rock types in the complex, and of sharply discordant contacts with the country rocks, all suggest that the emplacement of the pluton (and the creation of the necessary space for it) probably occurred by cauldron subsidence (Clough, *et al.,* 1909; Bussell, *et al.,* 1976). In this model, space for pluton emplacement is created by down-dropping a single, roughly cylindrical block along a steeply- or outward-dipping ring fault (Bussell, *et al.*, 1976).

10.2.2 Partial melting in the aureole: The sequence of metamorphic reactions in the pelitic rocks was dehydration reactions followed by fluid-present partial melting followed by fluid-absent solid-solid reactions and partial-melting reactions.

Partial melting of the (semi)pelitic rocks in the Etive aureole was not extensive. It is not easy to estimate the exact proportion of melt to restitic materials but a rough estimation based on hand specimens inspection and thin section investigations shows that the melt proportion is in range of 5-15%. The main limiting factor of partial

melting was probably a shortage firstly of water and later of biotite within the inner aureole.

Some of the leucosome veinlets are arranged parallel to the former S_2 crenulation cleavage. Muscovite and other phyllosilicates was originally aligned parallel to the S_2 crenulation cleavage, in the hinges of microfolds, during the regional metamorphic and deformational episode. This phenomenon provided a preferred distribution of the minerals in the rock. Melt first appeared in the chemically suitable materials (quartz-rich microlithons in the hinges of the microfolds). This process produced the tiny leucosome veinlets parallel to the S_2 crenulation cleavage.

Partial melting was accompanied by fracturing of the hornfels mesosomes, probably as a result of the volume increase brought about by fluid-absent melting reactions. The breccia-like migmatites ("agmatites") produced, contain interconnected leucosome veins up to ~5 cm long. During metamorphism these veins would have allowed limited migration of melts away from the sites at which they were produced; however there is no particular evidence to suggest that melt migration occurred on a large scale. Metabasite units within the pelites are only very rarely cut by leucosome veins. Thus, it seems very unlikely that there was any mixing of the anatectic melts produced within the aureole and the dioritic magma of the main pluton. Nevertheless, granitic and dioritic magmas would be perfectly miscible at diorite magmatic temperatures yielding a granodioritic hybrid, so the process is chemically possible and would in principle, be detectable. However it is doubtful whether the volumes of melt generated in the aureole could ever have been large enough to cause any significant and detectable shift in composition of the diorite. Careful geochemical traverses across the diorite towards the contact might help to resolve this issue.

10.2.3 Implications for fluid behaviour: The rocks of the Etive igneous complex and its aureole show evidence of a two-stage history of fluid interaction. During the thermal peak of contact metamorphism, the aureole rocks and the pluton appear to have been operating as separate systems. The rocks of the middle aureole experienced fluid-present conditions, presumably as a result of prograde dehydration reactions. At the same time, xenoliths within the Quarry Diorite were also experiencing fluid-present conditions, presumably as a result of fluid expulsion from

the crystallising magma. Between these two fluid-present regimes was a fluid-absent zone, the inner aureole (the Sil Zone), within which fluid-absent partial melting of pelitic rocks took place. Rocks as close as 15m from the contact were fluid-absent at this time and were therefore not affected by fluid of magmatic (dioritic) origin. This implies either (i) that the amounts of fluid from the crystallising diorite (in excess of the used up by hydration of Px to form Hbl) were very small and were only accessible to rocks in intimate contact with the magma, i.e. xenoliths, or (ii) that the inner aureole presented a very effective barrier to magmatic fluid. The inner aureole hornfelses probably had a very low permeability owing to the presence of anatectic melts, which could have helped to cause such a barrier. The steep contact probably also resulted in the channelling of any magmatically-derived fluids vertically upwards, perhaps to pond at the roof of the intrusion. This mechanism would probably have caused the intensive alteration of the roof rocks and therefore facilitated their subsequent weathering and removal. The meta-andesitic screen between Quarry Diorite and Cruachan granodiorite did not undergo melting during contact metamorphism and therefore had higher porosity and permeability than the pelitic and basic hornfelses. Thus it is possible that most of the magmatic fluid has been channelled through the meta-andesites.

There is clear evidence, throughout the complex, of a later phase of fluid interaction, manifested in the localised late-stage hydrothermal alteration of magmatic minerals in the igneous rocks themselves and of the high-temperature peak-metamorphic minerals in the hornfelses. Feldspars in both groups of rocks show localised evidence of sericitation, as do cordierites, corundums, etc. within the pelitic hornfelses. In the latter, this alteration is clearly retrogressive. It occurred long enough after the peak of contact metamorphism for the temperatures to have dropped blow the thermal stability of cordierite. This type of alteration is found throughout the aureole, even in the Sil Zone, which was fluid-absent at the peak of metamorphism. This type of alteration is not generally pervasive and tends to be restricted mainly to areas adjacent to cracks indicates that it has been caused by infiltration of hydrous fluids along fractures. Several possibilites exist for the origin of these fluids, some or all of which may have contributed:

(i) Residual fluids left over from the crystallisation of the Quarry Diorite.

(ii) Residual metamorphic fluids and fluids released by crystallisation of inner-aureole anatectic melt.

(iii) Far-travelled fluids released from other later intrusions of the complex (e.g. Cruachan Granodiorite, Starav Granite) as they crystallised.

(iv) Country-rock fluids involved in hydrothermal convection systems set up by the cooling igneous complex (e.g. Taylor and Forrester, 1968)

Detailed isotopic work is probably required to address this issue.

10.2.4 Problems of deducing reactions in inner-aureole rocks: The chemical composition-distance relations for the minerals in the metabasic rocks are not very clear for all major elements, but the phase relations permit one to deduce the reactions responsible for the development of the metamorphic zones and isograds in metabasites. The Na content of plagioclase in the high-grade, inner-aureole metabasites, adjacent to the contact, increases as the distance from the contact decreases. This observation is in contrast with the Ca-enrichment trend of plagioclases from the outer aureole towards the contact. This behaviour of plagioclase is not fully understood, but probably because of very low water activities in the inner-aureole metabasites, the projections from H_2O are not valid for these rocks; thus plagioclase shows abnormal behaviour.

The migration of tie-lines and tie-triangles in the quartz-bearing and quartz absent pelites is not systematic and the deduction of metamorphic reactions based on the tie-line migration, continuous reactions is not always possible. The presence of appreciable amounts of Ti and F in inner-aureole biotites and Zn in spinel might be the reason, because in this case the mineral phase relations are not in the pure KFMASH system. The low water activity in the inner-aureole rocks is an additional possible reason for non-systematic tie-line arrangements in AFM and SFM projections from Kfs, Qtz and H_2O as H_2O is probably no longer an excess component.

In general, cross-tie line relations in the pelitic rocks give a much clearer indication of the discontinuous metamorphic reactions than migrating tie-triangle do for continuous ones.

10.2.5 Implications of geothermometric and geobarometric results: The distribution of peak-contact-metamorphic temperatures indicates a very steep sub-horizontal thermal gradient of about 125°C/km for the aureole.

The pressure of contact-metamorphism in the southern segment of the aureole was 2±1.5 kbar. Assuming a lithostatic pressure gradient and an average density for overlying rocks of 2.7 g/cc, a pressure of 2±1.5 kbar corresponds to an emplacement depth of about 6.5 km.

Among the igneous rocks of the Etive complex is a screen of extrusive lavas of Silurian age indicating a shallow environment for the emplacement of the putonic rocks. The emplacement depth obtained by barometry of pelitic rocks is in agreement with this fact. The Ballachulish igneous complex, about 8km to the north of the Etive complex, was emplaced at a depth of 10km (Pattison and Harte, 1991). Considering similar ages for the Ballachulish and Etive complexes (Clayburn *et al.*, 1983; Troll and Weiss, 1991; Thirwall, 1988), the difference in the emplacement depth implies that the thickness of the overburden during the Siluro-Devonian time was not completely uniform. However, the rather similar pressures for contact metamorphism in the Ballachulish and the Etive aureoles shows that the thickness of the crust at about 400Ma was possibly not very variable over much of the south-west Dalradian.

10.3 Scope for future work

In order to find out the difference in the pressure of emplacement of the Etive complex in different parts and thus to assess whether or not there has been any tilting of the complex, it is necessary to find suitable assemblages for barometry from the northern and eastern parts of the aureole. More field geology work should be done in these two areas.

Further work on the volatile contents of cordierite should be done to capitalise on the present study. In particular further work on the H_2O contents of cordierites in quartz-bearing pelites from the Spinel Zone is needed before fluid-present melting can be demonstrated unequivocally. More generally, the CO_2 and H_2O contents of cordierites in graphitic and non-graphitic pelites should be compared to assess lithological control on aH_2O and aCO_2. Cordierites in semipilites interlayered with calc-silicates should also be examined to assess the effect of adjacent lithologies on these parameters.

There are extensive outcrops of calc-silicate rocks in the south-western part of the aureole. These merit more detailed study to assess temperature and pressure variations in the aureole and to constrain the compositions of metamorphic fluids. The calc-silicates are unlikely to have undergone partial melting, so the relationship

between metamorphic and magmatic fluids may well be different in that part of the aureole. For similar reason, the more continuous exposures of metabasic hornfelses in the western aureole should be studied.

More studies can be done on the degree of partial melting, mass-balance calculations for migmatites. More migmatites may remain to be discovered in the northern and eastern parts of the aureole.

Thermal modelling of the complex and its aureole will help to shed light on the heat regimes of the complex-aureole system and will better explain the details of petrologic and geochemical data obtained from the study of the contact-metamorphic rocks. In particular, thermal modelling of successive intrusions, with or without intervening country-rock screens, may yield useful insights into cumulative thermal metamorphism.

A potentially useful method for studying the thermal and hydrothermal responses of the country rocks to the emplacement of the hot magma would be the application of stable isotopes to the igneous rocks and the aureole. The data from such a study could be used for determining fluid flux, and fluid provenance both at the peak of thermal metamorphism and during cooling.

Appendix 1
XRF whole rock analysis

A1.1 Sample preparation

Rock specimens were cut into slices and weathered or fractured materials cut away and rejected. Slices were cleaned and powdered by means of a tungsten-carbide swing mill. To avoid contamination, the mill was flushed by grinding and rejecting a small amount of the sample prior to grinding of the required material. Pressed boric acid pellets were made from each sample, pellets contains 2 ± 0.05 grams of sample powder (Jenkins and De Vries, 1970). Thorough cleaning of all equipment involved took place between pressings.

A1.2 Analysis and processing

The pellets were analysed by X-Ray Fluorescence (XRF) using a Philips 1450 X–ray spectrometer in the Department of earth Sciences of Manchester University. Each sample was analysed for major elements and selected trace elements. Major elements were analysed using a Cr tube with a W sample support mask. Trace element analyses employed a Rh tube with an Al mask. Each run involved 3 samples in conjuction with a standard to correct for machine drift. The output was computer-processed against a selection of stored calibration standards covering a range of rock types from basaltic to granitic compositions. The resulting data were checked by hand to see which calibration range best encompassed the data for each sample. Where possible, quadratic calibration curves were used. Results are reported on a volatile-free basis and total Fe is recorded as FeO. Details of the technique used and the correction procedure are described by Brown *et al.*(1973)

A1.3 Limitation of the technique

XFR is an efficient method for the analyses of a large number of samples. Preparation of pressed pellets is relatively simple, and run times are short. Better quality analyses, particularly for some major elements, can be achieved by using fused beads rather

than pressed pellets, but this is much more time consuming procedure when a large number of samples is involved and was not though necessary for the project. In any case pressed pellets are required for trace element analysis. The advantage of this technique over ICP-AES and ICP-MS is that the concentration of Zr is likely to be more accurately recorded. This is because zircon is resistant to the digestion procedure employed in the preparation of ICP samples, and hence will be under-represented in any solutions prepared by this method.

A1.4 Quality assessment- comparison of internal standards

The quality of XRF data was assessed by running international standards as unknowns using the same standard sets as those used for Etive rocks. The results are reported below in terms of the absolute difference in weight % between the measured and accepted compositions.

	Measured composition (wt. %)				Actual composition (wt. %)				Difference (wt. %)			
Standard	AGV-1	GSP-1	NIM-G	BCR-1	AVC-1	GSP-1	NIM-G	BCR-1	AGV-1	GSP-1	NIM-G	BCR-1
SiO_2	60.51	68.12	75.87	55.43	60.07	67.89	76.40	56.72	0.44	0.23	-0.53	0.71
Al_2O_3	16.77	15.12	12.51	15.02	17.56	15.37	12.19	13.67	-0.79	-0.25	0.32	1.35
Fe_2O_3	6.81	4.14	1.92	11.85	6.88	4.36	2.02	13.46	-0.07	-0.22	-0.10	-1.61
MgO	1.26	1.07	0.20	2.26	1.56	0.97	0.06	3.48	-0.30	0.10	0.14	-1.22
CaO	5.11	2.00	0.81	6.57	4.99	2.04	0.78	6.95	0.12	-0.04	0.03	-0.38
Na_2O	4.31	2.78	3.50	3.72	4.34	2.82	3.39	3.28	-0.03	-0.04	0.11	0.44
K_2O	2.86	5.50	5.09	1.63	2.94	5.57	5.04	1.70	-0.08	-0.07	0.05	-0.07
TiO_2	1.07	0.65	0.10	2.10	1.06	0.66	0.09	2.20	0.01	-0.01	0.01	-010
MnO	0.23	0.10	0.09	0.26	0.10	0.04	0.02	0.18	0.13	0.06	0.07	0.08
P_2O_5	0.89	0.38	0.02	0.37	0.50	0.28	0.01	0.36	0.39	0.10	0.01	0.01
Total	99.81	99.86	100.11	99.23								

The probable maximum errors are given below:

Content of element in sample (wt% or ppm)	80%	40&	30%	20%	10%-5%	1%	10ppm
Relative error (%)	1	2	3	4	5	10	20

Appendix 2
Whole rock chemistry of igneous samples

CG = Cruachan Granodiorite, QD = Quarry Diorite, MG = Meall Odhar Granite,
BD = Below Detection Limit

Sample	7B, CG	4A, CG	5H, CG	21B, QD	31D, QD	3A, CG	3D, MG
Major elements, wt%							
SiO2	56.62	57.15	63.35	64.16	55.31	57.14	71.11
Al2O3	16.91	17.80	17.90	15.74	17.07	18.15	15.42
Fe2O3	1.55	3.34	0.99	1.21	1.46	1.66	0.87
FeO	4.00	2.98	2.58	3.14	3.76	4.30	0.78
MgO	4.59	3.66	1.53	3.40	5.95	3.72	0.66
CaO	5.59	6.30	3.55	4.00	8.83	5.60	0.83
Na2O	4.52	3.96	4.93	3.93	3.59	4.55	3.91
K2O	2.61	2.60	3.60	3.33	2.03	2.65	5.63
TiO2	0.94	1.19	0.76	0.66	1.07	1.19	0.36
P2O5	0.34	0.62	0.25	0.30	0.56	0.54	0.06
total	99.67	99.60	99.44	99.87	99.62	99.50	99.63
CIPW Norm							
Quartz	3.96	7.41	10.44	14.56	1.96	3	24.15
Corundum	-	-	-	-	-	-	1.51
Orthose	15.42	15.37	21.28	19.68	12.00	15.66	33.27
Albite	38.25	33.51	41.72	33.26	30.38	38.50	33.09
Anorthite	18.14	23.12	16.08	15.47	24.47	21.28	3.76
Diopside	6.11	3.53	0.05	2.10	12.79	2.70	-
Hypersthene	13.01	8.21	6.45	11.13	12.66	12.52	1.76
Magnetite	2.25	4.84	1.44	1.75	2.12	2.41	1.26
Apatite	0.81	1.47	0.59	0.71	1.33	1.28	0.14
Ilmenite	1.79	2.26	1.44	1.25	2.03	2.26	0.68
total	99.73	99.71	99.49	99.92	99.73	99.60	99.64
Trace elements, ppm							
Nb	15	17	8	14	10	16	13
Zr	295	345	522	229	217	459	396
Y	33	32	31	31	27	31	43
Sr	888	954	1094	892	1401	1105	677
Rb	61	79	75	71	38	62	118
Zn	48	68	44	42	47	68	36
Cu	BD	17	BD	8	BD	6	BD
Ni	22	BD	BD	BD	26	BD	BD
Cr	107	11	BD	52	103	12	BD
Ce	88	88	139	86	69	130	131
Nd	22	31	59	38	21	35	44
V	128	164	74	102	165	144	37
La	39	47	67	38	25	49	53
Ba	1263	1492	4005	1224	1222	2003	2004
Sc	17	18	5	9	18	17	5

Sample	17, QD	5G, MG	4B, MG	5J, MG	1A, CG	1D, CG	3F, CG
Major elements, wt%							
SiO2	61.90	76.58	76.54	64.62	58.59	59.94	58.57
Al2O3	16.25	12.68	12.51	17.99	18.19	16.26	18.67
Fe2O3		0.25	0.22	0.68	1.70	1.55	1.51
FeO	1.34	0.23	0.20	1.76	4.39	4.02	3.86
MgO	3.46	0.24	0.19	0.83	3.00	3.91	2.93
CaO	3.85	0.25	0.29	2.17	6.20	5.73	5.15
Na2O	4.66	3.59	3.22	4.88	4.02	4.08	4.85
K2O	4.54	5.33	5.84	5.47	2.22	2.86	2.32
TiO2	2.79	0.13	0.11	0.60	1.02	0.89	1.14
P2O5	0.68	BD	BD	0.12	0.56	0.47	0.50
total	0.30	99.28	99.12	99.12	99.89	99.71	99.50
	99.77						
CIPW Norm							
Quartz	9.19	34.40	34.55	8.95	8.63	7.98	5.60
Corundum	-	0.55	0.36	0.35	-	-	-
Orthose	16.49	31.50	34.51	32.33	13.12	16.90	13.71
Albite	38.42	30.38	27.25	41.29	34.02	34.53	41.04
Anorthite	15.72	1.24	1.44	10.06	25.03	17.61	22.32
Diopside	4.54	-	-	-	1.99	6.51	0.23
Hypersthene	11.52	0.60	0.48	3.75	11.48	11.22	11.14
Magnetite	1.94	0.36	0.32	0.99	2.46	2.25	2.19
Apatite	0.71	-	-	0.28	1.33	1.11	1.18
Ilmenite	1.29	0.25	0.21	1.14	1.94	1.69	2.17
total	99.82	99.28	99.12	99.14	99.99	99.80	99.59
Trace elements, ppm							
Nb	15	BD	15	14	20	16	24
Zr	269	124	130	736	243	270	534
Y	39	33	44	32	46	35	40
Sr	1275	77	121	1345	1363	988	1265
Rb	70	116	153	116	82	65	104
Zn	61	12	6	40	67	57	67
Cu	16	BD	BD	BD	24	3	BD
Ni	12	BD	BD	BD	13	2	BD
Cr	74	BD	BD	BD	91	51	6
Ce	80	52	60	287	100	95	126
Nd	34	12	16	104	39	33	23
V	104	23	12	64	156	137	138
La	42	47	35	126	36	48	53
Ba	1363	159	184	8567	1068	1280	1743
Sc	12	6	BD	11	22	18	12

Sample	5F, CG	5A, CG	5B, CG	19B, QD	23B, QD	Δ659A, QD	216, QD
Major elements, wt%							
SiO2	68.24	60.39	64.43	62.94	60.62	59.95	58.95
Al2O3	15.93	17.48	17.64	15.75	15.99	18.28	15.76
Fe2O3	0.76	1.26	0.81	2.50	1.43	1.62	1.48
FeO	1.99	3.26	2.09	2.22	3.69	2.76	4.49
MgO	1.42	3.77	1.71	3.77	4.77	2.76	6.36
CaO	2.71	4.90	3.32	4.42	4.93	5.73	5.71
Na2O	4.10	4.98	4.99	4.15	4.45	4.67	3.32
K2O	3.96	2.59	3.90	3.05	2.66	2.81	2.66
TiO2	0.43	0.73	0.53	0.69	0.77	0.91	0.82
P2O5	0.15	0.35	0.19	0.32	0.37	0.42	0.50
total	99.69	99.71	99.61	99.81	99.68	99.91	100.32
CIPW norm							
Quartz	20.63	5.56	10.50	13.46	7.25	6.84	7.54
Corundum	0.30	-	-	-	-	-	-
Orthose	23.40	15.31	23.05	18.02	15.72	16.61	15.72
Albite	34.69	42.14	42.23	35.12	37.66	39.52	28.09
Anorthite	12.56	17.69	14.22	15.34	15.80	20.62	20.25
Diopside	-	3.67	0.92	3.70	5.20	4.28	4.13
Hypersthene	5.85	11.37	6.11	8.53	13.71	7.06	19.53
Magnetite	1.10	1.83	1.17	3.62	2.07	2.35	2.15
Apatite	0.36	0.83	0.45	0.76	0.88	0.99	1.18
Ilmenite	0.82	1.39	0.01	1.31	1.46	1.73	1.56
total	99.72	99.77	99.64	99.87	99.75	99.99	100.14
Trace elements, ppm							
Nb	16	21	12	14	13	13	11
Zr	246	292	330	262	280	384	209
Y	38	37	33	37	37	39	39
Sr	747	1009	935	1118	1324	1614	1497
Rb	137	79	115	74	64	86	87
Zn	44	69	30	56	58	61	66
Cu	1	BD	5	10	11	4	50
Ni	BD	6	BD	11	26	11	83
Cr	33	63	7	64	90	46	158
Ce	63	99	115	78	113	102	82
Nd	26	33	31	39	30	34	35
V	61	108	65	104	122	110	137
La	28	40	43	42	41	42	33
Ba	1077	1375	3112	1252	1417	1650	1017
Sc	10	17	7	11	17	14	18

Sample	20, QD	Δ376, QD	Δ662, QD	Δ660, QD	116B, QD	193C, QD	31D, QD
Major elements, wt%							
SiO2	63.47	55.61	57.34	60.27	62.87	61.14	55.31
Al2O3	16.17	17.69	16.29	16.36	16.24	17.51	17.07
Fe2O3	1.16	1.73	1.80	1.43	1.35	1.15	1.30
FeO	3.17	4.73	4.93	3.90	3.67	3.14	3.53
MgO	3	5.31	5.06	4.09	2.86	2.86	5.95
CaO	3.96	6.99	6.43	5.33	4.17	4.88	8.83
Na2O	4.27	3.93	3.58	4.06	3.86	4.70	3.59
K2O	3.44	2.09	2.01	2.69	3.39	2.95	2.03
TiO2	0.69	1.05	0.95	0.76	0.75	0.82	1.07
P2O5	0.28	0.55	0.47	0.37	0.32	0.36	0.56
total	99.61	99.68	98.86	99.26	99.48	99.51	99.24
CIPW norm							
Quartz	12.21	2.58	7.34	8.88	13.45	8.02	2.09
Corundum	-	-	-	-	-	-	-
Orthose	20.33	12.35	11.88	15.90	20.03	17.43	1200
Albite	36.13	33.26	30.29	34.36	32.66	39.77	30.38
Anorthite	14.80	24.46	22.44	18.47	16.97	17.97	24.47
Diopside	2.59	5.61	5.41	4.68	1.49	3.34	12.78
Hypersthene	9.94	15.32	15.94	12.65	10.78	8.97	12.39
Magnetite	1.68	2.51	2.70	2.07	1.96	1.67	1.88
Apatite	0.66	1.30	1.11	0.88	0.76	0.85	1.33
Ilmenite	1.31	1.99	1.80	1.44	1.42	1.56	2.03
total	99.66	99.38	99.01	99.33	99.54	99.58	99.34
Trace elements, ppm							
Nb	14	16	12	15	12	17	10
Zr	286	314	256	271	314	345	217
Y	37	44	39	41	42	38	27
Sr	1036	1503	1571	1207	1109	1469	1401
Rb	90	61	54	74	105	79	38
Zn	55	78	83	67	87	57	47
Cu	27	49	50	30	15	14	BD
Ni	38	73	108	76	45	18	26
Cr	77	161	185	142	105	51	103
Ce	82	82	65	67	93	85	69
Nd	30	35	22	30	42	32	21
V	99	162	165	120	101	103	165
La	40	45	35	41	39	34	25
Ba	1252	1119	994	1029	1491	1363	1222
Sc	9	22	15	20	9	16	18

Sample	104, CG	102A, CG	97B, CG	1D, CG
Major elements, wt%				
SiO2	54.87	60.99	62.97	59.94
Al2O3	16.86	15.93	17.87	16.26
Fe2O3	2.18	1.47	1.07	1.49
FeO	4.75	3.61	2.33	3.67
MgO	6.27	4.70	2.11	3.91
CaO	6.49	4.96	3.73	5.73
Na2O	3.67	3.96	5.01	4.08
K2O	2.67	2.77	3.64	2.86
TiO2	1.32	0.85	0.86	0.89
P2O5	0.74	0.42	0.33	0.47
total	99.62	99.66	99.92	99.30
CIPW norm				
Quartz	1.22	9.95	8.92	8.25
Corundum	-	-	-	-
Orthose	15.78	16.37	21.51	16.90
Albite	31.06	33.51	42.40	34.53
Anorthite	21.10	17.51	15.52	17.61
Diopside	5.39	3.71	0.84	6.49
Hypersthene	17.78	13.94	6.83	10.65
Magnetite	3.16	2.13	1.55	2.16
Apatite	1.75	0.99	0.78	1.11
Ilmenite	2.51	1.61	1.63	1.69
total	99.76	99.76	99.98	99.39
Trace elements, ppm				
Nb	12	18	15	16
Zr	317	269	570	270
Y	44	43	32	35
Sr	1763	1191	1093	988
Rb	77	90	86	65
Zn	83	57	48	57
Cu	43	12	14	3
Ni	54	81	BD	2
Cr	120	157	9	51
Ce	66	60	142	95
Nd	35	29	35	33
V	185	123	75	137
La	20	37	60	48
Ba	1469	1013	2676	1280
Sc	19	15	4	18

Appendix 3

Electron microprobe

A3.1 Sample preparation

Polished, uncovered thin sections were made from the samples for analysis. These sections were coated with a 20 nm carbon film before analysis. Silver paint was used to ensure a viable electrical connection between the carbon coat and the frame in which thin section were mounted.

A3.2 Machines used

All samples were analysed for major elements using the modified Cambridge Instrument Geoscan microprobe at the Department of earth Sciences in the Manchester University. The machine is interfaced to an Oxford Instrument/Link Analytical QX-2000 energy dispersive X-ray analysis system and uses energy dispersive spectrometer (E.D.S.) analysis. The E.D.S. comprises a Kevex detector, a Harwell 2010 pulse processor and Link System electronics. Link System ZAF4/FLS software is used to convert X-ray spectra obtained from the specimen into chemical analyses. The detection limit of the machine is approximately 0.2 wt%. The following standards were used:

Si and Ca – Natural wollastonite
Al-Synthetic corundum
Fe- Synthetic fayalite
Mn- Synthetic periclase
Na- Natural jadeite
K- Natural orthoclase (Spencer A)
Ba- Natural barite
Ti- Synthetic rutile
Ni- Metallic nickel
Cr- Metallic chromium

A3.3 Operation Condition

15 kv electron beam accelerating voltage, checked regularly by means of a Faraday cage. Regular gain calibration were made using a stored spectrum file.

Beam diameter between 1-2 μm.

75 degree X-ray take-off angle

a 40 second acquisition time per analysis,

3 nA specimen current on cobalt metal,

2500 CPS output count rate from cobalt metal with 18% detection system dead time.

The Geoscan was calibrated for the following elements: Si, Ti, Cr. Fe, Mn, Mg, Ca, Na, K, and Zr.

Wave-length dispersive electron microprobe was used for analysing the F content in biotites.

Criteria for accepting microprobe data.

Mineral	Oxide (wt%)	No. of O in formula	Cation Total	Stoichiometric Criteria	
Plagioclase	98-102	8	4.90-5.10	(Si, Al)	3.96-4.04
				(Na, Ca, K)	0.98-1.02*
Alkali feldspar	98-102	8	4.90-5.10	(Si, Al)	3.96-4.04
				(Na, Ca, K)	0.98-1.02*
Garnet	98.102	24	15.70-16.00**	(Si, Al, Ti, Cr, Fe^{3+})	9.80-10.20
				(Fe^{2+}, Mn, Mg. Ca)	5.90-6.10
Cordierite	96.101	18	10.80-11.00	(Si, Al, Ti, Cr, Fe^{3+})	8.8-9.2
				(Fe^{2+}, Mn, Mg)	1.96-2.04
Pyroxene	98.102	6	3.96-4.00**		
Biotite	93-98	22		(K, Na, Ca)	1.70-2.00
Muscovite	93-102	22		(K, Na, Ca)	1.70-2.00
Spinel	98.102	4	2.94-3.00**	(Al, Ti, Cr, Fe^{3+})	1.96-2.04
				(Fe^{2+}, Mn, Mg, Zn)	0.98-1.02
Hornblende	95-99	23			

* Does not include Ba which was not analysed for on the Geoscan microprobe

** Cation totals systematically greater than these are taken to indicate the presence of Fe3+ and were recalculated to the ideal cation total

Microprobe analyses of igneous amphiboles

Sample															
Percentage Oxides															
SiO2	51.01	50.18	50.81	54.15	49.09	52.33	49.36	50.42	48.90	49.63	50.14	48.97	49.43	51.56	52.77
TiO2	0.93	1.15	1.07	0.29	1.29	0.67	1.31	0.99	1.26	0.92	1.09	1.38	1.08	0.70	0.77
Al2O3	4.34	4.79	4.54	2.26	5.59	3.56	5.31	4.49	5.63	4.87	4.99	5.83	5.10	3.96	3.55
Cr2O3	0.03	0.12	0.19	0.05	0.09	0.00	0.60	0.03	0.08	0.09	0.08	0.04	0.00	0.06	0.00
Fe2O3	0.00	0.00	0.00	0.00	0.00	0.00	0.00	0.46	0.00	0.43	0.00	0.00	0.00	0.00	0.00
FeO	12.28	12.24	12.18	10.36	12.76	11.75	12.68	11.47	13.13	12.34	12.33	12.72	12.33	12.01	11.71
MnO	0.34	0.27	0.35	0.28	0.35	0.45	0.39	0.33	0.39	0.58	0.37	0.30	0.30	0.33	0.39
MgO	15.08	15.50	15.48	17.22	14.91	16.16	14.80	15.76	15.03	15.08	14.94	15.17	15.38	15.86	16.23
CaO	11.90	11.69	11.83	12.44	11.53	12.13	11.51	11.68	11.71	11.75	12.09	11.74	11.38	11.99	11.75
ZnO	0.00	0.00	0.00	0.00	0.00	0.00	0.00	0.36	0.01	0.23	0.02	0.00	0.00	0.13	0.10
Na2O	1.11	1.30	1.08	0.76	1.47	0.94	1.35	0.76	1.46	1.07	1.08	1.75	1.63	0.97	1.02
K2O	0.03	0.12	0.19	0.11	0.49	0.24	0.41	0.29	0.41	0.38	0.38	0.45	0.47	0.33	0.28
Total	**97.05**	**97.36**	**97.72**	**97.92**	**97.57**	**98.23**	**97.18**	**97.04**	**98.01**	**97.36**	**97.51**	**98.35**	**97.10**	**97.90**	**98.57**
Number of Ions on the basis of 23 oxygens															
SI	7.45	7.32	7.37	7.74	7.20	7.52	7.26	7.34	7.13	7.26	7.32	7.13	7.27	7.46	7.57
Ti	0.10	0.13	0.12	0.03	0.14	0.07	0.14	0.11	0.14	0.10	0.12	0.15	0.12	0.07	0.08
Al	0.74	0.82	0.78	0.38	0.97	0.60	0.92	0.77	0.67	0.84	0.86	1.00	0.88	0.67	0.60
Cr	0.00	0.01	0.02	0.00	0.01	0.00	0.00	0.00	0.00	0.01	0.00	0.00	0.00	0.00	0.00
Fe3+	0.00	0.00	0.00	0.00	0.00	0.00	0.00	0.05	0.00	0.05	0.00	0.00	0.00	0.00	0.00
Fe2+	1.50	1.49	1.48	1.24	1.56	1.41	1.56	1.40	1.60	1.51	1.50	1.55	1.52	1.45	1.41
MnO	0.04	0.03	0.04	0.03	0.04	0.05	0.05	0.04	0.05	0.07	0.05	0.04	0.04	0.04	0.05
MgO	3.28	3.37	3.35	3.67	3.26	3.46	3.24	3.42	3.27	3.29	3.25	3.29	3.37	3.42	3.47
CaO	1.86	1.83	1.84	1.90	1.81	1.87	1.81	1.82	1.83	1.84	1.89	1.83	1.79	1.86	1.81
Zn	0.00	0.00	0.00	0.00	0.00	0.00	0.00	0.04	0.00	0.02	0.00	0.00	0.00	0.01	0.01
Na	0.31	0.37	0.30	0.21	0.42	0.26	0.38	0.21	0.41	0.30	0.31	0.49	0.46	0.27	0.28
K	0.00	0.02	0.03	0.02	0.09	0.04	0.08	0.05	0.07	0.07	0.07	0.08	0.09	0.06	0.05
Total	15.28	15.39	15.33	15.23	15.50	15.28	15.44	15.24	15.17	15.36	15.37	15.56	15.54	15.31	15.33
Sample				MM5K						MM17					
Percentage Oxides															
SiO2	50.23	49.82	51.53	49.97	48.07	49.30	50.08	49.49	48.88	50.78	49.94	49.66	49.84	49.45	49.75
TiO2	1.03	1.09	0.62	1.11	1.27	1.22	1.24	1.42	1.28	0.47	0.56	1.17	1.23	1.11	0.87
Al2O3	5.03	5.13	3.71	4.80	5.96	5.44	5.24	5.38	5.41	4.74	4.98	5.62	5.74	4.89	5.18
Cr2O3	0.00	0.08	0.06	0.01	0.04	0.03	0.12	0.07	0.00	0.09	0.02	0.14	0.05	0.00	0.13
Fe2O3	0.00	0.00	0.00	0.00	0.00	0.00	0.00	0.00	0.00	0.00	0.00	0.00	0.00	0.00	0.00
FeO	12.53	12.80	11.56	12.54	13.42	13.14	12.63	12.76	12.57	13.65	14.16	13.90	13.16	13.77	13.53
MnO	0.41	0.41	0.36	0.27	0.25	0.26	0.29	0.30	0.18	0.10	0.05	0.03	0.00	0.09	0.13
MgO	15.01	14.87	16.31	14.95	14.30	14.84	15.22	14.96	14.85	15.16	14.77	15.03	15.14	14.46	14.59
CaO	11.67	11.59	11.81	11.85	11.74	11.57	11.68	11.62	11.77	11.06	11.26	11.33	11.26	11.78	11.38
ZnO	0.00	0.05	0.00	0.00	0.00	0.00	0.00	0.00	0.00	0.22	0.00	0.26	0.27	0.00	0.00
Na2O	1.23	1.17	1.14	1.18	1.39	1.46	1.19	1.40	1.40	1.29	1.25	1.48	1.56	1.44	1.44
K2O	0.36	0.48	0.24	0.41	53.00	0.53	0.45	0.44	0.46	0.34	0.41	0.45	0.50	0.42	0.47
Total	**97.50**	**97.49**	**97.34**	**97.09**	**96.97**	**97.79**	**98.14**	**97.84**	**96.80**	**97.90**	**97.40**	**99.07**	**98.75**	**97.41**	**97.47**
Number of Ions on the basis of 23 oxygens															
Si	7.34	7.29	7.48	7.34	7.11	7.22	7.27	7.23	7.21	7.40	7.33	7.19	7.23	7.28	7.32
Ti	0.11	0.12	0.07	0.12	0.14	0.13	0.13	0.16	0.14	0.05	0.06	0.13	0.13	0.12	0.10
Al	0.87	0.88	0.63	0.83	1.04	0.94	0.89	0.93	0.94	0.81	0.86	0.96	0.98	0.85	0.89
Cr	0.00	0.00	0.00	0.00	0.00	0.00	0.01	0.00	0.00	0.01	0.00	0.02	0.00	0.00	0.01
Fe3+	0.00	0.00	0.00	0.00	0.00	0.00	0.00	0.00	0.00	0.00	0.00	0.00	0.00	0.00	0.00
Fe2+	1.53	1.60	1.40	1.54	1.66	1.61	1.53	1.56	1.55	1.66	1.74	1.68	1.60	1.70	1.66
MnO	0.05	0.05	0.04	0.03	0.03	0.03	0.03	0.04	0.02	0.01	0.00	0.00	0.00	0.01	0.02
MgO	3.27	3.25	3.53	3.27	3.15	3.24	3.29	3.26	3.27	3.29	3.23	3.24	3.27	3.18	3.20
CaO	1.83	1.82	1.84	1.86	1.86	1.82	1.82	1.82	1.86	1.72	1.77	1.76	1.75	1.86	1.79
Zn	0.00	0.00	0.00	0.00	0.00	0.00	0.00	0.00	0.00	0.02	0.00	0.03	0.03	0.00	0.00
Na	0.35	0.33	0.32	0.34	0.40	0.41	0.33	0.40	0.40	0.36	0.37	0.41	0.44	0.41	0.41
K	0.07	0.09	0.04	0.08	0.10	0.10	0.08	0.08	0.09	0.06	0.08	0.08	0.09	0.08	0.09
Total	**15.42**	**15.43**	**15.35**	**15.41**	**15.49**	**15.50**	**15.38**	**15.48**	**15.48**	**15.39**	**15.44**	**15.50**	**15.52**	**15.49**	**15.49**

Microprobe analyses of igneous biotites

Sampli MM5E												MM5H			
Percentage Oxides															
SiO2	36.59	36.61	37.09	36.94	36.64	36.54	36.59	37.17	36.87	36.50	35.60	36.23	35.95	36.74	37.05
Al2O3	13.08	13.62	13.61	13.20	13.36	13.84	13.08	13.66	13.68	13.61	13.56	13.31	13.62	13.75	13.81
FeO	17.18	17.05	17.18	17.54	17.37	18.24	17.18	17.80	17.67	16.93	17.62	17.25	18.16	17.06	17.58
MnO	0.00	0.07	0.00	0.00	0.00	0.00	0.00	0.00	0.00	0.00	0.00	0.03	0.11	0.08	0.00
MgO	13.14	12.59	12.75	12.87	12.81	12.26	13.14	13.36	12.88	13.02	12.96	13.54	12.26	12.97	12.80
CaO	0.11	0.01	0.14	0.12	0.14	0.07	0.11	0.10	0.05	0.12	1.67	0.14	0.10	0.05	0.22
TiO2	4.61	4.75	4.20	4.39	4.59	4.68	4.61	4.51	4.79	5.11	5.49	4.11	5.06	4.57	4.27
Na2O	0.35	0.46	0.43	0.49	0.45	0.47	0.35	0.54	0.62	0.58	0.50	0.45	0.42	0.49	0.49
K2O	9.17	9.03	9.27	9.16	9.17	9.01	9.17	9.15	9.16	9.31	7.41	8.60	8.98	9.28	9.13
Cr2O3	0.00	0.05	0.02	0.00	0.02	0.00	0.00	0.02	0.08	0.05	0.00	0.03	0.00	0.00	0.08
Total	94.23	94.24	94.69	94.71	94.55	95.11	94.23	96.31	95.80	95.23	94.81	93.69	94.66	94.99	95.43
Number of ions on the bsis of 22 Oxygens															
Si	5.16	2.60	5.65	5.65	5.60	5.56	5.16	5.58	5.56	5.53	5.42	5.57	5.50	5.58	5.61
Al	2.36	2.45	2.44	2.38	2.41	2.48	2.36	2.42	2.43	2.43	2.44	2.41	2.46	2.46	2.46
Fe	2.20	2.18	2.19	2.24	2.22	2.32	2.20	2.23	2.23	2.14	2.24	2.22	2.32	2.17	2.22
Mn	0.00	0.00	0.00	0.00	0.00	0.00	0.00	0.00	0.00	0.00	0.00	0.00	0.01	0.01	0.00
Mg	3.00	2.87	2.90	2.94	2.92	2.78	3.00	2.99	2.89	2.94	2.94	3.10	2.80	2.93	2.89
Ca	0.02	0.00	0.02	0.02	0.02	0.01	0.02	0.02	0.00	0.02	0.27	0.02	0.02	0.00	0.03
Ti	0.53	0.55	0.48	0.51	0.53	0.53	0.53	0.51	0.54	0.58	0.63	0.47	0.58	0.52	0.48
Na	0.10	0.14	0.13	0.14	0.13	0.14	0.10	0.16	0.18	0.17	0.15	0.13	0.12	0.14	0.14
K	1.79	1.76	1.80	1.79	1.79	1.75	1.79	1.75	1.76	1.80	1.44	1.69	1.75	1.80	1.76
Cr	0.00	0.00	0.00	0.00	0.00	0.00	0.00	0.00	0.00	0.00	0.00	0.00	0.00	0.00	0.01
Total	15.16	15.56	15.61	15.67	15.62	15.57	15.16	15.66	15.59	15.61	15.53	15.61	15.56	15.61	15.60

Sample				MM5K.A					MM5K.B					MM17	
Percentage Oxides															
SiO2	36.26	36.50	36.23	37.52	37.22	37.18	37.79	37.72	37.19	37.31	37.32	36.93	36.92	37.13	37.45
Al2O3	13.53	13.43	14.04	13.45	13.23	13.50	13.72	13.65	13.21	13.42	13.31	13.29	13.44	13.03	13.00
FeO	17.88	17.62	17.06	17.08	16.12	16.62	17.14	17.14	17.65	17.09	17.04	16.53	17.34	18.34	18.55
MnO	0.00	0.02	0.02	0.00	0.00	0.06	0.00	0.00	0.08	0.00	0.06	0.00	0.00	0.00	0.00
MgO	12.59	12.38	12.83	13.65	13.08	13.65	14.27	13.81	12.56	13.11	13.32	13.77	13.27	13.02	12.74
CaO	0.16	0.05	0.15	0.09	1.59	0.12	0.12	0.10	0.13	0.11	0.08	0.15	0.17	0.15	0.04
TiO2	4.42	4.40	4.98	4.41	5.81	4.57	4.06	4.08	4.87	4.47	4.26	4.23	4.14	3.71	3.72
Na2O	0.26	0.40	0.43	0.43	0.47	0.47	0.56	0.79	0.49	0.48	0.45	0.45	0.53	0.41	0.48
K2O	8.65	9.01	9.10	9.38	8.70	9.10	9.02	9.36	9.23	9.43	9.27	9.21	9.33	8.83	9.10
Cr2O3	0.09	0.03	0.01	0.03	0.19	0.00	0.00	0.10	0.00	0.02	0.00	0.00	0.00	0.00	0.00
Total	93.84	93.84	94.85	96.04	96.41	95.27	96.68	96.75	95.41	95.44	95.11	94.56	95.14	94.62	95.08
Number of ions on the bsis of 22 Oxygens															
Si	5.58	5.62	5.50	5.63	5.56	5.61	5.63	5.63	5.64	5.65	5.66	5.62	5.61	5.68	5.72
Al	2.45	2.44	2.51	2.38	2.33	2.40	2.41	2.40	2.36	2.40	2.38	2.37	2.41	2.35	2.34
Fe	2.30	2.27	2.17	2.14	2.01	2.10	2.13	2.14	2.24	2.16	2.16	2.11	2.20	2.35	2.37
Mn	0.00	0.00	0.00	0.00	0.00	0.00	0.00	0.00	0.01	0.00	0.00	0.00	0.00	0.00	0.00
Mg	2.89	2.84	2.90	3.05	2.91	3.07	3.17	3.07	2.84	2.96	3.01	3.13	3.00	2.97	2.90
Ca	0.03	0.00	0.02	0.01	0.25	0.02	0.02	0.02	0.02	0.02	0.01	0.02	0.03	0.02	0.00
Ti	0.51	0.51	0.57	0.49	0.65	0.52	0.45	0.46	0.56	0.51	0.48	0.48	0.47	0.43	0.43
Na	0.08	0.12	0.12	0.12	0.13	0.14	0.16	0.23	0.14	0.14	0.13	0.13	0.16	0.12	0.14
K	1.70	1.77	1.76	1.80	1.66	1.75	1.71	1.78	1.78	1.82	1.79	1.79	1.81	1.72	1.77
Cr	0.01	0.00	0.00	0.00	0.11	0.00	0.00	0.01	0.00	0.00	0.00	0.00	0.00	0.00	0.00
Total	15.55	15.57	15.55	15.62	15.61	15.61	15.68	15.74	15.59	15.66	15.62	15.65	15.69	15.64	15.67

Sample															
Percentage Oxides															
SiO2	37.96	36.97	37.14	37.90	38.09	37.28	36.87	36.93	37.42	36.98	37.59	37.32	36.79	36.84	37.85
Al2O3	12.77	12.72	13.23	12.93	12.92	13.06	13.03	13.14	12.94	13.13	13.25	13.06	12.83	13.04	12.85
FeO	16.63	18.19	18.87	16.82	16.68	17.71	19.03	18.35	17.19	17.38	17.44	17.60	19.02	19.17	17.40
MnO	0.00	0.00	0.00	0.00	0.00	0.00	0.00	0.00	0.00	0.00	0.00	0.00	0.00	0.00	0.00
MgO	14.10	12.76	13.05	14.25	13.83	13.43	12.65	12.71	14.09	13.49	14.12	13.41	12.56	12.39	13.49
CaO	0.09	0.08	0.05	0.20	0.11	0.09	0.18	0.18	0.12	0.15	0.16	0.11	0.13	0.17	0.09
TiO2	4.15	4.06	3.80	3.44	3.84	3.49	3.76	3.73	3.47	3.17	3.29	3.16	3.73	3.97	4.00
Na2O	0.49	0.41	0.46	0.55	0.51	0.52	0.50	0.47	0.54	0.38	0.68	0.54	0.56	0.53	0.48
K2O	8.94	9.22	9.30	9.18	9.16	9.22	9.09	9.09	9.08	9.21	9.25	9.22	9.35	9.10	9.13
Cr2O3	0.02	0.00	0.12	0.00	0.04	0.06	0.03	0.05	0.00	0.00	0.08	0.12	0.00	0.00	0.04
Total	95.15	94.41	96.02	95.57	95.18	94.86	95.14	94.66	94.85	93.89	95.86	94.54	94.97	95.21	95.33
Number of ions on the bsis of 22 Oxygens															
Si	5.72	5.69	5.64	5.72	5.75	5.68	5.65	5.66	5.70	5.69	5.67	5.71	5.65	5.64	5.73
Al	2.27	2.31	2.37	2.30	2.30	2.35	2.35	2.37	2.32	2.38	2.35	2.36	2.32	2.36	2.29
Fe	2.09	2.34	2.39	2.12	2.11	2.26	2.44	2.35	2.19	2.23	2.20	2.25	2.44	2.46	2.20
Mn	0.00	0.00	0.00	0.00	0.00	0.00	0.00	0.00	0.00	0.00	0.00	0.00	0.00	0.00	0.00
Mg	3.17	2.93	2.95	3.21	3.11	3.05	2.89	2.91	3.20	3.09	3.17	3.06	2.88	2.83	3.05
Ca	0.02	0.01	0.00	0.03	0.02	0.01	0.03	0.03	0.02	0.02	0.02	0.02	0.02	0.03	0.01
Ti	0.47	0.47	0.43	0.39	0.44	0.40	0.43	0.43	0.40	0.37	0.37	0.36	0.43	0.46	0.45
Na	0.14	0.12	0.13	0.16	0.15	0.15	0.15	0.14	0.16	0.11	0.20	0.16	0.17	0.16	0.14
K	1.75	1.81	1.80	1.77	1.76	1.79	1.78	1.78	1.76	1.81	1.78	1.80	1.83	1.78	1.76
Cr	0.00	0.00	0.01	0.00	0.00	0.00	0.00	0.00	0.00	0.00	0.01	0.01	0.00	0.00	0.00
Total	15.63	15.68	15.72	15.70	15.64	15.69	15.72	15.67	15.75	15.70	15.77	15.73	15.74	15.72	15.63

Sample			659									
Percentage Oxides												
SiO2	38.18	37.61	36.09	36.48	37.06	37.01	36.76	36.64	37.07	36.50	36.84	39.17
Al2O3	13.17	12.97	13.24	13.42	13.47	13.26	13.36	12.72	13.09	13.42	13.41	13.17
FeO	18.07	16.52	17.99	17.59	17.28	17.08	17.09	17.25	17.43	17.68	17.53	17.50
MnO	0.00	0.00	0.05	0.00	0.04	0.05	0.00	0.00	0.00	0.03	0.00	0.00
MgO	13.37	13.84	12.64	12.80	13.00	13.17	13.37	13.04	13.37	12.87	12.71	12.53
CaO	0.14	0.08	0.12	0.27	0.13	0.19	0.11	0.04	0.11	0.19	0.12	0.13
TiO2	3.82	4.24	4.86	4.51	4.34	4.48	3.72	4.31	4.07	4.66	4.49	5.02
Na2O	0.49	0.47	0.35	0.48	0.46	0.58	0.44	0.42	0.45	0.48	0.52	0.47
K2O	9.24	9.25	9.10	9.16	9.13	9.37	9.12	9.10	9.30	9.12	9.48	9.17
Cr2O3	0.00	0.00	0.00	0.02	0.00	0.03	0.00	0.00	0.06	0.05	0.09	0.03
Total	96.48	94.98	94.96	94.73	94.91	95.22	93.97	93.52	94.95	95.00	95.19	97.19
Number of ions on the basis of 22 Oxygens												
Si	5.72	5.69	5.55	5.58	5.63	5.61	5.65	5.67	5.65	5.56	5.59	5.58
Al	2.33	2.31	2.40	2.42	2.41	2.37	2.42	2.32	2.35	2.41	2.40	2.39
Fe	2.26	2.09	2.31	2.25	2.20	2.17	2.20	2.23	2.22	2.25	2.22	2.26
Mn	0.00	0.00	0.00	0.00	0.00	0.00	0.00	0.00	0.00	0.00	0.00	0.00
Mg	2.99	3.12	2.89	2.92	2.95	2.98	3.06	3.00	3.04	2.92	2.88	2.88
Ca	0.02	0.01	0.02	0.04	0.02	0.03	0.02	0.13	0.02	0.03	0.02	0.02
Ti	0.43	0.48	0.56	0.52	0.50	0.51	0.43	0.50	0.47	0.53	0.51	0.58
Na	0.14	0.14	0.10	0.14	0.14	0.17	0.13	0.13	0.13	0.14	0.15	0.14
K	1.77	1.78	1.78	1.79	1.77	1.81	1.78	1.80	1.81	1.77	1.84	1.80
Cr	0.00	0.00	0.00	0.00	0.00	0.00	0.00	0.00	0.00	0.00	0.01	0.00
Total	15.66	15.62	15.61	15.66	15.62	15.65	15.69	15.78	15.69	15.61	15.62	15.65

Sampl:	MM5E															
Percentage Oxides																
SiO2	62.56	62.71	62.46	64.69	60.45	60.06	62.80	62.60	62.42	57.62	63.16	62.13	63.71	65.47	64.58	64.54
Al2O3	22.97	23.32	23.76	22.35	24.23	24.63	23.43	23.43	23.73	27.09	23.51	23.47	22.48	18.66	18.97	18.82
FeO	0.39	0.19	0.30	0.22	0.16	0.26	0.15	0.22	0.35	0.17	0.23	0.31	0.24	0.10	0.11	0.06
MnO	0.00	0.00	0.00	0.00	0.00	0.00	0.07	0.00	0.00	0.00	0.00	0.11	0.00	0.00	0.01	0.00
MgO	0.00	0.11	0.12	0.00	0.00	0.05	0.01	0.02	0.05	0.00	0.00	0.00	0.00	0.11	0.18	0.04
CaO	4.55	4.79	4.80	3.39	6.13	6.64	4.75	4.82	4.96	9.07	4.68	4.92	3.84	0.09	0.16	0.09
TiO2	0.03	0.02	0.20	0.00	0.05	0.05	0.00	0.03	0.00	0.00	0.00	0.07	0.12	0.07	0.16	0.00
Na2O	8.87	8.84	8.41	9.76	7.95	7.78	8.96	8.81	8.32	6.47	8.81	8.64	9.08	1.11	1.53	1.66
K2O	0.24	0.12	0.49	0.15	0.20	0.12	0.37	0.32	0.38	0.07	0.38	0.31	0.24	15.18	14.39	14.23
Total	99.61	100.10	100.54	100.56	99.17	99.59	100.54	100.25	100.21	100.49	100.71	99.96	99.17	100.79	100.09	99.44
Number of Ions on the basis of 8 Oxygens																
Si	2.79	2.77	2.76	2.84	2.72	2.69	2.77	2.77	2.76	2.57	2.78	2.76	2.83	2.99	2.96	2.97
Al	1.21	1.22	1.24	1.16	1.28	1.31	1.22	1.22	1.24	1.43	1.22	1.24	1.18	1.00	1.02	1.02
Fe	0.01	0.00	0.01	0.01	0.00	0.00	0.00	0.00	0.01	0.00	0.01	0.00	0.01	0.01	0.00	0.00
Mn	0.00	0.00	0.00	0.00	0.00	0.00	0.00	0.00	0.00	0.00	0.00	0.00	0.00	0.00	0.00	0.00
Mg	0.00	0.00	0.00	0.00	0.00	0.00	0.00	0.00	0.00	0.00	0.00	0.00	0.00	0.00	0.01	0.01
Ca	0.22	0.23	0.23	0.16	0.29	0.32	0.22	0.23	0.23	0.43	0.22	0.23	0.18	0.01	0.01	0.00
Ti	0.00	0.00	0.00	0.00	0.00	0.00	0.00	0.00	0.00	0.00	0.00	0.00	0.00	0.00	0.00	0.00
Na	0.77	0.76	0.72	0.83	0.69	0.67	0.77	0.75	0.72	0.56	0.75	0.74	0.78	0.09	0.15	0.15
K	0.01	0.01	0.03	0.01	0.01	0.00	0.02	0.02	0.03	0.00	0.02	0.02	0.01	0.89	0.84	0.84
Total	5.00	4.99	4.99	5.01	4.99	4.99	5.00	4.99	4.99	4.99	5.00	4.99	4.99	4.99	4.99	4.99
Sample			MM5G													
Percentage Oxides																
SiO2	64.88	64.24	64.96	65.36	65.56	65.64	65.90	66.12	66.32	65.70	65.16	66.27	68.23	68.87	66.11	65.66
Al2O3	18.65	18.19	18.37	18.32	18.41	18.60	18.66	18.72	18.77	18.72	18.37	21.05	20.26	19.77	21.41	21.42
FeO	0.17	0.10	0.11	0.17	0.13	0.13	0.12	0.16	0.34	0.14	0.13	0.19	0.09	0.27	0.17	0.27
MnO	0.05	0.00	0.21	0.00	0.00	0.01	0.00	0.00	0.09	0.02	0.00	0.00	0.00	0.08	0.00	0.00
MgO	0.05	0.10	0.10	0.02	0.07	0.06	0.09	0.07	0.00	0.03	0.00	0.03	0.00	0.00	0.00	0.01
CaO	0.35	0.09	0.07	0.10	0.04	0.27	0.15	0.19	0.18	0.27	0.23	1.78	0.98	0.04	2.41	2.42
TiO2	0.14	0.12	0.00	0.00	0.00	0.00	0.00	0.00	0.02	0.00	0.08	0.09	0.04	0.06	0.00	0.00
Na2O	1.40	1.25	0.64	1.95	1.52	2.49	2.12	0.28	4.85	2.18	2.88	10.54	11.17	11.69	10.18	10.16
K2O	14.44	14.93	15.66	13.91	14.69	13.08	13.54	0.71	10.00	13.71	12.54	0.09	0.04	0.09	0.25	0.20
Total	100.13	99.04	100.12	99.83	100.42	100.29	100.58	5.00	100.57	100.77	99.39	100.06	100.81	100.87	100.53	100.14
Number of Ions on the basis of 8 Oxygens																
Si	2.98	2.99	2.99	3.00	3.00	3.00	3.00	3.00	2.99	2.99	2.99	2.92	2.97	2.99	2.90	2.88
Al	1.01	0.99	1.00	0.99	0.99	1.00	1.00	1.00	1.00	1.00	0.99	1.09	1.04	1.01	1.11	1.11
Fe	0.00	0.00	0.00	0.00	0.00	0.01	0.00	0.00	0.01	0.00	0.00	0.00	0.00	0.00	0.00	0.01
Mn	0.00	0.00	0.00	0.00	0.00	0.00	0.00	0.00	0.00	0.00	0.00	0.00	0.00	0.00	0.00	0.00
Mg	0.00	0.00	0.00	0.00	0.00	0.00	0.00	0.00	0.00	0.00	0.00	0.00	0.00	0.00	0.00	0.00
Ca	0.02	0.00	0.00	0.00	0.00	0.01	0.00	0.00	0.00	0.01	0.01	0.08	0.04	0.00	0.11	0.11
Ti	0.00	0.00	0.00	0.00	0.00	0.00	0.00	0.00	0.00	0.00	0.00	0.00	0.00	0.00	0.00	0.00
Na	0.13	10.12	0.07	0.18	0.14	0.22	0.19	0.28	0.42	0.19	0.26	0.90	0.94	0.98	0.86	0.87
K	0.85	0.89	0.92	0.82	0.86	0.76	0.79	0.71	0.58	0.80	0.73	0.00	0.00	0.01	0.01	0.01
Total	4.99	4.99	4.99	4.99	4.99	5.00	4.99	4.99	5.00	4.99	5.00	4.99	4.99	4.99	4.99	4.99

Microprobe analyses of igneous feldspars

Sample	MM5H															
Percentage Oxides																
SiO2	64.97	61.25	62.32	64.44	65.19	61.99	60.89	63.66	62.59	61.06	62.64	62.75	60.33	65.05	62.60	65.07
Al2O3	18.40	24.32	23.54	21.97	22.16	23.87	24.46	22.44	23.32	23.93	23.66	23.77	24.54	18.43	23.04	18.77
FeO	0.17	0.13	0.11	0.34	0.16	0.26	0.17	0.23	0.16	0.33	0.22	0.16	0.20	0.20	0.16	0.09
MnO	0.00	0.03	0.03	0.01	0.00	0.03	0.12	0.00	0.00	0.01	0.00	0.07	0.11	0.00	0.16	0.00
MgO	0.04	0.00	0.00	0.00	0.00	0.00	0.19	0.06	0.00	0.00	0.00	0.07	0.06	0.20	0.00	0.17
CaO	0.07	5.89	4.88	3.28	2.94	5.38	5.99	3.92	4.69	5.65	4.86	5.02	6.35	0.06	4.63	0.15
TiO2	0.02	0.06	0.00	0.00	0.02	0.00	0.00	0.05	0.00	0.13	0.00	0.08	0.11	0.00	0.06	0.00
Na2O	1.01	7.96	8.69	9.53	9.62	8.38	7.88	9.04	8.66	8.14	8.68	8.69	7.73	1.10	8.78	1.19
K2O	15.29	0.24	0.20	0.32	0.20	0.26	0.28	0.43	0.24	0.30	0.18	0.17	0.22	15.08	0.15	15.07
Total	99.97	99.88	99.77	99.89	100.29	100.17	99.98	99.83	99.66	99.55	100.24	100.78	99.65	100.12	99.56	100.51
Number of Ions on the basis of 8 Oxygens																
Si	3.00	2.73	2.77	2.85	2.86	2.73	2.71	2.82	2.78	2.73	2.77	2.76	2.70	2.99	2.79	2.98
Al	1.00	1.27	1.23	1.15	1.15	1.18	1.29	1.17	1.22	1.26	1.23	1.23	1.29	1.00	1.21	1.02
Fe	0.00	0.00	0.00	0.01	0.00	0.00	0.00	0.00	0.00	0.01	0.00	0.01	0.00	0.00	0.00	0.00
Mn	0.00	0.00	0.00	0.00	0.00	0.00	0.00	0.00	0.00	0.00	0.00	0.00	0.00	0.00	0.00	0.00
Mg	0.00	0.00	0.00	0.00	0.00	0.25	0.01	0.00	0.00	0.00	0.00	0.00	0.00	0.01	0.00	0.01
Ca	0.00	0.28	0.23	0.15	0.14	0.11	0.28	0.19	0.23	0.27	0.23	0.24	0.31	0.01	0.22	0.00
Ti	0.00	0.00	0.00	0.00	0.00	0.72	0.00	0.00	0.00	0.00	0.00	0.00	0.00	0.00	0.00	0.00
Na	0.09	0.69	0.75	0.82	0.82	0.01	0.69	0.78	0.75	0.71	0.75	0.75	0.67	0.09	0.76	0.10
K	0.90	0.02	0.01	0.02	0.02	0.00	0.01	0.03	0.01	0.02	0.01	0.00	0.02	0.89	0.00	0.88
Total	4.99	4.99	4.99	5.00	4.99	5.00	4.99	4.99	4.99	5.00	4.99	4.99	4.99	4.99	4.99	4.99
Sample							MM17									
Percentage Oxides																
SiO2	64.55	62.15	61.82	62.35	64.38	65.03	64.49	64.19	63.78	63.98	64.92	64.28	64.99	64.63	64.49	64.12
Al2O3	19.02	23.47	23.33	24.17	18.57	18.84	18.67	18.91	18.96	19.05	18.81	19.51	18.77	19.31	19.98	19.30
FeO	0.15	0.22	0.43	0.19	0.07	0.22	0.00	0.12	0.30	0.17	0.09	0.26	0.25	0.46	0.28	0.28
MnO	0.00	0.00	0.00	0.00	0.07	0.00	0.00	0.03	0.00	0.00	0.00	0.05	0.04	0.00	0.00	0.14
MgO	0.09	0.00	0.00	0.10	0.11	0.08	0.13	0.06	0.06	0.23	0.00	0.13	0.13	0.11	0.08	0.20
CaO	0.14	4.97	5.08	5.35	0.10	0.29	0.21	0.47	0.60	0.46	0.42	0.72	0.19	0.60	1.24	0.60
TiO2	0.04	0.00	0.00	0.02	0.00	0.65	0.17	0.48	0.47	0.49	0.34	0.58	0.33	0.56	0.39	0.58
Na2O	2.09	8.60	8.39	8.50	1.35	3.08	1.17	2.05	2.29	1.96	2.52	2.83	2.05	3.19	3.79	3.06
K2O	13.31	0.07	0.52	0.30	14.45	11.83	14.68	12.86	12.73	13.12	12.48	11.87	13.27	11.06	9.81	11.23
Total	99.39	99.48	99.57	100.98	99.10	100.02	99.52	99.18	99.19	99.46	99.58	100.23	100.02	99.92	100.06	99.51
Number of Ions on the basis of 8 Oxygens																
Si	2.98	2.77	2.76	2.74	2.98	2.96	2.98	2.96	2.95	2.95	2.98	2.94	2.97	2.95	2.92	2.94
Al	1.03	1.24	1.23	1.25	1.02	1.02	1.02	1.03	0.01	1.03	1.02	1.05	1.01	1.04	1.07	1.04
Fe	0.00	0.00	0.02	0.00	0.00	0.01	0.00	0.00	1.03	0.00	0.00	0.01	0.00	0.02	0.01	0.01
Mn	0.00	0.00	0.00	0.00	0.00	0.00	0.00	0.00	0.00	0.00	0.00	0.00	0.00	0.00	0.00	0.00
Mg	0.00	0.00	0.00	0.00	0.00	0.00	0.01	0.00	0.00	0.02	0.00	0.00	0.00	0.00	0.00	0.01
Ca	0.01	0.24	0.24	0.25	0.00	0.02	0.01	0.02	0.03	0.02	0.02	0.03	0.00	0.03	0.06	0.03
Ti	0.00	0.00	0.00	0.00	0.00	0.02	0.00	0.02	0.02	0.02	0.01	0.02	0.01	0.02	0.01	0.02
Na	0.19	0.74	0.73	0.73	0.13	0.27	0.10	0.18	0.21	0.17	0.22	0.25	0.18	0.28	0.33	0.27
K	0.78	0.00	0.03	0.02	0.85	0.68	0.86	0.76	0.75	0.77	0.73	0.69	0.78	0.64	0.57	0.66
Total	4.99	4.99	5.01	4.99	4.98	4.98	4.98	4.98	5.00	4.98	4.98	4.99	4.98	4.98	4.98	4.98

Microprobe analyses of igneous feldspars

Sample	MM17															
Percentage Oxides																
SiO2	62.14	62.14	61.41	58.61	55.70	62.33	61.80	58.67	61.80	60.81	55.13	62.60	57.63	62.78	57.12	61.82
Al2O3	23.42	23.73	23.63	25.36	27.35	23.46	23.93	25.86	23.65	0.28	28.09	23.54	26.43	24.13	26.49	24.04
FeO	0.26	0.41	0.35	0.39	0.31	0.26	0.23	0.28	0.47	25.06	0.52	0.32	0.40	0.29	0.49	0.38
MnO	0.00	0.00	0.02	0.00	0.00	0.00	0.08	0.02	0.00	0.00	0.09	0.00	0.00	0.00	0.12	0.00
MgO	0.02	0.02	0.00	0.00	0.16	0.00	0.00	0.15	0.00	0.00	0.01	0.02	0.09	0.00	0.04	0.17
CaO	5.02	5.09	5.42	7.23	9.86	4.90	5.12	7.55	5.16	6.11	10.74	4.88	8.28	5.02	8.60	5.16
TiO2	0.11	0.12	0.05	0.00	0.01	0.10	0.11	0.08	0.16	0.14	0.11	0.00	0.08	0.11	0.19	0.06
Na2O	8.31	8.64	8.38	7.28	6.05	8.71	8.62	7.26	8.27	7.75	5.56	8.71	6.69	8.51	6.48	8.60
K2O	0.42	0.26	0.26	0.25	0.12	0.20	0.22	0.21	0.25	0.19	0.13	0.28	0.15	0.23	0.17	0.28
Total	99.70	100.41	99.52	99.12	99.56	99.96	100.11	100.08	99.76	100.34	100.38	100.35	99.75	101.07	99.70	100.51
Number of Ions on the basis of 8 Oxygens																
Si	2.76	2.75	2.74	2.64	2.52	2.76	2.74	2.62	2.76	2.69	2.48	2.77	2.59	2.75	2.57	2.73
Al	1.23	1.24	1.24	1.35	1.46	1.23	1.25	1.36	1.24	1.31	1.49	1.23	1.40	1.24	1.40	1.25
Fe	0.01	0.01	0.01	0.01	0.01	0.01	0.00	0.01	0.02	0.01	0.02	0.01	0.01	0.01	0.02	0.01
Mn	0.00	0.00	0.00	0.00	0.00	0.00	0.00	0.00	0.00	0.00	0.00	0.00	0.00	0.00	0.00	0.00
Mg	0.00	0.00	0.00	0.00	0.01	0.00	0.00	0.01	0.00	0.00	0.00	0.00	0.00	0.00	0.00	0.01
Ca	0.24	0.24	0.26	0.35	0.48	0.23	0.24	0.36	0.25	0.29	0.52	0.23	0.40	0.24	0.41	0.24
Ti	0.00	0.00	0.00	0.00	0.00	0.00	0.00	0.00	0.00	0.00	0.00	0.00	0.00	0.00	0.00	0.00
Na	0.72	0.74	0.73	0.64	0.53	0.75	0.74	0.01	0.71	0.67	0.48	0.75	0.58	0.72	0.56	0.74
K	0.02	0.01	0.01	0.01	0.00	0.01	0.01	0.63	0.01	0.01	0.00	0.02	0.01	0.01	0.01	0.02
Total	4.98	4.99	4.99	5.00	5.01	4.99	4.98	5.00	4.99	4.98	4.99	5.01	4.99	4.98	4.98	5.00
Sample		MM5K.A														
Percentage Oxides																
SiO2	55.23	64.64	64.46	63.28	63.00	63.31	63.54	64.37	63.85	62.53	62.94	59.57	64.35	65.05	65.22	64.70
Al2O3	27.53	18.97	19.21	22.86	23.02	23.12	23.22	18.75	22.61	23.41	23.20	25.54	18.52	19.43	18.61	19.19
FeO	0.49	0.00	0.18	0.43	0.30	0.18	0.17	0.29	0.21	0.12	0.25	0.15	0.11	0.19	0.21	0.10
MnO	0.00	0.15	0.00	0.01	0.00	0.04	0.00	0.00	0.00	0.14	0.00	0.00	0.01	0.05	0.05	0.00
MgO	0.00	0.18	0.23	0.00	0.00	0.00	0.09	0.04	0.00	0.04	0.00	0.06	0.18	0.16	0.06	0.09
CaO	9.93	0.11	0.19	4.27	4.29	4.62	4.29	0.17	4.09	4.75	4.58	7.27	0.32	0.21	0.10	0.20
TiO2	0.09	0.00	0.18	0.08	0.02	0.00	0.09	0.27	0.13	0.00	0.05	0.03	0.08	0.26	0.00	0.17
Na2O	5.75	2.35	2.13	9.04	8.72	8.85	9.01	2.09	8.78	8.68	8.72	7.44	1.23	3.23	2.37	2.84
K2O	0.31	12.66	13.03	0.47	0.50	0.23	0.43	13.14	0.56	0.09	0.47	0.13	14.42	11.27	13.24	11.68
Total	99.33	99.06	99.61	100.44	99.85	100.35	100.84	99.12	100.23	99.76	100.21	100.19	99.22	99.85	99.86	98.97
Number of Ions on the basis of 8 Oxygens																
Si	2.51	2.97	2.95	2.79	2.79	2.79	2.79	2.97	2.82	2.77	2.78	2.65	2.98	2.96	2.99	2.97
Al	1.47	1.03	1.05	1.19	1.21	1.20	1.20	1.02	1.19	1.23	1.21	1.34	1.01	1.05	1.00	1.04
Fe	0.02	0.00	0.00	0.02	0.01	0.00	0.00	0.01	0.00	0.00	0.00	0.00	0.00	0.00	0.00	0.00
Mn	0.00	0.00	0.00	0.00	0.00	0.00	0.00	0.00	0.00	0.00	0.00	0.00	0.00	0.00	0.00	0.00
Mg	0.00	0.01	0.02	0.00	0.00	0.00	0.00	0.00	0.00	0.00	0.00	0.00	0.01	0.01	0.00	0.00
Ca	0.48	0.00	0.00	0.20	0.20	0.22	0.20	0.00	0.19	0.22	0.22	0.35	0.02	0.01	0.00	0.01
Ti	0.00	0.00	0.00	0.00	0.00	0.00	0.00	0.00	0.00	0.00	0.00	0.00	0.00	0.00	0.00	0.00
Na	0.51	0.22	0.19	0.77	0.75	0.76	0.77	0.19	0.75	0.75	0.75	0.64	0.11	0.29	0.21	0.26
K	0.02	0.75	0.76	0.03	0.03	0.01	0.02	0.78	0.03	0.00	0.03	0.00	0.85	0.65	0.77	0.69
Total	5.01	4.98	4.97	5.00	4.98	4.98	4.98	4.98	4.98	4.97	4.99	4.98	4.98	4.97	4.98	4.96

Sample MM5K.B											D659					
Percentage Oxides																
SiO2	59.42	60.34	60.72	62.23	65.29	62.92	62.07	62.75	62.97	62.30	61.30	61.61	53.87	54.46	60.99	57.14
Al2O3	25.29	24.92	24.62	23.45	18.74	23.17	23.46	23.14	22.94	23.60	24.13	24.53	29.11	28.84	24.38	27.03
FeO	0.31	0.17	0.21	0.27	0.20	0.26	0.20	0.31	0.37	0.30	0.17	0.18	0.26	0.26	0.22	0.08
MnO	0.00	0.00	0.08	0.00	0.00	0.02	0.00	0.00	0.06	0.00	0.02	0.00	0.00	0.00	0.04	0.01
MgO	0.04	0.00	0.00	0.00	0.15	0.00	0.11	0.00	0.00	0.00	0.04	0.15	0.16	0.15	0.00	0.02
CaO	7.05	6.62	6.16	4.60	0.19	4.55	5.14	4.47	4.32	4.91	5.63	5.69	11.34	10.94	5.97	8.92
TiO2	0.00	0.00	0.14	0.00	0.00	0.00	0.00	0.06	0.00	0.00	0.00	0.10	0.06	0.14	0.06	0.05
Na2O	7.39	7.77	7.75	8.87	1.74	8.91	8.51	8.89	8.98	8.56	8.18	8.65	4.89	5.09	8.07	6.20
K2O	0.22	0.18	0.33	0.21	14.47	0.26	0.20	0.22	0.17	0.21	0.20	0.19	0.02	0.20	0.32	0.16
Total	99.72	100.00	100.01	99.63	100.78	100.09	99.69	99.84	99.81	99.88	99.67	101.10	99.65	100.08	100.05	99.51
Number of Ions on the basis of 8 Oxygens																
Si	2.66	2.69	2.70	2.77	2.98	2.78	2.76	2.78	2.78	2.77	2.73	2.72	2.44	2.45	2.71	2.57
Al	1.33	1.31	1.29	1.23	1.00	1.21	1.23	1.21	1.20	1.24	1.27	1.27	1.55	1.53	1.28	1.43
Fe	0.01	0.00	0.00	0.01	0.00	0.01	0.00	0.01	0.01	0.01	0.00	0.00	0.01	0.01	0.00	0.00
Mn	0.00	0.00	0.00	0.00	0.00	0.00	0.00	0.00	0.00	0.00	0.00	0.00	0.00	0.00	0.00	0.00
Mg	0.00	0.00	0.00	0.00	0.01	0.00	0.00	0.00	0.00	0.00	0.00	0.01	0.01	0.01	0.00	0.00
Ca	0.34	0.32	0.29	0.22	0.01	0.22	0.24	0.21	0.20	0.23	0.27	0.27	0.55	0.53	0.28	0.43
Ti	0.00	0.00	0.00	0.00	0.00	0.00	0.00	0.00	0.00	0.00	0.00	0.00	0.00	0.00	0.00	0.00
Na	0.64	0.67	0.70	0.76	0.13	0.76	0.74	0.76	0.77	0.74	0.71	0.74	0.43	0.44	0.70	0.54
K	0.01	0.01	0.02	0.01	0.84	0.01	0.02	0.01	0.01	0.01	0.01	0.01	0.01	0.01	0.02	0.01
Total	4.99	5.00	5.00	5.00	4.97	4.99	4.97	4.98	4.97	5.00	4.99	5.02	5.00	4.98	4.99	4.98

Sample										
Percentage Oxides										
SiO2	61.73	58.37	61.73	56.68	62.43	53.78	59.78	53.78	61.68	53.54
Al2O3	23.77	26.69	24.45	27.31	23.36	29.39	25.62	29.21	23.93	29.33
FeO	0.09	0.16	0.13	0.34	0.10	0.18	0.17	0.09	0.20	0.11
MnO	0.00	0.00	0.14	0.00	0.00	0.00	0.00	0.00	0.06	0.00
MgO	0.00	0.03	0.00	0.04	0.00	0.02	0.02	0.21	0.00	0.04
CaO	5.30	8.40	5.75	9.45	4.80	11.89	6.92	11.70	5.53	11.66
TiO2	0.08	0.00	0.00	0.10	0.07	0.17	0.00	0.10	0.03	0.02
Na2O	8.43	6.73	8.10	6.04	0.29	4.72	7.41	5.00	8.19	4.70
K2O	0.29	0.17	0.30	0.18	0.10	0.15	0.22	0.11	0.32	0.17
Total	99.69	100.55	100.60	100.14	99.15	100.30	100.14	100.20	99.94	99.57
Number of Ions on the basis of 8 Oxygens										
Si	2.75	2.60	2.73	2.55	2.78	2.42	2.66	2.43	2.74	2.43
Al	1.25	1.40	1.27	1.45	1.22	1.56	0.00	1.55	1.25	1.57
Fe	0.00	0.00	0.00	0.01	0.00	0.00	1.34	0.00	0.00	0.00
Mn	0.00	0.00	0.00	0.00	0.00	0.00	0.00	0.00	0.00	0.00
Mg	0.00	0.00	0.00	0.00	0.00	0.00	0.00	0.01	0.00	0.00
Ca	0.25	0.40	0.27	0.45	0.23	0.57	0.33	0.57	0.26	0.57
Ti	0.00	0.00	0.00	0.00	0.00	0.00	0.00	0.00	0.00	0.00
Na	0.73	0.58	0.69	0.53	0.75	0.41	0.64	0.44	0.71	0.41
K	0.02	0.01	0.02	0.01	0.02	0.01	0.01	0.00	0.02	0.01
Total	5.00	4.99	4.98	5.00	5.00	4.97	4.98	5.00	4.98	4.99

Microprobe analyses of igneous orthopyroxene

Sample: MM17									
Oxides Percentage									
SiO2	52.73	52.46	52.40	53.24	52.78	52.34	52.03	52.03	52.77
TiO2	0.23	0.19	0.26	0.29	0.40	0.42	0.27	0.27	0.29
Al2O3	0.93	0.89	0.90	0.66	1.25	0.81	0.98	0.98	0.83
Cr2O3	0.07	0.15	0.05	0.05	0.00	0.14	0.13	0.13	0.07
Fe2O3	2.81	3.03	2.07	1.68	2.04	2.98	3.49	3.49	2.28
FeO	19.20	19.29	19.41	19.56	20.11	18.65	18.69	18.69	19.96
MnO	0.09	0.15	0.23	0.29	0.18	0.15	0.18	0.18	0.12
MgO	22.20	22.13	21.91	22.43	21.94	22.41	21.95	21.95	22.01
CaO	1.40	1.39	1.40	1.16	1.36	1.45	1.44	1.44	1.37
ZnO	0.16	0.00	0.19	0.00	0.06	0.25	0.00	0.00	0.12
Na2O	0.51	0.48	0.48	0.56	0.49	0.46	0.51	0.51	0.47
K2O	0.03	0.00	0.00	0.00	0.00	0.00	0.08	0.08	0.00
Total	100.36	100.16	99.31	99.93	100.61	100.70	99.76	99.76	100.30
Number of Ions on the basis of 6 Oxygens									
SiO2	1.95	1.95	1.96	1.97	1.95	1.94	1.94	1.94	1.96
TiO2	0.00	0.00	0.00	0.00	0.01	0.01	0.00	0.00	0.00
Al2O3	0.04	0.04	0.04	0.03	0.05	0.03	0.04	0.04	0.04
Cr2O3	0.00	0.00	0.00	0.00	0.00	0.00	0.00	0.00	0.00
Fe3+	0.08	0.08	0.06	0.05	0.06	0.08	0.10	0.10	0.06
Fe2+	0.59	0.60	0.61	0.61	0.62	0.58	0.58	0.58	0.62
MnO	0.00	0.00	0.00	0.01	0.00	0.00	0.00	0.00	0.00
MgO	1.22	1.22	1.22	1.24	1.21	1.24	1.22	1.22	1.22
CaO	0.06	0.05	0.06	0.05	0.05	0.06	0.06	0.06	0.05
ZnO	0.00	0.00	0.00	0.00	0.00	0.00	0.00	0.00	0.00
Na2O	0.04	0.03	0.04	0.04	0.03	0.03	0.04	0.04	0.03
K2O	0.00	0.00	0.00	0.00	0.00	0.00	0.00	0.00	0.00
Total	4.00	4.00	4.00	4.00	4.00	4.00	4.00	4.00	4.00

Microprobe analyses of igneous clinopyroxenes

Sample: MM17								D659							
Oxides Percentage															
SiO2	55.30	51.97	52.17	51.81	52.89	51.92	51.41	53.75	53.72	53.98	53.41	53.42	54.01	54.05	53.89
TiO2	0.42	0.36	75.00	0.56	0.40	0.55	0.68	0.15	0.24	0.14	0.22	0.22	0.23	0.21	0.17
Al2O3	1.51	1.27	1.88	1.65	1.32	1.49	1.78	0.83	0.74	0.90	0.87	0.95	0.84	0.94	0.85
Cr2O3	0.04	0.28	0.14	0.08	0.07	0.10	0.18	0.03	0.06	0.04	0.08	0.01	0.13	0.03	0.07
Fe2O3	0.00	4.77	4.00	3.14	2.39	2.49	2.39	1.13	2.38	0.62	2.38	3.19	1.26	1.63	1.87
FeO	9.76	4.95	7.28	8.04	7.93	7.98	8.16	7.65	5.91	7.53	6.17	5.58	6.73	6.61	6.28
MnO	0.16	0.00	0.02	0.12	0.23	0.05	0.00	0.35	0.45	0.31	0.48	0.60	0.53	0.51	0.53
MgO	12.83	15.04	14.15	13.78	14.23	14.06	13.76	13.52	13.63	14.08	13.86	14.58	14.73	14.66	14.43
CaO	19.58	21.43	20.13	20.31	20.82	20.32	20.19	22.44	22.97	22.45	22.91	21.94	21.76	21.63	22.28
ZnO	0.03	0.00	0.17	0.05	0.12	0.20	0.00	0.13	0.00	0.00	0.08	0.09	0.10	0.00	0.03
Na2O	0.79	0.70	0.99	0.79	0.69	0.70	0.76	0.74	0.94	0.64	0.70	0.80	0.71	0.83	0.75
K2O	0.00	0.00	0.00	0.00	0.03	0.01	0.00	0.00	0.00	0.00	0.01	0.00	0.00	0.00	0.00
Total	100.42	100.78	101.68	100.33	101.12	99.87	99.32	100.72	101.04	100.69	101.17	101.38	101.04	101.10	101.16
Number of ions on the basis of 6 Oxygens															
SiO2	2.06	1.92	1.92	1.93	1.95	1.94	1.93	2.00	1.98	1.99	1.97	1.96	1.98	1.98	1.98
TiO2	0.01	0.01	0.02	0.02	0.01	0.01	0.02	0.00	0.00	0.00	0.00	0.00	0.00	0.00	0.00
Al2O3	0.07	0.05	0.08	0.07	0.06	0.07	0.08	0.04	0.03	0.04	0.04	0.04	0.04	0.04	0.04
Cr2O3	0.00	0.00	0.00	0.00	0.00	0.00	0.00	0.00	0.00	0.00	0.00	0.00	0.00	0.00	0.00
Fe3+	0.00	0.13	0.11	0.09	0.07	0.07	0.07	0.03	0.07	0.02	0.07	0.09	0.03	0.04	0.05
Fe2+	0.30	0.15	0.22	0.25	0.24	0.25	0.26	0.24	0.18	0.23	0.19	0.17	0.21	0.20	0.19
MnO	0.00	0.00	0.00	0.00	0.00	0.00	0.00	0.01	0.01	0.01	0.01	0.02	0.02	0.02	0.02
MgO	0.71	0.83	0.77	0.77	0.78	0.78	0.77	0.74	0.75	0.77	0.76	0.80	0.81	0.80	0.80
CaO	0.78	0.85	0.79	0.81	0.82	0.81	0.81	0.90	0.91	0.89	0.90	0.86	0.85	0.85	0.88
ZnO	0.00	0.00	0.00	0.00	0.00	0.00	0.00	0.00	0.00	0.00	0.00	0.00	0.00	0.00	0.00
Na2O	0.06	0.05	0.07	0.06	0.05	0.05	0.05	0.05	0.07	0.05	0.05	0.06	0.05	0.06	0.05
K2O	0.00	0.00	0.00	0.00	0.00	0.00	0.00	0.00	0.00	0.00	0.00	0.00	0.00	0.00	0.00
Total	4.00	4.00	4.00	4.00	4.00	4.00	4.00	4.00	4.00	4.00	4.00	4.00	4.00	4.00	4.00

Appendix 5
Microprobe results of metamorphic minerals

Microprobe results from biotites in metabasites

Sample	MM166A							MM166B								
Oxides Percentage																
SiO2	38.21	37.34	38.29	38.15	36.82	38.00	37.94	38.03	37.85	37.76	37.65	37.27	37.39	38.02	37.61	37.52
TiO2	4.00	4.24	4.27	4.40	3.62	4.49	4.28	5.41	5.39	5.51	5.42	5.55	5.03	5.18	5.17	5.71
Al2O3	14.44	14.16	14.41	14.60	14.86	14.40	14.68	14.02	14.05	13.93	14.03	13.72	14.25	14.09	13.66	13.51
Cr2O3	0.33	0.41	0.11	0.54	0.25	0.33	0.34	0.34	0.39	0.38	0.58	0.34	0.49	0.38	0.43	0.49
FeO	11.09	11.35	11.36	11.84	13.81	11.78	11.84	13.24	13.25	13.30	13.22	13.07	13.19	13.22	13.74	13.25
MnO	0.00	0.00	0.00	0.00	0.00	0.00	0.00	0.00	0.00	0.00	0.00	0.00	0.00	0.00	0.00	0
MgO	17.38	16.60	17.00	16.75	16.47	16.67	16.76	15.42	15.49	15.35	15.25	14.98	15.23	15.56	14.83	15.21
CaO	0.06	0.15	0.09	0.13	0.14	0.09	0.19	0.04	0.12	0.18	0.18	0.07	0.14	0.12	0.05	0.08
Na2O	0.73	0.65	0.60	0.71	0.62	0.53	0.67	0.38	0.37	0.48	0.42	0.28	0.44	0.52	0.48	0.48
K2O	8.79	8.73	8.75	8.74	7.63	8.85	8.76	9.09	9.15	8.99	9.06	9.17	8.99	9.02	9.09	9.22
Total	95.05	93.43	94.70	95.86	94.23	95.17	95.48	95.98	95.92	95.04	95.72	94.46	95.16	96.11	95.60	95.47
Cation on the basis of 22 Oxygens																
SI	5.60	5.59	5.63	5.58	5.50	5.59	5.58	5.59	6.08	5.56	5.56	5.58	5.55	5.59	5.58	5.57
TI	0.44	0.48	0.47	0.48	0.41	0.50	0.47	0.59	0.65	0.61	0.60	0.62	0.56	0.27	0.64	0.64
AI	2.49	2.50	2.50	2.52	2.62	2.49	2.54	2.43	2.66	2.42	2.44	2.42	2.49	2.44	2.39	2.36
Cr	0.04	0.05	0.01	0.06	0.03	0.04	0.04	0.04	0.05	0.04	0.07	0.04	0.06	0.04	0.05	0.06
Fe	1.36	1.42	1.40	1.45	1.73	1.45	1.46	1.63	1.78	1.64	1.63	1.64	1.64	1.63	1.71	1.64
Mn	0.00	0.00	0.00	0.00	0.00	0.00	0.00	0.00	0.00	0.00	0.00	0.00	0.00	0.00	0.00	0
Mg	3.78	3.70	3.73	3.65	3.70	3.56	3.68	3.38	3.71	3.37	3.36	3.35	3.37	3.41	3.28	3.36
Ca	0.01	0.02	0.01	0.02	0.02	0.01	0.03	0.00	0.02	0.03	0.03	0.01	0.02	0.02	0.00	0.01
Na	0.21	0.19	0.17	0.20	0.18	0.15	0.19	0.11	0.12	0.14	0.12	0.08	0.13	0.15	0.14	0.14
K	1.64	1.67	1.64	1.63	1.46	1.66	1.64	1.70	1.87	1.69	1.71	1.75	1.70	1.69	1.72	1.75
Total	15.59	15.62	15.57	15.59	15.61	15.55	15.64	15.47	15.52	15.50	15.49	15.49	15.52	15.24	15.51	15.53
Sample		MM165						MM198B						MM141B		
Oxides Percentage																
SIO2	37.84	36.09	35.89	36.25	36.87	36.49	37.44	35.89	35.89	35.93	35.82	35.83	36.03	35.76	34.78	36.43
TiO2	5.85	5.10	4.92	4.39	5.12	5.06	3.33	5.20	6.32	6.20	5.39	5.40	5.32	5.17	4.48	6.06
Al2O3	13.99	13.89	13.75	13.84	13.96	14.11	13.14	13.74	13.57	13.47	13.58	13.72	13.65	13.86	14.09	13.59
Cr2O3	0.33	0.23	0.27	0.02	0.12	0.17	0.02	0.11	0.18	0.20	0.05	0.21	0.15	0.09	0.16	0.41
FeO	13.74	17.08	17.18	17.49	17.89	18.07	16.46	20.53	20.02	19.93	20.14	19.96	20.06	19.13	19.70	16.99
MnO	0.00	0.00	0.00	0.00	0.00	0.00	0.00	0.00	0.00	0.00	0.00	0.00	0.00	0.00	0.00	0
MgO	15.17	12.39	12.58	12.48	12.42	12.42	14.13	10.87	10.50	10.60	10.74	11.21	11.10	11.42	12.47	12.33
CaO	0.03	0.18	0.11	0.20	0.12	0.18	0.12	0.15	0.09	0.07	0.09	0.12	0.06	0.19	0.18	0.21
Na2O	0.50	0.36	0.53	0.36	0.31	0.52	0.52	0.33	0.24	0.27	0.36	0.52	0.41	0.54	0.60	0.57
K2O	8.97	8.95	9.17	8.65	9.14	9.21	8.58	9.14	9.31	9.20	9.15	8.94	8.89	8.12	6.89	8.45
Total	96.43	94.17	94.42	93.68	95.95	96.23	93.75	95.98	96.12	95.88	95.34	95.91	95.67	94.27	93.37	95.03
Cation on the basis of 22 Oxygens																
SI	5.55	5.53	5.51	5.60	5.57	5.51	5.72	5.50	5.48	5.51	5.52	5.49	5.52	5.51	5.41	5.52
TI	0.64	0.59	0.57	0.51	0.58	0.58	0.38	0.60	0.73	0.71	0.63	0.62	0.61	0.60	0.52	0.69
AI	2.42	2.51	2.49	2.52	2.48	2.51	2.37	2.48	2.44	2.43	2.47	2.48	2.46	2.52	2.58	2.43
Cr	0.04	0.02	0.03	0.00	0.01	0.02	0.00	0.01	0.02	0.02	0.00	0.02	0.02	0.01	0.01	0.05
Fe	1.68	2.19	2.20	2.26	2.26	2.28	2.10	2.63	2.56	2.56	2.60	2.56	2.57	2.47	2.56	2.16
Mn	0.00	0.00	0.00	0.00	0.00	0.00	0.00	0.00	0.00	0.00	0.00	0.00	0.00	0.00	0.00	0
Mg	3.32	2.83	2.88	2.87	2.79	2.79	3.22	2.48	2.39	2.42	2.47	2.56	2.53	2.63	2.89	2.79
Ca	0.00	0.03	0.02	0.03	0.02	0.02	0.02	0.02	0.01	0.01	0.02	0.01	0.01	0.03	0.03	0.03
Na	0.14	0.10	0.16	0.10	0.09	0.15	0.15	0.09	0.07	0.08	0.10	0.15	0.12	0.16	0.18	0.07
K	1.68	1.75	1.79	1.70	1.76	1.78	1.67	1.79	1.82	1.80	1.80	1.75	1.74	1.60	1.37	1.63
Total	15.47	15.55	15.65	15.59	15.56	15.64	15.63	15.60	15.52	15.54	15.61	15.64	15.58	15.53	15.25	15.47

Microprobe results from biotites in metabasites

Sample MM141B				
Oxides Percentage				
SiO2	35.73	36.37	36.79	36.70
TiO2	5.41	5.95	4.71	3.59
Al2O3	13.81	13.94	14.03	14.03
Cr2O3	0.29	0.30	0.39	0.36
FeO	17.29	17.03	16.55	17.62
MnO	0.00	0.00	0.00	0.00
MgO	12.95	12.54	13.55	13.28
CaO	0.14	0.11	0.12	0.22
Na2O	0.61	0.59	0.51	0.63
K2O	7.83	8.66	8.51	8.54
Total	94.06	95.50	95.04	94.98
Cation on the basis of 22 Oxygens				
Si	5.47	5.49	5.55	5.57
Ti	0.62	0.67	0.53	0.41
Al	2.49	2.48	2.49	2.51
Cr	0.03	0.04	0.04	0.04
Fe	2.21	2.15	2.09	2.24
Mn	0.00	0.00	0.00	0.00
Mg	2.95	2.82	3.04	3.00
Ca	0.02	0.01	0.01	0.03
Na	0.18	0.18	0.15	0.19
K	1.53	1.67	1.64	1.66
Total	15.50	15.51	15.56	15.65

Microprobe results of amphiboles in metabasites

Sample Number	MM148A							MM141B						MM166B		
Oxides Percentage																
SiO2	41.87	39.29	37.29	39.90	39.41	39.32	40.06	51.12	51.47	51.73	53.65	51.39	53.03	51.66	51.95	51.83
TiO2	0.55	1.06	1.66	0.91	0.79	1.21	0.78	0.12	0.13	0.20	0.11	0.20	0.08	1.21	1.37	1.23
Al2O3	15.02	16.66	18.83	17.04	16.84	17.05	16.63	4.97	3.58	2.78	1.65	4.42	2.91	4.87	4.44	4.72
Cr2O3	0.00	0.16	0.16	0.06	0.19	0.30	0.09	0.10	0.18	0.00	0.03	0.02	0.11	0.48	0.19	0.39
Fe2O3	1.43	2.67	4.37	1.69	3.84	2.74	3.00	0.45	0.00	0.00	0.00	0.00	0.02	0.00	0.00	0.00
FeO	10.36	10.26	9.28	10.33	8.84	9.28	9.67	13.87	14.38	18.65	18.14	14.60	16.10	9.98	9.87	9.42
MnO	0.03	0.01	0.00	0.00	0.10	0.00	0.00	0.10	0.25	0.00	0.48	0.24	0.27	0.00	0.00	0.00
MgO	13.13	11.30	11.00	11.88	12.13	11.85	12.12	14.31	14.41	11.61	16.05	13.99	15.23	16.94	17.59	17.03
CaO	12.44	12.71	12.30	12.72	12.31	12.79	12.69	12.20	11.21	11.52	7.03	11.93	9.84	11.78	11.47	11.87
ZnO	0.00	0.15	0.00	0.00	0.00	0.06	0.00	0.00	0.00	0.07	0.00	0.13	0.08	0.20	0.23	0.04
Na2O	3.02	2.53	2.44	2.76	2.52	2.56	2.64	0.88	0.50	0.51	0.46	0.78	0.41	0.76	0.83	0.84
K2O	0.23	0.71	0.67	0.66	0.61	0.60	0.64	0.06	0.05	0.00	0.00	0.11	0.04	0.38	0.36	0.32
Total	98.07		97.99	97.95		97.75	98.35	98.19	96.16	97.08	97.59	97.82	98.14	98.26	98.29	97.70
Cations per 22 Oxygens per formula unit																
Si	6.12	5.83	5.51	5.87	5.81	5.79	5.87	7.40	7.59	7.72	7.83	7.49	7.67	7.38	7.40	7.43
Ti	0.06	0.12	0.18	0.10	0.09	0.13	0.08	0.01	0.01	0.02	0.01	0.02	0.00	0.13	0.15	0.13
Al	2.59	2.92	3.28	2.95	2.92	2.96	2.87	0.85	0.62	0.49	0.28	0.76	0.49	0.82	0.75	0.80
Cr	0.00	0.02	0.02	0.00	0.02	0.03	0.01	0.01	0.02	0.00	0.00	0.00	0.01	0.05	0.02	0.04
Fe3+	0.16	0.30	0.49	0.19	0.43	0.30	0.33	0.05	0.00	0.00	0.00	0.00	0.00	0.00	0.00	0.00
Fe2+	1.27	1.27	1.15	1.27	1.11	1.14	1.19	1.68	1.77	2.33	2.21	1.78	1.95	1.19	1.18	1.13
Mn	0.00	0.00	0.00	0.00	0.01	0.00	0.00	0.01	0.03	0.00	0.06	0.03	0.03	0.00	0.00	0.00
Mg	2.86	2.50	2.42	2.60	2.67	2.60	2.65	3.09	3.17	2.58	3.49	3.04	3.29	3.60	3.73	3.64
Ca	1.95	2.02	1.95	2.00	1.94	2.02	1.99	1.89	1.77	1.84	1.10	1.86	1.53	1.80	1.75	1.82
Zn	0.00	0.02	0.00	0.00	0.00	0.00	0.00	0.00	0.00	0.00	0.00	0.01	0.00	0.02	0.02	0.00
Na	0.86	0.73	0.70	0.79	0.72	0.73	0.75	0.25	0.14	0.15	0.13	0.22	0.11	0.21	0.23	0.23
K	0.04	0.13	0.13	0.12	0.11	0.11	0.12	0.01	0.01	0.00	0.00	0.02	0.00	0.07	0.06	0.06
Total	15.89	15.86	15.82	15.91	15.83	15.84	15.87	15.26	15.15	15.15	15.13	15.24	15.12	15.28	15.29	15.29
Sample Number							MM198B								MM165	
Oxides Percentage																
SiO2	53.80	51.39	51.97	50.56	52.39	50.21	44.45	44.95	45.36	48.25	44.49	44.37	44.54	43.47	48.26	48.77
TiO2	0.57	1.43	1.23	1.64	1.45	1.85	2.21	2.13	2.14	1.23	2.16	2.25	2.24	2.33	1.47	1.32
Al2O3	2.78	4.98	4.45	5.62	4.67	5.66	8.03	8.65	8.24	6.22	8.41	8.67	8.69	8.95	6.18	5.87
Cr2O3	0.29	0.36	0.44	0.42	0.31	0.42	0.22	0.18	0.00	0.02	0.12	0.03	0.09	0.02	0.11	0.25
Fe2O3	0.00	0.00	0.00	0.00	0.00	0.00	0.00	0.00	0.00	0.00	0.00	0.00	0.00	0.00	0.00	0.00
FeO	9.41	9.96	9.84	10.19	9.87	9.90	17.46	16.91	17.35	17.90	17.47	17.58	17.57	17.79	14.12	14.06
MnO	0.03	0.01	0.00	0.00	0.00	0.00	0.00	0.00	0.00	0.00	0.00	0.00	0.00	0.00	0.00	0.00
MgO	18.30	17.15	17.41	16.19	17.24	16.31	11.13	11.03	11.35	11.83	11.06	10.86	10.84	10.03	13.78	14.15
CaO	11.35	11.84	11.43	11.74	11.56	11.88	10.93	11.57	11.17	11.03	11.35	11.34	11.34	10.98	11.06	10.78
ZnO	0.07	0.30	0.00	0.00	0.30	0.06	0.00	0.09	0.00	0.20	0.00	0.10	0.07	0.00	0.00	0.20
Na2O	0.64	0.81	0.98	0.94	0.83	0.99	1.59	1.50	1.43	1.12	1.66	1.52	1.47	1.49	1.24	1.09
K2O	0.15	0.27	0.21	0.41	0.26	0.39	0.82	0.81	0.73	0.32	0.83	0.86	0.84	0.91	0.46	0.36
Total	97.40	98.52	97.97	97.73	98.89	97.66	96.83	97.84	97.78	98.12	97.55	97.58	97.69	95.97	96.69	96.87
Cations per 22 Oxygens per formula unit																
Si	7.68	7.31	7.43	7.29	7.43	7.24	6.76	6.74	6.80	7.16	6.72	6.69	6.71	6.69	7.17	7.21
Ti	0.06	0.15	0.13	0.18	0.16	0.20	0.25	0.24	0.24	0.14	0.25	0.25	0.25	0.27	0.16	0.15
Al	0.47	0.83	0.75	0.96	0.78	0.96	1.44	1.53	1.45	1.09	1.49	1.54	1.54	1.62	1.08	1.02
Cr	0.03	0.04	0.05	0.05	0.03	0.05	0.03	0.02	0.00	0.00	0.01	0.00	0.01	0.00	0.01	0.03
Fe3+	0.00	0.00	0.00	0.00	0.00	0.00	0.00	0.00	0.00	0.00	0.00	0.00	0.00	0.00	0.00	0.00
Fe2+	1.12	1.18	1.18	1.23	1.17	1.19	2.22	2.12	2.17	2.22	2.20	2.22	2.21	2.29	1.75	1.74
Mn	0.00	0.00	0.00	0.00	0.00	0.00	0.00	0.00	0.00	0.00	0.00	0.00	0.00	0.00	0.00	0.00
Mg	3.89	3.64	3.71	3.48	3.64	3.51	2.52	2.47	2.53	2.62	2.49	2.44	2.43	2.30	3.05	3.12
Ca	1.74	1.80	1.75	1.81	1.76	1.84	1.78	1.86	1.79	1.75	1.83	1.83	1.83	1.81	1.76	1.71
Zn	0.00	0.03	0.00	0.00	0.03	0.00	0.00	0.01	0.00	0.02	0.00	0.01	0.00	0.00	0.00	0.02
Na	0.18	0.22	0.27	0.26	0.23	0.28	0.47	0.44	0.42	0.32	0.48	0.44	0.43	0.45	0.36	0.31
K	0.03	0.05	0.04	0.08	0.05	0.07	0.16	0.16	0.14	0.06	0.16	0.16	0.16	0.18	0.09	0.07
Total	15.20	15.27	15.31	15.34	15.28	15.35	15.63	15.59	15.56	15.38	15.64	15.61	15.59	15.62	15.44	15.38

Microprobe results of amphiboles in metabasites

Sample Number MM165							MM196A							
Oxides Percentage														
SiO2	49.32	50.33	46.97	47.46	50.19	48.19	48.81	49.71	50.82	50.57	50.36	51.84	51.10	50.35
TiO2	1.48	1.09	1.75	1.73	1.17	1.44	1.75	1.39	1.28	1.28	1.28	0.88	1.01	1.27
Al2O3	5.56	5.15	7.34	6.90	4.77	6.02	6.00	5.62	4.92	4.95	5.22	3.92	4.56	5.01
Cr2O3	0.04	0.10	0.28	0.37	0.06	0.29	0.46	0.15	0.28	0.23	0.28	0.15	0.13	0.15
Fe2O3	0.00	0.00	0.00	0.00	0.00	0.00	0.00	0.00	0.00	0.00	0.00	0.00	0.00	0.00
FeO	13.77	13.95	14.57	13.80	13.37	13.55	12.51	13.29	12.45	12.39	12.55	12.35	11.74	12.35
MnO	0.17	0.11	0.00	0.00	0.06	0.00	0.01	0.00	0.00	0.00	0.00	0.00	0.00	0.17
MgO	14.13	14.70	12.83	13.25	14.65	13.58	14.72	14.90	15.35	15.47	15.26	16.22	16.56	15.39
CaO	11.19	11.09	11.39	11.73	11.41	11.31	10.99	11.12	11.11	11.17	11.56	10.85	11.34	11.26
ZnO	0.25	0.00	0.00	0.18	0.12	0.11	0.15	0.06	0.00	0.04	0.07	0.07	0.20	0.17
Na2O	1.09	1.16	1.31	1.21	0.89	1.21	1.19	1.14	1.00	1.03	1.02	0.88	0.97	0.25
K2O	0.48	0.34	0.58	0.58	0.37	0.43	0.29	0.26	0.23	0.27	0.26	0.12	0.19	1.06
Total	97.50	98.02	97.02	97.22	97.09	96.13	96.90	97.64	97.47	97.40	97.85	97.28	97.81	97.43
Cations per 22 Oxygens per formula unit														
Si	7.26	7.34	7.00	7.04	7.37	7.20	7.19	7.25	7.40	7.37	7.31	7.52	7.36	7.34
Ti	0.16	0.12	0.19	0.19	0.13	0.16	0.19	0.15	0.14	0.14	0.14	0.09	0.11	0.14
Al	0.96	0.88	1.29	1.21	0.83	1.06	1.04	0.97	0.84	0.85	0.89	0.67	0.77	0.86
Cr	0.00	0.01	0.03	0.04	0.00	0.03	0.05	0.02	0.03	0.03	0.03	0.02	0.01	0.02
Fe3+	0.00	0.00	0.00	0.00	0.00	0.00	0.00	0.00	0.00	0.00	0.00	0.00	0.00	0.00
Fe2+	1.69	1.70	1.82	1.71	1.64	1.69	1.54	1.62	1.52	1.51	1.52	1.50	1.41	1.50
Mn	0.02	0.01	0.00	0.00	0.00	0.00	0.00	0.00	0.00	0.00	0.00	0.00	0.00	0.02
Mg	3.10	3.19	2.85	2.93	3.21	3.03	3.23	3.24	3.33	3.36	3.30	3.51	3.55	3.34
Ca	1.76	1.73	1.82	1.86	1.79	1.81	1.73	1.74	1.73	1.74	1.80	1.69	1.75	1.76
Zn	0.03	0.00	0.00	0.02	0.01	0.01	0.02	0.00	0.00	0.00	0.00	0.00	0.02	0.02
Na	0.31	0.33	0.38	0.35	0.25	0.35	0.34	0.32	0.28	0.29	0.29	0.25	0.27	0.07
K	0.09	0.06	0.11	0.11	0.07	0.08	0.05	0.05	0.04	0.05	0.05	0.02	0.03	0.20
Total	15.40	15.39	15.49	15.46	15.32	15.43	15.39	15.37	15.33	15.34	15.33	15.27	15.30	15.27

Microprobe results from plagioclases in metabasites

Sample MM141B														MM198B	
Oxides Percentage															
SiO2	45.78	45.45	45.69	46.40	45.89	45.41	44.91	45.22	44.99	46.47	45.62	45.13	44.70	55.32	54.74
TiO2	0.00	0.01	0.04	0.08	0.00	0.03	0.00	0.08	0.06	0.00	0.13	0.12	0.00	0.00	0.04
Al2O3	34.27	34.52	34.47	33.74	34.31	34.69	34.40	34.47	34.49	34.21	33.65	34.52	34.78	28.36	28.57
FeO	0.62	0.17	0.23	0.39	0.20	0.27	0.15	0.24	0.30	0.33	0.93	0.48	0.09	0.13	0.28
MnO	0.04	0.00	0.00	0.09	0.00	0.00	0.14	0.06	0.00	0.02	0.13	0.03	0.01	0.02	0.00
MgO	0.30	0.23	0.25	0.09	0.22	0.26	0.15	0.21	0.34	0.21	0.78	0.33	0.28	0.12	0.06
CaO	17.39	18.24	17.99	17.26	17.73	18.27	18.38	18.02	17.72	17.65	17.23	17.90	18.25	11.07	10.83
Na2O	1.22	1.18	1.29	1.59	1.43	1.33	1.11	1.28	1.31	1.78	1.52	1.11	0.97	5.28	5.39
K2O	0.01	0.04	0.07	0.00	0.00	0.00	0.00	0.00	0.00	0.00	0.22	0.11	0.07	0.16	0.18
Cr2O3	0.15	0.04	0.06	0.00	0.09	0.03	0.00	0.07	0.00	0.00	0.00	0.06	0.15	0.02	0.02
Total	99.77	99.77	99.97	99.59	99.69	100.23	99.11	99.66	99.13	100.51	100.20	99.80	99.26	100.70	99.98
Cations on the basis of 8 Oxygens															
Si	2.12	2.10	2.11	2.14	2.12	2.09	2.09	2.09	2.09	2.13	2.11	2.09	2.08	2.48	2.47
Ti	0.00	0.00	0.00	0.00	0.00	0.00	0.00	0.00	0.00	0.00	0.00	0.00	0.00	0.00	0.00
Al	1.87	1.88	1.87	1.84	1.87	1.88	1.89	1.88	1.89	1.85	1.83	1.88	1.91	1.50	1.52
Fe	0.02	0.00	0.00	0.01	0.00	0.01	0.00	0.00	0.01	0.01	0.04	0.02	0.00	0.00	0.01
Mn	0.00	0.00	0.00	0.00	0.00	0.00	0.00	0.00	0.00	0.00	0.00	0.00	0.00	0.00	0.00
Mg	0.02	0.02	0.02	0.00	0.01	0.02	0.01	0.01	0.02	0.01	0.05	0.02	0.02	0.00	0.00
Ca	0.86	0.90	0.89	0.85	0.88	0.90	0.92	0.89	0.88	0.87	0.85	0.89	0.91	0.53	0.52
Na	0.11	0.10	0.11	0.14	0.13	0.12	0.10	0.11	0.12	0.16	0.14	0.10	0.09	0.46	0.47
K	0.00	0.00	0.00	0.00	0.00	0.00	0.00	0.00	0.00	0.00	0.01	0.00	0.00	0.01	0.01
Cr	0.00	0.00	0.00	0.00	0.00	0.00	0.00	0.00	0.00	0.00	0.00	0.00	0.00	0.00	0.00
Total	5.00	5.01	5.01	5.00	5.01	5.02	5.01	5.02	5.02	5.03	5.04	5.02	5.01	5.00	5.01
Sample	MM198B														
Oxides Percentage															
SiO2	55.75	55.86	54.35	54.98	55.94	56.05	55.56	55.62	55.62	55.23	55.04	55.63	55.63	54.72	55.37
TiO2	0.04	0.02	0.05	0.07	0.00	0.03	0.03	0.00	0.07	0.00	0.05	0.01	0.01	0.02	0.00
Al2O3	28.28	27.90	29.22	28.96	28.22	28.63	28.60	27.68	27.76	28.37	28.29	28.08	28.08	28.12	28.25
FeO	0.34	0.30	0.47	0.25	0.19	0.29	0.27	0.14	0.16	0.28	0.09	0.16	0.16	0.22	0.21
MnO	0.00	0.00	0.00	0.01	0.05	0.02	0.10	0.05	0.08	0.02	0.04	0.00	0.00	0.00	0.06
MgO	0.10	0.00	0.09	0.19	0.06	0.22	0.05	0.00	0.09	0.31	0.21	0.04	0.04	0.08	0.04
CaO	10.69	10.52	11.55	10.93	10.63	10.98	10.89	10.11	10.29	10.56	10.53	10.39	10.39	10.62	10.57
Na2O	5.63	5.43	4.99	5.30	5.50	5.54	5.49	5.65	5.58	5.61	5.37	5.75	5.75	5.39	5.41
K2O	0.16	0.19	0.12	0.19	0.19	0.16	0.18	0.24	0.14	0.15	0.23	0.17	0.17	0.12	0.15
Cr2O3	0.00	0.00	0.07	0.00	0.09	0.07	0.07	0.08	0.00	0.00	0.09	0.00	0.00	0.02	0.04
Total	100.95	100.15	100.82	100.87	100.89	101.99	101.23	99.55	99.81	100.41	99.95	100.16	100.16	99.23	100.07
Cations on the basis of 8 Oxygens															
Si	2.49	2.51	2.44	2.46	2.50	2.48	2.48	2.52	2.51	2.48	2.48	2.50	2.50	2.48	2.49
Ti	0.00	0.00	0.00	0.00	0.00	0.00	0.00	0.00	0.00	0.00	0.00	0.00	0.00	0.00	0.00
Al	1.49	1.48	1.54	1.53	1.49	1.49	1.50	1.48	1.47	1.50	1.50	1.49	1.49	1.51	1.50
Fe	0.01	0.01	0.02	0.00	0.00	0.01	0.01	0.00	0.00	0.01	0.00	0.00	0.00	0.00	0.00
Mn	0.00	0.00	0.00	0.00	0.00	0.00	0.00	0.00	0.00	0.00	0.00	0.00	0.00	0.00	0.00
Mg	0.00	0.00	0.00	0.01	0.00	0.01	0.00	0.00	0.00	0.02	0.01	0.00	0.00	0.00	0.00
Ca	0.51	0.51	0.55	0.52	0.51	0.52	0.52	0.49	0.50	0.51	0.51	0.50	0.50	0.52	0.51
Na	0.49	0.47	0.43	0.46	0.48	0.48	0.48	0.50	0.49	0.49	0.47	0.50	0.50	0.47	0.47
K	0.00	0.01	0.00	0.01	0.01	0.00	0.01	0.01	0.00	0.00	0.01	0.01	0.01	0.00	0.00
Cr	0.00	0.00	0.00	0.00	0.00	0.00	0.00	0.00	0.00	0.00	0.00	0.00	0.00	0.00	0.00
Total	5.01	4.99	5.00	5.00	5.00	5.01	5.01	5.00	5.00	5.02	5.00	5.01	5.01	5.00	5.00

Microprobe results from plagioclases in metabasites

Sample MM196A									MM166B						
Oxides Percentage															
SiO2	48.45	51.06	49.90	54.95	50.09	50.81	48.45	51.08	57.31	55.19	55.88	56.27	57.25	56.45	55.93
TiO2	0.00	0.17	0.00	0.00	0.00	0.00	0.00	0.00	0.04	0.01	0.09	0.05	0.00	0.13	0.11
Al2O3	32.60	31.07	31.99	28.63	32.07	31.03	32.60	31.03	27.25	28.30	27.47	27.74	27.20	27.81	27.77
FeO	0.00	0.03	0.14	0.05	0.00	0.02	0.01	0.04	0.15	0.31	0.13	0.12	0.04	0.24	0.17
MnO	0.14	0.37	0.18	0.13	0.10	0.04	0.14	0.16	0.04	0.00	0.00	0.00	0.01	0.00	0.00
MgO	0.07	0.00	0.00	0.00	0.01	0.03	0.07	0.03	0.19	0.24	0.04	0.17	0.12	0.04	0.09
CaO	0.14	0.08	0.16	0.06	0.09	0.00	0.14	0.17	8.99	10.47	9.63	9.50	8.98	9.95	9.83
Na2O	15.84	14.01	15.20	11.22	14.86	14.22	15.84	14.06	6.43	5.59	5.74	5.96	5.50	5.77	5.93
K2O	2.71	3.65	3.14	5.28	3.19	3.44	2.71	3.54	0.07	0.06	0.13	0.08	0.75	0.18	0.17
Cr2O3	0.02	0.02	0.05	0.15	0.00	0.07	0.02	0.00	0.08	0.00	0.08	0.00	0.00	0.04	0.03
Total	99.99	100.40	100.76	100.48	100.42	99.66	99.99	100.11	100.56	100.04	99.13	99.84	99.76	100.58	100.03
Cations on the basis of 8 Oxygens															
Si	2.22	2.32	2.26	2.47	2.27	2.32	2.22	2.32	2.56	2.49	2.53	2.53	2.57	2.52	2.52
Ti	0.00	0.00	0.00	0.00	0.00	0.00	0.00	0.00	0.00	0.00	0.00	0.00	0.00	0.00	0.00
Al	1.76	1.66	1.71	1.52	1.72	1.67	1.76	1.66	1.43	1.50	1.47	1.47	1.44	1.47	1.47
Fe	0.00	0.00	0.00	0.00	0.00	0.00	0.00	0.00	0.00	0.01	0.00	0.00	0.00	0.00	0.00
Mn	0.00	0.01	0.00	0.00	0.00	0.00	0.00	0.00	0.00	0.00	0.00	0.00	0.00	0.00	0.00
Mg	0.00	0.00	0.00	0.00	0.00	0.00	0.00	0.00	0.01	0.02	0.00	0.01	0.00	0.00	0.00
Ca	0.01	0.00	0.01	0.00	0.00	0.00	0.00	0.01	0.43	0.50	0.47	0.46	0.43	0.48	0.47
Na	0.78	0.68	0.74	0.54	0.72	0.69	0.78	0.68	0.56	0.49	0.50	0.52	0.48	0.50	0.52
K	0.24	0.32	0.28	0.46	0.28	0.30	0.24	0.31	0.00	0.00	0.00	0.00	0.04	0.01	0.01
Cr	0.00	0.00	0.00	0.00	0.00	0.00	0.00	0.00	0.00	0.00	0.00	0.00	0.00	0.00	0.00
Total	5.02	5.00	5.01	5.00	5.00	4.99	5.02	5.00	5.00	5.01	4.99	4.99	4.97	4.99	5.00

Sample								MM165				
Oxides Percentage												
SiO2	56.46	55.79	56.23	57.14	58.32	57.29	56.49	49.87	49.30	53.64	52.41	49.95
TiO2	0.06	0.00	0.09	0.06	0.17	0.01	0.06	0.06	0.00	0.04	0.00	0.00
Al2O3	28.13	27.69	27.06	26.49	26.03	27.02	27.36	32.27	32.74	29.38	30.13	32.53
FeO	0.14	0.19	0.20	0.16	0.16	0.08	0.16	0.08	0.07	0.18	0.10	0.06
MnO	0.09	0.00	0.00	0.00	0.01	0.00	0.00	0.02	0.00	0.00	0.00	0.00
MgO	0.22	0.14	0.11	0.14	0.12	0.12	0.13	0.15	0.00	0.11	0.21	0.02
CaO	9.84	9.73	9.16	8.44	8.67	8.94	9.40	15.18	15.78	11.68	12.89	15.52
Na2O	5.98	5.94	5.90	6.33	5.99	6.47	5.98	3.03	2.70	4.85	4.29	2.91
K2O	0.06	0.11	0.62	0.32	0.92	0.15	0.13	0.05	0.02	0.16	0.00	0.01
Cr2O3	0.05	0.02	0.11	0.06	0.00	0.00	0.00	0.00	0.00	0.00	0.00	0.04
Total	101.03	99.51	99.41	99.10	100.29	100.07	99.67	100.73	100.69	100.06	100.05	101.03
Cations on the basis of 8 Oxygens												
Si	2.51	2.52	2.54	2.58	2.61	2.57	2.54	2.26	2.24	2.42	2.38	2.26
Ti	0.00	0.00	0.00	0.00	0.00	0.00	0.00	0.00	0.00	0.00	0.00	0.00
Al	1.48	1.47	1.44	1.41	1.37	1.43	1.45	1.73	1.75	1.57	1.61	1.73
Fe	0.00	0.00	0.00	0.00	0.00	0.00	0.00	0.00	0.00	0.00	0.00	0.00
Mn	0.00	0.00	0.00	0.00	0.00	0.00	0.00	0.00	0.00	0.00	0.00	0.00
Mg	0.01	0.01	0.00	0.00	0.00	0.00	0.00	0.01	0.00	0.00	0.01	0.00
Ca	0.47	0.47	0.44	0.41	0.41	0.43	0.45	0.74	0.77	0.57	0.63	0.75
Na	0.52	0.52	0.52	0.55	0.52	0.65	0.52	0.27	0.24	0.43	0.38	0.26
K	0.00	0.00	0.04	0.02	0.05	0.00	0.00	0.00	0.00	0.00	0.00	0.00
Cr	0.00	0.00	0.00	0.00	0.00	0.00	0.00	0.00	0.00	0.00	0.00	0.00
Total	5.00	5.00	5.00	4.99	4.99	5.00	4.99	5.01	5.00	4.99	5.01	5.00

Microprobe results of pyroxenes in metabasites

Sample Number MM196A												MM198B				
Oxides Percentage																
SiO2	52.69	52.93	52.79	52.85	53.09	52.83	52.89	52.94	52.79	52.66	52.55	51.84	51.88	51.50	52.91	52.19
TiO2	0.19	0.15	0.13	0.20	0.12	0.30	0.08	0.24	0.30	0.33	0.33	0.16	0.11	0.07	0.15	0.11
Al2O3	0.29	0.32	0.28	0.89	0.61	0.57	0.72	0.90	0.74	0.89	0.79	0.54	0.57	0.44	0.62	0.72
Cr2O3	0.04	0.07	0.00	0.30	0.16	0.15	0.31	0.17	0.29	0.20	0.16	0.09	0.02	0.03	0.11	0.13
Fe2O3	1.09	0.88	0.52	2.21	2.23	1.12	1.35	1.83	1.57	0.99	1.88	1.52	0.95	2.00	1.19	1.48
FeO	24.75	25.23	25.48	8.30	8.71	9.44	9.24	8.81	8.70	9.64	8.28	28.17	28.30	27.37	12.22	12.03
MnO	0.03	0.16	0.23	0.03	0.19	0.15	0.02	0.13	0.12	0.10	0.18	0.18	0.14	0.23	0.00	0.13
MgO	20.04	19.62	19.83	13.83	13.85	13.53	13.87	13.97	13.90	13.94	13.84	17.11	17.25	17.23	12.31	12.20
CaO	0.83	0.93	0.80	21.74	21.63	21.65	21.36	21.21	21.65	20.90	21.41	1.03	0.99	1.01	20.86	20.70
ZnO	0.00	0.00	0.00	0.00	0.00	0.00	0.00	0.00	0.00	0.00	0.00	0.00	0.00	0.00	0.00	0.00
Na2O	0.34	0.40	0.25	0.55	0.49	0.43	0.42	0.54	0.44	0.41	0.55	0.39	0.36	0.43	0.52	0.44
K2O	0.00	0.00	0.00	0.00	0.00	0.00	0.00	0.00	0.00	0.00	0.00	0.05	0.00	0.00	0.03	0.00
Total	100.31	100.69	100.31	100.89	101.08	100.17	100.27	100.75	100.50	100.06	99.98	101.07	100.56	100.33	100.93	100.15
Cations on the basis of 6 Oxygens																
Si	1.98	1.99	1.99	1.96	1.97	1.98	1.97	1.96	1.96	1.70	1.96	1.97	1.98	1.97	1.98	1.97
Ti	0.00	0.00	0.00	0.00	0.00	0.00	0.00	0.00	0.00	0.00	0.00	0.00	0.00	0.00	0.00	0.00
Al	0.01	0.01	0.01	0.04	0.03	0.02	0.03	0.04	0.03	0.04	0.03	0.02	0.03	0.02	0.03	0.03
Cr	0.00	0.00	0.00	0.00	0.00	0.00	0.00	0.00	0.00	0.00	0.00	0.00	0.00	0.00	0.00	0.00
Fe3+	0.03	0.02	0.01	0.06	0.06	0.03	0.04	0.05	0.04	0.03	0.05	0.04	0.03	0.06	0.03	0.04
Fe2+	0.78	0.79	0.80	0.26	0.27	0.29	0.29	0.27	0.27	0.30	0.26	0.90	0.90	0.88	0.38	0.38
Mn	0.00	0.00	0.00	0.00	0.00	0.00	0.00	0.00	0.00	0.00	0.00	0.00	0.00	0.00	0.00	0.00
Mg	1.12	1.10	1.11	0.76	0.76	0.75	0.77	0.77	0.77	0.78	0.77	0.97	0.98	0.98	0.69	0.69
Ca	0.03	0.04	0.03	0.86	0.86	0.87	0.85	0.84	0.86	0.84	0.86	0.04	0.04	0.04	0.84	0.84
Zn	0.00	0.00	0.00	0.00	0.00	0.00	0.00	0.00	0.00	0.00	0.00	0.00	0.00	0.00	0.00	0.00
Na	0.02	0.03	0.02	0.04	0.03	0.03	0.03	0.04	0.03	0.03	0.04	0.03	0.03	0.03	0.04	0.03
K	0.00	0.00	0.00	0.00	0.00	0.00	0.00	0.00	0.00	0.00	0.00	0.00	0.00	0.00	0.00	0.00
Total	4.00	4.00	4.00	4.00	4.00	4.00	4.00	4.00	4.00	4.00	4.00	4.00	4.00	4.00	4.00	4.00
Sample Number				MM141B												
Oxides Percentage																
SiO2	52.49	52.27	52.08	51.96	51.95	51.91	51.70	52.26	52.63	52.87	52.34	52.96	52.33	52.02	52.31	51.93
TiO2	0.13	0.05	0.18	0.19	0.31	0.16	0.09	0.05	0.11	0.16	0.15	0.29	0.09	0.15	0.17	0.22
Al2O3	0.72	0.83	0.91	0.44	0.57	0.25	0.26	0.31	0.52	0.55	0.19	0.63	0.56	0.50	0.66	0.56
Cr2O3	0.11	0.15	0.09	0.00	0.06	0.00	0.05	0.11	0.00	0.16	0.00	0.25	0.11	0.12	0.10	0.19
Fe2O3	2.42	1.40	3.63	2.63	1.51	0.83	2.63	2.51	2.30	1.48	1.76	0.73	1.46	1.29	1.79	1.17
FeO	11.09	11.31	9.51	25.38	26.12	26.94	24.91	25.38	23.92	24.70	24.55	10.68	10.89	14.66	11.67	12.59
MnO	0.24	0.00	0.12	0.42	0.38	0.43	0.54	0.29	0.36	0.14	0.38	0.00	0.16	0.29	0.27	0.32
MgO	12.43	12.41	12.63	18.26	17.95	18.23	18.34	18.48	19.69	19.79	19.50	13.10	12.64	10.28	12.25	11.90
CaO	21.13	20.96	21.20	1.18	1.08	1.13	1.11	1.04	0.85	0.78	0.89	21.73	21.55	21.46	20.97	20.83
ZnO	0.00	0.00	0.00	0.00	0.00	0.00	0.00	0.00	0.00	0.00	0.00	0.00	0.00	0.00	0.00	0.00
Na2O	0.50	0.49	0.68	0.53	0.54	0.19	0.50	0.56	0.55	0.48	0.40	0.37	0.31	0.34	0.45	0.32
K2O	0.00	0.00	0.00	0.00	0.00	0.00	0.00	0.00	0.00	0.00	0.01	0.00	0.00	0.00	0.00	0.00
Total	101.26	99.87	101.02	100.98	100.47	100.07	100.13	100.98	100.94	101.12	100.16	100.73	100.11	101.12	100.64	100.03
Cations on the basis of 6 Oxygens																
Si	1.96	1.98	1.95	1.97	1.97	1.98	1.97	1.97	1.97	1.98	1.98	1.98	1.97	1.98	1.97	1.97
Ti	0.00	0.00	0.00	0.00	0.00	0.00	0.00	0.00	0.00	0.00	0.00	0.00	0.00	0.00	0.00	0.00
Al	0.03	0.04	0.04	0.02	0.03	0.01	0.01	0.01	0.02	0.02	0.00	0.03	0.02	0.02	0.03	0.02
Cr	0.00	0.00	0.00	0.00	0.00	0.00	0.00	0.00	0.00	0.00	0.00	0.00	0.00	0.00	0.00	0.00
Fe3+	0.07	0.04	0.10	0.07	0.04	0.02	0.07	0.07	0.06	0.04	0.05	0.02	0.04	0.04	0.05	0.03
Fe2+	0.35	0.36	0.30	0.80	0.83	0.86	0.79	0.80	0.75	0.77	0.78	0.33	0.34	0.47	0.37	0.40
Mn	0.00	0.00	0.00	0.01	0.01	0.01	0.02	0.00	0.01	0.00	0.01	0.00	0.00	0.00	0.00	0.01
Mg	0.69	0.70	0.70	1.03	1.02	1.04	1.04	1.04	1.10	1.10	1.10	0.73	0.71	0.58	0.69	0.67
Ca	0.85	0.85	0.85	0.05	0.04	0.05	0.04	0.04	0.03	0.03	0.04	0.87	0.87	0.87	0.85	0.85
Zn	0.00	0.00	0.00	0.00	0.00	0.00	0.00	0.00	0.00	0.00	0.00	0.00	0.00	0.00	0.00	0.00
Na	0.04	0.04	0.05	0.04	0.04	0.01	0.04	0.04	0.04	0.03	0.03	0.03	0.02	0.02	0.03	0.02
K	0.00	0.00	0.00	0.00	0.00	0.00	0.00	0.00	0.00	0.00	0.00	0.00	0.00	0.00	0.00	0.00
Total	4.00	4.00	4.00	4.00	4.00	4.00	4.00	4.00	4.00	4.00	4.00	4.00	4.00	4.00	4.00	4.00

Microprobe results of pyroxenes in metabasites

Sample Number MM165								MM166B								
Oxides Percentage																
SiO2	51.80	52.31	51.97	52.42	51.80	53.22	52.51	53.62	53.87	53.84	53.77	53.80	53.94	53.82	53.68	53.44
TiO2	0.20	0.05	0.16	0.17	0.12	0.12	0.11	0.12	0.22	0.15	0.22	0.19	0.06	0.10	0.10	0.21
Al2O3	0.55	0.57	0.43	0.36	0.61	0.53	0.70	0.54	0.32	0.57	0.36	0.45	0.39	0.58	0.46	0.82
Cr2O3	0.10	0.00	0.09	0.10	0.00	0.15	0.09	0.13	0.05	0.00	0.02	0.00	0.00	0.09	0.00	0.23
Fe2O3	1.77	1.77	2.22	1.12	0.06	0.80	2.46	2.37	1.35	1.06	1.50	2.29	1.46	1.45	1.60	1.81
FeO	12.54	26.25	25.90	26.99	27.61	11.09	8.73	19.95	21.13	21.02	20.56	20.22	21.39	20.89	20.85	6.52
MnO	0.33	0.20	0.25	0.25	0.05	0.08	0.12	0.00	0.01	0.10	0.00	0.10	0.03	0.15	0.01	0.00
MgO	11.72	18.20	17.84	18.12	18.26	12.60	12.98	22.97	22.76	22.74	22.70	23.02	22.63	22.60	22.91	14.83
CaO	20.91	1.14	1.12	1.05	1.31	22.06	21.87	0.84	0.75	0.93	0.79	0.75	0.84	0.72	0.81	22.52
ZnO	0.00	0.00	0.00	0.00	0.00	0.00	0.00	0.00	0.00	0.00	0.00	0.00	0.00	0.00	0.00	0.00
Na2O	0.34	0.48	0.63	0.42	0.04	0.39	0.61	0.48	0.40	0.36	0.53	0.45	0.37	0.47	0.33	0.49
K2O	0.00	0.00	0.00	0.00	0.00	0.00	0.00	0.02	0.02	0.00	0.00	0.02	0.00	0.00	0.00	0.00
Total	100.25	100.97	100.61	100.99	99.87	101.07	100.20	101.04	100.89	100.77	100.45	101.30	101.11	100.88	100.76	100.87
Cations on the basis of 6 Oxygens																
Si	1.97	1.98	1.98	1.98	1.98	1.99	1.97	1.97	1.98	1.98	1.98	1.97	1.98	1.98	1.98	1.96
Ti	0.00	0.00	0.00	0.00	0.00	0.00	0.00	0.00	0.00	0.00	0.00	0.00	0.00	0.00	0.00	0.00
Al	0.02	0.02	0.02	0.02	0.03	0.02	0.03	0.02	0.01	0.02	0.02	0.02	0.02	0.02	0.02	0.03
Cr	0.00	0.00	0.00	0.00	0.00	0.00	0.00	0.00	0.00	0.00	0.00	0.00	0.00	0.00	0.00	0.00
Fe3+	0.05	0.05	0.06	0.03	0.00	0.02	0.07	0.06	0.04	0.03	0.04	0.06	0.04	0.04	0.04	0.05
Fe2+	0.40	0.83	0.82	0.85	0.88	0.35	0.27	0.61	0.65	0.65	0.63	0.62	0.66	0.64	0.64	0.20
Mn	0.01	0.00	0.00	0.00	0.00	0.00	0.00	0.00	0.00	0.00	0.00	0.00	0.00	0.00	0.00	0.00
Mg	0.66	1.03	1.01	1.02	1.04	0.70	0.72	1.26	1.25	1.25	1.25	1.26	1.24	1.24	1.26	0.81
Ca	0.85	0.05	0.05	0.04	0.05	0.88	0.88	0.03	0.03	0.04	0.03	0.03	0.03	0.03	0.03	0.89
Zn	0.00	0.00	0.00	0.00	0.00	0.00	0.00	0.00	0.00	0.00	0.00	0.00	0.00	0.00	0.00	0.00
Na	0.02	0.03	0.05	0.03	0.00	0.03	0.04	0.03	0.03	0.03	0.04	0.03	0.03	0.03	0.02	0.03
K	0.00	0.00	0.00	0.00	0.00	0.00	0.00	0.00	0.00	0.00	0.00	0.00	0.00	0.00	0.00	0.00
Total	4.00	4.00	4.00	4.00	4.00	4.00	4.00	4.00	4.00	4.00	4.00	4.00	4.00	4.00	4.00	4.00

Sample Number		MM166B				
Oxides Percentage						
SiO2	53.18	53.38	53.60	53.71	53.55	53.77
TiO2	0.18	0.24	0.31	0.28	0.28	0.20
Al2O3	0.94	0.56	0.77	0.74	1.01	0.77
Cr2O3	0.21	0.12	0.15	0.25	0.28	0.24
Fe2O3	1.53	1.43	1.40	1.12	1.14	0.14
FeO	7.53	6.61	6.72	7.10	7.51	7.99
MnO	0.07	0.20	0.16	0.00	0.22	0.00
MgO	14.97	14.93	14.95	14.91	14.89	15.09
CaO	21.12	22.43	22.55	22.26	21.77	22.26
ZnO	0.00	0.00	0.00	0.00	0.00	0.00
Na2O	0.52	0.40	0.42	0.49	0.45	0.23
K2O	0.00	0.00	0.00	0.00	0.00	0.00
Total	100.26	100.32	101.03	100.86	101.12	100.69
Cations on the basis of 6 Oxygens						
Si	1.97	1.97	1.97	1.97	1.97	1.98
Ti	0.00	0.00	0.00	0.00	0.00	0.00
Al	0.04	0.02	0.03	0.03	0.04	0.03
Cr	0.00	0.00	0.00	0.00	0.00	0.00
Fe3+	0.04	0.04	0.04	0.03	0.03	0.00
Fe2+	0.23	0.20	0.21	0.22	0.23	0.25
Mn	0.00	0.00	0.00	0.00	0.00	0.00
Mg	0.83	0.82	0.82	0.82	0.81	0.83
Ca	0.84	0.89	0.89	0.88	0.86	0.88
Zn	0.00	0.00	0.00	0.00	0.00	0.00
Na	0.04	0.03	0.03	0.03	0.03	0.02
K	0.00	0.00	0.00	0.00	0.00	0.00
Total	4.00	4.00	4.00	4.00	4.00	4.00

Microprobe results of biotites in pelites

Sample	MM169B							MM151								
Oxides																
SiO2	34.97	34.60	35.38	35.61	35.31	35.39	35.49	35.11	34.34	35.09	35.00	35.09	34.67	34.89	34.52	34.64
TiO2	3.95	3.38	4.44	3.98	3.65	3.99	4.03	4.62	4.42	4.78	4.37	4.89	4.68	4.64	4.47	3.29
Al2O3	17.10	17.42	17.24	17.11	17.76	16.87	17.18	18.40	18.80	18.52	19.20	18.44	18.65	18.37	18.82	18.76
Cr2O3	0.54	0.77	0.11	0.41	0.21	0.31	0.56	0.17	0.26	0.28	0.00	0.12	0.08	0.12	0.20	0.15
MnO	0.00	0.00	0.00	0.00	0.00	0.00	0.00	0.00	0.00	0.00	0.00	0.00	0.00	0.00	0.00	0.00
MgO	7.13	7.59	8.20	8.29	7.88	8.11	8.08	6.19	6.33	6.20	6.56	6.19	6.13	6.09	6.33	6.60
CaO	0.06	0.12	0.07	0.12	0.08	0.02	0.08	0.09	0.13	0.03	0.12	0.00	0.03	0.11	0.02	0.00
Na2O	0.52	0.28	0.45	0.27	0.51	0.46	0.41	0.44	0.36	0.42	0.42	0.32	0.36	0.43	0.36	0.18
K2O	9.04	8.95	9.17	9.40	9.26	9.21	9.28	9.39	9.39	9.38	9.45	9.30	9.21	9.39	9.40	9.39
FeO	23.36	22.00	22.00	20.66	21.00	21.74	20.95	22.41	22.30	22.82	21.28	22.16	21.77	22.13	22.28	21.75
Total	96.67	95.11	97.06	95.85	95.66	96.10	96.06	96.82	96.33	97.52	96.40	96.51	95.58	96.17	96.40	94.76
Number of atoms on the basis of 22 oxygens																
Si	5.37	5.38	5.36	5.45	5.42	5.43	5.42	5.36	5.27	5.33	5.33	5.36	5.34	5.36	5.29	5.38
Ti	0.46	0.39	0.51	0.46	0.42	0.46	0.46	0.53	0.51	0.54	0.50	0.56	0.54	0.54	0.51	0.38
Al	3.10	3.19	3.08	3.09	3.21	3.05	3.09	3.31	3.40	3.32	3.45	3.32	3.39	3.33	3.40	3.43
Cr	0.07	0.09	0.01	0.05	0.03	0.04	0.07	0.02	0.03	0.03	0.00	0.01	0.01	0.01	0.02	0.02
Mn	0.00	0.00	0.00	0.00	0.00	0.00	0.00	0.00	0.00	0.00	0.00	0.00	0.00	0.00	0.00	0.00
Mg	1.63	1.76	1.85	1.89	1.80	1.85	1.84	1.41	1.45	1.41	1.49	1.41	1.41	1.39	1.44	1.53
Ca	0.01	0.02	0.01	0.20	0.01	0.00	0.01	0.01	0.02	0.00	0.02	0.00	0.00	0.02	0.00	0.00
Na	0.15	0.08	0.13	0.08	0.15	0.14	0.12	0.13	0.11	0.12	0.12	0.09	0.11	0.13	0.11	0.05
K	1.77	1.77	1.77	1.84	1.81	1.80	1.81	1.83	1.84	1.82	1.84	1.81	1.81	1.84	1.84	1.86
Fe	3.00	2.86	2.79	2.64	2.70	2.79	2.68	2.86	2.86	2.90	2.71	2.83	2.80	2.84	2.86	2.83
Total	15.56	15.54	15.51	15.70	15.55	15.56	15.50	15.46	15.49	15.47	15.46	15.39	15.41	15.46	15.47	15.48
Sample	MM151	MM153									MM185B					
Oxides																
SiO2	34.88	34.49	34.38	34.67	34.72	34.45	34.70	33.89	34.64	34.08	33.96	33.98	33.64	34.32	33.62	33.89
TiO2	4.54	3.92	4.48	4.75	5.11	4.56	4.19	4.37	4.85	4.93	3.10	2.61	2.88	4.48	2.31	2.70
Al2O3	18.68	19.21	18.18	18.16	18.54	18.76	18.75	18.67	18.52	18.09	19.71	19.92	19.77	19.51	19.89	19.88
Cr2O3	0.14	0.07	0.12	0.09	0.05	0.09	0.10	0.06	0.08	0.09	0.06	0.01	0.07	0.07	0.11	0.14
MnO	0.00	0.00	0.00	0.00	0.00	0.00	0.00	0.00	0.00	0.00	0.00	0.00	0.00	0.00	0.00	0.00
MgO	6.22	5.65	5.92	5.89	5.55	5.39	5.87	6.05	5.51	6.22	5.72	6.27	5.98	5.59	6.59	6.40
CaO	0.09	0.12	0.90	0.03	0.10	0.09	0.06	0.03	0.02	0.15	0.12	0.14	0.07	0.07	0.04	0.04
Na2O	0.42	0.52	0.43	0.46	0.53	0.47	0.45	0.47	0.31	0.37	0.49	0.51	0.52	0.50	0.52	0.43
K2O	9.32	9.38	9.33	9.54	9.53	9.35	9.26	8.95	9.35	9.43	9.10	9.05	8.94	8.86	8.96	9.45
FeO	22.14	22.97	23.95	24.12	23.58	23.26	23.25	24.00	23.54	24.11	23.21	23.38	23.93	23.91	22.69	23.30
Total	96.43	96.33	97.69	97.71	97.71	96.42	96.63	96.49	96.82	97.47	95.47	95.87	95.80	97.31	94.73	96.23
Number of atoms on the basis of 22 oxygens																
Si	5.34	5.31	5.29	5.29	5.28	5.31	5.32	5.23	5.32	5.23	5.27	5.25	5.23	5.23	5.25	5.22
Ti	0.52	0.45	0.52	0.54	0.58	0.53	0.48	0.51	0.56	0.57	0.36	0.30	0.34	0.51	0.27	0.31
Al	3.37	3.49	3.29	3.26	3.33	3.41	3.39	3.39	3.35	3.27	3.61	3.63	3.62	3.51	3.66	3.61
Cr	0.02	0.00	0.01	0.01	0.00	0.01	0.01	0.00	0.00	0.01	0.00	0.00	0.00	0.00	0.01	0.02
Mn	0.00	0.00	0.00	0.00	0.00	0.00	0.00	0.00	0.00	0.00	0.00	0.00	0.00	0.00	0.00	0.00
Mg	1.42	1.30	1.36	1.34	1.26	1.24	1.34	1.39	1.26	1.42	1.32	1.44	1.38	1.27	1.53	1.47
Ca	0.01	0.02	0.02	0.00	0.02	0.01	0.01	0.00	0.00	0.02	0.02	0.02	0.01	0.01	0.00	0.00
Na	0.13	0.16	0.13	0.14	0.16	0.14	0.13	0.01	0.09	0.11	0.15	0.15	0.16	0.15	0.16	0.13
K	1.82	1.84	1.83	1.86	1.85	1.84	1.81	1.76	1.83	1.85	1.80	1.78	1.77	1.72	1.78	1.86
Fe	2.83	2.96	3.08	3.08	3.00	3.00	2.98	3.09	3.02	3.09	3.01	3.02	3.11	3.05	2.96	3.00
Total	15.46	15.53	15.53	15.52	15.48	15.49	15.47	15.38	15.43	15.57	15.54	15.59	15.62	15.45	15.62	15.62

Sample	MM185B					MM188D										
Oxides																
SiO2	33.72	34.18	33.59	34.03	33.84	36.75	36.21	36.84	35.83	36.20	35.95	36.40	36.00	35.56	36.95	35.91
TiO2	3.25	1.98	2.08	3.50	2.54	2.25	2.44	2.50	2.09	1.79	1.86	1.75	2.09	2.34	2.39	2.40
Al2O3	20.17	19.88	19.90	19.47	20.39	18.00	18.00	18.57	19.34	18.64	19.09	19.17	19.17	18.66	19.31	18.78
Cr2O3	0.15	0.15	0.07	0.39	0.18	0.09	0.00	0.08	0.06	0.00	0.00	0.06	0.07	0.00	0.10	0.01
MnO	0.00	0.00	0.00	0.00	0.00	0.00	0.00	0.00	0.00	0.00	0.00	0.00	0.00	0.00	0.00	0.00
MgO	6.41	6.99	6.77	6.26	6.30	11.43	11.06	11.26	10.91	11.71	11.18	11.39	11.42	10.78	11.11	10.99
CaO	0.09	0.11	0.13	0.05	0.08	0.03	0.00	0.11	0.05	0.04	0.17	0.03	0.08	0.07	0.17	0.00
Na2O	0.49	0.23	0.39	0.44	0.39	0.31	0.27	0.42	0.44	0.53	0.46	0.42	0.56	0.47	0.47	0.44
K2O	9.27	9.11	9.15	9.22	9.03	9.21	9.35	9.30	9.26	9.36	8.97	9.21	9.37	9.11	8.71	9.58
FeO	23.39	22.12	21.61	22.85	22.94	16.59	16.51	16.33	17.25	16.62	17.11	16.97	16.94	18.20	15.67	17.42
Total	96.94	94.75	93.69	96.21	95.69	94.66	93.84	95.41	95.23	94.89	94.79	95.40	95.70	95.19	94.88	95.53
Number of atoms on the basis of 22 oxygens																
SI	5.17	5.31	5.29	5.24	5.23	5.54	5.52	5.51	5.40	5.45	5.43	5.45	5.40	5.39	5.51	5.40
TI	0.37	0.23	0.25	0.40	0.29	0.25	0.28	0.28	0.24	0.20	0.21	0.20	0.24	0.27	0.27	0.27
Al	3.64	3.64	3.69	3.53	3.71	3.20	3.23	3.27	3.43	3.31	3.40	3.38	3.39	3.33	3.39	3.33
Cr	0.02	0.02	0.00	0.05	0.02	0.01	0.00	0.01	0.00	0.00	0.00	0.00	0.00	0.00	0.01	0.00
Mn	0.00	0.00	0.00	0.00	0.00	0.00	0.00	0.00	0.00	0.00	0.00	0.00	0.00	0.00	0.00	0.00
Mg	1.46	1.62	1.59	1.44	1.45	2.57	2.51	2.51	2.45	2.63	2.52	2.54	2.55	2.43	2.47	2.47
Ca	0.01	0.02	0.02	0.00	0.01	0.00	0.00	0.02	0.00	0.00	0.03	0.00	0.01	0.01	0.03	0.00
Na	0.14	0.07	0.12	0.13	0.12	0.09	0.08	0.12	0.13	0.15	0.14	0.12	0.16	0.14	0.13	0.13
K	1.81	1.81	1.84	1.81	1.78	1.77	1.82	1.78	1.78	1.80	1.73	1.76	1.79	1.76	1.66	1.84
Fe	3.00	2.88	2.84	2.94	2.96	2.09	2.11	2.04	2.17	2.09	2.16	2.12	2.13	2.30	1.95	2.19
Total	15.62	15.60	15.64	15.54	15.57	15.52	15.55	15.54	15.60	15.63	15.62	15.57	15.67	15.63	15.42	15.63
Sample	MM187														MM131B	
Oxides																
SiO2	33.80	33.80	33.99	33.94	34.35	33.21	34.24	33.58	34.13	34.70	34.14	33.61	33.31	33.44	33.19	33.12
TiO2	3.02	4.42	3.08	3.15	3.94	3.24	3.42	3.81	3.66	3.04	3.70	3.46	4.26	4.05	4.31	3.75
Al2O3	20.00	19.64	20.07	20.28	20.17	20.09	19.80	20.08	20.02	20.34	20.35	19.98	19.06	19.47	19.46	19.48
Cr2O3	0.08	0.08	0.00	0.02	0.02	0.16	0.28	0.10	0.10	0.02	0.06	0.25	0.16	0.15	0.11	0.15
MnO	0.00	0.00	0.00	0.00	0.00	0.00	0.00	0.00	0.00	0.00	0.00	0.00	0.00	0.00	0.00	0.00
MgO	6.88	6.27	6.45	6.86	6.74	6.69	6.33	6.67	6.82	6.91	6.68	6.43	6.42	6.39	5.94	6.37
CaO	0.16	0.16	0.05	0.08	0.20	0.11	0.15	0.08	0.13	0.15	0.10	0.16	0.19	0.13	0.05	0.07
Na2O	0.62	0.54	0.48	0.54	0.61	0.50	0.31	0.44	0.61	0.41	0.45	0.50	0.57	0.36	0.48	0.39
K2O	9.30	9.26	9.13	9.27	9.24	8.73	9.36	9.33	9.43	9.11	9.18	9.24	8.93	9.10	9.38	9.28
FeO	22.67	22.94	23.65	22.34	22.15	23.60	22.82	22.26	22.58	22.04	23.05	22.82	22.36	22.81	23.13	23.04
Total	96.53	97.11	96.90	96.48	97.42	96.33	96.71	96.35	97.48	96.72	97.71	96.45	95.26	95.90	96.05	95.65
Number of atoms on the basis of 22 oxygens																
SI	5.19	5.16	5.21	5.19	5.20	5.12	5.25	5.15	5.18	5.26	5.17	5.17	5.18	5.17	5.15	5.15
TI	0.35	0.51	0.35	0.36	0.45	0.37	0.39	0.44	0.42	0.35	0.42	0.40	0.50	0.47	0.50	0.44
Al	3.62	3.54	3.62	3.66	3.60	3.65	3.58	3.63	3.58	3.64	3.63	3.62	3.49	3.55	3.56	3.57
Cr	0.01	0.01	0.00	0.00	0.00	0.02	0.03	0.01	0.01	0.00	0.00	0.03	0.02	0.02	0.01	0.02
Mn	0.00	0.00	0.00	0.00	0.00	0.00	0.00	0.00	0.00	0.00	0.00	0.00	0.00	0.00	0.00	0.00
Mg	1.57	1.43	1.47	1.56	1.52	1.54	1.45	1.53	1.54	1.56	1.51	1.47	1.49	1.47	1.37	1.48
Ca	0.03	0.03	0.00	0.01	0.03	0.02	0.02	0.01	0.02	0.02	0.02	0.03	0.03	0.02	0.00	0.01
Na	0.18	0.16	0.14	0.16	0.18	0.15	0.09	0.13	0.18	0.12	0.13	0.15	0.17	0.11	0.14	0.12
K	1.82	1.81	1.78	1.81	1.78	1.72	1.83	1.83	1.82	1.76	1.77	1.81	1.77	1.79	1.86	1.84
Fe	2.91	2.93	3.03	2.86	2.81	3.04	2.93	2.86	2.86	2.80	2.92	2.94	2.91	2.95	3.00	2.99
Total	15.68	15.58	15.60	15.61	15.57	15.63	15.57	15.59	15.61	15.51	15.57	15.62	15.56	15.55	15.59	15.62

Sample	MM131B						MM197A									
Oxides																
SiO2	33.20	33.47	34.17	33.67	33.31	34.52	35.48	37.09	35.91	35.00	35.35	35.73	36.28	36.04	35.90	36.34
TiO2	4.49	4.57	4.47	3.70	4.29	3.32	4.72	4.10	4.55	4.58	4.41	4.10	4.20	3.88	4.14	4.11
Al2O3	19.55	18.95	18.79	19.35	18.95	18.79	16.13	16.45	16.75	16.76	17.26	16.81	16.95	16.74	16.65	16.73
Cr2O3	0.07	0.09	0.00	0.09	0.08	0.05	0.12	0.02	0.17	0.11	0.21	0.16	0.16	0.16	0.22	0.11
MnO	0.00	0.00	0.00	0.00	0.00	0.00	0.00	0.00	0.00	0.00	0.00	0.00	0.00	0.00	0.00	0.00
MgO	5.65	5.86	6.69	6.33	6.68	7.22	8.92	8.95	9.11	8.26	8.66	8.97	10.30	10.59	10.76	10.94
CaO	0.12	0.17	0.08	0.13	0.04	0.14	0.00	0.10	0.10	0.04	0.09	0.08	0.09	0.09	0.05	0.08
Na2O	0.47	0.52	0.34	0.46	0.51	0.45	0.41	0.36	0.47	0.45	0.42	0.49	0.40	0.55	0.49	0.41
K2O	9.30	9.46	9.44	9.39	9.17	9.49	9.32	9.11	9.03	9.14	9.29	9.47	9.48	9.32	9.47	9.43
FeO	23.88	22.98	22.78	23.01	22.46	22.15	21.26	20.33	20.51	20.50	21.60	21.00	19.21	18.87	18.57	18.26
Total	96.73	96.07	96.76	96.13	95.49	96.13	96.36	96.51	96.60	94.84	97.29	96.81	97.07	96.24	96.25	96.41
Number of atoms on the basis of 22 oxygens																
Si	5.13	5.19	5.23	5.20	5.18	5.31	5.42	5.59	5.43	5.41	5.35	5.43	5.44	5.44	5.42	5.46
Ti	0.52	0.53	0.51	0.43	0.50	0.38	0.54	0.46	0.52	0.53	0.50	0.47	0.47	0.44	0.47	0.46
Al	3.56	3.46	3.39	3.52	3.48	3.40	2.90	2.92	2.99	3.06	3.08	3.01	3.00	2.98	2.96	2.96
Cr	0.00	0.01	0.00	0.01	0.01	0.00	0.01	0.00	0.02	0.01	0.02	0.02	0.02	0.02	0.03	0.01
Mn	0.00	0.00	0.00	0.00	0.00	0.00	0.00	0.00	0.00	0.00	0.00	0.00	0.00	0.00	0.00	0.00
Mg	1.30	1.36	1.53	1.46	1.55	1.65	2.03	2.01	2.05	1.90	1.95	2.03	2.30	2.38	2.42	2.45
Ca	0.02	0.03	0.01	0.02	0.00	0.02	0.00	0.02	0.02	0.00	0.01	0.01	0.01	0.01	0.00	0.01
Na	0.14	0.16	0.10	0.14	0.15	0.13	0.12	0.11	0.14	0.14	0.12	0.14	0.12	0.16	0.14	0.12
K	1.83	1.87	1.84	1.85	1.82	1.86	1.82	1.75	1.74	1.80	1.79	1.84	1.81	1.79	1.82	1.81
Fe	3.08	2.98	2.92	2.97	2.92	2.85	2.72	2.56	2.60	2.65	2.73	2.67	2.41	2.38	2.34	2.29
Total	15.58	15.59	15.53	15.60	15.61	15.60	15.56	15.42	15.51	15.50	15.55	15.62	15.58	15.60	15.60	15.57
Sample	MM155							MM184B								
Oxides																
SiO2	36.31	36.00	35.04	35.45	35.36	36.73	36.15	41.24	34.24	33.89	34.45	34.66	35.73	35.25	34.60	34.25
TiO2	2.16	2.62	3.03	3.85	1.76	1.94	2.99	3.11	4.32	4.14	4.22	4.74	3.77	4.34	4.04	3.76
Al2O3	19.86	19.41	19.35	18.89	19.95	18.96	19.04	18.70	19.20	19.59	18.93	19.16	20.77	19.39	19.64	19.92
Cr2O3	0.13	0.90	0.08	0.10	0.12	0.01	0.12	0.14	0.01	0.18	0.13	0.10	0.11	0.03	0.04	0.09
MnO	0.00	0.00	0.00	0.00	0.00	0.00	0.00	0.00	0.00	0.00	0.00	0.01	0.00	0.00	0.00	0.00
MgO	9.31	7.91	6.27	7.38	8.38	9.74	8.57	8.04	8.93	8.46	9.00	9.28	8.58	9.37	9.06	8.87
CaO	0.00	0.12	0.05	0.02	0.06	0.16	0.08	0.00	0.09	0.02	0.12	0.00	0.02	0.13	0.00	0.05
Na2O	0.46	0.51	0.38	0.44	0.50	0.38	0.44	0.42	0.30	0.38	0.48	0.51	0.50	0.57	0.56	0.55
K2O	9.55	9.51	9.38	9.34	9.49	9.25	9.40	8.52	9.38	9.50	9.37	9.48	9.25	9.64	9.45	9.02
FeO	18.58	19.30	22.39	21.29	19.39	18.27	19.78	15.98	17.90	19.12	18.94	18.26	16.91	18.23	18.63	18.39
Total	96.36	96.28	95.97	96.76	95.01	95.44	96.57	96.15	94.37	95.28	95.64	96.20	95.64	96.95	96.02	94.90
Number of atoms on the basis of 22 oxygens																
Si	5.43	5.46	5.38	5.38	5.40	5.53	5.44	5.99	5.25	5.18	5.24	5.22	5.33	5.26	5.23	5.22
Ti	0.24	0.30	0.35	0.44	0.20	0.22	0.34	0.34	0.50	0.48	0.48	0.54	0.42	0.49	0.46	0.43
Al	3.50	3.47	3.50	3.38	3.59	3.36	3.38	3.20	3.47	3.53	3.40	3.40	3.65	3.41	3.50	3.58
Cr	0.02	0.01	0.01	0.01	0.01	0.00	0.01	0.02	0.00	0.02	0.02	0.01	0.01	0.00	0.00	0.01
Mn	0.00	0.00	0.00	0.00	0.00	0.00	0.00	0.00	0.00	0.00	0.00	0.00	0.00	0.00	0.00	0.00
Mg	2.08	1.79	1.43	1.67	1.91	2.19	1.92	1.74	2.04	1.93	2.04	2.08	1.91	2.09	2.04	2.02
Ca	0.00	0.02	0.01	0.00	0.01	0.03	0.01	0.00	0.01	0.00	0.02	0.00	0.00	0.02	0.00	0.00
Na	0.13	0.15	0.11	0.13	0.15	0.11	0.13	0.12	0.09	0.11	0.14	0.15	0.15	0.16	0.16	0.16
K	1.82	1.84	1.84	1.81	1.85	1.78	1.80	1.58	1.83	1.85	1.82	1.82	1.76	1.84	1.82	1.75
Fe	2.33	2.45	2.87	2.70	2.48	2.30	2.49	1.94	2.29	2.45	2.41	2.30	2.11	2.28	2.35	2.34
Total	15.55	15.49	15.50	15.52	15.60	15.52	15.52	14.93	15.48	15.55	15.57	15.52	15.34	15.55	15.56	15.51

Sample		MM143										MM188C				
Oxides																
SiO2	34.48	35.29	36.19	35.31	36.02	35.78	35.54	35.68	35.81	36.78	36.28	34.19	34.14	34.10	34.69	34.05
TiO2	4.32	4.26	3.83	4.35	4.42	4.32	4.31	3.46	3.86	3.17	4.06	3.95	2.89	3.34	4.27	3.62
Al2O3	18.73	17.33	17.91	17.36	17.49	17.65	17.72	17.55	17.35	18.77	17.43	19.54	19.93	19.84	18.86	19.98
Cr2O3	0.09	0.15	0.22	0.16	0.17	0.17	0.16	0.22	0.04	0.16	0.19	0.06	0.09	0.14	0.20	0.00
MnO	0.00	0.00	0.00	0.00	0.00	0.00	0.00	0.00	0.00	0.00	0.00	0.00	0.00	0.00	0.00	0.00
MgO	8.80	8.65	9.19	8.42	8.76	8.46	8.35	8.67	9.00	9.31	9.33	8.67	8.82	8.83	8.83	8.63
CaO	0.02	0.10	0.02	0.11	0.13	0.07	0.10	0.02	0.10	0.09	0.07	0.02	0.11	0.09	0.06	0.06
Na2O	0.52	0.48	0.51	0.32	0.44	0.45	0.46	0.54	0.42	0.47	0.52	0.42	0.44	0.46	0.39	0.44
K2O	9.37	9.21	9.54	9.41	9.45	9.36	9.28	9.41	9.37	8.30	9.35	9.32	9.32	9.49	9.52	9.50
FeO	18.83	19.90	19.85	20.23	19.64	20.03	20.74	19.32	19.73	17.90	19.82	18.97	18.33	18.47	19.37	18.95
Total	95.16	95.37	97.26	95.67	96.52	96.29	96.66	94.87	95.68	94.95	97.05	95.14	94.07	94.76	96.19	95.23
Number of atoms on the basis of 22 oxygens																
SI	5.27	5.40	5.42	5.40	5.43	5.43	5.39	5.47	5.46	5.54	5.44	5.22	5.27	5.23	5.26	5.20
TI	0.50	0.49	0.43	0.50	0.50	0.49	0.49	0.40	0.44	0.36	0.46	0.45	0.34	0.38	0.49	0.42
Al	3.37	3.13	3.16	3.13	3.11	3.16	3.17	3.17	3.12	3.33	3.08	3.52	3.62	3.59	3.37	3.60
Cr	0.01	0.02	0.03	0.02	0.02	0.02	0.02	0.03	0.00	0.02	0.02	0.00	0.01	0.02	0.02	0.00
Mn	0.00	0.00	0.00	0.00	0.00	0.00	0.00	0.00	0.00	0.00	0.00	0.00	0.00	0.00	0.00	0.00
Mg	2.00	1.97	2.05	1.92	1.70	1.91	1.89	1.98	2.05	2.09	2.09	1.97	2.03	2.02	1.99	1.97
Ca	0.00	0.02	0.00	0.02	0.02	0.01	0.02	0.00	0.02	0.01	0.01	0.00	0.02	0.01	0.01	0.01
Na	0.16	0.14	0.15	0.09	0.13	0.13	0.13	0.16	0.12	0.14	0.15	0.12	0.13	0.14	0.12	0.13
K	1.83	1.80	1.82	1.84	1.82	1.81	1.79	1.84	1.82	1.59	1.79	1.82	1.83	1.86	1.84	1.85
Fe	2.41	2.55	2.49	2.59	2.48	2.54	2.63	2.48	2.52	2.25	2.49	2.42	2.36	2.37	2.45	2.42
Total	15.55	15.52	15.55	15.51	15.21	15.50	15.53	15.53	15.55	15.33	15.53	15.52	15.61	15.62	15.55	15.60
Sample							MM171									
Oxides																
SiO2	34.66	33.65	34.17	33.62	33.73	34.52	33.19	33.10	33.50	34.53	34.14	33.75	33.91	33.37	33.70	33.64
TiO2	3.19	4.21	3.27	3.71	4.31	3.11	3.91	3.88	3.41	3.15	2.14	3.60	3.55	3.63	3.85	3.55
Al2O3	20.30	19.36	19.95	19.69	19.75	20.36	18.99	18.98	19.71	20.15	19.57	18.79	19.19	19.08	19.60	19.25
Cr2O3	0.08	0.04	0.17	0.00	0.15	0.08	0.04	0.02	0.07	0.00	0.06	0.10	0.00	0.00	0.05	0.07
MnO	0.00	0.00	0.00	0.00	0.00	0.00	0.00	0.00	0.00	0.00	0.00	0.00	0.00	0.00	0.00	0.00
MgO	8.80	8.57	9.13	8.38	8.33	9.02	6.58	6.59	6.02	5.80	6.11	6.24	5.54	5.57	6.27	6.20
CaO	0.07	0.02	0.09	0.10	0.10	0.11	0.11	0.08	0.13	0.21	0.17	0.17	0.12	0.15	0.08	0.02
Na2O	0.57	0.53	0.42	0.36	0.37	0.54	0.39	0.39	0.50	0.32	0.51	0.28	0.45	0.40	0.55	0.54
K2O	9.38	9.27	9.24	9.36	9.26	9.35	8.97	8.59	9.38	8.41	9.18	8.90	9.14	9.20	9.33	9.25
FeO	18.63	18.66	18.73	19.16	19.56	18.82	23.21	24.00	23.14	22.73	24.09	23.08	24.06	24.63	23.08	23.91
Total	95.68	94.31	95.17	94.38	95.56	95.91	95.39	95.63	95.86	95.30	95.97	94.91	95.96	96.03	96.51	96.43
Number of atoms on the basis of 22 oxygens																
SI	5.25	5.19	5.22	5.19	5.16	5.23	5.17	5.15	5.19	5.32	5.30	5.28	5.27	5.20	5.81	5.20
TI	0.36	0.49	0.38	0.43	0.49	0.35	0.46	0.45	0.40	0.36	0.25	0.42	0.41	0.43	0.45	0.41
Al	3.62	3.52	3.59	3.58	3.56	3.63	3.49	3.48	3.60	3.66	3.58	3.46	3.51	3.51	3.55	3.51
Cr	0.01	0.00	0.02	0.00	0.02	0.01	0.00	0.00	0.00	0.00	0.00	0.01	0.00	0.00	0.00	0.00
Mn	0.00	0.00	0.00	0.00	0.00	0.00	0.00	0.00	0.00	0.00	0.00	0.00	0.00	0.00	0.00	0.00
Mg	1.99	1.97	2.08	1.93	1.90	2.03	1.53	1.53	1.39	1.33	1.41	1.45	1.28	1.29	1.44	1.43
Ca	0.01	0.00	0.01	0.02	0.02	0.02	0.02	0.01	0.02	0.03	0.03	0.03	0.02	0.03	0.01	0.00
Na	0.17	0.16	0.12	0.11	0.11	0.16	0.12	0.12	0.15	0.09	0.15	0.08	0.13	0.12	0.16	0.16
K	1.81	1.82	1.80	1.84	1.81	1.80	1.78	1.70	1.85	1.65	1.82	1.78	1.81	1.83	1.83	1.82
Fe	2.36	2.40	2.39	2.47	2.50	2.38	3.02	3.12	3.00	2.93	3.13	3.02	3.12	3.21	2.97	3.09
Total	15.58	15.55	15.61	15.57	15.57	15.61	15.59	15.56	15.60	15.37	15.67	15.53	15.55	15.62	16.22	15.62

Sample					MM197B										MM181	
Oxides																
SiO2	33.81	33.58	33.76	33.72	34.97	35.15	35.76	35.44	34.96	34.96	35.03	34.63	34.75	35.08	34.80	34.94
TiO2	2.95	3.01	3.17	3.03	4.27	4.16	3.91	4.06	4.56	5.22	5.31	4.07	4.06	3.96	3.57	3.29
Al2O3	19.72	19.85	19.48	20.15	17.14	17.42	18.43	17.40	17.44	16.50	17.00	17.21	17.27	17.69	19.09	19.05
Cr2O3	0.02	0.05	0.09	0.04	0.37	0.39	0.26	0.27	0.20	0.13	0.09	0.13	0.20	0.30	0.04	0.08
MnO	0.00	0.00	0.00	0.00	0.00	0.00	0.00	0.00	0.00	0.00	0.00	0.00	0.00	0.00	0.00	0.00
MgO	6.38	6.21	6.23	6.32	7.87	7.89	7.27	7.68	7.61	7.15	7.72	7.48	7.70	7.65	7.89	7.46
CaO	0.17	0.12	0.13	0.16	0.09	0.09	0.09	0.06	0.13	0.07	0.00	0.00	0.02	0.10	0.03	0.13
Na2O	0.50	0.47	0.37	0.47	0.44	0.49	0.30	0.32	0.46	0.31	0.42	0.37	0.49	0.33	0.50	0.51
K2O	9.36	9.29	9.22	9.39	9.28	9.12	8.47	9.02	9.20	9.25	9.27	9.17	8.96	9.32	9.45	9.30
FeO	23.98	23.47	23.38	23.76	21.61	21.77	20.93	22.12	21.94	23.36	21.69	22.14	22.73	21.87	20.02	20.47
Total	96.89	96.05	95.83	97.04	96.04	96.48	95.42	96.37	96.50	96.95	96.53	95.20	96.18	96.30	95.39	95.23
Number of atoms on the basis of 22 oxygens																
Si	5.21	5.20	5.23	5.16	5.38	5.37	5.45	5.41	5.35	5.36	5.35	5.38	5.36	5.38	5.33	5.37
Ti	0.34	0.35	0.37	0.35	0.49	0.48	0.45	0.47	0.52	0.60	0.61	0.48	0.47	0.46	0.41	0.38
Al	3.58	3.63	3.56	3.64	3.11	3.14	3.31	3.13	3.14	2.98	3.06	3.15	3.14	3.20	3.44	3.45
Cr	0.00	0.00	0.01	0.00	0.04	0.05	0.03	0.03	0.02	0.02	0.01	0.02	0.02	0.04	0.00	0.00
Mn	0.00	0.00	0.00	0.00	0.00	0.00	0.00	0.00	0.00	0.00	0.00	0.00	0.00	0.00	0.00	0.00
Mg	1.46	1.43	1.44	1.44	1.80	1.80	1.65	1.75	1.74	1.63	1.76	1.73	1.76	1.75	1.80	1.71
Ca	0.03	0.02	0.02	0.03	0.02	0.01	0.01	0.01	0.02	0.01	0.00	0.00	0.00	0.02	0.00	0.02
Na	0.15	0.14	0.11	0.14	0.13	0.14	0.09	0.09	0.14	0.09	0.12	0.11	0.15	0.10	0.15	0.15
K	1.84	1.84	1.82	1.84	1.82	1.78	1.65	1.76	1.79	1.81	1.81	1.82	1.76	1.82	1.84	1.82
Fe	3.09	3.04	3.03	3.04	2.78	2.78	2.67	2.82	2.81	2.99	2.77	2.88	2.93	2.81	2.56	2.63
Total	15.70	15.65	15.59	15.64	15.57	15.55	15.31	15.47	15.53	15.49	15.49	15.57	15.59	15.58	15.53	15.53
Sample											MM141A					
Oxides																
SiO2	35.23	34.80	34.81	35.45	35.46	35.05	34.68	35.46	34.93	35.12	34.76	35.01	34.25	35.49	33.49	35.88
TiO2	3.61	3.58	3.24	2.85	2.82	3.09	3.82	3.59	4.07	3.02	3.26	3.51	2.39	3.87	2.69	3.65
Al2O3	18.97	19.45	19.55	19.39	20.26	19.32	19.38	19.72	19.22	19.20	18.70	18.49	19.59	18.34	19.03	18.50
Cr2O3	0.00	0.14	0.00	0.06	0.03	0.05	0.02	0.07	0.00	0.10	0.61	0.71	0.39	0.23	0.02	0.22
MnO	0.00	0.00	0.00	0.00	0.00	0.00	0.00	0.00	0.00	0.00	0.00	0.00	0.00	0.00	0.00	0.00
MgO	8.21	7.79	8.21	8.77	8.90	8.20	7.97	8.37	7.78	8.43	6.45	6.40	6.42	6.33	6.99	6.85
CaO	0.07	0.10	0.08	0.08	0.10	0.05	0.09	0.02	0.06	0.09	0.09	0.11	0.09	0.08	0.14	0.12
Na2O	0.61	0.46	0.58	0.51	0.47	0.49	0.47	0.52	0.45	0.41	0.37	0.39	0.42	0.42	0.69	0.49
K2O	9.29	9.49	9.35	9.27	9.53	9.46	9.61	9.53	9.33	9.45	9.33	9.38	9.25	9.32	8.17	9.30
FeO	20.32	20.63	20.80	19.66	20.01	19.82	20.51	20.51	20.73	20.18	22.47	22.38	23.27	21.87	23.39	22.03
Total	96.31	96.44	96.62	96.04	97.58	95.53	96.55	97.79	96.57	96.00	96.04	96.38	96.07	95.95	94.61	97.04
Number of atoms on the basis of 22 oxygens																
Si	5.33	5.28	5.27	5.36	5.28	5.35	5.27	5.29	5.30	5.35	5.36	5.37	5.30	5.43	5.24	5.42
Ti	0.41	0.41	0.37	0.32	0.32	0.35	0.44	0.40	0.46	0.35	0.38	0.40	0.28	0.44	0.32	0.41
Al	3.38	3.48	3.49	3.46	3.56	3.48	3.47	3.47	3.44	3.44	3.40	3.34	3.57	3.31	3.51	3.29
Cr	0.00	0.02	0.00	0.00	0.00	0.00	0.00	0.00	0.00	0.01	0.07	0.09	0.04	0.03	0.00	0.03
Mn	0.00	0.00	0.00	0.00	0.00	0.00	0.00	0.00	0.00	0.00	0.00	0.00	0.00	0.00	0.00	0.00
Mg	1.85	1.76	1.85	1.98	1.98	1.87	1.81	1.86	1.76	1.91	1.48	1.46	1.48	1.45	1.63	1.54
Ca	0.01	0.02	0.01	0.01	0.02	0.00	0.01	0.00	0.01	0.01	0.02	0.02	0.01	0.01	0.02	0.02
Na	0.18	0.14	0.17	0.15	0.13	0.14	0.14	0.15	0.13	0.12	0.11	0.12	0.12	0.13	0.21	0.14
K	1.79	1.84	1.81	1.79	1.81	1.84	1.86	1.81	1.81	1.83	1.84	1.84	1.82	1.82	1.63	1.79
Fe	2.57	2.62	2.63	2.49	2.49	2.53	2.61	2.55	2.63	2.57	2.90	2.87	3.01	2.80	3.06	2.78
Total	15.52	15.57	15.60	15.56	15.59	15.56	15.61	15.53	15.54	15.59	15.56	15.51	15.63	15.42	15.62	15.42

Sample	MM141			MM198C-F											MM146	
Oxides																
SiO2	34.74	35.79	35.43	36.71	37.12	36.97	37.46	36.35	36.71	36.35	36.98	35.93	36.47	36.04	34.06	33.70
TiO2	3.21	3.76	4.39	4.91	5.02	4.56	4.58	5.25	5.17	5.09	5.10	4.93	4.98	4.97	5.63	4.66
Al2O3	18.55	18.52	18.13	15.08	15.00	14.72	15.13	15.09	14.63	15.14	15.02	14.80	14.62	14.79	18.02	17.87
Cr2O3	0.38	0.18	0.27	0.17	0.10	0.17	0.18	0.39	0.06	0.64	0.43	0.31	0.33	0.24	0.88	0.69
MnO	0.00	0.00	0.00	0.00	0.00	0.00	0.00	0.00	0.00	0.00	0.00	0.00	0.00	0.00	0.00	0.00
MgO	6.65	6.66	6.73	13.39	14.59	14.63	15.02	13.07	13.81	13.75	13.93	14.02	13.99	12.46	5.62	5.98
CaO	0.11	0.04	0.02	0.20	0.19	0.19	0.24	0.18	0.14	1.00	0.16	0.18	0.14	0.11	0.00	0.11
Na2O	0.42	0.46	0.38	0.41	0.49	0.61	0.56	0.57	0.52	0.63	0.55	0.62	0.48	0.50	0.30	0.40
K2O	8.98	9.29	9.30	9.07	9.10	9.05	9.11	9.13	9.10	9.26	9.17	8.34	9.01	9.04	9.20	9.07
FeO	21.55	22.21	21.71	16.21	14.52	15.13	13.74	16.38	16.15	15.34	15.23	15.30	14.58	17.21	21.65	21.56
Total	94.59	96.91	96.36	96.15	96.13	96.03	96.02	96.41	96.29	97.20	96.57	94.43	94.60	95.36	95.36	94.04
Number of atoms on the basis of 22 oxygens																
Si	5.39	5.44	5.41	5.48	5.49	5.49	5.52	5.43	5.47	5.42	5.47	5.43	5.49	5.47	5.28	5.31
Ti	0.37	0.43	0.50	0.55	0.56	0.51	0.51	0.59	2.57	0.57	0.57	0.56	0.56	0.57	0.66	0.55
Al	3.39	3.32	3.26	2.65	2.62	2.58	2.63	2.66	0.00	2.66	2.62	2.64	2.59	2.64	3.29	3.32
Cr	0.05	0.02	0.03	0.02	0.01	0.02	0.02	0.05	0.00	0.07	0.05	0.04	0.04	0.03	0.11	0.09
Mn	0.00	0.00	0.00	0.00	0.00	0.00	0.00	0.00	3.07	0.00	0.00	0.00	0.00	0.00	0.00	0.00
Mg	1.54	1.51	1.53	2.98	3.22	3.24	3.30	2.91	0.02	3.05	3.07	3.16	3.14	2.82	1.30	1.40
Ca	0.02	0.00	0.00	0.03	0.03	0.03	0.04	0.03	0.00	0.02	0.02	0.03	0.02	0.02	0.00	0.02
Na	0.13	0.14	0.11	0.12	0.14	0.18	0.16	0.16	0.15	0.18	0.16	0.18	0.14	0.15	0.09	0.12
K	1.78	1.80	1.81	1.73	1.71	1.71	1.71	1.74	1.73	1.76	1.73	1.61	1.73	1.75	1.82	1.82
Fe	2.80	2.82	2.77	2.02	1.80	1.88	1.69	2.04	2.01	1.91	1.88	1.93	1.83	2.18	2.81	2.84
Total	15.47	15.48	15.42	15.58	15.58	15.64	15.58	15.61	15.02	15.64	15.57	15.58	15.54	15.63	15.36	15.47

Sample								255D	MM188D.PL							
Oxides																
SiO2	34.11	34.04	34.08	34.52	34.15	34.14	33.98	33.25	33.70	35.00	33.95	34.15	33.81	33.78	33.73	34.23
TiO2	4.50	4.38	2.98	5.28	4.53	5.56	3.79	1.88	3.86	4.56	3.10	4.24	3.59	3.89	3.84	3.47
Al2O3	17.65	17.77	17.75	17.21	17.49	16.93	18.00	17.27	19.69	19.05	20.04	18.98	19.69	19.89	19.23	19.53
Cr2O3	1.03	0.63	0.48	0.63	0.63	0.67	0.58	0.00	0.29	0.13	0.24	0.08	0.13	0.09	0.26	0.04
MnO	0.00	0.00	0.00	0.00	0.00	0.00	0.00	0.00	0.00	0.00	0.00	0.00	0.00	0.00	0.00	0.00
MgO	6.31	6.43	6.58	6.19	6.38	5.70	5.01	5.97	8.02	7.83	7.67	7.43	7.70	7.67	7.41	8.23
CaO	0.00	0.08	0.11	0.04	0.15	0.09	0.11	0.14	0.02	0.00	0.13	0.07	0.11	0.00	0.07	0.09
Na2O	0.29	0.37	4.30	0.36	0.37	0.36	0.43	0.48	0.38	0.45	0.44	0.29	0.28	0.42	0.50	0.46
K2O	9.22	9.13	9.06	9.22	9.30	8.92	9.05	7.83	9.42	9.32	9.25	9.25	9.41	9.10	9.29	9.14
FeO	22.33	21.88	22.15	21.86	21.39	22.47	24.00	26.88	20.16	19.78	21.70	20.09	20.91	20.12	21.14	20.05
Total	95.44	94.71	97.49	95.31	94.39	94.84	94.95	93.70	95.54	96.12	96.52	94.58	95.63	94.96	95.47	95.24
Number of atoms on the basis of 22 oxygens																
Si	5.31	5.32	5.39	5.36	5.36	5.36	5.34	5.62	5.18	5.31	5.18	5.28	5.19	5.20	5.21	5.25
Ti	0.53	0.52	0.35	0.62	0.53	0.66	0.45	0.24	0.45	0.52	0.36	0.49	0.41	0.45	0.45	0.40
Al	3.24	3.27	3.31	3.15	3.23	3.13	3.34	3.44	3.57	3.40	3.60	3.46	3.56	3.61	3.50	3.53
Cr	0.13	0.08	0.06	0.08	0.08	0.08	0.07	0.00	0.03	0.01	0.03	0.01	0.02	0.01	0.03	0.00
Mn	0.00	0.00	0.00	0.00	0.00	0.00	0.00	0.00	0.00	0.00	0.00	0.00	0.00	0.00	0.00	0.00
Mg	1.46	1.50	1.55	1.43	1.49	1.33	1.18	1.50	1.84	1.77	1.74	1.71	1.76	1.76	1.70	1.88
Ca	0.00	0.01	0.02	0.00	0.02	0.01	0.02	0.03	0.00	0.00	0.02	0.01	0.02	0.00	0.01	0.01
Na	0.09	0.11	0.13	0.11	0.11	0.11	0.13	0.16	0.11	0.13	0.13	0.09	0.08	0.13	0.15	0.14
K	1.83	1.82	1.82	1.83	1.86	1.79	1.81	1.69	1.85	1.80	1.80	1.82	1.84	1.79	1.83	1.79
Fe	2.91	2.86	2.93	2.84	2.81	2.95	3.16	3.75	2.59	2.51	2.77	2.60	2.68	2.59	2.73	2.57
Total	15.50	15.49	15.56	15.42	15.49	15.42	15.50	16.43	15.62	15.45	15.63	15.47	15.56	15.54	15.61	15.57

Sample		MM166D														MM134A
Oxides																
SiO2	33.77	35.67	34.64	35.12	34.93	34.84	34.70	34.94	34.50	34.75	35.29	34.70	34.93	34.93	35.44	35.73
TiO2	3.93	3.28	3.23	3.18	3.08	3.56	3.53	3.64	4.13	4.11	5.15	4.59	4.34	4.34	4.72	3.75
Al2O3	19.37	17.79	18.02	18.01	17.75	17.74	18.22	17.42	17.86	17.88	17.97	17.96	17.96	17.96	17.28	18.78
Cr2O3	0.15	0.12	0.02	0.04	0.05	0.06	0.00	0.00	0.09	0.03	0.06	0.03	0.08	0.08	0.05	0.12
MnO	0.00	0.00	0.00	0.00	0.00	0.00	0.00	0.00	0.00	0.00	0.00	0.00	0.00	0.00	0.00	0.03
MgO	7.27	9.04	8.91	9.00	8.94	8.56	8.97	9.11	8.34	8.89	8.62	9.04	9.22	9.22	9.18	9.07
CaO	0.13	0.18	0.08	0.11	0.09	0.10	0.13	0.05	0.12	0.04	0.14	0.12	0.08	0.08	0.06	0.17
Na2O	0.41	0.59	0.58	0.58	0.52	0.50	0.60	0.61	0.48	0.50	0.58	0.57	0.55	0.55	0.67	0.48
K2O	9.30	9.44	9.40	9.51	9.46	9.54	9.55	9.33	9.46	9.51	9.56	9.56	9.38	9.38	9.56	7.81
FeO	21.71	21.75	21.89	21.68	21.60	22.04	21.91	21.22	21.89	20.37	21.12	20.62	20.35	20.35	20.73	18.69
Total	96.04	97.86	96.77	97.23	96.42	96.94	97.61	96.32	96.87	96.08	98.49	97.19	96.89	96.89	97.69	94.63
Number of atoms on the basis of 22 oxygens																
Si	5.20	5.37	5.28	5.33	5.35	5.31	5.25	5.35	5.27	5.31	5.27	5.25	5.28	5.28	5.33	5.41
Ti	0.45	0.37	0.37	0.36	0.35	0.41	0.40	0.42	0.47	0.47	0.58	0.52	0.49	0.49	0.53	0.43
Al	3.51	3.16	3.24	3.22	3.20	3.19	3.25	3.14	3.22	3.22	3.16	3.20	3.20	3.20	3.06	3.35
Cr	0.02	0.01	0.00	0.00	0.00	0.00	0.00	0.00	0.01	0.00	0.00	0.00	0.01	0.01	0.00	0.01
Mn	0.00	0.00	0.00	0.00	0.00	0.00	0.00	0.00	0.00	0.00	0.00	0.00	0.00	0.00	0.00	0.00
Mg	1.67	2.03	2.03	2.04	2.04	1.94	2.02	2.08	1.90	2.02	1.62	2.04	2.08	2.08	2.06	2.05
Ca	0.02	0.03	0.01	0.02	0.01	0.02	0.02	0.00	0.02	0.00	0.02	0.02	0.01	0.01	0.00	0.03
Na	0.12	0.17	0.17	0.17	0.15	0.15	0.18	0.18	0.14	0.15	0.17	0.17	0.16	0.16	0.20	0.14
K	1.83	1.81	1.83	1.84	1.85	1.85	1.84	1.82	1.84	1.85	1.82	1.84	1.81	1.81	1.83	1.51
Fe	2.79	2.74	2.79	2.75	2.77	2.81	2.77	2.72	2.80	2.60	2.64	2.61	2.57	2.57	2.61	2.37
Total	15.61	15.69	15.72	15.73	15.72	15.68	15.73	15.71	15.67	15.62	15.28	15.65	15.61	15.61	15.62	15.30
Sample												MM166A				
Oxides																
SiO2	34.72	35.29	35.50	35.50	34.65	35.60	35.46	35.47	35.23	35.15	34.86	34.84	34.96	34.84	35.44	35.01
TiO2	4.37	4.05	4.21	4.16	4.30	3.87	4.91	5.02	4.36	3.91	3.39	5.64	5.40	5.21	5.29	5.35
Al2O3	17.22	17.70	17.78	17.47	17.34	17.79	17.30	17.30	16.30	16.37	17.24	16.28	16.34	16.48	16.81	16.62
Cr2O3	0.00	0.05	0.24	0.07	0.07	0.02	0.08	0.17	0.14	0.07	0.11	0.16	0.18	0.21	0.17	0.26
MnO	0.02	0.06	0.19	0.17	0.28	0.00	0.00	0.00	0.00	0.00	0.00	0.00	0.00	0.00	0.00	0.00
MgO	9.77	9.40	8.85	8.65	8.58	9.04	8.89	8.96	8.83	9.30	8.40	6.92	7.11	7.24	6.91	7.01
CaO	0.17	0.18	0.13	0.10	0.04	0.05	0.08	0.07	0.09	0.12	0.14	0.04	0.13	0.07	0.05	0.11
Na2O	0.55	0.57	0.48	0.47	0.47	0.42	0.49	0.50	0.40	0.47	0.52	0.44	0.48	0.45	0.46	0.32
K2O	8.44	9.32	9.05	9.47	9.18	9.41	9.43	9.36	8.97	9.03	8.96	9.17	9.21	9.25	8.68	9.30
FeO	19.10	19.34	18.98	19.00	18.20	18.60	19.03	19.07	21.17	19.72	21.45	23.29	22.78	23.34	21.95	22.80
Total	94.36	95.96	95.41	95.06	93.11	94.80	95.67	95.92	95.49	94.14	95.07	96.78	96.59	97.09	95.76	96.78
Number of atoms on the basis of 22 oxygens																
Si	5.33	5.35	5.40	5.43	5.40	5.44	5.39	5.38	5.43	5.44	5.39	5.36	5.37	5.35	5.44	5.38
Ti	0.50	0.46	0.48	0.48	0.50	0.44	0.56	0.57	0.50	0.45	0.39	0.65	0.62	0.60	0.61	0.62
Al	3.12	3.16	3.19	3.15	3.19	3.20	3.10	3.09	2.96	2.99	3.14	2.95	2.96	2.98	3.04	3.01
Cr	0.00	0.00	0.03	0.00	0.00	0.00	0.01	0.02	0.02	0.00	0.01	0.02	0.02	0.02	0.02	0.03
Mn	0.00	0.00	0.02	0.02	0.04	0.00	0.00	0.00	0.00	0.00	0.00	0.00	0.00	0.00	0.00	0.00
Mg	2.23	2.12	2.00	1.97	1.99	2.06	2.02	2.02	2.03	2.15	1.94	1.59	1.63	1.66	1.58	1.61
Ca	0.03	0.03	0.02	0.02	0.00	0.00	0.01	0.01	0.01	0.02	0.02	0.00	0.02	0.01	0.00	0.02
Na	0.16	0.17	0.14	0.14	0.14	0.12	0.15	0.15	0.12	0.14	0.15	0.13	0.14	0.13	0.14	0.09
K	1.65	1.80	1.75	1.85	1.83	1.83	1.83	1.81	1.76	1.78	1.77	1.80	1.80	1.81	1.70	1.82
Fe	2.45	2.45	2.41	2.43	2.37	2.38	2.42	2.42	2.73	2.55	2.77	3.00	2.93	3.00	3.04	2.93
Total	15.47	15.54	15.44	15.49	15.46	15.47	15.49	15.47	15.56	15.52	15.58	15.50	15.49	15.56	15.57	15.51

Sample	MM166A									MM149						
Oxides																
SiO2	35.14	35.27	34.86	35.05	34.97	35.33	35.23	34.69	34.73	34.25	33.69	34.69	34.97	34.66	34.78	34.79
TiO2	5.49	5.07	6.42	2.15	5.50	3.81	4.30	4.00	6.07	3.72	3.77	3.85	3.94	3.65	4.06	4.16
Al2O3	16.52	16.50	16.07	16.85	16.62	17.06	16.56	16.73	16.58	18.79	18.40	18.84	18.72	18.78	18.89	18.44
Cr2O3	0.22	0.10	0.18	0.03	0.12	0.11	0.20	0.19	0.23	0.02	0.04	0.06	0.10	0.01	0.01	0.13
MnO	0.00	0.00	0.00	0.00	0.00	0.00	0.00	0.00	0.00	0.00	0.00	0.00	0.00	0.00	0.00	0.00
MgO	7.01	7.14	9.32	11.32	9.84	8.51	8.05	8.36	9.10	6.99	7.07	7.17	6.94	7.25	7.05	6.92
CaO	0.02	0.11	0.14	0.11	0.11	0.05	0.12	0.02	0.00	0.12	0.08	0.05	0.00	0.08	0.09	0.11
Na2O	0.48	0.41	0.84	0.32	0.99	0.33	0.45	0.39	0.75	0.40	0.31	0.57	0.49	0.45	0.42	0.38
K2O	9.06	9.11	8.53	8.48	8.07	9.01	9.13	8.88	8.83	9.12	8.50	9.10	9.20	9.32	9.24	9.39
FeO	23.46	16.50	20.16	20.40	19.33	22.26	22.07	22.47	19.98	21.31	22.46	21.82	21.78	21.94	21.76	21.54
Total	97.40	90.21	96.52	94.71	95.55	96.47	96.11	95.73	96.27	94.72	94.32	96.15	96.14	96.14	96.30	95.86
Number of atoms on the basis of 22 oxygens																
Si	5.36	5.41	5.29	5.39	5.33	5.40	5.42	5.36	5.27	5.32	5.27	5.31	5.34	5.32	5.31	5.35
Ti	0.63	0.58	0.73	0.25	0.63	0.44	0.50	0.46	0.69	0.43	0.44	0.44	0.45	0.42	0.47	0.48
Al	2.97	2.98	2.87	3.06	2.98	3.07	3.00	3.05	2.97	3.44	3.39	3.40	3.37	3.40	3.40	3.34
Cr	0.03	0.01	0.02	0.00	0.01	0.01	0.02	0.02	0.03	0.00	0.00	0.00	0.01	0.00	0.00	0.02
Mn	0.00	0.00	0.00	2.60	0.00	0.00	0.00	0.00	0.00	0.00	0.00	0.00	0.00	0.00	0.00	0.00
Mg	1.60	1.63	2.11	2.60	2.23	1.94	1.85	1.93	2.06	1.62	1.65	1.64	1.58	1.66	1.61	1.59
Ca	0.00	0.02	0.02	0.02	0.02	0.00	0.02	0.00	0.00	0.02	0.01	0.00	0.00	0.01	0.01	0.02
Na	0.14	0.12	0.25	0.10	0.29	0.10	0.13	0.12	0.22	0.12	0.09	0.17	0.14	0.13	0.12	0.11
K	1.76	1.78	1.65	1.66	1.57	1.76	1.79	1.75	1.71	1.81	1.70	1.78	1.79	1.82	1.80	1.84
Fe	2.99	2.93	2.56	2.63	2.46	2.84	2.84	2.91	2.54	2.77	2.94	2.79	2.78	2.82	2.78	2.77
Total	15.48	15.46	15.50	18.31	15.52	15.56	15.57	15.60	15.49	15.53	15.49	15.53	15.46	15.58	15.50	15.52

Sample			
Oxides			
SiO2	35.35	34.88	34.87
TiO2	3.67	3.07	3.16
Al2O3	19.29	19.91	18.94
Cr2O3	0.07	0.07	0.07
MnO	0.00	0.00	0.00
MgO	6.72	6.79	7.35
CaO	0.11	0.13	0.00
Na2O	0.41	0.45	0.43
K2O	8.99	8.56	9.34
FeO	20.47	20.61	21.35
Total	95.08	94.47	95.51
Number of atoms on the basis of 22 oxygens			
Si	5.42	5.37	5.36
Ti	0.42	0.36	0.36
Al	3.48	3.61	3.43
Cr	0.00	0.00	0.00
Mn	0.00	0.00	0.00
Mg	1.53	1.56	1.68
Ca	0.02	0.02	0.00
Na	0.12	0.13	0.13
K	1.76	1.68	1.83
Fe	2.62	2.65	2.75
Total	15.37	15.38	15.54

Microprobe results of cordierite in pelites

Sample Number	MM133.C										134A					
Oxide Percentage																
SiO2	47.79	47.73	48.07	47.84	47.79	48.33	48.44	47.85	47.73	48.10	48.84	48.05	47.50	48.63	48.11	48.61
TiO2	0.10	0.04	0.00	0.00	0.03	0.12	0.00	0.00	0.00	0.06	0.00	0.00	0.10	0.00	0.00	0.00
Al2O3	32.54	32.47	33.04	32.67	32.51	32.79	32.80	32.62	32.89	33.06	32.77	32.38	32.07	32.84	32.62	33.03
Cr2O3	0.00	0.00	0.08	0.07	0.00	0.07	0.00	0.03	0.00	0.07	0.08	0.00	0.00	0.04	0.05	0.10
MnO	0.00	0.03	0.04	0.03	0.00	0.00	0.01	0.04	0.08	0.00	0.97	0.84	0.68	1.06	0.10	0.85
MgO	6.91	6.88	7.02	6.73	7.07	6.85	6.89	6.72	7.03	7.19	7.79	7.43	7.48	7.40	7.48	7.35
CaO	0.00	0.00	0.05	0.00	0.00	0.00	0.00	0.00	0.90	0.02	0.03	0.00	0.06	0.00	0.07	0.00
ZnO	0.00	0.00	0.03	0.00	0.40	0.05	0.00	0.09	0.00	0.31	0.08	0.13	0.00	0.00	0.30	0.14
Na2O	0.49	0.26	0.39	0.27	0.36	0.38	0.34	0.35	0.34	0.45	0.39	0.31	0.33	0.33	0.41	0.25
K2O	0.03	0.00	0.03	0.00	0.00	0.03	0.00	0.00	0.00	0.00	0.06	0.00	0.05	0.00	0.08	0.00
FeO	11.28	11.16	11.03	11.14	10.96	11.12	11.16	10.93	11.04	11.20	9.24	9.40	8.96	9.43	9.02	9.62
Total	99.14	98.57	99.78	98.75	99.12	99.74	99.64	98.63	100.01	100.46	100.25	98.54	97.23	99.73	98.24	99.95
Number of atoms in the formula unit on the basis of the 18 oxygens																
Si	4.97	4.98	4.95	4.98	4.96	4.98	4.99	4.98	4.95	4.93	4.98	4.99	4.99	4.99	4.97	4.98
Ti	0.00	0.00	0.00	0.00	0.00	0.00	0.00	0.00	0.00	0.00	0.00	0.00	0.00	0.00	0.00	0.00
Al	3.99	3.99	4.01	4.00	3.98	3.98	3.98	4.00	4.02	3.99	3.94	3.97	3.97	3.97	3.98	3.99
Cr	0.00	0.00	0.00	0.00	0.00	0.00	0.00	0.00	0.00	0.00	0.00	0.00	0.00	0.00	0.00	0.00
Mn	0.00	0.00	0.00	0.00	0.00	0.00	0.00	0.00	0.00	0.00	0.08	0.07	0.06	0.09	0.09	0.07
Mg	1.07	1.07	1.08	1.04	1.09	1.05	1.06	1.04	1.09	1.10	1.19	1.15	1.17	1.13	1.15	1.12
Ca	0.00	0.00	0.00	0.00	0.00	0.00	0.00	0.00	0.01	0.00	0.00	0.00	0.00	0.00	0.00	0.00
Zn	0.00	0.00	0.00	0.00	0.03	0.00	0.00	0.00	0.00	0.02	0.00	0.01	0.00	0.00	0.02	0.01
Na	0.10	0.05	0.08	0.05	0.07	0.08	0.07	0.07	0.07	0.09	0.08	0.06	0.07	0.07	0.08	0.05
K	0.00	0.00	0.00	0.00	0.00	0.00	0.00	0.00	0.00	0.00	0.00	0.00	0.00	0.00	0.01	0.00
Fe	0.98	0.97	0.95	0.97	0.95	0.96	0.96	0.95	0.96	0.96	0.79	0.82	0.79	0.81	0.78	0.82
Total	11.11	11.06	11.07	11.04	11.08	11.05	11.06	11.04	11.10	11.09	11.06	11.07	11.05	11.06	11.08	11.04
Sample Number						MM151									MM133.BR	
Oxide Percentage																
SiO2	48.35	48.79	48.78	48.04	48.95	47.86	47.80	48.03	48.07	47.71	47.87	47.70	47.57	47.90	48.87	48.32
TiO2	0.01	0.09	0.01	0.00	0.03	0.00	0.00	0.00	0.02	0.00	0.00	0.00	0.06	0.02	0.02	0.00
Al2O3	32.81	32.76	33.17	32.75	33.15	32.26	32.45	32.14	32.54	32.07	32.13	32.25	32.07	32.62	32.47	32.76
Cr2O3	0.00	0.07	0.00	0.00	0.01	0.00	0.00	0.05	0.05	0.00	0.00	0.03	0.03	0.03	0.00	0.12
MnO	0.68	0.76	0.98	1.00	0.90	0.06	0.00	0.04	0.00	0.00	0.02	0.00	0.00	0.00	0.28	0.32
MgO	7.71	7.76	7.67	7.79	7.54	6.25	6.36	6.31	6.60	6.31	6.36	6.41	6.26	6.74	7.55	7.70
CaO	0.00	0.00	0.02	0.08	0.03	0.03	0.00	0.00	0.03	0.00	0.00	0.00	0.00	0.00	0.07	0.00
ZnO	0.03	0.00	0.00	0.00	0.00	0.00	0.00	0.12	0.00	0.00	0.00	0.00	0.44	0.00	0.16	0.05
Na2O	0.34	0.46	0.36	0.37	0.17	0.42	0.35	0.32	0.36	0.20	0.29	0.42	0.27	0.41	0.34	0.41
K2O	0.00	0.05	0.00	0.00	0.00	0.04	0.02	0.00	0.00	0.00	0.05	0.00	0.00	0.00	0.00	0.08
FeO	9.38	9.06	9.15	8.99	9.49	11.90	11.83	11.97	12.04	11.60	11.80	11.90	11.72	11.70	9.66	9.90
Total	99.31	99.80	100.14	99.02	100.27	98.82	98.81	98.98	99.71	97.89	98.52	98.71	98.42	99.42	99.42	99.66
Number of atoms in the formula unit on the basis of the 18 oxygens																
Si	4.97	4.99	4.98	4.96	4.99	5.00	5.00	5.01	4.97	5.01	5.00	4.99	4.99	4.97	5.02	4.96
Ti	0.00	0.00	0.00	0.00	0.00	0.00	0.00	0.00	0.00	0.00	0.00	0.00	0.00	0.00	0.00	0.00
Al	3.98	3.95	3.99	3.99	3.98	3.97	3.99	3.95	3.97	3.97	3.96	3.98	3.96	3.99	3.93	3.97
Cr	0.00	0.00	0.00	0.00	0.00	0.00	0.00	0.00	0.00	0.00	0.00	0.00	0.00	0.00	0.00	0.01
Mn	0.06	0.07	0.08	0.09	0.08	0.00	0.00	0.00	0.00	0.00	0.00	0.00	0.00	0.00	0.02	0.03
Mg	1.18	1.18	1.17	1.20	1.14	0.97	0.99	0.98	1.02	0.90	0.99	1.00	0.98	1.04	1.16	1.18
Ca	0.00	0.00	0.00	0.00	0.00	0.00	0.00	0.00	0.00	0.00	0.00	0.00	0.00	0.00	0.00	0.00
Zn	0.00	0.00	0.00	0.00	0.00	0.00	0.00	0.01	0.00	0.00	0.00	0.00	0.03	0.00	0.01	0.00
Na	0.07	0.09	0.07	0.07	0.03	0.08	0.07	0.06	0.07	0.04	0.06	0.08	0.05	0.08	0.07	0.08
K	0.00	0.00	0.00	0.00	0.00	0.00	0.00	0.00	0.00	0.00	0.00	0.00	0.00	0.00	0.00	0.01
Fe	0.81	0.78	0.78	0.78	0.81	1.04	1.03	1.04	1.04	1.02	1.03	1.04	1.03	1.01	0.83	0.85
Total	11.07	11.06	11.07	11.09	11.03	11.06	11.08	11.05	11.07	10.94	11.04	11.09	11.04	11.09	11.04	11.09

Microprobe results of cordierite in pelites

Sample Number							MM197B									
Oxide Percentage																
SiO2	48.08	47.92	47.98	48.04	48.31	48.18	48.17	48.08	48.00	48.04	47.68	48.28	48.32	48.37	48.19	48.02
TiO2	0.00	0.00	0.00	0.00	0.00	0.03	0.00	0.02	0.00	0.33	0.00	0.09	0.04	0.01	0.00	0.00
Al2O3	32.77	32.52	32.31	32.28	32.69	32.58	32.45	32.61	32.46	32.34	32.40	32.51	32.33	32.23	32.69	32.30
Cr2O3	0.00	0.00	0.12	0.00	0.04	0.00	0.10	0.00	0.00	0.00	0.00	0.02	0.04	0.08	0.00	0.03
MnO	0.29	0.42	0.32	0.46	0.37	0.44	0.03	0.00	0.10	0.04	0.13	0.06	0.00	0.17	0.19	0.00
MgO	7.46	7.41	7.20	7.26	7.50	7.44	7.18	7.10	6.70	6.71	6.57	7.29	7.10	6.85	7.08	6.81
CaO	0.07	0.03	0.01	0.00	0.00	0.02	0.00	0.00	0.03	0.07	0.01	0.01	0.06	0.01	0.10	0.00
ZnO	0.04	0.00	0.02	0.06	0.15	0.02	0.09	0.00	0.00	0.00	0.00	0.00	0.11	0.05	0.14	0.14
Na2O	0.28	0.37	0.26	0.40	0.37	0.40	0.38	0.47	0.40	0.27	0.30	0.35	0.32	0.22	0.27	0.33
K2O	0.02	0.00	0.00	0.00	0.06	0.00	0.00	0.05	0.03	0.00	0.03	0.03	0.00	0.00	0.01	0.00
FeO	9.88	9.82	10.00	9.77	9.97	9.69	10.49	10.91	11.34	11.05	11.50	10.25	10.59	10.71	10.90	11.09
Total	98.89	98.49	98.22	98.27	99.46	98.80	98.89	99.24	99.06	98.85	98.62	98.89	98.91	98.70	99.57	98.72
Number of atoms in the formula unit on the basis of the 18 oxygens																
Si	4.98	4.99	4.99	5.00	4.98	4.99	4.99	4.98	4.98	4.99	4.98	5.00	5.00	5.02	4.98	5.00
Ti	0.00	0.00	0.00	0.00	0.00	0.00	0.00	0.00	0.00	0.03	0.00	0.00	0.00	0.00	0.00	0.00
Al	4.00	3.99	3.96	3.96	3.97	3.97	3.96	3.98	3.97	3.96	3.99	3.96	3.95	3.94	3.98	3.96
Cr	0.00	0.00	0.01	0.00	0.00	0.00	0.00	0.00	0.00	0.00	0.00	0.00	0.00	0.00	0.00	0.00
Mn	0.03	0.04	0.03	0.04	0.03	0.04	0.00	0.00	0.00	0.00	0.01	0.00	0.00	0.01	0.02	0.00
Mg	1.15	1.15	1.12	1.13	1.15	1.14	1.11	1.09	1.04	1.04	1.02	1.12	1.09	1.06	1.09	1.06
Ca	0.00	0.00	0.00	0.00	0.00	0.00	0.00	0.00	0.00	0.00	0.00	0.00	0.00	0.00	0.01	0.00
Zn	0.00	0.00	0.00	0.00	0.01	0.00	0.00	0.00	0.00	0.00	0.00	0.00	0.00	0.00	0.01	0.01
Na	0.05	0.08	0.05	0.08	0.07	0.08	0.08	0.09	0.08	0.05	0.06	0.07	0.06	0.04	0.05	0.07
K	0.00	0.00	0.00	0.00	0.00	0.00	0.00	0.00	0.00	0.00	0.00	0.00	0.00	0.00	0.00	0.00
Fe	0.85	0.85	0.87	0.85	0.86	0.84	0.91	0.94	0.98	0.96	1.00	0.89	0.92	0.93	0.94	0.96
Total	11.06	11.10	11.03	11.06	11.07	11.06	11.05	11.08	11.05	11.03	11.06	11.04	11.02	11.00	11.08	11.06
Sample Number		MM133.BR									MM134A					
Oxide Percentage																
SiO2	48.52	47.75	48.87	48.32	48.08	47.92	47.98	48.04	48.31	48.18	48.84	48.05	47.50	48.63	48.11	48.42
TiO2	0.00	0.00	0.02	0.00	0.00	0.00	0.00	0.00	0.00	0.03	0.00	0.00	0.10	0.00	0.00	0.00
Al2O3	32.66	32.14	32.47	32.76	32.77	32.52	32.31	32.28	32.68	32.58	32.77	32.38	32.07	32.84	32.62	32.73
Cr2O3	0.03	0.03	0.00	0.12	0.00	0.00	0.12	0.00	0.04	0.00	0.08	0.00	0.00	0.04	0.05	0.00
MnO	0.05	0.41	0.28	0.32	0.29	0.42	0.32	0.46	0.37	0.44	0.97	0.84	0.68	1.06	0.99	0.84
MgO	6.90	7.55	7.55	7.70	7.46	7.41	7.21	7.26	7.50	7.44	7.79	7.43	7.48	7.40	7.48	7.73
CaO	0.00	0.03	0.07	0.00	0.07	0.03	0.01	0.00	0.00	0.02	0.03	0.00	0.06	0.00	0.07	0.06
ZnO	0.09	0.00	0.16	0.05	0.04	0.00	0.02	0.06	0.15	0.02	0.08	0.13	0.00	0.00	0.30	0.00
Na2O	0.23	0.24	0.34	0.41	0.28	0.37	0.26	0.40	0.37	0.30	0.39	0.31	0.33	0.33	0.41	0.32
K2O	0.02	0.15	0.00	0.08	0.02	0.00	0.00	0.00	0.06	0.00	0.06	0.00	0.05	0.00	0.08	0.04
FeO	11.01	9.55	9.66	9.90	9.88	9.82	10.00	9.77	9.97	9.69	9.24	9.40	8.96	9.43	9.02	9.30
Total	99.51	97.85	99.42	99.66	98.89	98.49	98.23	98.27	99.45	98.70	100.25	98.54	97.23	99.73	99.13	99.44
Number of atoms in the formula unit on the basis of the 18 oxygens																
Si	5.00	4.99	5.02	4.96	4.98	4.99	4.99	5.00	4.98	4.99	4.98	4.99	4.99	4.99	4.97	4.98
Ti	0.00	0.00	0.00	0.00	0.00	0.00	0.00	0.00	0.00	0.00	0.00	0.00	0.00	0.00	0.00	0.00
Al	4.00	3.96	3.93	3.97	4.00	3.99	3.96	3.96	3.97	3.97	3.94	3.97	3.97	3.97	3.98	3.97
Cr	0.00	0.00	0.00	0.01	0.00	0.00	0.01	0.00	0.00	0.00	0.00	0.00	0.00	0.00	0.00	0.00
Mn	0.00	0.04	0.02	0.03	0.03	0.04	0.03	0.04	0.03	0.04	0.08	0.07	0.06	0.09	0.09	0.07
Mg	1.06	1.18	1.16	1.18	1.15	1.15	1.12	1.13	1.15	1.15	1.18	1.15	1.17	1.13	1.15	1.18
Ca	0.00	0.00	0.00	0.00	0.00	0.00	0.00	0.00	0.00	0.00	0.00	0.00	0.00	0.00	0.00	0.00
Zn	0.00	0.00	0.01	0.00	0.00	0.00	0.00	0.00	0.01	0.00	0.00	0.01	0.00	0.00	0.02	0.00
Na	0.05	0.05	0.07	0.08	0.06	0.08	0.05	0.08	0.07	0.08	0.08	0.06	0.07	0.07	0.08	0.06
K	0.00	0.02	0.00	0.01	0.00	0.00	0.00	0.00	0.00	0.00	0.00	0.00	0.00	0.00	0.01	0.00
Fe	0.95	0.83	0.83	0.85	0.85	0.85	0.87	0.85	0.86	0.84	0.79	0.82	0.79	0.81	0.78	0.80
Total	11.06	11.07	11.04	11.09	11.07	11.10	11.03	11.06	11.07	11.07	11.05	11.07	11.05	11.06	11.08	11.06

Microprobe results of cordierite in pelites

Sample Number								MM197A								
Oxide Percentage																
SiO2	48.42	48.61	48.35	48.79	48.78	48.04	48.95	48.62	48.63	47.88	47.94	48.53	48.16	47.87	48.05	48.54
TiO2	0.00	0.00	0.01	0.09	0.01	0.00	0.03	0.05	0.10	0.00	0.03	0.05	0.01	0.00	0.00	0.00
Al2O3	32.73	33.03	32.81	32.76	33.17	32.75	33.15	32.92	33.00	32.72	32.62	32.89	32.74	32.18	32.37	32.67
Cr2O3	0.00	0.09	0.00	0.07	0.00	0.00	0.01	0.00	0.05	0.00	0.00	0.02	0.00	0.03	0.06	0.12
MnO	0.84	0.85	0.68	0.76	0.98	1.00	0.90	0.09	0.02	0.11	0.20	0.06	0.22	0.00	0.05	0.11
MgO	7.73	7.35	7.70	7.76	7.67	7.79	7.54	6.85	7.09	7.01	6.78	6.93	6.71	7.32	6.67	7.43
CaO	0.06	0.00	0.00	0.00	0.02	0.08	0.03	0.01	0.00	0.03	0.00	0.02	0.04	0.01	0.09	0.00
ZnO	0.00	0.14	0.03	0.00	0.00	0.00	0.00	0.08	0.00	0.02	0.00	0.00	0.00	0.11	0.09	0.00
Na2O	0.32	0.25	0.34	0.46	0.36	0.37	0.17	0.22	0.39	0.45	0.20	0.34	0.34	0.37	0.24	0.16
K2O	0.04	0.00	0.00	0.05	0.00	0.00	0.00	0.02	0.00	0.00	0.00	0.01	0.00	0.00	0.31	0.06
FeO	9.30	9.62	9.38	9.06	9.15	8.99	9.49	11.13	11.14	11.44	10.81	11.27	11.46	10.37	10.09	10.44
Total	99.44	99.94	99.30	99.80	100.14	99.02	100.27	99.99	100.42	99.66	98.58	100.12	99.68	98.26	98.02	99.53
Number of atoms in the formula unit on the basis of the 18 oxygens																
Si	4.98	4.98	4.97	4.99	4.98	4.96	4.99	4.99	4.97	4.95	4.99	4.98	4.98	4.99	5.02	4.99
Ti	0.00	0.00	0.00	0.00	0.00	0.00	0.00	0.00	0.00	0.00	0.00	0.00	0.00	0.00	0.00	0.00
Al	3.97	3.99	3.98	3.95	3.99	3.99	3.98	3.98	3.98	3.99	4.00	3.98	3.99	3.95	3.98	3.96
Cr	0.00	0.00	0.00	0.00	0.00	0.00	0.00	0.00	0.00	0.00	0.00	0.00	0.00	0.00	0.00	0.01
Mn	0.07	0.07	0.06	0.07	0.08	0.09	0.08	0.00	0.00	0.01	0.02	0.00	0.02	0.00	0.00	0.00
Mg	1.18	1.12	1.18	1.18	1.17	1.20	1.14	1.05	1.08	1.08	1.05	1.06	1.03	1.14	1.04	1.14
Ca	0.00	0.00	0.00	0.00	0.00	0.00	0.00	0.00	0.00	0.00	0.00	0.00	0.00	0.00	0.01	0.00
Zn	0.00	0.01	0.00	0.00	0.00	0.00	0.00	0.00	0.00	0.00	0.00	0.00	0.00	0.00	0.00	0.00
Na	0.06	0.05	0.07	0.09	0.07	0.07	0.03	0.04	0.08	0.09	0.04	0.07	0.07	0.08	0.05	0.03
K	0.00	0.00	0.00	0.00	0.00	0.00	0.00	0.00	0.00	0.00	0.00	0.00	0.00	0.00	0.04	0.00
Fe	0.80	0.82	0.81	0.80	0.78	0.78	0.81	0.95	0.95	0.99	0.94	0.97	0.99	0.90	0.88	0.89
Total	11.06	11.04	11.07	11.08	11.07	11.09	11.03	11.01	11.06	11.11	11.04	11.06	11.08	11.06	11.02	11.02
Sample Number				MM181										MM188D.PL		
Oxide Percentage																
SiO2	48.20	47.90	48.24	47.84	48.16	47.86	47.89	48.13	47.78	48.00	48.41	48.65	48.30	47.70	48.42	48.04
TiO2	0.07	0.00	0.10	0.03	0.09	0.00	0.01	0.02	0.01	0.02	0.00	0.11	0.00	0.00	0.03	0.02
Al2O3	32.60	32.33	32.83	32.34	32.20	32.43	32.26	32.52	32.55	32.20	32.30	32.81	32.61	32.53	32.82	32.44
Cr2O3	0.00	0.03	0.00	0.04	0.00	0.03	0.00	0.09	0.09	0.13	0.00	0.00	0.01	0.16	0.00	0.00
MnO	0.09	0.25	0.08	0.15	0.06	0.14	0.12	0.00	0.05	0.06	0.07	0.19	0.15	0.00	0.00	0.05
MgO	6.78	6.32	6.85	6.60	6.60	6.62	6.30	6.48	6.40	6.28	6.28	7.43	6.71	7.92	7.69	7.67
CaO	0.05	0.00	0.00	0.04	0.00	0.00	0.04	0.00	0.10	0.00	0.00	0.02	0.01	0.02	0.06	0.00
ZnO	0.03	0.12	0.20	0.19	0.13	0.14	0.00	0.00	0.00	0.09	0.09	0.00	0.00	0.00	0.27	0.17
Na2O	0.31	0.30	0.24	0.39	0.30	0.32	0.19	0.33	0.35	0.34	0.26	0.34	0.32	0.40	0.45	0.29
K2O	0.01	0.04	0.00	0.00	0.01	0.05	0.04	0.04	0.06	0.00	0.00	0.02	0.00	0.05	0.00	0.00
FeO	11.23	11.51	11.00	10.79	11.00	11.46	11.55	11.38	11.82	11.41	11.54	10.15	11.38	9.40	9.13	9.38
Total	99.37	98.80	99.54	98.41	98.55	99.05	98.40	98.99	99.21	98.53	98.95	99.72	99.49	98.18	98.87	98.06
Number of atoms in the formula unit on the basis of the 18 oxygens																
Si	4.98	4.99	4.98	4.99	5.01	4.98	5.00	5.00	5.00	5.01	5.03	4.99	4.99	4.96	4.99	5.00
Ti	0.00	0.00	0.00	0.00	0.00	0.00	0.00	0.00	0.00	0.00	0.00	0.00	0.00	0.00	0.00	0.00
Al	3.97	3.97	3.99	3.98	3.95	3.98	3.97	3.98	3.99	3.96	3.96	3.97	3.97	3.99	3.99	3.98
Cr	0.00	0.00	0.00	0.00	0.00	0.00	0.00	0.00	0.00	0.01	0.00	0.00	0.00	0.01	0.00	0.00
Mn	0.00	0.02	0.00	0.01	0.00	0.01	0.01	0.00	0.00	0.00	0.00	0.02	0.01	0.00	0.00	0.00
Mg	1.04	0.98	1.05	1.02	1.02	1.03	0.98	1.00	0.99	0.98	0.97	1.14	1.03	1.23	1.18	1.19
Ca	0.00	0.00	0.00	0.00	0.00	0.00	0.00	0.00	0.01	0.00	0.00	0.00	0.00	0.00	0.00	0.00
Zn	0.00	0.00	0.02	0.01	0.01	0.01	0.00	0.00	0.00	0.00	0.00	0.00	0.00	0.00	0.02	0.01
Na	0.06	0.06	0.05	0.09	0.06	0.06	0.04	0.07	0.07	0.07	0.05	0.07	0.06	0.08	0.09	0.06
K	0.00	0.00	0.00	0.00	0.00	0.00	0.00	0.00	0.00	0.00	0.00	0.00	0.00	0.00	0.00	0.00
Fe	0.97	1.00	0.95	0.94	0.96	1.00	1.01	0.99	1.03	1.00	1.00	0.87	0.98	0.82	0.79	0.82
Total	11.02	11.02	11.04	11.04	11.01	11.07	11.01	11.04	11.09	11.03	11.01	11.06	11.04	11.09	11.06	11.06

Microprobe results of cordierite in pelites

Sample Number								MM188C								
Oxide Percentage																
SiO2	48.30	47.87	48.42	47.94	48.17	47.88	47.86	48.73	48.51	48.52	48.65	48.19	48.38	48.46	48.91	48.16
TiO2	0.00	0.00	0.03	0.04	0.03	0.00	0.00	0.05	0.00	0.03	0.03	0.00	0.00	0.08	0.00	0.02
Al2O3	32.83	32.43	32.80	32.84	32.64	32.74	32.69	33.18	33.09	32.81	32.93	32.55	32.80	32.91	32.93	32.75
Cr2O3	0.00	0.00	0.00	0.00	0.00	0.03	0.00	0.00	0.00	0.05	0.00	0.03	0.17	0.01	0.00	0.12
MnO	0.08	0.05	0.08	0.00	0.09	0.00	0.00	0.09	0.12	0.16	0.24	0.08	0.10	0.09	0.13	0.13
MgO	7.80	7.54	7.74	7.94	7.79	7.89	7.76	8.68	8.44	8.58	8.33	8.15	8.42	8.22	8.44	8.31
CaO	0.00	0.00	0.00	0.00	0.02	0.03	0.00	0.06	0.04	0.00	0.00	0.00	0.04	0.00	0.05	0.01
ZnO	0.00	0.14	0.00	0.00	0.19	0.00	0.00	0.10	0.00	0.00	0.01	0.15	0.00	0.26	0.00	0.11
Na2O	0.42	0.44	0.43	0.40	0.44	0.42	0.49	0.44	0.35	0.38	0.33	0.26	0.28	0.34	0.28	0.40
K2O	0.08	0.00	0.04	0.04	0.03	0.00	0.09	0.00	0.03	0.00	0.04	0.03	0.00	0.06	0.01	0.04
FeO	9.23	9.17	9.42	9.16	9.07	9.36	9.22	8.27	8.31	8.00	8.35	8.41	8.67	8.25	8.09	8.37
Total	98.74	97.64	98.96	98.36	98.47	98.35	98.11	99.60	98.89	98.53	98.91	97.85	98.86	98.68	98.84	98.42
Number of atoms in the formula unit on the basis of the 18 oxygens																
Si	4.99	4.99	4.99	4.97	4.99	4.97	4.97	4.96	4.98	4.99	4.99	5.00	4.98	4.98	5.01	4.97
Ti	0.00	0.00	0.00	0.00	0.00	0.00	0.00	0.00	0.00	0.00	0.00	0.00	0.00	0.00	0.00	0.00
Al	3.99	3.99	3.98	4.00	3.98	4.00	4.00	3.98	4.00	3.98	3.98	3.98	3.98	3.99	3.98	3.98
Cr	0.00	0.00	0.00	0.00	0.00	0.00	0.00	0.00	0.00	0.00	0.00	0.00	0.01	0.00	0.00	0.01
Mn	0.00	0.00	0.00	0.00	0.00	0.00	0.00	0.00	0.01	0.01	0.02	0.00	0.00	0.00	0.01	0.01
Mg	1.20	1.17	1.19	1.15	1.20	1.22	1.20	1.32	1.29	1.32	1.27	1.26	1.29	1.26	1.29	1.28
Ca	0.00	0.00	0.00	0.00	0.00	0.00	0.00	0.00	0.00	0.00	0.00	0.00	0.00	0.00	0.00	0.00
Zn	0.00	0.01	0.00	0.00	0.01	0.00	0.00	0.00	0.00	0.00	0.00	0.01	0.00	0.02	0.00	0.00
Na	0.08	0.09	0.09	0.08	0.09	0.08	0.10	0.09	0.07	0.07	0.07	0.05	0.06	0.07	0.06	0.08
K	0.01	0.00	0.00	0.00	0.00	0.00	0.01	0.00	0.00	0.00	0.00	0.00	0.00	0.00	0.00	0.00
Fe	0.80	0.80	0.81	0.80	0.79	0.81	0.80	0.70	0.71	0.69	0.72	0.73	0.75	0.71	0.69	0.72
Total	11.07	11.05	11.06	11.00	11.06	11.08	11.08	11.05	11.06	11.06	11.05	11.03	11.07	11.03	11.04	11.05
Sample Number			MM153									MM146				
Oxide Percentage																
SiO2	48.96	48.05	47.55	47.83	48.11	47.65	48.00	47.85	48.13	47.69	47.67	46.93	47.75	47.23	47.50	47.40
TiO2	0.00	0.01	0.03	0.07	0.00	0.18	0.00	0.00	0.05	0.11	0.00	0.05	0.00	0.02	0.08	0.13
Al2O3	33.05	32.72	32.20	31.91	32.45	32.18	32.10	32.12	32.33	32.14	31.86	31.45	32.45	32.03	32.03	31.57
Cr2O3	0.05	0.06	0.00	0.06	0.00	0.04	0.00	0.00	0.00	0.00	0.00	0.02	0.00	0.13	0.00	0.00
MnO	0.00	0.16	0.12	0.00	0.00	0.00	0.09	0.05	0.00	0.01	0.03	0.03	0.05	0.00	0.00	0.00
MgO	8.56	8.43	5.79	6.00	6.03	5.98	5.74	5.90	5.95	5.72	5.69	6.30	6.74	6.48	6.52	6.52
CaO	0.00	0.05	0.00	0.03	0.00	0.00	0.00	0.00	0.02	0.00	0.01	0.05	0.05	0.04	0.00	0.02
ZnO	0.00	0.03	0.00	0.00	0.15	0.00	0.00	0.17	0.00	0.13	0.14	0.22	0.00	0.00	0.22	0.00
Na2O	0.44	0.34	0.26	0.27	0.32	0.41	0.26	0.36	0.26	0.33	0.23	0.34	0.34	0.32	0.34	0.33
K2O	0.00	0.01	0.02	0.01	0.06	0.00	0.04	0.00	0.04	0.00	0.02	0.00	0.00	0.00	0.00	0.00
FeO	8.48	8.24	12.68	12.36	12.32	12.97	12.37	12.27	12.55	12.32	12.47	11.16	11.32	11.35	11.66	11.41
Total	99.54	98.10	98.65	98.54	99.44	99.41	98.60	98.72	99.33	98.45	98.12	96.55	98.70	97.60	98.35	97.38
Number of atoms in the formula unit on the basis of the 18 oxygens																
Si	4.99	4.97	4.99	5.01	5.00	4.98	5.03	5.00	5.00	5.00	5.02	5.00	4.98	4.98	4.98	5.01
Ti	0.00	0.00	0.00	0.00	0.00	0.01	0.00	0.00	0.00	0.00	0.00	0.00	0.00	0.00	0.00	0.01
Al	3.97	3.99	3.98	3.94	3.97	3.96	3.96	3.96	3.96	3.98	3.96	3.95	3.99	3.98	3.96	3.93
Cr	0.00	0.00	0.00	0.00	0.00	0.00	0.00	0.00	0.00	0.00	0.00	0.00	0.00	0.01	0.00	0.00
Mn	0.00	0.01	0.01	0.00	0.00	0.00	0.00	0.00	0.00	0.00	0.00	0.00	0.00	0.00	0.00	0.00
Mg	1.30	1.30	0.90	0.94	0.93	0.93	0.89	0.92	0.92	0.89	0.89	1.00	1.05	1.02	1.02	1.03
Ca	0.00	0.00	0.00	0.00	0.00	0.00	0.00	0.00	0.00	0.00	0.00	0.00	0.00	0.00	0.00	0.00
Zn	0.00	0.00	0.00	0.00	0.01	0.00	0.00	0.01	0.00	0.01	0.01	0.02	0.00	0.00	0.02	0.00
Na	0.09	0.07	0.05	0.05	0.06	0.08	0.05	0.07	0.05	0.07	0.05	0.07	0.07	0.06	0.07	0.07
K	0.00	0.00	0.00	0.00	0.00	0.00	0.00	0.00	0.00	0.00	0.00	0.00	0.00	0.00	0.00	0.00
Fe	0.72	0.71	1.11	1.08	1.07	1.12	1.08	1.07	1.09	1.08	1.01	0.99	0.99	1.00	1.02	1.00
Total	11.07	11.05	11.04	11.02	11.04	11.08	11.01	11.03	11.02	11.03	10.94	11.03	11.08	11.05	11.07	11.05

Microprobe results of cordierite in pelites

Sample Number															193D	
Oxide Percentage																
SiO2	47.83	47.48	47.83	47.38	47.43	47.98	47.26	47.18	47.41	46.87	47.27	47.06	47.08	47.00	48.33	48.39
TiO2	0.06	0.02	0.00	0.01	0.06	0.04	0.00	0.08	0.00	0.05	0.03	0.00	0.00	0.07	0.03	0.00
Al2O3	32.25	31.79	32.22	32.04	32.28	32.07	32.20	31.89	32.15	31.99	32.05	31.94	31.73	31.95	32.59	32.61
Cr2O3	0.00	0.00	0.02	0.00	0.00	0.00	0.00	0.07	0.07	0.00	0.00	0.00	0.00	0.10	0.00	0.11
MnO	0.00	0.01	0.00	0.11	0.00	0.00	0.09	0.08	0.00	0.00	0.03	0.00	0.03	0.08	0.15	0.07
MgO	6.59	6.66	6.52	6.62	6.46	6.48	6.42	6.49	6.44	6.40	6.52	6.40	6.53	6.39	8.00	7.87
CaO	0.00	0.00	0.00	0.00	0.00	0.05	0.00	0.00	0.07	0.03	0.00	0.00	0.01	0.00	0.00	0.06
ZnO	0.00	0.20	0.13	0.12	0.15	0.10	0.00	0.03	0.04	0.13	0.00	0.18	0.00	0.27	0.00	0.08
Na2O	0.30	0.34	0.20	0.32	0.21	0.26	0.40	0.26	0.50	0.30	0.22	0.41	0.23	0.26	0.43	0.27
K2O	0.03	0.00	0.02	0.03	0.07	0.00	0.03	0.00	0.03	0.00	0.04	0.00	0.00	0.03	0.00	0.00
FeO	11.76	11.59	11.72	11.70	11.73	11.73	11.51	11.57	11.69	11.55	11.33	11.27	11.42	11.57	9.13	8.99
Total	98.82	98.09	98.66	98.33	98.39	98.71	97.91	97.65	98.40	97.32	97.49	97.26	97.03	97.72	98.66	98.45
Number of atoms in the formula unit on the basis of the 18 oxygens																
Si	4.99	4.99	5.00	4.97	4.97	4.98	4.97	4.98	4.97	4.96	4.99	4.98	4.99	4.96	4.99	5.00
Ti	0.00	0.00	0.00	0.00	0.00	0.00	0.00	0.00	0.00	0.00	0.00	0.00	0.00	0.00	0.00	0.00
Al	3.97	3.94	3.97	3.96	3.99	3.98	3.99	3.97	3.97	3.99	3.99	3.99	3.97	3.98	3.97	3.97
Cr	0.00	0.00	0.00	0.00	0.00	0.00	0.00	0.00	0.00	0.00	0.00	0.00	0.00	0.00	0.00	0.00
Mn	0.00	0.00	0.00	0.01	0.00	0.00	0.00	0.00	0.00	0.00	0.00	0.00	0.00	0.00	0.01	0.00
Mg	1.02	1.04	1.01	1.04	1.01	1.02	1.00	1.02	1.00	1.01	1.02	1.01	1.03	1.00	1.23	1.21
Ca	0.00	0.00	0.00	0.00	0.00	0.00	0.00	0.00	0.00	0.00	0.00	0.00	0.00	0.00	0.00	0.00
Zn	0.00	0.02	0.01	0.01	0.01	0.00	0.00	0.00	0.00	0.01	0.00	0.01	0.00	0.02	0.00	0.00
Na	0.06	0.07	0.04	0.06	0.04	0.05	0.08	0.05	0.10	0.06	0.04	0.08	0.05	0.05	0.09	0.05
K	0.00	0.00	0.00	0.00	0.01	0.00	0.00	0.00	0.00	0.00	0.00	0.00	0.00	0.00	0.00	0.00
Fe	1.03	1.02	1.02	1.03	1.03	1.03	1.01	1.02	1.03	1.02	1.00	1.00	1.01	1.02	0.79	0.78
Total	11.07	11.08	11.05	11.08	11.06	11.06	11.05	11.04	11.07	11.05	11.04	11.07	11.05	11.03	11.08	11.01
Sample Number																MM187
Oxide Percentage																
SiO2	48.89	47.88	48.27	48.69	48.49	47.89	48.56	48.29	48.00	48.37	47.79	47.94	47.64	47.60	47.60	47.27
TiO2	0.04	0.05	0.00	0.00	0.02	0.07	0.00	0.00	0.11	0.00	0.00	0.00	0.00	0.00	0.00	0.04
Al2O3	33.21	32.56	32.93	33.06	32.81	32.52	33.10	32.85	32.78	33.05	32.47	32.65	32.19	32.64	32.64	32.34
Cr2O3	0.01	0.05	0.00	0.00	0.00	0.03	0.02	0.05	0.05	0.01	0.03	0.03	0.00	0.09	0.09	0.00
MnO	0.14	0.05	0.02	0.04	0.00	0.02	0.08	0.20	0.12	0.12	0.10	0.01	0.09	0.12	0.12	0.17
MgO	8.28	7.87	8.21	9.10	8.12	7.94	8.26	8.07	8.08	8.36	8.08	8.12	7.69	7.70	7.70	6.37
CaO	0.00	0.00	0.00	0.00	0.00	0.00	0.03	0.00	0.03	0.04	0.02	0.01	0.05	0.07	0.07	0.03
ZnO	0.00	0.00	0.03	0.00	0.00	0.16	0.19	0.04	0.04	0.29	0.00	0.00	0.00	0.00	0.00	0.00
Na2O	0.37	0.27	0.46	0.40	0.39	0.31	0.49	0.36	0.37	0.48	0.35	0.46	0.33	0.48	0.48	0.50
K2O	0.02	0.01	0.00	0.00	0.04	0.07	0.06	0.02	0.01	0.00	0.05	0.03	0.01	0.00	0.00	0.00
FeO	9.29	8.81	9.10	8.81	8.85	8.86	9.27	9.22	8.70	8.74	8.98	8.80	9.60	9.44	9.44	12.10
Total	100.25	97.55	99.02	100.10	98.72	97.87	100.06	99.10	98.29	99.46	97.87	98.05	97.60	98.14	98.14	98.82
Number of atoms in the formula unit on the basis of the 18 oxygens																
Si	4.97	4.99	4.97	5.00	5.00	4.98	4.95	4.97	4.96	4.95	4.97	4.98	4.99	4.96	4.96	4.95
Ti	0.00	0.00	0.00	0.00	0.00	0.00	0.00	0.00	0.00	0.00	0.00	0.00	0.00	0.00	0.00	0.00
Al	3.98	4.00	3.99	4.00	3.99	3.99	3.98	3.99	4.00	3.99	3.98	4.00	3.97	4.00	4.00	3.99
Cr	0.00	0.00	0.00	0.00	0.00	0.00	0.00	0.00	0.00	0.00	0.00	0.00	0.00	0.00	0.00	0.00
Mn	0.01	0.00	0.02	0.00	0.00	0.00	0.00	0.02	0.01	0.01	0.00	0.00	0.00	0.01	0.01	0.01
Mg	1.26	1.22	1.23	1.24	1.25	1.23	1.25	1.23	1.24	1.28	1.25	1.26	1.20	1.19	1.19	0.99
Ca	0.00	0.00	0.00	0.00	0.00	0.00	0.00	0.00	0.00	0.00	0.00	0.00	0.00	0.00	0.00	0.00
Zn	0.00	0.00	0.00	0.00	0.00	0.01	0.01	0.00	0.00	0.02	0.00	0.00	0.00	0.00	0.00	0.00
Na	0.07	0.05	0.07	0.08	0.08	0.06	0.10	0.07	0.07	0.09	0.07	0.09	0.07	0.10	0.10	0.10
K	0.00	0.00	0.00	0.00	0.00	0.00	0.00	0.00	0.00	0.00	0.00	0.00	0.00	0.00	0.00	0.00
Fe	0.79	0.77	0.79	0.75	0.76	0.77	0.79	0.79	0.75	0.75	0.78	0.76	0.84	0.82	0.82	1.06
Total	11.08	11.03	11.07	11.07	11.08	11.04	11.08	11.07	11.03	11.09	11.05	11.09	11.07	11.08	11.08	11.10

Microprobe results of cordierite in pelites

Sample Number																MM195(
Oxide Percentage																
SiO2	47.24	47.56	47.64	47.77	47.51	47.38	47.77	47.35	47.70	47.25	47.56	48.16	48.11	47.45	47.43	47.96
TiO2	0.03	0.08	0.20	0.00	0.00	0.04	0.02	0.02	0.00	0.00	0.04	0.00	0.00	0.04	0.00	0.03
Al2O3	32.20	32.59	32.43	32.58	32.34	32.32	32.45	32.28	32.47	32.56	32.37	32.85	32.75	32.22	32.30	32.69
Cr2O3	0.04	0.00	0.01	0.00	0.00	0.00	0.00	0.03	0.00	0.09	0.01	0.00	0.03	0.00	0.05	0.04
MnO	0.25	0.16	0.09	0.20	0.25	0.08	0.15	0.15	0.12	0.13	0.00	0.04	0.00	0.17	0.04	0.14
MgO	6.19	6.50	6.61	6.86	6.52	6.50	6.81	6.40	6.69	6.78	6.61	6.56	6.41	6.36	6.61	6.59
CaO	0.00	0.00	0.03	0.00	0.00	0.03	0.00	0.06	0.00	0.05	0.00	0.00	0.00	0.04	0.00	0.00
ZnO	0.00	0.08	0.03	0.00	0.04	0.00	0.00	0.00	0.17	0.09	0.17	0.00	0.37	0.00	0.04	0.08
Na2O	0.46	0.55	0.41	0.44	0.28	0.50	0.49	0.42	0.42	0.41	0.46	0.37	0.36	0.42	0.45	0.29
K2O	0.04	0.00	0.00	0.01	0.00	0.02	0.04	0.01	0.04	0.00	0.00	0.00	0.00	0.00	0.00	0.00
FeO	11.92	11.56	11.54	10.69	11.22	11.90	11.33	11.03	11.08	11.07	11.18	11.84	11.69	11.39	11.19	11.52
Total	98.37	99.08	98.99	98.55	98.16	98.77	99.06	97.75	98.69	98.43	98.40	99.82	99.72	98.09	98.11	99.34
Number of atoms in the formula unit on the basis of the 18 oxygens																
Si	4.97	4.97	4.97	4.98	4.98	4.96	4.97	4.98	4.98	4.94	4.97	4.97	4.98	4.98	4.97	4.97
Ti	0.00	0.00	0.00	0.00	0.00	0.00	0.00	0.00	0.00	0.00	0.00	0.00	0.00	0.00	0.00	0.00
Al	3.99	3.99	3.98	4.00	4.00	3.98	3.98	4.00	4.00	4.01	3.99	4.00	3.99	3.99	4.00	3.99
Cr	0.00	0.00	0.00	0.00	0.00	0.00	0.00	0.00	0.00	0.00	0.00	0.00	0.00	0.00	0.00	0.00
Mn	0.02	0.01	0.00	0.02	0.02	0.00	0.01	0.01	0.01	0.01	0.00	0.00	0.00	0.01	0.00	0.01
Mg	0.97	1.00	1.03	1.07	1.02	1.01	1.06	1.00	1.04	1.06	1.03	1.01	0.99	1.00	1.03	1.02
Ca	0.00	0.00	0.00	0.00	0.00	0.00	0.00	0.00	0.00	0.00	0.00	0.00	0.00	0.00	0.00	0.00
Zn	0.00	0.00	0.00	0.00	0.00	0.00	0.00	0.00	0.01	0.00	0.01	0.00	0.03	0.00	0.00	0.00
Na	0.09	0.11	0.08	0.09	0.06	0.10	0.10	0.09	0.09	0.08	0.09	0.07	0.07	0.09	0.09	0.06
K	0.00	0.00	0.00	0.00	0.00	0.00	0.00	0.00	0.00	0.00	0.00	0.00	0.00	0.00	0.00	0.00
Fe	1.05	1.00	1.00	0.93	0.98	1.04	0.98	0.97	0.97	0.97	0.98	1.02	1.01	1.00	0.98	1.00
Total	11.09	11.08	11.06	11.09	11.06	11.09	11.10	11.05	11.10	11.07	11.07	11.07	11.07	11.07	11.07	11.05
Sample Number													MM189A			
Oxide Percentage																
SiO2	47.80	48.31	47.82	47.95	47.72	47.76	48.05	47.76	48.04	48.35	48.37	47.97	48.11	47.67	47.92	47.39
TiO2	0.03	0.00	0.08	0.00	0.03	0.05	0.00	0.05	0.00	0.00	0.00	0.00	0.00	0.00	0.02	0.02
Al2O3	32.54	32.93	32.49	32.21	32.36	32.37	32.51	32.45	32.75	32.65	32.73	32.41	32.69	32.54	32.09	32.34
Cr2O3	0.06	0.00	0.11	0.00	0.04	0.00	0.00	0.00	0.00	0.09	0.00	0.04	0.12	0.00	0.06	0.00
MnO	0.20	0.21	0.18	0.28	0.15	0.26	0.08	0.25	0.16	0.30	0.12	0.12	0.17	0.18	0.00	0.08
MgO	6.38	6.93	6.64	6.52	6.98	6.83	6.88	6.76	7.14	6.95	7.11	6.90	7.65	7.21	6.72	6.80
CaO	0.04	0.00	0.00	0.02	0.03	0.01	0.03	0.12	0.05	0.00	0.02	0.01	0.03	0.00	0.01	0.03
ZnO	0.06	0.04	0.00	0.00	0.00	0.18	0.00	0.10	0.00	0.00	0.06	0.16	0.00	0.01	0.03	0.00
Na2O	0.32	0.32	0.37	0.37	0.40	0.28	0.37	0.32	0.32	0.32	0.37	0.27	0.41	0.37	0.51	0.29
K2O	0.02	0.01	0.00	0.02	0.00	0.00	0.00	0.00	0.00	0.00	0.03	0.00	0.03	0.02	0.02	0.02
FeO	11.74	11.26	11.51	11.35	10.46	10.62	10.59	10.88	10.79	10.59	10.83	11.04	9.66	10.19	10.83	10.84
Total	99.19	100.01	99.20	98.72	98.17	98.36	98.51	98.69	99.25	99.25	99.64	98.92	98.87	98.19	98.21	97.81
Number of atoms in the formula unit on the basis of the 18 oxygens																
Si	4.97	4.97	4.97	5.00	4.98	4.98	5.00	4.97	4.97	5.00	4.98	4.98	4.98	4.97	5.00	4.97
Ti	0.00	0.00	0.00	0.00	0.00	0.00	0.00	0.00	0.00	0.00	0.00	0.00	0.00	0.00	0.00	0.00
Al	3.99	3.99	3.98	3.96	3.98	3.98	3.98	3.98	3.99	3.98	3.97	3.96	3.99	4.00	3.95	4.00
Cr	0.00	0.00	0.00	0.00	0.00	0.00	0.00	0.00	0.00	0.00	0.00	0.00	0.01	0.00	0.00	0.00
Mn	0.02	0.02	0.02	0.02	0.01	0.02	0.00	0.02	0.01	0.03	0.01	0.01	0.01	0.02	0.00	0.00
Mg	0.99	1.06	1.03	1.01	1.09	1.06	1.07	1.05	1.10	1.07	1.09	1.07	1.18	1.12	1.05	1.06
Ca	0.00	0.00	0.00	0.00	0.00	0.00	0.00	0.01	0.00	0.00	0.00	0.00	0.00	0.00	0.00	0.00
Zn	0.00	0.00	0.00	0.00	0.00	0.01	0.00	0.00	0.00	0.00	0.00	0.01	0.00	0.00	0.00	0.00
Na	0.06	0.06	0.08	0.07	0.08	0.05	0.07	0.06	0.06	0.06	0.07	0.05	0.08	0.08	0.10	0.06
K	0.00	0.00	0.00	0.00	0.00	0.00	0.00	0.00	0.00	0.00	0.00	0.00	0.00	0.00	0.00	0.00
Fe	1.02	0.97	1.00	0.99	0.91	0.93	0.92	0.95	0.93	0.92	0.93	0.96	0.84	0.89	0.95	0.95
Total	11.05	11.07	11.08	11.05	11.05	11.03	11.04	11.04	11.06	11.06	11.05	11.04	11.09	11.08	11.05	11.04

Microprobe results of cordierite in pelites

Sample Number															MM184B	
Oxide Percentage																
SiO2	47.32	47.35	47.91	47.51	48.36	47.39	47.71	48.06	47.54	47.99	47.59	47.68	47.30	47.47	48.42	48.37
TiO2	0.00	0.01	0.00	0.00	0.00	0.00	0.02	0.00	0.00	0.00	0.00	0.00	0.00	0.04	0.02	0.02
Al2O3	32.80	31.87	32.19	32.44	32.84	32.24	32.20	32.46	31.92	32.84	32.54	32.31	32.31	32.31	33.01	32.73
Cr2O3	0.00	0.00	0.06	0.16	0.06	0.03	0.07	0.00	0.00	0.00	0.05	0.00	0.00	0.00	0.00	0.00
MnO	0.17	0.08	0.06	0.00	0.00	0.04	0.03	0.17	0.16	0.08	0.05	0.02	0.09	0.10	0.28	0.18
MgO	6.75	7.12	7.04	7.14	7.02	6.67	6.76	7.00	6.88	6.90	6.79	7.11	7.00	6.70	8.07	7.72
CaO	0.00	0.02	0.02	0.00	0.02	0.04	0.06	0.05	0.01	0.00	0.00	0.00	0.02	0.03	0.00	0.01
ZnO	0.00	0.03	0.00	0.00	0.00	0.00	0.00	0.00	0.07	0.00	0.00	0.00	0.09	0.14	0.00	0.11
Na2O	0.38	0.33	0.36	0.55	0.38	0.29	0.45	0.47	0.40	0.39	0.45	0.49	0.39	0.39	0.36	0.25
K2O	0.00	0.07	0.00	0.00	0.01	0.01	0.14	0.11	0.02	0.05	0.01	0.00	0.08	0.00	0.03	0.00
FeO	10.51	10.34	10.74	10.20	10.47	10.50	10.00	10.77	10.51	10.87	10.52	10.53	10.52	10.79	9.16	9.07
Total	97.93	97.22	98.38	98.00	99.16	97.21	97.44	99.09	97.51	99.12	98.00	98.14	97.80	97.97	99.35	98.46
Number of atoms in the formula unit on the basis of the 18 oxygens																
Si	5.01	5.00	4.99	4.97	5.00	4.99	5.00	4.98	5.00	4.97	4.98	4.99	4.96	4.98	4.97	4.99
Ti	0.00	0.00	0.00	0.00	0.00	0.00	0.00	0.00	0.00	0.00	0.00	0.00	0.00	0.00	0.00	0.00
Al	3.97	3.96	3.95	4.00	4.00	4.00	3.98	3.97	3.95	4.00	4.01	3.98	4.00	3.99	3.99	3.98
Cr	0.00	0.00	0.00	0.01	0.00	0.00	0.00	0.00	0.00	0.00	0.00	0.00	0.00	0.00	0.00	0.00
Mn	0.01	0.00	0.00	0.00	0.00	0.00	0.00	0.01	0.01	0.00	0.00	0.00	0.00	0.00	0.02	0.02
Mg	1.07	1.12	1.09	1.11	1.08	1.05	1.06	1.08	1.08	1.07	1.06	1.11	1.09	1.05	1.23	1.20
Ca	0.00	0.00	0.00	0.00	0.00	0.00	0.00	0.00	0.00	0.00	0.00	0.00	0.00	0.00	0.00	0.00
Zn	0.00	0.00	0.00	0.00	0.00	0.00	0.00	0.00	0.00	0.00	0.00	0.00	0.00	0.01	0.00	0.00
Na	0.08	0.07	0.07	0.11	0.08	0.06	0.09	0.09	0.08	0.08	0.09	0.10	0.08	0.08	0.07	0.05
K	0.00	0.01	0.00	0.00	0.00	0.00	0.02	0.01	0.00	0.00	0.00	0.00	0.01	0.00	0.00	0.00
Fe	0.93	0.91	0.94	0.89	0.91	0.93	0.88	0.93	0.92	0.94	0.92	0.92	0.92	0.95	0.79	0.78
Total	11.07	11.07	11.04	11.09	11.07	11.03	11.03	11.07	11.04	11.06	11.06	11.10	11.06	11.06	11.07	11.02
Sample Number											MM166A					
Oxide Percentage																
SiO2	47.90	48.62	48.71	48.40	48.39	48.60	48.21	48.23	49.06	48.03	48.02	48.29	48.08	48.08	48.16	47.99
TiO2	0.05	0.05	0.00	0.05	0.10	0.00	0.00	0.07	0.06	0.04	0.03	0.04	0.05	0.09	0.00	0.14
Al2O3	32.54	32.99	32.97	32.84	32.84	32.81	32.45	32.84	33.60	32.20	32.68	32.63	32.38	32.55	32.50	32.58
Cr2O3	0.00	0.00	0.00	0.00	0.05	0.00	0.00	0.07	0.07	0.00	0.00	0.05	0.05	0.00	0.03	0.03
MnO	0.32	0.52	0.45	0.29	0.20	0.24	0.24	0.31	0.13	0.36	0.12	0.00	0.00	0.10	0.05	0.17
MgO	8.09	8.19	8.15	8.16	8.08	8.21	8.09	8.14	8.41	7.88	6.43	6.36	6.42	6.55	6.56	6.57
CaO	0.00	0.00	0.00	0.01	0.00	0.05	0.00	0.02	0.05	0.00	0.04	0.05	0.00	0.00	0.01	0.05
ZnO	0.00	0.00	0.00	0.00	0.00	0.29	0.00	0.00	0.13	0.02	0.26	0.00	0.00	0.00	0.12	0.00
Na2O	0.34	0.44	0.30	0.39	0.41	0.40	0.23	0.35	0.42	0.38	0.43	0.30	0.32	0.38	0.40	0.25
K2O	0.00	0.09	0.06	0.00	0.01	0.00	0.05	0.00	0.00	0.00	0.00	0.01	0.00	0.00	0.00	0.03
FeO	9.35	8.31	8.58	8.57	9.14	8.36	8.53	8.45	8.90	8.70	11.92	11.76	12.00	11.69	11.24	11.77
Total	98.59	99.21	99.22	98.71	99.22	98.96	97.80	98.48	100.83	97.61	99.93	99.49	99.30	99.44	99.07	99.58
Number of atoms in the formula unit on the basis of the 18 oxygens																
Si	4.98	4.98	4.99	4.99	4.97	4.99	5.00	4.97	4.95	5.00	4.96	5.00	4.99	4.98	4.99	4.97
Ti	0.00	0.00	0.00	0.00	0.00	0.00	0.00	0.00	0.00	0.00	0.00	0.00	0.00	0.00	0.00	0.01
Al	3.99	3.98	3.99	4.00	4.00	3.97	3.97	4.00	3.99	3.96	3.98	3.98	3.96	3.98	3.97	3.97
Cr	0.00	0.00	0.00	0.00	0.00	0.00	0.00	0.00	0.00	0.00	0.00	0.00	0.00	0.00	0.00	0.00
Mn	0.03	0.04	0.04	0.03	0.02	0.02	0.02	0.03	0.02	0.03	0.01	0.00	0.00	0.00	0.00	0.01
Mg	1.25	1.25	1.25	1.25	1.24	1.26	1.25	1.25	1.26	1.22	0.99	0.98	0.99	1.01	1.01	1.01
Ca	0.00	0.00	0.00	0.00	0.00	0.00	0.00	0.00	0.00	0.00	0.00	0.00	0.00	0.00	0.00	0.00
Zn	0.00	0.00	0.00	0.00	0.00	0.02	0.00	0.00	0.01	0.00	0.02	0.00	0.00	0.00	0.00	0.00
Na	0.07	0.09	0.06	0.08	0.08	0.08	0.05	0.07	0.08	0.08	0.09	0.06	0.06	0.08	0.08	0.05
K	0.00	0.01	0.00	0.00	0.00	0.00	0.00	0.00	0.00	0.00	0.00	0.00	0.00	0.00	0.00	0.00
Fe	0.73	0.71	0.74	0.74	0.78	0.72	0.74	0.73	0.75	0.76	1.03	1.02	1.04	1.01	0.97	1.02
Total	11.05	11.06	11.07	11.09	11.09	11.06	11.03	11.05	11.06	11.05	11.08	11.04	11.04	11.06	11.02	11.04

Microprobe results of cordierite in pelites

Sample Number							MM171									
Oxide Percentage																
SiO2	47.79	47.84	48.02	47.31	47.95	48.25	47.54	47.47	47.48	47.67	47.61	48.20	47.40	47.89	47.42	47.16
TiO2	0.00	0.00	0.00	0.00	0.05	0.01	0.06	0.01	0.00	0.00	0.00	0.00	0.02	0.06	0.04	0.03
Al2O3	32.01	32.30	32.68	31.89	32.60	32.65	32.58	32.24	32.40	32.56	32.42	32.82	32.51	32.99	32.37	32.24
Cr2O3	0.07	0.05	0.00	0.12	0.00	0.00	0.00	0.10	0.00	0.00	0.09	0.05	0.00	0.00	0.00	0.00
MnO	0.02	0.07	0.19	0.06	0.06	0.14	0.18	0.34	0.24	0.21	0.18	0.30	0.28	0.24	0.23	0.09
MgO	6.20	6.32	6.57	6.18	6.52	6.71	6.08	5.91	5.96	5.89	6.21	6.55	6.19	6.74	6.49	6.03
CaO	0.03	0.01	0.10	0.00	0.08	0.00	0.04	0.00	0.01	0.04	0.00	0.02	0.00	0.01	0.00	0.01
ZnO	0.00	0.10	0.23	0.00	0.00	0.11	0.05	0.00	0.05	0.24	0.14	0.07	0.06	0.00	0.08	0.00
Na2O	0.25	0.39	0.43	0.36	0.38	0.33	0.32	0.34	0.42	0.44	0.36	0.33	0.29	0.59	0.51	0.39
K2O	0.01	0.04	0.00	0.02	0.00	0.00	0.00	0.03	0.01	0.02	0.01	0.00	0.02	0.00	0.02	0.00
FeO	12.02	12.08	11.88	12.00	11.56	11.76	12.24	12.14	12.33	12.59	12.27	11.85	11.76	11.68	11.64	13.47
Total	98.40	99.20	100.10	97.94	99.20	99.96	99.09	98.58	98.90	99.66	99.29	100.19	98.53	100.20	98.80	99.42
Number of atoms in the formula unit on the basis of the 18 oxygens																
Si	5.00	4.98	4.96	4.99	4.98	4.98	4.96	4.98	4.97	4.96	4.96	4.96	4.96	4.94	4.95	4.96
Ti	0.00	0.00	0.00	0.00	0.00	0.00	0.00	0.00	0.00	0.00	0.00	0.00	0.00	0.00	0.00	0.00
Al	3.95	3.96	3.98	3.97	3.99	3.97	4.00	3.99	4.00	4.00	3.98	3.98	4.01	4.00	3.98	4.00
Cr	0.00	0.00	0.00	0.01	0.00	0.00	0.00	0.00	0.00	0.00	0.00	0.00	0.00	0.00	0.00	0.00
Mn	0.00	0.00	0.02	0.00	0.00	0.01	0.02	0.03	0.02	0.02	0.02	0.03	0.02	0.02	0.02	0.00
Mg	0.97	0.98	1.01	0.97	1.00	1.03	0.94	0.92	0.93	0.91	0.97	1.00	0.97	1.04	1.01	0.95
Ca	0.00	0.00	0.01	0.00	0.00	0.00	0.00	0.00	0.00	0.00	0.00	0.00	0.00	0.00	0.00	0.00
Zn	0.00	0.00	0.02	0.00	0.00	0.00	0.00	0.00	0.00	0.02	0.01	0.00	0.00	0.00	0.00	0.00
Na	0.05	0.08	0.08	0.07	0.08	0.06	0.06	0.07	0.08	0.09	0.07	0.07	0.06	0.11	0.10	0.08
K	0.00	0.00	0.00	0.00	0.00	0.00	0.00	0.00	0.00	0.00	0.00	0.00	0.00	0.00	0.00	0.00
Fe	1.05	1.05	1.03	1.06	1.00	1.01	1.07	1.06	1.08	1.10	1.07	1.02	1.03	1.00	1.02	1.09
Total	11.02	11.05	11.11	11.07	11.05	11.06	11.05	11.05	11.08	11.10	11.08	11.06	11.05	11.11	11.08	11.08
Sample Number						MM166D										
Oxide Percentage																
SiO2	48.10	47.51	47.77	47.63	47.26	47.42	47.65	48.32	47.81	47.79	47.61	47.74	47.43	47.76	47.52	47.67
TiO2	0.00	0.00	0.00	0.00	0.02	0.03	0.06	0.00	0.01	0.07	0.00	0.00	0.06	0.00	0.00	0.09
Al2O3	32.63	32.96	32.69	32.33	32.23	32.55	32.41	32.78	32.62	32.54	32.75	33.02	32.72	32.57	32.79	32.67
Cr2O3	0.00	0.00	0.00	0.00	0.00	0.00	0.00	0.00	0.08	0.01	0.00	0.00	0.00	0.00	0.00	0.03
MnO	0.22	0.37	0.26	0.31	0.17	0.19	0.01	0.18	0.00	0.04	0.00	0.00	0.01	0.17	0.15	0.17
MgO	6.50	6.62	6.39	6.12	6.17	6.71	6.45	6.94	6.69	6.17	6.78	6.62	6.35	6.27	6.54	6.51
CaO	0.00	0.07	0.03	0.04	0.02	0.00	0.00	0.02	0.00	0.00	0.02	0.01	0.02	0.07	0.07	0.06
ZnO	0.00	0.11	0.39	0.00	0.00	0.28	0.00	0.04	0.00	0.00	0.00	0.00	0.15	0.00	0.30	0.02
Na2O	0.43	0.48	0.33	0.33	0.33	0.39	0.28	0.39	0.25	0.39	0.33	0.23	0.30	0.37	0.28	0.31
K2O	0.00	0.00	0.00	0.03	0.08	0.03	0.00	0.04	0.00	0.03	0.02	0.03	0.08	0.00	0.00	0.00
FeO	12.14	11.44	11.76	11.78	11.88	11.81	11.67	11.37	11.47	12.45	11.64	11.83	12.26	11.79	11.94	11.67
Total	100.02	99.56	99.62	98.57	98.16	99.41	98.53	100.08	98.93	99.49	99.15	99.48	99.38	99.00	99.59	99.20
Number of atoms in the formula unit on the basis of the 18 oxygens																
Si	4.97	4.93	4.96	4.99	4.97	4.93	4.98	4.97	4.97	4.97	4.95	4.95	4.94	4.98	4.93	4.95
Ti	0.00	0.00	0.00	0.00	0.00	0.00	0.00	0.00	0.00	0.00	0.00	0.00	0.00	0.00	0.00	0.00
Al	3.97	4.03	4.00	3.99	4.00	3.99	4.00	3.97	4.00	3.99	4.01	4.04	4.01	4.00	4.01	4.00
Cr	0.00	0.00	0.00	0.00	0.00	0.00	0.00	0.00	0.00	0.00	0.00	0.00	0.00	0.00	0.00	0.00
Mn	0.02	0.03	0.02	0.03	0.01	0.02	0.00	0.02	0.00	0.00	0.00	0.00	0.00	0.01	0.01	0.01
Mg	1.00	1.02	0.99	0.96	0.97	1.04	1.00	1.06	1.04	0.96	1.05	1.02	0.98	0.97	1.01	1.00
Ca	0.00	0.00	0.00	0.00	0.00	0.00	0.00	0.00	0.00	0.00	0.00	0.00	0.00	0.00	0.00	0.00
Zn	0.00	0.01	0.03	0.00	0.00	0.02	0.00	0.00	0.00	0.00	0.00	0.00	0.01	0.00	0.02	0.00
Na	0.09	0.01	0.07	0.07	0.07	0.08	0.06	0.08	0.05	0.08	0.07	0.05	0.06	0.07	0.06	0.06
K	0.00	0.00	0.00	0.00	0.01	0.00	0.00	0.00	0.00	0.00	0.00	0.00	0.01	0.00	0.00	0.00
Fe	1.05	0.99	1.02	1.03	1.04	1.03	1.02	0.98	1.00	1.08	1.01	1.03	1.07	1.03	1.04	1.01
Total	11.10	11.02	11.09	11.07	11.07	11.11	11.06	11.08	11.06	11.08	11.09	11.09	11.08	11.06	11.08	11.03

Microprobe results of cordierite in pelites

Sample Number					MM166C											
Oxide Percentage																
SiO2	47.92	47.71	47.77	47.34	48.04	48.18	47.77	47.91	48.73	48.63	49.00	48.24	48.67	48.97	48.37	48.83
TiO2	0.00	0.01	0.00	0.00	0.00	0.00	0.06	0.00	0.08	0.04	0.00	0.04	0.12	0.06	0.00	0.00
Al2O3	32.60	32.48	32.52	32.40	32.49	32.55	32.52	32.60	32.57	32.91	33.32	32.57	33.23	33.11	32.35	32.88
Cr2O3	0.02	0.04	0.00	0.05	0.00	0.02	0.00	0.03	0.06	0.05	0.04	0.03	0.03	0.00	0.03	0.00
MnO	0.14	0.18	0.13	0.05	0.06	0.14	0.11	0.09	0.09	0.00	0.15	0.15	0.13	0.09	0.08	0.00
MgO	6.84	6.58	6.57	6.63	5.87	6.23	6.00	5.87	6.27	6.40	6.19	5.33	5.46	5.78	5.85	6.58
CaO	0.03	0.06	0.10	0.04	0.01	0.00	0.02	0.00	0.02	0.01	0.03	0.02	0.05	0.00	0.06	0.03
ZnO	0.16	0.00	0.11	0.00	0.00	0.24	0.00	0.04	0.00	0.11	0.00	0.11	0.11	0.00	0.00	0.00
Na2O	0.29	0.28	0.38	0.36	0.18	0.37	0.29	0.40	0.32	0.22	0.26	0.25	0.24	0.46	0.29	0.17
K2O	0.00	0.03	0.00	0.03	0.00	0.00	0.00	0.00	0.00	0.00	0.02	0.00	0.00	0.00	0.00	0.00
FeO	11.60	11.64	11.58	11.76	12.54	12.00	12.30	12.56	12.21	12.55	12.64	13.66	13.82	13.42	12.80	11.82
Total	99.60	99.01	99.16	98.66	99.19	99.73	99.07	99.50	100.35	100.92	101.65	100.40	101.86	101.89	99.83	100.31
Number of atoms in the formula unit on the basis of the 18 oxygens																
Si	4.96	4.96	4.97	4.95	5.00	4.99	4.98	4.98	5.00	4.97	4.98	4.99	4.96	4.99	5.01	5.01
Ti	0.00	0.00	0.00	0.00	0.00	0.00	0.00	0.00	0.00	0.00	0.00	0.00	0.00	0.00	0.00	0.00
Al	3.98	3.98	3.99	3.99	3.99	3.97	4.00	3.99	3.94	3.97	3.99	3.97	3.99	3.97	3.95	3.98
Cr	0.00	0.00	0.00	0.00	0.00	0.00	0.00	0.00	0.00	0.00	0.00	0.00	0.00	0.00	0.00	0.00
Mn	0.01	0.01	0.01	0.00	0.00	0.01	0.01	0.00	0.00	0.00	0.01	0.01	0.01	0.00	0.00	0.00
Mg	1.06	1.02	1.02	1.03	0.91	0.96	0.93	0.91	0.96	0.98	0.94	0.82	0.83	0.88	0.90	1.00
Ca	0.00	0.00	0.01	0.00	0.00	0.00	0.00	0.00	0.00	0.00	0.00	0.00	0.00	0.00	0.00	0.00
Zn	0.01	0.00	0.00	0.00	0.00	0.02	0.00	0.00	0.00	0.00	0.00	0.00	0.00	0.00	0.00	0.00
Na	0.06	0.06	0.08	0.07	0.04	0.07	0.06	0.08	0.06	0.04	0.05	0.05	0.05	0.09	0.06	0.03
K	0.00	0.00	0.00	0.00	0.00	0.00	0.00	0.00	0.00	0.00	0.00	0.00	0.00	0.00	0.00	0.00
Fe	1.00	1.01	1.00	1.03	1.09	1.04	1.07	1.09	1.05	1.07	1.07	1.18	1.18	1.14	1.11	1.01
Total	11.08	11.04	11.08	11.07	11.03	11.06	11.05	11.05	11.01	11.03	11.04	11.02	11.02	11.07	11.03	11.03
Sample Number										MM185B						
Oxide Percentage																
SiO2	49.27	49.18	48.26	48.28	48.44	47.75	48.21	48.05	48.32	47.02	47.61	47.40	47.44	47.81	47.81	47.76
TiO2	0.03	0.00	0.04	0.08	0.00	0.00	0.00	0.01	0.00	0.05	0.00	0.08	0.00	0.00	0.00	0.03
Al2O3	33.42	33.26	32.53	32.65	33.06	32.51	32.84	32.43	32.65	31.94	32.18	31.82	32.15	32.19	32.19	32.23
Cr2O3	0.12	0.00	0.02	0.00	0.03	0.03	0.00	0.01	0.03	0.10	0.10	0.04	0.02	0.00	0.00	0.02
MnO	0.06	0.02	0.05	0.11	0.02	0.10	0.08	0.13	0.10	0.00	0.00	0.02	0.02	0.00	0.00	0.00
MgO	6.57	6.62	6.52	6.46	6.35	5.76	5.88	5.93	6.03	5.76	5.96	5.75	5.94	5.89	5.89	6.25
CaO	0.00	0.00	0.02	0.05	0.00	0.02	0.13	0.00	0.03	0.02	0.03	0.00	0.00	0.00	0.00	0.00
ZnO	0.26	0.09	0.00	0.00	0.10	0.35	0.09	0.04	0.18	0.07	0.00	0.00	0.16	0.18	0.18	0.00
Na2O	0.39	0.20	0.28	0.29	0.40	0.21	0.39	0.25	0.30	0.39	0.44	0.31	0.39	0.40	0.40	0.42
K2O	0.00	0.03	0.00	0.02	0.00	0.00	0.00	0.00	0.06	0.06	0.01	0.03	0.03	0.07	0.07	0.00
FeO	12.45	11.98	12.03	11.86	12.32	12.63	12.99	12.66	12.74	12.54	12.64	12.11	12.45	12.29	12.29	11.87
Total	102.57	101.38	99.75	99.80	100.72	99.36	100.61	99.51	100.44	97.95	98.97	97.56	98.60	98.83	98.83	98.58
Number of atoms in the formula unit on the basis of the 18 oxygens																
Si	4.96	4.99	4.99	4.98	4.97	4.98	4.97	4.99	4.98	4.97	4.98	5.01	4.98	5.00	5.00	5.00
Ti	0.00	0.00	0.00	0.00	0.00	0.00	0.00	0.00	0.00	0.00	0.00	0.00	0.00	0.00	0.00	0.00
Al	3.97	3.98	3.96	3.97	3.99	3.99	3.99	3.97	3.97	3.98	3.97	3.97	3.98	3.97	3.97	3.98
Cr	0.01	0.00	0.00	0.00	0.00	0.00	0.00	0.00	0.00	0.00	0.00	0.00	0.00	0.00	0.00	0.00
Mn	0.00	0.00	0.00	0.01	0.00	0.00	0.00	0.01	0.00	0.00	0.00	0.00	0.00	0.00	0.00	0.00
Mg	0.99	1.00	1.00	0.99	0.97	0.89	0.90	0.92	0.93	0.91	0.93	0.91	0.93	0.92	0.92	0.98
Ca	0.00	0.00	0.00	0.00	0.00	0.00	0.01	0.00	0.00	0.00	0.00	0.00	0.00	0.00	0.00	0.00
Zn	0.02	0.00	0.00	0.00	0.00	0.03	0.00	0.00	0.01	0.00	0.00	0.00	0.01	0.01	0.01	0.00
Na	0.08	0.04	0.06	0.06	0.08	0.04	0.08	0.05	0.06	0.08	0.09	0.06	0.08	0.08	0.08	0.09
K	0.00	0.00	0.00	0.00	0.00	0.00	0.00	0.00	0.00	0.00	0.00	0.00	0.00	0.01	0.01	0.00
Fe	1.05	1.02	1.04	1.02	1.06	1.10	1.12	1.10	1.10	1.11	1.11	1.07	1.09	1.08	1.08	1.04
Total	11.08	11.03	11.05	11.03	11.07	11.03	11.07	11.04	11.05	11.05	11.08	11.02	11.07	11.07	11.07	11.09

Microprobe results of cordierite in pelites

Sample Number							MM169B									
Oxide Percentage																
SiO2	47.71	47.79	47.91	47.53	47.22	48.03	47.92	48.12	48.07	47.96	48.07	48.33	46.93	48.22	47.91	47.84
TiO2	0.03	0.00	0.00	0.00	0.00	0.03	0.01	0.08	0.00	0.00	0.00	0.11	0.07	0.00	0.00	0.04
Al2O3	32.51	32.06	32.23	32.40	31.70	32.56	32.46	32.45	32.38	32.32	32.39	32.29	31.37	32.43	32.20	32.55
Cr2O3	0.00	0.00	0.00	0.00	0.05	0.00	0.00	0.05	0.00	0.00	0.00	0.00	0.01	0.01	0.12	0.00
MnO	0.02	0.00	0.07	0.05	0.00	0.04	0.10	0.00	0.02	0.21	0.19	0.02	0.09	0.00	0.00	0.02
MgO	6.26	6.42	6.57	6.44	5.85	6.38	6.60	6.35	6.40	6.51	6.15	6.43	6.39	6.65	6.46	6.57
CaO	0.00	0.00	0.04	0.00	0.01	0.00	0.00	0.00	0.00	0.00	0.00	0.00	0.03	0.02	0.00	0.00
ZnO	0.00	0.14	0.00	0.00	0.00	0.16	0.00	0.00	0.05	0.05	0.02	0.08	1.34	0.00	0.16	0.20
Na2O	0.43	0.26	0.44	0.43	0.48	0.35	0.30	0.24	0.43	0.41	0.34	0.39	0.49	0.37	0.23	0.31
K2O	0.05	0.00	0.03	0.00	0.94	0.03	0.00	0.00	0.04	0.02	0.02	0.00	0.00	0.00	0.01	0.00
FeO	11.75	11.11	11.32	11.55	11.52	11.71	11.87	11.55	11.84	11.68	12.17	11.65	11.52	12.32	11.56	11.89
Total	98.76	97.78	98.61	98.40	97.77	99.29	99.26	98.84	99.23	99.16	99.35	99.30	98.24	100.02	98.65	99.42
Number of atoms in the formula unit on the basis of the 18 oxygens																
Si	4.98	5.02	5.00	4.98	5.00	4.98	4.98	5.01	5.00	4.99	4.99	5.00	4.96	4.98	5.00	4.96
Ti	0.00	0.00	0.00	0.00	0.00	0.00	0.00	0.00	0.00	0.00	0.00	0.00	0.00	0.00	0.00	0.00
Al	4.00	3.97	3.97	4.00	3.96	3.98	3.97	3.98	3.97	3.96	3.97	3.94	3.91	3.95	3.96	3.98
Cr	0.00	0.00	0.00	0.00	0.00	0.00	0.00	0.00	0.00	0.00	0.00	0.00	0.00	0.00	0.01	0.00
Mn	0.00	0.00	0.00	0.00	0.00	0.00	0.00	0.00	0.00	0.02	0.02	0.00	0.00	0.00	0.00	0.00
Mg	0.97	1.00	1.02	1.00	0.91	0.99	1.02	0.99	0.99	1.01	0.95	0.99	1.00	1.02	1.00	1.02
Ca	0.00	0.00	0.00	0.00	0.00	0.00	0.00	0.00	0.00	0.00	0.00	0.00	0.00	0.00	0.00	0.00
Zn	0.00	0.01	0.00	0.00	0.00	0.01	0.00	0.00	0.00	0.00	0.00	0.00	0.10	0.00	0.01	0.01
Na	0.09	0.05	0.09	0.09	0.10	0.07	0.06	0.05	0.09	0.08	0.07	0.08	0.10	0.07	0.05	0.06
K	0.00	0.00	0.00	0.00	0.13	0.00	0.00	0.00	0.00	0.00	0.00	0.00	0.00	0.00	0.00	0.00
Fe	1.03	0.98	0.99	1.01	1.01	1.02	1.03	1.00	1.03	1.02	1.06	1.01	1.02	1.06	1.01	1.03
Total	11.07	11.03	11.07	11.08	11.11	11.05	11.06	11.03	11.08	11.08	11.06	11.02	11.09	11.08	11.04	11.06
Sample Number				MM149								MM143				
Oxide Percentage																
SiO2	48.02	48.49	48.52	47.84	47.73	48.03	47.91	47.77	47.19	47.72	48.27	48.52	48.00	48.29	48.68	49.12
TiO2	0.04	0.05	0.04	0.00	0.00	0.03	0.05	0.00	0.00	0.00	0.00	0.00	0.01	0.06	0.05	0.09
Al2O3	32.30	32.77	33.17	32.20	32.32	32.60	32.20	32.17	31.59	32.22	32.45	32.59	32.49	32.75	33.05	32.35
Cr2O3	0.01	0.02	0.00	0.04	0.01	0.03	0.06	0.03	0.00	0.00	0.03	0.00	0.00	0.09	0.07	0.04
MnO	0.08	0.00	0.08	0.16	0.16	0.23	0.09	0.31	0.22	0.39	0.26	0.19	0.11	0.07	0.07	0.09
MgO	6.49	6.49	6.65	6.66	6.28	6.62	6.63	6.96	6.33	6.42	6.85	7.54	6.31	7.44	7.51	7.37
CaO	0.00	0.00	0.00	0.04	0.02	0.00	0.00	0.00	0.00	0.01	0.00	0.05	0.00	0.00	0.04	0.04
ZnO	0.00	0.00	0.02	0.30	0.08	0.20	0.00	0.03	0.13	0.00	0.08	0.00	0.00	0.07	0.00	0.18
Na2O	0.47	0.29	0.16	0.33	0.24	0.39	0.36	0.53	0.20	0.38	0.41	0.29	0.41	0.36	0.24	0.18
K2O	0.00	0.00	0.04	0.00	0.00	0.03	0.00	0.00	0.00	0.03	0.01	0.02	0.01	0.00	0.00	0.00
FeO	11.76	11.69	11.74	11.27	11.11	11.06	11.23	11.08	11.15	11.40	11.05	10.23	12.05	10.23	10.18	9.67
Total	99.17	99.80	100.42	98.84	97.95	99.22	98.53	98.88	96.81	98.57	99.41	99.43	99.39	99.36	99.89	99.13
Number of atoms in the formula unit on the basis of the 18 oxygens																
Si	4.99	5.00	4.97	4.99	5.00	4.98	5.00	4.98	5.02	4.99	5.00	5.00	4.99	4.97	4.98	5.05
Ti	0.00	0.00	0.00	0.00	0.00	0.00	0.00	0.00	0.00	0.00	0.00	0.00	0.00	0.00	0.00	0.00
Al	3.96	3.98	4.00	3.96	4.00	3.98	3.96	3.95	3.96	3.97	3.96	3.96	3.98	3.98	3.98	3.92
Cr	0.00	0.00	0.00	0.00	0.00	0.00	0.00	0.00	0.00	0.00	0.00	0.00	0.00	0.00	0.00	0.00
Mn	0.00	0.00	0.00	0.01	0.01	0.02	0.00	0.02	0.02	0.03	0.02	0.02	0.01	0.00	0.00	0.01
Mg	1.00	1.00	1.01	1.03	0.98	1.02	1.03	1.08	1.00	1.00	1.06	1.16	0.98	1.14	1.15	1.14
Ca	0.00	0.00	0.00	0.00	0.00	0.00	0.00	0.00	0.00	0.00	0.00	0.00	0.00	0.00	0.00	0.00
Zn	0.00	0.00	0.00	0.02	0.00	0.01	0.00	0.00	0.01	0.00	0.00	0.00	0.00	0.00	0.00	0.01
Na	0.10	0.06	0.03	0.07	0.05	0.08	0.07	0.11	0.04	0.08	0.08	0.06	0.08	0.07	0.05	0.04
K	0.00	0.00	0.00	0.00	0.00	0.00	0.00	0.00	0.00	0.00	0.00	0.00	0.00	0.00	0.00	0.00
Fe	1.02	1.00	1.00	0.98	0.97	0.96	0.98	0.97	0.99	1.00	0.96	0.88	1.05	0.88	0.87	0.83
Total	11.07	11.04	11.01	11.06	11.01	11.05	11.04	11.11	11.04	11.07	11.08	11.08	11.09	11.04	11.03	11.00

Microprobe results of cordierite in pelites

Sample Number				MM141								MM131B				
Oxide Percentage																
SiO2	48.24	48.98	48.38	47.95	48.11	47.60	47.68	48.00	47.84	47.98	48.48	47.93	47.43	47.76	47.71	47.93
TiO2	0.06	0.00	0.02	0.04	0.00	0.00	0.00	0.00	0.00	0.00	0.00	0.03	0.00	0.00	0.04	0.00
Al2O3	32.91	32.81	32.72	32.51	32.72	32.55	32.01	32.39	32.66	32.49	32.47	32.47	3.98	32.25	32.31	32.44
Cr2O3	0.00	0.08	0.00	0.06	0.08	0.06	0.12	0.02	0.02	0.06	0.00	0.00	0.00	0.02	0.00	0.00
MnO	0.01	0.20	0.18	0.00	0.00	0.00	0.00	0.00	0.01	0.00	0.00	0.11	0.00	0.26	0.18	0.09
MgO	7.55	7.58	7.42	5.70	6.63	6.56	6.17	5.96	6.32	6.20	6.29	5.89	0.94	6.19	6.09	6.75
CaO	0.02	0.04	0.02	0.00	0.00	0.00	0.00	0.00	0.00	0.00	0.05	0.00	0.00	0.07	0.00	0.00
ZnO	0.09	0.09	0.00	0.00	0.00	0.13	0.06	0.00	0.00	0.04	0.03	0.02	0.01	0.17	0.12	0.00
Na2O	0.21	0.40	0.23	0.24	0.36	0.29	0.22	0.23	0.40	0.17	0.24	0.32	0.07	0.42	0.31	0.43
K2O	0.00	0.00	0.03	0.00	0.02	0.01	0.04	0.04	0.00	0.01	0.01	0.00	0.00	0.00	0.00	0.08
FeO	10.12	10.02	9.96	13.16	11.81	11.61	11.93	11.97	12.55	12.24	12.22	12.26	1.05	11.75	11.95	11.16
Total																
Number of atoms in the formula unit on the basis of the 18 oxygens																
Si	4.97	5.00	4.99	4.99	4.98	4.97	5.00	5.01	4.96	4.99	5.02	5.00	4.99	4.99	4.99	4.98
Ti	0.00	0.00	0.00	0.00	0.00	0.00	0.00	0.00	0.00	0.00	0.00	0.00	0.00	0.00	0.00	0.00
Al	3.99	3.95	3.98	3.99	3.99	4.00	3.96	3.99	3.99	3.98	3.96	3.99	3.98	3.97	3.98	3.98
Cr	0.00	0.00	0.00	0.00	0.00	0.00	0.01	0.00	0.00	0.00	0.00	0.00	0.00	0.00	0.00	0.00
Mn	0.00	0.02	0.01	0.00	0.00	0.00	0.00	0.00	0.00	0.00	0.00	0.01	0.00	0.02	0.02	0.00
Mg	1.16	1.15	1.14	0.88	1.02	1.02	0.97	0.93	0.98	0.96	0.97	0.92	0.94	0.96	0.95	1.05
Ca	0.00	0.00	0.00	0.00	0.00	0.00	0.00	0.00	0.00	0.00	0.00	0.00	0.00	0.00	0.00	0.00
Zn	0.00	0.00	0.00	0.00	0.00	0.01	0.00	0.00	0.00	0.00	0.00	0.00	0.01	0.01	0.01	0.00
Na	0.04	0.08	0.04	0.05	0.07	0.06	0.04	0.05	0.08	0.03	0.05	0.06	0.07	0.08	0.06	0.09
K	0.00	0.00	0.00	0.00	0.00	0.00	0.00	0.00	0.00	0.00	0.00	0.00	0.00	0.00	0.00	0.01
Fe	0.87	0.85	0.86	1.14	1.02	1.01	1.05	1.04	1.09	1.06	1.06	1.07	1.05	1.03	1.05	0.97
Total	11.03	11.05	11.02	11.05	11.08	11.07	11.03	11.02	11.10	11.02	11.06	11.05	11.04	11.06	11.06	11.08
Sample Number					MM198C											
Oxide Percentage																
SiO2	47.69	48.00	47.55	48.02	48.51	48.96	48.93	49.13	48.94	49.09	48.97	48.57	48.78	48.52	5.02	48.75
TiO2	0.00	0.00	0.00	0.04	0.05	0.02	0.00	0.08	0.00	0.09	0.00	0.00	0.06	0.00	0.00	0.07
Al2O3	32.05	32.61	32.58	32.60	32.47	32.70	32.57	33.00	32.92	33.02	32.93	32.25	32.60	32.42	3.94	32.67
Cr2O3	0.00	0.00	0.08	0.06	0.00	0.00	0.08	0.02	0.12	0.00	0.10	0.00	0.07	0.00	0.00	0.00
MnO	0.25	0.16	0.16	0.00	0.15	0.27	0.24	0.20	0.06	0.28	0.06	0.23	0.16	0.07	0.02	0.19
MgO	6.06	6.35	6.49	6.10	8.28	8.09	8.22	8.55	8.26	8.26	8.67	8.11	8.26	8.27	1.27	8.24
CaO	0.00	0.00	0.00	0.00	0.09	0.01	0.02	0.00	0.06	0.01	0.00	0.00	0.00	0.00	0.00	0.00
ZnO	0.03	0.08	0.00	0.32	0.00	0.29	0.00	0.00	0.00	0.00	0.10	0.22	0.09	0.00	0.00	0.00
Na2O	0.36	0.39	0.44	0.36	0.24	0.07	0.21	0.30	0.26	0.09	0.28	0.24	0.17	0.25	0.03	0.31
K2O	0.02	0.02	0.05	0.02	0.00	0.00	0.04	0.00	0.00	0.00	0.03	0.05	0.00	0.00	0.00	0.01
FeO	12.04	11.59	12.04	12.18	8.69	8.83	9.15	8.57	8.72	8.86	8.51	8.79	8.44	8.75	0.75	8.73
Total	98.50	99.20	99.39	99.70	98.48	99.24	99.46	99.85	99.34	99.70	99.65	98.46	98.63	98.28	11.03	98.97
Number of atoms in the formula unit on the basis of the 18 oxygens																
Si	5.00	4.98	4.95	4.98	5.00	5.01	5.01	5.00	5.00	5.00	4.99	5.02	5.01	5.01	5.02	5.00
Ti	0.00	0.00	0.00	0.00	0.00	0.00	0.00	0.00	0.00	0.00	0.00	0.00	0.00	0.00	0.00	0.00
Al	3.96	3.99	4.00	3.99	3.95	3.95	3.93	3.96	3.97	3.96	3.96	3.93	3.95	3.95	3.94	3.95
Cr	0.00	0.00	0.00	0.00	0.00	0.00	0.00	0.00	0.01	0.00	0.00	0.00	0.00	0.00	0.00	0.00
Mn	0.02	0.01	0.01	0.00	0.01	0.02	0.02	0.02	0.00	0.02	0.00	0.02	0.01	0.00	0.02	0.02
Mg	0.95	0.98	1.00	0.94	1.27	1.24	1.25	1.30	1.26	1.25	1.32	1.25	1.27	1.27	1.27	1.26
Ca	0.00	0.00	0.00	0.00	0.01	0.00	0.00	0.00	0.00	0.00	0.00	0.00	0.00	0.00	0.00	0.00
Zn	0.00	0.00	0.00	0.02	0.00	0.02	0.00	0.00	0.00	0.00	0.00	0.02	0.00	0.00	0.00	0.00
Na	0.07	0.08	0.09	0.07	0.05	0.01	0.04	0.06	0.05	0.02	0.05	0.05	0.03	0.05	0.03	0.06
K	0.00	0.00	0.00	0.00	0.00	0.00	0.00	0.00	0.00	0.00	0.00	0.00	0.00	0.00	0.00	0.00
Fe	1.06	1.00	1.05	1.06	0.75	0.76	0.78	0.73	0.75	0.75	0.72	0.76	0.73	0.76	0.75	0.75
Total	11.06	11.04	11.10	11.06	11.04	11.01	11.03	11.07	11.04	11.00	11.04	11.05	11.00	11.04	11.03	11.04

Microprobe results of garnet in pelites

Sample	MM134A.CG									MM134A.RG						
Oxides, wt%																
SiO2	37.32	37.25	37.47	37.02	37.30	37.56	37.30	36.93	37.13	37.34	37.78	38.07	38.09	37.70	37.19	37.24
TiO2	0.00	0.04	0.07	0.02	0.00	0.00	0.05	0.00	0.05	0.14	0.02	0.04	0.01	0.04	0.12	0.00
Al2O3	21.34	21.24	21.10	21.04	20.95	21.20	21.15	20.73	20.95	20.96	21.28	21.28	21.09	21.37	21.21	21.28
Cr2O3	0.00	0.09	0.00	0.12	0.05	0.11	0.05	0.00	0.12	0.01	0.00	0.00	0.00	0.00	0.09	0.00
Fe2O3	3.08	3.36	2.98	2.92	2.68	2.18	3.70	3.01	3.14	3.06	3.27	1.72	1.68	2.55	3.29	4.08
FeO	26.85	26.44	26.61	26.36	26.59	27.09	25.67	26.21	26.51	22.38	23.03	24.28	24.77	24.45	24.36	24.05
MnO	7.77	7.88	7.65	7.90	7.89	7.95	7.75	7.69	7.72	7.25	7.12	7.29	7.37	7.70	7.53	7.46
MgO	3.98	4.06	4.09	3.99	3.98	4.04	4.13	3.98	3.89	2.85	3.03	2.92	3.11	3.34	3.56	3.73
CaO	1.14	1.07	1.21	1.11	1.14	1.09	1.17	1.21	1.14	6.41	6.00	5.69	5.31	4.61	3.84	3.47
ZnO	0.00	0.07	0.00	0.07	0.00	0.00	0.26	0.00	0.16	0.00	0.06	0.11	0.00	0.03	0.03	0.00
Na2O	0.29	0.30	0.36	0.28	0.31	0.24	0.42	0.32	0.34	0.38	0.39	0.28	0.21	0.21	0.28	0.38
K2O	0.00	0.03	0.00	0.01	0.01	0.02	0.03	0.01	0.00	0.00	0.00	0.00	0.00	0.00	0.00	0.02
total	101.78	101.84	101.54	100.84	100.90	101.48	101.68	100.09	101.15	100.78	101.98	101.68	101.64	102.00	101.50	101.72
Number of cations on the basis of 12 oxygens																
Si	2.94	2.93	2.95	2.94	2.96	2.96	2.94	2.96	2.95	2.95	2.95	2.98	2.99	2.95	2.93	2.92
Ti	0.00	0.00	0.00	0.00	0.00	0.00	0.00	0.00	0.00	0.00	0.00	0.00	0.00	0.00	0.00	0.00
Al	1.98	1.97	1.96	1.97	1.96	1.97	1.96	1.96	1.96	1.95	1.96	1.97	1.95	1.97	1.97	1.97
Cr	0.00	0.00	0.00	0.00	0.00	0.00	0.00	0.00	0.00	0.00	0.00	0.00	0.00	0.00	0.00	0.00
Fe3+	0.18	0.20	0.18	0.17	0.16	0.13	0.22	0.18	0.19	0.18	0.19	0.10	0.10	0.15	0.19	0.24
Fe2+	1.77	1.74	1.75	1.75	1.77	1.79	1.69	1.75	1.76	1.48	1.50	1.59	1.63	1.60	1.60	1.58
Mn	0.52	0.53	0.51	0.53	0.53	0.53	0.52	0.52	0.52	0.49	0.47	0.48	0.49	0.51	0.50	0.50
Mg	0.47	0.48	0.48	0.40	0.47	0.47	0.48	0.47	0.46	0.34	0.35	0.34	0.36	0.39	0.42	0.44
Ca	0.10	0.09	0.10	0.09	0.10	0.09	0.10	0.10	0.10	0.54	0.50	0.48	0.45	0.39	0.32	0.29
Zn	0.00	0.00	0.00	0.00	0.00	0.00	0.01	0.00	0.00	0.00	0.00	0.00	0.00	0.00	0.00	0.00
Na	0.04	0.05	0.05	0.04	0.05	0.04	0.00	0.05	0.05	0.06	0.06	0.04	0.03	0.03	0.04	0.06
K	0.00	0.00	0.00	0.00	0.00	0.00	0.00	0.00	0.00	0.00	0.00	0.00	0.00	0.00	0.00	0.00
total	8.00	8.00	8.00	8.00	8.00	8.00	8.00	8.00	8.00	8.00	8.00	8.00	8.00	8.00	8.00	8.00
Sample				MM166A												
Oxides, wt%																
SiO2	37.72	37.53	37.43	37.03	37.26	37.48	37.49	37.39	37.06	37.18	37.72	37.27	37.24	37.14	37.16	37.34
TiO2	0.00	0.09	0.04	0.00	0.00	0.00	0.00	0.02	0.00	0.00	0.01	0.00	0.07	0.14	0.09	0.19
Al2O3	21.35	21.27	21.13	21.10	21.22	21.11	20.84	21.18	20.83	21.15	21.21	21.00	20.75	21.13	20.97	21.23
Cr2O3	0.09	0.00	0.06	0.09	0.06	0.10	0.07	0.03	0.08	0.03	0.09	0.03	0.00	0.22	0.00	0.00
Fe2O3	2.04	2.16	2.49	2.56	2.51	2.34	1.95	2.62	2.20	2.72	1.53	2.40	1.68	2.86	2.46	2.03
FeO	26.06	26.76	26.98	33.11	33.23	33.25	33.68	33.27	33.15	32.87	34.03	33.42	33.94	33.11	33.47	33.44
MnO	7.60	7.45	7.65	2.05	1.85	2.02	2.10	2.09	2.04	2.05	2.21	2.05	2.24	2.30	2.56	2.09
MgO	3.70	3.76	3.79	3.83	3.73	3.75	3.76	3.82	3.63	3.85	3.63	3.67	3.36	3.55	3.45	3.64
CaO	2.63	2.03	1.49	0.87	0.92	0.85	0.86	0.88	0.81	0.95	0.79	0.81	0.88	0.87	0.91	1.00
ZnO	0.14	0.11	0.01	0.00	0.00	0.00	0.32	0.10	0.32	0.00	0.28	0.24	0.00	0.24	0.09	0.00
Na2O	0.27	0.27	0.03	0.24	0.32	0.38	0.20	0.29	0.25	0.31	0.24	0.27	0.27	0.31	0.23	0.32
K2O	0.00	0.00	0.00	0.00	0.04	0.00	0.00	0.00	0.05	0.00	0.00	0.00	0.00	0.00	0.00	0.00
total	101.60	101.43	101.37	100.89	101.14	101.27	101.27	101.69	100.43	101.10	101.26	101.16	100.44	101.87	101.39	101.28
Number of cations on the basis of 12 oxygens																
Si	2.97	2.96	2.96	2.95	2.96	2.97	2.98	2.95	2.97	2.95	2.98	2.96	2.98	2.94	2.96	2.96
Ti	0.00	0.00	0.00	0.00	0.00	0.00	0.00	0.00	0.00	0.00	0.00	0.00	0.00	0.00	0.00	0.01
Al	1.98	1.98	1.97	1.98	1.98	1.97	1.95	1.97	1.97	1.98	1.98	1.97	1.96	1.97	1.97	1.98
Cr	0.00	0.00	0.00	0.00	0.00	0.00	0.00	0.00	0.00	0.00	0.00	0.00	0.00	0.01	0.00	0.00
Fe3+	0.12	0.13	0.15	0.15	0.15	0.14	0.12	0.16	0.13	0.16	0.09	0.14	0.10	0.17	0.15	0.12
Fe2+	1.71	0.77	1.78	2.20	2.21	2.20	2.24	2.20	2.22	2.18	2.25	2.22	2.28	2.19	2.23	2.22
Mn	0.51	0.50	0.51	0.14	0.12	0.14	0.14	0.14	0.14	0.14	0.15	0.14	0.15	0.15	0.17	0.14
Mg	0.43	0.44	0.45	0.45	0.44	0.44	0.45	0.45	0.43	0.45	0.43	0.43	0.40	0.42	0.41	0.43
Ca	0.22	0.17	0.13	0.07	0.08	0.07	0.07	0.07	0.07	0.08	0.07	0.07	0.08	0.07	0.08	0.08
Zn	0.00	0.00	0.00	0.00	0.00	0.00	0.02	0.00	0.02	0.00	0.02	0.01	0.00	0.01	0.00	0.00
Na	0.04	0.04	0.05	0.04	0.05	0.06	0.03	0.04	0.03	0.05	0.04	0.04	0.04	0.05	0.03	0.05
K	0.00	0.00	0.00	0.00	0.00	0.00	0.00	0.00	0.00	0.00	0.00	0.00	0.00	0.00	0.00	0.00
total	8.00	8.00	8.00	8.00	8.00	8.00	8.00	8.00	8.00	8.00	8.00	8.00	8.00	8.00	8.00	8.00

Microprobe results of garnet in pelites

Sample	MM166A									
Oxides, wt%										
SiO2	37.11	36.89	37.28	37.41	37.16	37.13	37.06	37.26	37.34	36.83
TiO2	0.10	0.02	0.00	0.08	0.02	0.08	0.02	0.09	0.00	0.12
Al2O3	21.08	20.84	20.78	20.82	20.76	20.76	21.00	20.95	20.92	21.02
Cr2O3	0.00	0.00	0.04	0.07	0.14	0.09	0.25	0.03	0.07	0.13
Fe2O3	2.67	1.43	2.41	2.18	2.71	2.69	2.48	3.04	2.17	2.90
FeO	33.29	33.93	32.94	33.46	33.35	33.08	34.23	33.22	33.53	32.43
MnO	2.32	2.45	2.04	2.16	1.89	1.99	2.11	2.18	1.92	2.18
MgO	3.58	3.49	3.69	3.66	3.79	3.67	2.85	3.60	3.67	3.60
CaO	0.91	0.86	0.83	0.89	0.93	0.97	0.89	0.88	0.90	0.91
ZnO	0.12	0.00	0.18	0.36	0.00	0.28	0.20	0.19	0.26	0.37
Na2O	0.25	0.08	0.38	0.25	0.25	0.29	0.34	0.31	0.25	0.34
K2O	0.00	0.00	0.00	0.00	0.03	0.00	0.00	0.01	0.03	0.00
total	101.45	100.01	100.57	101.34	101.02	101.03	101.44	101.77	101.07	100.84
Number of cations on the basis of 12 oxygens										
Si	2.95	2.97	2.98	2.97	2.96	2.96	2.96	2.95	2.97	2.94
Ti	0.00	0.00	0.00	0.00	0.00	0.00	0.00	0.00	0.00	0.00
Al	1.97	1.98	1.96	1.95	1.95	1.95	1.97	1.95	1.96	1.98
Cr	0.00	0.00	0.00	0.00	0.00	0.00	0.02	0.00	0.00	0.00
Fe3+	0.16	0.09	0.14	0.13	0.16	0.16	0.15	0.18	0.13	0.17
Fe2+	2.21	2.29	2.20	2.22	2.22	2.20	2.28	2.20	2.23	2.16
Mn	0.16	0.17	0.14	0.14	0.13	0.13	0.14	0.15	0.13	0.15
Mg	0.42	0.42	0.44	0.08	0.45	0.44	0.34	0.42	0.44	0.43
Ca	0.08	0.08	0.07	0.02	0.08	0.08	0.08	0.07	0.08	0.08
Zn	0.00	0.00	0.01	0.04	0.00	0.02	0.01	0.01	0.01	0.02
Na	0.04	0.01	0.06	0.00	0.04	0.04	0.05	0.05	0.04	0.05
K	0.00	0.00	0.00	0.04	0.00	0.00	0.00	0.00	0.00	0.00
total	8.00	8.00	8.00	8.00	8.00	8.00	8.00	8.00	8.00	8.00

Microprobe results of K-feldspars in pelites

Sample Number			MM166C							MM131.PL						
Oxides wt%																
SiO2	64.96	65.11	65.29	65.07	64.76	64.55	64.90	64.53	64.77	64.74	64.52	65.25	65.03	65.24	64.81	64.60
TiO2	0.16	0.10	0.24	0.25	0.15	0.13	0.21	0.13	0.10	0.25	0.30	0.09	0.26	0.16	0.02	0.22
Al2O3	18.79	18.63	19.01	18.66	18.53	18.54	18.65	18.63	18.78	18.67	18.77	18.56	18.86	18.97	19.02	18.90
Cr2O3	0.05	0.00	0.00	0.01	0.00	0.00	0.01	0.11	0.08	0.00	0.00	0.01	0.03	0.00	0.02	0.07
MnO	0.00	0.09	0.05	0.00	0.00	0.07	0.00	0.00	0.00	0.00	0.00	0.00	0.00	0.09	0.00	0.00
MgO	0.06	0.00	0.09	0.00	0.00	0.00	0.03	0.00	0.11	0.00	0.02	0.10	0.05	0.10	0.10	0.19
CaO	0.12	0.04	0.14	0.11	0.06	0.13	0.15	0.24	0.11	0.19	0.16	0.09	0.23	0.20	0.14	0.17
ZnO	0.00	0.14	0.02	0.11	0.12	0.00	0.04	0.00	0.00	0.09	0.10	0.00	0.00	0.26	0.14	0.02
Na2O	2.27	2.10	2.36	2.14	2.38	1.92	1.91	1.93	2.32	1.80	1.19	1.85	1.99	2.19	2.00	1.83
K2O	13.36	13.41	13.06	13.42	12.95	13.87	13.69	13.74	13.28	13.95	14.57	14.09	13.64	13.61	13.85	14.15
FeO*	0.00	0.00	0.06	0.09	0.03	0.02	0.28	0.00	0.02	0.14	0.11	0.15	0.12	0.05	0.08	0.16
total	99.77	99.62	100.32	99.86	98.98	99.23	99.87	99.31	99.57	99.83	99.74	100.19	100.21	100.87	100.18	100.31
Number of atoms in the formula unit on the basis of 8 oxygens																
Si	2.98	2.99	2.98	2.99	2.99	2.99	2.98	2.98	2.98	2.98	2.97	2.99	2.98	2.97	2.97	2.96
Ti	0.00	0.00	0.00	0.00	0.00	0.00	0.00	0.00	0.00	0.00	0.01	0.00	0.00	0.00	0.00	0.00
Al	1.02	1.01	1.02	1.00	1.00	1.01	1.01	1.02	1.02	1.01	1.02	1.00	1.02	1.02	1.03	1.02
Cr	0.00	0.00	0.00	0.00	0.00	0.00	0.00	0.00	0.00	0.00	0.00	0.00	0.00	0.00	0.00	0.00
Mn	0.00	0.00	0.00	0.00	0.00	0.00	0.00	0.00	0.00	0.00	0.00	0.00	0.00	0.00	0.00	0.00
Mg	0.00	0.00	0.00	0.00	0.00	0.00	0.00	0.00	0.00	0.00	0.00	0.00	0.00	0.00	0.00	0.01
Ca	0.00	0.00	0.00	0.00	0.00	0.00	0.00	0.01	0.00	0.00	0.00	0.00	0.01	0.01	0.00	0.00
Zn	0.00	0.00	0.00	0.00	0.00	0.00	0.00	0.00	0.00	0.00	0.00	0.00	0.00	0.00	0.00	0.00
Na	0.20	0.19	0.21	0.19	0.21	0.17	0.17	0.17	0.21	0.16	0.11	0.16	0.18	0.19	0.18	0.16
K	0.78	0.79	0.76	0.79	0.76	0.82	0.80	0.81	0.78	0.82	0.86	0.82	0.80	0.79	0.81	0.83
Fe	0.00	0.00	0.00	0.00	0.00	0.00	0.01	0.00	0.00	0.00	0.00	0.00	0.00	0.00	0.00	0.00
total	4.98	4.98	4.97	4.97	4.96	4.99	4.97	4.99	4.99	4.97	4.97	4.97	4.99	4.98	4.99	4.98
Sample Number				MM169B										MM134A		
Oxides wt%																
SiO2	65.23	64.81	65.00	66.12	65.29	65.39	64.98	65.23	65.47	65.76	65.06	65.33	64.84	64.52	63.69	65.50
TiO2	0.11	0.19	0.19	0.14	0.19	0.18	0.14	0.18	0.18	0.21	0.13	0.18	0.10	0.36	0.45	0.25
Al2O3	18.99	18.79	19.06	19.22	18.81	18.97	18.78	18.59	19.01	18.84	18.91	19.03	18.59	18.72	18.72	18.89
Cr2O3	0.00	0.05	0.10	0.00	0.01	0.05	0.05	0.07	0.11	0.09	0.01	0.00	0.00	0.00	0.00	0.04
MnO	0.00	0.03	0.00	0.08	0.08	0.06	0.04	0.00	0.02	0.00	0.03	0.00	0.02	0.10	0.00	0.00
MgO	0.19	0.08	0.17	0.11	0.10	0.02	0.09	0.05	0.00	0.10	0.04	0.09	0.02	0.08	0.03	0.08
CaO	0.22	0.22	0.08	0.11	0.15	0.16	0.18	0.07	0.16	0.14	0.05	0.03	0.14	0.15	0.15	0.10
ZnO	0.16	0.00	0.00	0.18	0.05	0.00	0.14	0.00	0.00	0.31	0.00	0.04	0.03	0.11	0.00	0.07
Na2O	1.97	1.25	2.22	2.34	2.10	2.25	2.41	2.22	1.92	2.28	2.37	2.12	2.00	1.51	1.77	1.64
K2O	13.91	14.88	13.53	13.24	13.85	13.41	13.44	13.70	14.00	13.73	13.26	13.61	13.85	14.41	13.64	14.32
FeO*	0.00	0.05	0.05	0.03	0.00	0.04	0.08	0.00	0.17	0.03	0.04	0.13	0.18	0.00	0.00	0.13
total	100.78	100.35	100.40	101.57	100.63	100.53	100.33	100.11	101.04	101.49	99.90	100.56	99.77	99.96	98.45	101.02
Number of atoms in the formula unit on the basis of 8 oxygens																
Si	2.97	2.97	2.97	2.98	2.98	2.98	2.97	2.99	2.98	2.98	2.98	2.98	2.98	2.97	2.97	2.98
Ti	0.00	0.00	0.00	0.00	0.00	0.00	0.00	0.00	0.00	0.00	0.00	0.00	0.00	0.01	0.02	0.00
Al	1.02	1.02	1.03	1.02	1.01	1.02	1.01	1.00	1.02	1.00	1.02	1.02	1.00	1.02	1.03	1.01
Cr	0.00	0.00	0.00	0.00	0.00	0.00	0.00	0.00	0.00	0.00	0.00	0.00	0.00	0.00	0.00	0.00
Mn	0.00	0.00	0.00	0.00	0.00	0.00	0.00	0.00	0.00	0.00	0.00	0.00	0.00	0.00	0.00	0.00
Mg	0.01	0.00	0.01	0.00	0.00	0.00	0.00	0.00	0.00	0.00	0.00	0.00	0.00	0.00	0.00	0.00
Ca	0.01	0.01	0.00	0.00	0.00	0.00	0.00	0.00	0.00	0.00	0.00	0.00	0.00	0.00	0.00	0.00
Zn	0.00	0.00	0.00	0.00	0.00	0.00	0.00	0.00	0.00	0.01	0.00	0.00	0.00	0.00	0.00	0.00
Na	0.17	0.11	0.20	0.20	0.19	0.20	0.21	0.20	0.17	0.20	0.21	0.19	0.18	0.13	0.16	0.14
K	0.81	0.87	0.79	0.76	0.81	0.78	0.78	0.80	0.81	0.79	0.77	0.79	0.81	0.86	0.81	0.83
Fe	0.00	0.00	0.00	0.00	0.00	0.00	0.00	0.00	0.00	0.00	0.00	0.00	0.00	0.00	0.00	0.00
total	4.99	4.98	5.00	4.96	4.99	4.98	4.97	4.99	4.98	4.98	4.98	4.98	4.97	4.99	4.99	4.96

Microprobe results of K-feldspars in pelites

Sample Number								MM171						MM146		
Oxides wt%																
SiO2	65.15	64.99	65.28	64.99	65.92	64.86	64.83	63.17	63.41	63.74	63.46	63.95	63.51	65.24	64.34	64.78
TiO2	0.18	0.27	0.30	0.28	0.32	0.32	0.17	0.29	0.32	0.27	0.37	0.25	0.28	0.22	0.20	0.23
Al2O3	18.68	18.79	19.04	18.93	19.04	18.74	18.77	20.68	19.04	18.94	20.29	19.72	19.54	18.97	18.65	18.63
Cr2O3	0.00	0.00	0.00	0.02	0.00	0.00	0.00	0.05	0.04	0.06	0.00	0.00	0.02	0.00	0.05	0.00
MnO	0.00	0.11	0.08	0.00	0.06	0.00	0.06	0.00	0.04	0.00	0.07	0.02	0.00	0.00	0.15	0.00
MgO	0.12	0.14	0.17	0.19	0.09	0.00	0.11	0.22	0.10	0.13	0.14	0.26	0.06	0.00	0.05	0.00
CaO	0.12	0.10	0.11	0.11	0.22	0.11	0.20	2.03	0.31	0.15	1.73	0.94	0.85	0.10	0.13	0.08
ZnO	0.12	0.00	0.00	0.00	0.00	0.19	0.00	0.00	0.00	0.00	0.12	0.18	0.18	0.00	0.07	0.00
Na2O	1.84	1.45	1.30	1.20	1.54	1.41	1.37	2.37	1.75	1.20	2.13	1.78	1.45	2.43	2.13	1.85
K2O	13.84	14.65	14.80	14.74	14.16	14.51	14.50	11.64	13.78	14.27	12.29	13.59	13.65	13.00	13.64	13.62
FeO*	0.05	0.13	0.03	0.10	0.10	0.08	0.12	0.28	0.00	0.19	0.14	0.00	0.13	0.00	0.00	0.15
total	100.10	100.63	101.11	100.56	101.45	100.22	100.13	100.73	98.79	98.95	100.74	100.69	99.67	99.96	99.41	99.34
Number of atoms in the formula unit on the basis of 8 oxygens																
Si	2.99	1.98	2.97	2.97	2.98	2.98	2.98	2.87	2.95	2.96	2.89	2.92	2.93	2.99	2.97	2.99
Ti	0.00	0.00	0.01	0.01	0.01	0.01	0.00	0.01	0.01	0.00	0.01	0.00	0.01	0.00	0.00	0.00
Al	1.00	1.01	1.02	1.02	1.02	1.01	1.02	1.11	1.04	1.04	1.09	1.06	1.06	1.02	1.01	1.01
Cr	0.00	0.00	0.00	0.00	0.00	0.00	0.00	0.00	0.00	0.00	0.00	0.00	0.00	0.00	0.00	0.00
Mn	0.00	0.00	0.00	0.00	0.00	0.00	0.00	0.00	0.00	0.00	0.00	0.00	0.00	0.00	0.00	0.00
Mg	0.00	0.00	0.01	0.01	0.00	0.00	0.00	0.01	0.00	0.00	0.01	0.02	0.00	0.00	0.00	0.00
Ca	0.00	0.00	0.00	0.00	0.01	0.00	0.01	0.10	0.01	0.00	0.08	0.05	0.04	0.00	0.00	0.00
Zn	0.00	0.00	0.00	0.00	0.00	0.00	0.00	0.00	0.00	0.00	0.00	0.00	0.00	0.00	0.00	0.00
Na	0.16	0.13	0.11	0.11	0.13	0.13	0.12	0.21	0.16	0.11	0.19	0.16	0.13	0.21	0.19	0.17
K	0.81	0.80	0.86	0.86	0.82	0.85	0.85	0.68	0.82	0.85	0.71	0.79	0.80	0.76	0.80	0.80
Fe	0.00	0.00	0.00	0.00	0.00	0.00	0.00	0.01	0.00	0.00	0.00	0.00	0.00	0.00	0.00	0.00
total	4.96	3.92	4.98	4.98	4.97	4.98	4.98	5.00	4.99	4.96	4.98	5.00	4.97	4.98	4.97	4.97
Sample Number			MM146				MM166D		MM195C							
Oxides wt%																
SiO2	65.04	65.55	65.48	64.83	65.26	65.08	63.77	64.63	64.89	64.59	64.98	64.17	64.42	63.92	64.64	65.07
TiO2	0.19	0.22	0.19	0.14	0.17	0.30	0.10	0.33	0.25	0.38	0.22	0.43	0.27	0.40	0.31	0.29
Al2O3	18.54	18.92	18.93	18.51	18.88	18.87	20.19	19.11	19.41	18.98	19.03	19.16	19.27	18.99	19.00	19.03
Cr2O3	0.00	0.08	0.00	0.00	0.05	0.00	0.00	0.00	0.00	0.04	0.00	0.00	0.06	0.00	0.00	0.00
MnO	0.10	0.00	0.00	0.00	0.00	0.21	0.00	0.07	0.00	0.00	0.03	0.02	0.00	0.00	0.00	0.00
MgO	0.00	0.06	0.03	0.10	0.13	0.13	0.21	0.00	0.20	0.00	0.13	0.00	0.01	0.03	0.09	0.13
CaO	0.17	0.06	0.12	0.04	0.12	0.11	1.49	0.08	0.09	0.25	0.10	0.20	0.19	0.13	0.19	0.08
ZnO	0.00	0.03	0.00	0.00	0.00	0.00	0.16	0.00	0.03	0.00	0.11	0.00	0.08	0.00	0.18	0.31
Na2O	1.62	2.17	1.92	2.05	2.15	2.15	3.09	1.61	1.68	1.77	1.65	1.70	1.72	1.83	1.77	1.64
K2O	14.29	13.71	13.81	13.80	13.63	13.39	10.82	13.95	14.47	14.06	14.15	13.94	13.80	13.76	13.98	14.37
FeO*	0.17	0.07	0.06	0.10	0.12	0.00	0.06	0.49	0.24	0.06	0.18	0.22	0.10	0.27	0.23	0.19
total	100.12	100.87	100.54	99.57	100.51	100.24	99.89	100.27	101.26	100.13	100.58	99.84	99.92	99.33	100.39	101.11
Number of atoms in the formula unit on the basis of 8 oxygens																
Si	2.99	2.98	2.99	2.99	2.98	2.98	2.91	2.97	2.95	2.96	2.97	2.96	2.96	2.96	2.96	2.97
Ti	0.00	0.00	0.00	0.00	0.00	0.01	0.00	0.01	0.00	0.01	0.00	0.01	0.00	0.01	0.01	0.01
Al	1.00	1.01	1.02	1.00	1.01	1.02	1.09	1.03	1.04	1.03	1.03	1.04	1.04	1.04	1.03	1.02
Cr	0.00	0.00	0.00	0.00	0.00	0.00	0.00	0.00	0.00	0.00	0.00	0.00	0.00	0.00	0.00	0.00
Mn	0.00	0.00	0.00	0.00	0.00	0.00	0.00	0.00	0.00	0.00	0.00	0.00	0.00	0.00	0.00	0.00
Mg	0.00	0.00	0.00	0.00	0.00	0.00	0.01	0.00	0.01	0.00	0.00	0.00	0.00	0.00	0.00	0.00
Ca	0.00	0.00	0.00	0.00	0.00	0.00	0.07	0.00	0.00	0.01	0.00	0.01	0.00	0.00	0.00	0.00
Zn	0.00	0.00	0.00	0.00	0.00	0.00	0.00	0.00	0.00	0.00	0.00	0.00	0.00	0.00	0.00	0.01
Na	0.14	0.19	0.17	0.18	0.19	0.19	0.27	0.14	0.15	0.16	0.15	0.15	0.15	0.16	0.16	0.15
K	0.84	0.79	0.80	0.81	0.79	0.78	0.63	0.82	0.84	0.82	0.82	0.82	0.81	0.81	0.82	0.83
Fe	0.00	0.00	0.00	0.00	0.00	0.00	0.00	0.02	0.00	0.00	0.00	0.00	0.00	0.01	0.00	0.00
total	4.97	4.97	4.98	4.98	4.97	4.98	4.98	4.99	4.99	4.99	4.97	4.99	4.96	4.99	4.98	4.99

Microprobe results of K-feldspars in pelites

Sample Numbe	MM155		MM197B								MM166A					
Oxides wt%																
SiO2	65.42	65.07	65.06	65.34	65.66	64.76	65.50	64.99	64.93	64.95	65.10	64.35	64.83	65.02	64.97	65.00
TiO2	0.09	0.00	0.27	0.16	0.25	0.10	0.11	0.19	0.21	0.26	0.18	0.29	0.27	0.08	0.08	0.13
Al2O3	18.53	18.23	18.92	18.63	19.01	18.63	18.91	18.95	18.67	18.91	18.93	18.58	18.89	18.98	18.80	18.83
Cr2O3	0.01	0.06	0.00	0.04	0.00	0.11	0.10	0.00	0.00	0.00	0.08	0.05	0.00	0.00	0.00	0.00
MnO	0.04	0.00	0.00	0.00	0.00	0.04	0.02	0.05	0.00	0.05	0.12	0.13	0.00	0.03	0.03	0.00
MgO	0.08	0.13	0.11	0.00	0.12	0.00	0.08	0.12	0.00	0.12	0.00	0.00	0.00	0.00	0.00	0.03
CaO	0.06	0.32	0.18	0.09	0.10	0.10	0.18	0.12	0.14	0.11	0.04	0.00	0.10	0.24	0.08	0.07
ZnO	0.00	0.05	0.00	0.08	0.00	0.21	0.00	0.00	0.00	0.06	0.15	0.27	0.16	0.17	0.15	0.19
Na2O	0.82	0.91	2.39	2.10	2.31	1.80	2.24	2.01	1.87	2.34	1.75	1.75	2.03	1.94	2.25	2.17
K2O	15.75	15.53	13.34	13.77	13.34	13.97	13.36	13.65	13.69	13.47	13.87	13.83	13.82	13.86	13.77	13.54
FeO*	0.15	0.00	0.14	0.05	0.04	0.05	0.05	0.09	0.11	0.00	0.21	0.04	0.00	0.00	0.15	0.00
total	100.95	100.30	100.41	100.26	100.83	99.77	100.55	100.17	99.62	100.27	100.43	99.29	100.10	100.32	100.28	99.96
Number of atoms in the formula unit on the basis of 8 oxygens																
Si	2.99	3.00	2.97	2.99	2.98	2.98	2.98	2.97	2.99	2.97	2.97	2.98	2.97	2.97	2.98	2.98
Ti	0.00	0.00	0.00	0.00	0.00	0.00	0.00	0.00	0.00	0.00	0.00	0.01	0.00	0.00	0.00	0.00
Al	1.00	0.99	1.02	1.00	1.02	1.01	1.01	1.02	1.01	1.02	1.02	1.01	1.02	1.02	1.01	1.02
Cr	0.00	0.00	0.00	0.00	0.00	0.00	0.00	0.00	0.00	0.00	0.00	0.00	0.00	0.00	0.00	0.00
Mn	0.00	0.00	0.00	0.00	0.00	0.00	0.00	0.00	0.00	0.00	0.00	0.00	0.00	0.00	0.00	0.00
Mg	0.00	0.00	0.00	0.00	0.00	0.00	0.00	0.00	0.00	0.00	0.00	0.00	0.00	0.00	0.00	0.00
Ca	0.00	0.02	0.00	0.00	0.00	0.00	0.00	0.00	0.00	0.00	0.00	0.00	0.00	0.02	0.00	0.00
Zn	0.00	0.00	0.00	0.00	0.00	0.00	0.00	0.00	0.00	0.00	0.00	0.01	0.00	0.00	0.00	0.00
Na	0.07	0.08	0.21	0.19	0.20	0.16	0.20	0.18	0.17	0.21	0.15	0.16	0.18	0.17	0.20	0.19
K	0.92	0.91	0.78	0.80	0.77	0.82	0.78	0.80	0.80	0.79	0.81	0.82	0.81	0.81	0.80	0.79
Fe	0.00	0.00	0.00	0.00	0.00	0.00	0.00	0.00	0.00	0.00	0.00	0.00	0.00	0.00	0.00	0.00
total	4.98	5.00	4.98	4.98	4.97	4.97	4.97	4.97	4.97	4.99	4.95	4.99	4.98	4.99	4.99	4.98
Sample Numbe	MM197A										MM131B					
Oxides wt%																
SiO2	65.77	65.18	65.22	65.41	64.93	65.34	65.04	64.88	64.99	64.74	65.03	65.28	64.50	64.69	65.00	64.30
TiO2	0.06	0.18	0.15	0.17	0.12	0.24	0.02	0.13	0.09	0.14	0.02	0.00	0.14	0.11	0.14	0.29
Al2O3	19.03	18.68	19.04	18.87	18.68	18.86	18.73	18.87	18.47	18.41	19.06	18.53	18.65	18.73	18.64	19.23
Cr2O3	0.00	0.08	0.05	0.07	0.05	0.00	0.06	0.00	0.01	0.08	0.00	0.04	0.17	0.03	0.00	0.02
MnO	0.02	0.02	0.00	0.00	0.00	0.04	0.00	0.00	0.00	0.02	0.00	0.00	0.04	0.00	0.10	0.00
MgO	0.09	0.00	0.05	0.07	0.00	0.00	0.00	0.00	0.00	0.11	0.10	0.04	0.17	0.11	0.00	0.08
CaO	0.09	0.10	0.17	0.14	0.04	0.09	0.15	0.15	0.06	0.03	0.09	0.12	0.06	0.13	0.16	0.14
ZnO	0.19	0.05	0.00	0.04	0.00	0.00	0.09	0.00	0.00	0.14	0.22	0.00	0.00	0.36	0.00	0.00
Na2O	2.27	2.24	2.45	2.61	2.22	2.23	1.85	2.45	2.37	1.28	1.67	1.30	1.08	1.18	2.45	1.79
K2O	13.45	13.49	12.95	13.09	13.46	13.50	13.60	13.05	13.42	14.78	14.54	14.90	14.97	14.99	13.24	14.10
FeO*	0.07	0.15	0.17	0.09	0.09	0.00	0.13	0.17	0.08	0.00	0.22	0.23	0.26	0.08	0.18	0.25
total	101.04	100.17	100.25	100.56	99.59	100.30	99.67	99.70	99.49	99.73	100.95	100.44	100.04	100.41	99.91	100.20
Number of atoms in the formula unit on the basis of 8 oxygens																
Si	2.98	2.99	2.98	2.98	3.00	2.99	2.99	2.99	3.00	2.99	2.97	2.99	2.97	2.97	2.98	2.95
Ti	0.00	0.00	0.00	0.00	0.00	0.00	0.00	0.00	0.00	0.00	0.00	0.00	0.00	0.00	0.00	0.01
Al	1.02	1.00	1.02	1.01	1.01	1.02	1.01	1.02	1.00	1.00	1.03	1.00	1.01	1.01	1.00	1.04
Cr	0.00	0.00	0.00	0.00	0.00	0.00	0.00	0.00	0.00	0.00	0.00	0.00	0.00	0.00	0.00	0.00
Mn	0.00	0.00	0.00	0.00	0.00	0.00	0.00	0.00	0.00	0.00	0.00	0.00	0.00	0.00	0.00	0.00
Mg	0.00	0.00	0.00	0.00	0.00	0.00	0.00	0.00	0.00	0.00	0.00	0.00	0.01	0.00	0.00	0.00
Ca	0.00	0.00	0.00	0.00	0.00	0.00	0.00	0.00	0.00	0.00	0.00	0.00	0.00	0.00	0.00	0.00
Zn	0.00	0.00	0.00	0.00	0.00	0.00	0.00	0.00	0.00	0.00	0.00	0.00	0.00	0.00	0.00	0.00
Na	0.20	0.20	0.22	0.23	0.20	0.20	0.16	0.22	0.21	0.11	0.15	0.12	0.10	0.10	0.22	0.16
K	0.78	0.79	0.75	0.76	0.79	0.79	0.80	0.76	0.79	0.87	0.85	0.87	0.88	0.88	0.78	0.83
Fe	0.00	0.00	0.00	0.00	0.00	0.00	0.00	0.00	0.00	0.00	0.00	0.00	0.01	0.00	0.00	0.01
total	4.98	4.98	4.97	4.98	5.00	5.00	4.96	4.99	5.00	4.97	5.00	4.98	4.98	4.96	4.98	5.00

Microprobe results of K-feldspars in pelites

Sample Numbe	MM141							MM187								
Oxides wt%																
SiO2	64.90	64.22	65.06	65.37	65.15	65.38	65.11	64.68	64.64	64.49	64.63	64.85	64.81	64.47	64.75	64.80
TiO2	0.26	0.31	0.20	0.19	0.26	0.22	0.08	0.39	0.40	0.22	0.20	0.28	0.30	0.41	0.28	0.24
Al2O3	18.73	18.81	18.99	19.11	18.90	19.12	18.92	19.45	19.33	19.45	19.22	19.21	19.64	19.26	19.67	19.17
Cr2O3	0.00	0.00	0.07	0.00	0.00	0.00	0.01	0.02	0.07	0.00	0.02	0.00	0.00	0.02	0.00	0.02
MnO	0.00	0.00	0.00	0.01	0.00	0.00	0.00	0.03	0.00	0.07	0.03	0.00	0.07	0.00	0.03	0.00
MgO	0.00	0.00	0.10	0.14	0.11	0.10	0.08	0.18	0.25	0.07	0.12	0.00	0.14	0.13	0.24	0.17
CaO	0.06	0.07	0.12	0.12	0.11	0.04	0.16	0.17	0.19	0.19	0.23	0.21	0.14	0.22	0.23	0.08
ZnO	0.00	0.15	0.00	0.00	0.00	0.00	0.08	0.00	0.22	0.20	0.00	0.00	0.00	0.00	0.00	0.00
Na2O	1.95	1.80	1.97	2.10	1.97	1.78	1.78	2.17	1.57	2.11	2.15	2.22	1.98	1.86	1.98	2.06
K2O	13.74	14.07	13.95	13.86	14.13	14.11	14.18	13.57	14.27	13.44	13.45	13.16	13.67	13.91	13.74	13.03
FeO*	0.15	0.19	0.28	0.02	0.18	0.08	0.10	0.03	0.01	0.01	0.06	0.07	0.13	0.10	0.00	0.03
total	99.79	99.62	100.74	100.92	100.81	100.83	100.50	100.69	100.95	100.25	100.11	100.00	100.88	100.38	100.92	99.60
Number of atoms in the formula unit on the basis of 8 oxygens																
Si	2.98	2.97	2.97	2.97	2.97	2.98	2.98	2.95	2.95	2.95	2.96	2.97	2.95	2.96	2.94	2.96
Ti	0.00	0.01	0.00	0.00	0.00	0.00	0.00	0.01	0.01	0.00	0.00	0.01	0.01	0.01	0.00	0.00
Al	1.01	1.02	1.02	1.02	1.02	1.03	1.02	1.04	1.04	1.05	1.04	1.04	1.05	1.04	1.05	1.03
Cr	0.00	0.00	0.00	0.00	0.00	0.00	0.00	0.00	0.00	0.00	0.00	0.00	0.00	0.00	0.00	0.00
Mn	0.00	0.00	0.00	0.00	0.00	0.00	0.00	0.00	0.00	0.00	0.00	0.00	0.00	0.00	0.00	0.00
Mg	0.00	0.00	0.00	0.00	0.00	0.00	0.00	0.01	0.02	0.00	0.00	0.00	0.00	0.00	0.02	0.01
Ca	0.00	0.00	0.00	0.00	0.00	0.00	0.00	0.00	0.00	0.00	0.01	0.01	0.00	0.01	0.01	0.00
Zn	0.00	0.00	0.00	0.00	0.00	0.00	0.00	0.00	0.00	0.00	0.00	0.00	0.00	0.00	0.00	0.00
Na	0.17	0.16	0.17	0.18	0.17	0.16	0.16	0.19	0.14	0.19	0.19	0.20	0.17	0.16	0.17	0.18
K	0.81	0.82	0.81	0.80	0.82	0.82	0.83	0.79	0.83	0.78	0.79	0.77	0.79	0.81	0.80	0.80
Fe	0.00	0.00	0.01	0.00	0.00	0.00	0.00	0.00	0.00	0.00	0.00	0.00	0.00	0.00	0.00	0.00
total	4.97	4.98	4.98	4.97	4.98	4.99	4.99	4.99	4.99	4.97	4.99	5.00	4.97	4.99	4.99	4.98

Sample Numbe	MM143								MM185B							
Oxides wt%																
SiO2	64.60	64.56	65.28	65.23	65.13	65.25	65.23	64.89	63.93	65.12	65.56	65.76	64.78	64.30	65.08	65.46
TiO2	0.14	0.16	0.13	0.22	0.23	0.18	0.17	0.16	0.60	0.42	0.08	0.17	0.30	0.41	0.11	0.33
Al2O3	19.17	18.78	18.55	18.73	18.66	18.73	19.02	18.51	19.13	18.70	18.79	18.89	18.73	18.82	18.56	19.09
Cr2O3	0.00	0.00	0.01	0.06	0.00	0.00	0.02	0.00	0.00	0.00	0.00	0.06	0.00	0.00	0.00	0.00
MnO	0.00	0.05	0.04	0.00	0.00	0.03	0.00	0.00	0.06	0.00	0.01	0.00	0.08	0.06	0.00	0.07
MgO	0.07	0.00	0.00	0.01	0.00	0.13	0.01	0.05	0.06	0.06	0.01	0.08	0.06	0.10	0.00	0.08
CaO	0.13	0.07	0.10	0.08	0.02	0.09	0.08	0.15	0.20	0.07	0.00	0.04	0.09	0.19	0.11	0.09
ZnO	0.00	0.00	0.14	0.05	0.02	0.16	0.00	0.00	0.08	0.00	0.00	0.34	0.06	0.21	0.27	0.22
Na2O	1.92	1.60	1.72	2.69	2.06	1.46	1.76	1.74	1.59	1.60	2.21	1.63	1.77	1.34	1.50	1.05
K2O	13.78	14.17	14.00	13.24	13.49	14.62	14.04	14.08	14.20	15.00	13.40	14.25	13.85	14.33	14.46	13.81
FeO*	0.07	0.08	0.12	0.00	0.11	0.13	0.03	0.00	0.12	0.14	0.00	0.03	0.00	0.10	0.03	0.11
total	99.88	99.47	100.09	100.31	99.72	100.78	100.36	99.58	99.97	101.11	100.06	101.25	99.72	99.86	100.12	100.31
Number of atoms in the formula unit on the basis of 8 oxygens																
Si	2.97	2.98	2.99	2.98	2.99	2.98	2.98	2.99	2.95	2.98	3.00	2.98	2.98	2.96	2.99	2.97
Ti	0.00	0.00	0.00	0.00	0.00	0.00	0.00	0.00	0.02	0.01	0.00	0.00	0.01	0.01	0.00	0.01
Al	1.04	1.02	1.00	1.00	1.01	1.00	1.03	1.00	1.04	1.01	1.01	1.01	1.01	1.02	1.00	1.02
Cr	0.00	0.00	0.00	0.00	0.00	0.00	0.00	0.00	0.00	0.00	0.00	0.00	0.00	0.00	0.00	0.00
Mn	0.00	0.00	0.00	0.00	0.00	0.00	0.00	0.00	0.00	0.00	0.00	0.00	0.00	0.00	0.00	0.00
Mg	0.00	0.00	0.00	0.00	0.00	0.00	0.00	0.00	0.00	0.00	0.00	0.00	0.00	0.00	0.00	0.00
Ca	0.00	0.00	0.00	0.00	0.00	0.00	0.00	0.00	0.01	0.00	0.00	0.00	0.00	0.00	0.00	0.00
Zn	0.00	0.00	0.00	0.00	0.00	0.00	0.00	0.00	0.00	0.00	0.00	0.01	0.00	0.00	0.00	0.00
Na	0.17	0.14	0.15	0.24	0.18	0.13	0.16	0.16	0.14	0.10	0.20	0.14	0.16	0.12	0.13	0.18
K	0.81	0.83	0.82	0.77	0.79	0.85	0.82	0.83	0.83	0.88	0.78	0.82	0.81	0.84	0.85	0.80
Fe	0.00	0.00	0.00	0.00	0.00	0.00	0.00	0.00	0.00	0.00	0.00	0.00	0.00	0.00	0.00	0.00
total	4.99	4.97	4.96	4.99	4.97	4.96	4.99	4.98	4.99	4.98	4.99	4.96	4.97	4.95	4.97	4.98

Microprobe results of K-feldspars in pelites

Sample Number			MM149			MM184B									MM188D.DL	
Oxides wt%																
SiO2	63.82	64.42	65.63	65.17	64.56	65.62	65.13	65.38	64.44	65.37	65.34	65.10	64.99	64.08	65.14	64.96
TiO2	0.37	0.37	0.24	0.24	0.20	0.13	0.10	0.26	0.33	0.02	0.19	0.15	0.08	0.02	0.03	0.04
Al2O3	19.00	18.84	18.65	18.92	18.65	18.74	18.51	19.28	19.31	18.59	18.98	18.23	18.61	18.11	18.97	18.61
Cr2O3	0.00	0.03	0.05	0.00	0.13	0.00	0.00	0.05	0.05	0.00	0.08	0.01	0.07	0.01	0.00	0.04
MnO	0.10	0.00	0.00	0.05	0.00	0.02	0.00	0.00	0.10	0.00	0.00	0.00	0.00	0.00	0.00	0.00
MgO	0.04	0.12	0.02	0.08	0.00	0.00	0.10	0.11	0.14	0.07	0.10	0.00	0.06	0.03	0.02	0.12
CaO	0.19	0.10	0.11	0.03	0.04	0.00	0.00	0.18	0.06	0.00	0.04	0.11	0.26	0.11	0.11	0.07
ZnO	0.00	0.10	0.08	0.00	0.08	0.28	0.00	0.13	0.00	0.00	0.10	0.11	0.02	0.00	0.00	0.00
Na2O	1.62	1.86	2.03	2.13	1.51	1.47	0.88	2.04	2.16	1.48	1.73	1.07	1.22	1.50	1.62	1.72
K2O	13.97	14.03	13.77	13.49	14.23	14.67	15.42	13.92	13.64	14.64	14.33	15.10	14.94	14.20	14.07	14.34
FeO*	0.13	0.14	0.00	0.16	0.00	0.14	0.09	0.15	0.25	0.27	0.17	0.05	0.06	0.09	0.20	0.00
total	99.24	100.01	100.58	100.27	99.40	101.07	100.23	101.50	100.48	100.44	101.06	99.93	100.31	98.15	100.16	99.90
Number of atoms in the formula unit on the basis of 8 oxygens																
Si	2.96	2.98	2.99	2.98	2.98	2.99	3.00	2.96	2.95	3.00	2.97	3.00	2.98	3.00	2.98	2.99
Ti	0.01	0.00	0.00	0.00	0.00	0.00	0.00	0.00	0.01	0.00	0.00	0.00	0.00	0.00	0.00	0.00
Al	1.04	1.00	1.00	1.02	1.01	1.00	1.00	1.03	1.04	1.00	1.02	0.99	1.00	1.00	1.02	1.01
Cr	0.00	0.00	0.00	0.00	0.00	0.00	0.00	0.00	0.00	0.00	0.00	0.00	0.00	0.00	0.00	0.00
Mn	0.00	0.00	0.00	0.00	0.00	0.00	0.00	0.00	0.00	0.00	0.00	0.00	0.00	0.00	0.00	0.00
Mg	0.00	0.00	0.00	0.00	0.00	0.00	0.00	0.00	0.00	0.00	0.00	0.00	0.00	0.00	0.00	0.00
Ca	0.01	0.01	0.00	0.00	0.00	0.00	0.00	0.00	0.00	0.00	0.00	0.00	0.01	0.00	0.00	0.00
Zn	0.00	0.00	0.00	0.00	0.00	0.00	0.00	0.00	0.00	0.00	0.00	0.00	0.00	0.00	0.00	0.00
Na	0.15	0.11	0.18	0.19	0.14	0.13	0.08	0.18	0.19	0.13	0.15	0.10	0.11	0.14	0.14	0.15
K	0.83	0.87	0.80	0.79	0.84	0.85	0.91	0.80	0.80	0.86	0.83	0.89	0.87	0.85	0.82	0.84
Fe	0.00	0.00	0.00	0.00	0.00	0.00	0.00	0.00	0.00	0.01	0.00	0.00	0.00	0.00	0.00	0.00
total	5.00	4.97	4.97	4.98	4.97	4.97	4.99	4.97	4.99	5.00	4.97	4.98	4.97	4.99	4.96	4.99
Sample Number								MM151								MM181
Oxides wt%																
SiO2	65.22	64.84	64.98	65.27	64.62	65.38	65.36	66.02	64.52	64.68	65.14	64.90	64.98	65.08	65.75	65.09
TiO2	0.17	0.19	0.16	0.19	0.14	0.12	0.10	0.12	0.19	0.12	0.23	0.24	0.18	0.12	0.16	0.07
Al2O3	18.58	18.67	18.47	18.53	18.42	18.52	18.57	19.12	18.44	18.72	18.75	19.03	19.11	18.73	18.80	18.76
Cr2O3	0.01	0.08	0.00	0.09	0.00	0.06	0.00	0.00	0.00	0.11	0.03	0.00	0.01	0.00	0.10	0.06
MnO	0.01	0.01	0.02	0.07	0.06	0.09	0.00	0.00	0.00	0.00	0.10	0.03	0.04	0.02	0.00	0.00
MgO	0.09	0.02	0.14	0.11	0.00	0.08	0.00	0.09	0.00	0.02	0.00	0.09	0.10	0.13	0.09	0.04
CaO	0.06	0.11	0.10	0.10	0.10	0.00	0.03	0.14	0.08	0.10	0.00	0.06	0.01	0.04	0.18	0.06
ZnO	0.22	0.00	0.00	0.15	0.06	0.00	0.00	0.00	0.09	0.00	0.00	0.00	0.00	0.03	0.00	0.05
Na2O	1.19	1.27	1.41	1.86	1.65	2.06	1.98	2.10	1.98	1.74	1.97	1.65	1.61	1.51	1.97	1.79
K2O	14.94	14.57	14.85	13.96	14.13	13.95	13.85	14.17	13.59	14.08	13.98	14.49	14.34	14.30	14.08	14.29
FeO*	0.00	0.08	0.00	0.00	0.23	0.03	0.08	0.06	0.23	0.10	0.05	0.00	0.06	0.03	0.08	0.16
total	100.49	99.84	100.13	100.33	99.41	100.29	99.97	101.82	99.12	99.67	100.25	100.49	100.44	99.99	101.21	100.37
Number of atoms in the formula unit on the basis of 8 oxygens																
Si	2.99	2.99	2.99	2.99	2.99	2.99	3.00	2.98	2.99	2.98	2.98	2.97	2.97	2.99	2.98	2.98
Ti	0.00	0.00	0.00	0.00	0.00	0.00	0.00	0.00	0.00	0.00	0.00	0.00	0.00	0.00	0.00	0.00
Al	1.00	1.01	1.00	1.00	1.00	1.00	1.00	1.02	1.00	1.02	1.01	1.03	1.03	1.01	1.00	1.01
Cr	0.00	0.00	0.00	0.00	0.00	0.00	0.00	0.00	0.00	0.00	0.00	0.00	0.00	0.00	0.00	0.00
Mn	0.00	0.00	0.00	0.00	0.00	0.00	0.00	0.00	0.00	0.00	0.00	0.00	0.00	0.00	0.00	0.00
Mg	0.00	0.00	0.01	0.00	0.00	0.00	0.00	0.00	0.00	0.00	0.00	0.00	0.00	0.00	0.00	0.00
Ca	0.00	0.00	0.00	0.00	0.00	0.00	0.00	0.00	0.00	0.00	0.00	0.00	0.00	0.00	0.00	0.00
Zn	0.00	0.00	0.00	0.00	0.00	0.00	0.00	0.00	0.00	0.00	0.00	0.00	0.00	0.00	0.00	0.00
Na	0.11	0.11	0.13	0.16	0.15	0.18	0.18	0.18	0.18	0.15	0.17	0.15	0.14	0.13	0.17	0.16
K	0.87	0.86	0.87	0.81	0.83	0.81	0.81	0.82	0.80	0.83	0.82	0.84	0.84	0.84	0.81	0.83
Fe	0.00	0.00	0.00	0.00	0.00	0.00	0.00	0.00	0.00	0.00	0.00	0.00	0.00	0.00	0.00	0.00
total	4.97	4.97	5.00	4.96	4.97	4.98	4.99	5.00	4.97	4.98	4.98	4.99	4.98	4.97	4.96	4.98

Microprobe results of K-feldspars in pelites

Sample Number									MM189A							
Oxides wt%																
SiO2	64.36	65.32	65.22	64.74	64.66	64.39	65.02	64.93	63.52	64.37	63.60	63.95	63.81	64.24	64.66	64.29
TiO2	0.24	0.21	0.13	0.16	0.19	0.27	0.16	0.10	0.40	0.36	0.45	0.39	0.25	0.32	0.34	0.32
Al2O3	18.74	18.76	18.83	18.87	18.45	18.79	18.76	18.77	18.93	18.90	19.03	18.72	18.89	18.77	19.06	19.25
Cr2O3	0.06	0.06	0.00	0.00	0.09	0.00	0.00	0.00	0.00	0.00	0.00	0.04	0.02	0.01	0.00	0.00
MnO	0.00	0.00	0.16	0.01	0.00	0.02	0.00	0.07	0.11	0.04	0.09	0.00	0.00	0.03	0.00	0.00
MgO	0.05	0.05	0.00	0.13	0.00	0.06	0.19	0.09	0.05	0.00	0.04	0.00	0.00	0.12	0.00	0.00
CaO	0.09	0.06	0.06	0.05	0.00	0.13	0.07	0.06	0.19	0.22	0.07	0.06	0.14	0.17	0.07	0.08
ZnO	0.00	0.00	0.29	0.00	0.26	0.05	0.00	0.00	0.17	0.00	0.00	0.10	0.25	0.19	0.00	0.00
Na2O	1.31	2.29	1.98	1.72	1.09	1.09	1.29	1.28	1.53	1.92	1.96	1.54	1.89	1.92	1.88	1.48
K2O	14.77	13.45	13.77	13.69	15.05	15.05	14.88	14.74	14.20	13.60	13.89	14.50	13.45	14.02	13.83	14.27
FeO*	0.02	0.10	0.00	0.00	0.15	0.04	0.11	0.02	0.02	0.16	0.04	0.00	0.06	0.00	0.18	0.10
total	99.64	100.30	100.44	99.37	99.94	99.89	100.48	100.06	99.12	99.57	99.17	99.30	98.76	99.79	100.02	99.79
Number of atoms in the formula unit on the basis of 8 oxygens																
Si	2.98	2.98	2.98	2.98	2.99	2.97	2.98	2.99	2.95	2.97	2.95	2.97	2.96	2.96	2.97	2.96
Ti	0.00	0.00	0.00	0.00	0.00	0.00	0.00	0.00	0.01	0.01	0.02	0.01	0.00	0.01	0.01	0.01
Al	1.02	1.01	1.01	1.02	1.00	1.02	1.01	1.02	1.04	1.03	1.04	1.02	1.03	1.02	1.03	1.05
Cr	0.00	0.00	0.00	0.00	0.00	0.00	0.00	0.00	0.00	0.00	0.00	0.00	0.00	0.00	0.00	0.00
Mn	0.00	0.00	0.00	0.00	0.00	0.00	0.00	0.00	0.00	0.00	0.00	0.00	0.00	0.00	0.00	0.00
Mg	0.00	0.00	0.00	0.00	0.00	0.00	0.01	0.00	0.00	0.00	0.00	0.00	0.00	0.00	0.00	0.00
Ca	0.00	0.00	0.00	0.00	0.00	0.00	0.00	0.00	0.01	0.01	0.00	0.00	0.00	0.00	0.00	0.00
Zn	0.00	0.00	0.01	0.00	0.00	0.00	0.00	0.00	0.00	0.00	0.00	0.00	0.00	0.00	0.00	0.00
Na	0.12	0.20	0.18	0.15	0.10	0.10	0.11	0.11	0.14	0.17	0.18	0.14	0.17	0.17	0.17	0.13
K	0.87	0.78	0.80	0.80	0.89	0.89	0.87	0.86	0.84	0.80	0.82	0.86	0.80	0.82	0.81	0.84
Fe	0.00	0.00	0.00	0.00	0.00	0.00	0.00	0.00	0.00	0.00	0.00	0.00	0.00	0.00	0.00	0.00
total	4.99	4.97	4.98	4.95	4.98	4.98	4.98	4.98	4.99	4.99	5.01	5.00	4.96	4.98	4.99	4.99

Sample Number				MM131DL							
Oxides wt%											
SiO2	65.51	65.70	65.15	64.83	64.66	64.65	64.56	64.90	64.62	65.17	64.60
TiO2	0.10	0.04	0.05	0.42	0.27	0.20	0.30	0.27	0.25	0.10	0.15
Al2O3	18.49	18.68	18.43	19.00	18.71	18.75	18.73	18.68	18.97	18.85	18.67
Cr2O3	0.02	0.02	0.00	0.00	0.00	0.06	0.00	0.00	0.14	0.00	0.00
MnO	0.00	0.00	0.02	0.04	0.00	0.00	0.01	0.00	0.00	0.12	0.00
MgO	0.07	0.09	0.00	0.09	0.18	0.07	0.10	0.09	0.19	0.01	0.09
CaO	0.01	0.00	0.05	0.18	0.19	0.17	0.16	0.10	0.15	0.19	0.17
ZnO	0.11	0.00	0.01	0.00	0.14	0.00	0.11	0.17	0.00	0.11	0.36
Na2O	1.06	1.74	0.96	1.83	1.55	1.26	1.65	1.61	1.89	1.69	1.13
K2O	15.21	14.37	15.41	13.75	14.40	14.79	13.97	14.25	13.68	14.23	14.73
FeO*	0.00	0.12	0.04	0.04	0.08	0.11	0.03	0.00	0.50	0.00	0.06
total	100.58	100.76	100.12	100.18	100.18	100.06	99.62	100.07	100.39	100.47	99.96
Number of atoms in the formula unit on the basis of 8 oxygens											
Si	3.00	2.99	3.00	2.97	2.97	2.98	2.97	2.98	2.96	2.98	2.98
Ti	0.00	0.00	0.00	0.01	0.01	0.00	0.01	0.00	0.00	0.00	0.00
Al	1.00	1.00	1.00	1.03	1.01	1.02	1.02	1.01	1.02	1.01	1.01
Cr	0.00	0.00	0.00	0.00	0.00	0.00	0.00	0.00	0.00	0.00	0.00
Mn	0.00	0.00	0.00	0.00	0.00	0.00	0.00	0.00	0.00	0.00	0.00
Mg	0.00	0.00	0.00	0.00	0.01	0.00	0.00	0.00	0.01	0.00	0.00
Ca	0.00	0.00	0.00	0.00	0.00	0.00	0.00	0.00	0.00	0.00	0.00
Zn	0.00	0.00	0.00	0.00	0.00	0.00	0.00	0.00	0.00	0.00	0.01
Na	0.09	0.15	0.08	0.16	0.14	0.11	0.15	0.14	0.17	0.15	0.10
K	0.89	0.84	0.91	0.80	0.84	0.87	0.82	0.83	0.80	0.83	0.87
Fe	0.00	0.00	0.00	0.00	0.00	0.00	0.00	0.00	0.02	0.00	0.00
total	4.98	4.98	4.99	4.97	4.98	4.98	4.97	4.96	4.98	4.97	4.97

Microprobe results of muscovites in pelites

Sample Numb	MM181					MM56A								MM56B	
Oxide %															
SiO2	45.77	46.97	45.61	45.71	45.67	47.31	48.03	46.28	46.58	47.21	46.66	47.97	46.05	47.93	47.40
TiO2	0.21	0.57	0.97	0.04	0.11	0.74	0.94	0.77	0.59	0.77	0.66	0.63	0.62	0.81	0.82
Al2O3	35.20	34.22	33.17	30.22	30.91	30.06	30.33	31.59	31.42	30.51	31.19	30.90	32.66	31.23	31.51
Cr2O3	0.00	0.00	0.00	0.04	0.11	0.00	0.00	0.00	0.07	0.00	0.00	0.05	0.12	0.00	0.10
MnO	0.00	0.00	0.00	0.00	0.00	0.00	0.00	0.01	0.00	0.00	0.03	0.03	0.00	0.00	0.00
MgO	0.63	1.04	1.57	2.93	3.29	1.91	1.82	1.34	1.29	1.79	1.41	1.89	1.12	1.90	1.75
CaO	0.03	0.11	0.01	0.14	0.00	0.02	0.08	0.04	0.05	0.07	0.08	0.04	0.05	0.00	0.09
ZnO	0.00	0.06	0.37	0.11	0.15	0.00	0.00	0.00	0.00	0.00	0.00	0.05	0.14	0.11	0.00
Na2O	0.71	0.55	0.47	1.05	0.29	0.47	0.26	0.51	0.59	0.54	0.62	0.55	0.38	0.63	0.47
K2O	10.44	10.32	10.46	9.56	9.37	10.34	10.27	10.26	10.18	10.20	10.21	10.10	10.45	10.26	10.50
FeO	0.87	1.31	2.58	4.24	4.91	3.34	2.51	3.01	3.23	3.26	2.80	3.27	2.42	2.67	2.68
total	93.86	95.15	95.21	94.04	94.81	94.19	94.24	93.81	94.00	94.35	93.66	95.48	94.01	95.54	95.32
Number of cations on the basis of 22 oxygens															
Si	6.18	6.26	6.15	6.28	6.22	6.45	6.50	6.32	6.35	6.42	6.37	6.43	6.26	6.41	6.37
Ti	0.02	0.06	0.10	0.00	0.01	0.08	0.10	0.08	0.06	0.08	0.07	0.06	0.06	0.08	0.08
Al	5.60	5.37	5.27	4.89	4.96	4.83	4.84	5.09	5.05	4.89	5.02	4.88	5.23	4.93	4.99
Cr	0.00	0.00	0.00	0.00	0.01	0.00	0.00	0.00	0.01	0.00	0.00	0.00	0.01	0.00	0.01
Mn	0.00	0.00	0.00	0.00	0.00	0.00	0.00	0.00	0.00	0.00	0.00	0.00	0.00	0.00	0.00
Mg	0.13	0.21	0.32	0.60	0.67	0.39	0.37	0.27	0.26	0.36	0.29	0.38	0.23	0.38	0.35
Ca	0.00	0.01	0.00	0.02	0.00	0.00	0.01	0.00	0.00	0.01	0.01	0.00	0.01	0.00	0.01
Zn	0.00	0.00	0.04	0.01	0.01	0.00	0.00	0.00	0.00	0.00	0.00	0.00	0.01	0.01	0.00
Na	0.19	0.14	0.12	0.28	0.08	0.12	0.07	0.13	0.15	0.14	0.16	0.14	0.10	0.16	0.12
K	1.80	1.75	1.80	1.68	1.63	1.80	1.77	1.79	1.77	1.77	1.78	1.73	1.81	1.75	1.80
Fe	0.10	0.15	0.29	0.49	0.56	0.38	0.28	0.34	0.37	0.37	0.32	0.37	0.27	0.30	0.30
total	14.02	13.95	14.09	14.25	14.15	14.05	13.94	14.02	14.02	14.04	14.02	13.99	13.99	14.02	14.03
Sample Number								MM255D							
Oxide %															
SiO2	47.39	47.39	49.03	47.26	46.83	46.32	48.46	46.32	48.17	48.28	48.13	48.54	47.91	47.78	46.27
TiO2	0.83	0.78	0.61	0.83	0.74	0.88	0.77	0.80	0.65	0.86	0.95	0.84	0.85	1.11	0.74
Al2O3	31.82	31.49	30.50	31.53	31.98	32.10	30.89	32.23	30.18	30.39	30.13	29.80	30.26	30.49	32.75
Cr2O3	0.00	0.00	0.00	0.05	0.08	0.00	0.06	0.02	0.06	0.00	0.00	0.00	0.00	0.12	0.00
MnO	0.04	0.00	0.00	0.00	0.00	0.02	0.00	0.00	0.01	0.00	0.10	0.00	0.11	0.00	0.07
MgO	1.85	1.68	2.17	1.70	1.60	1.36	2.18	1.49	2.11	2.21	2.00	2.26	1.93	2.15	1.36
CaO	0.02	0.01	0.09	0.06	0.12	0.10	0.05	0.10	0.08	0.08	0.19	0.12	0.14	0.11	0.18
ZnO	0.00	0.04	0.00	0.00	0.00	0.00	0.07	0.00	0.00	0.00	0.00	0.00	0.00	0.00	0.00
Na2O	0.34	0.34	0.33	0.37	0.44	0.58	0.42	0.80	0.58	0.80	0.73	0.67	0.64	0.73	0.84
K2O	10.64	10.51	10.41	10.46	10.54	10.55	10.56	9.88	10.00	10.03	9.98	9.75	10.06	9.94	9.91
FeO	2.06	2.63	2.29	2.54	2.50	2.31	2.46	2.21	2.64	2.50	2.50	2.78	2.23	2.67	2.34
total	94.99	94.87	95.43	94.80	94.83	94.22	95.92	93.85	94.48	95.15	94.71	94.76	94.13	95.10	94.46
Number of cations on the basis of 22 oxygens															
Si	6.36	6.38	6.53	6.37	6.32	6.29	6.45	6.29	6.50	6.47	6.48	6.53	6.48	6.42	6.25
Ti	0.08	0.08	0.06	0.08	0.07	0.09	0.08	0.80	0.07	0.09	0.10	0.08	0.09	0.11	0.07
Al	5.03	5.00	4.79	5.00	5.09	5.14	4.85	5.16	4.80	4.80	4.78	4.72	4.83	4.83	5.21
Cr	0.00	0.00	0.00	0.00	0.00	0.00	0.01	0.00	0.00	0.00	0.00	0.00	0.00	0.01	0.00
Mn	0.00	0.00	0.00	0.00	0.00	0.00	0.00	0.00	0.00	0.00	0.01	0.00	0.01	0.00	0.01
Mg	0.37	0.34	0.43	0.34	0.32	0.27	0.43	0.30	0.42	0.44	0.40	0.45	0.39	0.43	0.27
Ca	0.00	0.00	0.01	0.01	0.02	0.01	0.00	0.01	0.01	0.01	0.03	0.02	0.02	0.01	0.03
Zn	0.00	0.00	0.00	0.00	0.00	0.00	0.00	0.00	0.00	0.00	0.00	0.00	0.00	0.00	0.00
Na	0.09	0.09	0.08	0.10	0.11	0.15	0.11	0.21	0.15	0.21	0.19	0.17	0.17	0.19	0.22
K	1.82	1.81	1.77	1.80	1.81	1.83	1.79	1.71	1.72	1.71	1.71	1.67	1.74	1.70	1.71
Fe	0.23	0.30	0.25	0.29	0.28	0.26	0.27	0.25	0.30	0.28	0.28	0.31	0.25	0.30	0.26
total	13.98	14.00	13.92	13.99	14.02	14.04	13.99	14.73	13.97	14.01	13.98	13.95	13.98	14.00	14.03

Microprobe results of spinels in pelites

Sample	MM197B								MM197A							
Oxide																
SiO2	0.00	0.15	0.19	0.12	0.50	0.17	0.29	0.36	0.01	0.20	0.19	0.09	0.09	0.17	0.04	0.00
TiO2	0.13	0.08	0.00	0.09	0.17	0.08	0.05	0.12	0.77	0.45	0.06	0.28	0.25	0.09	0.18	0.41
Al2O3	52.49	54.53	54.31	54.63	54.16	52.74	52.62	52.24	54.39	54.51	56.04	55.60	55.10	54.35	55.01	54.48
Cr2O3	0.00	0.19	0.16	0.12	0.00	0.20	0.20	0.14	0.27	0.32	0.06	0.03	0.19	0.74	0.05	0.69
Fe2O3	8.79	6.09	6.29	6.59	5.64	8.27	8.35	8.36	5.09	5.35	4.62	4.61	5.19	5.33	5.11	4.83
FeO	36.63	35.81	35.28	36.23	36.73	36.31	37.07	36.79	36.54	36.98	35.63	35.59	34.43	34.70	35.85	36.15
MnO	0.00	0.00	0.00	0.00	0.00	0.00	0.00	0.00	0.00	0.00	0.00	0.00	0.00	0.00	0.00	0.00
MgO	2.33	3.11	3.28	3.01	2.87	2.35	2.18	2.45	2.78	2.66	2.95	2.95	3.29	2.75	2.93	2.77
CaO	0.09	0.01	0.14	0...08	0.02	0.08	0.06	0.07	0.07	0.00	0.02	0.02	0.00	0.05	0.07	0.05
ZnO	0.28	0.31	0.15	0.27	0.38	0.92	0.69	0.23	0.64	0.61	1.41	1.17	1.80	2.21	0.69	0.37
K2O	0.02	0.03	0.05	0.01	0.00	0.03	0.02	0.07	0.00	0.00	0.00	0.02	0.01	0.00	0.00	0.04
Total	100.76	100.31	99.85	101.07	100.47	101.15	101.53	100.83	100.56	101.08	100.98	100.36	100.35	100.39	99.93	99.79
Number of atoms on the basis of 4 oxygens																
Si	0.00	0.00	0.00	0.00	0.01	0.00	0.00	0.01	0.00	0.00	0.00	0.00	0.00	0.00	0.00	0.00
Ti	0.00	0.00	0.00	0.00	0.00	0.00	0.00	0.00	0.02	0.01	0.00	0.00	0.00	0.00	0.00	0.00
Al	1.80	1.85	1.85	1.84	1.84	1.80	1.79	1.79	1.85	1.85	1.89	1.88	1.87	1.85	1.88	1.86
Cr	0.00	0.00	0.00	0.00	0.00	0.00	0.00	0.00	0.00	0.00	0.00	0.00	0.00	0.02	0.00	0.02
Fe3+	0.19	0.13	0.14	0.14	0.12	0.18	0.18	0.18	0.11	0.12	0.10	0.10	0.11	0.12	0.11	0.10
Fe2+	0.89	0.86	0.85	0.87	0.89	0.88	0.90	0.89	0.88	0.89	0.85	0.85	0.83	0.84	0.86	0.88
Mn	0.00	0.00	0.00	0.00	0.00	0.00	0.00	0.00	0.00	0.00	0.00	0.00	0.00	0.00	0.00	0.00
Mg	0.10	0.13	0.14	0.13	0.12	0.10	0.09	0.11	0.12	0.11	0.13	0.13	0.14	0.12	0.13	0.12
Ca	0.00	0.00	0.00	0.00	0.00	0.00	0.00	0.00	0.00	0.00	0.00	0.00	0.00	0.00	0.00	0.00
Zn	0.00	0.00	0.00	0.00	0.01	0.02	0.01	0.00	0.01	0.01	0.03	0.02	0.04	0.05	0.01	0.00
K	0.00	0.00	0.00	0.00	0.00	0.00	0.00	0.00	0.00	0.00	0.00	0.00	0.00	0.00	0.00	0.00
Total	3.00	3.00	3.00	3.00	3.00	3.00	3.00	3.00	3.00	3.00	3.00	3.00	3.00	3.00	3.00	3.00

Sample	MM197A						MM171									MM189A
Oxide																
SiO2	0.08	0.12	0.75	0.06	0.00	0.06	0.02	0.00	0.09	0.01	0.00	0.02	0.00	0.00	0.04	0.07
TiO2	0.17	0.00	0.00	0.12	0.00	0.06	0.00	0.00	0.12	0.01	0.08	0.00	0.09	0.17	0.07	0.05
Al2O3	54.33	55.68	55.02	54.42	54.73	53.72	57.37	56.92	56.32	57.31	57.10	56.91	57.93	56.33	57.27	56.85
Cr2O3	0.87	0.17	0.32	0.20	0.02	0.06	0.26	0.38	0.26	0.32	0.14	0.48	0.08	0.33	0.42	0.19
Fe2O3	5.27	5.53	2.96	6.24	6.15	7.33	2.81	3.00	2.62	3.30	3.13	3.14	3.19	3.62	2.71	2.90
FeO	36.03	34.47	35.86	35.97	35.74	35.83	36.94	36.75	36.81	36.54	36.63	36.39	37.04	36.94	37.09	34.52
MnO	0.00	0.00	0.00	0.00	0.00	0.00	0.26	0.00	0.00	0.00	0.14	0.00	0.00	0.00	0.00	0.00
MgO	2.78	3.17	3.01	2.96	3.10	2.88	2.61	2.30	2.31	2.50	2.83	2.65	2.76	2.23	2.68	2.77
CaO	0.00	0.01	0.00	0.08	0.03	0.10	0.00	0.10	0.00	0.00	0.00	0.20	0.04	0.03	0.03	0.00
ZnO	0.48	2.09	0.93	0.25	0.05	0.39	0.00	0.62	0.30	0.83	0.04	0.46	0.51	0.77	0.02	2.47
K2O	0.04	0.03	0.00	0.01	0.00	0.00	0.00	0.00	0.06	0.09	0.00	0.02	0.00	0.04	0.02	0.03
Total	100.05	101.27	98.85	100.31	99.82	100.43	100.27	100.07	98.89	100.91	100.09	100.21	101.64	100.46	100.35	99.85
Number of atoms on the basis of 4 oxygens																
Si	0.00	0.00	0.02	0.00	0.00	0.00	0.00	0.00	0.00	0.00	0.00	0.00	0.00	0.00	0.00	0.00
Ti	0.00	0.00	0.00	0.00	0.00	0.00	0.00	0.00	0.00	0.00	0.00	0.00	0.00	0.00	0.00	0.00
Al	1.85	1.87	1.88	1.85	1.87	1.83	1.93	1.93	1.93	1.92	1.93	1.92	1.93	1.91	1.93	1.93
Cr	0.02	0.00	0.00	0.00	0.00	0.00	0.00	0.01	0.00	0.00	0.00	0.01	0.00	0.00	0.01	0.00
Fe3+	0.11	0.12	0.06	0.14	0.13	0.16	0.06	0.06	0.06	0.07	0.07	0.07	0.07	0.08	0.06	0.06
Fe2+	0.87	0.82	0.87	0.87	0.86	0.87	0.88	0.88	0.89	0.87	0.88	0.87	0.87	0.89	0.89	0.83
Mn	0.00	0.00	0.00	0.00	0.00	0.00	0.00	0.00	0.00	0.00	0.00	0.00	0.00	0.00	0.00	0.00
Mg	0.12	0.13	0.13	0.13	0.13	0.12	0.11	0.10	0.10	0.11	0.12	0.11	0.12	0.10	0.11	0.12
Ca	0.00	0.00	0.00	0.00	0.00	0.00	0.00	0.00	0.00	0.00	0.00	0.00	0.00	0.00	0.00	0.00
Zn	0.01	0.04	0.02	0.00	0.00	0.00	0.00	0.01	0.00	0.02	0.00	0.01	0.01	0.02	0.00	0.05
K	0.00	0.00	0.00	0.00	0.00	0.00	0.00	0.00	0.00	0.00	0.00	0.00	0.00	0.00	0.00	0.00
Total	3.00	3.00	3.00	3.00	3.00	3.00	3.00	3.00	3.00	3.00	3.00	3.00	3.00	3.00	3.00	3.00

Microprobe results of spinels in pelites

Sample	MM186A							MM166C								
Oxide																
SiO2	0.05	0.36	0.36	0.02	0.00	0.08	0.00	0.10	0.07	0.07	0.16	0.22	0.03	0.40	0.04	0.10
TiO2	0.19	0.04	0.04	0.29	0.15	0.15	0.09	0.09	0.03	0.03	0.12	0.00	0.17	0.36	0.15	0.09
Al2O3	56.25	57.83	57.83	57.26	57.66	57.29	56.71	56.85	56.77	56.77	56.71	56.64	55.03	56.63	55.41	56.85
Cr2O3	0.25	0.14	0.14	0.11	0.09	0.07	0.16	0.14	0.02	0.02	0.00	0.01	0.09	0.15	0.27	0.14
Fe2O3	3.07	1.55	1.55	2.84	2.24	2.73	3.51	2.83	3.97	3.97	3.69	4.56	5.00	2.97	4.92	2.83
FeO	34.68	34.91	34.91	34.33	33.86	33.96	34.02	34.80	36.94	36.94	36.68	37.35	36.76	37.26	37.44	34.80
MnO	0.00	0.00	0.00	0.00	0.00	0.00	0.00	0.00	0.00	0.00	0.00	0.00	0.00	0.00	0.00	0.00
MgO	2.81	3.25	3.25	3.37	3.47	3.52	3.34	2.82	2.42	2.42	2.61	2.41	2.38	2.52	2.09	2.82
CaO	0.00	0.03	0.03	0.00	0.01	0.05	0.02	0.01	0.07	0.07	0.01	0.04	0.00	0.00	0.07	0.01
ZnO	2.16	1.89	1.89	1.95	2.14	2.03	1.93	2.22	0.77	0.77	0.73	0.73	0.51	0.97	0.03	2.22
K2O	0.00	0.01	0.01	0.05	0.00	0.00	0.02	0.00	0.00	0.00	0.06	0.04	0.00	0.08	0.00	0.00
Total	99.46	100.01	100.01	100.22	99.62	99.88	99.80	99.86	101.06	101.06	100.77	102.00	99.97	101.34	100.42	99.86
Number of atoms on the basis of 4 oxygens																
Si	0.00	0.01	0.01	0.00	0.00	0.00	0.00	0.00	0.00	0.00	0.00	0.00	0.00	0.01	0.00	0.00
Ti	0.00	0.00	0.00	0.00	0.00	0.00	0.00	0.00	0.00	0.00	0.00	0.00	0.00	0.00	0.00	0.00
Al	1.92	1.94	1.94	1.92	1.94	1.93	1.92	1.93	1.91	1.91	1.91	1.89	1.88	1.90	1.88	1.93
Cr	0.00	0.00	0.00	0.00	0.00	0.00	0.00	0.00	0.00	0.00	0.00	0.00	0.00	0.00	0.00	0.00
Fe3+	0.07	0.03	0.03	0.06	0.05	0.60	0.08	0.06	0.08	0.08	0.08	0.10	0.11	0.06	0.11	0.06
Fe2+	0.84	0.83	0.83	0.82	0.81	0.81	0.82	0.84	0.88	0.88	0.88	0.88	0.89	0.89	0.90	0.84
Mn	0.00	0.00	0.00	0.00	0.00	0.00	0.00	0.00	0.00	0.00	0.00	0.00	0.00	0.00	0.00	0.00
Mg	0.12	0.14	0.14	0.14	0.15	0.15	0.14	0.12	0.10	0.10	0.11	0.10	0.10	0.11	0.09	0.12
Ca	0.00	0.00	0.00	0.00	0.00	0.00	0.00	0.00	0.00	0.00	0.00	0.00	0.00	0.00	0.00	0.00
Zn	0.05	0.04	0.04	0.04	0.04	0.04	0.04	0.05	0.02	0.02	0.01	0.01	0.01	0.02	0.00	0.05
K	0.00	0.00	0.00	0.00	0.00	0.00	0.00	0.00	0.00	0.00	0.00	0.00	0.00	0.00	0.00	0.00
Total	3.00	3.00	3.00	3.00	3.00	3.00	3.00	3.00	3.00	3.00	3.00	3.00	3.00	3.00	3.00	3.00
Sample	MM166C							MM146								
Oxide																
SiO2	0.32	0.29	0.18	0.20	0.18	0.32	0.07	0.10	0.08	0.07	0.20	0.14	0.10	0.55	0.13	0.19
TiO2	0.03	0.16	0.11	0.09	0.04	0.04	0.08	0.09	0.12	0.13	0.00	0.06	0.07	0.07	0.03	0.15
Al2O3	56.36	55.47	57.12	56.14	56.31	56.04	55.93	56.85	57.74	56.65	56.39	56.26	56.58	58.71	57.20	56.85
Cr2O3	0.15	0.14	0.04	0.11	0.07	0.00	0.14	0.14	0.06	0.04	0.11	0.20	0.07	0.05	0.09	0.12
Fe2O3	3.58	3.15	3.19	3.06	3.19	4.08	4.05	2.83	3.21	3.43	3.88	3.62	4.42	0.00	3.73	3.48
FeO	37.24	37.12	36.53	36.65	37.00	36.84	36.51	34.80	36.17	35.74	35.89	37.19	36.38	35.48	36.10	36.31
MnO	0.00	0.00	0.00	0.00	0.00	0.00	0.00	0.00	0.00	0.00	0.00	2.78	0.00	0.00	0.00	0.00
MgO	2.07	2.00	2.64	2.30	2.13	2.51	2.39	2.82	2.99	3.08	2.98	0.05	2.83	2.43	3.26	3.03
CaO	0.00	0.06	0.00	0.00	0.03	0.00	0.03	0.01	0.07	0.00	0.00	0.86	0.00	0.00	0.01	0.00
ZnO	1.11	0.90	1.25	0.65	0.71	0.96	0.78	2.22	0.98	0.65	0.70	0.80	0.73	0.68	0.45	0.70
K2O	0.08	0.00	0.00	0.08	0.05	0.00	0.03	0.00	0.03	0.02	0.05	0.00	0.05	0.04	0.02	0.02
Total	100.94	99.29	101.06	99.28	99.71	100.79	100.01	99.86	101.45	99.81	100.20	102.16	101.23	98.01	101.02	100.85
Number of atoms on the basis of 4 oxygens																
Si	0.01	0.01	0.00	0.00	0.00	0.01	0.00	0.00	0.00	0.00	0.01	0.00	0.00	0.02	0.00	0.00
Ti	0.00	0.00	0.00	0.00	0.00	0.00	0.00	0.00	0.00	0.00	0.00	0.00	0.00	0.00	0.00	0.00
Al	1.90	1.90	1.92	1.92	1.92	1.89	1.90	1.93	1.92	1.92	1.90	1.90	1.90	2.00	1.91	1.91
Cr	0.00	0.00	0.00	0.00	0.00	0.00	0.00	0.00	0.00	0.00	0.00	0.00	0.00	0.00	0.00	0.00
Fe3+	0.08	0.07	0.07	0.07	0.07	0.09	0.09	0.06	0.07	0.07	0.08	0.08	0.09	0.00	0.08	0.07
Fe2+	0.89	0.90	0.87	0.89	0.89	0.88	0.88	0.84	0.85	0.86	0.86	0.89	0.86	0.86	0.85	0.86
Mn	0.00	0.00	0.00	0.00	0.00	0.00	0.00	0.00	0.00	0.00	0.00	0.07	0.00	0.00	0.00	0.00
Mg	0.09	0.09	0.11	0.10	0.09	0.11	0.10	0.12	0.13	0.13	0.13	0.00	0.12	0.10	0.14	0.13
Ca	0.00	0.00	0.00	0.00	0.00	0.00	0.00	0.00	0.00	0.00	0.00	0.03	0.00	0.00	0.00	0.00
Zn	0.02	0.02	0.03	0.01	0.01	0.02	0.02	0.05	0.02	0.01	0.02	0.02	0.01	0.01	0.00	0.01
K	0.00	0.00	0.00	0.00	0.00	0.00	0.00	0.00	0.00	0.00	0.00	0.00	0.00	0.00	0.00	0.00
Total	3.00	3.00	3.00	3.00	3.00	3.00	3.00	3.00	3.00	3.00	3.00	3.00	3.00	3.00	3.00	3.00

Microprobe results of spinels in pelites

Sample	MM146											MM133				
Oxide																
SiO2	0.22	0.01	0.02	0.12	0.11	0.20	0.31	0.12	0.00	0.04	0.00	0.00	0.54	0.07	0.00	0.00
TiO2	0.10	0.00	0.12	0.10	0.05	0.04	0.03	0.11	0.18	0.15	0.19	0.00	0.02	0.00	0.02	0.06
Al2O3	56.94	56.01	55.02	56.49	56.72	56.59	56.82	55.76	55.53	55.57	55.61	58.55	58.08	58.40	58.71	59.84
Cr2O3	0.13	0.11	0.27	0.09	0.21	0.11	0.06	0.13	0.06	0.15	0.48	0.07	0.00	0.03	0.05	0.07
Fe2O3	3.68	3.76	3.82	3.43	3.50	3.43	3.06	3.40	4.37	4.56	3.51	2.66	1.15	2.68	2.00	0.59
FeO	36.33	35.23	35.06	36.04	36.00	35.79	36.12	35.99	35.76	35.93	35.77	34.88	35.44	34.75	35.03	34.43
MnO	0.00	0.00	0.00	0.00	0.00	0.00	0.00	0.00	0.00	0.00	0.00	0.01	0.00	0.00	0.00	0.09
MgO	2.77	2.74	2.58	2.73	2.88	2.50	2.65	2.40	2.47	2.50	2.57	3.82	3.73	3.75	3.64	3.66
CaO	0.00	0.00	0.07	0.00	0.00	0.02	0.00	0.00	0.02	0.00	0.00	0.11	0.00	0.01	0.00	0.02
ZnO	1.45	1.27	1.15	0.78	0.98	1.77	1.58	1.25	1.21	1.21	1.12	0.65	0.78	0.89	0.92	1.70
K2O	0.00	0.00	0.00	0.07	0.00	0.05	0.00	0.00	0.05	0.05	0.00	0.02	0.00	0.08	0.00	0.00
Total	101.62	99.13	98.11	99.85	100.45	100.50	100.63	99.16	99.65	100.16	99.25	100.77	99.74	100.66	100.37	100.46
Number of atoms on the basis of 4 oxygens																
Si	0.00	0.00	0.00	0.00	0.00	0.00	0.01	0.00	0.00	0.00	0.00	0.00	0.01	0.00	0.00	0.00
Ti	0.00	0.00	0.00	0.00	0.00	0.00	0.00	0.00	0.00	0.00	0.00	0.00	0.00	0.00	0.00	0.00
Al	1.90	1.91	1.90	1.91	1.91	1.91	1.91	1.91	1.90	1.89	1.90	1.94	1.94	1.94	1.96	1.98
Cr	0.00	0.00	0.00	0.00	0.00	0.00	0.00	0.00	0.00	0.00	0.01	0.00	0.00	0.00	0.00	0.00
Fe3+	0.08	0.08	0.08	0.07	0.07	0.07	0.07	0.07	0.09	0.10	0.08	0.06	0.02	0.06	0.04	0.01
Fe2+	0.86	0.85	0.86	0.87	0.86	0.86	0.86	0.87	0.87	0.87	0.87	0.82	0.84	0.82	0.83	0.81
Mn	0.00	0.00	0.00	0.00	0.00	0.00	0.00	0.00	0.00	0.00	0.00	0.00	0.00	0.00	0.00	0.00
Mg	0.12	0.12	0.11	0.12	0.12	0.11	0.11	0.10	0.11	0.11	0.11	0.16	0.16	0.16	0.15	0.15
Ca	0.00	0.00	0.00	0.00	0.00	0.00	0.00	0.00	0.00	0.00	0.00	0.00	0.00	0.00	0.00	0.00
Zn	0.03	0.03	0.02	0.02	0.02	0.04	0.03	0.03	0.03	0.03	0.02	0.01	0.02	0.02	0.02	0.03
K	0.00	0.00	0.00	0.00	0.00	0.00	0.00	0.00	0.00	0.00	0.00	0.00	0.00	0.00	0.00	0.00
Total	3.00	3.00	3.00	3.00	3.00	3.00	3.00	3.00	3.00	3.00	3.00	3.00	3.00	3.00	3.00	3.00

Sample					MM169B						MM166D					
Oxide																
SiO2	0.30	0.00	0.00	0.02	0.00	0.29	0.34	0.10	0.10	0.16	0.00	0.00	0.00	0.00	0.03	1.41
TiO2	0.19	0.08	0.07	0.09	0.00	0.12	0.04	0.15	0.12	0.15	0.00	0.00	0.02	0.90	0.02	0.08
Al2O3	57.72	58.42	58.33	58.25	56.59	56.52	55.88	56.27	56.86	55.82	58.18	57.41	57.31	56.16	57.78	56.22
Cr2O3	0.11	0.16	0.01	0.06	0.30	0.26	0.23	0.30	0.17	0.33	0.08	0.26	0.19	1.45	0.06	0.19
Fe2O3	1.71	1.34	2.25	2.12	3.46	2.35	3.01	3.06	2.81	3.63	2.56	2.66	3.00	2.19	2.66	0.08
FeO	34.05	35.73	34.98	34.97	35.64	34.65	36.76	36.51	36.61	36.24	34.77	35.84	35.10	36.48	35.64	36.99
MnO	0.00	0.00	0.00	0.04	0.00	0.00	0.00	0.00	0.00	0.00	0.00	0.00	0.00	0.00	0.00	0.00
MgO	3.76	3.44	3.45	3.37	2.29	2.66	2.28	2.30	2.38	2.53	3.45	3.19	3.52	3.13	3.41	3.02
CaO	0.00	0.04	0.06	0.02	0.02	0.02	0.04	0.01	0.00	0.07	0.00	0.00	0.00	0.04	0.01	0.00
ZnO	1.78	0.09	1.18	1.36	2.07	2.83	0.96	1.11	0.97	0.84	1.44	0.11	0.42	0.60	0.36	1.00
K2O	0.06	0.00	0.00	0.00	0.00	0.00	0.00	0.02	0.04	0.05	0.00	0.04	0.03	0.06	0.00	0.00
Total	99.68	99.30	100.33	100.30	100.37	99.70	99.54	99.83	100.06	99.82	100.48	99.51	99.59	101.01	99.97	98.99
Number of atoms on the basis of 4 oxygens																
Si	0.01	0.00	0.00	0.00	0.00	0.01	0.01	0.00	0.00	0.00	0.00	0.00	0.00	0.00	0.00	0.04
Ti	0.00	0.00	0.00	0.00	0.00	0.00	0.00	0.00	0.00	0.00	0.00	0.00	0.00	0.02	0.00	0.00
Al	1.94	1.96	1.95	1.95	1.92	1.92	1.91	1.91	1.93	1.90	1.94	1.94	1.93	1.88	1.94	1.91
Cr	0.00	0.00	0.00	0.00	0.00	0.00	0.00	0.00	0.00	0.01	0.00	0.00	0.00	0.03	0.00	0.00
Fe3+	0.04	0.03	0.05	0.04	0.07	0.05	0.07	0.07	0.06	0.08	0.05	0.06	0.06	0.05	0.06	0.00
Fe2+	0.81	0.85	0.83	0.83	0.86	0.84	0.89	0.88	0.88	0.87	0.82	0.86	0.84	0.87	0.85	0.89
Mn	0.00	0.00	0.00	0.00	0.00	0.00	0.00	0.00	0.00	0.00	0.00	0.00	0.00	0.00	0.00	0.00
Mg	0.16	0.15	1.15	0.14	0.10	0.11	0.10	0.10	0.10	0.11	0.15	0.14	0.15	0.13	0.14	0.13
Ca	0.00	0.00	0.00	0.00	0.00	0.00	0.00	0.00	0.00	0.00	0.00	0.00	0.00	0.00	0.00	0.00
Zn	0.04	0.00	0.02	0.03	0.04	0.06	0.02	0.02	0.02	0.02	0.03	0.00	0.01	0.01	0.01	0.02
K	0.00	0.00	0.00	0.00	0.00	0.00	0.00	0.00	0.00	0.00	0.00	0.00	0.00	0.00	0.00	0.00
Total	3.00	3.00	3.00	3.00	3.00	3.00	3.00	3.00	3.00	3.00	3.00	3.00	3.00	3.00	3.00	3.00

Microprobe results of spinels in pelites

Sample	MM166D														
Oxide															
SiO2	0.06	0.00	0.10	0.11	0.05	0.03	0.03	0.12	0.09	0.00	0.12	0.09	0.00	0.00	0.06
TiO2	0.02	0.00	0.00	0.01	0.07	0.10	0.14	0.07	0.05	0.00	0.00	0.07	0.00	0.06	0.05
Al2O3	57.08	57.79	57.88	57.54	57.11	57.02	57.44	58.78	57.62	57.25	57.99	57.02	57.53	57.90	57.48
Cr2O3	0.10	0.11	0.02	0.19	0.25	0.92	0.01	0.22	0.34	0.34	0.43	0.52	0.14	0.34	0.04
Fe2O3	3.37	3.56	2.71	3.07	3.40	2.46	3.54	2.16	2.46	3.44	2.30	2.42	3.57	2.93	2.93
FeO	36.27	34.84	35.78	37.42	36.56	36.97	37.21	37.20	36.29	36.43	36.99	36.41	36.73	35.87	36.86
MnO	0.00	0.00	0.00	0.00	0.00	0.00	0.00	0.00	0.00	0.00	0.00	0.00	0.00	0.00	0.00
MgO	2.83	3.71	3.46	2.58	2.81	2.59	2.60	3.06	2.93	2.92	2.78	2.77	2.69	3.38	2.63
CaO	0.09	0.50	0.04	0.00	0.00	0.04	0.04	0.05	0.03	0.04	0.05	0.02	0.00	0.07	0.02
ZnO	0.57	0.32	0.29	0.32	0.64	0.38	0.53	0.04	0.54	0.24	0.43	0.55	0.56	0.41	0.27
K2O	0.01	0.00	0.00	0.00	0.00	0.00	0.01	0.00	0.04	0.04	0.00	0.00	0.05	0.01	0.07
Total	100.40	100.83	100.28	101.24	100.89	100.51	101.55	101.70	100.39	100.70	101.09	99.87	101.27	100.97	100.41
Number of atoms on the basis of 4 oxygens															
Si	0.00	0.00	0.00	0.00	0.00	0.00	0.00	0.00	0.00	0.00	0.00	0.00	0.00	0.00	0.00
Ti	0.00	0.00	0.00	0.00	0.00	0.00	0.00	0.00	0.00	0.00	0.00	0.00	0.00	0.00	0.00
Al	1.92	1.92	1.94	1.92	1.92	1.92	1.92	1.94	1.93	1.92	1.93	1.93	1.92	1.93	1.93
Cr	0.00	0.00	0.00	0.00	0.00	0.02	0.00	0.00	0.00	0.01	0.01	0.01	0.00	0.01	0.00
Fe3+	0.07	0.08	0.06	0.07	0.07	0.05	0.07	0.05	0.05	0.07	0.05	0.05	0.08	0.06	0.06
Fe2+	0.87	0.82	0.85	0.89	0.87	0.88	0.88	0.87	0.86	0.87	0.88	0.87	0.87	0.85	0.88
Mn	0.00	0.00	0.00	0.00	0.00	0.00	0.00	0.00	0.00	0.00	0.00	0.00	0.00	0.00	0.00
Mg	0.12	0.16	0.15	0.11	0.12	0.11	0.11	0.13	0.12	0.12	0.12	0.12	0.11	0.14	0.11
Ca	0.00	0.01	0.00	0.00	0.00	0.00	0.00	0.00	0.00	0.00	0.00	0.00	0.00	0.00	0.00
Zn	0.01	0.00	0.00	0.00	0.01	0.01	0.01	0.00	0.01	0.00	0.01	0.01	0.01	0.01	0.01
K	0.00	0.00	0.00	0.00	0.00	0.00	0.00	0.00	0.00	0.00	0.00	0.00	0.00	0.00	0.00
Total	3.00	3.00	3.00	3.00	3.00	3.00	3.00	3.00	3.00	3.00	3.00	3.00	3.00	3.00	3.00

Appendix 6
F content of biotites in pelites from WD microprobe analyses

F contents of biotites in pelites (atom per formula unit). SD= standard deviation.

MM181	MM56A	MM188C	MM171	MM184B	MM166A	MM197A
0.24	0.14	0.20	0.22	0.26	0.35	0.45
0.25	0.11	0.18	0.15	0.28	0.33	0.39
0.26	0.12	0.16	0.11	0.26	0.41	0.48
0.26	0.13	0.16	0.16	0.23	0.37	0.42
0.25	0.15	0.19	0.16	0.28	0.34	0.55
0.22	0.12	0.24	0.16	0.21	0.37	0.42
0.22	0.10	0.19	0.17	0.29	0.33	0.42
0.23	0.10	0.20	0.10	0.23	0.34	0.39
0.15		0.15	0.09	0.29	0.31	0.31
0.23		0.23		0.28	0.23	
Mean=0.23	Mean=0.12	Mean=0.19	Mean=0.15	Mean=0.26	Mean=0.34	Mean=0.42
SD=0.03	SD=0.02	SD=0.03	SD=0.04	SD=0.03	SD=0.04	SD=0.06

Appendix 7
Ion Probe Set-up

A7.1 Sample Preparation: Sample preparation for ion probe analysis is significantly more stringent than for the electron microprobe (Hinton, 1995). Samples prepared as polished thin sections and were cut down to 1 inch round slides. Prior to coating, samples were ultrasonically cleaned to remove polishing compounds and chemicals from the surface and cracks. The surface of the samples were coated with a conducting layer of gold (~20 nm thick). Gold was chosen not carbon since CO_2 in cordierite was important component to be analysed. Also gold is mono-isotopic, poorly ionising and has a high mass, molecular complexes with gold should not therefore generate significant interference (Hinton, 1995).

A7.2 Standards: Two cordierite standards were used for study of CO_2 and H_2O in unknown cordierites from the Etive aureole. These are Cordierite AMNH and Cordierite 8-90.

Cordierite AMNH is from the American Museum of Natural History and was sampled from a gem mine in Zimbabwe. It has 1.56 wt% H_2O and ca. 0.6 wt% CO_2.

8-90 was donated by Prof. V. Schenk (Kiel-Germany) and is from the Serre Massif, Calabria. It has ca. 1.3 wt% CO_2 and 0.8 wt% H_2O. In both cases CO_2 has been independently measured by stepped heating mass spectrometry; for 8-90 CO_2 has also been measured by coulometric titration.

H_2O has been independently measured by Karl Fischer titration (8-90) and by H-extraction + manometry (both AMNH and 8-90). AMNH has had its H_2O done in triplicate at SURRC by H-extraction, and its CO" done in duplicate at Royal Holloway by stepped heating (S.L. Harley, personal communications).

A7.3 Ion Probe Setting-Up: The ion microprobe in the Grant Institute of Geology in Edinburgh was used for secondary ion mass spectrometry of H and C in cordierite. The machine is a highly modified Cameca ims-4f ion microprobe. The ion microprobe was operated for 5 days measuring secondary negative ions using an O^-

(negative) primary beam. The primary beam energy was approximately 10.5 keV whereas the extraction energy was 4.5 keV. The net impact energy of the ions onto the surface was 6 keV. The sample voltage offset was set such that only ions with energies ranging from 55 to 95 eV were measured (i.e. 75±20 eV) The position of the energy window was checked using the low-energy tail of the energy distribution (i.e. determined voltage offset required to reduce the secondary ion intensity by a factor of 10 and then sample voltage offset 100 eV above this). This routinely meant that the offset was set at 60 eV. Secondary ions were measured sequentially on an electron multiplier ion counting system. Count rates measured for H and C were ratioed to ^{28}Si.

The instrument was operated for 1 day measuring positive secondary ions. In this case the net primary beam impact energy was 15 keV (10.5+4.5). The energy offset was determined in the same way as for negatives but since the sample charging is less under positive ion bombardment, the offset is routinely about 75 eV. Count rates for H were ratioed to ^{30}Si since ^{28}Si would have overloaded are detector system.

In general the higher energy of the negative–positive combination results in higher beam densities and better beam focus than the negative-negative combination. The negative secondaries are used principally for C analyses, the yield of C^- being much higher than C^+. Also doubly charged molecular interferences such as $^{24}Mg^{2-}$ are not observed whereas $^{24}Mg^{2+}$ is the dominant species at mass 12 in the positive ion mass spectrum. For H there is little to choose between positives and negatives; generally it is easier to tune the instrument and primary beam focus using positive secondary ions.

Carbon and hydrogen abundances have been determined using the ion probe. SIMS $^{12}C/^{28}Si$, $^{1}H/^{28}Si$ and $^{1}H/^{30}Si$ isotopic ratios obtained using both negative and positive beams (separately in different working sessions) and measured on 25μm spot analyses of reference samples (standards), have been used to drive CO_2 and H_2O calibration curves (Fig.'s Ap1, Ap2 and Ap3). Obtained isotopic ratios from unknown cordierites from the Etive aureole were tested against standard cordierites in all SIMS sessions. Background level for H_2O and CO_2 are 0.025 and 0.322 wt% respectively and analytical precision is to ±0.06 wt%.

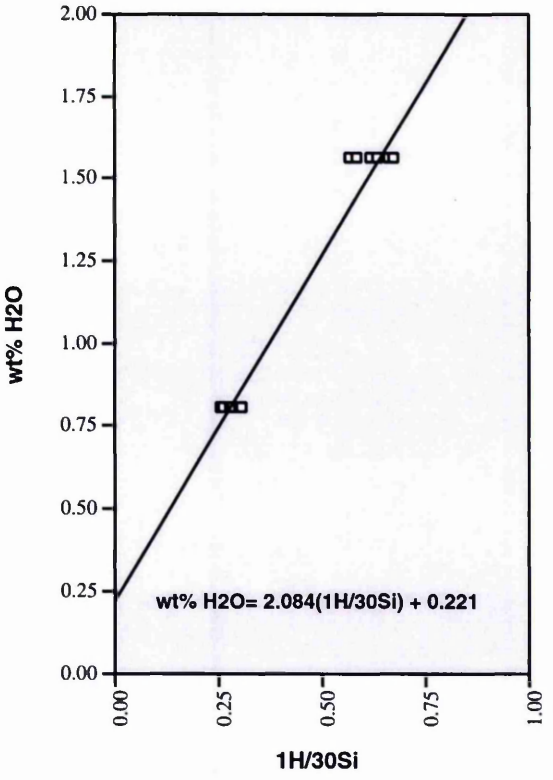

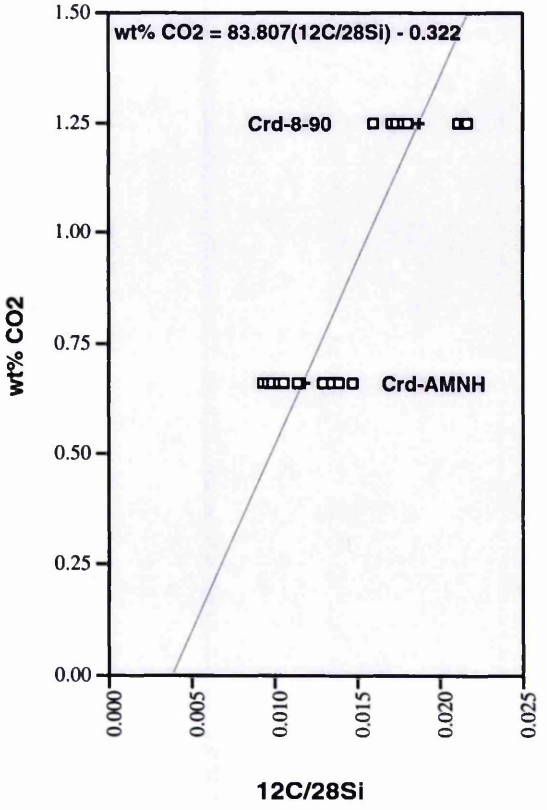

Fig A7.1 Calibration curves for CO2 and H2O in standard cordierites.

Appendix 8

Activity models for biotite, garnet and plagioclase

A8.1 Biotite: Activity models for biotite used in this study, from Patino Douce et al. (1993) are:

$$a_{phlogopite} = 9.481 X^2_{M2_{Mg}} X_{M1_{Mg}} X_{IV_{Al}} X^3_{Si} X_K X^2_{OH}$$

$$a_{annite} = 9.481 X^2_{M2_{Fe}} X_{M1_{Fe}} X_{IV_{Al}} X^3_{Si} X_K X^2_{OH}$$

A8.2 Garnet: Activity models for garnet used in this study, from Berman (1990) are:

$$a_{Gr} = (X_{Gr} \cdot \gamma_{Gr})^3$$
$$a_{Py} = (X_{Py} \cdot \gamma_{Py})^3$$
$$a_{Alm} = (X_{Alm} \cdot \gamma_{Alm})^3$$

Where Gr=grossular, Py=Pyrope and Alm+almandine. The activity coefficient (γ) is given by:

$3RtlnY_{Gr}$

$$\begin{aligned}
&= W_{112}(2X_1X_2 - 2X_1^2X_2) + W_{122}(X_2^2 - 2X_1X_2^2) \\
&+ W_{113}(2X_1X_3 - 2X_1^2X_3) + W_{133}(X_3^2 - 2X_1X_3^2) \\
&+ W_{114}(2X_1X_4 - 2X_1^2X_4) + W_{144}(X_4^2 - 2X_1X_4^2) \\
&+ W_{223}(-2X_2^2X_3) + W_{233}(-2X_2X_3^2) \\
&+ W_{224}(-2X_2^2X_4) + W_{224}(-2X_2X_4^2) \\
&+ W_{334}(-2X_3^2X_4) + W_{344}(-2X_3X_4^2) \\
&+ W_{123}(X_2X_3 - 2X_1X_2X_3) + W_{124}(X_2X_4 - 2X_1X_2X_4) \\
&+ W_{134}(X_3X_4 - 2X_1X_3X_4) + W_{234}(-2X_2X_3X_4)
\end{aligned}$$

$3RTlnY_{Py}$

$$= W_{112}(X_1^2 - 2X_1^2X_2) + W_{122}(2X_1X_2 - 2X_1X_2^2)$$
$$+ W_{113}(-2X_1^2X_3) + W_{133}(-2X_1X_3^2)$$
$$+ W_{114}(-2X_1^2X_4) + W_{144}(-2X_1X_4^2)$$
$$+ W_{223}(2X_2X_3 - 2X_2^2X_3) + W_{233}(X_3^2 - 2X_2X_3^2)$$
$$+ W_{224}(-2X_2X_4 - 2X_2^2X_4) + W_{244}(X_4^2 - 2X_2X_4^2)$$
$$+ W_{334}(-2X_3^2X_4) + W_{344}(-2X_3X_4^2)$$
$$+ W_{123}(X_1X_3 - 2X_1X_2X_3) + W_{124}(X_1X_4 - 2X_1X_2X_4)$$
$$+ W_{134}(2X_1X_3X_4) + W_{234}(X_3X_4 - 2X_2X_3X_4)$$

$3RT\ln\gamma_{Alm}$

$$= W_{112}(-2X_1^2X_2) + W_{122}(-2X_1X_2^2)$$
$$+ W_{113}(X_1^2 - 2X_1^2X_3) + W_{133}(2X_1X_3 - 2X_1X_3^2)$$
$$+ W_{114}(-2X_1^2X_4) + W_{144}(-2X_1X_4^2)$$
$$+ W_{223}(X_2^2 - 2X_2^2X_3) + W_{233}(2X_2X_3 - 2X_2X_3^2)$$
$$+ W_{224}(-2X_2^2X_4) + W_{244}(-2X_2X_4^2)$$
$$+ W_{334}(2X_3X_4 - 2X_3^2X_4) + W_{344}(X_4^2 - 2X_3X_4^2)$$
$$+ W_{123}(X_1X_2 - 2X_1X_2X_3) + W_{124}(-2X_1X_2X_4)$$
$$+ W_{134}(X_1X_4 - 2X_1X_3X_4) + W_{234}(X_2X_4 - 2X_2X_3X_4)$$

where 1=grossular, 2=pyrope, 3=almandine and 4=spessartine.

R=gas constant and the interaction parameters (e.g. W_{123}) are:

Parameter	W_H(J/mol)
112	21 560
122	69 200
113	20 320
133	2620
223	230
233	3720
123	58 825
124	45 424
134	11 470
234	1975

A8.3 Plagioclase: Activity model for plagioclase used in this study, from Elkins and Grove (1990) is:

$$a_{An} = X_{An}.\exp\{(W_{Or\,Ab}[X_{Ab}X_{Or}(\tfrac{1}{2} - X_{An} - 2X_{Ab})]$$
$$+ W_{AbOr}[X_{Ab}X_{Or}(\tfrac{1}{2} - X_{An} - 2X_{Or})]$$
$$+ W_{AbAn}[2X_{Ab}X_{An}(1 - X_{An}) + X_{Ab}X_{Or}(\tfrac{1}{2} - X_{An})]$$
$$+ W_{AnAb}[X_{Ab}^2(1 - 2X_{An}) + X_{Ab}X_{Or}(\tfrac{1}{2} - X_{An})]$$
$$+ W_{OrAn}[2X_{Or}X_{An}(1 - X_{An}) + X_{Ab}A_{Or}(\tfrac{1}{2}X_{An})]$$
$$+ W_{AnOr}[X_{Or}^2(1 - 2X_{An}) + X_{Ab}X_{Or}(\tfrac{1}{2} - X_{An})]$$
$$+ W_{OrAbAn}[X_{Or}X_{Ab}(1 - 2X_{An})])/RT\}$$

Where An=anorthite, Ab=albite and Or=Orthoclase and the interaction parameters are:

	W_H	W_H
W_{AbOr}	18810	18810
W_{OrAb}	27320	27320
W_{AbAn}	28226	7924 (525)
W_{AnAb}	8471	0.0
W_{OrAn}	47396	40317 (460)
W_{AnOr}	52468	38974 (292)
W_{AbOrAn}	8700	12545 (965)

Allen, J. M. and Goldie, R. 1978. Coexisting amphiboles from the Noranda area, Quebec: extension of the actinolite-hornblende miscibility gap to iron-rich bulk compositions. *American Mineralogist*, **63**, 205-209.

Almond, D. C., 1964. Metamorphism of Tertiary lavas in Strathraird, Skye. *Transactions of the Royal Society of Edinburgh*, **45**, 413-435.

Anderson, J. G. C., 1937. The Etive granite complex. *Quarterly Journal of the Geological Society of London*, **93**, 487-532.

Anderson, D.J, Lindsley, D. H. and Davidson, P. M., 1993. QUILF: A pascal program to assess equilibria among Fe-Mg-Mn-Ti oxides, pyroxene, olivine and quartz. *Computers and Geosciences,* **19,** 9, 1333-1359.

Anderton, R., 1975. Tidal Flat and shallow marine sediments from the Craignish Phyllites, Middle Dalradian, Argyll, Scotland. *Geological Magazine*, **112,** 337-340.

Anderton, R., 1976. Tidal-shelf sedimentation: an example from the Scottish Dalradian. *Sedimentology*, **23**, 429-458.

Anderton, R., 1979. Slopes, submarine fans and syn-depositional faults: sedimentology of parts of the Middle and upper Dalradian in the S.W. Highlands of Scotland. In: Harris, A. L., Holland, C. H., and Leake, B. E. (eds) The British Caledonian-reviewed. *Special publication of the Geological Society of London*, **8**, 483-488.

Anderton, R., 1980. Did Iapetus start to open during the Cambrian? *Nature,* **286,** 706-708.

Anderton, R., 1985. Sedimentation and tectonics in the Scottish Dalradian. *Scottish Journal of Geology,* **93,** 487-533.

Anderton, R., 1988. Dalradian slides and basin development: a radical interpretation of stratigraphy and structure in the SW and Central Highlands of Scotland. *Journal of the Geological Society of London*, **145**, 669-678.

Anovits, L. M. and Essene, E. J., 1987. Phase equilibria in the system $CaCO_3$-$MgCO_3$-$FeCO_3$. *Journal of Petrology*, **28**, 389-414.

Applegate, J. D. R. and Hodges, K. V., 1994. Empirical evaluation of solution models for pelitic minerals and their application to thermobarometry, *Contributions to Mineralogy and Petrology*, **117**, 56-65.

Ashcroft, W. A., Kneller, B. C., Leslie, A. G. and Munro, M., 1984. Major shear zones and autochthonous Dalradian in the north-east Scottish Caledonides. *Nature,* **310,** 760-762.

Ashcroft, W. A. and Boyd, R.,1976. The Belhelvie mafic igneous intrusion, Aberdeenshire-a reinvestigation. *Scottish Journal of Geology*, **12**, 1-14.

Ashworth, J. R., 1975. The sillimanite zone of the Huntly-Portsoy area in the north-east Dalradian, Scotland. *Geological Magazine,* **112,** 113-136.

Ashworth, J. R. & Chinner, G., A., 1978. Coexisting garnet and cordierite in migmatites from the Scottish Caledonides. *Contribution to Mineralogy and Petrology*, **65**, 379-394.

Ashworth, J. R. and Tyler, I. M., 1983. The distribution of metamorphic temperatures around the Strontian granodiorite. *Geological Magazine,***120,** 281-290.

Ashworth, J. R., 1985. Introduction. In: *Migmatites (ed. Ashworth, J. R.),* pp. 1-31. Blackie, Glasgow.

Askyuk, A.M. and Zhukhovskaya, T.N., 1994, Experimental calibration of the phlogopite fluorimeter at 500-700°C and 1-4 kbar and estimated HF concentrations of fluids associated with marble: some examples. *Geochimica et Cosmochimica Acta*, **58,** 4305-4317.

Atherton, M. P., 1964. The garnet isograd in pelitic rocks and its relationship to metamorphic facies. *American Mineralogist,* **49,** 1331-1349.

Atherton, M. P., 1968. The variation in garnet, biotite, and chlorite composition in medium grade pelitic rocks from the Dalradian, Scotland, with particular reference to the zonation in garnet. *Contributions to Mineralogy and Petrology*, **18**, 347-371.

Atherton, M. P., 1977. The metamorphism of the Dalradian rocks of Scotland. *Scottish Journal of Geology,* **13,** 331-370.

Avchenko, O. V., 1986. Interpreting pressure and temperature estimates derived from mineral assemblages and from geothermobarometers: *International Geology Review,* **28**, 1269-1277.

Bailey, E. B., 1910. Recumbent folds in the schists of the Scottish Highlands. *Quarterly Journal of the Geological Society of London*, **66**, 586-620.

Bailey, E. B., 1917. The Islay Anticline (Inner Hebrides). *Quarterly Journal of Geological Society of London*, **72**, 132-164.

Bailey, E. B., 1922. The structure of the south-west Highlands of Scotland. *Quarterly Journal of Geological Society of London,* **78,** 82-127.

Bailey, E. B., 1925. Perthshire tectonics: Loch Tummel, Blair Atholl and Glen Shee. *Transactions of the Royal Society of Edinburgh*, **53**, 671-698.

Bailey, E. B., 1934. West Highland Tectonics: Loch Leven to Glen Roy. *Quarterly Journal of Geological Society of London,* **90,** 462-523.

Bailey, E. B., 1938. Eddies in mountain structure. *Quarterly Journal of the Geological Society of London*, **94**, 607-625.

Bailey, E. B., 1940. Discussion of paper by A. Allison: Loch Awe succession and tectonics: Kilmartin-Tayvalich-Danna. *Quarterly Journal of Geological Society of London,* **96,** 423-449.

Bailey, E. B., 1960. The geology of Ben Nevis and Glencoe and the surrounding country (2nd edition). *Memoir of the Geological Survey, Scotland,* Sheet 53 (Scotland).

Bailey, E. B. & McGregor, 1912. The Glen Orchy Anticline, Argyllshire. *Quarterly Journal of the Geological Society of London*, **68**, 164-179.

Bailey, E. B. and Maufe, H. B., 1916. The geology of Ben Nevis and Glencoe and the surrounding country. *Sheet 53, Memoir of Geological Survey of Scotland, Edinburgh.*

Bailey, E. B. and Maufe, H. B., 1960. The geology of Ben Nevis and Glen Coe and the surrounding country: explanation of sheet 53. *Mem. Geological Society of Scotland, Edinburgh:* H.M.S.O., 307 pp.

Baker, A. J., 1985. Pressure and temperature of metamorphism in the eastern Dalradian. *Journal of the Geological Society of London,* **142**, 137-148.

Baker, A. J. and Droop, G. T. R., 1983. Grampian metamorphic conditions deduced from the mafic granulites and sillimanite-K-feldspar gneisses in the Dalradian of Glen Muick, Scotland. *Journal of the Geological Society of London,* **140,** 489-497.

Baltatzis, E., 1979. Staurolite forming reactions in the eastern Dalradian of Scotland. *Contributions to Mineralogy and Petrology*, **69**, 193-200.

Bamford, D., Nunn, K., Prodehl, C., and Jacob, B., 1977. LISPB-III. Upper crustal structure of northern Britain. *Journal of the Geological Society of London,* **133,** 481-488.

Barker, F., 1979. Trondhjemite: Definition, environment and hypotheses of origin. In: Barker, F. (ed.) Trondhjemites, dacites and related rocks. Elsevier, Amsterdam, pp. 1-12.

Barritt, S. D., 1983. The controls of radioelement distribution in the Etive and Cairnogrom granites: implications for heat production. Ph.D. thesis, Open University, unpublished.

Barrow, G., 1893. On an intrusion of muscovite biotite gneiss in the south-east Highlands of Scotland and its accompanying metamorphism. *Quarterly Journal of the Geological Society of London,* **49,** 330-358.

Batchelor, R. A., 1987. Geochemical and petrological characteristics of the Etive granitoid complex, Argyll. *Scottish Journal of Geology*, **23**, 227-249.

Batchelor R. A., Armstrong, D. C. and McDonald, M., 1992. Composition of fluid in quartz: discrimination of magma pulses in a Caledonian granitoid. *Mineralogical Magazine*, **56**, 335-342.

Beddoe, Stephens B., 1990. Pressure and temperature of Dalradian metamorphism and the andalusite-kyanite transformation in the Northern Grampians. *Scottish Journal of Geology*, **26**, 3-14.

Bell, K., 1968. Age relations and provenance of the Dalradian Series of Scotland. *Bulletin of the Geological Society of America*, **79**, 1167-1194.

Bendall, C. A., 1995. A geochronological, structural and metamorphic study of parts of the Central and South-west Dalradian. *Ph.D. thesis, University of Manchester, unpublished.*

Berg, J. H. and Docka, J. A., 1983. Geothermometry in the Kiglapait contact aureole, Labrador. *American Journal of Science*, **283**, 414-434.

Berman, R. G., 1988. Internally-consistent thermodynamic data for minerals in the system Na_2O-K_2O-CaO-MgO-FeO-Fe_2O_3- Al_2O_3-SiO_2-TiO_2-H_2O-CO_2. *Journal of Petrology*, **29**, 445-522.

Berman, R. G., 1990. Mixing properties of Ca-Mg-Fe-Mn garnets. *American Mineralogist*, **75**, 328-344

Berman, R. G. and Brown, T. H., 1988. A general method for thermobarometric calculations, with a revised garnet solution model and geological application. *Geological Society of America Abstracts with Programs*, **20**, A98.

Bhattacharya, A., Mohanty, L., Maji, A., Sen, S. K. and Raith, M., 1992. Non-ideal mixing in the phlogopite-annite binary: constraints from experimental data on Mg-Fe partitioning and a reformulation of the biotite-garnet geothermometer. *Contributions to Mineralogy and Petrology*, **111**, 87-93.

Bickle, M. J. and Powell, R., 1977. Calcite-dolomite geothermometry for iron-bearing carbonates. *Contributions to Mineralogy and Petrology*, **59**, 281-292.

Blundy, J. D. & Holland, T. J. B., 1990. Calcic amphiboles equilibria and a new amphibole-plagioclase geothermometer. *Contributions to Mineralogy and Petrology*, **104**, 208-224.

Boberski, C. and Schreyer, W., 1990, Synthesis and water contents of Fe^{2+}-bearing cordierites: *European Journal of Mineralogy*, **2**, 565-584.

Booth, J. E., 1984. Structural, stratigraphic and metamorphic studies in the SE Dalradian Highlands. *Unpublished Ph.D. thesis*, University of Edinburgh.

Borradaile, G. J., 1970. The west limb of the Loch Awe syncline and the associated cleavage fan. *Geological Magazine,* **107,** 459-467.

Borradaile, G. J., 1973. Dalradian structure and stratigraphy of the northern Loch Awe district, Argyllshire. *Transactions of the Royal Society of Edinburgh,* **69,** 1-21.

Bowman, J. R. and Essene, E. J., 1982. P-T-X(CO2) conditions of contact metamorphism in the Black Butte aureole, Elkhorn, Montana. *American Journal of Science*, **282**, 311-340.

Boyd, F. R., 1969. Electron-probe study of diopside inclusions from kimberlite. *American Journal of Science*, **267-A**, 50-69.

Boyd, F. R., 1973. A pyroxene geotherm. *Geochemica et Cosmochemica Acta*, **37**, 2533-2546.

Bradbury, H. J., 1985. The Caledonian metamorphic core: an Alpine model. *Journal of the Geological Society of London,* **142,** 129-136.

Bradbury, H. J., Smith, R. A. and Harris, A. L., 1976. 'Older' granites as time-markers in Dalradian evolution. *Journal of the Geological Society of London,* **132,** 677-684.

Bradbury, H. J., Harris, A. L. and Smith, R. A., 1979. Geometry and emplacement of nappes in the Central Scottish Highlands. In: Harris, A. L., Holland, C. H., and Leake, B. E. (Eds.) The Caledonides of British Isles- reviewed, 213-220. *Special publication of the Geological Society of London..*

Brown, E., H., 1977. The crossite content of Ca-amphiboles as a guide to pressure of metamorphism. *Journal of Petrology*, **18**, 53-72.

Brown, J. F., 1975. Rb-Sr studies and related chemistry on the Caledonian calc-alkaline igneous rocks of NW Argyllshire. Ph.D. thesis, University of Oxford, unpublished.

Brown, P. E., 1991. Caledonian and earlier magmatism. In; Geology of Scotland (3^{rd} edition) 229-295. Craig,G. Y. (edt), London, The Geological Society of London.

Brown, P. E., Miller, J. A, Grasty, R. L., and Fraser, W. E., 1965. Pottasium-argon ages of some aberdeenshire granites and gabbros. *Nature, London*, **207**, 1287-1288.

Brown, P. E., Miller, J. A. and Grasty, K. L. 1968. Isotopic age of late Caledonian granitic intrusions in the British Isles. *Proceedings of the Yorkshire Geological Society*, **36**, 251-276.

Brown, W. L. and Parsons, I., 1981. Towards a more practical two-feldspar geothermometer. *Contributions to Mineralogy and Petrology*, **76**, 369-377.

Buddington, A. F., 1948. Origin of granitic rocks of the northwest Adirondacks. *Geological Society of America Memoir,* **28,** 21-43.

Bucher-Nurminen, K., 1982. On the mechanism of contact aureole formation in dolomitic country rock by the Adamello intrusion (northern Italy). *American Mineralogist,* **67**, 1101-1107.

Burnham, C.W., Holloway, J.R. and Davis, N.F., 1969. Thermodynamic properties of water to 1000°C and 10000 bars. *Geological Society of America Special Paper*, **132.**

Busrewil M., T., Pankhurst, R. J. and Wadworth, W. J., 1973. The igneous rocks of the Bogancloch area, NE Scotland. *Scottish Journal of Geology*, **9**, 165-176.

Bussell, M. A., Pitcher, W. S. and Wilson, P. A., 1976. Ring complexes of the Peruvian coastal batholith: a longstanding subvolcanic regime. *Canadian Journal of Earth Science*, **13**, 1020-1030.

Carey, J.W., 1995. A thermodynamic formulation of hydrous cordierite. *Contributions to Mineralogy and petrology*, **119**, 155-165.

Carrington, D. P. and Harley, S. L., 1996. Cordierite as a monitor of fluid and melt H_2O content in the lower crust: an experimental calibration. *Geology*, **24**, 647-650.

Carswell, D. A., 1990. Eclogite Facies Rocks, Blackie, New York.

Chappel, B. W., and White, A. J. R., 1974. Two contrasting granite types. *Pacific. Geology*, **8**, 173-174.

Chatterjee, N., M., and Johannes, W., 1974. Thermal stability and standard thermodynamic properties of synthetic $2M_1$-muscovite, $KAl_2[AlSi_3O_{10}(OH)_2]$. *Contributions to Mineralogy and Petrology*, **48**, 89-114.

Chinner, G. A., 1960. Pelitic gneisses with varying ferrous/ferric ratios from Glen Clova, Angus, Scotland. *Journal of Petrology*, **1**, 178-217.

Chinner, G. A., 1962. Almandine in thermal aureole. *Journal of Petrology*, **3**, 310-340.

Chinner, G. A., 1965. The Kyanite isograd in Glen Colva, Angus, Scotland. Mineralogical Magazine, **34,** 132-143.

Chinner, G. A., 1966. The distribution of pressure and temperature during Dalradian metamorphism. *Quarterly Journal of the Geological Society of London,* **122,** 159-186.

Chinner, G. A., 1967. Chloritoid and the isochemical character of Barrow's zones. *Journal of Petrology,* **8,** 268-282.

Cho, M., and Liou, J. G., 1987. Prehnite-pumpelluite to greenschist facies transition in the Karmutsen metabasalts, Vancouver Island, British Colombia. *Journal of Petrology*, **28**, 417-443.

Clark, D. B., 1992. Granitoid Rocks. *Chapman and Hall. London.*

Clayburn, J. A. P., 1981. Age and petrogenetic studies of some magmatic and metamorphic rocks in the Grampian Highlands. *Unpublished Ph.D. thesis*, University of Oxford.

Clayburn, J. A. P., Harmon, R. S., Pankhurst, R. J., and Brown, J. F., 1983. Sr, O and Pb isotope evidence for the origin and evolution of the Etive Igneous Complex, Scotland. *Nature*, **303**, 492-497.

Clemens J. D. & Wall, V. J., 1981. Crystallisation and origin of some peraluminous (S-type) granitic magmas. *Cantributions to Mineralogy and Petrology,* **14,** 111-132.

Clemens, J. D. & Vielzeuf, D., 1987. Constraints on melting and magma production in the crust. *Earth and Planetary Science Letters,* **86,** 287-306.

Clemens, J. D. and Droop, G. T. R., 1998. Fluid, P-T paths and the fates of anatectic melts in the Earth's crust. *Lithos*, **44,** 21-36.

Clough, C. T., 1897. The geology of Cowal. *Mem. of Geological Survey of Scotland.*

Clough, C. T., Maufe, H. B. and Bailey, E. B., 1909. The cauldron subsidence of Glen Coe and associated igneous phenomena. *Quarterly Journal of the Royal Society of London*, **65**, 611-678.

Compton, R. R., 1960. Contact metamorphism in Santa Rosa Range, Nevada. *Geological Society of America Bulletin*, **71**, 1383-1416.

Darbyshire, D. P. F. and Beer, K. E.,1988. Rb-Sr age of the Bennachie and Middleton granites, Aberdeenshire. *Scottish Journal of Geology*, **24**, 189-193.

Davidson, P. M., Grover, J. E. and Lindsley, D. H., 1982. $(Ca,Mg)_2SiO_6$ clinopyroxenes: a solution model based on non-convergent site-disorder. *Contributions to Mineralogy and Petrology*, **80**, 88-102.

Davis, B. T. C. and Boyd, F. R., 1966. The join $Mg_2Si_2O_6$-$CaMgSi_2O_6$ at 30 kilobars pressure and its application to pyroxenes from kimberlites. *Journal of Geophys. Research*, **71**, 3567-3576.

Deer, W. A., Howie, R. A. and Zussman, J., 1992. An Introduction to the Rock Forming Mineral, Harlow, London.

Dempster, T. J., 1983. Studies of orogenic evolution in the Scottish Dalradian. *Unpublished Ph.D. thesis*, University of Edinburgh.

Dempster, T. J., 1985. Uplift patterns and orogenic evolution in the Scottish Dalradian. *Journal of the Geological Society of London,* **142,** 111-128.

Dempster, T. J. and Harte, B., 1986. Polymetamorphism in the Dalradian of the Central Highlands. *Geological Magazine,* **123,** 95-104.

Dewey, J. F., 1969. Evolution of the Appalachian/Caledonian orogen. *Nature,* **222,** 124-129.

Dewey, J. F. & Pankhurst, R. J.1970. The evolution of the Scottish Caledonides in relation to their isotopic age pattern. *Transactions of the Royal Society of Edinburgh,* **68,** 361-389.

Dickerson, R., P. and Holdaway, M., J., 1989. Acadian metamorphism associated with the Lexington batholith, Bingham, Maine. *American Journal of science*, **289**, 945-974.

Downie, C., Lister, T. R., Harris, A. L. and Fettes, D. J., 1971. A palynological investigation of the Dalradian rocks of Scotland. *Report of the Institute of the Geological Sciences, London,* **No. 71/9,** 30pp.

Droop. G. T. R., 1987. A general equation for estimating Fe^{3+} concentration in ferromagnesian silicates and oxides from microprobe analyses, using stoichiometric criteria. *Mineralogical Magazine*, **51**, 431-435.

Droop, G. T. R. & Charnley, N. R., 1985. Comparative geobarometry of pelitic hornfelses associated with the Newer Gabbros: a preliminary study. *Journal of the Geological Society of London,* **122,** 53-62.

Droop, G. T. R. and Treloar, P. J., 1981. Pressure of metamorphism in the thermal aureole of the Etive Complex. *Scottish Journal of Geology,* **17,** 85-102.

Droop. G. T. R. and Harte, B., 1995. The effect of Mn on the phase relations of medium-grade pelites: Constraints from natural assemblages on petrogenetic grid topology. *Journal of Petrology*, **36**, 1549-1578.

Elkins, L. T. and Grove, T. L., 1990. Ternary feldspar experiments and thermodynamic models. *American Mineralogist*, **75**, 544-559.

Ellis, D. J and Green, D. H., 1985. Garnet-forming reactions in mafic granulites from Enderby Land, Antarctica-Implications for Geothermometry and Geobarometry. *Journal of Petrology*, **26(3)**, 633-662.

England, P. C. and Richardson, S. W., 1977. The influence of erosion upon the mineral facies of rocks from different metamorphic environments. *Journal of the Geological Society of London*, **134**, 201-213.

Ernst, W. G., 1976. Petrologic phase equilibria. W. H. Freeman, San Francisco.

Eskola, P., 1914. On the petrologyof the Orijarvi region of southwestern Finland. *Bull. Comm. Geol. De Finland* **40.**

Eskola, P., 1915. On the relation between chemical and mineralogical composition in the metamorphic rocks of the Orijarvi region. *Bull. Comm. Geol. Finland* **44**, 167-225.

Essene, E. J., 1989. The current status of thermobarometry in metamorphic rocks. In: Daly, J. S., Cliff, R. A. and Yardley, B. W. D. (eds) Evolution of metamorphic belts. Blackwell Scientific Publications, Oxford, 1-44.

Evans, N. H. and Speer, J. A., 1984. Low-pressure metamorphism and anatexis of Carolina Slate Belt phyllites in the contact aureole of the Lilesville Pluton, North Carolina, U.S.A. *Contributions to Mineralogy and Petrology*, **12**, 25-62.

Eyles, C. H. and Eyles, N., 1983. Glaciomarine model for upper Precambrian diamictites of the Port Askaig Formation, Scotland. *Geology*, **11**, 692-696.

Fairchild, I. J., 1980. Stages in a Precambrian dolomitisation, Scotland: cementing versus replacement textures. *Sedimentology*, **27**, 631-650.

Fairchild, I. J., 1985. Petrography and carbonate chemistry of some Dalradian dolomitic metasediments: preservation of diagenetic textures. *Journal of the Geological Society of London*, **142**, 167-185.

Ferry, J. M., 1978. Fluid interaction between granite and sediment during metamorphism, South-Central Maine. *American Journal of Science*, **278**, 1025-1056.

Ferry, J. M., 1992. Regional metamorphism of the Waits River Formation, eastern Vermont; delination of a new type of giant metamorphic hydrothermal system. *Journal of Petrology*, **33,1**, 45-94.

Ferry, J. M., Mutti, L. J. and Zuccala, G. J., 1978. Contact metamorphism/hydrothermal alteration of Tertiary basalts from the Isle of skye, northwest Scotland. *Contributions to Mineralogy and Petrology*, **95**, 166-181.

Ferry, J. M. and Spear, F. S., 1978. Experimental calibration of the partitioning of Fe and Mg between biotite and garnet. *Contributions to Mineralogy and Petrology*, **66**, 113-117.

Ferry, J. M., Mutti, L., J., and Zuccala, G. J., 1987. Contact metamorphism/hydrothermal alteration of Tertiary basalts from the Isle of Skye, northwest Scotland. *Contributions to Mineralogy and Petrology*, **95**, 166-181.

Fettes, D. J., 1979. The metamorphic map of the British and Irish Caledonides. In: A. J. Harris et al. (Eds.) The Caledonides of the British Isles, Reviewed, *Geological Society of London Special Publication No. 8*, pp. 323-337. *Scottish Academic Press, Edinburgh.*

Fettes, D. J., Graham, C. M., Harte, B. and Plant, J. A., 1986. Lineaments and basement domains, an alternative view of Dalradian evolution. *Journal of the Geological Society of London*, **143**, 453-464.

Fisher, G. W., 1973. Nonequilibrium thermodynamics and a model for diffusion-controlled metamorphic processes. *American Journal of Science,* **273,** 897-924.

Fleuty, M. J., 1964. The description of folds. *Proceedings of the Geological Association*, **75**, 461-492.

Fraser, D. G., 1977. Thermodynamics in geology. D. Reidel Publishing Company, Dordrecht.

Fraser, D. G. and Lawless, P. J., 1978. Palaeogeotherms: implication of disequilibrium in garnet lherzolite xenoliths. Nature, **273**, 220-222.

Frost, M. J., 1962. Metamorphic grade and iron-magnesium distribution between coexisting garnet-biotite and garnet-hornblende. *Geological Magazine*, **99**, 427-438.

Frost, C. D. and O'Nions, R. K., 1985. Caledonian magma genesis and crustal recycling. *Journal of Petrology*, **26**, 515-544.

Furnham, M. L. and Lindsley, D. H., 1988. Ternary-feldspar modeling and thermometry. *American Mineralogist*, **73**, 201-215.

Ganguly, J. and Saxena, S. K., 1984. Mixing properties of aluminosilicate garnets: constraints from natural and experimental data and applications to geothermo-barometry. *American Mineralogist*, **69**, 88-97.

Ghiorso, M. S., 1984. Activity/composition relations in the ternary feldspars. *Contributions to Mineralogy and Petrology*, **87**, 282-296.

Glover, B. W. 1993. The sedimentology of the Neoproterozoic Grampian Group and the significance of the Fort William Slide between Spean Bridge and Rubha Cuilcheanna, Inverness-shire. *Scottish Journal of Geology*, **29**, 29-43.

Goldman, J. R. and Albee, A. L., 1977. Correlation of Fe/Mg partitioning between garnet and biotite with $^{18}O/^{16}O$ partitioning between quartz and magnetite. *American Journal of Science*, **277**, 750-761.

Goldschmidt, V., M., 1911. Die Kontakt metamorphose in kristianiagebiet. *Lkr. Videnskselsk, Kristiana* **1**, 483 p.

Goodman, S. and Winchester, J., A., 1993. Geochemical variations within metavolcanic rocks of the Dalradian Farragon Beds and adjacent formations. *Scottish Journal of Geology*, **29**, 131-141.

Gower, P. J., 1973. The middle-upper Dalradian boundary with special reference to the Loch Tay Limestone. *Unpublished Ph.D. thesis*, University of Liverpool.

Graham, C. M., 1976. Petrochemistry and tectonic significance of Dalradian metabasaltic rocks of the S.W. Scottish Highlands. *Journal of the Geological Society of London,* **132,** 61-84.

Graham, C. M., 1986. The role of the Cruachan Lineament during Dalradian evolution. *Scottish Journal of Geology,* **22,** 257-270.

Graham, C. M. and., Bradbury, H. J., 1981. Cambrian and late Precambrian basaltic igneous activity in the Scottish Dalradian: a review. *Geological Magazine*, **118**, 27-37.

Graham, C. M., Greig, K. M., Sheppard, S. M. F. and Turi, B. 1983. Genesis and mobility of the H_2O-CO_2 fluid phase during regional greenschist and epidote amphibolite facies metamorphism: a petrological and stable isotope study in the Scottish Dalradian. *Journal of the Geological Society of London,* **140,** 577-599.

Grant, J. A., 1985. Phase equilibria in partial melting of pelitic rocks. In: *Migmatites*, J. R. Ashworth (editor), 86-144. Blackie, Glasgow.

Grant, J. A. and Frost, B. R., 1990. Contact metamorphism and partial melting of pelitic rocks in the aureole of the Laramie anorthosite complex, Morton Pass, Wyoming. *American Journal of Science*, **290**, 425-427.

Grapes, R. H. and Graham, C. M., 1978. The actinolite-hornblende series in metabasites and the so-called miscibility gap: A review. *Lithos*, **11**, 85-97.

Green, N. L. and Usdansky, S. I., 1986. Ternary-feldspar mixing relations and thermobarometry. *American Mineralogist*, **71**, 1100-1108.

Gresens, R. L., 1967. Composition-volume relationship of metasomatism. *Chemical Geology*, **2,** 47-55.

Gribble, C. D., 1966. The thermal aureole of the Haddo House norite in Aberdeenshire. *Scottish Journal of Geology*, **3**, 306-313.

Gribble, C. D., 1967. The basic intrusive rocks of Caledonian age in the Haddo House and Arnage districts, Aberdeenshire. *Scottish Journal of Geology*, **3**, 125-136.

Gribble, C. D., 1968. The cordierite-bearing rocks of the Haddo House and Arnage District, Aberdeenshire. *Contributions to Mineralogy and Petrology*, **17**, 315-330.

Groom, D. R. and Hall, A., 1974. The geochemistry of the Devonian lavas of the northern Lorne Plateau, Scotland. *Mineralogical Magazine*, **39**, 621-640.

Guidotti, C. V. 1984. Micas in metamorphic rocks. In: Bailey., S. W. (ed) , Micas. *Reviews in Mineralogy*. Volume **13**. Mineralogical Society of America.

Gunn, A. G., Styles, M. T., Stephenson, D., Shaw, M. H. and Rollin, K. E., 1990. Platinum-group elements in ultramafic rocks of the Upper Deveron Valley, near Huntly, Aberdeenshire. Mineral Reconnaissance report, British Geological Survey, No. 115.

Gunter, A. E., 1977, Annual Meeting of the Geologists Association of Canada, Abstract. **22.**

Hackler, R. T. and Wood, B. J., 1984. Experimental determination of Fe and Mg exchange between garnet and olivine and estimation of Fe-Mg garnet mixing properties. *American Mineralogist*, **74**, 994-999.

Hall, J., 1985. Geophysical constraints on crustal structure in the Dalradian region of Scotland. *Journal of the Geological Society of London*, **142**, 149-155.

Hall, J., Brewer, J. A., Matthews, D. H. and Warner, M. R., 1984. Crustal structure across the Caledonides from the "WINCH" seismic reflection profile: influence on the evolution of the Midland Valley of Scotland. *Transactions of the Royal Society of Edinburgh*, **75**, 97-109.

Halliday, A. N., Graham, C. M., Aftalion, M. and Dymoke, P., 1989. The depositional age of the Dalradian Supergroup: U-Pb and Sm Nd isotopic studies of the Tayvallich Volcanics, Scotland. *Journal of the Geological Society of London,* **146,** 3-6.

Halliday, A. N., Aftalion, M., Van Breeman, O., and Jocelyn, J., 1979. Petrogenetic significance of Rb-Sr and U-Pb isotopic systems in 400 Ma old British Isles granitoids and their hosts. In: The Caledonides of the British Isles-reviewed. Harris, A. L., Holland, C., H., and Leake, B. E. (editors). 653-661. *Special Publication of the Geological Society of London*, No. 8.

Hammarstrom, J. M. and Zen, E-an, 1986. Aluminium in hornblende: an empirical geobarometer. *American Mineralogist*, **71**, 1297-1313.

Harker, A., 1909. The natural history of igneous rocks. *Methen, London.*

Harker, A., 1952. Metamorphism (3rd ed.) London.

Harley, S.L., 1994. Cordierite as a sensor of fluid and melt distribution in crustal metamorphism. *Mineralogical Magazine*, **58A**, 374-375.

Harmon, R. S., 1983. Oxygen and strontium isotopic evidence regarding the role of continental crust in the origin and evolution of British Caledonian granites. In: Atherton, M. P., Gribble, C. D. (editors) *Migmatites, melting and metamorphism*, Shiva, Kent, pp 62-79.

Harmon, R. S. and Halliday, A. N., 1980. Oxygen and strontium isotope relationships in the British late Caledonian granites. *Nature,* **283**, 21-25.

Harmon, R. S., Pankhurst, R. J., Plant, J. A., and Simpson, P. R., 1984. Petrogenesis of the Cairngorm granite, east-central Grampian Highlands, scotland. In: *Open magmatic system.* 72-73. *Proceedings of ISEM field conference*. Duncan, M. A., Grove, T. L. and Hildreth, W. (editors). (Dallas, Texas: Southern Methodist University).

Harper, C. T., 1967. The geological interpretation of potassium-argon ages of metamorphic rocks from the Scottish Highlands. *Scottish Journal of Geology,* **3,** 46-66.

Harris, A. L., 1963. Structural investigations in the Dalradian rocks between Pitlochry and Blair Atholl. *Transactions of the Edinburgh Geological Society*, **19**, 256-278.

Harris, A. L., Bradbury, H. J. and Mc Gonigal, M. H., 1976. The evolution and transport of the Tay nappe. *Scottish Journal of Geology*, **12**, 103-113.

Harris, A. L., Baldwin, C. T., Bradbury, H. J., Johnson. H. D. and Smith, R. A., 1978. Ensialic basin sedimentation: the Dalradian Supergroup. In: Bowes and Leake (Eds.)

Crustal evolution in north-western Britain and adjacent regions. Seel House Press, Liverpool.

Harris, A. L. & Pitcher, W. S., 1975. The Dalradian Supergroup. In: Harris, A. L. *et al.*, (eds). A correlation of Precambrian rocks in the British Isles. *Special Report of the Geological Society of London*, **6**, 52-75.

Harrison, T. N., and Hutchinson, J., 1987. The age and origin of the Eastern Grampian Newer Granites. *Scottish Journal of Geology*, **23**, 269-282.

Harte, B., 1975. Determination of a pelitic petrogenetic grid for the eastern Scottish Dalradian. *Year Book of the Carnegie Institute, Washington,* **74,** 438-446.

Harte, B., 1988. Lower Palaeozoic metamorphism in the Moine-Dalradian belt of the British Isles. In: Harris *et. al.* (Eds.) The Caledonian-Appalachian Orogen. *Geological Society of London,* **38,** 123-134.

Harte, B. and Johnson, M. R. W., 1969. Metamorphic history of Dalradian rocks in Glens Clova, Esk and Lethnot, Angus, Scotland. *Scottish Journal of Geology,* **5,** 54-80.

Harte, B. and Graham, C. M., 1975. The graphical analysis of greenschist to amphibolite facies mineral assemblages in metabasites. *Journal of Petrology*, **16**, 347-370.

Harte, B. and Hudson, N. F. C., 1979. Pelitic facies series and the temperature and pressure of Dalradian metamorphism in E Scotland. In: A. J. Harris et al. (Eds.) The Caledonides of the British Isles, Reviewed, *Geological Society of London Special Publication No. 8*, pp. 323-337. *Scottish Academic Press, Edinburgh.*

Harte, B., Booth, J. E., Dempster, T. J., Fettes, D. J., Mendrum, J. R. and Watts, D., 1984. Aspects of the post depositional evolution of the Dalradian and Highland Boundary rocks in the Southern Highlands of Scotland. *Transactions of the Royal Society of Edinburgh,* **75,** 151-163.

Harte, B., Pattison, D. R. M. and Linklater, C. M., 1991. Field relations and petrography of partially melted pelitic and semi-pelitic rocks. In: Equilibrium and kinetics in contact metamorphism: The Ballachulish Igneous Complex and its thermal aureole. (eds. Voll, G., Töpel, J., Pattison, D. R. M. and Seifert, F.) Springer-Verlag, Heidelberg.

Harwood, D. S., 1966. Geology of the Cupsuptic quadrangle, Maine. *U. S. Geological Survey, Open File Report*, 259 p.

Haselton, H. T. and Newton, R. C., 1980. Thermodynamic properties of pyrope-grossular garnets and their stabilities at high temperatures and high pressures. *Journal of Geophys. Research*, **85**, 6973-6982.

Haselton, H. T., Hovis, G. L., Hemingway, B. S. and Robie, R. A., 1983. Calorimetric investigation of the excess entropy of mixing in analbite-sanidine solid solutions:

lack of evidence for Na, K short-range order and implications for two-feldspar thermometry. *American Mineralogist.* **68**, 398-413.

Haslam, H. W. and Kimbell, G. S., 1981. Disseminated copper-molybdenum mineralisation near Ballachulish, Highland region. *Mineral Reconnaissance Report, British Geological Survey*, No. 43.

Helgeson, H. C., Delany, J. M., Nesbitt H. W. and Bird, D. K., 1978. Summary and critique of the thermodynamic properties of rock-forming minerals. *American Journal of Science*, **278A**, 1-299.

Heuss-Aβbichler, S. and Masch, L., 1991. Microtextures and reaction mechanisms of carbonate rocks: A comparison between the thermoaureoles of Ballachlish and Monzoni (Italy). In: Equilibrium and kinetics in contact metamorphism: The Ballachulish Igneous Complex and its aureole. (eds. Voll, G., Topel, J., Pattison, D. R. M. and Seifert, F.). Springer-Verlag: Heidelberg.

Hickman, A. H., 1975. The stratigraphy of late Precambrian metasediments between Glen Roy and Lismore. *Scottish Journal of Geology,* **11,** 117-142.

Hickman, A. H. and Wright, A. E., 1983. Geochemistry and chemostratigraphical correlation of slates, marbles and quartzites of the Appin Group, Argyll, Scotland. *Transactions of the Royal Society of Edinburgh: Earth Sciences*, **73**, 251-278.

Highton, A., J., 1992. The tectonostratigraphical significance of pre-750 Ma metagabbros within the northern Central Highlands, Inverness-shire. *Scottish Journal of Geology*, **28**, 71-76.

Hinton, R. W., 1995. Ion microprobe analysis in geology. In: Microprobe Techniques in the Earth Sciences. Pott, P. J., Bowles, F. W., Reed, S. J. B. and Cave, M. R. (editors). *The Mineralogical Society Series*, **6**,. Chapman and Hall, London.

Hinxman, L. W., Carruthers, R. G. and MacGregor, M., 1923. The geology of Corrour and the Moor of Rannoch. Memoir of the Geological Survey. Scotland, Sheet 54 (Scotland).

Hipkin, R. G. and Hussain, A., 1983. Regional gravity analysis: North Britain. *Report of Institute of Geological Science, London,* **82.**

Hodges, K. V. and Spear, F. S., 1982. Geothermometry, geobarometry and the Al2SiO5 triple point at Mt. Moosilauke, New Hampshire. *American Mineralogist.* **67**, 1118-1134.

Hoersch, A. L., 1981. Progressive metamorphism of the chert-bearing Durness Limestone in the Beinn an Dubhaich aureole, Isle of Skye, Scotland: A re-examination. *American Mineralogist*, **66**, 491-506.

Hoisch, T. D., 1991. Equilibria within the mineral assemblage quartz+muscovite+ biotite+garnet+plagioclase, and implications for the mixing properties of octahedrally-coordinated cations in muscovite and biotite. *Contributions to Mineralogy and Petrology*, **108**, 43-54.

Holdaway, M. J., 1971. Stability of andalusite and the aluminum silicate phase diagram. *American Journal of Science*, **271**, 97-131.

Holdaway, M. J. and Lee, S. M., 1977. Fe-Mg cordierite stability in high-grade pelitic rocks based on experimental, theoretical and natural observations. *Contributions to Mineralogy and Petrology*, **63**, 175-198.

Holland, T. J. B. and Blundy, J., 1994. Non-ideal interactions in calcic amphiboles and their bearing on amphibole-plagioclase thermometry. *Contributions to Mineralogy and Petrology*, **116**, 433-447.

Holland, T. J. B. and Powell, R.,1985. An internally consistent thermodynamic data set with uncertainties and correlations: 2 Data and results. *Journal of Metamorphic Geology*, **3(4)**, 343-370.

Holland, T. J. B. and Powell, R., 1990. An enlarged and updated internally consistent thermodynamic dataset with uncertainties and correlations: the system K_2O-Na_2O-CaO-MgO-MnO-FeO-Fe_2O_3-Al_2O_3-TiO_2-SiO_2-C-H_2-O_2. *Journal of Metamorphic Geology*, **8**, 89-124.

Holland, T. J. B. and Powell, R., 1998. An internally consistent thermodynamic data set for phases of petrological interest. *Journal of Metamorphic Geology*, **16**, 309-343.

Holland, T. J. B., Navrotsky, A. and Newton, R. C., 1979. Thermodynamic parameters of $CaMgSi_2O_6$-$Mg_2Si_2O_6$ pyroxenes based on regular solution and cooperative disordering models. *Contributions to Mineralogy and Petrology*, **69**, 337-344.

Hollister, L. S., Grissom, G. C., Peters E. K., Stowell, H. H. and Sisson, V. B., 1987. Confirmation of the empirical correlation of aluminum in hornblende with pressure of solidification of calc-alkaline plutons. *American Mineralogist*, **72**, 231-239.

Holmquist, P. J., 1921. Typen und Nomenklatur der Adergesteine. *Geologiska Föreningens i Stockholm Förhandlingar*, **43**, 613-631.

Holness, M. B., 1992. Metamorphism and fluid infiltration of the calc-silicate aureole of the Beinn an Dubhaich Granite, Skye. *Journal of Petrology*, **33**, 1261-1293.

Hubbert, M. K. and Rubey, W. W., 1959. Role of fluid pressure in mechanics of overthrust faulting I. Mechanics of fluid-filled porous solids and its application to overthrust faulting. *Geological Society of America Bulletin*, **709**, 115-166.

Hudson, N. F. C., 1980. Regional metamorphism of some Dalradian pelites in the Buchan area, northeast Scotland. *Contributions to Mineralogy and Petrology*, **73**, 39-51.

Hudson, N. F. C., 1985. Conditions of Dalradian metamorphism in the Buchan area. *Journal of the Geological Society of London*, **142**, 63-76.

Hudson, N. F. C. and Harte, B., 1985. K_2O-poor, aluminous assemblages from the Buchan Dalradian, and the variety of ortho amphibole assemblages in aluminous bulk composition in the amphibolite facies. *American Journal of Science,* **285,** 224-266.

Indares, A. and Martignole, J., 1985. Biotite-garnet geothermometry in the granulite facies: the influence of Ti and Al in biotite. *American Mineralogist*, **70**, 272-278.

Ishii, T., 1975. The relation between temperature and composition of pigeonite in some lavas and their application to geothermometry. *Mineral. J. (Jpn)*, **8**, 48-57.

Jenkins, R. and De Vries, J. L., 1970. Practical X-ray spectrometry. *Phillips technical library, Macmillan.*

Jenkins, D. M., Holland, T. J. B. and Clare, A. K., 1991. Experimental determination of the pressure-temperature stability field and thermochemical properties of synthetic tremolite. *American Mineralogist*, **76**, 458-469.

Joesten, R. L., 1991. Kinetics of Coarsening and diffusion-controlled mineral growth. *In: Contact Metamorphism*, Kerrick, D. M. (ed.). *Reviews in Mineralogy*, **26**, Mineralogical Society of America

Johannes, W., 1983. On the origin of layered migmatites. In: *Migmatites, Melting and Metamorphism* (eds Atherton, M. P. & Gribble, C. D.), pp. 234-248. Shiva Publishing, Nantwich, UK.

Johannes, W., 1984. Beginning of melting in the granite system Qz-Or-Ab-An-H_2O. *Contributions to Mineralogy and Petrology*, **86**, 264-273.

Johannes, W., 1988. What controls partial melting in migmatites? *Journal of Metamorphic Geology,* **6,** 451-465.

Johnson, M. R. W., 1962. Relations of movement and metamorphism in the Dalradians of Banffshire. *Transactions of the Geological Society of Edinburgh*, **19,** 29-64.

Johnson, M. R. W., 1963. Some time relations of movement and metamorphism in the Scottish Highlands. *Geologie Mijnb.* ,**42,** 121-142.

Johnson, M. R. W., 1991. Dalradian. In: Craig, G. Y. (editor) *Geology of Scotland,3rd edition,* pp. 125-160. The Geological Society, London.

Johnstone, G., S., 1975. The Moine Succession. In: A correlation of Precambrian rocks in the British Isles. Harris, A. L., and others (editors) pp 30-42. *Special Report of the Geological Society of London*, No. 6.

Johnstone, G. S and Smith, D. I., 1965. Geological observations concerning the Breadalbane Hydroelectric Project, Perthshire. *Bulletin of the Geological Survey of Great Britain*, No. **22**, 1-52.

Kerrich, R., Beckinsale, R. D. and Durham, J. J., 1977. The transition between deformation regimes dominated by intercrystalline diffusion and intercrystalline creep evaluated by oxygen isotope thermometry. *Tectonophysics*, **38**, 241-257.

Kerrick, D. M. 1977. The genesis of zoned skarns in the Sierra Nevada, California. *Journal of Petrology*, **18**, 144-181.

Kerrick, D. M., 1990. The Al_2SiO_5 polymorphs. *Review in Mineralogy, Mineralogical Society of America*, **22.**

Kerrick, D. M., 1991. Overview of contact metamorphism. In: *Contact Metamorphism*, Kerrick, D. M. (ed.). *Reviews in Mineralogy*, **26**, Mineralogical Society of America.

Kerrick, D. M. and Darken, L. S., 1975. Statistical thermodynamic models for ideal oxide and silicate solid solution with application to plagioclase. *Geochemica et Cosmochemica Acta*, **39**, 1431-1442.

Kerrick, D. M., Lasaga, A. C. and Raeburn, S. P., 1991. Kinetics of heterogeneous reactions. In: *Contact Metamorphism*, Kerrick, D. M. (ed.). *Reviews in Mineralogy*, **26**, Mineralogical Society of America

Klein, C., 1969. Two amphibole assemblages in the system actinolite-hornblende-glaucophane. *American Mineralogist.* **54,** 212-237.

Klein, G. DE V., 1970. Tidal origin of a Precambrian quartzite- the Lower Fine-Grained Quartzite (Middle Dalradian) of Islay, Scotland. *Journal of Sedimentary Petrology,* **40,** 973-985.

Kneller, B. C., 1988. The geology of part of Buchan. Unpublished Ph.D. thesis, University of Aberdeen.

Kneller, B., C., and Aftalion, M., 1987. The isotopic and structural age of the Aberdeen Granite. *Journal of the Geological Society of London*, **144**, 717-721.

Knill, J. L., 1959. Palaeocurrents and sedimentary facies of the Dalradian metasediments of the Craignish-Kilmelfort district. *Proceedings of the Geological Association of London,* **70,** 273-284.

Knill, J. L., 1963. A sedimentary history of the Dalradian Series. In: Johnson, M. R. W. and Stewart, F. H. (Eds,) *The British Caledonides.* Oliver & Boyd, London and Edinburgh.

Kretz, R., 1981. Site-occupancy interpretation of the distribution of Mg and Fe between orthopyroxene and clinopyroxene in metamorphic rocks. *Canadian Mineralogist,* **19,** 493-500.

Kretz, R., 1982. Transfer and exchange equilibria in a portion of the pyroxene quadrilateral, as deduced from natural and experimental data. *Geochimica et Cosmochimica Acta*, **46**, 411-421.

Kretz, R., 1983. Symbols for rock forming minerals. *American Mineralogist,* **68,** 277-279.

Kunyioshi, S., and Liou, J., G., 1976. Contact metamorphism of the Karmutsen Volcanics, Vancouver Island, British Colombia. *Journal of Petrology*, **17**, 73-99.

Kurepin, V.A., 1985. H_2O and CO_2 contents of cordierite as an indicator of thermodynamic conditions of formation. *Geochemistry International*, **22**, 148-156.

Kynaston, H. and Hill, J. B., 1908. The geology of the country near Oban and Dalmally. *Memoir of the Geological Survey, Scotland*, Sheet 45 (Scotland).

Labotka, T. C., Papike, J. J. and Vaniman, D. T., 1981. Petrology of contact metamorphosed argillite from the Rove Formation, Gunflint Trail, Minnesote. *American Mineralogist*. **66**, 70-86.

Labotka, T. C., Nabelek, P. I. and Papike, J. J., 1988. Fluid infiltration through the Big Horse Limestone member in the Notch Peak contact-metamorphic aureole. *American Mineralogist*, **73**, 1302-1324.

Labotka, T. C., White, T. C. and Papike, J. J., 1984. The evolution of water in the contact-metamorphic aureole of the Duluth Complex, northeastern Minnesota. *Geological Society of America Bulletin*, **95**, 788-804.

Lamb, W.M. and Valley, J.W., 1985, C-O-H fluid calculations and granulite genesis, *in* Tobi, A.C. and Touret, J.R.L., eds., The deep Proterozoic crust in the north Atlantic provinces: Dordrecht, D. Reidel, p. 119-131.

Lambert, R. St. J., 1959. The mineralogy and metamorphism of the Moine Schists of the Morar and Kroydart districts of Inverness-shire. *Transactions of the Royal Society of Edinburgh,* **63**, p. 553.

Lambert, R. St. J. and McKerrow, W. S., 1976. The Grampian Orogeny. *Scottish Journal of Geology,* **12,** 271-292.

Lambert, R. St. J., Holland, J. E. and Leggett, J. K., 1981. Petrology and tectonic setting of some Ordovician volcanic rocks from the Southern Uplands of Scotland. *Journal of the Geological Society of London,* **138,** 421-436.

Lambert, R. St. J., Holland, J. G. and Winchester, J. A., 1982. A geochemical composition of the Dalradian Leven Schist and the Grampian Division Monadhliath Schist of Scotland. *Journal of the Geological Society of London*, **139**, 71-84.

Leake, B. E., 1971. On aluminous and edenitic hornblendes. *Mineralogical Magazine*, **38**, 389-407.

Leake, B. E., 1978. Nomenclature of amphiboles. *Mineralogical Magazine*, **42**, 533-563.

Leake, B. E., 1982. Volcanism in the Dalradian. 45-50 In: Igneous rocks of the British Isles. Southerland, D. S. (editor). John Wiley and Sons, Chichester.

Le Maitre R. W., Bateman P., Dudek A., Keller J., Lameyer Le Bas M. J., Sabine P. A.,

Schmid R., Sorensen H., Streckeisen, A., Wooley A. R. and Zanettin B., 1989. A classification of igneous rocks and glossary of terms. *Blackwell, Oxford.*

Lindsley, D. H., 1983. Pyroxene thermometry. *American Mineralogist*, **68**, 477-493.

Lindley, D. H. and Anderson, D. J., 1983. A two-pyroxene thermometer. *Proc. 13th Lunar Planet. Sci. Conf. Part 2, J. Geophys. Res.* **88** Sup. A887-A906.

Lindsley, D. H., Grover, J. E. and Davidson, P. M., 1981. The thermodynamics of the $Mg_2Si_2O_6$-$CaMgSi_2O_6$ join: a review and an improved model. *Adv. Phys. Geochem.* **1**, 149-175.

Litherland, M., 1970. The stratigraphy and structure of the Dalradian rocks around Loch Creran, Argyll. *Unpublished Ph.D. thesis*, University of Liverpool.

Litherland, M., 1980. The stratigrapgy of the Dalradian rocks around Loch Creran, Argyllshire. *Scottish Journal of Geology*, **16**, 105-123.

Litherland, M., 1982. The structure of Loch Creran Dalradian and a new model for the SW Highlands. *Scottish Journal of Geology*, **18**, 205-225.

Loomis, T. P., 1972a. Contact metamorphism of pelitic rocks by the Ronda ultramafic intrusion, southern Spain. *Geological Society of America Bulletin*, **83**, 2449-2474.

Loomis, T. P., 1972b. Coexisting aluminium silicate phases in contact metamorphic aureole. *American Journal of Science*, **272**, 933-945.

Loomis, T. P., 1975. Reaction zoning of garnet. *Contributions to Mineralogy and Petrology.* **52**, 285-305.

MacCulloch, J., 1817. Observations on the mountain Cruachan in Argyllshire, with some remarks on the surrounding country. *Transactions of the Geological Society of Great Britain*, **4**, 117-138.

Manning, C. E. and Bird, D. K., 1991. Porosity evolution and fluid flow in the basalts of the Skaergaard magma-hydrothermal system, east Greenland. *American Journal of Science*, **291**, 201-257.

Masch, L. and Heuss-Aβbichler, S., 1991. Decarbonation reactions in siliceous dolomites and impure limestones. In: G. Voll, J. Topel, D. R. M. Pattison and F. Seifert, (eds.), Equilibrium and kinetics in Contact Metamorphism: The Ballachulish Igneous Complex and its Aureole. Springer-Verlag, Berlin.

Mason, D. R. 1991 CIPWNorm program for Macintosh, version 3.3. .

Mather, J. D., 1970. The biotite isograd and the lower greenschist facies in the Dalradian rocks of Scotland. *Journal of Petrology,* **11,** 253-275.

McCallien, W. J.,1927. Preliminary account of the post-Dalradian geology of Kintyre. *Transactions of the Geological Society of Glasgow*, **18**, 40-126.

McCallien, W., J., 1929. The metamorphic rocks of Kintyre. *Transactions of the Royal Society of Edinburgh*, **56**, 409-436.

Mc Donough, W. F., Sun, S., Ringwood, A. E., Jagoutz E. and Hofmann, A. W., 1991. K, Rb, and Cs in the earth and moon and the evolution of the earth's mantle. *Geochemica et Cosmochemica Acta*, Ross Taylor Symposium volume.

McLellan, M., 1985. Metamorphic reactions in the kyanite and sillimanite zones of the Barrovian type area. *Journal of Petrology*, **26**, 789-818.

McLennan, E. L., 1985. Metamorphic reactions in the kyanite and sillimanite zones of the Barrovian type area. *Journal of Petrology*, **26**, 789-818.

Mehnert, K. R., 1968. *Migmatites and the Origin of Granitic Rocks.* Elsevier, Amsterdam.

Mendum, J. R. & Fettes, D. J., 1985. The Tay Nappe and associate folding in the Ben Ledi-Loch Lomond area. *Scottish Journal of Geology*, **21**, 41-56.

Mercier, J.-C. C., 1976. Single-pyroxene geothermometry and geobarometry. *American Mineralogist*, **61**, 603-615.

Miller, J. A. and Brown, P. E., 1965. Potassium-argon age studies in Scotland. *Geological Magazine*, **102**, 106-134.

Mirwald, P.W. and Schreyer, W., 1977. Die stabile und metastabile Abbaureaktion von Mg-Cordierit in Talk, Disthen und Quarz und ihre Abhangigkeit vom leichgewichtswassergehalt des Cordierits. *Fortschr. Mineral*, **55**, 95-97.

Mirwald, P.W., Maresch, W.V. and Schreyer, W., 1979. Der Wassergehalt von Mg-Cordierite zwischen 500° und 800°C sowie 0.5 und 11 kbar. *Fortschritte der Mineralogie,* **57**, Bh. 1, 101-102.

Moles, N. R., 1985. Metamorphic conditions and uplift history in central Perthshire: evidence from mineral equilibria in the Foss celsian-barite-sulphide deposit. *Journal of the Geological Society of London*, **142**, 39-52.

Moore, J, M., Jr., 1960 Phase relation in the contact aureole of the Onawa Puton, Maine. Ph.D. Dissertation, Massachusetts Institute of Technology, 187 pp.

Moore, J. N. and Kerrick, D. M., 1976. Equilibria in siliceous dolomites of the Alta aureole, Utah. *American Journal of Science*, **276,** 502-524.

Munro, M., 1965. Some structural features of the Caledonian granitic complex at Strontian, Argyll. *Scottish Journal of Geology*, **9**, 99-108.

Munro, M., 1970. A reassessment of the 'younger' basic igneous rocks between Huntly and Portsoy based on new borehole evidence. *Scottish Journal of Geology*, **6**, 41-52.

Munro, M., 1984. Cumulate relations in the 'Younger Basic' masses of the Huntly-Portsoy area, Grampian region. *Scottish Journal of Geology*, **20**, 343-359.

Munro, M., 1986a. Mylonite zones in the Insch 'Younger Basic' Mass. *Scottish Journal of Geology*, **22**, 132-136.

Munro, M., 1986b. Geology of the country around Aberdeen. *Memoir of the British Geological Survey*, Sheet 77 (Scotland).

Munro M. and Gallaghar, J. W., 1984. Disruption of the 'Younger Basic' masses in the Huntly-Portsoy area, Grampian Region. *Scottish Journal of Geology*, **20**, 361-382.

Newton, R.C. and Wood, B.J., 1979. Thermodynamics of water in cordierite and some petrologic consequences of cordierite as a hydrous system. *Contributions to Mineralogy and Petrology*, **68**, 391-405.

Newton, R. C., Charlu, T. V. and Kleppa, O. J., 1980. Thermochemistry of the high structural state plagioclases. *Geochimica et Cosmochimica Acta.*, **44**, 933-941.

Nichols, G. T., Berry, R. F. and Green, D. H., 1992. Internally consistent gahnitic spinel-cordierite-garnet equilibria in the FMASHZn system: geothermobarometry and applications. *Contributions to Mineralogy and Petrology*, **111**, 362-377.

Nicol, J., 1852. On the geology of the southern portion of the peninsula of Cantyre, Argyllshire. *Quarterly Journal of the Geological Society of London*, **8**, 406-425.

Nicolas, A. and Jackson, M., 1982. High temperature dikes in peridotites: Origin by hydraulic fracturing. *Journal of Petrology*, **23**, 568-582.

Nockolds, S. R., 1934. The contaminated tonalite of Loch Awe, Argyll. *Ibid*, **105**, 302-321.

O'Conner, J. T., 1965. A classification for quartz-rich igneous rocks based on feldspar ratios. *U.S. Geological Survey Professional paper*, **525B**, B79-B84.

Oki, Y., 1958. Thermally metamorphosed rocks in the northern Kiso mountain range, Central Japan. *Journal of the Geological Society of Japan*, **64**, 1-12.

Oki, Y., 1961. Metamorphism in the northern Kiso Range, Nagano Prefecture, Japan. *Japanese Journal of Geology and Geophysics*, **32**, 479-496.

Okrusch, M., 1969. Die Gneishornfelse um Steinach in der Oberpfalz. *Contributions to Mineralogy and Petrology*, **22**, 32-71.

Okrusch, M., 1971. Garnet-cordierite-biotite equilibria in the Steinach aureole, Bavaria. *Contributions to Mineralogy and Petrology*, **32**, 1-23.

Olsen, S. N., 1985. Mass balance in migmatites. In: *Migmatites* (ed. Ashworth, J. R.), pp. 145-179. Blackie, Glasgow.

Orville, P. M., 1972. Plagioclase cation exchange equlibria with aqueous chloride solution: results at 700°C and 2000 bars in the presence of quartz. *American Journal of Science*, **272**, 234-272.

Pankhurst, R. J., 1970. The geochronology of the basic igneous complexes. *Scottish Journal of Geology*, **6**, 83-107.

Pankhurst, R. J., 1974. Rb-Sr whole-rock chronology of Caledonian events in northeast Scotland. *Bulletin of the Geological Society of America*, **85**, 345-350.

Pankhurst, R. J., 1979. Isotope and trace element evidence for the origin and evolution of Caledonian granites in the Scottish Highlands. 18-33, in: Origin of granite batholites: geochemical evidence. Atherton, M. P. and Tarney, J. (editors). Shiva, Orpington.

Pantin, H. M., 1961. The stratigraphy and structure of the Blair Atholl-Bena'Gloe area, Perthshire, Scotland. *Transactions of the Royal Society of New Zealand*, **88**, 597-622.

Parsons, I. and Brown, W. L., 1983. A TEM and microprobe study of a two-perthite alkali gabbro: implications for the ternary feldspar system. *Contributions to Mineralogy and Petrology*, **82**, 1-12.

Patiño Douce, A. E., and Johnstone, A. D., 1991. Phase equilibria and melt productivity in the pelitic system: implications for the origin of peraluminous granitoids and aluminous granites. *Contributions to Mineralogy and Petrology,* **107,** 202-218.

Patiño Douce, A. E., Johnstone, A. D. & Rice, J. M., 1993. Octahedral excess mixing properties in biotite: a working model with applications to geothermometry and geobarometry. *American Mineralogist*, **78**, 113-131.

Pattison, D. R. M., 1991. P-T-a(H_2O) conditions in the thermal aureole. In: Equilibrium and kinetics in contact metamorphism: The Ballachulish Igneous Complex and its aureole. (eds. Voll, G., Topel, J., Pattison, D. R. M. and Seifert, F.). Springer-Verlag: Heidelberg.

Pattison, D. R. M., 1987. Variation in Mg/(Mg+Fe), F, and (Fe,Mg)Si=2Al in pelitic minerals in the Ballachulish thermal aureole, Scotland. *American Mineralogist*, **72,** 255-272.

Pattison, D. R. M. and Tracy, R. J., 1991. Phase equilibria and thermobarometry of metapelites. In: Contact metamorphism., Kerrick, D. M. (ed). *Reviews in Mineralogy,* **26,** Mineralogical Society of America.

Pattison, D. R. M. and Harte, B., 1985. A petrogenetic grid for pelites in the Ballachulish aureole and other Scottish thermal aureoles. *Journal of the Geological Society of London*, **142**, 7-28.

Pattison, D. R. M. and Harte, B., 1988. Evolution of structurally contrasting anatectic migmatites in the 3-kbar Ballachulish aureole, Scotland. *Journal of Metamorphic Geology,* **6,** 475-494.

Pattison, D. R. M. and Harte, B., 1991. Petrography and mineral chemistry of pelites. In: Equilibrium and kinetics in contact metamorphism: The Ballachulish Igneous

Complex and its aureole. (eds. Voll, G., Topel, J., Pattison, D. R. M. and Seifert, F.). Springer-Verlag: Heidelberg.

Pattison, D. R. M. and Voll, G., 1991. Regional geology of the Ballachulish area. In: Equilibrium and kinetics in contact metamorphism: The Ballachulish Igneous Complex and its aureole. (eds. Voll, G., Topel, J., Pattison, D. R. M. and Seifert, F.). Springer-Verlag: Heidelberg.

Peacock, J. D., Berridge, N. G., Harris, A. L. and May, F., 1968. The geology of the Elgin district. *Memoir of the Geological Survey of Scotland*, Sheet 95 (Scotland).

Pearce, J. A. and Cann, J. R., 1971. Ophiolite origin investigated by discriminant analysis using Ti, Zr and Y. *Earth and Planetary Sciences Letters*, **12,** 339-349.

Pearce, J. A. and Cann, J. R., 1973. Tectonic setting of basic volcanic rocks determined using trace element analyses. *Earth and Planetary Science Letters*, **19,** 290-300.

Pearce, J. A., Harris, N. B. W. and Tindle, A. G., 1984. Trace element discriminant diagrams for the tectonic setting of granitic rocks. *Journal of Petrology*, **25**, 956-983.

Perchuk, L. L. and Lavrent'eva, I. V., 1983. Experimental investigation of exchange equilibria in the system cordierite-garnet-biotite. In: Saxena, S. K. (ed) Kinetics and equilibrium in mineral reactions. Springer, New York, 199-239.

Perkins, E. H., Brown, T. H. and Berman, R. G., 1986. PTX-SYSTEM: Three programs for calculation of pressure-temperature-composition phase diagrams. *Computers and Geosciences*, **12**, 749-755.

Philbrick, S. S., 1936. The contact metamorphism of the Onawa Pluton, Piscataquis County, Maine. *American Journal of Science*, **231**, 1-40.

Phillips, W. E. A., Stillman, C. J. and Murphy, T., 1976. A Caledonian plate tectonic model. *Journal of the Geological Society of London,* **32,** 579-609.

Piasecki, M. A. J., 1980. New light on the Moine rocks of the Central Highlands of Scotland. *Journal of the Geological Society of London,* **137,** 41-59.

Piasecki, M. A. J. and van Breemen, O., 1979a. A Morarian age for the 'Younger Moines' of central and western Scotland. *Nature*, **278**, 734-736.

Piasecki, M. A. J. and van Breemen, O.. 1979b. The 'Central Highland Granulites'-cover-basement tectonics in the Moine. In: Harris, A. L., Holland, C. H., and Leake, B. E. (Eds.) The Caledonides of British Isles- reviewed. *Special publication of the Geological Society of London.*

Piasecki, M. A. J. and Temperley, S., 1988. The Central Highland Division. 46-53, In: Later Protrozoic stratigraphy of the Northern Atlantic Regions. Winchester, J. A. (editor). Blackie, New York.

Pidgeon, R. T. & Aftalion, M., 1978. Cogenetic and inherited zircon U-Pb systems in granites: Palaeozoic granites of Scotland and England. In: Bowes, D. R. & Leake, B. E. (eds). Crustal evolution in northwestern Britain and adjacent regions. *Geological Journal, Special Issue*, **10**, 183-220.

Pigage, L. C. and Greenwood, H. J., 1982. Internally consistent estimates of pressure and temperature: The staurolite problem. *American Journal of Science*, **282**, 943-969.

Pitcher, W., S. and Berger, A. R., 1972. The geology of Donegal: a study of granite emplacement. *Wiley and Sons, Interscience*: New York.

Piwinskii A. J. and Wyllie, P. J., 1968. Experimental studies of igneous rock series; a zonal pluton in the Wallowa Batholith, Oregon. *Gournal of Geology*, **76**, 205-234.

Plant, J. A., 1986. Models for granites and their mineralising systems in the British and Irish Caledonides. In: Geology and genesis of mineral deposits in Ireland. Andrew, C. J. (editor). Pp 121-156. Dublin, *Irish Association for Economic Geology.*

Plant, J., Brown, G. C., Simpson, P. R. and Smith, R. T., 1980. Signature of metalliferous granites in the Scottish Caledonides. *Trans. Inst. Min. Metall.* **89B**, 198-210.

Platten, I. M., 1982. Partial melting of feldspatic quartzite around late Caledonian minor intrusions in Appin, Scotland. *Geological Magazine,* **119(4),** 413-419.

Platten, I. M., 1983. Partial melting of semipelites and the development of marginal breccias around a late Caledonian minor intrusion in the Grampian Highlands of Scotland. *Geological Magazine,* **120(1),** 37-49.

Platten, I. M.,1991. Zoning and layering in diorites of the Scottish Caledonian Appinite suite. *Geological Journal*, **26**, 329-348.

Poldervaart, A. and Hess, H. H., 1951. Pyroxenes in crystallisation of basaltic magmas. *Journal of Geology*, **59**, 472-489.

Powell, D., 1974. Stratigraphy and structure of the Western Moine and the problem of Moine orogenesis. *Journal of the Geological Society of London*, **130**, 575-590.

Powell, C. McA., 1979. A morphological classification of rock cleavage. *Tectonophysics*, **58,** 21-34.

Powell, D. & Phillips, W. E. A., 1985. Time and deformation in the Caledonian orogen of Britain and Ireland. In: Harris (Ed.) The Nature and timing of orogenic activity in the Caledonian rocks of the British Isles. *Geological Society of London Mem.*, **9,**17-39.

Powell, R., Condliffe, D. M. and Condliffe, E., 1984. Calcite-dolomite thermometry in the system $CaCO_3$-$MgCO_3$-$FeCO_3$: an experimental study. *Journal of Metamorphic Geology*, **2**, 33-41.

Powell, R. & Holland, T. J. B., 1988. An internally consistent thermodynamic dataset with uncertainties and correlation: 3, Application to geobarometry, worked examples and a computer program. *Journal of Metamorphic Geology*, **6**, 173-204.

Powell, R. & Downes, J., 1990. Garnet porphyroblasts-bearing leucosomes in metapelites: mechanisms, phase diagrams, and an example from Broken Hill, Australia. In: *High-temperature Metamorphism and Crustal Anatexis* (eds. Ashworth, J. R. & Brown, M.), pp.105-123, Unwin Hyman, UK.

Pringle, J., 1940. The discovery of Cambrian trilobites in the Highland Border rocks near Callander, Perthshire. *Advanc. Sci. London,* **1,** 252.

Rast, N., 1958. The tectonics of the Schiehallion Complex. *Quarterly Journal of the Geological Society of London*, **114**, 25-46.

Rast, N., 1963. Structure and metamorphism of the Dalradian rocks of Scotland.In: Johnson, M. R. W. and Stewart, F. H. (Eds,) *The British Caledonides.* Oliver & Boyd, London and Edinburgh.

Rast, N. & Litherland, M., 1970. The correlation of the Ballachulish and Perthshire (Iltay) Dalradian successions. *Geological Magazine*, **107**, 259-272.

Read, H. H., 1923. The geology of Banff, Huntly, Turriff. *Mem. Geological Survey of Scotland.*

Read, H. H., 1936. The stratigraphical order of the Dalradian rocks of the Banffshire coast. *Geological Magazine,* **73,** 468-473.

Read, H. H., 1961. Aspects of the Caledonian magmatism in Britain. *Proceedings of the Liverpool and Manchester Geological Society*, **2**, 653-683.

Read, H. H., 1952. Metamorphism and migmatization in the Ythan Valley, Aberdeenshire. *Transactions of the Geological Society of Edinburgh,* **15,** 265-279.

Read, H. H., 1955. The Banff Nappe. *Proceedings of Geological Association of London,* **66,** 1-29.

Reinhardt, J. and Rubenach, M. J., 1989. The temperature-time relationship across metamorphic zones: Evidence from porphyroblast-matrix relationships in progressively deformed metapelites. *Tectonophysics*, **158,** 141-161.

Reverdatto, V. V., 1973. The facies of contact metamorphism. In Sobolov, V. S. (ed.) *Dept. Geol. Publication* **233**, Canberra, 263 p.

Rice, J. M., 1977b. Contact metamorphism of impure dolomitic limestone in the Boulder aureole, Montana. *Contributions to Mineralogy and Petrology*, **59**, 237-259.

Richardson, S. W. & Powell, R., 1976. Thermal causes of the Dalradian metamorphism in the central Highlands of Scotland. *Scottish Journal of Geology,* **12,** 237-268.

Richardson, S. W., Gilbert, M. C. and Bell, P. M., 1969. Experimental determination of kyanite-andalusite and andalusite-sillimanite equilibria: the aluminium silicate triple point. *American Journal of Science*, **267**, 259-272.

Roberts, J. L., 1966. The emplacement of the Main Glencoe Fault-Intrusion at Stob Mhic Mhartuin. *Geological Magazine*, **103**, 299-316.

Roberts, J. L., 1974a. The structure of the Dalradian rocks in the SW Highlands of Scotland. *Journal of the Geological Society of London*, **130**, 93-124.

Roberts, J. L., 1974b. The evolution of the Glencoe Cauldron. *Scottish Journal of Geology*, **10**, 269-282.

Roberts, J. L. & Treagus, J. E., 1975. The structure of the Moine and Dalradian rocks in the Dalmally district of Argyllshire, Scotland. *Geological Journal*, **10**, 59-74.

Roberts, J. L. & Treagus, J. E., 1977. Polyphase generation of nappe structures in the Dalradian rocks of the SW Highlands of Scotland. *Scottish Journal of Geology*, **13**, 237-254.

Roberts, J. L. & Treagus, J. E., 1979. Stratigraphical and structural correlation between the Dalradian rocks of SW and Central Highlands of Scotland. In: *The Caledonides of the British Isles-reviewed.* Pp. 199-204. Harris, A. L., Holland, C. H., and Leake, B. E., (editors). *Special Publication of the Geological Society of London*, No. 8.

Robertson, S., 1991. Older granites in the south-eastern Scottish Highlands. *Scottish Journal of Geology*, **27**, 21-26.

Robertson, S.,1994. Timing of Barrovian metamorphism and 'Older Granite' emplacement in relation to Dalradian deformation. *Journal of the Geological Society of London*, **151**, 5-8.

Rock, N. M. S., 1991. *Lamprophyres*. Blackie, Glasgow and London.

Rock, N. M. S., Cooper, C. and Gaskarth, J. W., 1986a. Late Caledonian subvolcanic vents and associated dykes in the Kirkcudbright area, Galloway, SE Scotland. *Proceedings of the Yorkshire Geological Society,* **46,** 29-38.

Rock, N. M. S., Gaskarth, J. W. and Rundle, C. C., 1986b. Late Caledonian dyke swarms in southern Scotland: a regional zone of primitive K-rich lamprophyric and associated vents. *Journal of Geology,* **96,** 505-522.

Rogers, G., Dempster, T. J., Bluck, B. J. and Tanner, P. W. G., 1989. A high-precision U/Pb age for the Ben Vuirich granite: implications for the evolution of the scottish Dalradian Supergroup. *Journal of the Geological Society of London*, **146**, 789-798.

Rogers, G., and Dunning, G., R.,1991. Geochronology of appinitic and related granitic magmatism in the W Highlands of Scotland: constraints on the timing of

transcurrent fault movement. *Journal of the Geological Society of London*, **148**, 17-27.

Rosenbusch, H., 1877. Die Steiger Schiefer und ihre Contactzonean den Granitten von Barr-Andlau und Hohwald. *Abh. Geol. Specialkarte Elsass-Lothr.* **1**, 79-393.

Ross, M. and Huebner, J. S., 1975. A pyroxene thermometer based on temperature-composition relationships of naturally occuring orthopyroxne, pigeonite, and augite. (extended abstract), *International Conference on Geothermometry and Geobarometry, Pennsylvania State University*, Oct. 5-10, 1975.

Russ-Nabelek, C., 1989. Isochemical contact metamorphism of mafic schist, Laramie anorthosite Complex, Wyoming: Amphibole composition and reactions. *American mineralogist*, **74**, 530-549.

Sabine, P. A., 1963. The Strontian granite complex, Argyllshire. *Bull. Geol. Surv. Gt. Br.* **20**, 6-42.

Saxena, S. K., 1969. Silicate solid-solution and geothermometry 3. Distribution of Fe and Mg between coexisting garnet and biotite. *Contributions to Mineralogy and Petrology*, **22**, 259-267.

Saxena, S. K., 1976. Two pyroxene thermometer: A model with an approximate solution. *American Mineralogist*, **61**, 643-652.

Saxena, S. K. and Nehru, C. E., 1975. Enstatite-diopside solvus and geothermometry. *Contributions to Mineralogy and Petrology*, **49**, 259-267.

Seck, H. A., 1971a. Koexistierende Alkalifeldspäte und Plagioklase im System $NaAlSi_3O_8$-$KAlSi_3O_8$-$CaAl_2Si_2O_8$-H_2O bei Temperaturen von 650° C bis 900° C. *N. Jb. Miner. Abh,*. **115**, 315-345.

Seck, H. A., 1971b. Der Einfluss des Drucks auf die Zusammensetzung koexistierender Alkalifeldspäte und plagioklase im System $NaAlSi_3O_8$-$KAlSi_3O_8$-$CaAl_2Si_2O_8$-H_2O. *Contribution to Mineralogy and Petrology*, **31**, 67-86.

Sederholm, J. J., 1907. Om granit och gneis. English summary: On granite and gneiss. *Bulletin Commision Géologique de Finland,* **23,** 1-90.

Sederholm, J. J., 1913. Die Entstehung der migmatitishen Gesteine. *Geologische Rundschau*, **4,** 174-185.

Sederholm, J. J., 1934. On migmatites and associated Precambrian rocks of southwestern Finland. *Bulletin Commision Géologique de Finland,* **107,** 1-68.

Sederholm, J. J., 1967. *Selected Works: Granites and Migmatites.* Oliver and Boyd, Edinburgh.

Seifert, F., 1970. Low-temperature compatibility relations of cordierite in haplopelites of the system K_2O-MgO-Al_2O_3-SiO_2-H_2O. *Journal of Petrology*, **11**, 73-99.

Seifert, F., 1976. Stability of the assemblage cordierite+K-feldspar+quartz. *Contributions to Mineralogy and Petrology*, **57**, 179-185.

Seki, Y., 1957. Petrological study of hornfelses in the central part of the median zones of Kitakami Mountainland, Iwate Prefecture. *Science Reports of Saitama University* **2**, 307-361.

Sengupta, P., Dasgupta, S., Bhattacharya, P. K. and Mukherjee. M., 1990. An orthopyroxene-biotite geothermometer and its application in crustal granulites and mantle-derived rocks. *Journal of Metamorphic Geology*, **8**, 191-197.

Shackleton, R. M., 1958. Downward-facing structures of the Highland Border. *Quarterly Journal of the Geological Society of London*, **113**, 361-392.

Shand, S. J., 1974. Eruptive rocks, their genesis, composition, classification and their relation to ore-deposits, 3rd edition, *J. Wiley and Sons, New York*, 488pp.

Shaw, H. R., 1963. The four-phase curve sanidine-quartz-liquid-gas between 500 and 4000 bars. *American Mineralogist*, **48**, 883-896.

Shiba, M., 1988. Metamorphic evolution of the southern part of Hidaka Belt, Hokkaido, Japan. *Journal of Metamorphic Geology*, **6**, 273-296.

Shive, P. N., Yei, Y., Frost, B. R. and Swapp, S., 1991. Effects of prograde metamorphism on magmatic properties of basalts. *Transactions of American Geophysics Union*, **72**, 100.

Sivaprakash, S., 1982. Geothermometry and geobarometry of Dalradian metapelites and metabasites from the Central Scottish Highlands. *Scottish Journal of Geology*, **18**, 109-124.

Skevington, D., 1971. Palaeontological evidence on the age of the Dalradian deformation and metamorphism in Ireland and Scotland. *Scottish Journal of Geology,* **7,** 285-288.

Smith, J. V. and Schreyer, W., 1962. Location of argon and water in cordierite. *Mineralogical Magazine*, **33**, 226-236.

Spear, F. S., 1978. Petrogenetic grid for amphibolites from the Post Pond and Ammonoosuc Volcanics. *Carnegie Institute Washington year book*, **77**, 805-808.

Spear, F. S., 1981. An experimental study of hornblende stability and compositional variability in amphibolite. *American Journal of Science*, **281**, 697-734.

Spear, F. S., 1993. Metamorphic phase equilibria and pressure-temperature time paths. *Mineralogical Society of America*, Monograph.

Spear, F. S. & Florence, F. P., 1992. Thermobarometry in granulites: pitfalls and new approaches, *Pre-Cambrian Research*, **55**, 209-241.

Speer, J. A., 1981. The nature and magnetic expression of isograds in the contact aureole of the Liberty Hill pluton, South Carolina: Part II *Geological Society of America Bulletin*, **92**, Part I, 603-609, Part II, 1262-1358.

Speer, J. A., 1982 Metamorphism of the pelitic rocks of the Snyder Group in the contact aureole of the Kiglapait layered intrusion, Labrador: Effects of buffering partial pressure of water. *Canadian Journal of Earth Science*, **19**, 1888-1909.

Spencer, A. M., 1971. Late Precambrian glaciation in Scotland. *Mem. Geological Society of London*, **6,** 100 pp.

Spencer, A. M., 1981. The late Precambrian Port Askaig Tillite in Scotland. In: *Earth's pre-Pleistocene glacial record.* pp. 632-636. Hambrey, M. J. and Harland W. B. (editors). *Cambridge University Press.*

Spencer, M. O. and Pitcher, W. S., 1968. Occurrence of the Portaskaig Tillite in north-east Scotland. *Proceedings of the Geological Society of London*, **1650,** 195-198.

Spencer, A. M. and Spencer, M.O., 1972. The Late Precambrian-Lower Cambrian Bonahaven Dolomite of Islay and its stromatolites. *Scottish Journal of Geology,* **8,** 269-282.

Spry, A., 1969. Metamorphic Textures. *Pergamon Press.* Oxford, 350 pp.

Stephens, W. E. and Halliday, A. N., 1984. Geochemical contrast between late Caledonian plutons of northern, central and southern Scotland. *Transactions of the Royal Society of Edinburgh*, **75**, 259-273.

Stephenson, D. and Gould, D., 1995. *The Grampian Highlands* (4th edition). British Geological Survey.

Stevens, G., Clemens, J. D. & Droop, G. T. R., 1997. Melt production during granulite-facies anatexis: experimental data from "primitive" metasedimentary protoliths. *Contributions to Mineralogy and Petrology,* **128,** 352-370.

Streckeisen, A., 1976. To each plutonic rock its proper name. *Earth Sciences Review*, **12**, 1-33.

Sturt, B. A., 1961. The geological structure of the area south of Loch Tummel. *Journal of the Geological Society of London,* **117,** 131-156.

Sturt, B. A. and Harris, A. L., 1961. The metamorphic history of the Loch Tummel area, Central Perthshire. *Liverpool Manchester Geological Journal*, **2**, 689-711.

Summerhayes, C. P., 1966. A geochronological and strontium isotope study of the Garabal Hill-Glen Fyne igneous complex, Scotland. *Geological Magazine*, **134**, 41-44.

Tanner, P. W. G. and Leslie, A. G., 1994. A pre-D2 age for the 590 Ma Ben Vurich Granite from the Dalradian of Scotland. *Journal of the Geological Society of London*, **151**, 209-212.

Taylor, S. R. and McLennan, S. M., 1985. *The continental crust.: its composition and evolution*. Blackwell, Oxford.

Temperley, S. 1989. The Grampian Highlands of Scotland; an orogenic analogue to the Adelaide fold belt of South Australia. *Abstract, Geological Society of Australia*, **24**, 146-147.

Thirwall, M. F., 1981. Implications for Caledonian plate tectonic model of chemical data from volcanic rocks of the British Old Red Sandstone. *Journal of the Geological Society of London*, **138**, 123-138.

Thirwall, M. F., 1982. Systematic variation in chemistry and Nd-Sr isotopes across a Caledonian calc-alkaline volcanic arc: implications for source materials. *Earth and Planetary Science Letters*, **58**, 27-50.

Thirwall, M. F., 1986. Lead isotope evidence for the nature of the mantle beneath Caledonian Scotland. *Earth and Planet. Sci. Lett.* 80, 55-70.

Thomas, P. R., 1979. New evidence for a Central Highland Root Zone. In: Harris, A. L., Holland, C. H., and Leake, B. E. (Eds.) The Caledonides of British Isles- reviewed. *Special publication of the Geological Society of London.*

Thomas, P. R., 1980. The stratigraphy and structure of the Moine rocks N of the Schiehallion Complex, Scotland. *Journal of the Geological Society of London,* **137,** 469-482.

Thomas, P. R. and Treagus, J. E., 1968. The stratigraphy and structure of the Glen Orchy area, Argyllshire, Scotland. *Scottish Journal of Geology*, **4**, 121-134.

Thompson, A. B., 1976. Mineral reactions in pelitic rocks: II. Calculation of some P-T-X(Fe-Mg) phase relations. *American Journal of Science*, **276**, 401-424.

Thompson, J. B., Jr., 1957. The graphical analysis of mineral assemblages in pelitic schists. *American Mineralogist,* **42,** 842-858.

Tilley, C. E., 1924. Contact-metamorphism in the Comrie area of the Perthshire Highlands. *Quarterly Journal of the Geological Society of London*, **80**, 22-71.

Tilley, C. E., 1925. A preliminary survey of metamorphic zones in the Southern Highlands of Scotland. *Quarterly Journal of the Geological Society of London,* **81,** 100-112.

Tracy, R. J., Jaffe, H. W. and Robinson, P., 1978. Monticellite marble at Cascade Mountain, adirondack Mountain, New York. American Mineralogist, **63**, 991-999.

Tracy, R. J., Robinson, P. and Thompson, A. B., 1976. Garnet composition and zoning in the determination of temperature and pressure of metamorphism, Central Massachusetts. *American Mineralogist*, **61**, 762-775.

Treagus, J. E., 1987. The structural evolution of the Dalradian of the Central Highlands of Scotland. *Transactions of the Royal Society of Edinburgh,* **78,** 1-15.

Treagus, J. E., 1991. Fault displacement in the Dalradian of the Central Highlands. *Scottish Journal of Geology,* **27** (2), 135-145.

Treagus, J. E. and King, G., 1978. A Complete Lower Dalradian succession in the Schiehallion district, Central Perthshire. *Scottish Journal of Geology,* **4,** 157-166.

Treloar, P. J., 1981. Garnet-biotite-cordierite thermometry and barometry in the Cashel thermal aureole, Connemara, Ireland. *Mineralogical Magazine*, **44**, 183-189.

Troll G. and Weiss, S., 1991. Structure, petrography and emplacement of plutonic rocks. *In: Equilibrium and kinetics in contact metamorphism; the Ballachulish igneous complex and its aureole.* Voll, G., Toepel, J. Pattison, D. R. M. and Seifert, F. (editors), Springer Verlag, Berlin.

Tullis, J. and Yund, R. A., 1980. Hydrolytic weakening of experimentally deformed Westerly Granite and Hale Albite rock. *Journal of Structural Geology*, **2**, 439-451.

Turnell, H. B., 1985. Palaeomagnetism and Rb-Sr age of the Ratagan and Comrie intrusions. *Geophysical Journal of the Royal Astronomical Society*, **83**, 363-378.

Tuttle, O. F. and Bowen, N. L., 1958. Origin of granite in the light of experimental studies in the system $NaAlSi_3O_8$-$KAlSi_3O_8$-SiO-H_2O. *Geological Society of America, Mem.*, **74.**

Tyler, I. M. and Ashworth, J. R., 1982. Sillimanite-potash feldspar assemblages in graphitic pelites, Strontian area, Scotland. *Contributions to Mineralogy and Petrology,* **81,** 18-29.

Upton, P. S., 1986. A structural cross-section of the Moine and Dalradian rocks of the Braemar area. *Report of the British Geological Survey*, **17**, No.1, 9-19.

Valley, J. W. and Essene, E., J., 1980. Calc-silicate reactions in Adirondack marble: The role of fluids and solid solution. *Geological Society of America Bulletin*, **91**, 114-117, 720-815.

Van Breeman, O. and Piasecki, M. A. J., 1983. The Glen Kyllachy granite and its bearing on the Caledonian orogeny in Scotland. *Journal of the Geological Society of London*, **140**, 47-62.

Vernon, R. H., 1979. Formation of late sillimanite by hydrogen metasomatism (base-leaching) in some high-grade gneisses. *Lithos*, **12**, 143-152.

Vielzeuf, D., 1983. The spinel and quartz associations in high grade xenoliths from Tallante (S. E. Spain) and their potential use in geothermometry and barometry. *Contributions to Mineralogy and Petrology*, **82**, 301-311.

Vielzeuf, D. & Holloway, J. R., 1988. Experimental determination of the fluid-absent melting reactions in the pelitic system: consequences for crustal differentiation. *Contributions to Mineralogy and Petrology,* **98,** 257-276.

Von Platen, H., 1965. Experimental anatexis and genesis of migmatites. In: *Controls of Metamorphism* (eds Pitcher, W. S. & Flynn, G. W.), pp. 213-218. Oliver and Boyd, London.

Vry, J.K., Brown, P.E. and Valley, J.W., 1990. Cordierite volatile content and the role of CO_2 in high-grade metamorphism. *American Mineralogist*, **75**, 71-88.

Wadsworth, W. J., 1991. Silicate mineralogy of the Belhevie cumulates, NE Scotland. *Mineralogical Magazine*, **55**, 113-119.

Waters, D. J. & Whales, C. J., 1984. Dehydration melting and the granulite transition in metapelites from southern Namaqualand, S. Africa. *Contributions to Mineralogy and Petrology,* **88,** 269-275.

Watkins, K. P., 1985. Petrogenesis of Dalradian albite porphyroblast schists. *Journal of the Geological Society of London*, **140,** 601-618.

Watson, J. V., 1964. Conditions in the metamorphic Caledonides during the period of late-orogenic cooling. *Geological Magazine*, **101**, 457-465.

Watson, J. V., 1984. The ending of the Caledonian orogeny in Scotland. *Journal of the Geological Society of London,* **141,** 193-214.

Weaver, B. and Tarney, J., 1984. Empirical approach to estimating the composition of the continental crust. *Nature*, **310,** 575-577.

Weiss, S. and Troll, G., 1989. The Ballachulish igneous complex Scotland: Petrography, mineral chemistry , and order of crystallisation in the Monzodiorite-Quartz Diorite and suite and in the Granite. *Journal of Petrology*, **30**, 1069-1115.

Wells, P. R. A., 1977. Pyroxene thermometry in simple and complex systems. *Contributions to Mineralogy and Petrology*, **62**, 129-139.

Wells, P. R. A. and Richardson, S. W., 1979. Thermal evolution of metamorphic rocks in the Central Highlands of Scotland. In: Harris, A. L., Holland, C. H., and Leake, B. E. (Eds.) The Caledonides of British Isles- reviewed. *Special publication of the Geological Society of London.*

Wen, S. and Nekvasil, H., 1994. SOLVOCALC Computer Program for feldspar thermometry.

Westbrook, G. K. and Borrodaile, G. J., 1978. The geological significance of the magnetic anomalies in the region of Islay. *Scottish Journal of Geology,* **14,** 213-224.

White, A. J. R., 1966. Genesis of migmatites from the Palmer region of South Australia. *Chemical Geology*, **1,** 165-200.

Williamson, W. O., 1935. The composite gneiss and contaminated granodiorite of Glen Shee, Perthshire. *Quarterly Journal of the Geological Society of London*, **91**, 382-422.

Wilson, J. R. and Leake, B. E., 1972. The petrochemistry of the epidiorite of the Tayvallich Peninsula, North Knapdale, Argyllshire. *Scottish Journal of Geology*, **8,** 215-252.

Winchester, J. A. and Glover, B. W., 1988. The Grampian Group, Scotland. In: Winchester, J. A. (Ed.) *Later Proterozoic stratigraphy of the Northern Atlantic regions.* Blackie, Glasgow and London, 146-161.

Wones, D. R. and Eugster, H. P., 1965. The stability of phlogopite in the presence of quartz and diopside. In: Fraser, D. G. (ed.) *Thermodynamics and Geology*, Reidel Dortrecht, 229-247.

Wones, D. R. and Gilbert, M. C., 1982. Amphibole in the igneous environment. In: Veblen, D. R. and Ribbe, P. H. (editors). Amphiboles: Petrology and phase relations. *Mineralogical Society of America, Review in Mineralogy*, **9B**, 325-389.

Wood, B. J. and Banno, S., 1973. Garnet-orthopyroxene and garnet-clinopyroxene relationships in simple and complex systems. *Contributions to Mineralogy and Petrology*, **42**, 109-124.

Wood, B. J. and Fraser, D. G., 1977. Elementary thermodynamics for geologists. Oxford University Press, Oxford

Wood, D. A., Tarney, J., Varet, J., Saunders, A. D., Bougault, H., Joron, J. L., Treuil, M. and Cann, J. R., 1979. Geochemistry of basalts drilled in the North Atlantic by IPOD Leg 49: implications for mantle heterogeneity. *Earth and Planetary Science Letters*, **42**, 77-97.

Worden, R. H., Droop, G. T. R. and Champness, P. E., 1992. The influence of crystallography and kinetics on phengite breakdown reactions in a low-pressure metamorphic aureole. *Contributions to Mineralogy and Petrology*, **110**, 329-345.

Wright, A. E., 1988. The Appin Group. In: Winchester, J. A. (Ed.) *Later Proterozoic stratigraphy of the Northern Atlantic regions.* Blackie, Glasgow and London, 146-161.

Wyllie, P. J. & Tuttle, O. F., 1961. Hydrothermal melting of shales. *Geological Magazine,* **98,** 56-66.

Zaleski, E., 1983. The geology of Strathspey and Lower Findhorn granitoid-a study involving field relations, petrography, mineralogy, geochemistry and geochronology. *Unpublished M.Sc. thesis*, University of St Andrews.

Zaleski, E., 1985. Regional and contact metamorphism within the Moy Intrusive Complex. Contributions to Mineralogy and Petrology, **89**, 296-306.